Integrated Performance and Potential Assessment of Floating Solar PV Systems in Indian Tropical Region: Field Experimentation, Modelling and Evaporation Management

THESIS

Submitted in partial fulfilment of the requirements for the degree of

DOCTOR OF PHILOSOPHY

by

KARMENDRA KUMAR AGRAWAL
2017PHXF0105P

Under the Supervision of

Dr Ravi Kant Mittal
Dr Shibani Khanra Jha
Dr Ajit Pratap Singh

BITS Pilani
Pilani | Dubai | Goa | Hyderabad

BIRLA INSTITUTE OF TECHNOLOGY AND SCIENCE, PILANI

2024

BIRLA INSTITUTE OF TECHNOLOGY AND SCIENCE, PILANI

CERTIFICATE

This is to certify that the thesis titled **Integrated Performance, and Potential Assessment of Floating Solar PV Systems in Indian Tropical Region: Field Experimentation, Modelling, and Evaporation Management** submitted by **Karmendra Kumar Agrawal** ID No **2017PHXF0105P** for award of Ph.D. of the Institute embodies original work done by him under our supervision.

Signature of the Supervisor:

DR RAVI KANT MITTAL
Professor
Department of Civil Engineering
Birla Institute of Technology and Science, Pilani, Pilani Campus
Date:

Signature of the Co Supervisor:

DR SHIBANI KHANRA JHA
Associate Professor
Department of Civil Engineering
Birla Institute of Technology and Science, Pilani, Pilani Campus
Date:

Signature of the Co Supervisor:

DR AJIT PRATAP SINGH
Senior Professor
Department of Civil Engineering
Birla Institute of Technology and Science, Pilani, Pilani Campus

Date:

ABSTRACT

Energy consumption stands as a pivotal determinant of economic growth and national development. With fossil fuels reigning as the primary energy source, powering approximately 70% of global energy production, concerns over greenhouse gas emissions loom large. The combustion of these fuels releases pollutants, exacerbating climate change and setting the stage for natural disasters like floods, droughts, and earthquakes. To avert such catastrophic outcomes, the imperative for an efficient, clean, and secure energy system becomes apparent for future generations.

However, the widespread adoption of Photovoltaic (PV) technology is hindered by its significant land requirements. Deploying solar power plants on agricultural land not only diverts precious land from farming activities for decades but also poses a loss to humanity's food supply. Alternatively, if the land is less fertile, it could be utilized for forest, residential, or industrial development. Enter the innovative solution of Floating Solar PV systems (FSPV), where solar panels are installed over water bodies, offering a viable alternative to land-based installations. FSPV not only mitigates land usage concerns but also enhances panel performance by operating at lower temperatures, thereby improving energy generation efficiency and reducing evaporation losses from water bodies.

Despite its potential, there remains a scarcity of studies on the technical feasibility, evaporation reduction, module performance, and economic viability of FSPV systems globally. This research endeavours to address these gaps by investigating the technical potential, evaporation loss reduction, module operating temperatures, module performance, and economic aspects of floating solar PV systems in the tropical region of Uttar Pradesh.

Floating Solar Photovoltaic (FSPV) systems are anticipated to exhibit superior efficiency compared to ground-mounted PV systems, largely due to their lower operating temperatures. To investigate this, an experimental FSPV setup was devised, featuring solar panels positioned at varying heights above the water surface. Results from the study reveal that FSPV modules can reduce module temperatures by up to 4°C-7°C under diurnal conditions. Assessing performance in terms of power output, the study underscores the importance of optimizing panel height over water bodies to maximize power generation. Recommendations include raising FSPV modules to their optimal height, with systems positioned at 500 mm above water surface yielding 1.8%-3.78% higher power output compared to ground-mounted PV systems, representing the highest among all panels tested.

The literature offers limited insight into module temperature prediction models for FSPV. Hence, Regression models were developed to predict the temperature of Floating Solar Photovoltaic (FSPV) modules, building upon the existing Kings model used for ground-mounted panels. These models were tailored to the experimental setup of solar panels installed on water bodies at BITS Pilani, India. Utilizing various parameters including ambient temperature, solar insolation, wind velocity, water temperature, and humidity, the regression and modified Kings models were employed to forecast the operating temperature of solar PV installations over water bodies. Among the developed models, the one-degree regression models incorporating three parameters exhibited superior performance compared to those with four or five parameters.

The study demonstrates that the annual power output estimates generated by the best-performing model align within an error margin of less than 0.2% compared to recorded data. Notably, research findings indicate that solar PV panels installed over water bodies boast an annual power output 2.5% higher than ground-mounted systems. These newly developed regression and modified Kings models offer reliable predictions for the operating temperature of solar PV installations over water bodies. Remarkably, only three meteorological parameters—ambient temperature, solar insolation, and wind velocity—are required to accurately predict module temperature in this context.

Extending the research, a comprehensive assessment was conducted at Rajghat Dam in Uttar Pradesh to estimate the technical potential of floating photovoltaic power generation, water conservation, and the preservation of agricultural land. The study revealed a power potential of 6513 MWp with 25% coverage of the total submergence area at Rajghat dam, yielding an annual power generation of 10,623,501 MWh. Additionally, an annual evaporation loss reduction of 1395 cubic meters per MWp (equivalent to 0.9 litres per kWh) was identified as an added benefit. Economic assessment indicated a Levelized Cost of Energy (LCOE) of $0.036/kWh (INR 2.61/kWh) with an 8.55% internal rate of return (IRR), indicating favourable conditions for large-scale deployment of Floating Solar Photovoltaic (FSPV) plants. Based on these findings, the study estimated the FSPV installation potential over major reservoirs of Uttar Pradesh to be 37,762 MWp with 25% area coverage, and 15,093 MWp with 10% area coverage.

Furthermore, the study estimated the evaporation reduction resulting from the deployment of FSPV systems above water surfaces and identified the best panel height above water bodies to maximize evaporation reduction. These insights were extended to evaluate the impact of FSPV installations on reducing evaporation over the major dams in the tropical region of

Uttar Pradesh, India. Experimental results revealed that the greatest evaporation reduction occurred with panels positioned 300 mm above the water surface, resulting in a reduction of 23.44%. Extending these findings to 28 major dams in Uttar Pradesh, an annual water saving of 92.56 million cubic meters (MCM) was projected with FSPV coverage of 25%. Notably, estimations suggested that a 1 MWp FSPV installation could provide water for 67 individuals annually in a tropical region, assuming a consumption rate of 100 liters per capita per day (lpcd).

Limited research has been conducted on estimating evaporation from water surfaces covered with photovoltaic (PV) panels, particularly in the context of Floating Solar Photovoltaic (FSPV) installations. This study focuses on the development of regression models for evaporation estimation under various conditions, leveraging experiments conducted in Pilani, India. It scrutinizes the dynamics of evaporation and validates estimation models, while also examining the impact of different meteorological parameters on evaporation rates to aid in model selection based on data availability and accuracy.

Expanding the study evaluates evaporation rates at 28 dam sites, comparing rates under uncovered and FSPV-covered conditions. Utilizing developed 4-parametric regression models, evaporation rates were assessed at these sites, both with and without PV panel coverage. The highest evaporation rates were recorded at Ohan dam, measuring 2126.53 mm/year for open sky and 1567.63 mm/year for covered with PV panels. Conversely, Kalagarh dam exhibited the lowest rates, at 1783.29 mm/year and 1283.32 mm/year, respectively. Notably, a substantial reduction in evaporation was observed when dam surfaces were covered with PV panels, ranging from 26.28% to 29.95% reduction at Ohan Dam and Pahuj dam, respectively.

Choosing to deploy Floating Solar Photovoltaic (FSPV) panels at dam locations requires more than just understanding changes in water surface area; it also involves evaluating installation expenses. Coverage recommendations for FSPV panels over water surfaces have been made by analysing evaporation reduction across twenty-eight dam sites, aiding in the decision-making process. Key factors such as the capacity of FSPV installations, cost implications, evaporation savings, and potential annual energy production have been thoroughly examined to support decision-makers and practitioners. To simplify the decision-making process, intuitive charts have been created that allow professionals to easily identify the best coverage strategy, installation capacity, associated costs, and estimated energy production tailored to their specific needs and limitations.

Beyond merely understanding water surface area changes, deploying FSPV panels at dam locations necessitates meticulous evaluation of installation expenses and associated benefits. Analysis of evaporation reduction across various dam sites informs decision-making processes, guiding recommendations for FSPV panel coverage. Factors such as installation capacity, cost implications, evaporation savings, and potential energy production are thoroughly examined to provide actionable insights for decision-makers. Through the creation of intuitive decision-making charts, tailored to specific needs and limitations, professionals are equipped with invaluable tools for making informed decisions regarding FSPV installations, serving both water preservation and energy generation goals effectively.

Keywords: Floating solar, Performance, panel operating temperature, potential, evaporation reduction, decision making.

ACKNOWLEDGEMENTS

Foremost, I offer my gratitude to my Mother and Father, who have brought me to this world and have laid for me a strong foundation so that I work miracles in my life while weaving my life amid the many challenges I come across from time to time. They have been watching over me and blessing me. Their teachings and sacrifices continue to inspire and motivate me at every step of my life. I have inherited my interest and curiosity in knowing things retrospectively from my father since my childhood.

I am indebted to the UP Irrigation and Water Resources Department for providing me with the invaluable opportunity to pursue this research Endeavour. This has significantly helped me with my professional growth. I promise to make certain value addition to the department with the newly obtained qualification. My exceptional admiration is reticent for Mr. T Venkatesh (Former, Additional Chief Secretary) for facilitating my respite from departmental responsibilities, and to Mr. Anil Garg (Principal Secretary) for advocating the worth of this work at the governmental level and its immense contribution in policy formulation for the benefit of Uttar Pradesh and its people.

This is a heartfelt acknowledgment of Dr. Ravi Mittal, whose exceptional mentorship and steadfast encouragement played a pivotal role during my PhD journey. His profound knowledge and commitment shone brightly in the detailed organization and implementation of experiments at BITS Pilani, facilitating the steady advancement of my research activities. The priceless input of Dr. Mittal has significantly enhanced my academic journey, leaving a lasting impact on my intellectual progress and evolution.

I would like to express my profound gratitude to Dr. Shibani Khanra Jha, my respected co-guide, for her invaluable mentorship and unwavering support during my educational journey. Dr. Jha's deep expertise and wholehearted dedication were especially apparent in her thorough revision of my work, enhancing its clarity and consistency. Her perceptive advice and beneficial suggestions have greatly improved the quality of my research and have been pivotal in both my personal growth and scholarly progress. I am deeply thankful for her guidance and help.

I am deeply grateful to Dr. Ajit Pratap Singh, my co-guide, for graciously accepting my request for guidance despite his demanding schedule. His extensive expertise and forward-thinking ideas proved to be invaluable assets to this research endeavor. Dr. Singh's profound understanding of the subject matter and innovative insights greatly enriched the development and execution of the project. His steadfast support and mentorship have been instrumental in shaping my academic journey, and I am deeply appreciative of his contributions.

I would like to be grateful to Prof. Anupam Singhal, Head of the Department, for his priceless support in effecting my thesis. I am also indebted to Prof. Anshuman, former Head, Department of Civil Engineering, BITS- Pilani, Pilani Campus. I would like to convey my recognition to the members of the Doctoral Advisory Committee (DAC), Prof. R Srinivas, and Prof. Selva Balaji M, Department of Civil Engineering, BITS- Pilani, Pilani Campus, for their precious annotations and opinion on the thesis effort.

I express gratitude to Prof. V. Ram Gopal Rao (Vice Chancellor, BITS- Pilani) and Prof. S. K. Barai (Director, BITS- Pilani, Pilani Campus) for permitting and facilitating my pursuance of doctoral thesis. I would also like to express gratefulness to Prof. A. K. Sarkar (Former Director BITS- Pilani, Pilani Campus) for his rallying round me and encouragement. Special credit to Prof. Shamik Chakraborty (Associate Dean, Academic Research Division).

I convey my earnest admiration for Dr. Sanjay Vashishtha for igniting the spark of research within me and for his mentorship right through the research progression. I extend my sincere thanks to Mr. Mudit Consul for his initial brainstorming, gentle guidance and imposing confidence and trust in my research pursuits.

To my family members who stood by me with unwavering encouragement and support, I express my heartfelt appreciation. A special mention goes to my wife, Mani Agrawal, who selflessly assumed additional responsibilities to enable me to complete this work. I am profoundly grateful for her sacrifices and unwavering kindness, generosity, and selflessness. I also extend my gratitude to my children, Maitreyi and Kartika, for their understanding and standing by us during this extremely busy and hard time.

I extend my appreciation to First Green for their munificent support, without which this research would not have been feasible. Special appreciation to Mr. Saurabh Gupta for his invaluable aid in data analysis. I am deeply obliged to Mr. Kamal Shrawan for his devoted efforts in maintaining the instruments and field setup over four consecutive years, his commitment and earnestness are truly commendable.

Lastly, I express my gratitude to BITS Pilani for providing me with the opportunity to conduct my research and for providing the necessary infrastructure and support.

Karmendra Kumar Agrawal

This work is lovingly dedicated to my parents:

Shri Suresh Chandra Agrawal

&

Smt. Urmila Agrawal

Whose endless dedication in serving others as also relentless hard work, and unflinching commitment to ensure education for everyone have deeply inspired me. They have imbued me with the importance of knowledge, have constantly supported my abilities, and fostered a passion for learning in me.

TABLE OF CONTENTS

List of Figures

List of Tables

List of Symbols and Abbreviations

Symbols

A_s - surface area of water body (Acres)

A_M - area of the module in m^2

C_F - floater material cost ($)

C_n - net cash flow ($)

C_I - total investment cost ($)

C_{OM} - operation and maintenance cost ($)

C_{cloud} - cloud fraction

c_p - specific heat of water at constant pressure (1.013×10^{-3} MJ kg^{-1} $^oC^{-1}$)

D_{FPV} - discounting factor

d - number of days in month

D - hours of daylight

d_r - inverse relative distance Earth-Sun

D_{TA} - total annual hours of daylight

$\overline{E}_{ws}$ - mean evaporation rate from the water body

E_{FPV} - energy produced and supplied to the grid by the system in its lifetime (kWh)

$\overline{E}_p$ - mean evaporation rate from the pan

E - evaporation rate from uncovered water surface

$e_{0(T)}$ - saturation vapour pressure at temperature T ^oC

$e_{0(Tmax)}$ - saturation vapour pressure at daily maximum temperature

$e_{0(Tmin)}$ - saturation vapour pressure at daily minimum temperature

e_a - actual vapour pressure in hPa

E_p - evaporation rate from PV panel covered water surface

e_s - mean saturation vapour pressure at ambient temperature (hPa/mbar)

ET - evapotranspiration rate

e_w - mean saturated vapour pressure at water temperature (hPa/mbar)

f(u) - wind speed function

F_{in} - heat flux from water inflow

F_{out} - heat flux from water outflow

F_p - heat flux due to precipitation

G - soil heat flux

G_{sc} - solar constant (0.0820 $MJm^{-2}min^{-1}$ or 1370 Wm^{-2})

Gsub - heat conduction between water and its substrate

G_T - solar irradiance incident on module surface (W/m^2)

$G_{T\ NOCT}$ - solar irradiance incident on module surface at NOCT condition (W/m^2)

H - sensible heat flux

h_w - wind- convection heat transfer coefficient (Wm^{-2} K^{-1})

$h_{w,\ NOCT}$ - wind- convection heat transfer coefficient at NOCT condition (Wm^{-2} K^{-1})

I - annual heat Index (non-dimensional) = $\sum i$, i = $(T_a)^{1.514}$

I_1 - pyranometer recorded value at angle θ_1

I_k - insurance cost ($)

J - number of day in the year between 1 (1 January) and 365 or 366 (31 December)

k - Ross coefficient ($K\ m^2\ W^{-1}$)

n - actual duration of sunshine (hour), life of the project

N - maximum possible duration of sunshine or daylight hour (hour)

n/N - relative sunshine duration

K_c - empirical constant

$\bar{p}_a$ - mean saturated vapour pressure of air at reference height

$\bar{p}_p$ - mean saturated vapour pressure of air at the surface of pan

$\bar{p}_s$ - mean saturated vapour pressure of air at water surface temperature

P - atmospheric pressure (kPa)

Q - net water stored

Q_n - net radiation (W/m^2), net change in heat/ energy stored in the water body

Q_s - solar radiation (W/m^2)

Q_x - change in heat/ energy stored in the water body (W/m^2)

R_D - degradation rate in a year

R - mean rate of precipitation

r_a - bulk aerodynamic resistance in s/m

R_a - extra – terrestrial radiation (MJ m^{-2} day^{-1})

Rh - relative humidity in %

Rh_{max} - maximum relative humidity in %

Rh_{min} - minimum relative humidity in %

Rhp - relative humidity below panel %

$R_{l(down)}$ - cloudy sky downward longwave radiation

$R_{l,\ down}$ - longwave radiation emitted by atmosphere

$R_{l,\ up}$ - longwave radiation emitted by earth

$R_{l0(upward)}$ - clear sky longwave radiation emitted by earth

$R_{lo,\ down}$- downward longwave radiation emitted during clear sky

R_n - net radiation (MJ m^{-2} day^{-1})

R_n' - net radiation in units of equivalent depth of water (mm day^{-1})

R_{nl} - net longwave radiation

R_{ns} - net incoming shortwave radiation (MJ m^{-2} day^{-1})

r_s - bulk surface resistance in s/m

R_s - shortwave or solar radiation (MJ m^{-2} day^{-1})

$R_{s(cmp11)}$- pyranometer (CMP11) recorded shortwave reading

R_s(pp) - pyranometer recorded shortwave reading at Pilani solar power plant

R_{so} - clear sky radiation

s - fraction of measured solar radiation to clear sky radiation

SVD - saturated vapour density at mean air temperature (g/m^3)

T_a, T - ambient/ air temperature (ºC), ºF for Jensen- Haize and Stephens-Stewart

T_{aK} - ambient/ air temperature (K)

T_b - base temperature of water

T_c - cell temperature (ºC)

$T_{c,ref}$ - reference cell temperature (ºC)

$T_{max,K}$ - maximum absolute Ambient/ air Temperature (K) during 24 hours

$T_{min,K}$ - minimum absolute Ambient/ air Temperature (K) during 24 hours

T_{mod}, T_p, T_{pv} - module/panel temperature (ºC)

$T_{mod,ref}$, T_{ref} - reference module temperature (ºC)

T_{modK} - module temperature (K)

T_o - temperature of evaporated water

T_w, T_s - water temperature (ºC)

U - heat exchange coefficient of module (Wm^{-2} $°C^{-1}$)

u - wind speed

U_0 - empirically determined coefficient (25 Wm^{-2} K^{-1})

U_1 - empirically determined coefficient (6.84 Wm^{-3} sK^{-1})

u_3 - wind speed measured at 3 m height above ground surface (m/s)

U_L - overall thermal loss coefficient ($Wm^{-2} K^{-1}$)
u_w - wind speed (miles/hour)
V - voltage (Volt)
v - wind speed measured at 2 m height (km/h)
v_f - free stream wind speed in the windward side of the PV array (m/s)
V_{ig} - ground water seepage inflow rate
V_{is} - surface water inflow rate
V_{oc} - open circuit voltage
V_{og} - ground water seepage outflow rate
V_{os} - surface water out flow rate
VPD - vapour pressure deficit
V_w, u_2 - wind speed measured at 2 m height (m/s)
V_{wz}, u_z - wind speed measured at z m height above ground surface (m/s)
V_1 - benchmark wind speed in the definition of NOCT temperature
α_L - albedo of longwave
α_s - albedo of shortwave
β_{power} - power variation coefficient with respect to module temperature in %/°C
β_{ref} - efficiency correction coefficient for reference temperature (% $^oC^{-1}$)
ε_{clear} - clear sky emissivity
ε_e - effective emissivity of the atmosphere (under all sky condition)
ε_{land} - emissivity of land surface
η_c , η_m - cell/module electrical efficiency
η_{mp} - maximum power point efficiency of module
$\eta_{mp\,ref}$ - reference maximum power point efficiency of module
η_{ref} - electrical efficiency at reference temperature
θ_1 - angle of inclination of pyranometer with respect to ground
$\mu_{\eta,mp}$ - maximum power point efficiency temperature coefficient
ρ_a - density of air (kg/m^3)
ω_s - sunset hour angle (radian)
$\propto$ - solar absorptance of PV layer
f - coefficient ($^oC\ m^2\ W^{-1}$)
w - wind speed measured at 10 m height (m/s)
z - elevation above mean sea level (m), height of measurement above ground surface [m]
Δ - slope of saturation vapour curve at air temperature (k Pa $^oC^{-1}$, Pa $^oC^{-1}$)
α - albedo of surface
β - Bowen ratio
γ - psychometric constant (k Pa $^oC^{-1}$)
δ - solar declination (radian)
ε - ratio of molecular weight of water vapour to dry air (0.622)
κ - constant of proportionality
λ - latent heat of vaporisation (2.45 MJ/kg at 20 ^{o}C)
ξ, C - mass transfer coefficient
ρ - density of water (1000 kg/m^3)
σ - Stefan Boltzmann constant (4.903×10^{-9} MJ $K^{-4}\ m^{-2}\ day^{-1}$)
τ - transmittance of glazing
ω - mounting coefficient
ϕ - latitude (radian)
ϖ - Pristley Constant (≈1.26)

Abbreviations

AHP - Analytic Hierarchy Process
ANN - Artificial Neural Network
ASHRAE - American Society of Heating, Refrigerating and Air-Conditioning Engineers
ASTM - American Society for Testing and Materials
BREB - Bowen-Ratio Energy-Budget
CAPEX- Capital Expenditures
CdTe - Cadmium Telluride
CERC - Central Electricity Regulatory Commission
CMP11 – Pyranometer by Kipps and Zones make
CWC - Central Water Commission
DC - Direct Current
FPPP - Floating Photovoltaic Power Plant
FRL - Full Reservoir Level
FSPV, FPV - Floating Solar Photo Voltaic
GEC - Green Energy Corridor
GM - Ground Mounted
GMPV - Ground Mounted Photo Voltaic
HDPE - High density Polyethylene
HIT - Heterojunction with an Intrinsic Thin layer
IEA - International Energy Agency
IEEFA - Institute for Energy Economics and Financial Analysis
IPCC - Intergovernmental Panel on Climate Change
IRR - Internal Rate of Return
LCOE - Levelized Cost of Energy
MCM - Million Cubic Meter
MNRE - Ministry of New and Renewable Energy
NOCT - Nominal Operating Cell Temperature
NPV - Net Present Value
NTE - Nominal Terrestrial Environment
OFR - On-Farm Reservoir
OPEX - Operation and Maintenance Expenditure
PHES - Pumped Hydro Energy Storage
PSH - Pumped Storage Hydroelectric
PV - Photovoltaic
RES - Renewable Energy Sources
RMSE - Root Mean Square Error
ROMT - Realistic Nominal Module Temperature
rRMSE- Relative value of Root Mean Square Error
SCADA- Supervisory Control and Data Acquisition
SOC - Standard Operating Conditions
SPV - Submerged Photo Voltaic
SRC - Standard Reporting Conditions
SRE - Standard Reference Environment
STC - Standard Testing Conditions
TMC - Thousand Cubic Meter
TRE - Test Reference Environment
USD - US Dollar
WMO - World Meteorological Organization
Wp - Watt peak

Chapter 1

Introduction

Traditionally, solar developers in India have explored utility-scale solar project development as land-based projects. Though photovoltaic modules are the most promising technology in the field of renewable energy, installation of these panels needs huge land investment, which is a massive loss from the point of view of agriculture and farming activities. Moreover, land-based solar PV is less efficient due to the high impact of module temperature. This chapter classifies and describes the floating photovoltaic system, its configuration, and the working methodology and compares the potential, social, environmental, and economic benefits of installing Floating solar PV (FSPV) with land-based PV installation. Also, it describes the potential of installing floating solar PV modules in different parts of the world and in India. This chapter also underlined the impact of weather conditions and other factors on the performance of floating solar PV modules.

1.1 Background

Energy consumption is one of the major deciding factors for the economic growth and development of any country. The energy demand grows proportionally with the population of a country. India is a country that covers 18% of the world's population and 2.4% of the world's land, which makes India the largest country in terms of population. It is the third largest consumer of energy after China and the United States of America, (IEA,2021). Fig 1.1 shows the energy consumption in India from 1990-2021, India Energy Information, (Enerdata,2022). It indicates a fourfold increase in energy use since 1990. There is a decrease in energy demand in the year 2020 due to the lockdown and other restrictions. About half of all commercial energy used in India is consumed by the industrial sector, which is the country's largest energy consumer, (Kumar et al.,2014). As per the reports of IEA, (Kala, 2022), energy use will grow at a rate of 6.5% annually from 2022 due to increased residential and industrial consumptions.

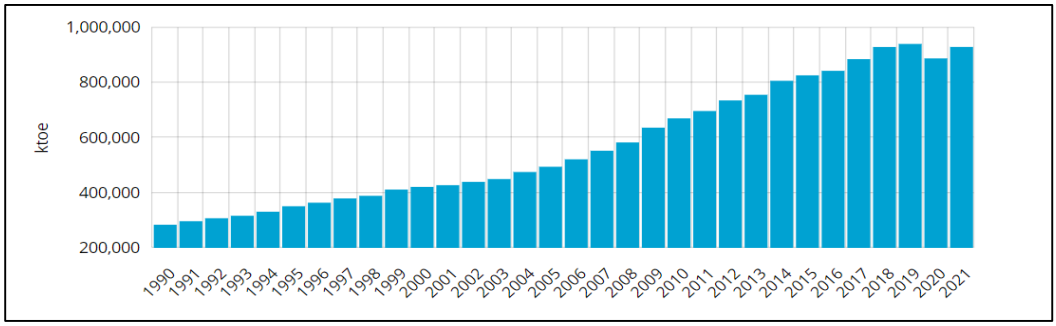

Figure 1.1. Energy consumption in India, 1990-2021 (Source: India Energy Information, Enerdata,2022)

Coal is regarded as the main source of energy because it is used to produce power in about 70% of all cases. Indian coal, however, is of poor quality and needs to be improved in order to fulfill demand. As a result, the government began importing coal to satisfy its need for energy and to foster a competitive environment that not only drives down the price of fuel but also fosters technological advancement. Around 48% of India's energy demand is fulfilled through import. The biggest threat to the country is its dependency on other countries for energy sources which can be reduced by switching to alternative energy sources. Natural gas and oil have become more widely used over time and replaced coal with the ability to generate two-thirds of energy consumption as the primary source of energy. Overall, due to a 33% rise in demand, fossil fuels will control the energy market and produce 85% of the world's electricity over the next 30 years. Despite having an abundance of fossil fuels available for electricity generation, burning of these energy sources releases greenhouse gases into the atmosphere, which worsens climatic conditions. Scientists have predicted that the world will experience natural disasters like floods, drought, earthquakes, etc., if the earth's temperature goes on increasing continuously. For this, an efficient, clean, and secure energy system is imperative for future generations.

Recently, India has deployed a phenomenal amount of renewable energy-based installations. Table 1.1. shows the power-generating capacity of different fuel types as of Feb 28, 2023, prepared by Central Electricity Authority of India, in its report (Power Sector at a Glance All India,2023). Approximately 42.6 % of energy demand is fulfilled by non-fossil fuel resources, of which 15.6 % of energy is generated by solar energy plants, (Power Sector at a Glance All India,2023), which can be due to a drop in utility-scale solar PV installation cost by 84%, (Acharya and Devraj,2019). India set a lofty objective in 2016 to produce 100 GW of solar power by 2022, of which 27% of the target would be unmet, (The Economic Times, 12April 2022). This is because solar PV installation takes a lot of land, and expanding project sizes necessitates big, contiguous land lots, which can be difficult in many circumstances.

The government of India has targeted to produce 500GW of energy from renewable energy by 2030, of which 280 GW would come from solar, 140GW from wind, and rest from other sources, (Ministry of Power ,12April 2022). India requires at least 65,000 square kilometers of land to install solar and wind power projects to meet the net-zero target by 2050 through the widespread adoption of renewable energy projects, (Mongabay ,10September 2021). A certain amount of global temperature rise, and other climatic impacts are already unavoidable due to past emissions. According to the Intergovernmental Panel on Climate Change (IPCC,2018), the global temperature rise must be kept to 1.5°C in order to avoid catastrophic health effects and millions of fatalities brought on by climate change. The study by Institute

for Energy Economics and Financial Analysis (IEEFA), (Charles Worringham,2021), notes the potential for land-use conflict to arise over renewable energy installations, even in sparsely populated areas. In addition to this, there was doubt over India's transmission system to sustain the increase in intermittent renewable energy production. To handle the lack of grid infrastructure, India is implementing a transmission network of the Green Energy Corridor (GEC) that connects states to states that lack renewable energy generation potential, (Ministry of New and Renewable Energy,2022). In order to overcome the land concern and due to the presence of enormous water bodies in a country like India (approx. 70,000 km^2), (Acharya and Devraj,2019), recommended to develop power by offshore winds, rooftop solar and solar on water bodies.

Table 1.1. Installed Power Generation Capacity as on February 28th, 2023.

Source	Fuel type	Installed Capacity (MW)	Installed Capacity (%)
Fossil Fuel	Coal	2,04,435	49.7
	Natural	24,824	6.1
	Lignite	6,620	1.6
	Diesel	589	0.1
	Total	**2,36,469**	**57.4%**
Non-Fossil Fuel	Hydro	46,850	11.4
	Wind	42,015	10.2
	Solar	64,381	15.6
	Cogeneration	10,218	2.5
	Nuclear	6780	1.6
	Small Hydro	4,983	1.2
	Waste to Energy	523	0.1
	Total	**1,75,743**	**42.6%**

(Source: Central Electricity Authority (CEA), Power Sector at a Glance All India,2023)

1.1.1 Floating Photovoltaic System

Floating solar photovoltaic (FSPV), also referred to as floatovoltaics, can be the most favorable alternative to overcome the shortcomings of the land-based PV system. Floating solar PV panels are those power generating system which is fitted on a frame that floats on the surface of water bodies such as Irrigation dams, water reservoirs, lakes, tailing ponds, ocean, and water treatment plants to achieve the current requirement varying from a few Kilo Watt (kW) to several Mega Watt (MW) with series and parallel connection. The module temperature of these systems is a function of wind speed and the temperature of a water body.

The floating solar power plant has modules and inverters like the ground-mounted solar power plant. The main difference between the two is the module mounting and appurtenant

structures. In order to maintain their position, these structures are anchored and moored to the ground, as shown in Figure. 1.2 Components other than modules and inverters of floating solar PV plants are the following:

1. Floating platform/ structure (Pontoon): This is the main component of the FSPV which supports the PV panels and keeps them floating over the water. The most common material used for this purpose globally is High Density Polyethylene (HDPE). However, other materials are also being used at certain places. Various designs have been developed by companies and are being used as per their requirements.
2. PV module support structure:
    - Floats: The float is a buoyant body that rests above the water and acts as a solar panel installation base. It also includes components for the fixing of mooring cables.
    - Upright Stands: When mounted to the float, this acts as a base component that produces an angle of inclination for the solar panels.
    - Bridges: The bridge is a component that connects floats to one another and serves as a foothold during construction and maintenance.
    - Binding Bands: The binding band fixes and floats together. Two varieties are available to match the wind pressure load.
    - Anchor Bolts: These bolts anchor the solar panel brackets to the floats.
    - Solar Panel Brackets: The fixing brackets are fixed with float bolts and act as support fitting to fix the solar panels in place.
3. Anchoring and Mooring system: The FSPV plants installed on the water are subjected to seasonal water level variation as well as wind pressures during their lifetime. To keep the FSPV plant stable and anchored at its intended location, Anchoring and Mooring system is designed. This system design requires a Bathymetry survey, water level fluctuation, soil conditions, and the location. Various types of Mooring systems have been used worldwide, such as Quays, Wharf, Jetties, Piers, Anchor buoys, and Mooring buoys.
4. Balance of System: Components other than those mentioned above, such as Cable, Combiner box, Switch board, Transformer, SCADA, etc., are termed as the balance of the system, and are the same as the ground-mounted system. However, cables used in the FSPV plants differ from the ground-mounted solar PV plant because the cables are in constant contact with water. The length requirement of the cable is also higher in the case of FSPV and needs to be UV resistant.

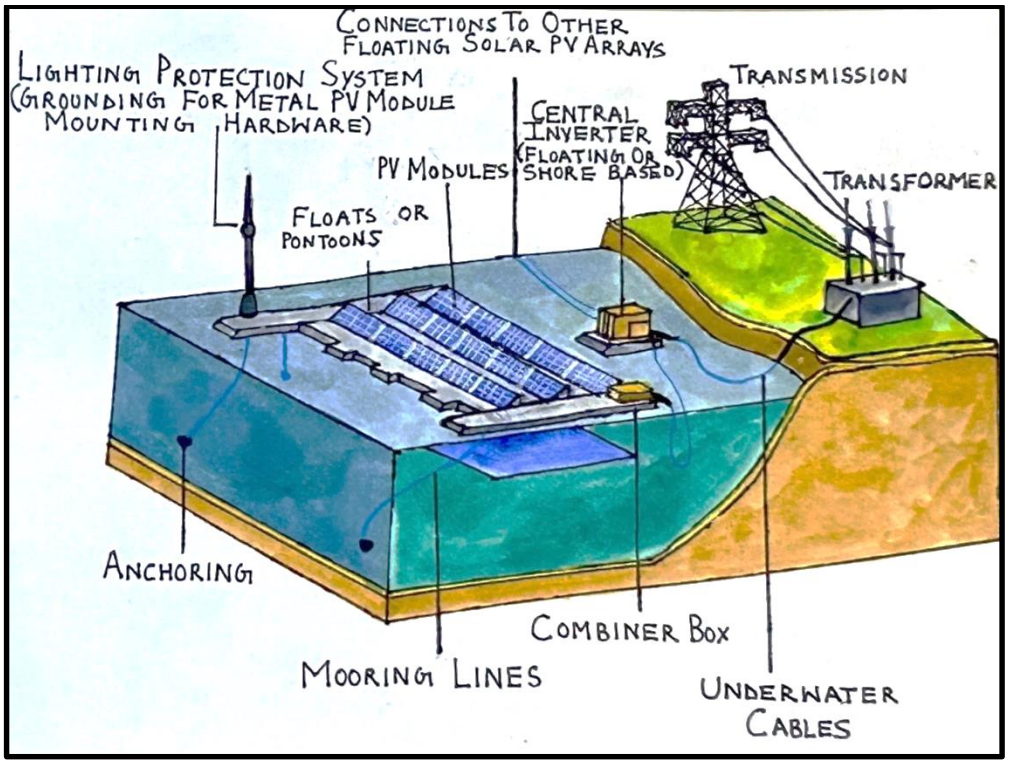

Figure. 1.2. Schematic diagram of a Floating solar photovoltaic system (Courtsey Kartika Agrawal)

1.1.2. Benefits of Floating Solar PV system

In recent years, there has been significant development in solar PV technology, and using this PV technology as a floating solar technology option to generate renewable electricity benefits in several ways. Some of the important are listed below:

1. The foremost advantage of this type of panel is to avoid land occupancy which can be otherwise used for agriculture, mining, and tourism purposes (Micheli,2022; Kichou, 2022; Essak and Ghosh,2022; Rizvi et al., 2022).

2. Due to the evaporative cooling effect, the ambient temperature near a water body is often lower than the ambient temperature on land (Liu et al.,2018; Kumar et al.,2021; Micheli,2022; Rahaman et al.,2023), and that wind speed tends to be higher over open water surfaces than on land resulting in higher generation efficiency and energy yield of PV panels (Majid et al.,2014 ; Choi, 2014; Sahu et al.,2016; Yadav et al., 2016; Liu et al.,2017; Kamuyu et al.,2018; Singh et al.,2019; Dzamesi et al.,2024).

3. Covering a portion of a water reservoir with floating solar panels minimizes the amount of solar radiation that reaches the water's surface and restricting the interaction of the wind with the water resulting in a reduction in the water evaporation losses as well as algae growth, thereby improving the overall water quality (Lee et al., 2014; Santafé et al., 2014; Wästhage, 2017; Singh et al.,2019; Farrar et al.,2022).

4. Floating solar PV plants are exposed to less dust than ground-mounted solar PV facilities because the wind over water includes less dust than the wind over land (Sarver et al., 2013).
5. Installation of solar PV on water bodies will help in providing sufficient electricity to develop micro-irrigation systems where availability of power is a major constraint, to take up water from canals to irrigation fields to provide last mile- connectivity.
6. As the electricity will be injected from the floating solar installation to the load centers, this will relieve the grid and reduce the transmission and distribution losses to a significant extent.

1.1.3. Floating Solar Operational Issues

The following issues need to be addressed during the design and installation of the floating solar PV system:

1. In order to withstand the strong forces of waves, floods, cyclones, and winds and stay afloat, the floating solar should be perfectly designed and resist these forces of nature for a period of 25 years. There are currently no clear standards or technical recommendations for FSPV components because the technology is still in its development stage.
2. Difficulty in handling operation and maintenance issues such as replacement of electrical parts, inspecting parts such as mooring and anchoring, cables, wiring issues and requirement of personnel with special training.
3. One of the most important factors in determining the actual potential and developing FSPV is the availability of water body data. There are no comprehensive water body statistics that include details on water surface area, water level changes, regional weather patterns, historical changes in the water surface, information on regional biodiversity, etc.
4. Large-scale FSPV plant deployment has unknown long-term effects on regional biodiversity.
5. Since the system is surrounded by water, the strength of the PV modules is poor due to corrosion.
6. There is a safety issue in transporting energy from water to the load center as the electric cables connected are placed underwater.

1.1.4. Economics Aspect

The development of structure accounts for almost 25% of the project cost, which is relatively low compared to land-based installation costs, (IEA,2021). Overheating of components is low in floating PV, resulting in low maintenance costs. World Bank floating solar market report (2019) has recommended $0.011/Wp as the operation and maintenance cost for floating solar since the HDPE thermoplastic floats have poor ultraviolet resistance resulting in premature deterioration, which adds cost to the system.

1.1.5. Environmental Aspect

As per the report, floating solar does not utilize chemicals and herbicides, hence less polluting technology. Floating solar also avoids using precious agricultural land, causing less deforestation, (India Energy Information, Enerdata,2022). There is also a reduction in algae growth by shading the water from the sun, which results in reduced photosynthesis. Since the modular individual float, which is to be joined to make a large section, is prefabricated and does not require civil work to manufacture and prepare the site, unlike land-based PV system, these systems have no manufacturing and construction impact on the environment. However, the large-scale installation of FSPV plants affect the diverse marine life underwater and water quality due to the breakdown of chemicals and other transport activities in the city. Therefore, it is crucial to consider every aspect of a reservoir before installing a large-scale solar plant on the water because these impacts are site-specific and vary from location to location.

1.2. Potential of solar floating photovoltaic system

The potential of solar floating photovoltaics has been widely investigated by different researchers, (Kumar et al.,2014; IEA,2021; Kala,2022). Many nations, including the United States, Japan, China, Korea, India, Brazil, Singapore, Norway, and the United Kingdom, have installed floating solar panels. Floating solar could be extremely helpful in regions with inadequate grid infrastructure, such as sub-Saharan Africa and some developing regions of Asia. The first floating solar plant was built in Aichi Prefecture, Japan, with an installed capacity of 20 kWp in 2007, (Delacroix et al.,2023). Since then, numerous nations have installed small floating power-generating units for research purposes. The first commercial floating solar plant, with an installed capacity of 175 kWp, was constructed at the Far Niente Winery in California, USA, later in 2008, (Trapani et al.,2015).

Floating PV gained significant momentum in 2018. According to the World Bank report (2019), the total installed capacity worldwide increased 100-fold by 2018, reaching 1.3 GWp,

as illustrated in Fig. 1.3. Out of which, most of the floating plants were deployed in China with an installed capacity of 960 MWp, followed by Japan (210 MWp), Korea (79 MWp), Taiwan (26 MWp), United Kingdom (13 MWp), India (2.7 MWp), Others (23.3 MWp), (Acharya and Devraj,2019). Most of these plants were installed on man-made reservoirs mainly built for wastewater treatment, rainwater harvesting, industrial basins, etc. Worldwide installed FSPV power grew from 3GW in 2020 to 13GW in 2022, surpassing a prediction of 10 GW by 2025 (Bloomberg,2023; Hopson and Christopher,2020).

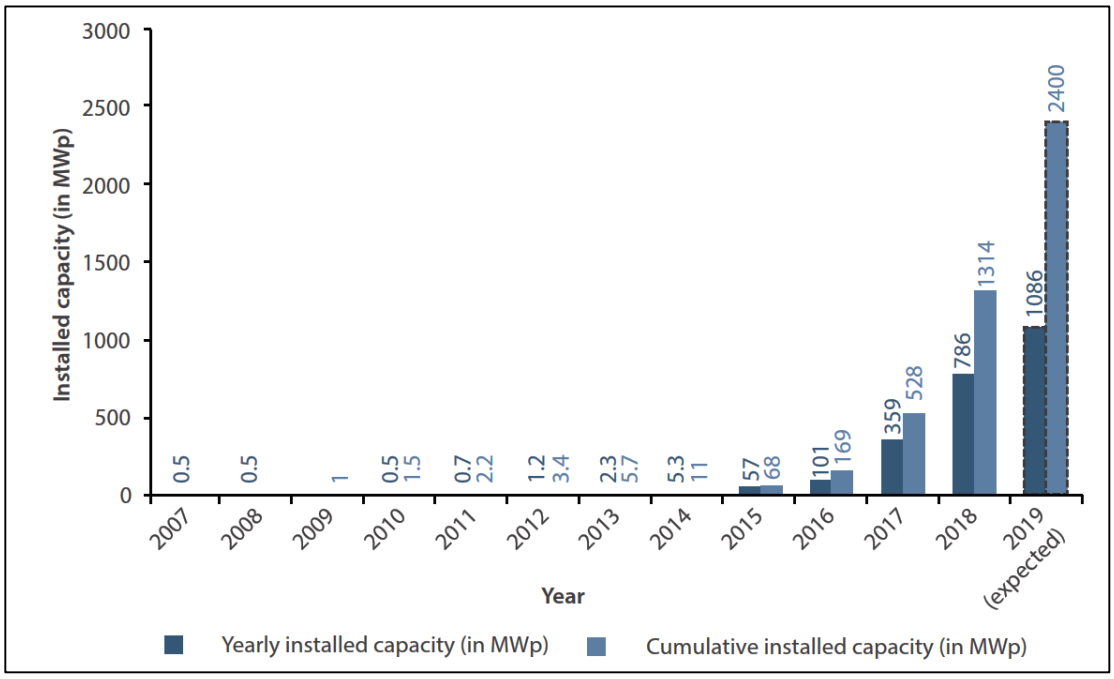

Figure 1.3. Worldwide installed capacity of the Floating solar plant (Source: (Acharya and Devraj, 2019)

India has the potential to become one of the largest centers for floating solar PV (FSPV) projects, with 5,264 dams covering almost 14,000 square kilometers and innumerable water bodies (India RE-navigator, 2018). The first research-based floating PV with an installed capacity of 10 kWp was constructed in 2015 at Kolkata by the Ministry of New and Renewable Energy (MNRE), India. Since then, numerous small-scale projects were deployed in different parts of India with a capacity ranging from 100 kWp to 500 kWp. In 2019, the country's FSPV installed capacity was 2.7 MWp (Charles & Majid, 2023). The total installed capacity in India as of December 2023 was 434 MWp. First large-scale floating plant of 25 MWp capacity was commissioned at Simhadri National thermal power plant, Visakhapatnam in 2021 and 92 MWp capacity was commissioned at Kayakulum, Kerela in 2022. The Ramagundam Floating solar power plant one of the largest floating solar plants with an installed capacity of 100 MW developed by NTPC in the Southern Region, is operational

since 2022. While Largest floating solar power plant of 278 MWp is functioning since 2023 at Omkareshwar dam, Madhya Pradesh (India), (Omkareshwar,2023).

1.3. Impact of weather parameters on PV modules

Temperature is one of the important parameters that have a significant role in determining the long-term performance and efficiency of the PV modules. It is a variable factor and has a strong dependency on different parameters. The following variables have been considered to study their effects on PV module temperature:

Ambient Temperature

Solar modules are manufactured at standard test conditions, and their performance varies due to different weather conditions. Therefore, it is the foremost parameter that influences the module temperature, (Emery et al.,1996). Various studies have been done by researchers with different climatic conditions of different regions and show a linear relationship between module temperature and ambient temperature, (King and Eckert,1996; Muzathik,2014; Bhattacharya et al.,2014; Wang et al.,2016). Hence, a lower ambient temperature is desirable. It can be seen from the literature that ambient temperature is maximum for the month of March to June due to high solar radiation while minimum from December to February in most of the regions. Usually, the ambient temperature on land is higher compared to the vicinity of the water body.

Solar Irradiance

It is another factor that is in direct proportion to the module temperature. High solar intensity leads to high module temperature which in turn decreases the module efficiency, (Abe et al.,2020; Sandnes and Rekstad,2002).

Relative Humidity

This is among the most variable meteorological data that varies for a whole year. Humidity affects solar efficiency in two ways:

- An increase in air humidity decreases the solar radiation reaching the solar panels due to water vapor accumulated on the surface of the panels which in turn reduces the power output and efficiency, (Gwandu and Creasey,1995; Omubo-Pepple et al.,2009; Darwish et al.,2013; Panjwani and Narejo,2014; Ayadi et al.,2019).
- Solar panels installed in hot and humid climate conditions are more prone to rust which deteriorates their performance over time (Bhattacharya et al.,2014).

Speed and Direction of Wind

This is one of the most overlooked parameters in the research that has a significant impact, especially when solar radiation and power output are high. This is because both the sun and the energy conversion process increase the temperature of the panel, thereby reducing the power output and efficiency of the PV system. Wind energy generally reduces the overheating effect of solar panels, which also increases the lifespan of the system, (Veldhuis et al.,2013; Chandra et al.,2018; Magare et al.,2018). Moreover, wind speed is higher on water than on land, which has the added advantage of low cell temperature and high energy yield to PV modules.

Photovoltaic Module Orientation

To harness the highest intensity of sunlight for a maximum period of time, the arrangement of solar panels in terms of their placement and tilt angle is as important as choosing the right type of solar panel (Kapoor and Garg, 2021b). Foster et al. (2009) revealed that maximum power is obtained when the incoming sunrays are focused on the panel perpendicularly. Lorens (2017) stated the geographic location of a solar panel is towards the South Pole for panels installed in northern hemisphere wheras PV panels installed in southern hemisphere fetches maximum energy when faces north pole.

Tilt angle is another important consideration to be taken care of for optimal energy production in a year. It is to be set equal to or closer to geographical latitude. Low tilt angles are prone to more problems, thereby yielding low power output and efficiency.

Dust and Sand Deposition on PV Module

Dust is the minute form of particles (size less than 500μm), mostly visible or non-visible solid material. Mainly, dust comes from construction sites, transportation, industries, and dust storms. This is the main contributing environmental issue that decreases the conversion of solar intensity to solar electricity, (Adinoyi et al.,2013). The performance of PV modules varies with the specific size and mass of dust and sand deposition. The performance of the PV module reduces with increases in the mass of dust particles, and as the size of particles decreases, relatively less sunlight reaches the surface of the panel, thereby deteriorating the energy yield (Sarver et al.,2013).

Photovoltaic Module Material

In order to improve the efficiency and reduce the cost of the PV modules, material selection is an important parameter, (Green and Bremner,2017). The most used semiconductor material

is silicon (Zhao et al.,1998). The very important property to investigate for a PV semiconductor is its 'Bandgap' that denotes the wavelength of light material it can absorb, (Shockley and Queisser,1961). If the wavelength of incoming radiation matches the semiconductor spectrum, then the efficiency of the panel increases, (Bird and Riordan,1986; Richards,2006).

1.4. Motivation

Due to the effects of rising energy consumption, such as the depletion of fossil fuels, escalating global warming, and greenhouse gas emissions, Renewable Energy Sources (RES) must be developed and used globally. One of the most practical renewable energy sources now-a-days is solar energy and that photovoltaic power generation is the most common application. The most common type of solar PV installation today is a ground-based installation, which typically has a land-use engagement for a long period of time. Moreover, India is an agriculture-intensive country sustaining almost 18% of the world's population over a total surface area of 2.4% of the world. Further, India plans to generate 500 GW of electricity from renewable sources by 2030, with solar photovoltaics (PV) accounting for the majority of that total and requiring 65000 km^2 of land for installation. For a nation like India, which has to provide not only for the basic needs of 1.31 billion people but also for their jobs and basic amenities, this amount of land is unaffordable. In addition to this, there is a loss of water due to evaporation. Therefore, the Ministry of New and Renewable Energy (MNRE), Government of India undertook a noble initiative to construct canal top solar power plants.

The present research is motivated by the MNRE, New Delhi initiative of the construction of solar PV plants over water bodies and the novel research and technical advancement required in the domain of floating Solar PV that cannot be utilized otherwise to restrict land-use and water evaporation loss. Since these plants are deployed on a fraction of the total water bodies, a practical approach is required to assess the water evaporation losses. Furthermore, in-depth research is required to address the technical challenges associated with FSPV in order to form an alternative to conventional solar PV.

First of its kind in Uttar Pradesh, a canal top solar power plant of 5.92 MWp was constructed over Jakhlaun Pump Canal off taking from Rajghat dam, in Lalitpur district. This plant was proposed on top of Jakhlaun Pump Canal, (village Bandarguda Jakhlaun, district Lalitpur, Uttar Pradesh) in intermediate stretches from chainage 0.100 Kms. To 12.00 Kms. based on the suitability of topography for installation of PV Panels. The geographic co-ordinates of the Jakhlaun Canal Top PV Plant at the pumping station are Longitude: 24º33' 2" N Latitude:

78º15’ 59” E. The project expected energy generation of 6.21 MU and 4.54 MU from 3.42 MW and 2.5 MW plants respectively.

The project was motivated by the factors such as: to reduce Uttar Pradesh's dependence on fossil fuel resources, to optimize utilisation of land & reduce evaporation losses from canal, to ensure the future of sustainable energy use, to reduce CO_2 emissions and the nation's carbon footprint and promote environmental, social and economically sustainable development.

This installation undertook the quest for developing floating solar power plants in Uttar Pradesh. Therefore, a case study of FSPV over Rajghat Dam is being done in the present work. Secondly, limited research has been reported globally to estimate the water conservation or water evaporation loss reduction relative to the height of the panel installed. The present research is driven by the motivations discussed above.

1.5. Objectives of the Present Research

After a thorough literature survey, the following objectives have been set for the present research work.

- To design and develop a field experimental setup to collect meteorological and PV panel performance data.
- To conduct a performance study between ground-mounted solar panels and those installed on a water body at varying heights based using field data.
- To develop predictive models for panel temperature utilizing meteorological and PV panel performance data and to analyze the significance of various meteorological parameters.
- To assess floating solar photovoltaic (FSPV) potential and Water Conservation by conducting a similar case study in tropical regions, viz. a case study for Rajghat Dam and a Potential assessment for Uttar Pradesh, India.
- To assess evaporation reduction due to FSPV installations in some major dams located in the tropical region in Uttar Pradesh, India using experimental data.
- To understand important insights about evaporation dynamics using experimental data in predictive evaporation models for open and PV-covered water bodies.

- The proposed research work is an attempt to help the government bodies to formulate technical guidelines and policies to implement on large-scale plants to ensure the quality and safety of local biodiversity.

The experimental setup of solar panels on the water body will help to estimate the important data of the water body, which is crucial to assess the potential of FSPV implementation. Moreover, it helps determine the exact position of the panel to be installed for the maximum reduction in evaporation loss. The objectives made herein would create a base for further research and development activities in the field of floating solar power generation.

1.6. Organization of the Thesis

The thesis has been organized into nine chapters. The following is a summary of the proposed thesis' chapter-by-chapter contributions:

Chapter 1: Introduction

Chapter 1 presents a broad overview of India's energy scenario and power consumption. It also discusses the goal and associated concern that the Indian government has set for the year 2050 and emphasizes the significance of solar PV installations on water and their advantages due to decreased evaporation. An overview of the impact of weather parameters on PV modules was highlighted in this Chapter. Also, the existing status of the floating solar system in India and other parts of the world has been discussed and the need for potential research on the floating solar system is explored. Accordingly, the motivation for the present research and the objectives and scope of the proposed work are established.

Chapter 2: Literature Background

Chapter 2 of the thesis presents and discusses the literature and previous studies done to predict module operating temperature and its impact on PV module efficiencies. The literature review also focuses on previous studies done to assess the impact of floating modules in reducing water evaporation losses in water bodies as well as their economic aspects. The status of FSPV potentials is also studied from both Indian and global perspectives.

Chapter 3: Design and Development of Experimental Setup

Chapter 3 of the thesis describes the experimental layout and design of the floating solar photovoltaic system setup at BITS, Pilani, India, to understand the effects of water bodies on the operating temperature of PV modules as well as the reduction in water evaporation losses through PV modules installed over water bodies. The data collected for the present work was

from April 2020 to till date. The proposed work analyses the data for the assessment of the accuracy of thermal models for solar panel temperature as well as evaporation loss reduction as per the Indian climatic conditions. The regression equations for panel temperature over the water body is proposed in the present work.

Chapter 4: Performance Assessment of Floating Solar PV Systems

Chapter 4 of the thesis presents the results for module temperature on ground and over water bodies. Performance study between ground-mounted solar panels and those installed on a water body at varying heights is conducted using field data. Additionally, the PV modules were assessed for their power output and analyzed to recommend the best panel height for maximizing PV performance.

Chapter 5: Predictive Model Development for Panel Temperature of Solar PV over Water Bodies

Chapter 5 of this thesis delves into the development of predictive models for panel operating temperature and performance assessment of PV panels by utilizing experimental data. efficient temperature model was recommended, and critical parameters were identified. A comparative study of PV panels over water bodies and ground-mounted PV panels was carried out to quantify the benefits of FSPV. Based on these findings, recommendations were made for the deployment of FSPV compared to ground-mounted PV in tropical climatic conditions.

Chapter 6: Assessment of Floating Solar Photovoltaic (FSPV) Potential and Water Conservation: A Case Study of Rajghat Dam and Prospective Assessment of Major Dams in Uttar Pradesh, India

Chapter 6 presents the technical feasibility, estimates evaporation loss reduction and levelized cost of electricity for installing solar PV on the Rajghat Dam. Based on this case study, a prospective assessment of floating solar PV installation potential is carried out over major dams in the tropical region, of Uttar Pradesh, India.

Chapter 7: FSPV Installations at Varying Heights: Evaporation Reduction Estimation for Major Dams of Tropical Region of Uttar Pradesh, India

Chapter 7 of the thesis discusses the results of evaporation loss beneath the panel and open to the sky using an evaporimeter for the Indian atmospheric conditions. A comparison is made to estimate the reduction in evaporation loss concerning changing heights of the panels installed above the evaporimeter and panel height with the highest evaporation loss reduction

is recommended. Based on these results, evaporation reduction due to FSPV installations in the major dams located in the tropical region in the state of Uttar Pradesh, India was estimated.

Chapter 8: Evaporation Dynamics: Analysis of experimental data and Model Development for open and PV-covered water bodies.

Chapter 8 delves into identifying critical parameters to study the evaporation dynamics. Then various predictive evaporation models using experimental data for open and PV-covered water bodies are developed. The evaporation estimates derived from these models are compared with recorded evaporation rates. Finally, the best evaporation models are recommended for open and PV-covered water bodies. Validation of the recommended models is performed for major dams located in the tropical region, of Uttar Pradesh, India.

Chapter 9: Conclusions and Future Scope

Chapter 9 summarizes the key findings of the thesis such as the significant potential of FSPV and, the benefits of FSPV installations primarily in energy generation and water conservation.

The current study also provides the future scope of work such as optimization of FSPV system design for enhanced performance and socio-economic and environmental impact and risk assessment of FSPV adoption along with limitations of the study.

Chapter 2

Literature Background

Recent Advancements in FSPV Technology and Regulatory Frameworks

Floating solar PV systems are the appropriate environment-friendly alternatives to play their leading role in reducing greenhouse gas emissions in the power sector and water evaporation loss reduction in the water sector. Floating Solar Photovoltaic (FSPV) technology has emerged as a promising renewable energy solution since its inception in 2007, when the first system was installed in Aichi, Japan, with a modest capacity of 20 kW for research purposes (Trapani, 2015). Initially, the technology experienced slow growth, with global installed capacity remaining minimal around 2008. However, the landscape began to shift significantly after 2017 as awareness of its advantages grew, sparking rapid advancements in both capacity and innovation (Xiong, 2023).

From 2018 to 2020, the global installed capacity of FSPV more than doubled, increasing from 1.1 GWp to 2.6 GWp (World Bank, 2019). By 2021, this figure had surpassed 3 GW, driven largely by the Asia-Pacific region, particularly China, which leads the global market with over 2.7 GWp of installed capacity. Europe follows as the second-largest market, with the Netherlands alone contributing over 200 MWp out of a regional total exceeding 250 MWp (DNV, 2022). By 2023, the cumulative global installed capacity had reached 4.6 GWp, showcasing the growing significance of FSPV in the renewable energy sector.

The rapid development of FSPV technology is attributed to its unique benefits, including reduced land-use competition, enhanced energy generation efficiency due to cooling effects, and high projected returns on investment (Micheli, 2022; Rosa-Clot, 2020; Xiong, 2023). Future projections highlight sustained momentum, with estimates suggesting global capacity could reach 13 GWp by 2025 and exceed 20 GWp by 2030 under medium growth scenarios (IEA-PVPS, 2021; Deloitte, 2019; DNV, 2023; Tina et al., 2023).

Policy frameworks have been instrumental in facilitating this growth, particularly in countries like China, Japan, and India, where subsidies, feed-in tariffs, and public-private partnerships have accelerated adoption (IRENA, 2021). The introduction of clear guidelines for design, environmental assessments, and hybridization with existing energy infrastructure has further strengthened the case for FSPV deployment. Notable trends include the integration of FSPV systems with hydroelectric plants, advancements in energy storage solutions, and the use of predictive models for optimization (Zhao et al., 2024; Singh et al., 2024).

Despite these advancements, FSPV technology still faces challenges, such as potential environmental impacts on aquatic ecosystems, the durability of floating structures under extreme weather conditions, and scalability issues requiring detailed feasibility studies (Armstrong et al., 2024; Ghosh, 2023). These challenges underscore the need for comprehensive regulatory frameworks and innovative solutions to enable sustainable and widespread adoption. This review explores the recent advancements in FSPV technology, focusing on regulatory frameworks, emerging trends, and the challenges that need to be addressed. By identifying knowledge gaps and addressing them through the present study, this research aims to contribute to the development of a robust and scalable FSPV ecosystem that aligns with global renewable energy goals.

This chapter is organized to address the detailed review of the studies of floating solar systems in global scenarios, the recent advancements of floating solar systems in Indian scenarios, and the methodologies adopted to evaluate module temperature of the floating solar system, the methodologies adopted to evaluate evaporation loss reduction, the economics aspects of floating solar plants. Finally, the chapter presents the research gaps and scope of the current study.

2.1. Studies on floating solar systems in the global scenario

This section evaluates the floating potential of different reservoirs of the world deployed on some parts of the reservoir in terms of power generation, water evaporation reduction, and CO_2 emission reduction. Furthermore, it evaluates the benefits of a hybrid system from technical and economic aspects.

Kougias et al. (2016), examined the possibility of water infrastructure in Mediterranean islands to support solar PV systems. Their research indicates that solar PV systems installed over water bodies can save about 3000 m^3 of water per MW. Kim et al. (2016), reviewed the new findings in the field of floating PV systems and the deployment of floating photovoltaic power plants in Korea between 2009 and 2014. Among them, the floating PV power plants established before 2011 may be regarded as test beds for research. The Korean Power GENCOs in Korea were the first to introduce commercial floating PV power projects after 2011. The author concluded that the installation of floating PV power generation systems with multi-megawatt sizes may continue to lead the way for innovative renewable energy technologies if the Korean government continues to encourage them.

Liu et al. (2017), have studied the power generation effectiveness of floating PV systems and a thorough examination of the benefits and possibilities of floating PV systems in China. In

order to achieve a higher generating efficiency, they have advised that sun and wind conditions should be taken into account during the actual construction of FPV systems. Under comparable environmental conditions, the results show that the FPV's generation efficiency would be 1.58 to 2.00% higher than that of a terrestrial PV system. The potential capacity of FPV systems in China would be 160 GW, covering an area of 2500 sq km of water surface and saving of evaporation losses was projected to be 2 x 1027 m^3.

Durkovíc & Durišíc (2017), explored a theoretical plan for supplying a portion of the electrical energy consumed by the aluminium factory in Montenegro from a large floating photovoltaic power plant (FPPP) installed on part of Skadar lake, which was at a distance of six km from the KAP. Also, the author proposed to install 18 FPPP with a capacity of 5 MWp each, oriented toward the south, and tilted at an ideal angle of 30^o in the area and an innovative azimuth angle control technique. The findings reveal that the total energy need met by the proposed FPPP, was 186.05 MWh which was roughly 31.29% more than a conventional PV power plant with equivalent installed power that is located on land. The reduction in water evaporation, which is roughly 5.41 million m^3 per year, is one of the key ecological benefits of building the FPPP. Safarini et al. (2017), simulated the performance of a solar island in the UAE and evaluated the power increase with reference to different tilt angles and tracking of solar radiation. The different scenarios employed for the power generation were: No tracking and zero tilt angle, Fixed tracking and 22^o tilt angle, and the third one was, 22^o slanted with the option of tracking. When compared to several tracking modules, the solar island concept offers a substantial benefit over traditional solar tracking systems by allowing the entire system to be rotated as a unified structure. However, in order to assess the viability of solar islands, thorough financial research is required. Rosa-Clot et al. (2017) investigated the potential for integrating the Floating PV plants with the existing basins for wastewater treatment in Australia with a view to energy production, water saving, and environmental and economic benefits. The author estimated 15000-25000 m^3 saving of water with each MWp installation of solar panels. Moreover, if the cost of floating solar was the same as for land-based plants, the amount of energy harvested is higher due to the cooling effect, which can increase the annual energy yield by up to 10%. In comparison to fixed Vs sun tracking solutions for wastewater basins, the author concluded that the fixed option offers the most benefits.

Dizier (2018), optimized the technical and economic aspects of the floating solar PV system incorporating active cooling strategies in Taiwan in order to maximize the power generation and minimize the cost of the system. This study intends to model various cooling methods for

the suggested system in order to comprehend the effects on the side of energy generation. Due to the abundance of water bodies and the affordable pricing of hydraulic equipment, the author concluded that Taiwan has significant interest from around the world in creating FPV power plants with cooling systems to produce electricity at a reduced cost.

Liu et al. (2018), have analyzed the technical, economic and environmental aspects of deploying a 1 MWp floating solar PV system on the freshwater Tengeh reservoir of Singapore. The total of eight systems comprises of different configuration of PV modules, inverters and floating structures and compared its performance with the rooftop PV system performance. The result shows that the FPV system PRs are up to 10% higher than Singapore's normal rooftop systems, ranging from 80% to just above 90%. Chico Hermanu et al. (2019), modelled and designed a 1 MWp floating solar PV plant on the three reservoirs in Indonesia to assess the potential of installing the FSPV plant and produced beneficial outcomes by using an electricity selling price of Rp 2609/kWh. Sudhakar (2019), reviewed the benefits of FPV plants in the form of a SWOT analysis. The study highlights the advantages of the FPV system as compared to the ground-mounted system. Liu et al. (2019), evaluated the benefits of integrating FPV and pump storage power systems and quantitatively assessed the potential of the integrated system in electricity generation and conservation of water and land resources. They performed a dual objective optimization to maximize the benefit of electricity generation and to minimize the energy imbalance at the same time. The methodology was applied to a 2 GW FPV farm and 1 GW pumped storage power system. The results indicated that the integrated FPV pumped storage power system has great potential for gaining the benefits of electricity generation and reducing energy imbalance. Additionally, this system saved 20.16 sq. km of land and 19.06 million cubic meter of water in a year due to the reduction in evaporation loss and the proposed IFPV-PSPS system. Zubair et al. (2020), have estimated the potential for FPV in Pakistan and found it to be 190 GW against the nationally installed capacity of a total of 28 GW from all sources. The finest place for FPV in Pakistan, according to the analytic hierarchy process (AHP), is Chinna Creek in Karachi which has 6.1 kWh/m^2 /day of solar irradiance and yields 2345 kWh/kW of energy. Rodrigues et al. (2020), simulated the potential for FPV power generation in the tropical Gaviao reservoir in northeastern Brazil. Based on the investigation, the net power generated was 879,221 MWh, water evaporation loss reduction was around $2.6*10^6$ m^3/year, and the system's construction expenditure was fully recovered in 8 years, thereby meeting 1.5 % demand of the people of Fortaleza. Nebey et al. (2020), estimated the energy harvesting potential of the water bodies of Amhara regional state with an FSPV system using a

geographic information system for generating electric power and identified the factors that affect the usability area of Angereb, Rib, and Koga irrigation dams. The result reveals that the key parameters for analyzing the usability of floating solar PV power location were distance from land, distance from forest, water surface size, and depth. Additionally, it shows that the Angereb, Rib, and Koga irrigation dams have useable surface areas of 63.83%, 61.09%, and 57.2%, respectively. Haas et al. (2020), studied the impact of floating solar PV on the micro-algal formation and hydropower revenue at the Rapel reservoir in central Chile. Also, in order to maintain a balance between the health of the environment and cost, an optimal range of solar module cover was identified and presented. The author recommends covering 40-60% of the lake surface in order to keep algal concentrations within limit without incurring revenue losses. Kumar et al. (2020), investigated the thermodynamic performance of photovoltaic modules in both the water and land environment through energy and exergy analysis. In order to comprehend the exergy performance, three amorphous silicon thin-film PV modules placed using ground-mounted PV (GMPV), floating PV (FPV), and submerged PV (SPV) methods are taken for experimentation. The result demonstrated that the exergy efficiency of the SPV system was found to be 3.07% and 43.65% higher than that of the FPV and GMPV installation methods respectively. Perera & Wen (2020) utilized and designed a novel anchoring concept using a constant-length cable and evaluated the performance of a 3 MW floating solar PV system through Matlab/Simulink. The results of the case study show that the payback term for the investment is 15 years, which is still very long. Baptista & Vargas (2020) evaluated the energy potential of a floating solar power plant in the Gouvaes dam, which is a part of the Tamega hydropower complex being built in northern Portugal by the Iberdrola Company and found the possibilities for integrating it into the Portuguese power grid. The result of the case study shows that the investment must be recovered over 15 years, which is still a very long time. Sulaeman et al. (2021), assessed the effectiveness of installing an FSPV system with the existing hydropower plant in the Amazon basin to compensate for the current underproduction of dams. Additionally, the relationship between PV output and system load was evaluated and the findings reveal that the overall investment in FPV improves system reliability remarkably and reduces load at peak demand periods. Lopes et al. (2022), investigated the technical potential of FPVs in artificial water bodies of Brazil utilizing 1% of its area at the national and state levels using the QGIS software to locate water bodies and obtain its meteorological data. The findings demonstrate that covering 1% of the identified potential locations can generate energy equivalent to over 12.5% of the country's current electricity generation and roughly 16% of Brazil's electricity consumption. Elminshawy et al. (2022), constructed and tested the performance of a partially submerged

floating PV system under actual wind conditions in Port Said, Egypt experimentally in order to analyze the optimal energy yield, module temperature, wind speed and direction, and geometric configuration. The results reveal that the partially submerged PV system reduces 14.16 % module temperature, thereby increasing 18.20% electrical power.

2.2. Studies on floating solar systems in the Indian scenario

This section reviews the viability and suitability of deploying the floating PV system on an Indian reservoir with different operating conditions from geographical, technical, economic and environmental aspects.

Singh et al. (2019), carried out a feasibility study for the installation of a 2 MW FSPV system in Pondicherry (Puducherry), India. The active area for the proposed work is 13,416 m^2, with a total of 1677 modules and 6708 panels of 300 KW each being installed. With a cost of USD 1.6 million and a payback period of 6 years, the total average annual power generation is 2685 MWh. The energy produced will be used to power electric transportation systems. Gurfude & Kulkarni (2019) investigated the performance of 1 MW FPV system coupled with a solar tracker at Ambazari lake, Nagpur, to evaluate energy yield and CO_2 emission reduction. The findings reveal that 18,71,229.186 kWh of power was generated with fixed tilt equal to latitude, 22,02,749.886 kWh with 1-axis tracking and 23,62,076.129 kWh with 2-axis tracking annually. Kumar et al. (2021), assessed the potential of FSPV in India, and it was discovered that 124 GWp of gross potential might be produced. The total gross potential, however, comes out to 111.9 GWp when calculations are based on 10% coverage, water depth under 80 m, and a global horizontal irradiance greater than or equal to 1800 kWp/m^2. The gross potential of FPV, when classified based on yearly irradiance between 1900 and 2000 kWp/m^2, would be 71.74 GWp, while for irradiance more than 2000 kWp/m^2, the potential estimated might be 7.4 GWp. Kapoor and Garg, (2021a) focuses on accurately determining solar potential and managing solar plants using IoT, big data, remote sensing, and GIS within a cloud computing environment. Nagananthini & Nagavinothini (2021) estimated the floating potential of the Vaigai reservoir located in Tamil Nadu, India with various tilt angles, orientation and tracking mechanism in terms of power generation, water evaporation loss reduction and CO_2 reduction. The results demonstrated that covering 30% of reservoir with 1.14 MW capacity of FPV plant, generates 1.9 GWh of energy, saved 42731.56 m^3 of water, and reducing 44734.62 tons of CO_2 emissions annually at an optimum tilt angle. Pakyala (2021), assessed the performance of 1 MW floating solar PV system in terms of energy generation, performance ratio, capacity utilization factor, cost analysis, evaporation reduction and carbon dioxide emission at the reservoir in Visakhapatnam, India.

Further, the author compared the performance of FPV with the 1 MW ground mounted PV system and found that an increase in power generation by 1.5-3% and saving in 42 million liters of water. In contrast to the price of ground-mounted power generation, the cost of electricity generation was slightly higher at 4.1 Rs/kWh. REC Group (2022), developed the unique canal-top, grid-connected solar plants with suspended structure installed with a capacity of 8,414,000 kWh using 16,680 REC Peak Energy 72 solar panels on two spreads, covering about 1.25 km from Rajgarh to Ajnod village downstream on Sidwhan and Ghaggar canals in the state of Punjab, India. With a combined average performance ratio of more than 80, this project reduces the amount of land needed for agriculture, while also saving millions of liters of water that might be used for irrigation purposes. Kapoor and Garg, (2021c) assesses canal-top solar potential in Roorkee Tehsil, India, using remote sensing, GIS, and cloud computing. Mamatha & Kulkarni (2022) estimated the power generation, CO_2 reduction and water evaporation loss due to the deployment of a pontoon-type floating solar PV structure on the Indian hydropower reservoir. The results show that existing hydropower plants may double their installed power capacity and generate 52% more electricity with a total coverage of 4% area of hydroelectric reservoirs, thereby, saving 837 million m^3 of water and adding 1.566 TWh of hydroelectric power annually. Shyam & Kanakasabapathy (2022) proposed a system that integrates a stand-alone floating solar PV (FPV) system and a pumped storage hydroelectric (PSH) system in hilly areas to estimate levelized cost of solar energy and levelized cost of stored energy. The two optimization techniques namely, linear programming and particle swarm optimization were used for finding optimal scheduling and sizing of the system. In comparison to the grid-connected system, the proposed system reduces 0.8518 Rs/kWh for solar energy and 4.2713 Rs/kWh for stored energy, thereby operating in a subsidized static tariff environment. Rizvi et al. (2023) proposed an FSPV–grid integrated system for Bhilai Steel Plant (BSP). They assessed power generation, area requirements, net present cost (NPC), levelized cost of energy (LCOE), grid interactions, internal rate of return (IRR), return on investment (ROI), payback periods, and pollutant emissions. Their results indicate that the FSPV–grid system can meet the steel plant's energy needs more cost-effectively than the current grid-only system, while also offering economic and environmental benefits. Makhija et al. (2024) examines the feasibility of a 2,500 MW floating PV (FPV) system on Gangrel Dam, Chhattisgarh, India, comparing it with a nearby on-ground PV (OPV) system. FPV can help maintain water quality, reduce land use, and minimize water evaporation.

2.3. Floating solar PV Module temperature and Performance

The PV module performance is governed by module temperature. Hence, it is an important parameter to be examined. Various formulations have been developed to estimate the ground-mounted PV module temperature. Very few studies have been published to estimate the temperature of PV modules on water bodies. This section reviews the numerous studies published to assess the performance and module temperature on ground and water bodies.

2.3.1. Performance of Floating solar PVs

Ferrer-Gisbert et al. (2013), investigated the performance of a full-scale floating solar PV system constructed on the agricultural reservoir of Alicante, Spain, covering 7% of its surface area and found it technically and economically feasible. Also, there was a reduction in the water evaporation rate. Cazzaniga et al. (2018), scrutinizes the effectiveness of photovoltaic (PV) systems installed on floating platforms. It explores various design approaches aimed at enhancing the efficiency and economic feasibility of floating photovoltaic (FPV) installations. It highlights FPV designs that leverage additional functionalities such as tracking, cooling, and concentration. The outcomes of experimental evaluations are shared, revealing a significant boost in performance attributable to the advantageous effects of tracking and cooling. Abeykoon et al. (2018), quantitatively determined the impact of temperature on the Hambantota Solar Power Station using polycrystalline silicon solar cells of 4783.48 m^2 area to generate electricity in conditions of a realistic environment. The study result shows that low operating cell temperature leads to increased efficiency of solar panels. The findings reveal that the conversion efficiency under environmental conditions was 11.9% with a temperature coefficient of 0.04% per degree Celsius. Sukarso and Kyung (2020) examined the floating solar PV system from an economic and technological point of view using remote sensing results to estimate FPV efficiency and quantify energy generation from the system and compare it to a ground-based solar PV system. The results indicated that FPV efficiency was approximately 0.61% greater than GPV. Furthermore, the levelized cost of electricity (LCOE) was also reduced by 3.37 cents/kWh and the internal rate of return (IRR) was increased by 6.08% when FPV and GPV were compared in the baseline scenario. Tina et al. (2021), simulated the performance of bifacial and mono-facial PV modules installed on water surface with active and passive cooling and on rooftop and validated their findings with the experimental results obtained with FPV system installed in the Enel Innovation Lab by Enel Green Power, Catania (Italy). The results demonstrate that active cooling in FPVs increases the collected energy by 9.7% and 9.5% for the bifacial and mono-facial respectively. Kapoor and Garg, (2018) aims to develop an approach for assessing solar

potential using cloud computing to improve energy planning.El Hammoumi et al. (2021), designed and evaluated the performance of small-scale FSPV systems operating under Moroccan conditions for research purposes and compared its performance with the land-mounted PV modules. The energy production from floating systems at various tilt angles is also examined by the author. In comparison to ground-mounted modules, the test results show that FPV module temperatures were 2.74^{o}C lower and generated 2.33% more energy. Moreover, the author also confirmed that the FPV system would produce the highest energy at the optimum tilt angle. Osama et al. (2022), proposed and examined the performance of a novel partially submerged floating system on a calm water surface operating under the hot climatic conditions of Egypt and compared its performance with the land-based PV system. The thermal and electrical performance of the recommended PSFPV module was assessed in relation to its submerged length, which ranged from 4 to 24 cm. The results demonstrate that the PSFPV system attains 15.10 % less operating temperature and 20.76 % more electrical power output. The total cost of electricity decreases from 0.075 $/kWh to 0.067 $/kWh with an increase in submerged length from 4 cm to 24 cm. Nisar et al. (2022), conducted an experimental analysis of the performance of mono-crystalline and polycrystalline PV modules mounted on water bodies and on the ground. The author also assessed the water evaporation from fully and partially submerged PV modules and discovered a 28% and 17% reduction in evaporation loss, respectively. With a tilt angle of 0^{o}, the floating PV generates 20–28% more energy than the ground-mounted PV cells. Rizvi et al. (2024) outlines a framework for determining the generating capacity needed for the steel industry, focusing on solar photovoltaics (PV). It proposes using floating solar photovoltaics (FSPV) on two unused reservoirs at a steel plant to improve economic and technical efficiency.

2.3.2. Module temperature of solar PVs: Ground-mounted and FSPVs

King (1997) addressed the issues of measurement and determined the temperature coefficients for short-circuit current, maximum power current, open-circuit voltage and maximum power voltage in order to know how module and array electrical performance for irradiance other than standard solar irradiance of 1000 W/m^2. King et al. (2004), developed a simplified empirically based thermal model that has been successfully used for concentrator modules with finned heat sinks, flat-plate modules installed in an open rack, and flat-plate modules with insulated rear surfaces emulating building integrated settings. The model has shown to be quite adaptable and completely appropriate for system engineering and design objectives with the temperature uncertainty to be less than 3% impact on the module's production of electricity. Koehl et al. (2011), proposed a simplified analytical and statistical

model to evaluate realistic nominal module temperature from meteorological data such as wind speed, ambient temperature, and solar irradiance and validated the simulated results with measured results at different sites. The author concluded that the models can simulate the transient temperature demands on modules at locations and sites where the necessary weather data is available.

Kamuyu et al. (2018) derived the floating PV module operating temperature equation coefficients using the data collected at an interval of five minutes for one year. In comparison to the actual temperature of the PV module, there was a deviation in the simulated results with an error range between 2% to 4% depending on the number of coefficients. Kaplanis & Kaplani (2018) derived the PV module temperature equation both at a steady state and transient conditions and validated with the experimental values. With the same model after validation, the author studied the effect of different parameters namely, ambient temperature, wind speed, solar irradiance on the performance and the mounting geometries of PV modules. The predicted model results were more accurate as compared to results obtained from six other models and applied to any site and environmental conditions. Barry et al. (2020) developed a dynamic temperature model as a function of ambient temperature, shortwave and longwave irradiance and wind speed by extending an existing parametric steady-state model using an exponential smoothing kernel to include the effect of the heat capacity of the system and validated with the measured data obtained from three PV modules deployed in Allgau region, Germany using non-linear optimization. The author reveals that the dynamic model's root-mean-square error between measured and modelled module temperature is lowered to 1.58 K on average, while the greatest instantaneous error is decreased from 20.02 K to 6.58 K when compared to steady-state model.

2.3.3. Predictive model for solar PV Module temperature

Ross (1976), developed the following model given by Equation (2.1) based on the thermal properties of modules, where the solar insolation is directly proportional to the difference between the temperature of the module and the ambient temperature,

$$T_{mod} = T_a + kG_T \tag{2.1}$$

where, T_{mod} is module temperature in °C, T_a is the ambient temperature in °C, G_T is solar insolation in W/m^2, k an empirical parameter called Ross coefficient depends on the properties of the module such as shape, size, encapsulation, technology, mounting type and environmental conditions. The natural light test procedure for determining the nominal operating cell temperature (NOCT) given by (Stultz and Wen, 1977), is utilized extensively

to understand and characterize the thermal performance of PV modules. The Nominal Operating Cell Temperature (NOCT) is the module cell temperature under operating conditions in the Nominal Terrestrial Environment (NTE) which is defined for the following parameters: Insolation = 800W/m^2, Air Temperature = 20°C, Wind Average Velocity = 1 m/s, Mounting - Tilted, Open Back, Open Circuit. ASTM method of determining the NOCT test procedure is based on gathering actual measured cell temperature data via thermocouples attached directly to the cells of interest, for a range of environmental conditions similar to the NTE. The data are then presented in a way that allows accurate and repeatable interpolation of the NOCT temperature.

Evans & Florschuetz (1978), studied the role of sunlight concentration in reducing the cost of electricity for terrestrial photovoltaic systems. Computer modelling was developed to compare the silicon cell with gallium arsenide cells in concentrating system, operations of a PV system in low insolation and the effect of wind-dependent thermal conductance on the performance of a passively cooled system. Results show that concentrating systems give better results in low solar radiation locations and wind effects should be considered in modelling in locations having large wind speed deviations from the yearly mean. Stultz (1979), summarised the NOCT measurements of different types of PV modules and illustrated the trend in NOCT. Care in thermal design and cost considerations could achieve the NOCT in the range of 43°C to 48°C range. With a minimum temperature difference (NOCT-28°C), a maximum NOCT efficiency of 0.94 can be obtained for flat plate configuration. Evans (1981) presented a procedure for long-term, the monthly average electrical output of passively cooled max power tracked photovoltaic arrays. This procedure applies to both south-facing, fixed flat arrays and 2-D tracked concentrators. The procedure combines the array with the local monthly mean temperature and the monthly KT (ratio of the total radiation on the horizontal to the extra-terrestrial radiation) to yield a monthly average array efficiency which, when multiplied by the monthly array insolation gives the electrical energy output.

Risser & Fuentes (1983) proposed the regression equation for module temperature with solar insolation, ambient temperature, and wind velocity as variables. The developed model is given by Equation (2.2),

$$T_{mod} = 0.899\,T_a + 3.12 + 0.025G_T - 1.30\,V_w. \qquad (2.2)$$

They also proposed the following linear regression model given by Equation (2.3). for estimating module back temperature, utilizing three meteorological parameters solar insolation, ambient temperature, and wind velocity,

$$T_{mod} = 1.31\,T_a + 3.81 + 0.0282G_T - 1.65\,V_w. \quad (2.3)$$

where, T_{mod} is module temperature in °C, T_a is the ambient temperature in °C, G_T is solar insolation in W/m^2, V_w is wind velocity in m/s.

Schott (1985), proposed Equation (2.4) to estimate module back temperature, using only two parameters ambient temperature and solar insolation. This equation is verified for wind speed between 1m/s to 1.5 m/s and temperature range from $0℃\ to\ 35℃$,

$$T_{mod} = T_a - 1 + 0.028G_T\,. \quad (2.4)$$

Ross & Smokler (1986) proposed the following Equation (2.5), for wind speed greater than 1 m/s with a constant coefficient of heat loss, to estimate module temperature,

$$T_{mod} = T_a + 0.035G_T. \quad (2.5)$$

Servant (1986), proposed to estimate the module temperature by utilizing meteorological parameters. The Equation (2.6) is given below,

$$T_{mod} = T_a + a\,G_T\,(1 + b\ T_a)(1 - c\,V_w) \quad (2.6)$$

where, T_{mod} is module temperature in °C, T_a is the ambient temperature in °C, G_T is solar insolation in W/m^2, V_w is wind velocity in m/s, while $a, b\ and\ c$ are the empirical constants. The empirical constants a and b are estimated first with meteorological data having wind velocity below 1 m/s and then empirical constant c is estimated.

Irodionov et al. (1989), proposed the following Equation (2.7) to estimate the back temperature of the PV module,

$$T_{mod} = 0.7 + 0.0155G_T + T_a. \quad (2.7)$$

They utilized only solar irradiation and temperature to estimate the PV module temperature.

Lasnier & Ang (1990) proposed the following Equation (2.8) for estimating PV module back temperature (T_{mod}),

$$T_{mod} = 30.006 + 0.0175(G_T - 150) + 1.14(T_a - 25) \quad (2.8)$$

where T_a is the ambient temperature in $°C$. G_T is the global solar radiation in W/m^2.

Markvart (2000), proposed the following Equation (2.9) with three parameters i.e. solar insolation, ambient temperature, and wind velocity,

$$T_{mod} = 0.943\,T_a + 4.3 + 0.028G_T - 1.528\,V_w \quad (2.9)$$

the coefficient of heat losses was not considered in the equation.

Nordmann & Clavadetscher (2003) compared the performance of grid-connected and stand-alone PV systems from 5 countries of different geographic locations. The effect of elevated cell temperature on the annual performance of different mounting namely freestanding, roof-mounted, and integrated PV facades, was studied. The sloped roof-mounted panel resulted in the highest temperature losses approx. 11.7% losses while the lowest temperature loss was observed as 1.7% to 5% losses, in free-standing and flat roofs.

Mondol et al. (2005), proposed the following Equation (2.10), for wind speed greater than 1 m/s with a constant coefficient of heat loss, to estimate module back temperature,

$$T_{mod} = T_a + 0.031G_T\ . \quad (2.10)$$

Notton et al. (2005), developed a simulation model because PV module cell temperature depends on PV cell material, the module, and the surrounding environment. The model is based on electrical analogy, developed for a double-glass multi-crystalline photovoltaic module, and validated with experimental data.

Mattei et al. (2006), developed a model based on the energy balance that takes place in a module. The module temperature is estimated by Equation (2.11),

$$T_{mod} = \frac{U\ T_a + G_T[(\propto\tau) - \eta_{ref} - \beta_{power}\,\eta_{ref}\ T_{mod,ref}]}{U - \beta_{power}\,\eta_{ref}\,G_T} \quad (2.11)$$

where, T_{mod} is module temperature in °C, T_a is the ambient temperature in °C, G_T is solar insolation in W/m^2, U is the heat exchange coefficient of module depends on wind speed, $\propto$ is cell absorption coefficient, τ is glass transmittance, η_{ref} is the module efficiency at reference temperature $T_{mod,ref}$ = 25 °C and at solar irradiance of 1000 W/m^2, while β_{power} is the power variation coefficient with respect to module temperature in %/°C.

Chenni et al. (2007), proposed the following Equation (2.12) for the assessment of the back temperature of the polycrystalline module,

$$T_{mod} = 0.943\,T_a + 0.028\,G_T - 1.528V_w. \quad (2.12)$$

The model for the cell output features has been developed in terms of solar irradiance, wind velocity and temperature environment change. The modelling process configures the computer simulation model to model cell output. The model was tested on three modules manufactured with different materials.

Mondol et al. (2007), proposed the following Equation (2.13), for wind speed greater than 1 m/s with a constant coefficient of heat loss, to estimate module back temperature,

$$T_{mod} = T_a + 0.031G_T - 0.058. \quad (2.13)$$

Faiman (2008) demonstrated that Hottel–Whillier–Bliss (HWB) equation normally used for the analysis of flat plate solar collectors, can be utilized to predict PV module temperature. The equation was utilized for predicting seven different modules manufactured from different materials. The equation developed for the PV module does not depend on the type of material. They considered the hypothesis of thermal stagnation, a condition when thermal power drops to zero and the thermal collector reaches maximum temperature. An approximated Equation (2.14) given, is derived as below,

$$\mathrm{T_{modK}} = \mathrm{T_a} + \frac{G_T}{(U_0 + U_1 . V_w)} \quad (2.14)$$

where, $\mathrm{T_{modK}}$ is the module temperature in K, $\mathrm{T_a}$ is the ambient temperature in K, $\mathrm{G_T}$ is the global solar irradiation incident on the module surface ($\mathrm{W/m^2}$), V_w is the wind speed in m/s, $\mathrm{U_0}$ coefficient describing the effect of radiation on the module temperature in $\mathrm{W/Km^2}$ and $\mathrm{U_1}$ describes the cooling by wind ($\mathrm{Ws/\,Km^3}$). Value of $U_0 = 25.0\ \mathrm{Wm^{-2}K^{-1}}$ and $U_1 = 6.84\mathrm{Wm^{-3}sK^{-1}}$ was suggested for ground-mounted PV installation.

Skoplaski et al. (2008), proposed Equation (2.15) to estimate module back temperature for wind speed V_f greater than 1 m/s, as the error rate is higher by this equation for wind speed below 1 m/s

$$T_{mod} = T_a + (\frac{0.25}{5.7+3.8V_f})G_T . \quad (2.15)$$

Skoplaski & Palyvos (2009) proposed the following Equation (2.16) For estimating the module back, the temperature of the p-Si PV module,

$$T_{mod} = T_a + (\frac{0.32}{8.91+2V_f})G_T. \quad (2.16)$$

The equation is based on 3 variables namely solar insolation, ambient temperature, and wind velocity. The error rate for this equation is high for wind speed values below 1 m/s.

Kurtz et al. (2009), proposed an exponential Equation (2.17) for estimating module back temperature,

$$T_{mod} = T_a + G_T * e^{-3.473-0.0594V_w} \quad (2.17)$$

they also utilized the three meteorological parameters of solar insolation, ambient temperature and wind velocity to estimate the back temperature of the module.

Akyuz et al. (2012), proposed the following three-parameter equation as shown in Equation (2.18) for estimating module back temperature,

$$T_{mod} = 0.95\,T_a + 3.1 + 0.025G_T - 0.3\,V_w\,. \quad (2.18)$$

In this study conducted in Turkey, the PV energy efficiency of a conventional photovoltaic (PV) system is formulated at the maximum amount of sun energy applied to the Photovoltaic system. The novel approach for determining PV energy efficiency considered the incidence angle and the day of the year as parameters.

Almaktar et al. (2013), developed a regression model to estimate PV module temperature for poly and mono-crystalline technologies in tropical climates such as Malaysia. For hourly and daily module temperature prediction, two models were developed as given below:

For hourly module temperature, the model developed is given by Equation (2.19),

$$T_{mod} = 0.409\,T_a + 30.60 + 0.014G_T - 0.377\,V_w - 0.15Rh. \quad (2.19)$$

For daily module temperature, the model developed is given by Equation (2.20),

$$T_{mod} = 0.859\,T_a + 15.22 + 0.01G_T - 0.967\,V_w - 0.093Rh. \quad (2.20)$$

These models utilized atmospheric parameters, hourly global solar radiation, ambient temperature, relative humidity, wind speed and module temperature.

Muzathik (2014), proposed following linear regression model given by Equation (2.21) for estimating module back temperature, utilizing three meteorological parameters solar insolation, ambient temperature, and wind velocity,

$$T_{mod} = 0.943\,T_a + 0.35229 + 0.0195G_T - 1.528\,V_w. \quad (2.21)$$

Segado et al. (2014), proposed two models to estimate module temperature; in the first model, they proposed a modification to the NOCT model by introducing the wind factor to account for the impact of wind, given by following Equation (2.22),

$$T_{mod} = T_a + \frac{G_T}{800W/m^2}(NOCT - 20℃) + a(V_W - V_1) \quad (2.22)$$

where, T_{mod} is module temperature in °C, T_a is the ambient temperature in °C, G_T is solar insolation in W/m^2, NOCT is nominal operating cell temperature in °C, a an empirical parameter, expressed in °C s m^{-1}, V_W the wind velocity in m/s and V_1 the benchmark wind speed appears in the definition of NOCT temperature i.e. 1 m/s.

In the second model, another parameter was introduced to account for the relation between the temperature increase and the incident solar insolation given by following Equation (2.23),

$$T_{mod} = T_a + b[\frac{G_T}{800W/m^2}(NOCT - 20℃)] + a(V_W - V_1) \quad (2.23)$$

where, b is another dimensionless empirical constant.

Coskun et al. (2016), proposed Equation (2.24) with input variables, global solar insolation, ambient temperature, and wind velocity. The equation to estimate polycrystalline module temperature is

$$T_{mod} = 1.4\,T_a + 0.01(G_T - 500) - V_w^{0.8}\,. \quad (2.24)$$

In the above study, Photovoltaic (PV) panel surface temperature has been estimated by utilizing the artificial neural network (ANN) method. The ANN is trained by inputting solar insolation, ambient temperature and wind data, and the surface temperature of the PV panel is output obtained.

Du et al. (2016), developed theoretical models for predicting Photovoltaic (PV) panel temperature was evaluated for realistic scenarios by studying the effects of solar irradiance, wind speed and ambient temperature on the PV panel temperature. There is a time lag of 50-250 seconds in the thermal response of solar cells of Si thickness of 100-500 μm in steady weather conditions. For solar cells with a temperature coefficient in the range of −0.21%∼−0.50%, they reported an approximate efficiency loss between 2.9% and 9.0%.

Coskun et al. (2017), studied 17 implicit correlation equations for predicting module temperature by utilizing climatic parameters such as ambient temperature, solar radiation, and wind speed from a solar plant. The correlations were modified, and new implicit correlations were proposed for temperature deviation trends based on solar radiation.

Sohani et al. (2022), reviewed machine learning techniques applied to PV systems to predict performance and detect faults. The review provides insight into various machine learning methods that can be applied for the estimation of module temperature. This technique is still in a nascent stage.

2.4. Assessment of evaporation losses and evaporation loss reduction of the floating solar system

Surface water evaporation is a complex phenomenon, and various factors affect the water evaporation from the open water surface, some of these factors include water surface area, temperature, vapour pressure difference, wind effect, atmospheric pressure and quality of water. This section reviewed the research work on evaporation loss estimation from water surface open to sky and due to FSPV installion over water surface and evaporation reduction due to installation of FSPV.

Penman (1948) has experimentally demonstrated that the aerodynamic approach to estimating water evaporation is insufficient. He has also established that energy balance is a very effective method. The experimental findings were used to analyze data from four geographically dispersed sites in the United States and Europe. When the results for turf were used, they showed good agreement with estimates of evaporation from catchment areas in the British Isles. Penman (1956) developed a method for calculating the rate of evaporation for a hypothetical open water surface. It is based on equations for the balance of water and energy. It is based on water balance and energy balance equations. Eagleman (1967) proposed an equation to calculate evapotranspiration rates depending on temperature and relative humidity, and he compared the outcomes with those of five other equations with the same number of factors. Also, it evaluated the pan coefficient corresponding to relative humidity and established a relationship between potential evapotranspiration and actual evapotranspiration. With the proposed equation, the author obtained improved results, but it was inaccurate when applied to an equation involving additional meteorological data. Chandra et al. (1988), investigated the impact of meteorological factors on pan evaporation, including air temperature, relative humidity, wind speed, and number of daylight hours. According to the trend of the parameters produced through single and multiple linear regression analysis, the three-season prediction equations were chosen. The research shows that there is a strong correlation between the climatic conditions and pan evaporation. Singh et al. (1992), studied the correlation between evaporation from a US Class A open pan evaporimeter and other meteorological variables at Hisar, India. The evaporation rate at Hisar was greatly affected by all five meteorological variables namely, wind speed, maximum and minimum temperature, relative humidity, sunshine hours per day, and solar radiation at the 1% level. the results reveal that evaporation was positively correlated with wind speed, sunshine hours, mean air temperature, and solar radiation, while it was negatively correlated with relative humidity. With respect to the correlation coefficient, relative humidity had the highest value ($r = 0.78$). When all the significant meteorological characteristics were considered, the maximum coefficient of determination was obtained as 0.96. Singh & Xu (1997) proposed seven generalized equations for estimating free surface evaporation and validated them with the results of pan evaporation taken monthly from the four sites of climatological stations in north-western Ontario, Canada. The findings demonstrated that all equations were consistent with observed evaporation and that the influence of wind speed on monthly evaporation was minimal. The calculated evaporation, however, did not correlate well with the actual values when an equation containing parameters from one site was used to calculate evaporation at another location. Shrivastava et al. (2001), developed a statistical

correlation between pan evaporation and the climatic parameters of Jabalpur using the linear regression technique. According to the analysis, the rate of evaporation is significantly influenced by the maximum temperature and the relative humidity in the morning. In addition to the relative humidity, it has been discovered that evaporation and the number of rainy days have a negative correlation. The morning relative humidity has the highest coefficient of determination value of 0.95, followed by the highest temperature which is 0.94. The best multiple regression model at Jabalpur has R2 = 0.99 as the coefficient of determination for estimating pan evaporation. Rosenberry et al. (2007), used 14 alternative evaporation methods to assess the evaporation loss on the mirror lake, a 0.15 km^2 water body in New Hampshire, Northeastern USA, for the six open-water seasons. The results were compared to Bowen-ratio energy-budget (BREB) approach values, which are considered to be the industry standard. The results from the Priestley-Taylor, De Bruin-Keijman, and Penman techniques had the best comparisons with the results from the BREB. However, each of the three approaches calls for measurements of net radiation, air temperature, change in heat stored in the lakes, and vapour pressure, making them all relatively data-intensive. The results from linear regression of air temperature offer better result (i.e. 73% variance) as compared to linear regression of solar radiation and air temperature (i.e. 74% variance) corresponding to BREB values. Sahoo et al. (2009), examined the rate of water evaporation from 15 existing models that use flux gradient, energy balance, and mass transfer methodologies for estimation. The models were based on a regular-sized open on-farm reservoir (OFR). They discovered that the evaporation rate predicted by the Priestley-Taylor, de Bruin-Keijman, and Bowen Ratio Energy Budget (BREB) models, as well as the OFR, is quite close to the actual evaporation measured by a class A pan evaporimeter. McJannet et al. (2011), measured the amount of evaporation from huge bodies of water using a scintillometer to calculate sensible and latent heat flux. They compared the latent heat flux estimations obtained from the scintillometer and the Eddy covariance system, which displayed excellent agreement under various weather circumstances. In addition to this, the proposed methodology required less instrumentation than the alternative scintillometer calculation approach. Shirgure (2012), reviewed the multiple linear regression techniques with various meteorological factors to estimate evaporation losses from rivers, canals, open water bodies, etc. and concluded that most models may produce accurate results when used under climatic conditions similar to those for which they were developed. Rim (2016) proposed a pan evaporation estimation equation utilizing just the temperature data by comparing the results of the proposed equation with the results obtained using an evaporimeter for the 12 water reservoirs in Korea. The author also validated the results of the proposed equation in 44 research regions with both

temperature-based equations and equations based on other meteorological data and observed better results using the same equation.

Cooley Keith (1983) reviewed several techniques for reducing evaporation on water surfaces and discovered that floating covers were more efficient than suspended ones. He estimated during field tests that using floating covers of foamed wax blocks, continuous wax and foamed rubber reduced evaporation losses between 36% and 84% during 8 years, and the estimate of the lowest cost for saving was USD 0.08-0.13 per kl per year. Youssef & Khodzinskaya (2019) reviewed the published work of the last 14 years (2004 to 2018) with a particular emphasis on the physical, chemical, and biological techniques of reducing evaporation from water surfaces and found that physical methods using floating or suspended covers save 70 to 95% of water, while use of chemicals like WaterSavr can save only 20-40% of water. Additionally, it was observed that biological techniques like floating plants, wind blockers, and palm fronds significantly reduced water evaporation.

Melvin et. al. (2015), carried out an experimental investigation to determine the impact of floating solar panels on reducing water evaporation in Singapore reservoirs and also investigated the potential effects of varying the height of the solar panel above the water body on the rate of evaporation. The floating solar panel above reservoirs is simulated by a prototype that is based on the idea of evaporation pans. The findings of the experiment demonstrated that solar panels suspended above water bodies can reduce evaporation rates by about 30%. However, there is no discernible relationship between the height of the solar panel above the water's surface and the rate of evaporation. The typical daily evaporation rate, as determined by the experimental setup, is approximately 7 mm/day; however, by covering a water body's surface with solar panels, this rate is lowered to approximately 5 mm/day. Kumar & Kumar (2019) evaluated the outdoor performance of three commercially available PV technologies namely, Multi-crystalline Silicon (Multi-Si), Heterojunction with an intrinsic thin layer (HIT), and Cadmium Telluride (CdTe) above water bodies experimentally for large scale installations in the hot and humid climate and collect the data for six months. The author also estimates the evaporation loss reduction and compares the performance of water-based PV technologies with its ground-based performance. They found that the average performance ratio of water bodies based HIT and Multi-Si modules was lower than their respective ground-based modules while the CdTe module over water bodies outperformed the ground-based modules. Furthermore, installing PV panels above the water's surface is found to reduce evaporation by 29.1%. Sharma & Kothari (2016) have examined the potential of combining the floating solar power plant in conjunction with the Pumped

hydro energy storage (PHES) and hydroelectric system for the large reservoirs of India. The results reveal that integrating FSPV+PHES & Hydroelectric can be used to generate an uninterrupted 13 GW of green power throughout the year, thereby reducing evaporation loss by 1692 MCM annually. Around 60 GWp of FSPV and 30 GW of PHES must be installed to do this. Mittal et al. (2017), examined the water evaporation reduction of four lakes in Rajasthan covering 5 %, 10 %, 15% and 20 % of the area of the reservoir. It was estimated that using FPV panels on water bodies would save 64 million to 496 million litres of water annually. Wasthage (2017) explored the performance of a floating solar PV system through a case study of a Shrimp solar farm in Thailand. According to the findings, floating PV systems provide greater reliability and efficiency than ground-mounted PV systems while also reducing water evaporation. Farfan & Breyer (2018) have proposed that combining FSPV plants and hydropower reservoirs would operate as a virtual battery consistent with meeting electricity demand with solar energy during peak irradiation hours while balancing the grid with hydropower during low or no irradiation times and creating zero effect area for the deployment of PV power plants. They calculated that 4400 GW of FPV power potential could be deployed globally at 25% reservoir coverage, producing around 6270 TWh of electricity and preventing 74 billion cubic metres of water from evaporating. An increase in hydropower generation was found due to a decrease in evaporation loss by 6.3 %. Bontempo et al. (2021), proposed evaporative models using the design of an experiment and linear regression method for estimating the daily evaporation rate in the free water basin and compared them with the experimental results obtained using an evaporimeter. The findings show that for covering 30% area with an FPV system, the reduction rate, for the suspended system, flexible modules system, and for those systems that completely cover the surface beneath the modules were 18%, 42% and 49% respectively. Kumar et al. (2021), reviewed the challenges and explored the feasibility of a floating PV system by incorporating the water climate effect from the view of its performance, degradation, economics and environmental aspects. In addition to this, the author also discussed the various cooling techniques and evaporation rate of floating PV systems and found that full water coverage can reduce the evaporation rate by 49% while installing the FPV at a fixed height minimizes the rate of evaporation by 30%.

2.5. Studies on the economics of floating solar PVs

The size and characteristics of the water basin where FPV had been installed have a significant impact on the plant's economics. The only differences from a ground-mounted PV plant were the costs of the floating structures, the preliminary survey necessary for

deployment in bigger reservoirs or canals, and its installation. In order to assess the cost of installing an FPV system for various scenarios, the research work was also reviewed in the context of economics.

Castro-Santos et al. (2016), established a generic methodology for calculating the life-cycle cost and levelized cost of energy (LCOE) of floating offshore renewable energy devices employing wave energy and wind energy devices for the two locations namely, Agucadoura and Sao Pedro de Moel in Portugal. The result reveals that the exploitation cost is the most significant expense in terms of the life cycle of a floating offshore renewable energy farm, followed by the manufacturing cost and installation cost. In addition to this, for LCOE, Aguçadoura is preferable for floating offshore wave energy while Sao Pedro de Moel is the finest choice for floating wind energy. Wästhage (2017), compared the LCOE (Levellised cost of energy) of a typical ground-mounted solar PV grid-connected system with the LCOE of floating solar PV Systems. The LCOE of a grid-connected system is lower than that of a floating solar PV system. However, the other benefits such as water evaporation loss reduction and land use reduction compensate for the higher cost. Barbuscia (2018), developed a simulation model of a floating solar PV system on a Portuguese dam to calculate the levelized cost of energy and conducted a sensitivity analysis on the power plant's major cost-influencing factors namely, capacity, modules cost, floating mounting structure cost, and plant location in order to reduce the cost of energy. The sensitivity analysis indicates the exponential-decreasing trend of the cost of energy for growing system capacity. Oliveira-Pinto & Stokkermans (2020) proposed a method for calculating the energy output of various FPV technologies, taking into account the cooling effect's advantage by modifying the heat loss factor (U-Value) in PVsyst and providing the global overview of the industry while showcasing the various technologies and highlighting the benefits, potential, and restrictions of FPV applications. The author also analyzed the economic feasibility of the two FPV systems and the in-land reference system for the three sites. The results reveal that the LCOE varied from 96.2 to 50.3 euros per megawatt-hour (MWh), depending on the technology used and the amount of solar radiation that the location receives and the payback period for both the FPV ranges between 4 to 8 years while that of in-land reference system lies between 3 to 6 years. Niaki & Davoodi (2020) analyzed the technical and economic aspects of a system combining a hydropower plant and a floating PV system in the Sardasht region in West Azerbaijan region and obtained optimal values of load, water level and equipment cost using Homer software. The results show that the FPV power production was 208 kWp under maximum load conditions for two water levels of 25m and 27m, while the net power cost and

the LCOE were 4226727 $ and 0.0359 $/kWh, respectively. Gorjian et al. (2021), reviewed the technical advancement and economic and environmental impact of floating solar energy conversion systems and compared them with ground-mounted PV technology. The findings demonstrated that FPV can be implemented on the water bodies to increase power and reduce water evaporation simultaneously. However, salt deposition and algal-bloom growth on offshore sites could degrade its performance. The total cost of the floating system was 25% more than the ground-mounted system, but with an increase in capacity of the plant from 52 kW to 2 MW, the levelized cost of energy decreased up to 85 %.

Zahedi et al. (2021), reviewed various cleaning techniques such as water-based and water-free approaches from the technical and economic prospects of floating power generation technology and found no specific cycle for cleaning and the environmental conditions determine the cleaning cycle of the FPV system.

2.6. Status of FSPV installations across the world

The study of FSPVs installed across the world is also taken into consideration for this research and some of the examples of such installations are highlighted below in Table 2.1 for reference.

Table 2.1. World Overview of Installed Floating Solar PV Plants

Country	Name of plant	Capacity (MWp)	Year of development	Area covered in ha	Area covered per MWp in m^2	Technology/Developer
Japan	Sakayatame Ike	0.633	2019	0.6359	10046	Hydrelio (Ciel & Terre)
Taiwan	Kaohsiung	9.994	2018	9.2000	9206	Hydrelio (Ciel & Terre)
Israel	Ashdot	0.269	2018	0.2285	8494	Hydrelio (Ciel & Terre)
Colorado US	Walden	0.074	2018	0.0686	9276	Hydrelio (Ciel & Terre)
New Jersey US	Sayreville	4.403	2019	4.1286	9377	Hydrelio (Ciel & Terre)
China	Anhui CECEP	70.005	2019	60	8572	Hydrelio (Ciel & Terre) Three Gorges (2022)
UK	Queen Elizabeth II	6.338	2016	6.4	10097	Hydrelio (Ciel & Terre)
Cambodia	CMIC	2.835	2019	2.4027	8475	Hydrelio (Ciel & Terre)
China	Guqiao Huainan	150	2017	-	-	Sungrow
China	Panji Huainan	150	2018	-	-	Beijing Northman, Zhongya Hefei Jintech New energy co ltd, Anhui ZNZC New Energy co. Ltd., CJ Institute China
China	Liuzhuang Yingshang	130	2018	-	-	Anhui ZNZC New Energy co. Ltd., Shanghai Qihua Wharf Engineering co ltd etc.

Country	Name of plant	Capacity (MWp)	Year of development	Area covered in ha	Area covered per MWp in m^2	Technology/Developer
China	Xinji Huainan	102	2017	-	-	Sungrow
China	Weishan Jining	100	2018	-	-	Sungrow
China	Huancheng Jining	50	2018	-	-	Sungrow Huancheng Jining (2017)
China	Panji Huainan	40	2017	-	-	Sungrow
China	Renlou Huaibei	40	2017	-	-	Shanghai Qihua Wharf Engineering co ltd etc.
China	Huaibei Anhui	32.686	2018	33.7511	10326	Ciel and Terre
China	Weishan Jining	31	2017	-	-	Sungrow
China	Xinji Huainan	20	2016	-	-	Xinyi Solar Holdings
Korea Rep.	Gunsan North Jeolla	18.7	2018	-	-	Scotra Co Ltd.
Japan	Yamakura Chiba	13.744	2018	13.7600	10012	Ciel and Terre
China	Anhui Fuyang Southern Wind-solar-storage,	650	2023	520	8000	China Three Gorges New Energy (Group) CO LTD
China	Wenzhou Taihan, Zhejiang	550	2021	493.3333	8969.7	Astroenergy Garanovic (2021)
Taiwan	Changbing, Changhua	440	2023			Ciel and Terre HEXA Renewables Changbing (2023)
China	Dezhou Dingzhuang, Shandong	320	2021	-	-	Huaneng International Lee (2022)
Indonesia	Cirata, Purwakarta,West Java	192	2023	200	10416.67	Perusahaan Listrik Negara (PLN) Nusantara Power Cirata (2019)
China	Three Gorges, Huainan City, Anhui	150	2017	-	-	Sungrow Three gorges(2022)
India	NTPC Ramagundam, Peddapalli, Telangana	100	2022	200	20000	BHEL Ramagundam (2022)
Singapore	Tangeh	60	2021	45	7500	Sembcorp Industries Martin (2021)
China	Yuanjiang Yiyang, Hunan	100	2019			Sungrow Yuanziang yiyang (2019)
Thailand	304 Industrial Park, Prachinburi	60	2023	-	-	Sungrow developer China Energy engineering (CEEC) and national Power Supply Public Co. Thailand (NPS) Garanovic (2023)

Country	Name of plant	Capacity (MWp)	Year of development	Area covered in ha	Area covered per MWp in m^2	Technology/Developer
Vietnam	Da Mi Reservoir, Binh Thuan Province	47.5	2019	50	10526.32	Da Nhim-Ham Thuan-Da Mi Hydropower Da Mi Reservoir (2019)
Thailand	Sirindhorn dam, Ubon Ratchathani	45	2021	70	15555.56	Electricity Generating Authority of Thailand(EGAT) Sirindhorn dam (2021)
South Korea	Hapcheon dam, South Gyeongsang	40	2021	-	-	Hanwha Q CELLS Korea Hapcheon dam (2021)
China	Anhui GCL	32		-	-	Ciel& Terre Anhui GCL (2023)
Israel	HaBonim Reservoir, Ma'ayan Tzvi	31	2023	58.7	18935.48	Teralight with subsidiary menorah Synergy Largue (2023)
India	NTPC Simhadri, Vizag, Andhra Pradesh	25	2021	60	24000	BHEL Gupta (2022)
Thailand	Ubol Ratana dam, Khon Kaen	24	2024	-	-	EGAT Ubol Ratana dam (2024)
India	NTPC Kayamkulam, Kerala	92	2022	-	-	Tata Power and BHEL Kayamkulam (2022)
Austria	Former sand pit site, Grafenworth	24.5	2023	14	5714.3	ECOwind and EVN Garanovic (2023-2)
China	Qintang Guigang, Guping Guangxi	20	2019	-	-	Sungrow Qintang (2019)
France	Lazer, Hautes-Alpes	20	2023	-	-	EDF Renewables Dasgupta (2023)
Israel	Burgata	13.5	2022	-	-	INBAR and EDF Renewables Burgata (2022)
New Jersey,USA	NJAW Canoe Brook, Millburn	8.9	2022	-	-	CIEL & TERRE New Jersey (2022)
India	Omkareshwar Dam (Madhya Pradesh)	278	2023	-	-	Rewa Ultra Mega Solar Limited (RUMSL) Omkareshwar (2023)

2.7. Research gaps and scope of the current study

In this chapter, several research on the technical potential assessment of PV systems installed on diverse water bodies around the world and in India, both theoretically and experimentally were studied and presented. The approaches chosen by many researchers to evaluate module temperature, module performance, evaporation loss reduction, and the economics of floating

solar PV systems were also discussed in this chapter. Based on the thorough study of the literature background, the following research gaps are identified:

- Based on the literature background, a few studies have been reported for FSPV installations in tropical regions. Performance assessment of floating solar PV systems and comparative study with ground-mounted PV based on the recorded data is not studied for Uttar Pradesh, a tropical region. To fill this gap, the current study proposes to assess the performance of floating solar PV systems for major dams/reservoirs of Uttar Pradesh and compare them with ground-mounted PVs based on the data from field experimentations.
- A comparative study of PV modules is not addressed extensively based on experimental evidence for ground-mounted and floating PVs. The research proposed to conduct extensive experiments and collection of meteorological and PV performance data by design and development of experimental setup.
- Limited study of FSPV potential assessment is performed in India but region-wise study, especially in the context of Uttar Pradesh is not performed and reported so far. The case study for one reservoir and further extension to assess the FSPV potential for major dams/reservoirs of Uttar Pradesh is conducted.
- Predictive models for module temperature of ground-mounted PV panels are mainly focused in previous studies, however limited studies of predictive models for module temperature of FSPV panels are reported; especially since there are no studies in the context of India. The development of predictive models for the module temperature of FSPV based on the recorded data from the field setup is proposed.
- Studies on model development for the assessment of evaporation and evaporation reduction due to FSPV installations and comparative studies with the open sky are limited. Based on the recorded data from the developed experimental setup, predictive model development, analysis and estimation of evaporation, evaporation reduction including comparative studies between water surface covered by PV module and water surface open to the sky and the impact of seasonal and annual variations, evaporation reduction assessment for major dams/reservoirs of Uttar Pradesh is proposed in this research.
- The performance study of FSPVs for various tilt angles and tracking are reported in limited studies. However, the impact of the height of the panel above the water surface is not taken into consideration for analyzing the panel performance and evaporation reduction. The study proposes a field setup for FSPVs with varying heights to record the

desired meteorological and panel performance data for analyzing the impact of panel heights. The study is proposed to extend in identifying the panel heights above the water surface for maximizing power generation and evaporation reduction. Also, the scope is further extended to estimate the performance and evaporation reduction for major dams/reservoirs of Uttar Pradesh.

- The decision-making strategies and tools to assess the plant capacity, area coverage, installation cost, power generation and evaporation reduction are not available currently. Based on the outcomes of the current research, the study also proposes to develop decision-making tools for technocrats, field engineers, researchers, stakeholders, and policymakers to achieve the desirable targets for various scenarios considering the plant capacity, area coverage, installation cost, power generation and evaporation reduction.

Chapter 3

Design and Development of Experimental Setup

Abstract

The increasing prominence of floating solar photovoltaic (FSPV) technology in power generation signifies its transition to a mainstream energy solution, albeit still in its early developmental stages. Consequently, meticulous evaluation of FSPV performance and its potential to reduce evaporation rates becomes imperative. However, existing literature reveals a scarcity of comprehensive data. It necessitates a holistic approach towards experimentations and data collection for key parameters to facilitate insightful analysis and to develop a predictive model for panel temperature, assess PV panel performance, evaluate evaporation reduction attributed to FSPV installations, and extrapolate findings to major dams in tropical regions. Key parameters (solar irradiance, wind speed, ambient temperature, module temperature, water temperature, dry and wet bulb temperature, evaporation loss, relative humidity, open circuit voltage, and current) are identified based on reported literature, and the experimental setup was designed and developed for collecting these parameters for various scenarios. The experimental setup was installed at Birla Institute of Technology and Science (BITS), Pilani, Rajasthan, India at 28° 21' 34.1316" N, 75° 35' 17.2896" E, at an elevation of 299 m above mean sea level. Over three years, data was systematically collected both manually and through sensors by ensuring that instruments, equipment, and data collection procedures were aligned with the identified parameters. The results of this study have the potential to contribute significantly to the field of renewable energy, water resource management and would aid in the development of new and innovative solutions for sustainable water conservation and energy generation.

3.1. Introduction

For this scientific investigation, data collection is the foundation upon which our research objectives are established. It involves a methodical process of collecting, recording, and analyzing empirical evidence or observations that are relevant to our research topic. In the context of this work, which focuses on investigating the performance and potential of floating solar photovoltaic (FSPV) systems in tropical regions, data collection is of utmost significance. This work focuses on the intricacies surrounding FSPV technology and its implications for renewable energy usage in tropical climates by carefully gathering and

analysing data on various parameters such as solar irradiance, panel temperature, power output, meteorological parameters and evaporation rates.

To provide a comprehensive context for these endeavours, the research background is delved to identify the key meteorological and thermal parameters that influence the performance of photovoltaic (PV) panels and evaporation process, as outlined in Chapter 1. It is believed that this foundational understanding is crucial because it serves as the bedrock for designing and developing the experimental setup, which forms the central focus of discussion in this chapter. By analysing existing literature and theoretical frameworks, the necessary groundwork for the data collection efforts is established, which is essential for insightful analyses in the subsequent chapters. The insights presented in this chapter will be instrumental in advancing the research.

3.2. Critical parameters for Data Collection: Background and Rationale

3.2.1. Various Thermal Models for Panel temperature

Thermal models help to predict the power, efficiency and temperature of the PV module utilising the meteorological parameters such as solar irradiance, ambient temperature and wind speed. Researchers have developed a great variety of correlations (both implicit and explicit) with different complexity due to the growing solar market. Even though many models have been created and researched on the evaluation of PV module temperature, these studies are far from sufficient to provide criteria for choosing appropriate models for PV technologies as these formulations were developed for some specific region and hence needs to be checked and corrected for adopting into the Indian conditions based on the experimental results. Some of the thermal models used for estimating the PV module temperature are listed in Table 3.1. Out of the six models, one of the PV module temperature estimation models for the floating PV system were derived by (Kamuyu et al.,2018).

Table 3.1. List of thermal models with meteorological data requirement for PV module temperature estimation

Thermal Models (Ref.)	Installation Type	Meteorological Data Required
Kings Model (King et al.,1997)	Ground Mounted	Solar irradiance, wind speed, ambient temperature
Faiman Model (Faiman,2008)	Ground Mounted	Solar irradiance, wind speed, ambient temperature
Kaplani Model (Kaplani and Kaplani,2014)	Ground Mounted	Solar irradiance, ambient temperature
Kurtz Model (Kurtz et al.,2009)	Ground Mounted	Solar irradiance, wind speed, ambient temperature

Thermal Models (Ref.)	Installation Type	Meteorological Data Required
Skopolaki Model (Skoplaki and Palyvos,2009)	Ground Mounted	Solar irradiance, wind speed, ambient temperature
Koehl Model (Koehl et al.,2011)	Ground Mounted	Wind speed
Kamuyu Model (Kamuyu et al.,2018)	Water Mounted	Solar irradiance, wind speed, ambient temperature, water temperature

3.2.2. Various Evaporation Estimation Methods

This study reviewed available literature from national and international case studies for estimation of evaporation. Evaporation is a process in which liquid water converts into gaseous vapour below the boiling point by the transfer of energy from the environment and the movement of the wind. Surface water evaporation is a complex phenomenon and are affected by various factors such as water surface area, temperature, vapour pressure difference, wind speed, atmospheric pressure, size of water body and quality of water. Evaporation can be quantified in several ways based on the method used described in Figure. 3.1.

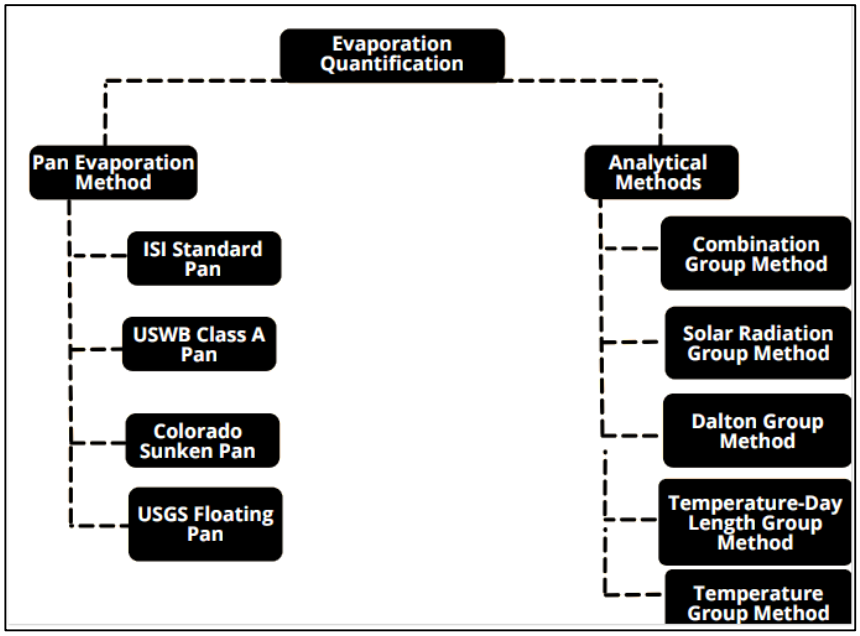

Figure. 3.1. Classification of methods for quantification of rate of evaporation

3.2.2.1. Pan Evaporation Method

In Pan Evaporation, an experimental observation using an evaporimeter is taken at a regular interval of time to estimate and quantify water evaporation, water temperature, ambient temperature, humidity, wind velocity, precipitation, sunshine hour. Based on the dimension and material of the pan, it is classified into four categories shown in Figure 3.2. Despite being the most direct method used globally, this approach has the following drawbacks.

1. The heat storage capacity and the heat transfer characteristic of a pan differs from a reservoir.
2. The height of a rim in the evaporation pan affects wind action and casts shadow over the water surface in the pan.

Therefore, to obtain the evaporation from a huge lake under the same meteorological and exposure circumstances, evaporation obtained from a pan must be corrected by using Equation (3.1).

Lake Evaporation = Pan Evaporation x Pan Coefficient (3.1)

Therefore, pan coefficient can be simply defined as ratio of evaporation on water body to evaporation on pan. In general, the coefficients depend on the pan's type, location, and the type of the water body. They may also change over time.

The ratio of the bulk mass transfer equations of the lake and the pan is used to calculate pan conversions and is given by Equation (3.2) (Finch and Hall ,2001).

$$\overline{E}_{ws} = K_c \cdot \left(\frac{\overline{p}_s - \overline{p}_a}{\overline{p}_p - \overline{p}_a} \right) \cdot \overline{E}_p \quad (3.2)$$

Where, K_c is the empirical constant, $\overline{E}_{ws}$ is mean evaporation rate from the water body, $\overline{E}_p$ is mean evaporation rate from the pan, $\overline{p}_s$ is the mean saturated vapour pressure of air at water surface temperature, $\overline{p}_p$ is the mean saturated vapour pressure of air at the surface of pan, $\overline{p}_a$ is the mean saturated vapour pressure of air at reference height.

ISI Standard pan

The ISI Standard Pan shown in Figure 3.2, also known as Modified Class A pan, specified by IS: 5973, is the most preferred pan in India. The unit comprises of a wide cylindrical pan with a dimension of 1220 mm in diameter and 255 mm in depth built of 20-gauge (0.914 mm) copper sheet that has been painted white on the outside and tinned on the inside. A stilling well consists of two reference cylindrical rod fixed in the middle- and one-gauge rod. It suppresses swirls that may be present in the main section of the pan, resulting in an uninterrupted water surface around the point of the fixed-point gauge. A fixed-point gauge indicates the level of water. The pan is positioned on a square wooden platform that is 1225 mm wide and 100 mm high above the ground to allow for unobstructed airflow beneath the pan. In order to prevent water loss from the pan owing to outside agents like birds and animals, it is covered with hexagonal wire mesh of standard size. A clamp is used to secure a

thermometer to the pan's side, allowing the bulb to sink 50 mm below the water's surface to measure the water's surface temperature.

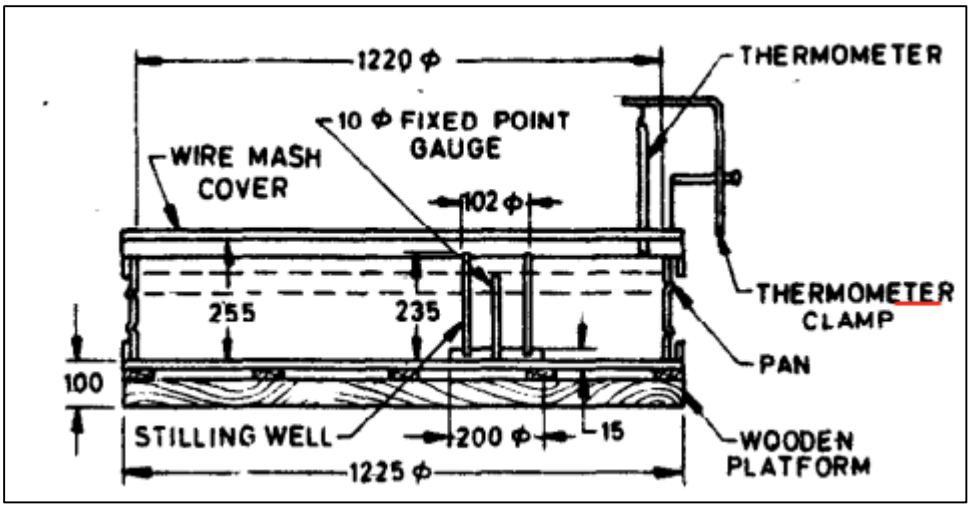

Figure. 3.2. ISI Standard Pan

US Weather Bureau Class A Pan

The US Class A pan is cheaper, easier to install, simple to clean and leak-detective. However, it suffers with a drawback of having its sides exposed to the sun. As a result, it heats up more quickly than pans buried in the ground, thereby increases evaporation. It is a circular pan having 1207 mm diameter and 254 mm depth. It is placed on a wooden open platform that is located on the ground. The evaporation is measured by measuring the depth of water in a stilling well with a hook gauge.

Colorado Sunken Pan

These were square pan having 914 mm length and 457 mm depth placed on the ground with the rim 51mm above the ground level. These pans are difficult to clean, detect leak and overestimate evaporation due to the heat transfer from the surrounding soil.

US Geological Survey Floating Pan

These were square pan having 900 mm length and 450 mm depth and were supported by drum floats in the middle of a raft that measures 4.25 x 4.87 m. The pans were set afloat in the lake with a goal to simulate the characteristics of a huge body of water. The drawbacks of the above-mentioned pan include measuring challenges and frequent splashing.

3.2.2.2. Analytical Method

The analytical models used to estimate the evaporation losses from the meteorological parameters are classified into four categories depending on the parameters they require or

terms they quantify (described in Figure 3.1). The ‘‘combination’’ methods quantify both energy and advective terms while Solar radiation & Temperature group rely on measurement of solar radiation and air temperature. The Dalton group mandates the measurement of wind speed, water surface temperature, air temperature, and air humidity. As the name implies, the Temperature and Day Length group requires the measurement of both air temperature and day length, whereas the Temperature group simply needs to know the air temperature. Each of these models was developed at various locations around the world and the best method suited for tropical areas like India was determined. Some methods were modified to estimate better evaporation loss. These models were studied and observed data were utilised to estimate evaporation from these models. The list of evaporative models applied for estimating the evaporation loss in the present work is shown in Table 3.2.

Keeping in view the need to estimate the evaporation loss reduction due to installation of floating solar PV over water bodies, present study has undertaken a pilot case study at BITS Pilani to quantify the evaporation loss through pan evaporation in normal condition and reduction in evaporation while covering the water with solar panels for floating solar PV plants and second objective to optimise the height of panels above water to maximise the evaporation loss reduction. Different approaches for measuring evaporation loss were used to validate the phenomenon, and the optimal formula for Indian meteorological circumstances was provided. Another objective of the study is to quantify evaporation loss reduction at potential water bodies for harnessing floating solar PV installation in the state of Uttar Pradesh. The consideration in this pilot case study will serve as a guide for evaluating the potential for floating solar PV technology at state and national level.

Table 3.2. List of evaporative models for estimating evaporation loss

Group	Methodology	Meteorological Data Required	Applicability
Combination Group	Penmann (PM)	Temperature, relative humidity, wind and net radiation	Daily
	Pristley-Taylor (PT)	Net radiation	>10 days
	De Bruin-Keijman (DK)	Net radiation	Daily
	Brutsaert-Stricker (BS)	Temperature, relative humidity, wind speed and net radiation	Daily
	De Bruin	Wind speed	>10 days
Solar radiation Mathod	Makkink (MK)	Solar radiation	Monthly
	Stephens-Stewart (SS)	Solar radiation and Air temperature	Monthly
	Jensen-Haise (JH)	Solar radiation and Air temperature	>5 days
Dalton Group	Ryan-Harleman (RH)	Ambient temperature, air temperature, wind speed, saturated vapour pressure of air	Daily

Group	Methodology	Meteorological Data Required	Applicability
Temperature –Day Length Group	Hamon	Air temperature, Total hours of daylight	Daily
	Blaney-Criddle	Air temperature, Total hours of daylight, Total annual hours of daylight at a specific latitude	Monthly
Temperature Group	Papdakis (PD)	Air temperature	Monthly

3.3. Experimental Material and Methodology

The research was carried out at Birla Institute of Technology and Science (BITS), Pilani, Rajasthan, India at 28° 21' 34.1316" N, 75° 35' 17.2896" E, at an elevation of 299 m above mean sea level to ascertain the FSPV module's performance under actual outside circumstances. The research area has a continental climate that is semi-arid, typical of Northwestern India. The summer season begins in April and lasts through June. During the hottest and driest months of May and June, the maximum temperatures can exceed 42°C. They are followed by the monsoon months of July, August, and early September, during which temperatures drop slightly and humidity levels climb significantly. In the monsoon months of July and August, Pilani experiences less rainfall. Warm days and mild to chilly evenings are common between the months of late October to early March. January is the coldest month in Pilani with the minimum temperature touching -2 ^{o}C at night.

Four multi-crystalline Si modules MS 320/24 from Mehar Solar Technologies Limited with 72 cells are chosen for the present study. The technical specifications of the PV module used in the present study are given in Table 3.3. The module area and efficiency is 1.9345 m^2 and 16.1% respectively. The experimental test rig consists of four photovoltaic modules such that three PV modules were installed at different heights above water surface namely, 30 cm, 50 cm and 100 cm and one ground-mounted PV system, Pyranometer, Temperature sensors, air and humidity sensor, Data Logger, digital anemometer. The principal instruments used for this research and their specifications are shown in Table 3.4. The following manual instruments were used in conjunction with these instruments: a manual anemometer, a sunshine recorder, four evaporimeters, four water temperature thermometers, a dry bulb and wet bulb thermometer, a maximum and minimum thermometer. Data from the experimental site was collected manually as well as automatically through sensors. Over the course of three years, data was manually collected for three separate time slots (8:30 a.m., 2:00 p.m., and 5:30 p.m.) and automatically through sensors with 15-minute and 1-minute time intervals. Figure 3.3. shows the experimental setup of FSPV and ground-mounted PV module at Pilani.

3.3.1. Collection of Operating Data of the Experimental Setup Rig.

Various sensors and instruments were installed to measure solar irradiance, wind speed, ambient temperature, module temperature, water temperature, dry and wet bulb temperature, evaporation loss, relative humidity. The data taker DT85 data logger interfaces with the SDI-12 sensor network to record the meteorological parameters with a 1 minute and 15 minutes time step shown in Figure 3.4. However, following data was recorded manually for the three time slots (8:30am, 2:30pm, 5:30pm) –

- Sunshine Hours (h) recorded once daily at 8:30 am
- Wind speed and direction (m/s)
- Maximum and minimum air temperature (^oC) recorded once daily at 8:30 am
- Ambient temperature (^oC)
- Dry and wet bulb temperature (^oC)
- Water temperature (^oC)
- Rainfall measurement (mm) recorded once daily at 8:30 am
- Evaporation (mm) recorded once daily at 8:30 am
- Data collected in one minute and fifteen-minute intervals via sensors are:
- Ambient Temperature (^oC)
- Humidity (%Rh)
- wind speed (km/h)
- wind direction (-)
- Panel temperature (^oC)
- water temperature (^oC)
- Solar Insolation (W/m^2)

Table 3.3. Technical Specification of PV Module at STC (1000 W/m^2; 25 ^{o}C, AM 1.5G)

Type	**Mehar Solar**
Name	**Multi C-Si 32/0818**
Maximum Power	312 W
Open circuit Voltage	46.07 V
Short circuit Current	8.85 A
Maximum Voltage	37.15 V
Maximum Current	8.39 A
Cell Efficiency Module Efficiency	17.8 % 16.1%

Table 3.4. Principal Instruments and its Specification

Type	**Instruments**	**Function**	**Make & Model**	**Accuracy**
Automatic-Type	Pyranometer	To measure solar irradiance	Kipp & Zonen CMP 11	>98%
	Digital Anemometer	To measure wind speed and direction	AA-WS-50_4-20 AA-WD-360_4-20	±3% FS
	Air Temperature Sensor	To measure ambient temperature (both maximum and minimum)	AARHT1K-4-20 PT100 RTD	±0.1°C
	Temperature Sensor	To measure water and panel temperature	PT100 RTD Pt100(3-wire)	±0.2°C, Class A
	Humidity sensor	To record humidity	WS08P	±2 % Rh
	Data Logger	To automatically monitor and record environmental parameters over time,	DT 85 series 4 DataTaker	-
Manual-Type	Thermometer	To measure ambient and water temperatures	ZEAL	1°C
	Dry and Wet Bulb Thermometer	To estimate humidity	ZEAL	1°C
	Rain Gauge	To measure rainfall	Standard or Funnel Rain Gauge	0.1mm
	Evaporimeter Anemometer Sunshine Recorder	To measure evaporation loss To measure wind speed and direction To measure Bright Sunshine hour	ISI Standard Class A Pan Campbell–Stokes recorder	- -0.23h

Figure. 3.3. Experimental test rig at BITS, Pilani, Pilani Campus, Rajasthan India

Figure 3.4. Recording of meteorological parameters with 1 and 15-minute interval.

3.3.2. Parametric Analysis of Floating Solar PV System

In the preceding sections, we detailed the instrumentation required to measure diverse parameters critical for assessing Floating Solar PV installations. Now, we will discuss existing calculation methods of key parameters utilizing different models. Through rigorous analysis in the following chapters, we aim to gain comprehensive insights into the performance, efficiency, and feasibility of Floating Solar PV systems in the Indian context.

3.3.2.1. Module Temperature

It is well known through literature and described in Chapter 2 that the operating temperature of a PV module is a dependent parameter. There are many correlations developed to estimate the operating temperature of PV cells/modules based on the type of mounting system which are classified as: Ground-mounted and Water-surface mounted.

The following mathematical expression Equation (3.3), derived by (King et al.,2004), is used to determine the operating temperature (T_{mod}) of ground-mounted solar PV panels as a function of solar irradiance, ambient temperature (T_a), and wind speed.

$$\boldsymbol{T_{mod} = T_a + G_T exp^{(a + bw)}} \quad (3.3)$$

Where, G_T is solar irradiance incident on module surface, (W/m^2), and '*a'* is a dimensionless coefficient establishing the upper limit for module temperature at low wind speeds and high solar irradiance, while '*b'* describes cooling by the wind and has dimension (s/m) and 'w' is wind speed measured at 10 m height in m/s. These empirically determined coefficients are representative of different module types and mounting configurations.

Kings model was simplified by (Kurtz et al.,2009) and substitutes the value of coefficient a & b as shown in Equation (3.4)

$$\boldsymbol{T_{mod} = T_a + G_T exp^{(-3.473\ -0.0594w)}} \quad (3.4)$$

Another notable expression proposed by (Faiman,2008) for estimating the operating temperature of ground-mounted solar PV panels is given in Equation (3.5)

$$\boldsymbol{T_{modK} = T_{aK} + {G_T}/{(U_0 + U_1 V_{w3.5})}} \quad (3.5)$$

Where, U_0, U_1 are empirically determined coefficients with average values 25 Wm^{-2} K^{-1} and 6.84 Wm^{-3} sK^{-1} respectively. This model was validated by (Koehl et al.,2011) and suggested a simplified way to determine a Realistic Nominal Module Temperature (ROMT) instead of Nominal Operating Cell Temperature (NOCT) given in Equation (3.6).

$$ROMT = 20 + 800/ (U_0 + U_1 V_{w3}) \quad (3.6)$$

Another remarkable empirical model was established by (Skoplaki et al.,2008)

$$T_c = \frac{T_a + \left(\frac{G_T}{G_{NOCT}}\right) \times \frac{h_{wNOCT}}{h_w} \left(T_{NOCT} - T_{a,NOCT}\right) \left[1 - \frac{\eta_{ref}}{(\tau\alpha)} (1 + \beta_{ref} T_{ref})\right]}{1 - \frac{\beta_{ref}\eta_{ref}}{(\tau\alpha)} \left(\frac{G_T}{G_{NOCT}}\right) \left(\frac{h_{w,NOCT}}{h_w}\right) \left(T_{NOCT} - T_{a,NOCT}\right)} \quad (3.7)$$

Equation (3.7) was further simplified by (Skoplaki et al., 2008) with the three basic environmental conditions with wind speed v_f >0 m/s and applies to free standing frames may be written as in Equation (3.8)

$$T_{mod} = T_a + \left(\frac{0.32}{8.91+2.0 v_f}\right) G_T \quad (3.8)$$

(Kaplani & Kaplanis ,2014) correlates the PV module operating temperature is given in Equation (3.9)

$$T_{mod} = T_a + f G_T \quad (3.9)$$

Where, f is the coefficient (ºC m^2 W^{-1}) and G_T global solar radiation intensity on the surface of the PV module (W/m^2) solar radiation intensity.

(Kamuyu et al.,2018), proposed an explicit equation for estimating the floating PV module operating temperature considering ambient temperature, wind velocity, solar irradiance and water temperature and is given in Equation (3.10)

$$T_{mod}=1.8081+0.9282T_a+0.021G_T-1.2210w+0.0246T_w \quad (3.10)$$

3.3.2.2. Evaporation Losses

The following Table 3.5 describes the various sets of mathematical expressions given in Equation (3.11 - 3.25) for estimating the evaporation loss.

Table 3.5. Mathematical expression for estimating the evaporation loss.

Evaporative Model	Mathematical Expression	Equation No.
COMBINATION METHOD		
(Priestley & Taylor,1972)	$E = \left(\varpi . \frac{\Delta}{\Delta+\gamma} . \frac{Q_n - Q_x}{\lambda\rho}\right)$ *86.4	(3.11)
(De Bruin & Keijman,1979)	$E = \left(\frac{\Delta}{0.85\Delta + 0.63\gamma} . \frac{Q_n - Q_x}{\lambda\rho}\right) * 86.4$	(3.12)
(Monteith,1965).	$E = \frac{1}{\lambda}\left(\frac{\Delta\,(R_n - G) + \rho_a c_p (e_s - e_a)/r_a}{\Delta + \gamma\left(1 + \frac{r_s}{r_a}\right)}\right)$	(3.13)
(Brutsaert & Stricker,1979).	$E = \left((2\varpi - 1)\left(\frac{\Delta}{\Delta+\gamma} . \frac{Q_n - Q_x}{\lambda\rho}\right) * 86.4\right) - \left(\frac{\gamma}{\Delta+\gamma} . 0.26 . (0.5 + 0.54 V_w) . (e_s - e_a)\right)$	(3.14)
(DeBruin,1978)	$E = 1.192\left(\frac{\varpi}{\varpi - 1}\right)\left(\frac{\gamma}{\Delta+\gamma}\right)\frac{(2.9 + 2.1 V_w)(e_s - e_a)}{\lambda.\rho} * 86.4$	(3.15)
SOLAR RADIATION METHOD		
(Jensen & Haise,1963).	$E = (0.014\, T_a - 0.37)(3.523 \times 10^{-2} Q_s)$	(3.16)
(Makkink & Heemst,1974)	$E = 52.6 * \left(\frac{\Delta}{\Delta+\gamma} . \frac{Q_s}{\lambda.\rho}\right) - 0.12$	(3.17)
(Stephens & Stewart,1963).	$E = (0.0082 T_a - 0.19)(3.495 \times 10^{-2} Q_s)$	(3.18)
DALTON GROUP METHOD		
(Harbeck,1958).	$E = \xi . u_w . (e_w - e_a) \times 25.4$	(3.19)
where,	$\xi = \frac{0.00338}{A_s^{0.05}}$	(3.20)
(Ryan et al.,1973).	$E = \frac{(2.7(T_w - T_a)^{0.333} + 3.1\, V_w) . (e_w - e_a) * 86.4}{\lambda.\rho}$	(3.21)
TEMPERATURE-DAYLENGTH GROUP METHOD		
(Blaney & Criddle,1962)	$E = (0.0173\, T_a - 0.314)(T_a) * \left(\frac{D}{D_{TA}}\right) * 25.4$	(3.22)
(Hamon,1960)	$E = 0.55 * \left(\frac{D}{12}\right)^2 (Pt) * 25.4$	(3.23)
TEMPERATURE GROUP		
(Papadakis,1965).	$E = 0.5625 * (e_{max} - (e_{min} - 2))\left(\frac{10}{d}\right)$	(3.24)
(Thornthwaite,1948).	$E = \left(1.6\left(\frac{10 T_a}{I}\right)^{6.75\times10^{-7} I^3 - 7.71\times10^{-5} I^2 + 1.79\times10^{-2} I + 0.49}\right)\left(\frac{10}{d}\right)$	(3.25)

where,

E = evaporation in mm/day

ϖ= Priestley Constant (≈1.26)

Δ = slope of saturated vapour pressure curve at air temperature (Pa/^{o}C)/ (kPa/^{o}C)

ρ = density of water (1000 kg/m^3)

λ =Latent heat of vaporization (MJ/kg)

γ = Psychometric constant (kPa/^{o}C)/ (Pa/^{o}C)

ρ_a = density of air (kg/m^3)

Q_n = Net radiation (W/m^2)

Q_x = change in heat stored in the water body (W/m^2)

Q_s = solar radiation (W/m^2)

r_s = bulk surface resistance in s/m

r_a = bulk aerodynamic resistance in s/m

V_w = Wind speed measured at 2 m height (m/s)

e_s = mean saturated vapour pressure at air/ambient temperature (hPa/ mbar) (kPa)

e_a - actual vapour pressure (hPa/ mbar) (kPa)

e_w = mean saturated vapour pressure at water temperature (hPa/mbar)

e_{max} = Vapour saturation pressure at maximum temperature (mb)

e_{min} = Vapour saturation pressure at minimum temperature (mb)

R_n = Net radiation (MJ/m2/day)

G = soil heat flux density (MJ/m2/day)

T_a = Ambient/ air Temperature (^{o}C)

T_w = Water Temperature (^{o}C)

c_p = specific heat of air (MJ/kg/ ^{o}C)

ξ = Mass transfer coefficient (a coefficient of proportionality)

A_s = Surface area of water body (Acres)

u_w = wind speed (miles/hour)

D= Hours of Daylight

D_{TA}= Total annual hours of daylight

Pt = saturated vapour density = 4.95 $\frac{e^{0.062T_a}}{100}$

I = Annual heat Index (non-dimensional) = $\sum i$, i = $(T_a)^{1.514}$

where, T_a = mean air temperature (°C) for Thronthwaite, Blaney- Criddle and °F for Jensen-Haize and Stephens-Stewart

d = Number of days in month

3.3.2.3. Power Output

The electrical power output (P_{pv}) in W for the solar PV system may be defined as given in Equation (3.26)

$$\text{Power output } P_{pv} = G_T x\, A_M x\, \eta_{Mref}(1 - \beta_{power} x(T_{pv} - T_{ref})) \quad (3.26)$$

where GT is solar insolation in W/m^2, A_M= Area of the module in m^2, η_{Mref} = module efficiency at NOCT, β_{power} = power variation coefficient with respect to module temperature in %/°C, T_{pv}= module temperature in °C and T_{ref} = NOCT temperature 25°C. Substituting the value of module temperature developed by numerous authors in Equation (3.26), electrical power generated can be estimated and compared for the ground-based PV module. For estimating the power generated by floating PV modules, substituting value of T_{mod} by Equation (3.10) into Equation (3.26).

3.3.2.4. Module Efficiency

The general expression for PV module efficiency (η_{el}), given by (Abeykoon et al.,2018) and (Florschuetz,1979*), can be written as*

$$\eta_{el} = \eta_{ref}\left[1 - \beta_{ref}\left(T_{pv} - T_{ref}\right)\right] \quad (3.27)$$

Where, β_{ref} = efficiency correction coefficient for reference temperature (°C^{-1}) and η_{ref} = electrical efficiency of the module for the reference temperature T_{ref}. Substituting the value of module temperature developed by numerous authors in Equation (3.27), we can estimate and compare the efficiency of ground- mounted PV modules. For estimating the efficiency of floating PV modules, substituting Equation (3.10) into Equation (3.27).

3.3.3. Proposed Linear Regression Model

The present study proposes the regression modelling for prediction of module operating temperature and evaporation estimation under different environmental conditions. the evaporation models with and without coverage of PV panel shall be developed, It also identifies the minimum number of parameters that impacts the prediction of module temperature and evaporation estimations. Further evaporation models shall be tested for different site conditions.

3.3.3.1. Accuracy Estimation of Models

In the proposed work, the accuracy of the above-mentioned models was assessed through two indices that is, Coefficient of Determination (R^2) and Root Mean Square Error (RMSE), taken together, they might provide an in-depth analysis of the PV module model. The R^2 indicates how closely the simulated data match the measured data or the fitted regression line. If the simulation model or fitted regression line has an R^2 value of 1, it precisely approximates the measured data. Hence, higher value of R^2 model gives better result for a specific application. RMSE demonstrates the short-term performance of a simulation model. When RSME equals to 0 means the model fully fits the measured data. According to ASHRAE Guideline 14-2014, if the relative value of root mean square error (rRMSE) is less than 30%, respectively, the simulation model is satisfactory in terms of accuracy. The following Equation (3.28 – 3.30) are used to calculate the values of R^2, RMSE, and rRSME (Finch and Hall ,2001):

$$R^2 = 1 - \frac{\sum_{i-1}^{k}(M_i - S_i)^2}{\sum_{i=1}^{k}(M_i - \overline{M})^2} \tag{3.28}$$

$$RSME = \sqrt{\left(\frac{\sum_{i=1}^{k}(M_i - S_i)^2}{k}\right)} \tag{3.29}$$

$$rRSME = \sqrt{\left(\frac{\sum_{i=1}^{k}(M_i - S_i)^2}{k}\right)} \Big/ \overline{M} \tag{3.30}$$

3.3.4. Assessment of floating solar Potential

Technical potential for floating solar is assessed in terms of the solar PV capacity installation (MW) and potential energy generation (MWh). The assessment has been conducted for the pilot case study of Rajghat Dam. This is further expanded into the study area of the state of Uttar Pradesh. The floating solar potential has been assessed, considering topographic limitations and environmental constraints. The primary benefit of assessing technical potential is in establishing benchmark estimates of solar PV capacity to be deployed. The key assumptions in estimating technical potential are physical constraints as location, topographic constraints, dead storage level in the driest month. The energy yield from the assessed potential of floating solar installation at water bodies has been assessed using the PVsyst software with the local solar irradiation data. The step-by-step methodology of potential assessment is provided in the following flowchart shown in Figure 3.5.

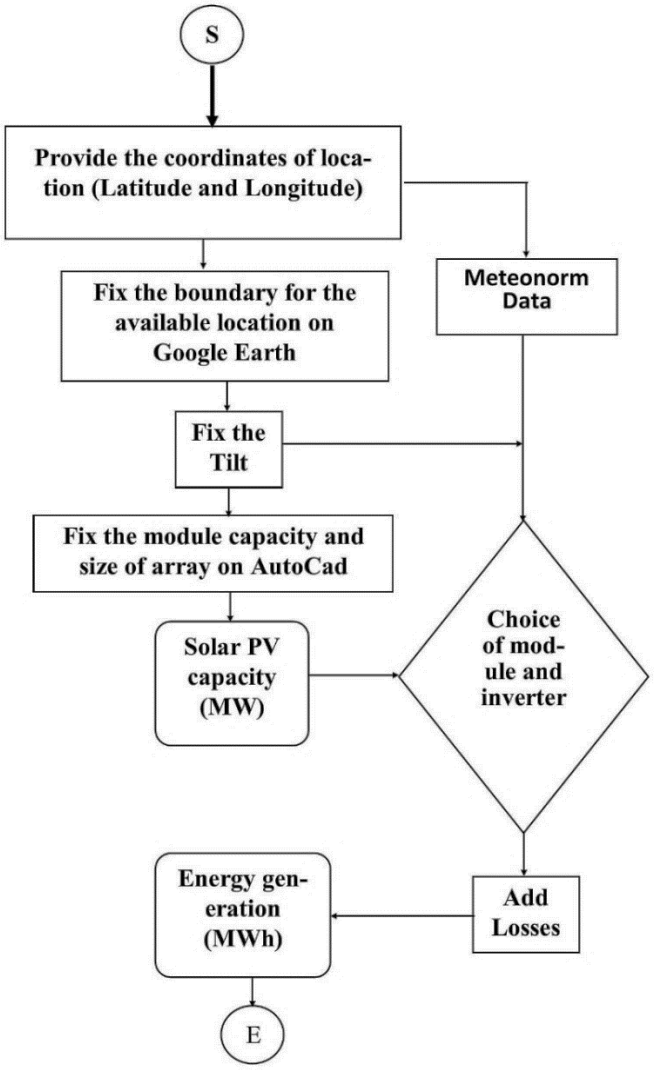

Figure 3.5. Flowchart to Assess the Potential of Rajghat dam

3.3.5. Assessment of Evaporation Loss Reduction

Around the world, numerous techniques have been tried and developed to lessen evaporation. According to a study conducted by (Yao et al.,2010), the floating covers among these solutions can save 68–76% of water. Covering the parts of water bodies by FPV plants, reduces evaporation from these ponds/reservoirs. In various literatures, evaporative models were compared with design of experiment (DoE) model and linear regression model was developed by them. Experimental data also validated the model developed considering different typology of FSPV as well as different coverage of water body. Based on present availability of literature, the present study estimates evaporation loss reduction by the methodology of (Bontempo Scavo et al., 2021) for 25% of the coverage area, which is based on preliminary results of the experiment.

3.3.6. Assessment of Financial Outcomes

The economic assessment of the Solar power plant is based on 2 expenditures namely: Capital Expenditures (CAPEX) and Operation and Maintenance Expenditure (OPEX). The total CAPEX for floating solar PV system depends upon the location, water body depth, variation, and system size. The O&M cost varies depending on the site conditions, which have several factors such as annual variation in water level, wind speed and wind pressure, inspection of mooring cables and anchoring system at regular interval. The economic assessment has been carried out in terms of Levelized Cost of Energy (LCOE) and Internal rate of return (IRR). According to standards set forth by the Central Electricity Regulatory Commission (CERC), the cost of materials, installation, and project costs are determined using current market prices to determine the tariff for renewable energy systems in India (Acharya & Devraj,2019). The levelized cost of energy can be estimated by Equation (3.31).

$$LCOE_{FPV} = \left(\frac{C_I + C_F + \sum_{k=1}^{n} \frac{C_{OM} + I_k}{(1-D_{FPV})^k}}{\sum_{k=1}^{n} \frac{E_{FPV.}(1-R_D)^k}{(1-D_{FPV})^k}} \right) \tag{3.31}$$

Where, C_I is the total investment cost (\$), C_F is the floater material cost (\$), C_{OM} is the operation and maintenance cost (\$), I_k is the insurance cost (\$), D_{FPV} is the discounting factor, E_{FPV} is the energy produced and supplied to the grid by the system in its lifetime (kWh), R_D is the degradation rate in a year and n is the life of the project.

Another financial metric, known as net present value (NPV) in (\$) is used to determine the system's entire cash flow in terms of present monetary worth and is given by Equation (3.32).

$$NPV_{FPV} = \sum_{k=1}^{n} \frac{C_n}{(1-D_{FPV})^k} - C_I \quad (3.32)$$

Where, C_n is the net cash flow ($).

The rate at which net present value falls to zero is known as the internal rate of return. This helps to calculate the discount rate. The time needed to repay the initial investment is indicated by the payback period. It represents the period 'n' when the cash flow become positive. It is estimated as given by Equation (3.33).

$$\sum_{k=1}^{n} \frac{C_n}{(1-D_{FPV})^k} = 0$$

(3.33)

3.4. Presentation of recorded data

Data was collected from 2020 to 2023 and sample data is presented in the subsequent section categorically.

3.4.1. Manual Data

3.4.1.1. Evaporation assessment data

Table 3.6 (a) Sample data for rainfall and wind (March 2021)

Date	Time	Rainfall Manual (Non recording type) mm	Wind			
			Initial Reading	Reading after 3 Minute	Speed Km./hr	Direction
1	2	3	4	5	6	7
01.03.21	8.30AM	0	92840	92841	20	NW
	2.30PM	0	92912	92914	40	NW
	5.30PM	0	93017	93018	20	WS
02.03.21	8.30AM	0	93042	93043	20	NE
	2.30PM	0	93242	93243	20	NE
	5.30PM	0	93358	93359	20	NE
03.03.21	8.30AM	0	93371	93372	20	NW
	2.30PM	0	93550	93551	20	NE
	5.30PM	0	93631	93632	20	NW
04.03.21	8.30AM	0	93646	93647	20	NW
	2.30PM	0	93758	93759	20	NE
	5.30PM	0	93853	93854	20	NW

Date	Time	Rainfall Manual (Non recording type) mm	Wind			
			Initial Reading	Reading after 3 Minute	Speed Km./hr	Direction
05.03.21	8.30AM	0	93886	93887	20	NE
	2.30PM	0	94014	94015	20	NE
	5.30PM	0	94112	94113	20	NW
06.03.21	8.30AM	0	94127	94128	20	NW
	2.30PM	0	94286	94287	20	NE
	5.30 PM	0	94398	94399	20	NW

Table 3.6 (b) Sample data for Dry Bulb and Wet Bulb Temperature (March 2021)

Date	Time	Open Air Temperature		Air Temperature at evaporimeter with solar panel above 30cm		Air Temperature at evaporimeter with solar panel above 50cm		Air Temperature at evaporimeter with solar panel above 100cm	
		Dry Bulb °C	Wet Bulb °C	Dry Bulb (Td1) ºC	Wet Bulb (Tw1) ºC	Dry Bulb (Td2) ºC	Wet Bulb (Tw2) ºC	Dry Bulb (Td3) ºC	Wet Bulb (Tw3) ºC
1	2	3	4	5	6	7	8	9	10
01.03.21	8.30 AM	18	14	18	14	18	17	18	18
	2.30 PM	32	17	30	16	30	27	36	24
	5.30 PM	27	16	26	15	26	24	-	22
02.03.21	8.30 AM	16	11	16	11	16	15	16	11
	2.30 PM	31	16	29	15	29	26	31	18
	5.30 PM	30	16	28	14	23	25	31	20
03.03.21	8.30 AM	19	13	18	12	19	12	19	13
	2.30 PM	35	18	33	17	33	20	34	20
	5.30 PM	31	17	31	17	31	29	36	24
04.03.21	8.30 AM	20	13	20	13	20	13	20	14
	2.30 PM	36	19	34	18	34	30	37	22
	5.30 PM	31	20	30	18	29	26	32	23

Date	Time	Open Air Temperature		Air Temperature at evaporimeter with solar panel above 30cm		Air Temperature at evaporimeter with solar panel above 50cm		Air Temperature at evaporimeter with solar panel above 100cm	
		Dry Bulb °C	Wet Bulb °C	Dry Bulb (Td1) ºC	Wet Bulb (Tw1) ºC	Dry Bulb (Td2) ºC	Wet Bulb (Tw2) ºC	Dry Bulb (Td3) ºC	Wet Bulb (Tw3) ºC
05.03.21	8.30 AM	20	16	20	16	20	19	20	16
	2.30 PM	34	18	33	16	33	27	35	26
	5.30 PM	30	18	29	16	28	25	38	22
06.03.21	8.30 AM	19	14	19	14	19	18	19	14
	2.30 PM	36	19	34	18	34	31	36	22
	5.30 PM	30	18	29	17	29	25	32	21

Note: "-"represents missing data.

Table 3.6 (c) Sample data for ambient temperature, water temperature and pan evaporation (March 2021)

Date	Time	Temperature		Water Temperature				Evaporation			
		Maximum °C	Minimum °C	With Solar Panel at 30 Cm. above Evaporimeter °C	With Solar Panel at 50 Cm. above Evaporimeter °C	With Solar Panel at 100 Cm. above Evaporimeter °C	Open to Sky °C	With Solar Panel at 30 Cm. above Evaporimeter °C mm	With Solar Panel at 50 Cm. above Evaporimeter mm	With Solar Panel at 100 Cm. above Evaoorimeter mm	Open to Sky °C mm
1	2	3	4	5	6	7	8	9	10	11	12
01.03.21	8.30 AM	32	11	14	14	14	13	4.00	4.20	4.20	4.400
	2.30 PM	-	-	23	23	24	25				
	5.30 PM	-	-	22	22	23	24				
02.03.21	8.30 AM	30	9	13	13	13	12	3.20	3.40	3.60	4.00
	2.30 PM	-	-	19	20	21	22				
	5.30 PM	-	-	20	21	22	24				
03.03.21	8.30 AM	31	9	13	13	12	12	3.60	4.00	4.00	4.20
	2.30 PM	-	-	20	21	22	24				
	5.30 PM	-	-	22	23	24	26				

Date	Time	Temperature		Water Temperature				Evaporation			
		Maximum °C	Minimum °C	With Solar Panel at 30 Cm. above Evaporimeter °C	With Solar Panel at 50 Cm. above Evaporimeter °C	With Solar Panel at 100 Cm. above Evaporimeter °C	Open to Sky °C	With Solar Panel at 30 Cm. above Evaporimeter °C mm	With Solar Panel at 50 Cm. above Evaporimeter mm	With Solar Panel at 100 Cm. above Evaoorimeter mm	Open to Sky °C mm
1	2	3	4	5	6	7	8	9	10	11	12
04.03.21	8.30 AM	34	13	15	15	15	14	4.00	4.20	4.40	4.60
	2.30 PM	-	-	22	23	24	25				
	5.30 PM	-	-	23	24	25	26				
05.03.21	8.30 AM	36	12	16	16	16	15	4.00	4.20	4.20	4.60
	2.30 PM	-	-	22	23	24	25				
	5.30 PM	-	-	23	24	25	26				
06.03.21	8.30 AM	34	12	15	15	15	14	4.00	4.00	4.20	4.60
	2.30 PM	-	-	22	23	24	25				
	5.30 PM	-	-	23	24	25	26				

3.4.2. Sensor Data

3.4.2.1. Panel Temperature Data

Table 3.7 (a) Water and Panels Temperature data collected on 06th – 07th April (8:00 am – 8:00 am)

Time	Water temperature when panel 30 cm above the water surface (ºC)	Panel temperature when panel 30 cm above the water surface (ºC)	Water temperature when panel 50 cm above the water surface (ºC)	Panel temperature when panel 50 cm above the water surface (ºC)	Water temperature when panel 100 cm above the water surface (ºC)	Panel temperature when panel 100 cm above the water surface (ºC)	Water temperature when no panel above the water surface (ºC)	Panel temperature when mounted above ground surface (ºC)
06/04/21 8:00	20.721	27.336	20.184	27.285	20.280	27.973	20.327	25.724
06/04/21 8:15	20.891	29.021	20.274	28.877	20.614	29.601	20.441	26.765
06/04/21 8:30	21.121	31.755	20.442	31.463	21.840	33.178	20.623	29.199
06/04/21 8:45	21.579	33.081	21.021	32.612	21.883	33.500	21.101	28.257
06/04/21 9:00	21.692	33.387	20.984	32.712	22.121	33.505	21.244	29.077
06/04/21 9:15	22.046	38.284	21.284	36.658	22.783	37.663	21.683	30.890
06/04/21 9:30	22.631	42.353	21.543	40.262	23.724	41.739	21.993	33.337
06/04/21 9:45	22.930	43.640	21.953	41.508	23.774	42.456	22.639	33.362

Time	Water temperature when panel 30 cm above the water surface (ºC)	Panel temperature when panel 30 cm above the water surface (ºC)	Water temperature when panel 50 cm above the water surface (ºC)	Panel temperature when panel 50 cm above the water surface (ºC)	Water temperature when panel 100 cm above the water surface (ºC)	Panel temperature when panel 100 cm above the water surface (ºC)	Water temperature when no panel above the water surface (ºC)	Panel temperature when mounted above ground surface (ºC)
06/04/21 10:00	23.451	47.994	22.382	45.185	24.493	45.944	23.234	34.982
06/04/21 10:15	23.575	47.375	22.521	44.861	24.269	45.129	23.734	34.823
06/04/21 10:30	24.002	51.646	22.921	48.786	25.144	49.757	24.217	37.687
06/04/21 10:45	24.284	53.502	23.082	50.436	25.118	50.350	24.833	37.052
06/04/21 11:00	24.754	56.716	23.445	54.149	25.970	55.117	25.526	38.996
06/04/21 11:15	24.991	57.127	23.846	54.572	25.718	54.385	26.023	38.550
06/04/21 11:30	25.207	56.635	24.026	53.855	26.191	54.420	26.602	39.899
06/04/21 11:45	25.381	59.017	24.223	56.124	26.419	57.169	27.182	40.598
06/04/21 12:00	25.620	60.362	24.612	58.111	26.810	59.025	27.719	40.968
06/04/21 12:15	25.924	62.417	24.929	59.458	27.124	60.803	28.345	42.046
06/04/21 12:30	26.046	62.166	25.066	59.301	26.887	59.548	28.828	40.222
06/04/21 12:45	26.201	61.356	25.320	58.941	27.120	59.144	29.342	41.257
06/04/21 13:00	26.442	61.633	25.590	59.143	27.669	59.729	29.772	42.674
06/04/21 13:15	26.632	61.486	25.849	59.495	27.687	60.355	30.363	41.758
06/04/21 13:30	26.720	58.453	26.031	56.612	27.951	57.149	30.644	40.578
06/04/21 13:45	27.048	64.324	26.303	61.367	28.544	63.056	31.208	42.170
06/04/21 14:00	27.119	61.912	26.503	59.556	28.494	60.314	31.449	41.823
06/04/21 14:15	27.433	63.859	26.859	61.661	28.606	63.376	31.941	41.153
06/04/21 14:30	27.371	57.318	26.950	56.319	28.546	56.628	32.149	40.966
06/04/21 14:45	27.859	60.577	27.345	58.980	29.465	60.629	32.495	42.398
06/04/21 15:00	27.968	57.757	27.536	56.377	29.314	56.776	32.628	40.342
06/04/21 15:15	28.156	57.941	27.768	55.348	29.797	57.413	32.923	40.588
06/04/21 15:30	28.515	58.286	28.116	57.546	29.695	58.734	33.104	41.734
06/04/21 15:45	28.751	56.843	28.237	55.915	30.600	55.084	33.327	41.538
06/04/21 16:00	28.855	55.165	28.529	54.279	29.932	54.540	33.349	40.643
06/04/21 16:15	28.801	51.970	28.605	51.396	30.037	52.506	33.365	40.826

Time	Water temperature when panel 30 cm above the water surface (ºC)	Panel temperature when panel 30 cm above the water surface (ºC)	Water temperature when panel 50 cm above the water surface (ºC)	Panel temperature when panel 50 cm above the water surface (ºC)	Water temperature when panel 100 cm above the water surface (ºC)	Panel temperature when panel 100 cm above the water surface (ºC)	Water temperature when no panel above the water surface (ºC)	Panel temperature when mounted above ground surface (ºC)
06/04/21 16:30	28.850	48.185	28.681	48.089	29.707	49.210	33.161	39.205
06/04/21 16:45	29.050	47.311	28.715	46.153	30.346	48.246	33.009	39.694
06/04/21 17:00	28.956	44.974	28.730	43.381	30.686	46.257	32.669	38.402
06/04/21 17:15	28.887	41.675	28.583	41.582	29.792	42.645	32.352	37.726
06/04/21 17:30	28.882	39.694	28.469	40.121	29.121	40.446	32.024	37.139
06/04/21 17:45	28.753	37.844	28.260	38.352	28.608	37.759	31.600	37.016
06/04/21 18:00	28.584	35.686	27.919	36.151	28.678	36.141	31.249	36.513
06/04/21 18:15	28.278	33.990	27.743	34.647	28.021	34.878	30.699	35.869
06/04/21 18:30	28.031	32.197	27.531	32.947	28.216	33.219	30.377	34.959
06/04/21 18:45	27.853	30.500	27.356	31.477	27.935	31.642	30.083	33.806
06/04/21 19:00	27.665	29.494	27.191	30.461	27.688	30.582	29.764	32.725
06/04/21 19:15	27.541	29.195	27.040	30.127	27.055	30.315	29.547	32.913
06/04/21 19:30	27.319	29.104	26.813	30.124	26.652	30.361	29.132	32.690
06/04/21 19:45	27.184	28.944	26.571	29.820	26.540	29.957	28.857	32.091
06/04/21 20:00	26.949	27.900	26.466	28.766	26.554	28.864	28.643	30.434
06/04/21 20:15	26.799	26.835	26.313	27.794	26.140	28.010	28.389	30.158
06/04/21 20:30	26.637	27.966	26.048	28.879	25.888	29.131	28.162	31.113
06/04/21 20:45	26.442	28.116	25.792	28.890	25.400	29.081	27.794	30.983
06/04/21 21:00	26.240	28.029	25.460	28.846	25.085	29.148	27.342	31.127
06/04/21 21:15	26.031	28.156	25.247	28.907	24.997	29.145	27.155	30.754
06/04/21 21:30	25.864	27.985	24.992	28.662	24.703	28.898	26.905	30.540
06/04/21 21:45	25.662	27.802	24.764	28.530	24.522	28.863	26.653	30.326
06/04/21 22:00	25.416	28.621	24.543	28.955	24.403	29.105	26.339	29.235
06/04/21 22:15	25.129	27.161	24.450	27.440	23.936	27.581	26.051	27.833
06/04/21 22:30	24.884	26.257	24.216	26.527	23.529	26.678	25.709	26.940
06/04/21 22:45	24.627	25.472	24.042	25.784	23.464	25.914	25.492	26.254

Time	Water temperature when panel 30 cm above the water surface (ºC)	Panel temperature when panel 30 cm above the water surface (ºC)	Water temperature when panel 50 cm above the water surface (ºC)	Panel temperature when panel 50 cm above the water surface (ºC)	Water temperature when panel 100 cm above the water surface (ºC)	Panel temperature when panel 100 cm above the water surface (ºC)	Water temperature when no panel above the water surface (ºC)	Panel temperature when mounted above ground surface (ºC)
06/04/21 23:00	24.350	24.983	23.823	25.288	23.170	25.452	25.179	25.834
06/04/21 23:15	24.270	24.331	23.670	24.672	22.953	24.819	24.952	25.256
06/04/21 23:30	24.111	23.800	23.491	24.120	22.742	24.262	24.507	24.749
06/04/21 23:45	23.831	22.887	23.297	23.210	22.500	23.378	24.498	23.822
07/04/21 0:00	23.592	22.440	23.092	22.710	22.146	22.866	24.099	23.190
07/04/21 0:15	23.273	21.966	22.834	22.186	22.021	22.284	23.794	22.545
07/04/21 0:30	23.068	21.442	22.576	21.744	21.384	21.873	23.493	22.349
07/04/21 0:45	22.844	21.029	22.435	21.307	21.448	21.383	23.280	21.863
07/04/21 1:00	22.460	20.584	22.206	20.815	20.952	20.930	22.927	21.295
07/04/21 1:15	22.393	20.187	22.000	20.469	20.626	20.589	22.813	21.053
07/04/21 1:30	22.055	20.073	21.790	20.340	20.836	20.436	22.569	21.003
07/04/21 1:45	21.916	19.831	21.610	20.113	20.302	20.232	22.325	20.821
07/04/21 2:00	21.763	19.443	21.410	19.817	20.389	19.927	22.129	20.717
07/04/21 2:15	21.694	19.105	21.321	19.502	20.277	19.572	21.898	20.572
07/04/21 2:30	21.503	18.799	21.115	19.192	20.199	19.243	21.741	20.390
07/04/21 2:45	21.398	18.519	21.033	18.962	20.074	19.058	21.630	20.362
07/04/21 3:00	21.266	18.151	20.911	18.655	20.056	18.716	21.473	19.957
07/04/21 3:15	21.111	17.751	20.810	18.348	20.214	18.390	21.352	19.631
07/04/21 3:30	21.159	18.004	20.741	18.559	20.005	18.623	21.234	19.766
07/04/21 3:45	21.049	17.766	20.640	18.421	19.655	18.512	21.114	19.705
07/04/21 4:00	20.983	18.159	20.558	18.761	19.773	18.814	21.028	20.285
07/04/21 4:15	20.824	18.036	20.457	18.774	19.627	18.859	20.871	20.082
07/04/21 4:30	20.758	17.796	20.289	18.393	19.768	18.463	20.798	19.778
07/04/21 4:45	20.673	17.242	20.238	17.840	19.656	17.942	20.612	19.210
07/04/21 5:00	20.563	16.780	20.179	17.397	19.412	17.567	20.578	19.326
07/04/21 5:15	20.524	17.226	20.040	17.844	19.196	18.001	20.450	19.658

Time	Water temperature when panel 30 cm above the water surface (ºC)	Panel temperature when panel 30 cm above the water surface (ºC)	Water temperature when panel 50 cm above the water surface (ºC)	Panel temperature when panel 50 cm above the water surface (ºC)	Water temperature when panel 100 cm above the water surface (ºC)	Panel temperature when panel 100 cm above the water surface (ºC)	Water temperature when no panel above the water surface (ºC)	Panel temperature when mounted above ground surface (ºC)
07/04/21 5:30	20.481	17.181	19.981	17.801	19.351	17.958	20.344	19.393
07/04/21 5:45	20.349	16.954	19.917	17.567	19.050	17.631	20.174	19.030
07/04/21 6:00	20.191	16.569	19.810	17.099	18.884	17.208	20.109	18.887
07/04/21 6:15	20.004	15.662	19.685	16.210	18.885	16.225	19.899	17.728
07/04/21 6:30	19.758	15.677	19.545	16.357	18.470	16.479	19.816	17.952
07/04/21 6:45	19.810	16.616	19.543	17.228	18.748	17.440	19.787	18.886
07/04/21 7:00	19.934	18.120	19.535	18.606	19.326	18.957	19.812	19.780
07/04/21 7:15	20.062	19.671	19.586	20.033	19.384	20.602	19.767	20.604
07/04/21 7:30	20.088	21.316	19.656	21.764	19.202	22.315	19.762	22.328
07/04/21 7:45	20.231	22.962	19.748	23.380	19.626	23.917	19.799	23.544
07/04/21 8:00	20.441	24.589	19.913	25.223	20.386	25.650	19.804	24.314
07/04/21 8:15	20.537	25.634	20.147	26.979	21.028	27.475	19.867	25.638
07/04/21 8:30	20.560	26.875	20.300	28.315	21.204	30.265	19.945	26.261

3.4.2.2. Panel characteristic data

Table 3.7 (b) Panel open circuit voltage and current data collected on 06th – 07th April (8:00 am – 8:00 am)

Date	Panel 1 Voltage (V)	Panel 2 Voltage (V)	Panel 3 Voltage (V)	Panel 4 Voltage (V)	Supply Voltage (V)	Panel 1 current (A)	Panel 2 current (A)	Panel 3 current (A)	Panel 4 current (A)
06/04/21 8:00	18.695	20.471	18.677	20.603	11.633	0.030	-0.033	0.063	-0.082
06/04/21 8:15	18.674	20.488	18.718	20.655	11.633	-0.035	-0.059	0.073	-0.054
06/04/21 8:30	18.901	20.729	18.923	20.858	11.633	-0.006	-0.070	0.096	-0.084
06/04/21 8:45	18.620	20.378	18.564	20.490	11.633	0.080	-0.013	0.076	-0.142
06/04/21 9:00	18.714	20.486	18.668	20.600	11.781	0.055	-0.020	0.077	-0.130
06/04/21 9:15	18.759	20.521	18.710	20.622	11.633	0.077	-0.019	0.115	-0.202
06/04/21 9:30	18.782	20.550	18.706	20.624	11.633	0.138	0.000	0.134	-0.298
06/04/21 9:45	18.729	20.500	18.685	20.573	11.633	0.043	-0.007	0.157	-0.312
06/04/21 10:00	18.686	20.502	18.673	20.590	11.633	-0.048	-0.007	0.187	-0.310

Date	Panel 1 Voltage (V)	Panel 2 Voltage (V)	Panel 3 Voltage (V)	Panel 4 Voltage (V)	Supply Voltage (V)	Panel 1 current (A)	Panel 2 current (A)	Panel 3 current (A)	Panel 4 current (A)
06/04/21 10:15	18.554	20.366	18.535	20.439	11.633	-0.107	0.014	0.158	-0.285
06/04/21 10:30	18.337	20.149	18.301	20.210	11.633	0.000	0.042	0.175	-0.390
06/04/21 10:45	18.573	20.420	18.562	20.480	11.633	-0.167	0.017	0.301	-0.423
06/04/21 11:00	17.883	19.696	17.805	19.732	11.633	-0.036	0.053	0.190	-0.434
06/04/21 11:15	18.357	20.205	18.318	20.248	11.633	-0.090	0.046	0.278	-0.470
06/04/21 11:30	18.274	20.135	18.241	20.200	11.633	-0.119	0.060	0.219	-0.414
06/04/21 11:45	18.185	20.036	18.120	20.058	11.633	-0.054	0.105	0.235	-0.516
06/04/21 12:00	18.090	19.899	17.990	19.947	11.633	0.002	0.077	0.156	-0.420
06/04/21 12:15	18.090	19.944	18.020	19.978	11.633	-0.040	0.175	0.149	-0.438
06/04/21 12:30	17.996	19.848	17.944	19.910	11.633	-0.053	0.091	0.174	-0.415
06/04/21 12:45	17.939	19.772	17.871	19.822	11.633	-0.006	0.076	0.192	-0.426
06/04/21 13:00	17.908	19.728	17.816	19.760	11.633	0.104	0.169	0.247	-0.525
06/04/21 13:15	18.130	19.962	18.023	19.975	11.633	0.063	0.157	0.199	-0.593
06/04/21 13:30	18.100	19.929	18.019	19.983	11.633	0.125	0.132	0.220	-0.446
06/04/21 13:45	17.866	19.743	17.815	19.845	11.633	0.036	0.115	0.153	-0.334
06/04/21 14:00	17.824	19.876	17.771	19.958	11.633	0.029	0.141	0.169	-0.365
06/04/21 14:15	17.578	19.723	17.511	19.810	11.633	0.038	0.154	0.105	-0.260
06/04/21 14:30	18.226	20.072	18.155	20.155	11.633	0.103	0.107	0.166	-0.360
06/04/21 14:45	17.953	19.785	17.900	19.905	11.633	0.180	0.117	0.155	-0.299
06/04/21 15:00	18.037	19.943	17.996	20.041	11.633	0.068	0.108	0.151	-0.316
06/04/21 15:15	17.873	19.887	17.872	20.026	11.633	0.154	0.191	0.194	-0.247
06/04/21 15:30	18.051	19.843	17.954	19.939	11.633	0.148	0.120	0.108	-0.305
06/04/21 15:45	18.053	19.816	18.009	19.959	11.633	0.102	0.043	0.171	-0.347
06/04/21 16:00	18.103	19.858	18.059	20.026	11.633	0.147	0.026	0.202	-0.293
06/04/21 16:15	18.181	19.905	18.137	20.058	11.633	0.149	0.064	0.177	-0.296
06/04/21 16:30	18.262	19.875	18.229	20.151	11.633	0.157	0.074	0.142	-0.214
06/04/21 16:45	18.184	19.947	18.127	20.075	11.633	0.155	-0.161	0.193	-0.193

Date	Panel 1 Voltage (V)	Panel 2 Voltage (V)	Panel 3 Voltage (V)	Panel 4 Voltage (V)	Supply Voltage (V)	Panel 1 current (A)	Panel 2 current (A)	Panel 3 current (A)	Panel 4 current (A)
06/04/21 17:00	18.137	19.874	18.100	20.039	11.633	0.093	0.058	0.142	-0.200
06/04/21 17:15	18.137	19.917	18.055	19.961	11.633	0.130	0.124	0.233	-0.374
06/04/21 17:30	17.882	19.684	17.792	19.709	11.633	0.107	0.154	0.185	-0.268
06/04/21 17:45	17.762	19.559	17.590	19.518	11.633	0.133	0.209	-0.001	-0.183
06/04/21 18:00	17.279	18.962	17.196	19.117	11.633	0.058	0.033	0.039	-0.083
06/04/21 18:15	16.583	18.348	16.608	18.523	11.633	0.001	0.023	0.015	-0.032
06/04/21 18:30	15.676	17.485	15.747	17.679	11.781	0.005	0.019	0.009	-0.018
06/04/21 18:45	13.346	15.297	13.633	15.527	11.633	0.006	0.016	0.006	-0.009
06/04/21 19:00	7.619	10.358	8.447	10.256	11.633	0.006	0.014	0.006	-0.004
06/04/21 19:15	-1.177	0.289	-1.022	0.628	11.633	0.009	0.014	0.009	-0.010
06/04/21 19:30	-1.462	0.020	-1.488	0.153	11.633	0.010	0.016	0.011	-0.006
06/04/21 19:45	-1.467	0.010	-1.492	0.147	11.781	0.011	0.015	0.012	-0.011
06/04/21 20:00	-1.470	0.004	-1.495	0.131	11.633	0.010	0.017	0.010	-0.010
06/04/21 20:15	-1.470	-0.001	-1.493	0.124	11.781	0.012	0.018	0.009	-0.010
06/04/21 20:30	-1.491	-0.008	-1.512	0.114	11.633	0.011	0.019	0.012	-0.007
06/04/21 20:45	-1.494	-0.024	-1.518	0.104	11.633	0.009	0.017	0.010	-0.010
06/04/21 21:00	-1.484	-0.014	-1.505	0.108	11.633	0.012	0.014	0.013	-0.016
06/04/21 21:15	-1.494	-0.031	-1.517	0.104	11.633	0.012	0.013	0.012	-0.015
06/04/21 21:30	-1.495	-0.019	-1.514	0.101	11.633	0.014	0.019	0.014	-0.009
06/04/21 21:45	-1.501	-0.030	-1.519	0.097	11.633	0.014	0.019	0.014	-0.007
06/04/21 22:00	-1.502	-0.025	-1.516	0.102	11.633	0.013	0.019	0.014	-0.011
06/04/21 22:15	-1.493	-0.031	-1.511	0.106	11.781	0.013	0.020	0.012	-0.008
06/04/21 22:30	-1.503	-0.036	-1.514	0.103	11.633	0.013	0.021	0.013	-0.011
06/04/21 22:45	-1.504	-0.038	-1.519	0.088	11.633	0.015	0.023	0.015	-0.007
06/04/21 23:00	-1.518	-0.037	-1.525	0.083	11.633	0.012	0.020	0.012	-0.011
06/04/21 23:15	-1.520	-0.043	-1.532	0.072	11.633	0.011	0.020	0.011	-0.012
06/04/21 23:30	-1.524	-0.048	-1.532	0.074	11.633	0.008	0.020	0.008	-0.011

Date	Panel 1 Voltage (V)	Panel 2 Voltage (V)	Panel 3 Voltage (V)	Panel 4 Voltage (V)	Supply Voltage (V)	Panel 1 current (A)	Panel 2 current (A)	Panel 3 current (A)	Panel 4 current (A)
06/04/21 23:45	-1.533	-0.052	-1.535	0.067	11.633	0.013	0.022	0.012	-0.012
07/04/21 0:00	-1.538	-0.055	-1.531	0.074	11.633	0.008	0.021	0.008	-0.010
07/04/21 0:15	-1.537	-0.059	-1.539	0.059	11.633	0.013	0.022	0.015	-0.009
07/04/21 0:30	-1.543	-0.068	-1.547	0.051	11.633	0.007	0.017	0.006	-0.013
07/04/21 0:45	-1.551	-0.077	-1.558	0.038	11.781	0.006	0.017	0.007	-0.013
07/04/21 1:00	-1.551	-0.077	-1.554	0.042	11.781	0.014	0.018	0.014	-0.017
07/04/21 1:15	-1.565	-0.082	-1.557	0.041	11.633	0.014	0.024	0.014	-0.010
07/04/21 1:30	-1.564	-0.086	-1.559	0.043	11.633	0.015	0.026	0.015	-0.010
07/04/21 1:45	-1.575	-0.105	-1.574	0.020	11.633	0.014	0.025	0.014	-0.009
07/04/21 2:00	-1.572	-0.091	-1.574	0.020	11.633	0.014	0.024	0.015	-0.010
07/04/21 2:15	-1.576	-0.098	-1.576	0.019	11.633	0.014	0.024	0.013	-0.011
07/04/21 2:30	-1.578	-0.101	-1.580	0.011	11.633	0.013	0.023	0.014	-0.010
07/04/21 2:45	-1.577	-0.107	-1.579	0.026	11.781	0.014	0.026	0.015	-0.010
07/04/21 3:00	-1.592	-0.100	-1.588	0.012	11.633	0.014	0.026	0.015	-0.009
07/04/21 3:15	-1.590	-0.105	-1.593	0.015	11.781	0.013	0.025	0.013	-0.009
07/04/21 3:30	-1.593	-0.106	-1.588	0.006	11.633	0.013	0.025	0.014	-0.008
07/04/21 3:45	-1.595	-0.107	-1.590	0.015	11.633	0.011	0.024	0.013	-0.010
07/04/21 4:00	-1.588	-0.101	-1.589	0.010	11.633	0.016	0.021	0.016	-0.015
07/04/21 4:15	-1.588	-0.101	-1.585	0.008	11.633	0.016	0.021	0.015	-0.014
07/04/21 4:30	-1.587	-0.102	-1.589	0.007	11.633	0.015	0.020	0.016	-0.013
07/04/21 4:45	-1.586	-0.104	-1.581	0.008	11.633	0.015	0.020	0.016	-0.010
07/04/21 5:00	-1.592	-0.109	-1.590	0.008	11.633	0.014	0.020	0.014	-0.015
07/04/21 5:15	-1.593	-0.109	-1.588	0.004	11.633	0.014	0.019	0.014	-0.016
07/04/21 5:30	-1.533	-0.058	-1.501	0.095	11.633	0.013	0.025	0.014	-0.009
07/04/21 5:45	1.828	3.242	2.011	3.654	11.633	0.013	0.024	0.014	-0.012
07/04/21 6:00	12.296	14.548	12.865	14.678	11.633	0.011	0.024	0.009	-0.001
07/04/21 6:15	15.883	17.730	16.030	17.894	11.633	0.003	0.018	-0.001	-0.007

Date	Panel 1 Voltage (V)	Panel 2 Voltage (V)	Panel 3 Voltage (V)	Panel 4 Voltage (V)	Supply Voltage (V)	Panel 1 current (A)	Panel 2 current (A)	Panel 3 current (A)	Panel 4 current (A)
07/04/21 6:30	17.243	19.031	17.276	19.170	11.633	0.003	0.017	-0.004	-0.007
07/04/21 6:45	17.834	19.607	17.830	19.734	11.633	0.007	0.009	-0.008	-0.012
07/04/21 7:00	18.046	19.848	18.054	19.964	11.633	0.007	0.007	-0.008	-0.010
07/04/21 7:15	18.321	20.087	18.287	20.225	11.633	0.024	-0.005	-0.018	0.003
07/04/21 7:30	18.429	20.183	18.377	20.333	11.633	0.022	-0.016	-0.044	0.024
07/04/21 7:45	18.413	20.198	18.363	20.324	11.633	0.023	-0.003	-0.040	0.019
07/04/21 8:00	18.429	20.399	18.489	20.530	11.633	-0.050	-0.011	-0.091	0.100
07/04/21 8:15	18.491	20.501	18.562	20.618	11.633	-0.065	0.025	-0.093	0.088
07/04/21 8:30	18.588	20.674	18.761	20.807	11.633	-0.167	-0.126	0.212	-0.105

3.4.2.3. Meteorological Data

Table 3.7 (c) Atmospheric data collected on 06th – 07th April (8:00 am – 8:00 am)

Date	Air temp at 10 cm height above water (ºC)	Air temp at 35cm height above water (ºC)	Ambient Temperature (ºC)	Humidity (%)RH	Solar Radiation (W/m^2)	Wind Speed (km/h)	Wind Direction (º)
06/04/21 8:00	24.196	24.210	24.643	29.930	134.392	0.005	11.722
06/04/21 8:15	25.387	25.425	25.586	29.229	163.063	3.492	10.484
06/04/21 8:30	27.203	27.292	26.905	28.799	254.677	3.833	50.583
06/04/21 8:45	27.606	27.728	27.731	27.651	172.854	4.292	42.719
06/04/21 9:00	28.124	28.230	28.119	26.953	195.120	0.008	8.970
06/04/21 9:15	29.985	30.018	29.612	26.466	276.733	3.723	55.853
06/04/21 9:30	31.951	31.832	31.333	25.687	373.582	4.309	45.654
06/04/21 9:45	32.703	32.585	32.024	24.396	369.200	4.997	65.147
06/04/21 10:00	33.208	33.556	33.070	23.826	480.489	0.008	45.713
06/04/21 10:15	33.503	34.071	33.284	22.574	374.342	4.702	75.672
06/04/21 10:30	34.721	35.141	34.519	22.242	419.164	4.122	234.842
06/04/21 10:45	35.367	36.438	34.956	21.396	593.153	5.344	127.325
06/04/21 11:00	37.797	38.953	36.102	21.042	376.193	0.009	49.278
06/04/21 11:15	36.830	37.970	36.738	20.114	598.394	4.894	20.148

Date	Air temp at 10 cm height above water (ºC)	Air temp at 35cm height above water (ºC)	Ambient Temperature (ºC)	Humidity (%)RH	Solar Radiation (W/m^2)	Wind Speed (km/h)	Wind Direction (º)
06/04/21 11:30	38.450	39.336	36.834	19.539	555.619	5.364	61.594
06/04/21 11:45	39.878	39.772	37.275	18.971	588.617	4.857	55.571
06/04/21 12:00	37.745	38.060	37.514	18.420	573.848	0.007	134.762
06/04/21 12:15	39.327	39.592	38.316	17.863	674.652	3.634	109.308
06/04/21 12:30	38.149	38.534	38.041	17.436	576.927	4.241	146.109
06/04/21 12:45	38.284	38.607	37.993	17.000	548.653	4.763	123.657
06/04/21 13:00	38.972	39.366	38.549	16.585	550.921	0.006	232.425
06/04/21 13:15	38.215	38.457	38.477	16.290	681.175	3.854	169.761
06/04/21 13:30	38.037	38.298	38.368	16.008	549.465	4.956	243.656
06/04/21 13:45	39.216	39.704	39.252	16.009	656.742	3.312	124.281
06/04/21 14:00	38.417	38.797	38.760	15.719	635.803	0.007	193.491
06/04/21 14:15	38.342	38.699	39.335	15.582	617.071	2.501	164.947
06/04/21 14:30	37.675	37.926	38.783	15.151	598.757	4.976	124.468
06/04/21 14:45	38.923	39.270	39.063	15.149	570.390	2.866	239.933
06/04/21 15:00	37.556	37.827	38.920	14.863	509.046	0.003	113.932
06/04/21 15:15	38.734	39.061	38.907	14.716	506.084	2.839	213.132
06/04/21 15:30	38.525	38.832	39.501	14.714	490.631	2.181	141.015
06/04/21 15:45	38.479	38.692	39.807	14.290	426.580	3.254	78.515
06/04/21 16:00	38.254	38.311	40.233	14.149	389.055	0.006	79.916
06/04/21 16:15	37.598	37.735	39.325	13.865	288.959	3.756	30.317
06/04/21 16:30	37.255	37.242	39.156	13.722	280.823	4.559	10.980
06/04/21 16:45	37.962	38.039	39.260	13.767	254.200	4.371	283.688
06/04/21 17:00	36.882	36.932	38.582	13.720	202.475	0.006	11.021
06/04/21 17:15	36.804	36.877	38.414	13.438	161.894	4.821	36.343
06/04/21 17:30	36.584	36.631	38.182	13.289	114.424	4.720	12.030
06/04/21 17:45	36.687	36.753	37.758	13.018	90.565	5.154	4.802

Date	Air temp at 10 cm height above water (ºC)	Air temp at 35cm height above water (ºC)	Ambient Temperature (ºC)	Humidity (%)RH	Solar Radiation (W/m^2)	Wind Speed (km/h)	Wind Direction (º)
06/04/21 18:00	36.165	36.309	37.450	12.170	41.424	0.007	236.512
06/04/21 18:15	35.804	35.983	36.978	11.597	18.807	5.753	11.420
06/04/21 18:30	34.392	34.634	36.265	11.449	5.268	4.247	55.646
06/04/21 18:45	33.301	33.678	35.303	11.310	-4.018	2.750	55.616
06/04/21 19:00	32.650	32.801	34.527	11.308	-4.939	0.002	32.501
06/04/21 19:15	33.067	33.326	33.834	11.453	-5.228	2.249	12.271
06/04/21 19:30	32.797	32.951	33.512	11.598	-5.743	2.717	5.633
06/04/21 19:45	32.231	32.489	33.302	11.597	-5.770	3.199	21.424
06/04/21 20:00	31.244	31.387	32.762	11.600	-7.153	0.002	-9.705
06/04/21 20:15	30.245	30.441	31.704	11.878	-7.391	0.830	12.721
06/04/21 20:30	31.056	31.122	31.940	12.169	-6.048	3.551	20.299
06/04/21 20:45	31.097	31.176	31.819	12.170	-6.207	3.915	13.253
06/04/21 21:00	31.210	31.283	31.705	12.307	-7.757	0.007	57.024
06/04/21 21:15	30.901	31.003	31.557	12.306	-6.928	4.456	12.431
06/04/21 21:30	30.419	30.547	31.381	12.306	-6.220	4.766	11.789
06/04/21 21:45	30.276	30.357	31.032	12.449	-6.707	4.040	31.942
06/04/21 22:00	29.165	29.159	30.397	13.724	-7.564	0.004	159.784
06/04/21 22:15	27.758	27.719	28.573	15.862	-7.104	7.202	149.429
06/04/21 22:30	26.868	26.830	27.622	17.575	-6.460	7.076	121.698
06/04/21 22:45	26.203	26.164	26.921	18.829	-6.712	6.526	169.766
06/04/21 23:00	25.796	25.748	26.476	19.823	-6.448	0.013	168.063
06/04/21 23:15	25.188	25.114	25.935	20.808	-5.763	4.258	67.757
06/04/21 23:30	24.710	24.653	25.288	22.094	-7.239	5.734	159.275
06/04/21 23:45	23.788	23.704	24.429	23.250	-6.911	4.985	77.710
07/04/21 0:00	23.185	23.110	23.762	24.958	-6.398	0.016	105.238
07/04/21 0:15	22.528	22.447	23.230	26.383	-6.504	8.915	210.150

Date	Air temp at 10 cm height above water (ºC)	Air temp at 35cm height above water (ºC)	Ambient Temperature (ºC)	Humidity (%)RH	Solar Radiation (W/m^2)	Wind Speed (km/h)	Wind Direction (º)
07/04/21 0:30	22.348	22.269	22.815	27.377	-8.106	7.151	59.387
07/04/21 0:45	21.911	21.796	22.431	28.139	-9.420	5.416	109.306
07/04/21 1:00	21.356	21.220	21.847	29.121	-7.435	0.014	80.921
07/04/21 1:15	21.087	20.966	21.512	29.925	-7.275	5.234	211.814
07/04/21 1:30	21.014	20.912	21.449	30.864	-8.667	5.443	313.955
07/04/21 1:45	20.848	20.772	21.297	31.329	-7.419	5.508	190.219
07/04/21 2:00	20.749	20.666	21.273	31.773	-8.469	0.003	238.155
07/04/21 2:15	20.672	20.588	21.131	32.192	-8.246	2.556	148.560
07/04/21 2:30	20.456	20.373	21.017	32.457	-9.088	3.072	209.400
07/04/21 2:45	20.379	20.307	20.865	32.918	-8.955	2.204	261.235
07/04/21 3:00	20.040	19.943	20.725	33.253	-8.798	0.000	260.652
07/04/21 3:15	19.766	19.644	20.494	33.604	-6.878	0.376	238.162
07/04/21 3:30	19.740	19.673	20.543	34.177	-7.233	0.604	147.879
07/04/21 3:45	19.795	19.681	20.455	34.466	-8.508	0.425	260.728
07/04/21 4:00	20.239	20.162	20.708	34.929	-9.981	0.003	238.176
07/04/21 4:15	20.019	19.970	20.765	34.928	-8.889	1.635	283.314
07/04/21 4:30	19.833	19.743	20.560	35.211	-10.007	0.854	260.696
07/04/21 4:45	19.192	19.130	20.236	35.486	-9.060	0.264	12.538
07/04/21 5:00	19.443	19.361	19.779	35.893	-8.981	0.000	12.572
07/04/21 5:15	19.558	19.477	20.113	36.461	-10.665	0.259	326.149
07/04/21 5:30	19.395	19.314	20.109	36.629	-8.467	0.632	305.761
07/04/21 5:45	19.324	19.232	19.860	37.037	-9.625	0.576	327.817
07/04/21 6:00	18.998	18.895	19.583	37.312	-3.554	0.000	-11.704
07/04/21 6:15	17.836	17.746	18.948	37.753	-1.974	0.000	-12.182
07/04/21 6:30	17.940	17.868	18.527	38.573	8.955	0.089	280.727
07/04/21 6:45	18.649	18.495	18.736	39.322	21.309	0.202	235.803

Date	Air temp at 10 cm height above water (ºC)	Air temp at 35cm height above water (ºC)	Ambient Temperature (ºC)	Humidity (%)RH	Solar Radiation (W/m^2)	Wind Speed (km/h)	Wind Direction (º)
07/04/21 7:00	19.771	19.671	19.706	39.620	34.854	0.000	32.780
07/04/21 7:15	20.595	20.491	20.496	39.789	56.627	0.000	32.691
07/04/21 7:30	21.519	21.544	21.758	40.043	81.447	0.000	32.647
07/04/21 7:45	22.370	22.312	22.961	39.329	86.666	0.880	213.427
07/04/21 8:00	23.764	23.710	23.828	38.607	143.143	0.001	258.427
07/04/21 8:15	24.337	24.412	24.610	38.049	178.289	1.705	235.962
07/04/21 8:30	24.233	24.382	24.786	37.339	222.524	2.222	145.671

3.5. Discussions

Data were collected from the field set up from April 2020 to March 2023 in the format as shown in sections 3.3. Manual data were collected from the field setup every day at 8:30 am, 2:30 pm and 5:30 pm. During the pandemic COVID-19, the manual data collection was interrupted and to overcome such situation and to collect panel performance data, further sensor-based data log components were added in the field setup. Sensor data were collected at the interval of 1 and 15 minutes. These data were transferred by data logger to the central server. Digital data files were prepared from manual records. Sample records of manual data were presented here for reference in the Table 3.6. (a) to 3.6. (c) and sensor data were presented in Table 3.7. (a) to 3.7. (c). However, complete data is available on the server as mentioned above.

Data collected from Pilani indicates that the maximum temperature occurs during April, May, and June, reaching a peak of 44°C in May. The winter months, December, and January, recorded a minimum temperature of 1°C. Wind velocity in Pilani is generally low, reaching up to 1 m/s during summer and decreasing to 0.15 m/s in winter. Average sunshine hours are 9 hours in summer and 7 hours in winter. Summer months, particularly April and May, have the lowest humidity, with maximum humidity around 30% and minimum humidity at 15%. In contrast, humidity is higher during the monsoon and winter months. Detailed discussions and data presentations are provided in the subsequent chapters.

3.6. Challenges

The development and collection of data from the experimental setup was full of challenges. Some of the challenges are enumerated below:

- Engaging manual staff amidst extreme climatic conditions and collecting and recording data for 365 consecutive days presented a formidable challenge for this field study.
- Furthermore, the task of collecting and recording data across a multitude of parameters, particularly three times daily, led to potential human error. Despite the best efforts to maintain accuracy, the sheer volume of data collection necessitated meticulous attention to detail to mitigate inaccuracies.
- The unforeseen emergence of the COVID-19 pandemic disrupted the smooth and continuous flow of data collection and recording. Health and safety protocols, as well as logistical challenges, imposed by the pandemic posed significant hurdles to the progress of the study.
- Instrument malfunctioning emerged as a persistent challenge, impeding the continuous recording of sensor data. Moreover, frequent network failures resulted in the loss of valuable sensor data, further complicating the data collection process.
- Compounding these challenges was the remote location of our study area, which presented difficulties in maintaining and replacing field instruments as needed. Accessing and transporting equipment to and from the study site required micro planning and coordination.
- Additionally, the absence of trained technical personnel posed a significant challenge. The lack of qualified individuals proficient in data recording and capable of addressing day-to-day instrumental malfunctions hindered the smooth execution of the field experimentations.

Enduring the rigors of such demanding environments, tested the resilience and dedication towards these research objectives by overcoming obstacles.

3.7. Adaptability of experimental design to environmental conditions and data integrity measures

The experimental design for Floating Solar Photovoltaic (FSPV) systems has been meticulously crafted to provide reliable insights into their performance and their role in reducing evaporation. Given the dynamic nature of environmental conditions, the setup is designed to be highly adaptable, ensuring the robustness of collected data while allowing for extrapolation to larger applications, such as large-scale dams in tropical regions.

3.7.1 Adaptability to climate variability

To address the wide range of climatic variations, the experimental setup incorporates sensors and materials specifically chosen for their resilience to extreme weather conditions. For solar irradiance monitoring, a CMP11 pyranometer has been installed, which operates within a temperature range of -40°C to +80°C. It can record solar luminous flux up to 4000 W/m² and has a rapid response time of less than 5 seconds, making it well-suited for environments with fluctuating solar conditions. The temperature sensors operate within a range of -40°C to +60°C with a high accuracy of ±0.1°C and include features to prevent overheating. Similarly, humidity sensors with a range of -40°C to +60°C and accuracy of ±2% RH are employed to capture reliable data under varying humidity levels, from 0% to 100%. For rainfall measurement, a tipping bucket rain gauge with 0.25 mm accuracy is used. Wind speed and direction sensors are capable of measuring speeds from 0.5 to 50 m/s and directions from 0° to 360°, with an accuracy of ±3%, operating reliably between -20°C and +85°C. Materials used in the setup are resistant to extreme temperatures, ensuring long-term durability and consistent performance. The system's ability to monitor environmental parameters over extended periods enables it to capture seasonal trends such as monsoons, winter fog, and summer heatwaves, providing a comprehensive understanding of FSPV performance across diverse conditions.

3.7.2 Geographical and topographical adaptability

The experimental design is also adaptable to varying geographical and topographical conditions. It is suitable for deployment in high-altitude regions or coastal areas with significant altitude variations. Minor adjustments, such as sensor recalibration to accommodate pressure and temperature changes in elevated regions, ensure accurate data collection. For instance, the setup at Birla Institute of Technology and Science (BITS), Pilani, located at 28°21'34.1316"N and 75°35'17.2896"E with an elevation of 299 meters above mean sea level, accounts for diverse climatic conditions, including high solar irradiance, fluctuating temperatures, and variable wind speeds.

3.7.3 Comprehensive environmental monitoring

The experimental setup is designed to measure a wide array of critical environmental and operational parameters. These include solar irradiance, wind speed, ambient and module temperatures, and relative humidity. The inclusion of such diverse measurements ensures that the setup captures the subtleties of varying weather patterns and their effects on FSPV system performance. To ensure reliable operation under extreme conditions, data collection is carried

out using a hybrid approach that combines manual methods with automated sensor-based recording. This dual approach mitigates the risk of data loss or anomalies caused by sensor disruptions and ensures the continuity of data collection. Additionally, the system is designed to simulate and record data across a range of scenarios, including diurnal and seasonal variations, ensuring that the results are applicable to a broader range of environmental conditions.

3.7.4 Ensuring data integrity for modelling

The integrity of the collected data is critical for the development of accurate predictive models and meaningful analyses. Instruments are carefully aligned to minimize errors caused by shading, misalignment, or external interference, ensuring consistency in measurements. Quality assurance is maintained through regular cross-referencing of manual measurements with sensor data to validate accuracy. Advanced data loggers are employed to store data with high temporal resolution, while backup systems are in place to prevent loss due to equipment failure or power outages. All data collection and handling processes adhere to standardized protocols to minimize inconsistencies across different conditions, enhancing comparability and repeatability. Techniques such as noise filtering and outlier analysis further improve data reliability, while statistical validation ensures the dataset is robust enough for advanced modelling and analysis.

3.8. Summary and Recommendations

The chapter concludes by highlighting the approach taken in identifying critical parameters through an extensive review of existing literature and reports. This process was crucial in laying the groundwork for the successful design and execution of the experiment. By aligning the instruments, equipment, and data collection procedures with these identified parameters, essential data on evaporation, panel performance, and meteorological conditions were systematically gathered over a period of three years. The collected data underwent thorough processing to meet the analytical requirements of the research, facilitating insightful analysis and meaningful conclusions regarding the performance and potential of floating solar photovoltaic systems in tropical regions. The results of this study have the potential to contribute significantly to the field of renewable energy, water resource management and would aid in the development of new and innovative solutions for sustainable water conservation and energy generation.

Based on the challenges faced and strategies taken to overcome the hurdles, the following recommendations are suggested.

Automation and Remote Monitoring: Implement automated data collection systems and remote monitoring capabilities to reduce the reliance on manual engagement and mitigate the risks associated with extreme climatic conditions as implemented in this study.

Backup Systems and Redundancy: Install backup systems and redundancy measures for critical instruments and data recording devices to mitigate the impact of instrument malfunctioning and network failures. This may involve setting up redundant sensors, power supplies, and communication channels to ensure continuous data collection and recording.

Training and Capacity Building: Impart training and capacity-building opportunities for field personnel to enhance their technical skills and proficiency in data recording and instrument maintenance.

By implementing these recommendations, researchers can mitigate the challenges associated with field study in extreme climatic conditions and remote locations for successful execution of field study to achieve research objectives.

Chapter 4

Performance Assessment of Floating Solar PV Systems

Abstract

Floating Solar Photovoltaic (FSPV) systems are expected to perform relatively at a higher efficiency level as compared to ground-mounted PV systems. The major factor affecting the operating efficiency of a solar panel is the operating temperature of the PV panel which is relatively lower as compared to ground-mounted PV system. To accomplish this, an experimental setup of the FSPV system has been developed which consists of solar panels operating at different heights above the water surface. The findings from the current study indicate that FSPV modules can reduce the module temperature by up to 4°C-7°C. The performance of FSPV has been analyzed under diurnal conditions. The performance has been assessed in terms of power output by utilizing module parameters. The results highlight the power output from solar panels under varying heights helps to optimize the operating heights of the solar panels over the water bodies to achieve maximum power output. Therefore, it is also advised for FSPV to raise the PV modules to their optimal height. The FSPV systems at 500 mm height provided 1.8-3.78% higher power output than ground-mounted PV systems, maximum of all the panels above water.

Keywords: Floating solar Photovoltaic (FSPV), operating height, power output, ground-mounted

4.1. Introduction

Photovoltaic (PV) systems have become one of the world's most promising energy-producing technologies in recent years. These technologies transform solar energy into electricity, aiding in the transition to sustainable energy sources while reducing the negative environmental effects of conventional fossil fuel-based energy sources. They offer energy independence and financial advantages because they are easily scalable and can be deployed almost anywhere that gets sunlight.

The Floating Solar Photovoltaic (FSPV) system is one specific form of PV system that has drawn the attention of both researchers and business professionals (Kassem et. al.,2023; Owhaib et. al.,2022; Tan et.al.,2021). As the name implies, FSPV systems entail mounting PV panels on floating platforms above the water surface. These systems offer several significant advantages over traditional ground-mounted PV systems, and they constitute a distinctive innovation within the renewable energy environment.

The potential for increased efficiency of FSPV systems is one of their key benefits. PV panels used on FSPV systems often function at lower temperatures than their ground-mounted equivalents since water bodies typically have a cooling effect. Given that the efficiency of PV panels is inversely correlated with their operating temperature, this is a major advantage. Lower operating temperatures result in greater energy conversion efficiencies, which, in turn, provide more power. Even more, FSPVs can also be deployed at various heights above the water surface to maximize power production and further improve system efficiency, this variable height parameter can be tuned.

The chapter presents the experimental setup along with the site's location, the local climate, and the technical details of the PV modules used. The approach used in the experiment is described, along with the various heights of the PV panels above the water's surface and the technique for calculating power output using module specifications. The study explains the impact of temperature and height of panels above the water surface on the power generation of FSPVs, while also drawing comparisons with ground-mounted solar arrays. A thorough analysis suggests the best operating heights for maximum power output and implications for the application of the FSPV technology.

Several factors influence the performance of a PV panel. Temperature is the most important factor influencing electrical performance. In general, it can be claimed that a PV module works better when it is operating at a lower temperature. Several factors influence the operating temperature of a PV panel, including incident solar radiation, ambient temperature, wind speed, relative humidity etc. (Dörenkämper M,2021). Kalogirou and Tripanagnostopoulos (2006), found that monocrystalline and polycrystalline PV panels lose 0.45% to 0.25% of their efficiency for every degree of temperature increase.

The FPV system is more effective than the on-ground PV system in terms of energy yield due to reduced soiling losses, as well as reduced operating temperature (Mekhilef,2012; Choi,2014), investigated FSPV systems with capacities of 2.4kW, 100kW, and 500kW in comparison to ground-mounted PV systems and reported FPV system has an 11% higher generating efficiency than an overland PV system.

Liu et al. (2017), developed a 3D finite element model to estimate the temperature of PV module installed over water surface and land and estimated the change in efficiency of power generation of FSPV and OPV (over land PV) in China. A difference of 3.5^0C was observed in operating temperature between a floating and a terrestrial PV cell. According to the study, the efficiency of floating PV systems can rise by 1.58-2.00% when compared to standard

terrestrial PV systems due to the water-cooling effect. El Hammoumi et. al. (2021), conducted experiments on small-scale FSPVs in Moroccan operational circumstances to assess and compare electrical and thermal performances of an FSPVS to those of a ground-mounted PV system. The experiment was designed with varying tilt angles of panels. The FSPVS module temperature was always lower than that of the ground-mounted solar modules up to 2.74^0C and FSPVS produces up to 2.33% more energy per day than the typical ground-mounted solar panels. It was also observed that at an appropriate tilt angle energy yield is maximum. FSPV modules adjusted to 30^0 (ideal tilt angle of Fez city) generated 43.5% more energy throughout the 3-hour test. Nisar et. al. (2021), studied the performance of FSPV with varying tilt angles and observed front panel temperature is 2-4% lower than the ground-mounted panels. Semeskandeh et. al. (2022), reported through simulation that the production capacity and panels' efficiency increased for FSPV panels by 19.47% and 27.98% respectively compared to ground-mounted PV systems. Kim et. al. (2020), studied the installation of a 500-kW FPV system using a high-durability steel structure in South Korea and reported 10% higher energy production by the FSPV system compared to the ground-mounted PV system. Sukarso and Kim (2020), studied the FSPV system's performance of the FSPV plant in the West Java province of Indonesia and reported that the efficiency of the FSPV system was 0.61% higher than that of the ground-mounted PV system based on simulation study utilizing water temperature. Febrian (2023), studied the performance of the floating photovoltaic system with passive cooling by thermosiphon. The floating photovoltaic system generated 4.52% higher power than ground ground-mounted photovoltaic system while the floating photovoltaic system with passive cooling by thermosiphon generated 7.86% higher power than the ground-mounted photovoltaic system. Sutanto (2022), estimated the energy capacity and capacity factor of different types of solar panels namely monocrystalline, polycrystalline, and thin film at Cirata Reservoir in Indonesia.

Despite the obvious advantages of the FSPV systems, experimental research on how changing the operating height above the water surface affects power output requires research attention. A few experimental studies conducted on this subject to date have shown a positive association between power output and particular FSPV module operating heights, but these findings still require confirmation. The focus of the current research effort is to address this information gap.

The experimental research in this study investigates the performance of FSPVs mounted at varying heights above the water's surface. The main objective is to assess how module height

may affect power production, which will help researchers design FSPV installation optimization solutions.

4.2. Experimentation and data collection

Four solar modules made up the experimental test rig; three of them were set at different heights above the water's surface - 300 mm, 500 mm, and 1000 mm; while the fourth was a ground-based PV system as per the detail provided in Chapter 3. These heights were chosen to study because the range of viable heights for FSPV systems was thought to be represented by them. The PV modules were selected based on their effectiveness, dependability, and robustness, as well as their compatibility with the design of the test rig and the experimental specifications.

A data logger connected to various sensors furnishes the panel performance data at 15- and 1-minute time intervals. The experimental setup for FSPV and a ground-mounted or reference PV module is shown in Figure 4.1. The current experimental captures the climatic factors including solar irradiance, ambient temperature, and wind speed to measure the energy yield of PV modules. The FSPV performance assessment methodology and schematic design of the experimental setup are shown in Figures 4.2 and 4.3 respectively.

Figure. 4.1. Experiment setup of Floating Solar Photovoltaic (FSPV) system at BITS Pilani campus, India

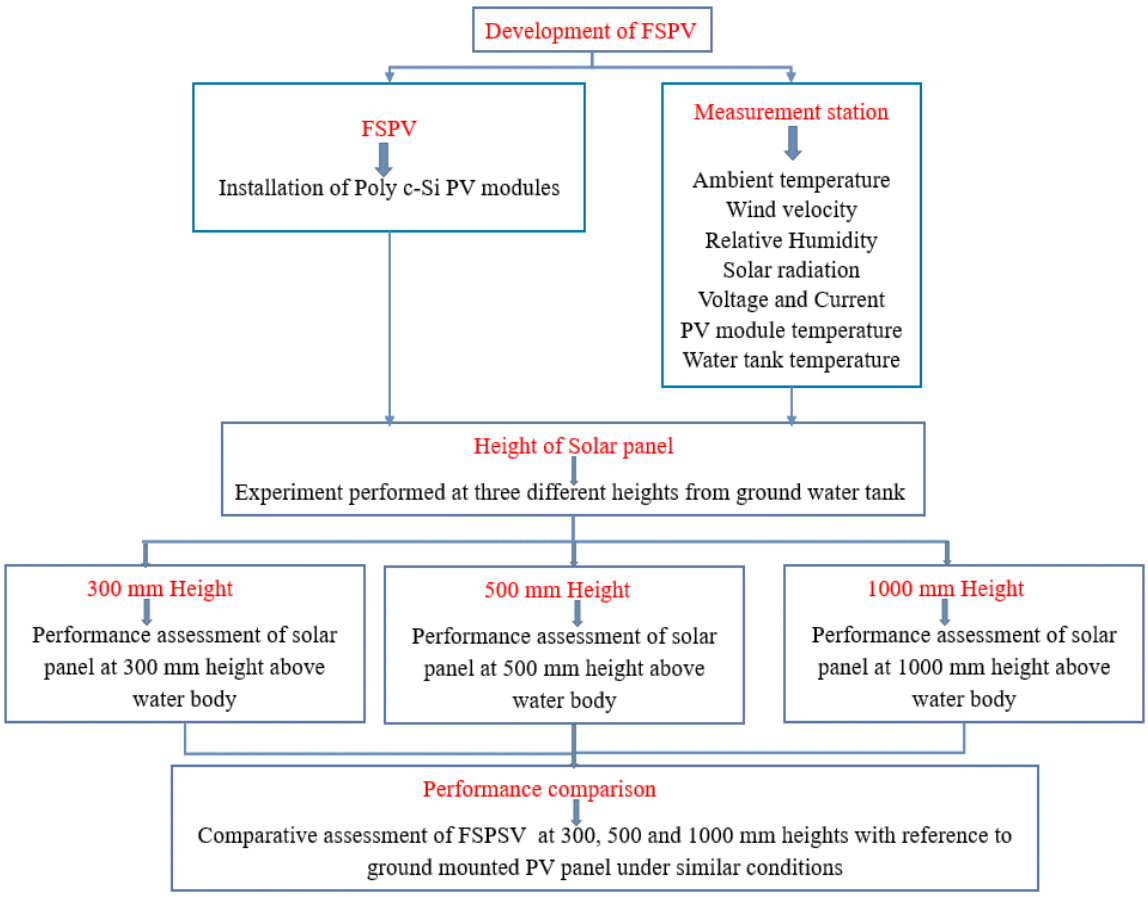

Figure 4.2. Methodology of performance assessment of FSPVsystem.

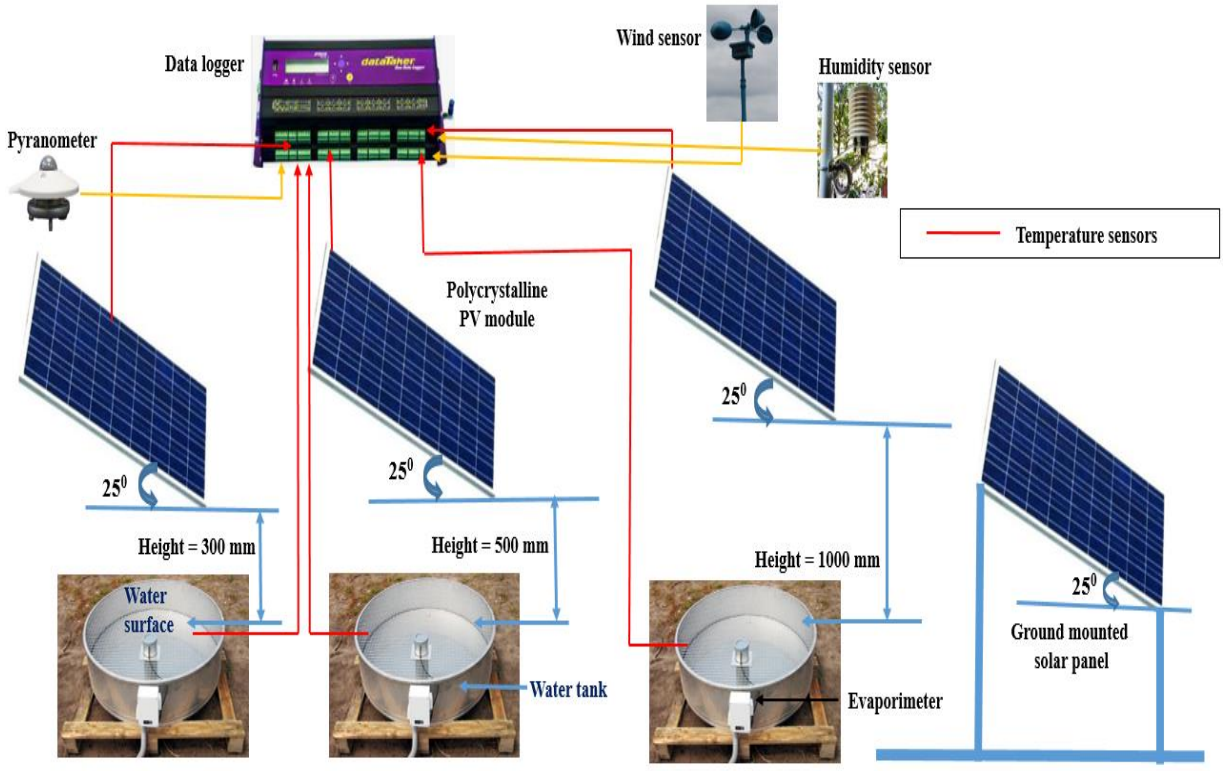

Figure 4.3. Outline of experimental setup of FSPV system.

4.3. Methodology

The methodology and experimental techniques used in the study are described in detail in this part. Additionally, it explains the justification for positioning PV panels at various heights above the water's surface and outlines the procedures for determining the power output using module specifications. In general, the float height ranges between 150-300 mm and taking this into account, the minimum panel height considered in this study is 300mm, however, the study extends to other panel heights (500mm, 1000mm) to capture the influence of panel heights on module temperature and subsequent power generation. Among the four modules including the ground-mounted, the fourth module, which served as a reference module placed on land and the other three were mounted at various heights (300mm, 500mm, and 1000mm) above the water surface. To test the impact of various panel heights on the overall performance and energy yield of the PV systems, several PV panel heights were varied above the water's surface. In order to find the height that maximizes energy output, the energy yields at various heights were compared. As the range of heights namely 300mm, 500mm, and 1000mm studied, represents a realistic scenario for deployment of FSPVs, given different constraints such as anchoring requirements, water level variations, and maintenance accessibility, the heights for the floating PV systems were adopted.

4.4. Results and Discussions

The following part will expand on the findings and engage in a thorough discussion to explore the ramifications of the discoveries. The climatic conditions and meteorological data from the experimental days related to the FSPV study are discussed. The temperature changes of the modules throughout the experiment are examined which explores a theoretical assessment of the power yield from FSPV and ground-mounted PV modules at various heights from the water surfaces, considering the operational parameters of the module via the experimental setup.

4.4.1. Meteorological Data from the Experimentation

The meteorological data from the experimentations are collected for three varying heights (300, 500, and 1000 mm) of panels above the water surface to compare the FSPV system to the terrestrial or reference PV system. The winter season, December 16–18, 2020, and the summer season, May 3–5, 2021, were each represented by a three-day experimental sequence.

On the trial days during the summer, the highest recorded ambient temperature, relative humidity, and wind speed were 40.07°C, 34.36%, and 2.47 m/s, respectively, can be observed in Figure 4.4. As shown in Figure 4.4, the minimum ambient temperature, relative humidity,

and wind speed were all 28.88°C, 16.15%, and 0.43 m/s. In contrast, on the test days during the winter, the highest ambient temperature, relative humidity, and wind speed were, respectively, 20.75°C, 83.99%, and 1.25 m/s, can be noted in Figure 4.5. As shown in Figure 4.5, the lowest recorded values for the ambient temperature, relative humidity, and wind speed were 3.57°C, 39.10%, and 0.30 m/s. It is observed that the highest or lowest temperature is nearly 20°C higher during the summer while relative humidity is on a considerably much lower side representing nearly the condition of "Loo" prevalent in tropical regions.

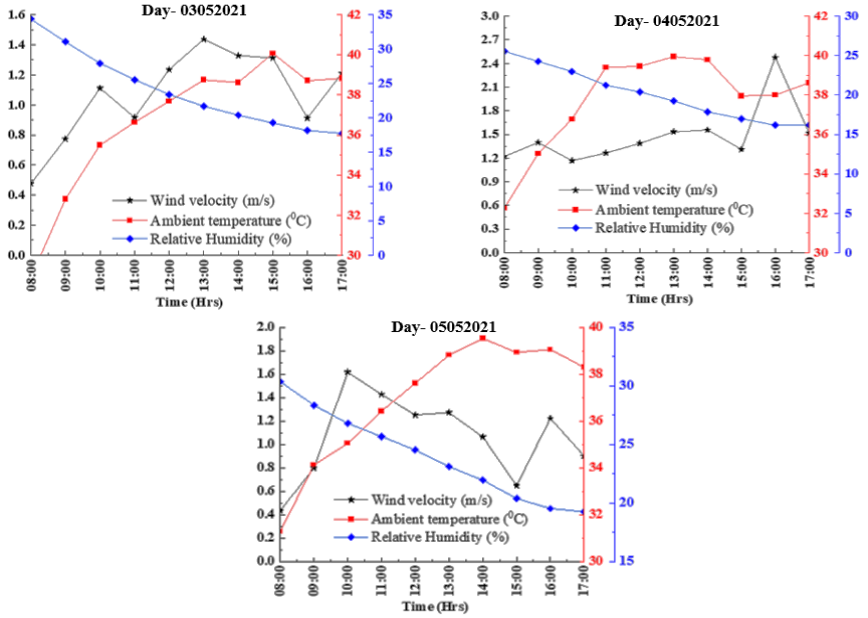

Figure 4.4. Meteorological conditions during summer representing diurnal variations

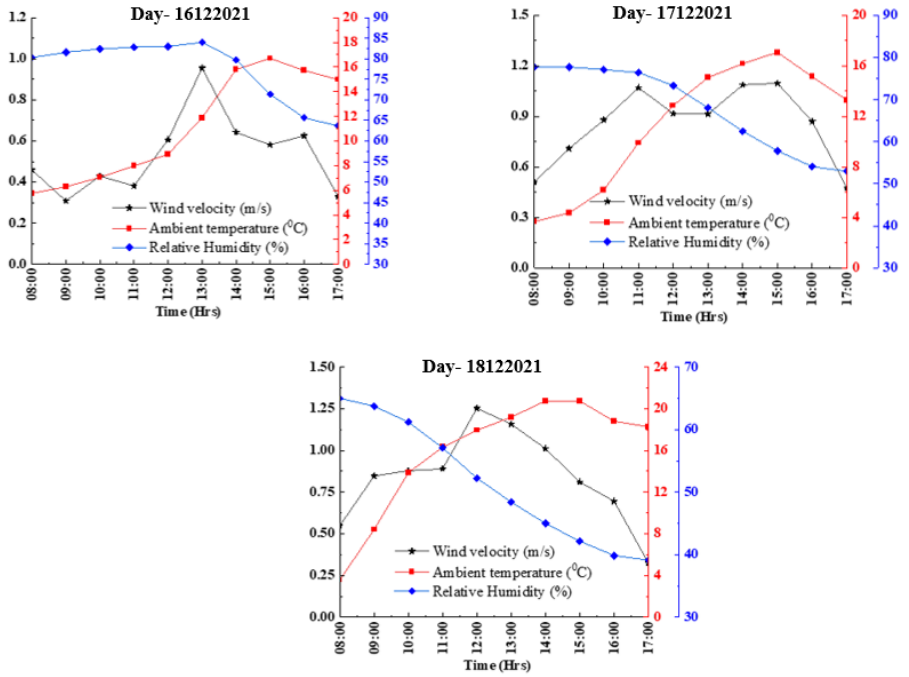

Figure 4.5. Meteorological conditions during winter representing diurnal variations

Mekhilef et al. (2012), highlighted the impact of meteorological conditions such as relative humidity, temperature, and wind velocity on solar cell efficiency. The increased wind velocity leads to better heat dissipation from the solar cells and leads to an increase in cell efficiency. For the present observations, the seasonal variations i.e., diurnal conditions of FSPV modules have been analyzed. In the comparison of both summer and winter conditions on test days of the experiment, the average wind velocity, relative humidity, and ambient temperature were 1.07 m/s, 24%, and 36.64°C during summers. In the same way, the average wind velocity, relative humidity, and ambient temperature were 0.53 m/s, 51%, and 15.78°C respectively during winters. The results show wind velocity and ambient temperatures during summers are almost 50% higher than in the winters. The relative humidity during summers was 53% lower than the winter conditions in Indian conditions. Hence, the maximum cooling effect on module operating temperature was obtained during the summers.

4.4.2. Temperature behavior of FSPV Module with panel heights

Table 4.1 presents the experimental observations concerning the FSPV module at 500 mm height from the water surface. The parameters like the temperature of the PV module, wind speed, ambient temperature, relative humidity, and solar radiation, were monitored and measured. Based on these measured parameters, power production was estimated.

Table 4.1. Experiment observations of the FSPV module at 500 mm height from the water surface

Day 05.05.2021	**PV module temperature**	**Wind speed (km/h)**	**Ambient temperature (^{0}C)**	**Relative Humidity (%)**	**Solar Radiation (W/m^2)**	**Power (W)**
Time (Hrs)	**Height from water surface 500 mm**					
10:00	47.59	4.79	35.08	27	476.44	53.89
11:00	53.83	4.75	36.12	26	595.98	65.09
12:00	59.98	3.97	36.76	25	**659.08**	69.45
13:00	61.40	4.34	38.44	23	638.02	66.67
14:00	59.17	3.92	39.00	22	634.48	67.18
15:00	58.97	3.26	39.73	21	579.09	61.39

It is clear from Table 4.1 that the FSPV system's module temperature changed greatly during the day; rising from 47.59°C at 10:00 to 61.40°C at 13:00; while the ambient temperature steadily rose from 35.08°C at 10:00 to 39.73°C at 15:00. Throughout the day, the wind's velocity varied and ranged between 3.26 and 4.79 km/h.

Solar radiation, a significant factor in the power output, peaked at a value of 659.08 W/m^2 at 12:00 and then gradually decreased throughout the afternoon. In parallel, the FSPV module's

power production peaked at the value of 68.68 W at 12:00, aligned with the peak solar radiation, and then progressively dropped to 60.83 W at 15:00. By the end of the observation period, the relative humidity had decreased from 27% at the beginning of the measurements to 21%. This dataset serves as a driver for a thorough investigation of how meteorological factors affect the FSPV module's performance.

The module operating temperature has been measured through thermocouples mounted on the backside of solar panels. The data has been measured on the FSPV modules as well as ground-mounted solar modules. The module operating temperature FSPV and ground-mounted modules have been compared for both, the winter as well as summer seasons. The data has been monitored and recorded for 24x7, however, in the results and discussion the data has been plotted only for a typical day from 10.00 hrs-15.00 hrs ideal for solar PV generation. The module operating temperature and ambient temperature for a typical summer day for all four modules at 300mm, 500mm, and 1000mm above water level and ground-mounted are shown in Figure 4.6. During summer and winter test days, the highest PV module temperatures were 69.45°C and 48.61^{0}C, respectively.

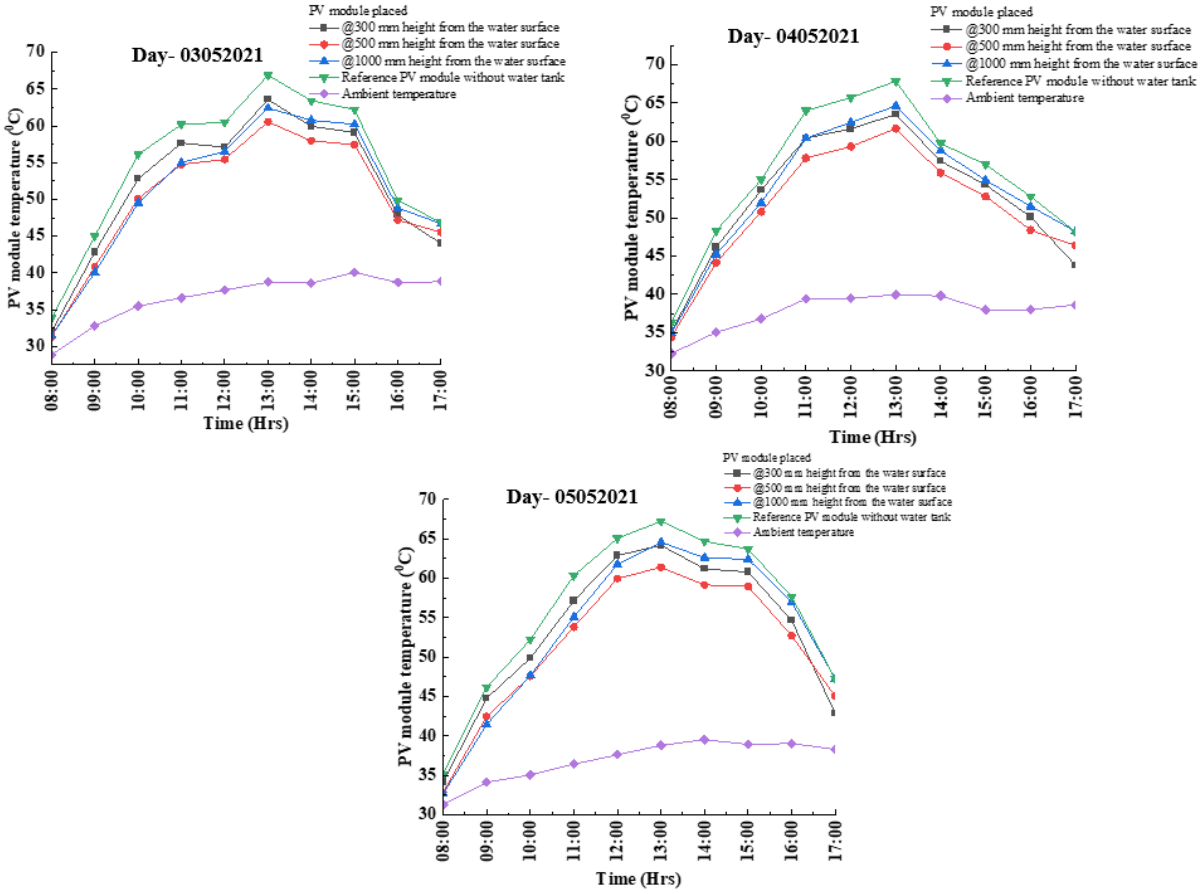

Figure 4.6. PV Module temperature variations during summer conditions

4.4.2.1. Temperature characteristics of FSPV at 300 mm panel height

The FSPV module operating temperature reached a high of 64.77 °C on day 03.05.2021, at a height of 300 mm above the water surface. The operating temperature of the ground-mounted PV module attained a maximum temperature of 67.94^{o}C, with a temperature difference of 3.17°C between the ground mounted reference PV modules and FSPV modules. The maximum difference between module operating temperature of FSPV and reference PV modules on days 04.05.2021 and 05.05.2021 between 12:00-13:00 hours. During this period, the highest ambient temperature was 40.50 °C. However, the highest module operating temperature difference between ambient and FSPV modules was determined to be 26.46 °C. As a result, the average temperature difference between the ground-mounted PV and FSPV modules was 2.95°C.

Furthermore, on day 16.12.2020, the FSPV module operating temperature reached as high as 40.19°C at a height of 300 mm above the water surface. The operating temperature of the ground-mounted PV module achieved a maximum temperature of 42.71 °C, with a temperature difference of 2.51 °C between the operating temperature of the reference PV and FSPV modules. Similarly, during 12:00-13:00 hours on days 17.12.2020 and 18.12.2020, the largest difference between the operating temperature of FSPV and reference PV modules was 3.42 °C, 3.19 °C. During the winter test days, the maximum ambient temperature was 20.77 °C. However, the highest temperature difference between ambient and FSPV modules was determined to be 25.55 °C. In winter, the average temperature difference between the reference PV and FSPV modules was 3.04 °C.

4.4.2.2. Temperature Characteristics of FSPV at 500 mm panel height

The peak period of solar radiation was 13:00-14:00 hours on day 04.05.2021 at a 500 mm height from the water surface. In comparison, the FSPV operating temperature attained a maximum temperature of 61.78°C, with a temperature differential of approximately 6.16 °C between the module operating temperature of the reference PV and FSPV modules. Similarly, the temperature variation on the other days was 5.17°C and 7.01°C. During the summer season, the average module operating temperature of the FSPV module is 6.11°C lower than that of the ground-mounted PV module.

Around 13:00 hours on day 16.12.2020, at a 500 mm height from the water's surface. In comparison, the operating temperature of the FSPV module attained a maximum temperature of 39.53°C, with a temperature difference of roughly 3.18°C between the operating temperature of the reference PV and FSPV modules. Similarly, the temperature deviations on

the other days were 3.61°C and 3.93°C. During winter test days, the module operating temperature of the FSPV module is 3.57°C lower than the ground-mounted PV module.

4.4.2.3. Temperature Characteristics of FSPV at 1000 mm panel height

In the same way, for 1000 mm panel height, during the peak time of sun radiation about 13:00-14:00 hours, the FSPV module operating temperature reached 63.76°C during the summer season. During summer, the average temperature difference between the ground-mounted PV and FSPV modules is approximately 3.41°C. During winter, this temperature difference is 3.23°C. The module operating temperature variation of panels with varying heights above water and ground-mounted for typical summer day 05.05.2021 and winter day 17.12.2020 is shown in Figure 4.7(a)-(b).

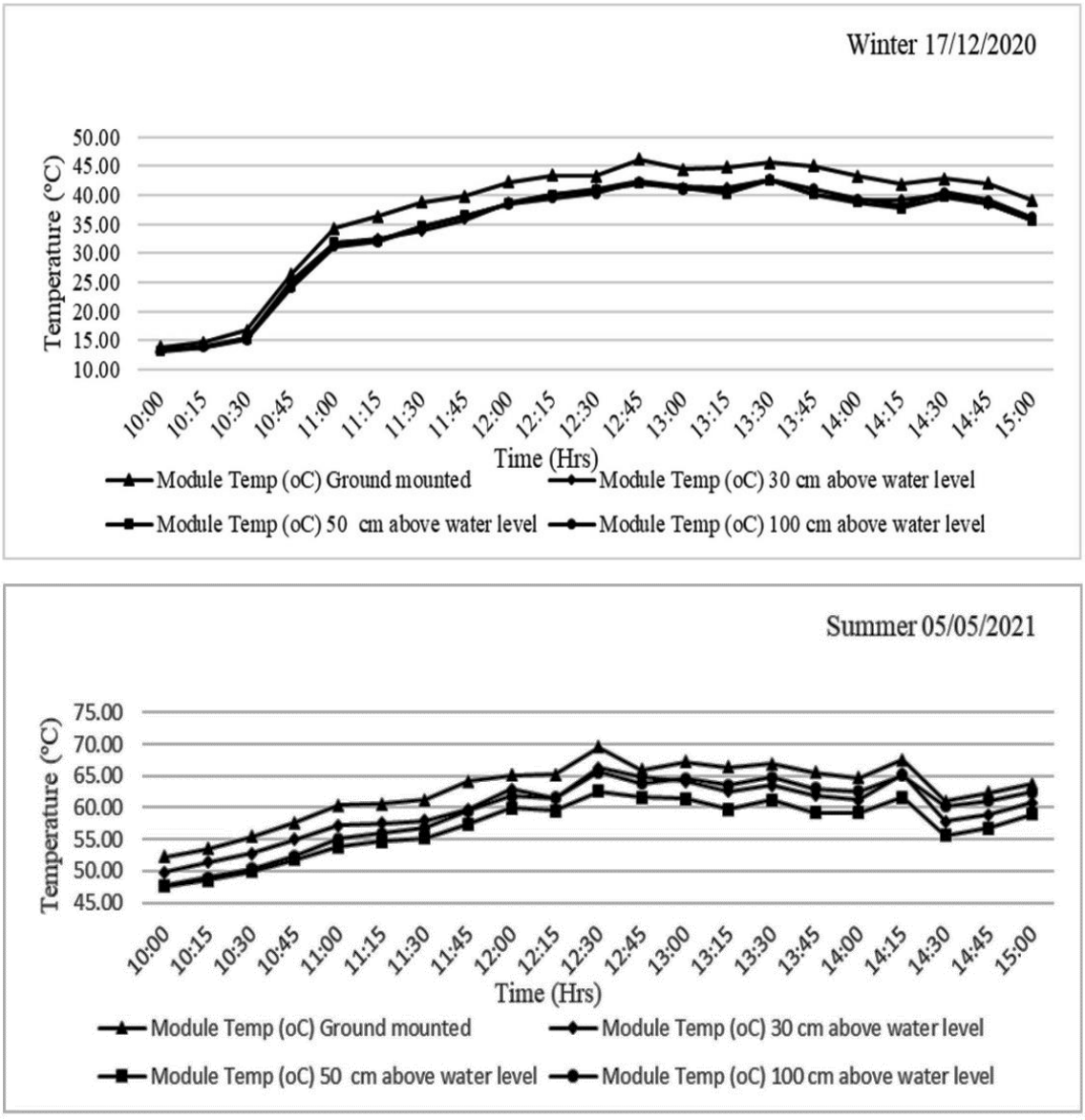

Figure 4.7. Module operating temperature of ground-mounted and floating solar PV panels at varying heights for (a)summer and (b)winter

4.4.3. Power Output of FSPV modules

The electrical efficiency of the PV module η_c depends on the module temperature T_{pv} and is given by Equation 4.1 (Florschuetz,1979)

$$\eta_c = \eta_{ref}\left[1 - \beta_{ref}\left(T_{pv} - T_{ref}\right)\right] \quad (4.1)$$

Where, β_{ref}= efficiency correction coefficient for reference temperature ($^oC^{-1}$) and η_{ref} = electrical efficiency of the module for the reference temperature T_{ref}.

Though the open circuit voltage (V_{oc}) of PV modules has been measured, however, the instantaneous power output from the PV modules has been estimated based on the theoretical assessment of the instantaneous power output and applying the temperature correction using the following Equation 4.2.

$$\text{Power output} = G_T x\, A_M x\, \eta_{Mref}(1 - \beta_{Mref} x(T_{pv} - T_{ref})) \quad (4.2)$$

where G_T is solar insolation in W/m^2, A_M= Area of the module in m^2, η_{Mref} = module efficiency at NOCT, β_{Mref} = power temperature coefficient in %, T_{pv}= module temperature in °C and T_{ref} = NOCT temperature 25°C. For present case module area A_M= 0.9880 m^2, η_{Mref}= 15.4%, β_{Mref} = 0.5% W/°C. The voltage output has been recorded with sensors. The variation of V_{oc} with temperature for a typical day for an FSPV panel 500 mm above water level is shown in Figure 4.8.

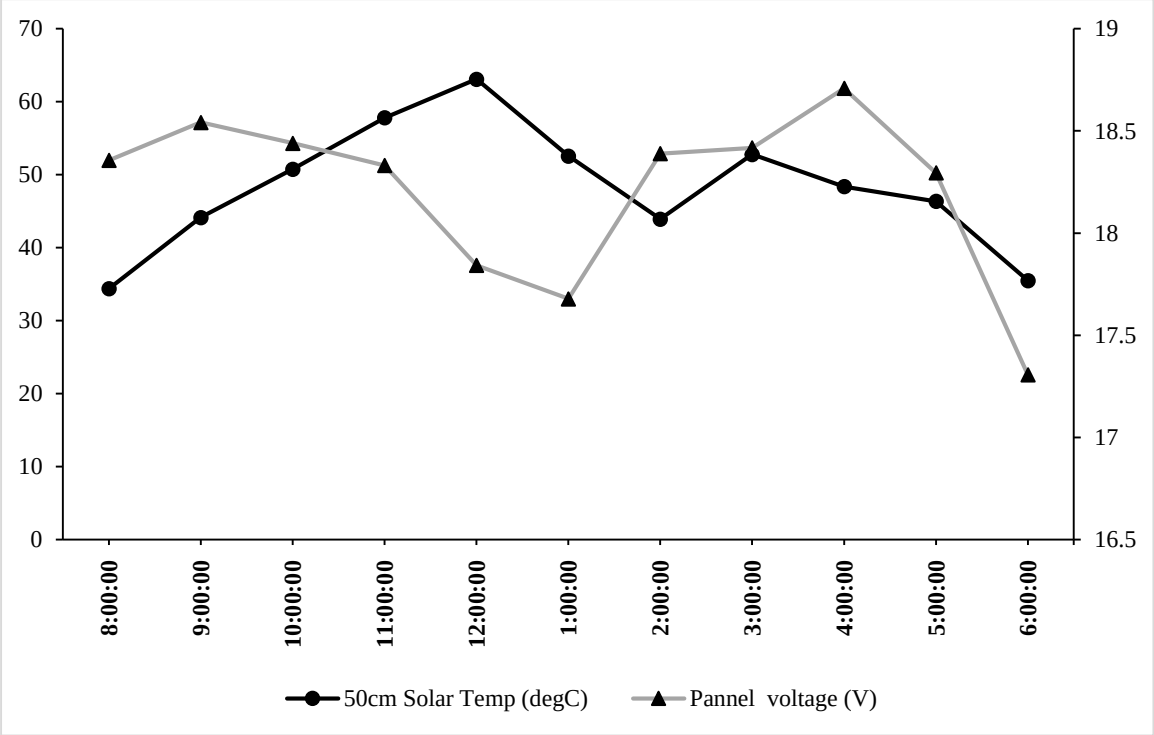

Figure 4.8. Voltage variation with temperature of FSPV panel of height 500mm

4.4.3.1. Power Output of FSPV panel at 300 mm Height

Trends of power produced from the FSPV panel at 300 mm height are shown in Figure 4.9 during summer. Maximum values of power produced are observed at 12.45 hrs. On 05.05.2021, the FSPV poly-crystalline module produced 70.20 W and the ground-mounted PV module produced 69.69 W at solar radiation of 686 W/m^2. On 04.05.2021, between 12:00-13:00 hrs, FSPV modules produced 84.22 W and ground-mounted PV modules produced 82.62 W at solar radiation of 824 W/m^2. Similarly, on 03.05.2021, the FSPV module produced 71.08 W and the ground-mounted PV module produced 69.50W at solar radiation of 687 W/m^2. Hence, it is concluded that the FSPV average power output is increased by 1.7 % with the ground-mounted PV module during summer.

Trends of power produced from the panel at 300 mm height are shown in Figure 4.10 for winters. Maximum values of power produced are observed between 13:00-14:00 hrs. On day 16.12.2020, the FSPV module produced 84.03 W and the ground-mounted PV module produced 82.16 W at solar radiation of 678 W/m^2. On 17.12.2020, between 12:00-13:00 hrs FSPV modules produced 92.03 W and ground-mounted PV modules produced 90.55 W at solar radiation of 787 W/m^2. Similarly, on 18.12.2020, the FSPV module produced 91.61 W, and the ground-mounted PV module produced 89.72 W at a solar radiation of 788 W/m^2. Hence, it concluded that the FSPV average power output was increased by 1.69 % with the reference PV module during winter test days.

4.4.3.2. Power Output of FSPV panel at 500 mm Height

Trends of power produced from FSPV panel at 500 mm height from the water surface are shown in Figure 4.9 during summer. Maximum values of power produced were observed between 12:00-13:00 hrs. During day 03.05.2021, the FSPV module produced 72.07 W and the ground-mounted PV module produced 69.50 W at solar radiation of 687 W/m^2. On 04.05.2021, between 12:00-13:00 hrs FSPV modules produced 85.50 W and ground-mounted PV modules produced 82.62 W at solar radiation of 824 W/m^2. Similarly, on 05.05.2021, the FSPV module produced 71.54 W and the reference PV module produced 69.69 W at solar radiation of 686 W/m^2. Hence it is concluded that the FSPV average power output was increased by 3.78 % with ground-mounted PV module during summer test days.

Trends of power produced from the FSPV panel at 500 mm height from the water surface are shown in Figure 4.10 for winters. Maximum values of power produced are observed between 13:00-14:00 hrs. On day 16.12.2020, the FSPV polycrystalline module produced 83.90 W and the ground-mounted PV module produced 82.16 W at solar radiation of 707 W/m^2. On

17.12.2020, between 12:00-13:00 hrs FSPV modules produced 92.15 W and ground-mounted PV modules produced 90.55 W at solar radiation of 787 W/m^2. Similarly, on 18.12.2020, the FSPV module produced 91.78 W and the ground-mounted PV module produced 89.72 W at a solar radiation of 788 W/m^2. Hence, it concluded that the FSPV average power output was increased by 1.8 % with ground-mounted PV module during winter test days.

4.4.3.3. Power Output of FSPV panel at 1000 mm Height

Trends of power produced from the FSPV panel at 1000 mm height from the water surface are shown in Figure 4.9 for the summer season. Maximum values of power produced are observed between 12:00-13:00 hrs. On 03.05.2021, the FSPV polycrystalline module produced 71.22 W and the ground-mounted PV module produced 69.50 W at solar radiation of 687 W/m^2. On 04.05.2021, between 12:00-13:00 hrs FSPV modules produced 84.02 W and ground-mounted PV modules produced 82.62 W at solar radiation of 824 W/m^2. Similarly, on 05.05.2021, the FSPV module produced 70.59 W and the ground-mounted PV module produced 69.69 W at a solar radiation of 686 W/m^2. Hence it concluded that the FSPV average power output was increased by 2.08 % with reference PV module during summer test days.

Trends of power produced from the FSPV panel at 1000 mm height from the water surface are shown in Figure 4.10 for winter. Maximum values of power produced are observed between 13:00-14:00 hrs. On day 16.12.2020, the FSPV polycrystalline module produced 83.56 W and the ground-mounted PV module produced 82.16 W at solar radiation of 707 W/m^2. On day 17.12.2020, between 12:00-13:00 hrs FSPV modules produced 92.23 W and ground-mounted PV modules produced 90.55 W at solar radiation of 787 W/m^2. Similarly, on day 18.12.2020, the FSPV module produced 91.61 W and the ground-mounted PV module produced 89.72 W at solar radiation of 788 W/m^2. Hence, it is concluded that the FSPV average power output is increased by 1.72 % with ground-mounted PV modules during winter test days.

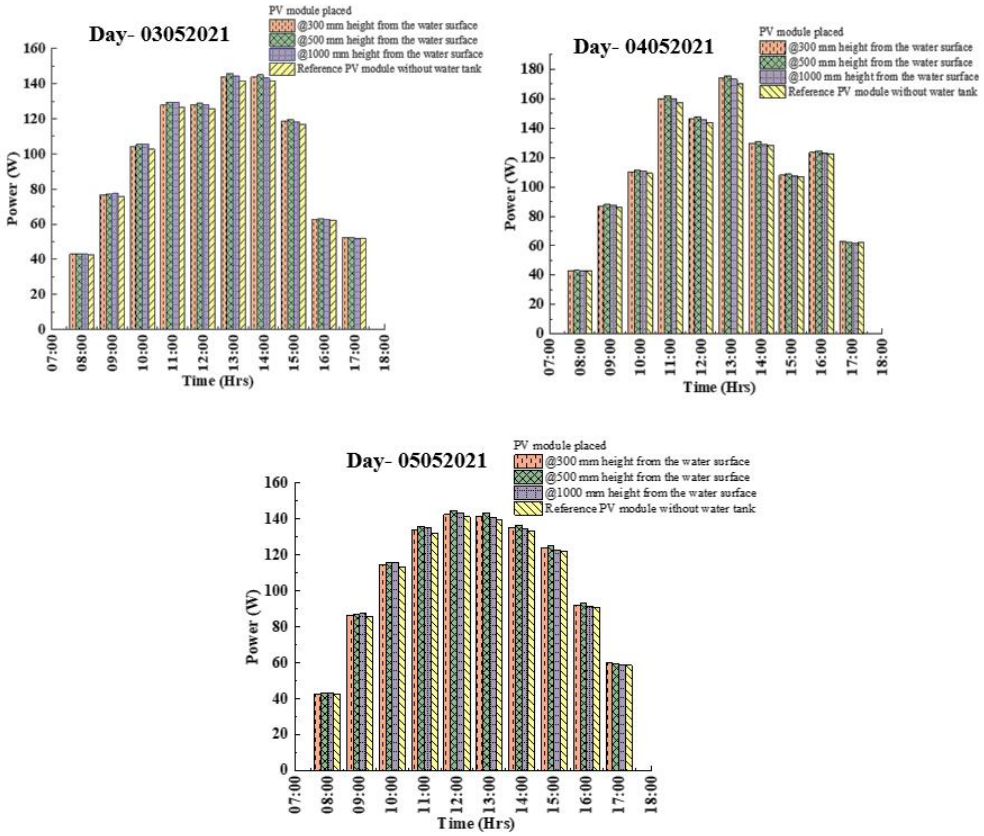

Figure 4.9. The power output of ground-mounted PV panels and floating solar PV panels at varying heights above water during summer.

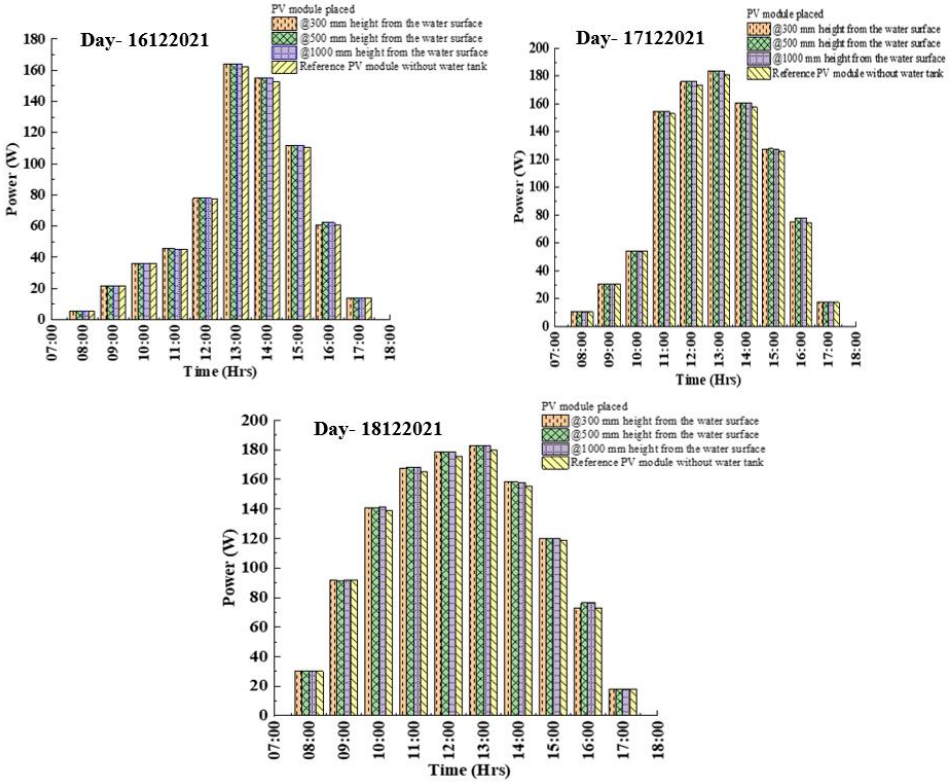

Figure 4.10. The power output of ground-mounted PVpanel and floating solar PV panels at varying heights above water during winter

4.4.3.4. FSPV panel performance

Figure 4.11(a)-(b) shows the variation in the performance of the power output of FSPV at varying heights above the water and ground-mounted panels for a typical summer and winter day, respectively. It is observed that module operating temperature of FSPV is lower than the ground-mounted PV panels while the power output of FSPV is higher than ground-mounted PV panels. However, it can be observed that a panel having height 500 mm above water is best, having module operating temperature lowest among all the panels and power output is highest among FSPV panels. Figure 4.12(a)-(b) further illustrates the superior power output performance of the FSPV panel situated 500 mm above the water surface compared to the ground-mounted panel during both seasons. Notably, the power output of the FSPV panel 500mm above the water increased by an average of 3% compared to the ground-mounted panels.

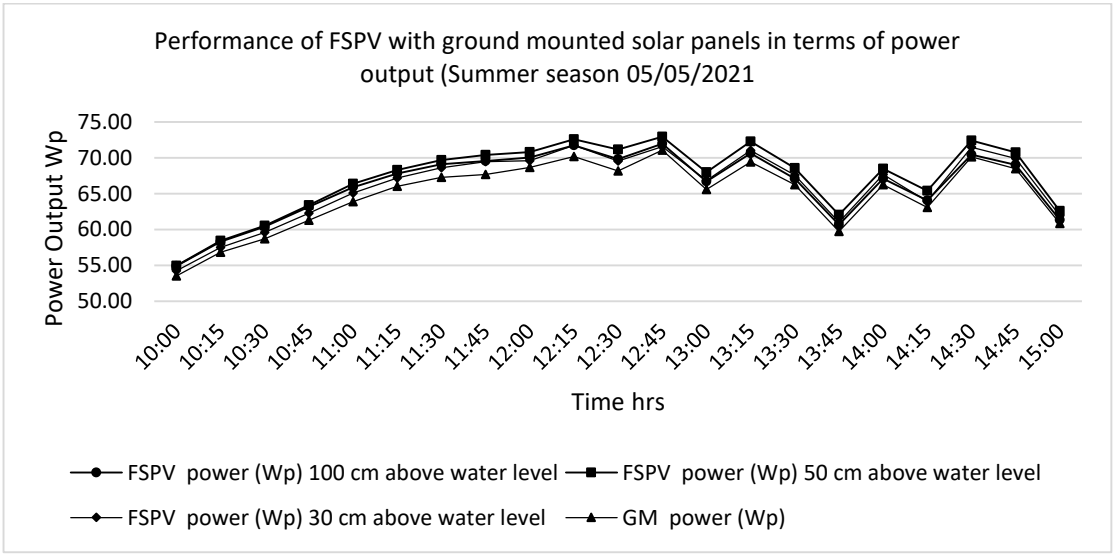

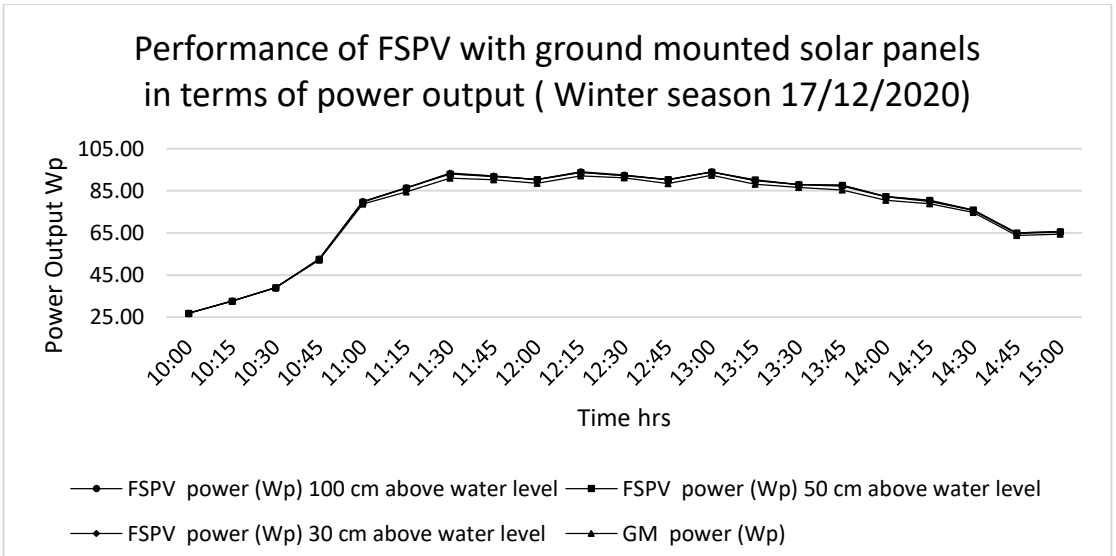

Figure 4.11. Power output performance for a typical day (a) summer (b) winter

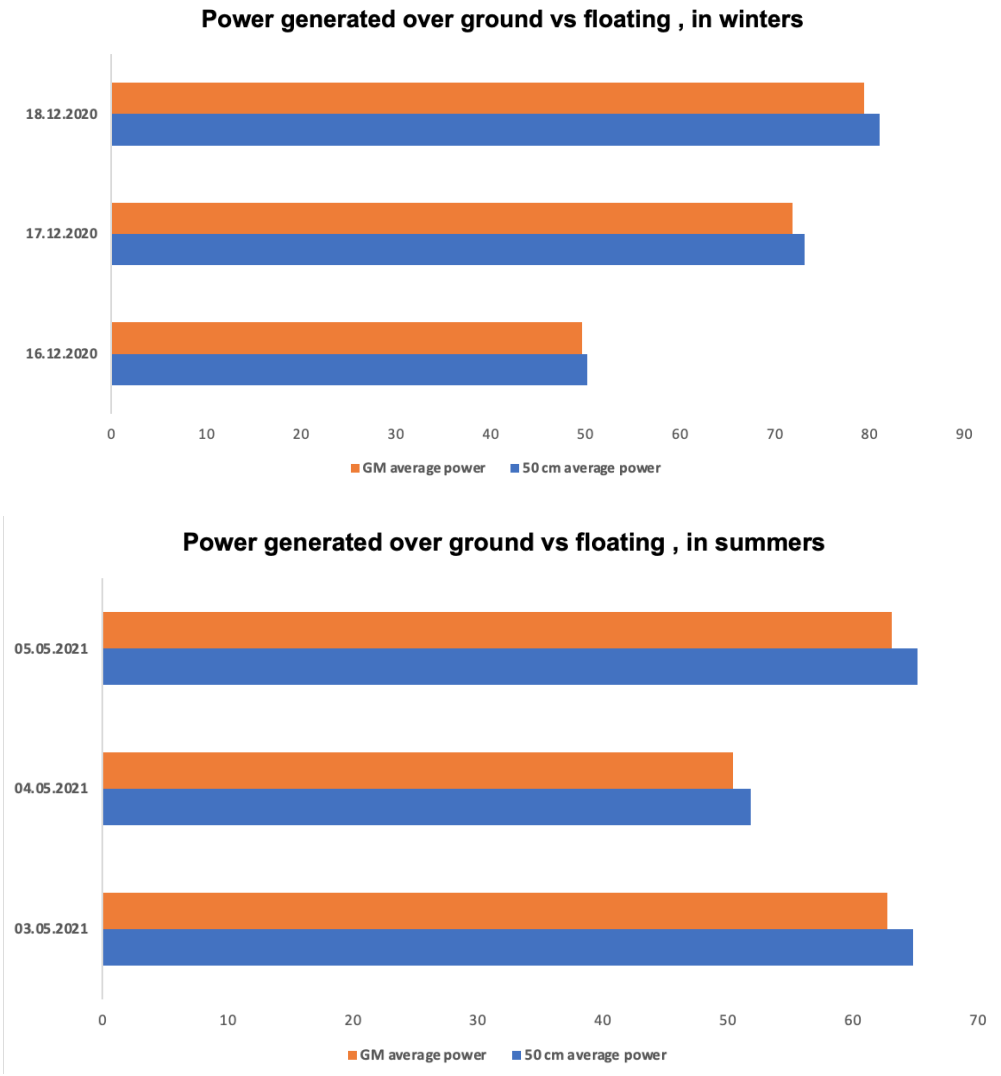

Figure 4.12. The power output performance of the FSPV panel at 500 mm above water and ground-mounted panel during (a) summer (b) winter

The results derived from the study present a compelling argument for the use of Floating Solar Photovoltaic (FSPV) systems in enhancing solar energy efficiency. They reveal a marked improvement in both temperature regulation and power output compared to the traditional ground-mounted systems. The cooling effect of water significantly contributes to a decrease in module operating temperature, enhancing the efficiency of power conversion. The study established that even with varying heights above the water surface (300 mm, 500 mm, and 1000 mm), FSPV systems consistently outperformed ground-mounted systems. It is noteworthy, that while all heights demonstrated the benefits of FSPV technology, the best performance observed with FSPV modules set at 500 mm above the water surface. This could be due to the optimal balance between the cooling effect of the water and exposure to sunlight at this height.

Based on the evidence presented by the experiment results, it can be concluded that an elevation of 500 mm above the water surface is optimal for maximum power output. At this height, FSPV modules achieve a low operating temperature while maintaining high insolation, maximizing power production. However, 500 mm appears to be the sweet spot; other factors such as safety, system stability, local weather patterns, and potential water level fluctuations might require adjustments to this height in real-world scenarios. This highlights the need for further research and site-specific assessments to determine the most suitable heights for FSPV installations.

4.5. Summary and Recommendations

In this chapter, a thorough analysis and comparison of the floating solar photovoltaic (FSPV) systems' performance in comparison to traditional ground-mounted PV systems in the climatic conditions of tropical regions like India were conducted. The experimental study is focused on the characteristics of temperature and electricity generation from the FSPV modules mounted at various heights above the water surface. The modules are installed at varying heights of 300mm, 500mm and 1000 mm above water bodies to establish the best-performing height. The following are the principal findings:

- During the winter season, though there is a temperature difference between module temperatures of a ground-mounted solar panel and a floating or FSPV solar panel, as high as about 4^0C during peak sun time. However, an average temperature variation of 3.25 ^{0}C was observed throughout the period.
- During winter the average power output of FSPV solar panels is 1.73% higher as compared to ground-mounted solar panels. It highlights that due to minor variations in the module operating temperature and lower operating temperature during winters the power output from solar panels does not change significantly.
- During summer season the temperature variation is significantly observed among the FSPV panels at varying height with respect to water levels. It may be noted that the lowest module temperature observed is on the solar panel installed over 500 mm above the water body. It is also observed that reducing the gap between water body and the solar panel does not lead to further reduction of operating temperature of solar panels. This is due to the fact that the reduced gap between water body and solar panels leads to reduced ventilation and the net effect is the higher operating temperature of panel, as in the case of the results shown for the module operating 300 mm above water level.

- While comparing the performance of the FSPV module with ground-mounted PV modules, it is found that the operating temperature of FSPV is about 10% lower compared to ground-mounted solar panels for panels at 500 mm and about 6% for panels at other heights at peak solar hour.
- The average power output of FSPV is also 2.5% higher as compared to typical ground-mounted solar panels during summer. However, the maximum power output was 3.78% higher for the FSPV panel at 500mm above the water level.
- The panels should be installed 500 mm above water bodies to maximize the power output and minimize module operating temperature.

The following recommendations are suggested based on the findings of this study:

- The height above the water's surface must be taken into consideration while installing FSPV devices. Considering both power output and module temperature reduction, our research indicates that a height of 500 mm is the most efficient. This optimal height should be taken into account in future FSPV installations.

Chapter 5

Predictive Model Development for Panel Temperature of Solar PV over Water Bodies

Abstract

Solar panel efficiency is highly dependent on its operating temperature. Technological developments have led to the installation of PV modules over the water bodies due to high efficiency and other benefits. The operating performance of solar panels over water bodies through field studies is the subject area of recent research. Investigation and comparison of the solar panel operating performance on water bodies with the ground-mounted solar PV installation were made. Regression models have been developed, and the existing exponential model for panel temperature has been modified based on the experimental setup of solar panels on water bodies at BITS Pilani, India. The linear, nonlinear, and exponential regression models were used to predict the operating temperature of solar PV installation over water bodies. Models for various parameters (ambient temperature, solar insolation, wind velocity, water temperature, humidity) were developed. The one-degree regression models with three parameters outperformed those of four and five. The study found that the annual power output estimates of the best model is within an error of less than 0.2% of power estimation from recorded data. According to research, solar PV panels installed over water bodies have an annual power output that is 2.59% higher than those installed on ground-mounted systems. The newly developed regression and modified Kings models can be used to predict the operating temperature of solar PV installation over water bodies. Only three meteorological parameters, ambient temperature, solar insolation, and wind velocity, can accurately predict the module temperature.

Keywords: Ground mounted solar PV, Floating solar PV, Temperature model, Regression Analysis, exponential module temperature model

5.1. Introduction

The experimental investigation as described in the Chapters 3 and 4 compares the operating performance of solar PV modules mounted above water bodies to those installed on the ground. This chapter further utilizes the outcomes to forecast the operating temperature of solar PV installations over water bodies; to develop predictive regression models and an adaptation of the exponential model for panel temperature prediction. These models consider many variables, such as the ambient temperature, solar insolation, wind speed, water temperature, and humidity.

With a focus on the significance of operating temperature, the study aims to increase understanding of the impact of various installation conditions on the performance of solar PV modules. The study will also contribute to the body of knowledge by examining the relative effectiveness of floating PV installations vs traditional ground-mounted PVs.

Based on the experimental investigation and recorded data collected for consecutive 3 years, this chapter analyses the data for predictive modelling. A thorough comparison of the operating performance of PV modules over water bodies vs those on the ground-mounted is provided by the developed models, experimental setup, and data-gathering techniques employed. This chapter also attempts to provide insightful information for the efficient deployment and use of PV systems in various climatic situations by relying on this information.

With the ever-increasing demand for energy, vastly eradicating stocks of fossil fuels and higher levels of environmental pollution have developed the need to look for alternative energy systems. Solar power is a clean and renewable energy resource available in abundance and free. The high availability of solar power near the equator line has led to the development of photovoltaic Cells. Many large-scale Photo Voltaic (PV) Cells are installed on the earth's surface and over the water bodies. Agrawal et al. (2022), Essak & Ghosh (2022), and Huang et al. (2023) reported many benefits of floating (water-mounted) PV such as temperature reduction, no cost for land, evaporation reduction, reduced soiling etc. The performance of these PV Cells depends on many factors, such as ambient temperature, solar insolation, and wind velocity. These factors are assumed to be influence factors of the process and affect the performance measures. Hence, it becomes important to predict the operating temperature of PV modules, and many studies have focused on predicting the operating temperature of PV modules.

While solar PV has become a mature technology, large-scale global installations are taking place on ground mounted as well as on water bodies. The performance of solar panels is highly dependent on their normal operating cell temperature. It is important to predict the operating temperature of PV modules. Hence, many studies have focused on predicting the operating temperature of PV modules. Schott (1985) and Servant (1986) proposed an implicit equation, while Ross & Smokler (1986), Lasnier & Ang (1990), and Mondol et al. (2005) proposed an explicit equation for module operating temperature using meteorological parameters. Coskun et al. (2017) used an artificial neural network to predict PV module operating temperature. Skoplaki et al. (2008) and Skoplaki & Polyvos (2009) developed an equation for predicting module operating temperature, showing high function error for wind

speed below one m/s. Muzathik et al. (2014) used simple correlation while Risser & Fuentes (1983) used linear regression to predict PV module operating temperature. Kings et al. (2004), Mattie et al. (2006), Chenni et al. (2007), Kurtz et al. (2009), and Akyuz et al. (2012), developed PV module operating temperature prediction model utilizing three meteorological parameters solar insolation, ambient temperature, and wind velocity. Almaktar et al. (2013) proposed a module operating temperature model for the tropical region, using only ambient temperature, while Kalogirou (2013) and Irodionov et al. (1989) developed the model using ambient temperature and solar insolation to predict module operating temperature. Mora Segado et al. (2015) developed a prediction model for PV modules of different technology under the climatic conditions of southern Spain using meteorological parameters. Kaplani & Kaplani (2020) developed a module operating temperature model based on the energy balance equation for all environmental conditions.

Koehl et al. (2011) proposed a Realistic Nominal Module Temperature (ROMT) based on observed field data, whereas Faiman (2008) provided a modified HWB equation to predict the module temperature. Barry et al. (2020) developed a dynamic model of photovoltaic module temperature as a function of atmospheric conditions. Du et al. (2016) developed a theoretical model, while Duffie & Beckman (2020) proposed an equation based on Nominal Operating Cell Temperature (NOCT), Sohani & Sayyaadi (2020) employed genetic programming for predicting solar PV panel temperature. All these models utilize meteorological parameters (solar insolation, ambient temperature, and wind velocity) to predict module temperature. Evans and Florschuetz (1978), Evans (1981), and Notton et al. (2005) developed equations to assess PV panel efficiency. All the studies focused on assessing the operating performance of PV modules on ground-mounted solar installation. However, limited work has been done to predict the operating performance of PV panels over water bodies. Kamuyu et al. (2018) and Tina et al. (2021) developed floating solar PV installation models for panel temperature estimation. Kamuyu et al. (2018) developed the regression model for the Korean region based on the experimental data with meteorological parameters (wind speed, ambient temperature, water temperature, and solar insolation). Tina et al. (2021) developed and validated mathematical models for estimating the performance of bifacial and mono-facial PV modules installed on water surfaces in Catania, Italy. The above studies on performance evaluation of solar PV installation over water bodies have focused on module temperature aspects.

Despite multiple studies conducted for predicting PV module operating temperature under different weather conditions on ground-mounted installations, limited studies were reported

for predicting the solar panel operating temperature on water bodies under different weather conditions. This study aims to develop an experimental-based regression model for evaluating the operating temperature of PV panels installed over water bodies operating under different weather conditions. Based on the literature review and subsequent research gap, an attempt has been made to bridge the gap by investigating the following objectives:

- Identify the influencing factors and performance measures of floating and ground-mounted solar PV installation.
- Develop mathematical models by application of regression analysis with varying parameters.
- Apply regression model analysis to predict the operating temperature of floating solar PV installation and estimation of power output.

5.2. Existing module operating temperature and performance models

The solar energy absorbed by a module is partly converted into electricity and the balance is converted into thermal energy. Thermal energy increases the cell's temperature if thermal energy is not dissipated properly. The maximum power point efficiency of a module depends on cell temperature, which can be expressed by Equation (5.1) (Florschuetz,1979):

$$\eta_{mp} = \eta_{mp.ref} + \mu_{\eta,mp}(T_c - T_{c,ref}) \quad (5.1)$$

Where η_{mp} is the maximum power point efficiency of the module and $\mu_{\eta,mp}$ is the maximum power point efficiency temperature coefficient. T_c is cell temperature and $\eta_{mp.ref}$ and $T_{c,ref}$ is the reference maximum power point efficiency and reference cell temp i.e., NOCT, conditions respectively. Energy balance on a unit area of the module, cooling by losses to the surroundings is given by Equation (5.2) (Evans and Florschuetz,1978):

$$(\tau\alpha)G_T = \eta_c G_T + U_L(T_c - T_a) \quad (5.2)$$

where $\tau\alpha$ is the effective transmittance-absorption product when multiplied by the incident radiation yields absorbed energy and η_c is module efficiency to convert incident radiation into electrical energy. The loss coefficient U_L includes the losses by convection and radiation from top and bottom and by conduction through the mounting framework to ambient temperature T_a. G_T is the incident solar insolation on the plane of the module and Tc is the cell temperature.

Module temperature plays an important role in maximum power point efficiency; therefore, estimation of panel temperature is the prime objective. Various models for PV panel temperature prediction were developed by various authors (Rauschenbach,1980; King et

al.,2004; Skoplaki et al.,2008; David Faiman,2008; Kurtz et al.,2009; Koehl et al.,2011) for ground mounting, which has been discussed in chapter 2. These models can be categorised as linear regression, non-linear regression, and exponential expressions.

Most widely used ground mounted PV panel temperature prediction model was presented by King et al. (2004), which is exponential model. The original general expression for module temperature is given by Equation (5.3)

$$T_{mod} = T_a + G_T e^{(a+bw)} \quad (5.3)$$

where G_T is solar irradiance incident on module surface (W/m^2), and a is a dimensionless coefficient establishing the upper limit for module temperature at low wind speeds and high solar irradiance, while b (s/m) describes cooling by the wind and w wind speed (m/s) measured at 10 m height. These empirically determined coefficients are representative of different module types and mounting configurations.

The above-stated model and models available in literature were developed for ground-mounted PV installation, so they could not be utilized to predict module temperature above water bodies. Kamuyu et al. (2018), suggested two linear regression models namely T_{m1} and T_{m2} for predicting modules temperature mounted over water for floating solar PV installations. Model T_{m1} was developed considering meteorological parameters ambient temperature, wind speed, and solar irradiance while model T_{m2} was developed by considering water temperature as an additional parameter in addition to parameters of model T_{m1}. The module operating temperature models T_{m1} and T_{m2} are given in Equations (5.4) and (5.5) respectively:

$$T_{m1} = 2.0458 + 0.9458T_a + 0.0215\,G_T - 1.2376w \quad (5.4)$$

$$T_{m2} = 1.8081 + 0.9282T_a + 0.021G_T - 1.2210w + 0.0246T_w \quad (5.5)$$

where, T_a the ambient temperature in ^{0}C, G_T solar irradiance in W/m^2, w wind speed in m/s and T_w is the water temperature in ^{0}C.

These empirical formulations have been developed for the Korean region which will not fetch results with the same accuracy for other regions. So, these models need to be checked and corrected for adoption in this region based on the experimental results. To develop temperature prediction models for floating solar in Indian conditions, an experimental setup was established at the Birla Institute of Technology and Science (BITS) Pilani, Pilani campus, India; data were collected, and predictive models were developed. The data was collected for consecutive three years and regression and exponential models have been

developed based on the available data. A comparative study among the Kamuyu et al. (2018) model, and regression models was carried out. The results are analyzed concerning seasonal variations. The impact of variation in different meteorological parameters (such as wind speed, ambient temperature, water temperature, humidity, and solar insolation) has also been assessed on the accuracy of the panel operating temperature.

5.3. Modeling procedure

Experimental Setup was used for collecting data for the input to modeling of the temperature of the PV modules. These experiments aimed to create models that would predict the temperature of photovoltaic (PV) panels based on specific meteorological parameters.The experimental set-up, which has the test rig consisting of PV modules, served as the basis for this. The information included a variety of parameters, including the air temperature (T_a) in degree celcius, the water temperature (T_w) in degree celcius, the solar insolation (G_T) in W/m^2, the wind speed (v) in km/hr, and the relative humidity (Rh) in %. Though the test rig consisted of four solar panels, however, the modeling is done based on ground-mounted solar panels, and a comparison with the best performing floating solar panel at 500 mm height over the water body.

5.3.1. Exponential model using experimental data.

In the first experiment, set of coefficients in Equation (5.3) were obtained for predicting floating PV panel temperature. The coefficients were determined for the FSPV panel as well as the ground-mounted panel with the original three meteorological parameters solar radiation, ambient temperature, and wind speed.

With an emphasis on solar radiation, water temperature, and wind speed, the second experiment attempted to estimate the panel temperature in response to meteorological factors. In this investigation, alternate models were created using water surface temperature (Tw) instead of ambient temperature (Ta) and then new coefficients were derived. A fitting exercise using the current data to find the coefficients of exponential equation (5.3) and the R-square values resulting from those coefficients are given in Table 5.1. These findings were analyzed, comparing predicted and actual temperatures for both ground-mounted and water-mounted panels, and evaluating the necessity of adapting the current empirical models to local conditions.

Table 5.1. New coefficients and R^2 values for exponential regression model for ground-mount and floating PV

Type of Mounting	R^2	Variables	Model Nomenclature
Ground mounted	0.737	G_T, v, T_a	GM1
Water mounted	0.955	G_T,v , T_a	F1
Water mounted	0.94	G_T, v, T_w	F2

Equation (5.6) shown below referred to as model GM1 in Table 5.1 was used beyond ground-mounted panels to forecast temperatures for panels mounted above water. A greater correlation than ground-mounted panels was demonstrated by the resulting R^2 value of 0.848, which suggests a more precise forecast of panel temperatures over water.

$$T_{mod} = T_a + G_T e^{(-3.085-0.032v)} \quad (5.6)$$

The modified Equation (5.7), hereinafter named F1 model, with new coefficient for water mounting panel were developed considering original variables namely ambient temperature, solar insolation, and wind velocity.

$$T_{mod} = T_a + G_T e^{(-3.359-0.022v)} \quad (5.7)$$

The model was further modified by substituting water temperature for ambient temperature in original equation and Equation (5.8), hereinafter named F2 model, was developed for water-mounted panels.

$$T_{mod} = T_a + G_T e^{(-2.998-0.025v)} \quad (5.8)$$

The R^2 values for model F1 and F2 were obtained as 0.955 and 0.94 respectively as detailed in Table 5.1.

5.3.2. Linear and quadratic models using experimental data

The operating temperatures of solar panels are predicted in this section by a thorough investigation of regression modelling, with a special emphasis on water-mounted panels. The newly determined coefficients and incorporate ambient temperature into the model, exponential equation has shown to be reliable in estimating the temperature of these panels. However, it is better suited for analysis with fewer meteorological parameters because it only includes three variables: solar insolation, wind speed, and ambient temperature.

The exponential equations, despite being straightforward and useful, ignores the importance of humidity, a vital element that could significantly impact panel temperatures, particularly

diurnal and seasonal variations like early in the morning and during the rainy season. Given that floating solar panels are mounted above bodies of water, it is assumed significant to take humidity into account. In present study regression model with inclusion of humidity and water temperature was planned and developed both linear and nonlinear regression models, to evaluate this impact on panel temperature prediction.

With the Solar Panel Temperature (ºC) as the dependent variable (target variable), the regression analysis included a wide range of independent variables, namely Ambient Temperature (ºC), Water Temperature (ºC), Solar Insolation (W/m^2), Wind Speed (km/h), and Humidity (%).

Models were developed considering three variables (ambient temperature, solar insolation, and wind speed), four variables (adding water temperature), and five variables (adding humidity) in the regression analysis. Additionally, to test the nonlinearity, if any, the nonlinear models were also developed.

Table 5.2 displays various regression models, R-square values, variables, and model nomenclatures that go with them. One-year meteorological and panel temperature data with 15-minute interval as discussed in Chapter 3, is used to test each model. All models performed well, in terms of R^2 values greater than 0.93.

Table 5.2. Linear Regression models for floating PV

Model	R-square value	Variables	Model Nomenclature
Linear Regression Degree 01	0.956	G_T,v, T_a	F3
Linear Regression Degree 01	0.93	G_T,v, R_h, T_w	F4
Linear Regression Degree 01	0.96	G_T,v, R_h, T_a, T_w	F5
Linear Regression Degree 02	0.96	G_T,v,T_a	F6
Linear Regression Degree 02	0.944	G_T,v, R_h, T_w	F7
Linear Regression Degree 02	0.963	G_T,v, T_a, T_w, R_h	F8

A-Linear Regression models F3, F4 and F5 are represented in Equations (5.9-5.11) respectively.

$$T_{mod} = -0.337 + 0.034\mathrm{G_T} - 0.056\mathrm{v} + 0.995\mathrm{T_a} \quad (5.9)$$

$$T_{mod} = 8.736 + 0.927\mathrm{T_w} + 0.043\mathrm{G_T} - 0.027\mathrm{v} - 0.105\mathrm{R_h}. \quad (5.10)$$

$$T_{mod} = -6.833 - 0.491\mathrm{T_w} + 0.03\mathrm{G_T} - 0.068\mathrm{v} + 1.526\mathrm{T_a} + 0.08\mathrm{R_h} \quad (5.11)$$

B-Linear Regression models F6, F7 and F8 are represented in Equations (5.12-5.14) respectively.

$$T_{mod} = -3.116 + 0.044G_T + 0.71v + 1.156T_a - 0.001G_Tv - 0.104v^2 + 0.003vT_a - 0.004T_a^2 \quad (5.12)$$

$$T_{mod} = 3.961 + 1.008T_w + 0.082G_T + 1.852v - 0.153R_h - 0.002T_w^2 - 0.015vT_w + 0.003T_wR_h - 0.002vG_T - 0.129v^2 - 0.009vR_h + 0.001R_h^2 \quad (5.13)$$

$$T_{mod} = -9.506 - 0.39T_w + 0.044G_T + 1.038v + 1.487T_a + 0.116R_h + 0.029T_w^2 + 0.001T_wG_T - 0.015vT_w - 0.053T_wT_a + 0.002R_hT_w - 0.001vG_T - 0.001T_aG_T - 0.094v^2 + 0.008vT_a - 0.004vR_h - 0.001T_aR_h + 0.023T_a^2 \quad (5.14)$$

where, T_w =Water temperature in °C, G_T = Solar insolation in W/m^2, T_a = Ambient temperature in °C, v = Wind velocity in km/h, R_h = Relative humidity in %.

5.4. Results and Discussions

5.4.1 Testing the models for seasonal adequacy

The suitability of each model was examined during several seasons. These models were tested for gauging the temperature of a panel mounted 500 mm above water surface. Figure 5.1 shows the temperature forecasts from all eight models for a typical May Day with maximum solar insolation together with the actual temperature. Table 5.3 displays the root mean square error (RMSE) of each model's temperature estimate.

Table 5.3. Maximum and minimum RMSE for temperature predicted by models

RMSE	**Models**							
	F1	F2	**F3**	F4	F5	F6	F7	F8
Maximum	5.64	8.26	**5.50**	9.43	8.19	6.95	22.38	22.07
Minimum	1.96	2.65	**1.67**	2.34	5.49	2.54	11.35	11.90

With a maximum error of 5.5 degrees and a minimum error of 1.67 degrees, Model F3 was found to be the best model in terms of root mean square error (RMSE). This strong performance is noteworthy, especially because several models were created to study the impacts of water temperature and humidity. But in the analysis, the simplest model with a three-parameter namely ambient temperature, solar insolation, and wind speed proved to be more useful. The models with fewer parameters outperformed those that took extra factors like humidity and water temperature into account.

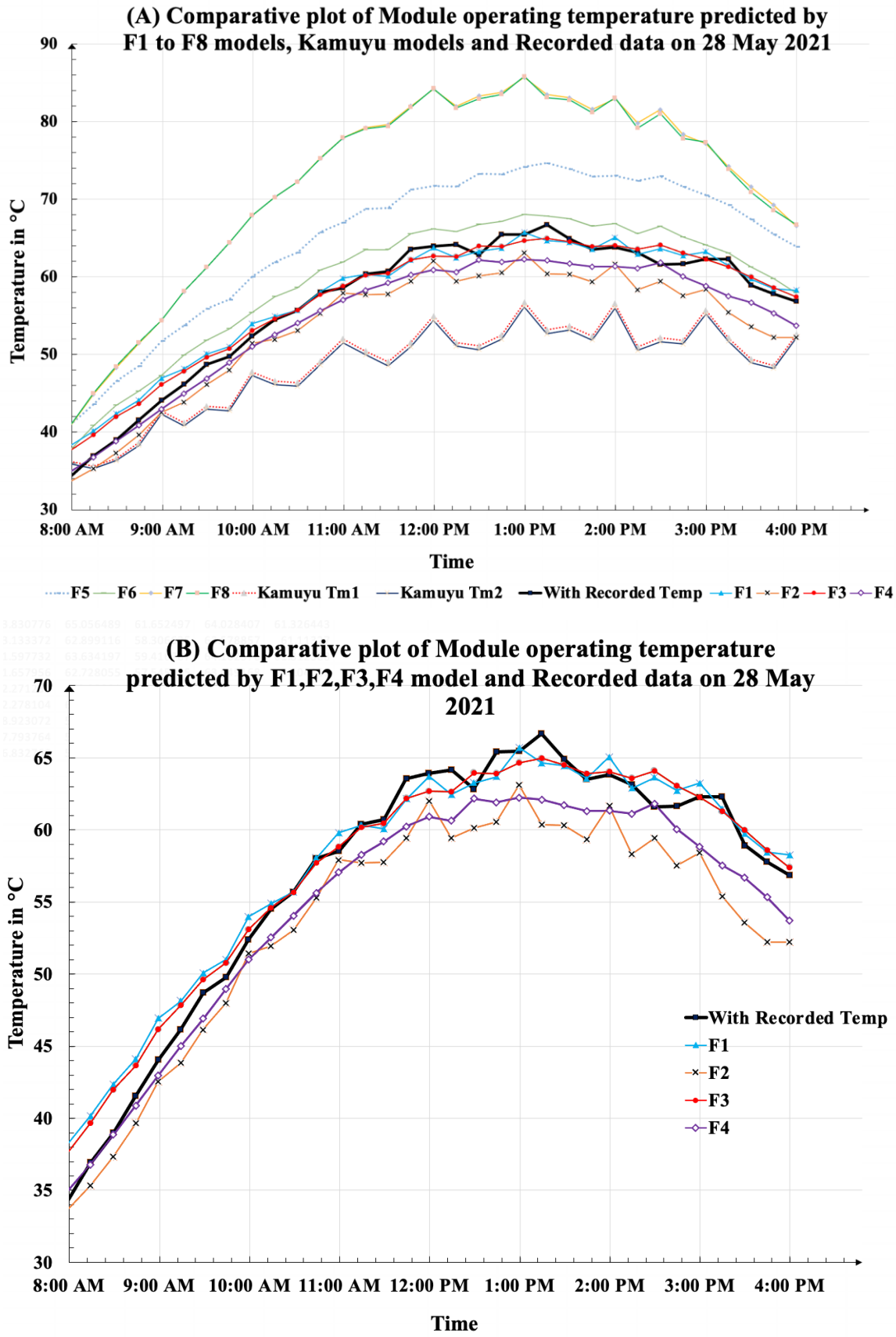

Figure 5.1. Predicted panel temperature for the typical day with maximum solar insolation in May 2021 (a) All eight models, Kamuyu et al. (2018) models and recorded temperature (b) Four best performing models F1,F2,F3,F4 and recorded panel temperature.

5.4.1.1. Seasonal Evaluation and model identification for best performance

The three main seasons experienced in India—summer (March to June), monsoon (July to September), and winter (October to February)—were used to subject the regression models to extensive testing. Table 5.4 shows how the models' performance varied with the seasons. For example, the correlation coefficient varied from 0.87 for F5 in the summer to 0.98 for F1 in the winter, while the R^2 value ranged from 0.75 for F5 to 0.95 for F1, with the lowest and highest values again occurring in the summer and winter, respectively.–With a maximum inaccuracy as reflected in terms of RMSE in summer of 7.3 degrees and a lowest error in winter of 2.74 degrees, Model F3 consistently shows the highest performance.

Table 5.4. RMSE of temperature prediction for different seasons

RMSE	**Models**							
	F1	F2	**F3**	F4	F5	F6	F7	F8
Summer	7.42	7.21	**7.30**	8.27	10.81	8.99	20.21	20.07
Monsoon	2.61	3.66	**2.74**	3.36	5.31	3.31	13.50	13.34
Winter	3.11	4.19	**3.07**	3.95	5.28	3.74	11.58	13.04
Correlation coefficient								
Summer	0.90	0.89	**0.90**	0.90	0.87	0.89	0.88	0.87
Monsoon	0.97	0.95	**0.97**	0.96	0.97	0.97	0.93	0.92
Winter	0.98	0.95	**0.97**	0.96	0.97	0.97	0.95	0.93
R^2								
Summer	0.81	0.79	**0.81**	0.81	0.75	0.79	0.77	0.75
Monsoon	0.94	0.90	**0.94**	0.92	0.93	0.93	0.87	0.85
Winter	0.95	0.91	**0.95**	0.91	0.94	0.95	0.90	0.87

Predictive model development should consider regional climatic trends because of the seasonal fluctuations in model performance. A well-balanced model that can handle the variety of climatic conditions throughout the year is important, and Model F3, which consistently outperformed all other models across all seasons, is a good example. The plots of predicted panel temperature with respect to recorded panel temperature for Model F3 are plotted and annexed in Appendix A5. The plots of the summer months (May and June), winter (January and February) and monsoon season (July and August) are shown in Figure 5.2.

The plots shown in Figure 5.2 outline the robustness of model F3, it not only predicts well in all the seasons, but it also captures higher temperatures of 65 degrees with equal precision as lower temperatures of 2 degrees during winters. The high humidity during monsoon is well captured by the model, visible from the plot of monsoon months July and August.

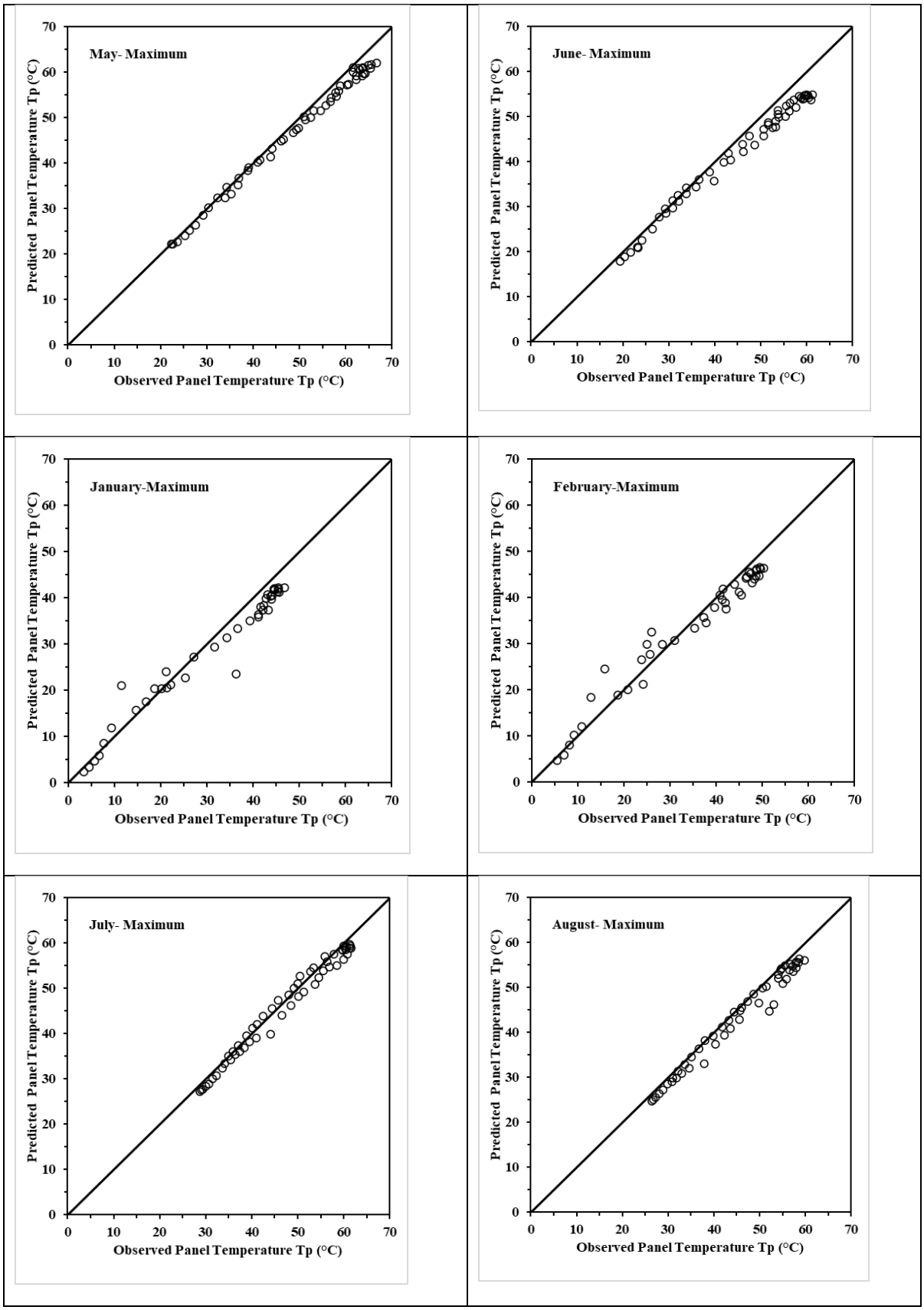

Figure 5.2. Plots of predicted panel temperature by model F3 with respect to recorded panel temperature for summer months (May and June), winter (January and February) and monsoon season (July and August).

The RMSE during summer, winter and monsoon are in proportion of the temperature of the panels. The temperature during summers is as high as 70 degrees while temperature during winters remains in the range of 45 degrees, so the model is performing equally well in all the seasons.

Overall, results highlight the necessity of incorporating seasonal environmental variability into predictive models for solar panel temperature to ensure dependable and accurate power estimation annually.

5.4.2 Evaluation of power output from developed models

The models were tested for power estimation to see the impact of error in the prediction of temperature. The power is estimated using Equation 5.15 given below:

$$Power = G_T \text{x}\, A_M \text{x}\, \eta_{Mref}(1 - \beta_{Mref} \text{x}(T_M - T_{ref})) \quad (5.15)$$

where G_T is solar insolation in W/m^2, A_M = Area of the module in m^2, η_{Mref} = module efficiency at NOCT, β_{Mref} = power temperature coefficient in %, T_M = module temperature in °C and T_{ref} = NOCT temperature 25°C. For present case module area A_M = 1.9345 m^2, η_{Mref} = 16.1%, β_{Mref} = 0.5% W/°C.

Power estimations were done for the highest and lowest solar insolation days on two typical days within each month. This was based on information gathered over a 12-month period. The estimated power production was then contrasted with the temperature data gathered from the modules and the temperature forecasts from the different models, as shown in Table 5.5.

Table 5.5. Power estimate of 24 days in a year (April 2021- March 2022) using maximum and minimum insolation days in each month and percentage error w.r.t recorded data

	Recorded data	**Model F1**	**Model F2**	**Model F3**	**Model F4**	**Model F5**	**Model F6**	**Model F7**	**Model F8**
Power Estimated (Wh)	20372	20293	20303	**20362**	20309	19639	19999	18435	18410
% above/ below the Recorded data		-0.53	-0.49	**-0.20**	-0.46	-3.74	-1.98	-9.64	-9.76

A typical May Day with maximum solar insolation is depicted in Figure 5.3 along with the expected temperature for that day using data from all eight models. it is clear as indicated in Table 5.5 that Model F3 produced the accurate power estimation. It's interesting to note that both Model F2 and Model F4, which comes second in accuracy, consider water temperature rather than ambient temperature.

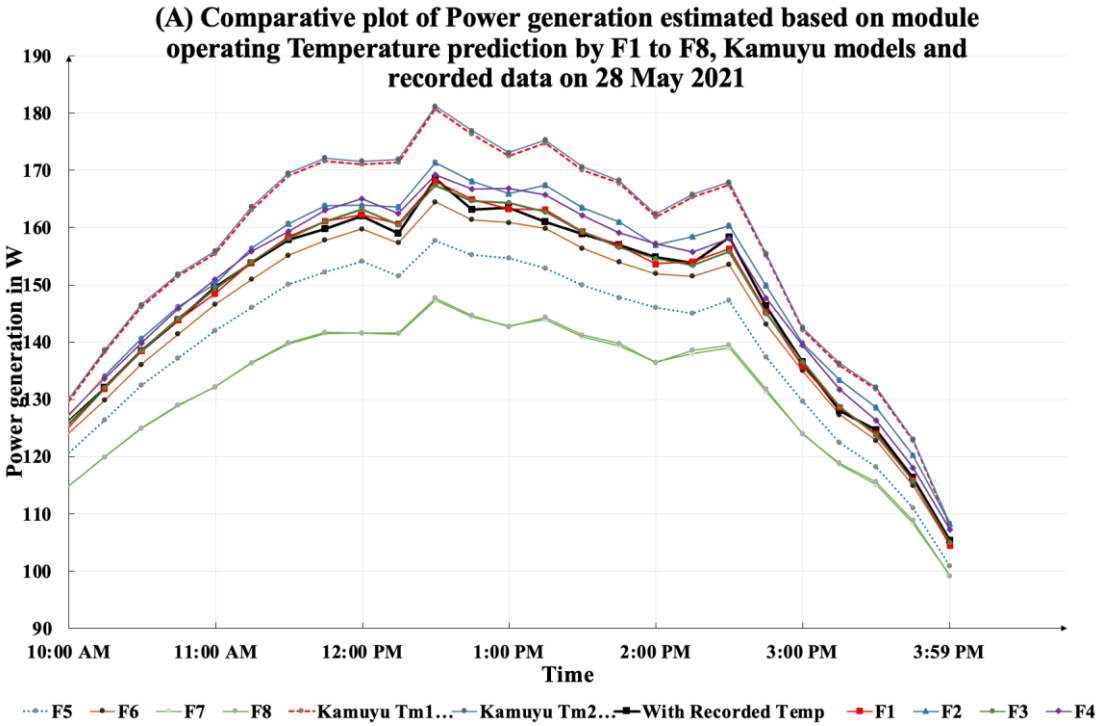

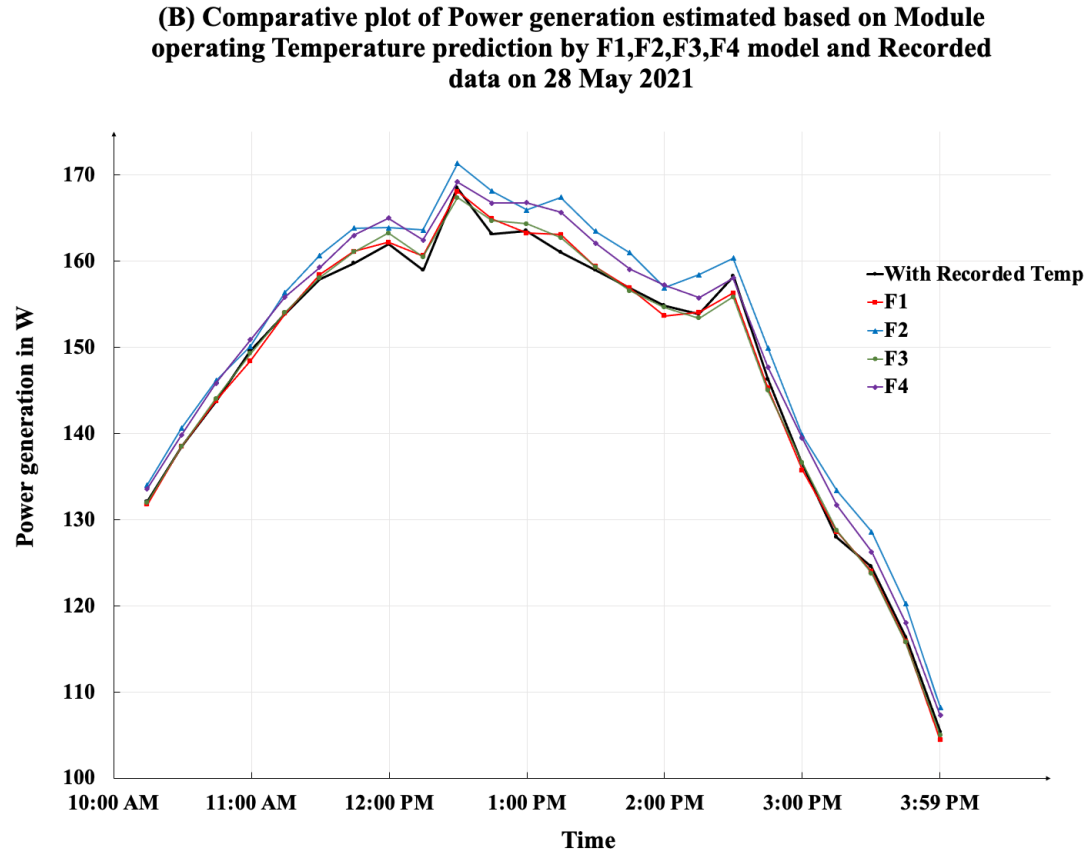

Figure 5.3. Power estimate for a typical day of maximum insolation in May 2021 (A) from recorded panel temperature data, estimates from F1 to F8 model, and the models from Kamuyu et al. (2018) (b) from recorded panel temperature data estimates from best-performing temperature models F1, F2,F3,F4 model.

In addition to this, the model by Kamuyu et al. (2018), for floating PVs' module operating temperature was used to estimate the power production. With the Tm1 model as given in Equation 5.4, this model's power estimation error was 4.10%, while with the Tm2 model given by Equation 5.5, it was 4.31%.

Figure 5.3 displays the power estimate from recorded panel temperature data, estimates from F1-F8 models, and the models from Kamuyu et al. (2018).

5.4.2.1. Assessment of power output from developed models: seasonal variation

Across several seasons, the power output calculated from the module operating temperature of all the models was also investigated. Seasonal variations on power estimate of 24 days in a year (April 2021- March 2022) using maximum and minimum insolation days in each month and percentage error with respect to recorded data are given in Table 5.6.The model tested for seasonal variation in power prediction shows a variation of -1.19% in summer to 0.07% in winter for model F1, while model F2 shows a variation of -1.10% in summer to 0.12% in winter. Model F3 is also three parametric using solar insolation, wind velocity, and ambient temperature shows lowest variation of -0.35 in summer and 0.59 in winter. Model F4 is four parametric using solar insolation, wind velocity, humidity, and water temperature. Model F4 shows a variation of -1.09% in summer to 0.34% in winter. Other models, F5, F6, F7, and F8, vary from -1.49% to -10.44%. These models were developed to observe the effect of humidity, water temperature, and nonlinearity. These models were developed to observe the effect of humidity, water temperature, and nonlinearity. The nonlinear regression models are not representing any improvement in the prediction even with all five variables. Thus, the linear models with three variables are the best representative models.

Table 5.6. Seasonal variations on power estimate (April 2021- March 2022)

Season	Power parameter	Recorded data	Model F1	Model F2	Model F3	Model F4	Model F5	Model F6	Model F7	Model F8
Summer	Power Estimated in Wh	7809	7716	7723	**7782**	7724	7474	7604	6994	7000
	% above or below the Recorded data		-1.19	-1.10	**-0.35**	-1.09	-4.29	-2.63	-10.44	-10.36
Monsoon	Power Estimated in Wh	5317	**5296**	5295	5261	5284	5125	5238	4785	4795
	% above or below the Recorded data		**-0.39**	-0.41	-1.05	-0.62	-3.61	-1.49	-10.00	-9.82
Winter	Power Estimated in Wh	7276	**7281**	7285	7319	7301	7040	7157	6656	6615
	% above or below the Recorded data		**0.07**	0.12	0.59	0.34	-3.24	-1.64	-8.52	-9.08
Annual	Power Estimated in Wh	20402	20293	20303	**20362**	20309	19639	19999	18435	18410
	% above or below the Recorded data		-0.53	-0.49	**-0.20**	-0.46	-3.74	-1.98	-9.64	-9.76

The results of this investigation showed that the most accurate predictions were made using three-parameter models that included solar insolation, wind speed, and either ambient or water temperature. The prediction was worsened by two-degree regression models, and the prediction was not improved by adding all five parameters. Additionally, the impact of water temperature was not much stronger than that of ambient temperature. These findings help to improve the design and operation of solar energy systems by offering helpful insights into the critical variables determining power output.

5.4.3. PV panel operating temperature variations: comparison of floating vs. Ground-mounted PV panels

The goal of the comparative study is to look at how the operating temperatures of floating and ground-mounted photovoltaic (PV) panels differ. The temperature measurements of both panel types across several seasons must be analyzed to fully comprehend the significance of these variances.

The seasonal maximum, minimum, and average panel operating temperatures for solar panels of floating and ground-mounted panels are shown in Table 5.7.

Table 5.7. Seasonal maximum, minimum, and average panel operating temperature of floating and Ground mounted panels

Season	**Summer**		**Winter**		**Monsoon**	
	Panel over water bodies (°C)	**Panel over** Ground **Mount (°C)**	**Panel over water bodies (°C)**	**Panel over Ground Mount (°C)**	**Panel over water bodies (°C)**	**Panel over Ground Mount (°C)**
Maximum Temperature	66.68	70.86	59.57	63.73	65.55	70.87
Minimum Temperature	14.02	13.45	-0.86	-1.37	24.26	24.38
Average Temperature	**39.50**	46.77	**25.71**	29.06	**38.33**	39.77

Despite the numbers mentioned above, it is not immediately clear how these temperature changes affect power production. Equation 5.15 was used to predict power output for both types of panels while taking the potential impact of temperature on power generation into account.

The power output was then calculated using the reported temperatures for both types of panels. Two typical days of maximum and minimum solar insolation in each month were used to determine the power production. Data collected over the course of a year was used to get these results are provided in Table 5.8.

Table 5.8. Power generation for maximum and minimum solar insolation day in a year (April 2021-March 2022)

Month	Power generated (floating) maximum insolation day (Wh)	Power generated (floating) minimum insolation day (Wh)	Power generated (GM)maximum insolation day (Wh)	Power generated (GM) minimum insolation day (Wh)
Apr-21	1280.7	555.5	1238.4	541.0
May-21	1258.1	188.7	1226.7	188.3
Jun-21	1295.1	747.2	1258.6	758.2
Jul-21	1261.7	462.5	1293.1	458.6
Aug-21	1283.9	361.6	1248.5	355.8
Sep-21	1120.9	504.2	1090.7	491.8
Oct-21	1219.9	292.1	1194.3	288.6
Nov-21	953.9	634.6	926.2	622.4
Dec-21	981.7	203.1	952.1	201.7
Jan-22	1105.3	213.1	1066.9	211.5
Feb-22	1245.0	427.6	1198.2	422.9
Mar-22	1307.4	1038.0	1256.7	946.3

The projected power generation for each month is shown graphically in Figure 5.4. The findings demonstrate that floating solar panels provide 2.59% more power generation yearly than PV systems that are installed on the ground. This finding implies that ground-mounted PV panels maintain an average temperature that is roughly six degrees higher than floating PV panels. Due to the substantial lowering of temperature, floating PV systems clearly outperform ground-mounted ones in terms of power output.

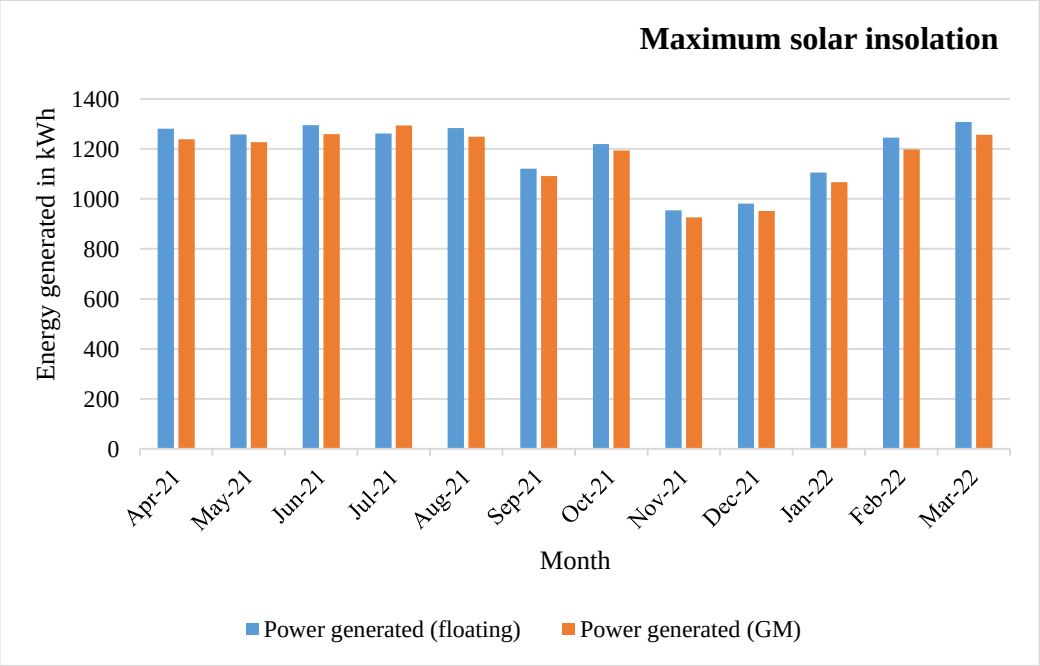

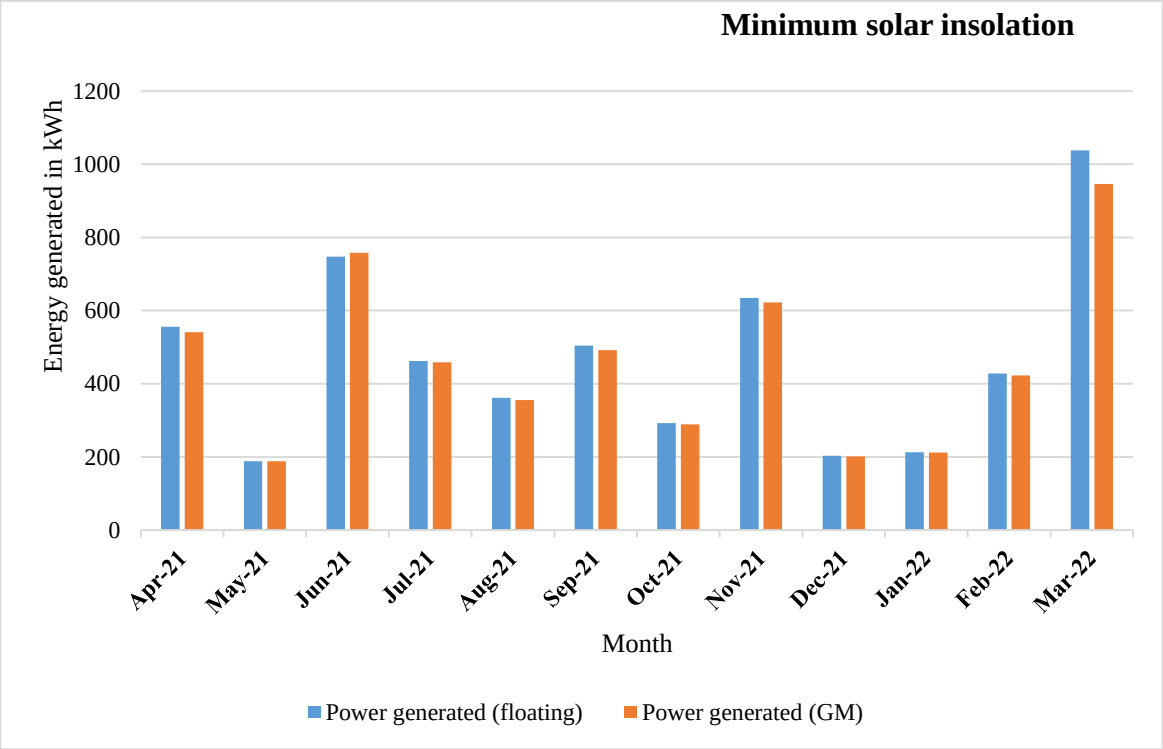

Figure 5.4. Monthly power generation of Ground-mounted and floating PV installation for (a) maximum and (b) minimum solar insolation day of each month from April 21-March 22.

5.5. Summary and Recommendations

The study found that the average operating temperature of modules mounted over the ground is six degrees higher than those mounted over water. Regression analysis was used to develop and validate models for predicting the operating temperature of floating solar PV modules. The models incorporated various meteorological parameters, including ambient temperature, solar insolation, wind velocity, water temperature, and humidity. The study concluded that-

- The three parametric models, F1 and F3, which utilized ambient temperature, solar insolation, and wind velocity, predicted panel operating temperature the best, with a maximum root mean square error (RMSE) of 5.64°C and 5.50°C, respectively. On the other hand, three parametric models replacing ambient temperature with water temperature, F2 and F4, predicted panel operating temperature less accurately, with a maximum RMSE of 8.26°C and 9.43°C, respectively.
- The study also found that the one-degree regression model with all five parameters did not add to the accuracy of the prediction model. However, the two-degree regression models were complex, with an RMSE of more than 20°C.

- Finally, the study found that best model is F3 which can be used to predict the operating temperature of the panel and power estimates, assessing the module's overall performance.
- The use of floating solar PV installation instead of ground-mounted PV installation, as it can provide a higher power output of 2.59 % annually. It was found that lowering the temperature can increase power production and reduce the soiling of panels.

Based on the outcomes of this study following recommendations are proposed:

- Floating solar PV systems should be preferred to ground-mounted ones due to lowering of operating temperatures by 6 ^{o}C. The study found that floating solar PV installations consistently produced 2.59 % more power than ground-mounted solar PV installations. Additionally, a possible decrease in panel soiling may result in lower maintenance expenses, increasing the cost-effectiveness of such systems.
- The temperature predictions made by the predictive model F3, which used ambient temperature as a parameter, were the most accurate. In order to estimate operating temperatures for floating PV installations, it can therefore be very useful tool.

Chapter 6

Assessment of Floating Solar Photovoltaic (FSPV) Potential and Water Conservation: A Case Study of Rajghat Dam and Prospective FSPV Potential Assessment of Major Dams in Uttar Pradesh, India

Abstract

Widely acceptable Photovoltaic (PV) technology faces the challenge of substantial land requirement. However, emerging PV technology over water bodies through floating solar panels can resolve this challenge and additionally leads to operation of the panels at low temperature, improving the energy generation efficiency and insulating water bodies to account for reduction in evaporation loss. In this work, simulation tasks are performed to assess the technical potential of floating photovoltaic power generation and discusses the sustainable system of floating solar PV technology in terms of prospective PV potential, conservation of water and potential to conserve agriculture land bank. The study estimates, power potential of 6513 MW_p for 25% coverage of total submergence area at Rajghat dam located in the Southern part of Uttar Pradesh, India, and annual power generation of 10,623,501 MWh. The study also reports annual evaporation loss reduction of 1395 cubic meter per MWp (or 0.9 l per kWh) as an additional benefit. In terms of economic assessment, the Levelized cost of energy (LCOE) is reported as $ 0.036/kWh (INR 2.61/kWh) with 8.55% internal rate of return (IRR), a very encouraging parameter for large scale deployment of FSPV plants. Based on these findings, the study estimated the FSPV installation potential over major reservoirs of Uttar Pradesh to be 37,762 MWp with 25% area coverage, and 15,093 MWp with 10% area coverage. Further, the study recommends FSPV installation over water bodies, justified by considerable savings in water evaporation losses and avoiding use of cultivable land for solar PV Installation purpose.

6.1. Introduction

The study presented in this chapter explores the potential advantages of floating solar PV (FSPV) installations over water bodies and evaluates the possibilities for implementing them. The research investigates the technical potential and economic viability of FSPV focusing on the potential benefits of this innovative approach to renewable energy production. In order to assess the possibilities of floating solar PV technology, a case study is done on the Rajghat Dam in Uttar Pradesh, India. Because of its sizeable open space and the presence of an existing hydroelectric power plant right next to it, the Rajghat Dam makes a great case study location.

The primary objective of this chapter is to provide a general overview of the significance of evaluating the possibility of installing floating solar PV on water bodies, particularly in the context of the Rajghat Dam. Recent studies have shown that it is now feasible to use underutilized water locations for renewable energy production by installing solar panels on water bodies like dams and reservoirs. This approach offers numerous advantages, including increased solar energy capacity, optimal use of land resources, and potential water conservation (Nguyen et al,2021).

Due to its features and existing infrastructure, the Rajghat Dam is an important site for the case study. The dam's 39 MW hydroelectric power-producing capacity now feeds energy to the neighbourhood grid via the nearby 132 KV GSS (CEA, 2018). Due to the lower FLH (Full Load Hours) of the hydropower plant compared to conventional hydropower plants and the principal use of the dam as a source of irrigation, the present hydropower plant runs at a lower capacity than anticipated (CEA,2018).

The Rajghat Dam offers a chance to increase power generation capacity while complementing the work of the current hydroelectric facility with floating solar PV arrays. It is conceivable to perform load balancing, enhance grid stability overall, and maximize the use of the water body for renewable energy generation by integrating floating solar PV with the infrastructure (Nguyen et al.,2021). Given that the hydropower plant operates at its peak during the monsoon season when solar power generation is at its lowest, this integration is an efficient way to fulfill the daily and seasonal changes in electricity demand (CEA,2018). On the other hand, the floating solar power plant would produce the most solar energy during the summer, when the Rajghat dam's water storage capacity is at its lowest (CEA,2018).

For several reasons, evaluating the potential of floating solar PV over water bodies is very important. Firstly, it enables the use of large water surfaces for solar energy production without requiring additional land use or raising environmental issues like those caused by ground-mounted solar facilities. This aspect is particularly valuable in regions with limited available land for large-scale renewable energy projects. Secondly, floating solar PV installations have demonstrated higher energy yields compared to their ground-mounted counterparts due to the cooling effect of water and the potential for increased solar irradiance reflection. This higher energy yield contributes to increased renewable energy generation and reduces dependence on fossil fuel-based power generation.

Additionally, the integration of floating solar PV with water features offers a chance to address problems with water resource management. Floating solar panels can lower water

evaporation loss by covering a portion of the water's surface, saving water supplies and increasing overall water availability (Rosa-Clot et al.,2017; Bontempo Scavo et al.,2021). This element is especially important in water-stressed tropical areas like Budelkhand/Vindhyachal region of Uttar Pradesh, where water scarcity impacts many industries, including agriculture and drinking water delivery.

In brief, it is critical to evaluate the potential of floating solar PV on water bodies, particularly at the Rajghat Dam in Uttar Pradesh, India, in order to maximise the production of renewable energy, improve the management of water resources, increase grid stability, and promote sustainable development (Rosa-Clot et al.,2017). The methods used to evaluate the potential will be covered in detail in the following sections of this chapter that follow. The chapter also delves into the technical and economic issues and offers the findings and discussions.

6.2. Methodology

A thorough methodology and strategy were used to examine the floating solar PV (FSPV) potential of the Rajghat Dam in Uttar Pradesh, India. Drawing on pertinent literature and research in the Indian context, this part provides a thorough overview of the methodology, data sources, tools, and parameters taken into account in the evaluation.

The methodology's first phase entailed acquiring relevant information about the Rajghat Dam location. Reports from the Central Electricity Authority (CEA,2018), which offered details on the size of the dam and the amount of power produced by the current hydroelectric power plant, were among the data sources. Meteonorm weather data has been used to ensure correct input for the analysis by providing historical weather data and sun irradiance levels. The water surface was also visualized and used as a tool in the assessment process using satellite data from sources like Google Earth and AutoCAD from Autodesk.

The following stage entailed evaluating the Rajghat Dam's FSPV's technical and geographical potential. Taking into account elements including shade, inter-row spacing, and structural constraints, this research sought to calculate the maximum capacity of FSPV installations that could be accommodated on the water surface. This was accomplished by using the popular PVsyst software (PVsyst SA,2021), which enables the simulation of a variety of parameters including module tilt degrees, orientation, and system losses. When taking into account the unique features of the Rajghat Dam site and the FSPV system, PVsyst offers precise predictions of the potential for energy production.

Studies and approaches that have already been conducted were used to evaluate the possible advantages of FSPV in minimizing water evaporation. Youssef & Khodzinskaya (2019), did a thorough assessment of several techniques for reducing evaporation from water surfaces. Urban Water Security Research Alliance studies conducted by Yao et al. (2010) showed that floating covers can conserve 68–76% of water by reducing evaporation loss.

By placing solar panels over water features in Singapore reservoirs, Melvin & Xiang (2015) discovered a 30% decrease in evaporation loss rates. Rosa-Clot et al. (2017), showed that enclosing lagoons with floating solar PV systems can reduce evaporation by 90%. Bontempo Scavo et al.(2021), quantified the evaporation loss reduction based on the coverage area of FSPV installations. The Rajghat Dam's potential for evaporation reduction was estimated utilizing the information from these studies.

After that, an economic analysis was done to determine whether FSPV on the Rajghat Dam would be a financially viable alternative. In this analysis, levelized cost of energy (LCOE), operation and maintenance (O&M) costs, and capital expenditures (CAPEX) costs were taken into account. Utilizing the CAPEX, OPEX, discount rate, system lifetime, and capacity utilization factor (CUF), the levelized cost of energy (LCOE) was determined. The discount rate, which reflects the opportunity cost of capital, was established at a 12% level following industry norms. Given the normal operating lifespan of solar PV systems, a 25-year system lifespan was anticipated. Based on the local solar irradiation levels and system losses, the CUF, which represents the actual energy generation as a percentage of the system's rated capacity, was estimated. The cost of electricity generated by the FSPV system over its lifetime, including capital and operating costs, was revealed by the LCOE analysis.

A thorough evaluation of the FSPV potential on the Rajghat Dam was made possible by the technique used in this study. An integrated understanding of the advantages and viability of applying FSPV on water bodies in the Indian tropical setting was made possible through the integration of technical analysis, evaporation reduction assessment, and economic analysis.

6.3. Results and Discussions

6.3.1. Technical potential

To determine the viability and capacity of implementing FSPV systems at this location, the technical potential of floating solar PV (FSPV) installation over the Rajghat Dam in Uttar Pradesh, India, was assessed. The dam provides enough room for FSPV installations, with a maximum dam height of 39 m and a water depth of 33 m at full reservoir level (FRL). About 242 km^2 of the water spread at FRL is ideal for the installation of solar PV. To assess the

technical potential, various factors such as location, topography, solar irradiance, and ambient temperature were considered. The coordinates of the Rajghat Dam were used to calculate solar path as shown in Figure 6.1 and analysed the solar insolation using PVsyst 7.0 software (Mateonorm database). The software provided valuable data on horizontal insolation and surface temperature for each month of the year shown in the Table 6.1. These variables are essential for evaluating the dam's solar energy capacity and figuring out the technical feasibility of installing FSPVs.

Table 6.1. Horizontal insolation and ambient temperature at Rajghat Dam.

Month	**Ambient Temperature (°C)**	**Horizontal Solar insolation Monthly (kWh/m^2)**	**Horizontal Solar insolation Daily average (kWh/m^2 /day)**
January	16.51	124.2	4.01
February	20.19	143.1	5.11
March	26.06	184.4	5.95
April	30.95	194.7	6.49
May	34.53	207.4	6.69
June	31.79	174.1	5.80
July	28.29	147.1	4.75
August	27.02	142.1	4.58
September	27.47	154.4	5.15
October	26.58	159.9	5.16
November	21.84	129.7	4.32
December	18.20	122.8	3.96
Year	**25.81**	**1883.8**	**5.16**

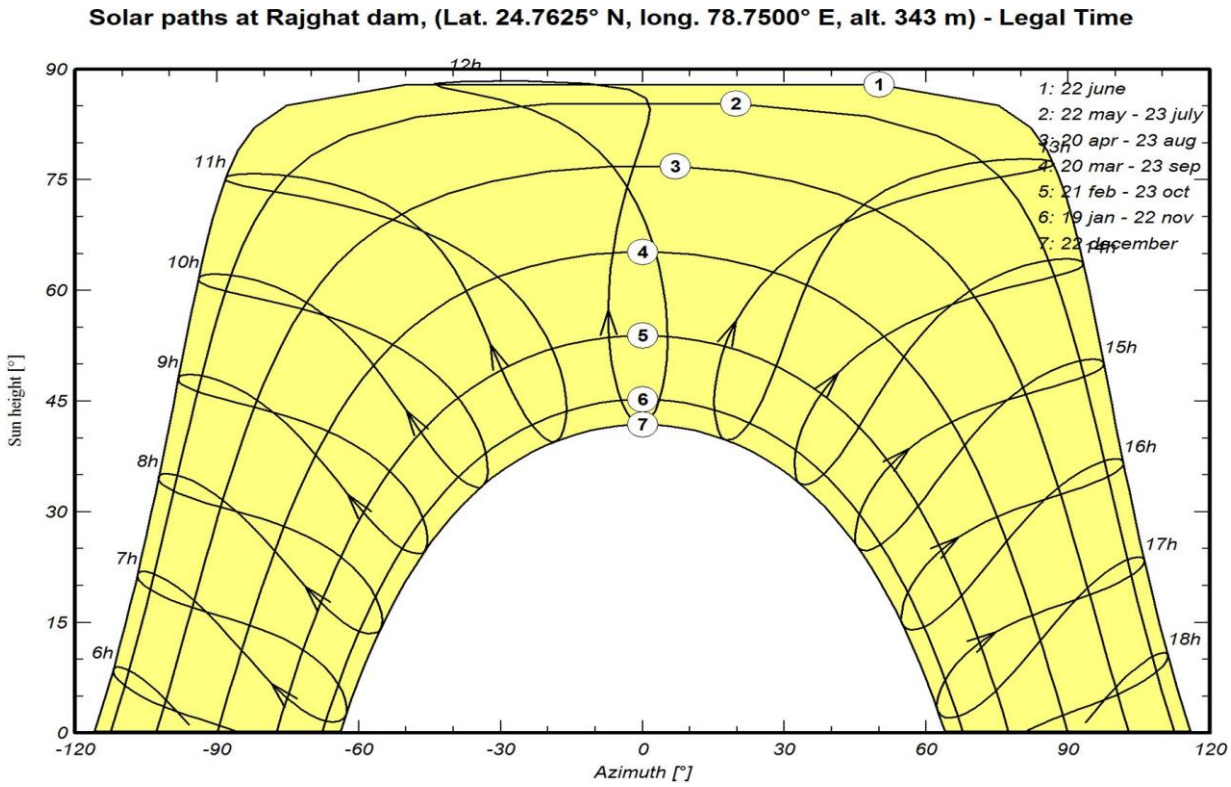

Figure 6.1. Solar path at Rajghat dam (PVsyst 7.0)

Based on the suggested surface area distribution, the technical capability of FSPV on the Rajghat Dam was assessed. For PV installations on water bodies, previous research by Perez et al. (2018) and Acharya & Devraj (2019) revealed varying percentages of surface area use. As a result of the Rajghat Dam's unique features, it was determined that 25% of the total submerged area at FRL, or roughly 6,052 hectares (24,210 ha at FSL) (Uttar Pradesh Irrigation and Water Resources Department data), could be covered by a floating solar PV installation.

The accessible surface area for FSPV installations was modelled using Google Earth and AutoCAD software to determine geographic potential. For the modelling process, 350 Wp monocrystalline technology PV modules with a 17.7% efficiency were taken into consideration. A surface area of about 2 m^2 was represented by each module. On the 6,052 hectares of usable surface, there are 6,513 MWp in total installed PV capacity. The approximate 3,450 hectares of buildable space were taken into account in this capacity estimate, while the remaining 3,063 hectares were set aside for the transportation of boats and other machinery for operation and maintenance as shown in Figure 6.2. When taking into account logistical needs, the utilisation of about 14.25% of the total submerged area was sufficient.

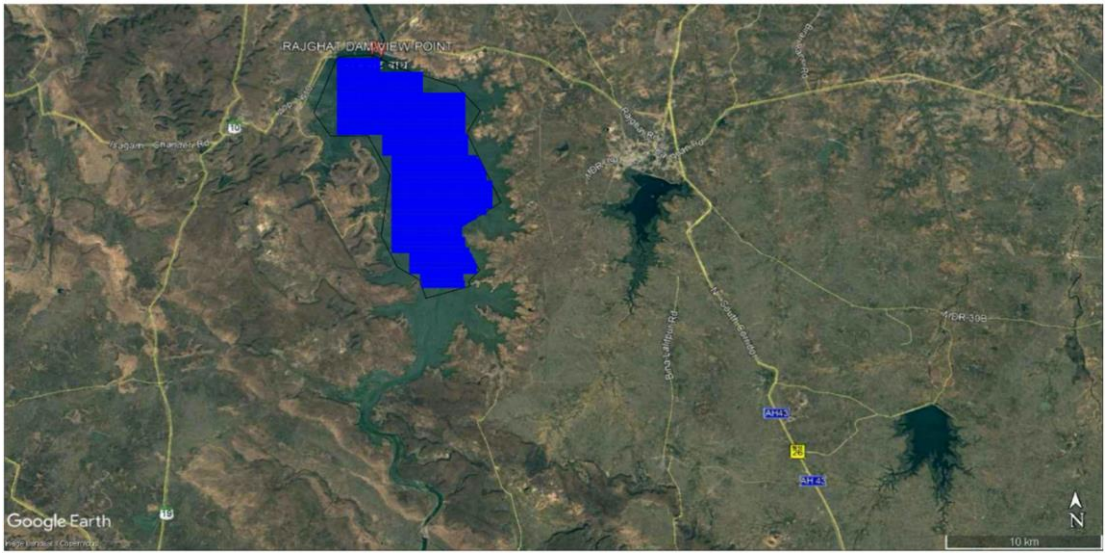

Figure. 6.2. PV Modules superimposed on water surface (Source: Google Earth and Auto cad from Autodesk).

The annual energy production from the FSPV systems was estimated as part of the technical potential assessment. A total of 10,623 GWh of energy and 6.05 GW of electricity were estimated to be produced annually by the Rajghat Dam. As a result, the FLHpv (Factor of Load and Hour=EL/PH, where EL is yearly energy production in GWh and PH is peak power in GW) was 1,756 hours, and 1.76 GWh of energy was produced per ha annually.

Furthermore, it is significant to remember that the Rajghat Dam already includes a hydropower facility with a 45 MW capacity. Effective power generation and grid integration are made possible by the integration of FSPV systems with the existing hydropower plant. According to the CEA (2018), report, the power generated from this plant was 87.6 MU in 2018. The FLH of a hydropower plant is 1946 hrs which is typically lower than the normally expected from hydropower plants. The power generation per sq. meter of submerged area is 0.1858 W, which is significantly lower than the power generation of FPV. This may be due to the reason that the reservoir is primarily built for irrigation purpose. The electricity generated from the floating solar power plant can be fed to the existing GSS. The floating solar power plant can run in tandem with the existing hydropower plant which represents an effective integration to meet the daily and seasonal demand variation. The hydropower plant will operate at its peak during monsoon season when solar power generation is minimal. The solar power generation from floating solar power plants shall be at its peak during the summer season when water availability in Rajghat dam reduces significantly. Further, it can be noted that the floating solar capacity installation is larger than the existing hydropower generation; the surplus power from floating solar can be used through a pumped hydro storage system for the successful integration of solar PV with the grid. The evaluation of the Rajghat Dam's technological potential offers important insights into the installed capacity, usable surface

area, and energy generation capability of FSPV systems. The findings highlight the suitability of the location for large-scale FSPV implementation, taking into account the geographical and environmental factors of the site.

6.3.2. Reduction in evaporation losses due to FSPV

The reduction of evaporation losses from water bodies is a critical aspect of water resource management, particularly in tropical regions facing water scarcity. Floating solar PV (FSPV) installations have emerged as a promising solution to mitigate evaporation and conserve water resources. Various studies have explored the potential of FSPV in reducing evaporation, offering valuable insights into the effectiveness of this approach.

Youssef & Khodzinskaya (2019), conducted a comprehensive review of evaporation reduction techniques and highlighted the significance of floating covers. According to their findings, floating covers can save a substantial amount of water, ranging from 68% to 76%. However, the implementation cost of such techniques can be a limiting factor. FSPV plants, characterized by their installation on water bodies such as reservoirs, dams, and ponds, play a crucial role in reducing evaporation. These installations not only shield the water surface from solar radiation but also act as windbreakers, influencing the evaporation process. Melvin & Xiang (2015), conducted a study on the impact of solar panels on water evaporation in Singapore reservoirs. Their findings revealed that FSPV installations can effectively reduce evaporation rates by approximately 30%.

Another study by Rosa-Clot et al. (2017), focused on covering lagoons with FSPVs and evaluating evaporation reduction compared to open surfaces. Using the Penman-Monteith equation, they estimated a remarkable 90% reduction in evaporation when lagoons were covered with FSPVs. Furthermore, Perez et al. (2018), investigated the water conservation potential of FSPV by analyzing 128 reservoirs in the United States with complete FSPV coverage. They reported a significant conservation of 28,000 million cubic meters of water.

Bontempo Scavo et al. (2021), conducted an in-depth analysis of various FSPV typologies and their evaporation reduction potential. Their research involved comparing evaporative models with a design of experiment (DoE) model, leading to the development of a reliable linear regression model. Their findings revealed that the evaporation reduction for suspended-type FSPV installations ranged from 6% to 60% based on coverage percentages, while direct contact floats exhibited an estimated evaporation reduction ranging from 18% to 100%.

In the context of the Rajghat Dam, the assessment of evaporation reduction considered a coverage area of 25% based on our experimental results. This estimation suggests that the

installation of a 6,513 MWp FSPV system at the Rajghat Dam could potentially save approximately 9.084 million cubic meters of water from evaporation losses. Such a reduction amounts to about 0.47% of the total reservoir capacity holds significant implications for water conservation efforts. The estimated evaporation reduction translates to approximately 1,395 litres per kilowatt peak (l/kWp) of installed FSPV capacity.

6.3.3 Economic Assessment

The economic assessment of the floating solar PV (FSPV) system at Rajghat Dam in the Indian context involves analyzing key economic metrics to determine the financial viability and feasibility of the project. Considering the specific conditions and market factors in India, the levelized cost of energy (LCOE) and internal rate of return (IRR) are important indicators used to assess the economic aspects of the FSPV system.

The geography, water body depth, system size, and market conditions all have an impact on the FSPV system's capital expenditure (CAPEX). In order to examine the project's financial sustainability and feasibility, major economic variables are analyzed for the floating solar PV (FSPV) system at Rajghat Dam in the Indian setting.

As per the information on PV investment costs, retreat from public press releases total CAPEX for FPV system in 2018 ranged between $0.8 and $1.2 per watt-peak, depending on the location, water body depth and variation, and system size (World bank Group,2019). In March 2018, India-based West Bengal Power Development Corporation Limited awarded EPC (Engineering, Procurement and Construction) bid for a 5 MWp FPV system to Ciel & Terre International on the basis lowest quote of Rs. 269.12 million (no grant provided), which corresponds to about $4.13 million or $0.83/Wp (average annual ex- change rate)(Ciel & Terre,2018). The economic assessment of the Solar power plant is based on 2 expenditures namely: Capital Expenditures (CAPEX) and Operation and Maintenance costs (OPEX).

6.3.3.1. Capital expenditure

A comparison of CAPEX available in the literature for floating solar and fixed tilt is given in Table 6.2. Some researchers have also estimated cost of fixed tilt FPV, (Rosa-Clot et al. (2017), have suggested $1.119/Wp at 2017 price level while Chico et al.(2019), have utilized Rp 31,600/Wp (Rp 13,200 = $1 US) for estimating cost of 1 MWp floating solar PV plant in Indonesia. Various researchers from different countries have estimated the cost of FPV plants ranging from USD 0.5–2.39/Wp during the period of 2015–2018. The EPC cost for India's first large scale FSPV at Kayamkulam, Kerala (India) based on tenders received in 2018 is USD 0.50/Wp. The costs achieved for EPC are site-specific and have certain hidden costs, so

the same cost cannot be utilized for estimation purposes. So, a cost analysis has been done based on market surveys and experience.

Table 6.2. Comparison of CAPEX for Floating and Ground Mounted Solar System

CAPEX Component	World Bank Floating Solar Market Report*	TERI Report (Acharya & Devraj,2019)
	FPV 50 MWp ($/Wp)-2018	FPV 70 MWp ($/Wp)-2018#
Modules	0.25	0.19
Inverters	0.06	0.06
Mounting System	0.15	0.16
BOS	0.13	0.06
Design, Construction, T&C	0.14	0.01
Total CAPEX	0.73	0.50

 # $1 = Rs. 70.09, assumed for 2018 by TERI

** World Bank Group (2019)*

6.3.3.2. Cost analysis of floating solar PV plants

The Floating Solar PV (FSPV) plants utilize mono or polycrystalline modules and string or central inverters are being utilized, however, central inverters are recommended for large-scale plants. A standard PV module price of $ 0.22/Wp and a cost of the central inverter of $ 0.03 have been utilized for estimating the Levelized cost of electricity. The cost analysis is given in Table 6.3 and shown in Figure 6.3.

Module Mounting Structure (MMS) involves civil construction as well as structure, anchoring and mooring system which depends on parameters such as bathymetry, water level variation, wind and wave characteristics, type of bank and water quality and level of salinity. These parameters are site-specific and cost varies from project to project. However, based on queries made with companies working in this field cost of floating structures including anchoring and mooring ranges between $0.12/Wp and $0.22/Wp. An average cost of $ 0.14/ Wp has been utilized for the Levelised cost of electricity.

The balance of the system includes equipment such as a combiner box, switchboard, transformer, cable and monitoring system SCADA. A cost of $0.13/Wp has been adopted based on experience and quarries. The higher cost of cable is due to high insulation to check current leakage, cable routing and slack requirement for constant movement of floating installation would be required. Installation, commissioning and other expenses based on experience and queries have been taken as $0.08/Wp. The cost enumerated above is for a fixed mounting structure.

Table 6.3. Cost analysis of floating solar PV plants.

S. No	Parameter	Cost ($/Wp)
1	PV Panel	0.22
2	Inverter	0.03
3	Mounting Structure, Design, civil construction	0.14
4	Electrical/Balance of system	0.13
5	Installation cost, land cost and other expenses	0.08
	Total	**0.60**

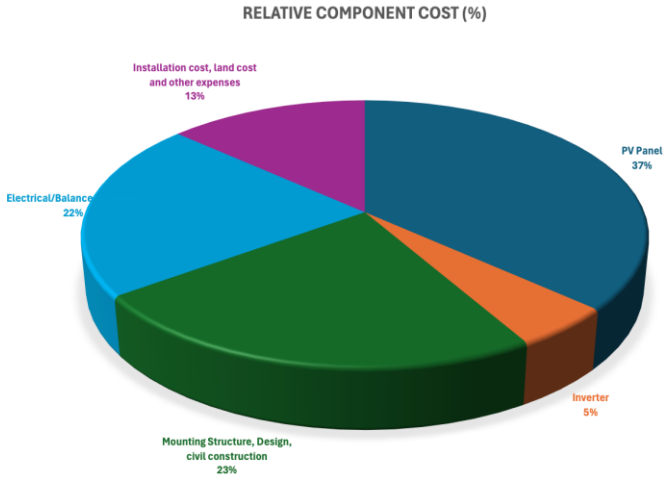

Figure. 6.3. Cost component of floating solar PV plant.

6.3.3.3. Operation cost (OPEX)

This cost includes operation and maintenance (O&M), insurance, inverter replacement cost and leasing cost of water body. Leasing cost of water bodies have wide variation across the globe, so this component has not been considered in the financial calculations. The O&M cost varies depending on the site conditions, which have several factors such as annual variation in water level, wind speed and wind pressure, inspection of mooring cables and anchoring system at regular interval. Replacement of parts or equipment is complicated and time consuming and it also involves safety issues, which potentially adds to maintenance cost.

World Bank Group and Energy Sector Management Assistance Program; Solar Energy Research Institute of Singapore (2019) have recommended $0.011/Wp as the O&M cost for floating solar. Floating PV is in the nascent stage of development and not much data is available, so a value suggested by World Bank floating solar market report (2019) as 0.3% of the system price, paid annually and adjusted to the inflation rate, which is same as for the utility scale ground mounted PV projects. Inverter manufacturer normally offers warranty for 5–12 years, so during operation period proposed for project i.e. 20 years at least once the inverter has to be replaced. World Bank floating solar market report (2019) have suggested a cost of $0.039/Wp for inverter maintenance cost. So OPEX proposed by World Bank floating

solar market report (2019) as $0.072/Wp. (Ciel et terre.,2020) have utilized 3% of CAPEX as OPEX for estimating LCOE, for which no reasoning is given, while (Barbuscia ,2018) have suggested ₵4.26/kWh as OPEX. However, (Barbuscia ,2018) has proposed breakup for OPEX cost; he suggested four components with their weightage, 69% for management and ad- ministration, 12% annual monitoring and maintenance, 17% onsite re- placement and works and 3% major replacements and works onshore. He also assumed 6 onsite visual inspection and module cleaning per year, 4 technical periodic maintenances (mainly for structure and inverters) per year and 2 under water visual inspections with Remotely Operated Vehicle, per year. For present study OPEX has been considered as $0.072/Wp based on market survey and experience, which is also suggested by World Bank floating solar market report (2019) based on detail analysis of existing data.

6.3.3.4. Levelised cost of energy (LCOE)

In order to determine the suitability of technologies discussed above, the cost components such as capital cost, Operation & Maintenance cost, interest rate, Capacity Utilization Factor (CUF) etc. were compared with generated income. An economic assessment has been carried out in terms of Levelized Cost of Energy (LCOE) and Internal rate of return (IRR).

6.3.3.5. Sensitivity analysis of Levelized Cost of energy (LCOE)

A sensitivity analysis of the financial assessment has been conducted, with Table 6.4 illustrating the variation in LCOE across different cost components.

Table 6.4. Variation of LCOE with changes in different cost components

% change in component	Variation in LCOE due to variation in CAPEX (%)	Variation in LCOE due to variation in CUF(%)	Variation in LCOE due to variation in DISCOUNT RATE (%)	Variation in LCOE due to variation in DEBT % in (%)	Variation in LCOE due to variation in OPEX (%)	Variation in LCOE due to variation in INTEREST ON DEBT (%)
0	0	0	0	0	0	0
10	8.05	-9.20	0.77	-10.73	1.92	3.07
20	15.71	-16.86	1.53	-21.46	3.83	6.13
30	23.37	-22.99	2.30	-32.18	5.36	9.20
40	31.03	-28.74	2.68		7.28	12.64
50	38.70	-33.33	3.45		9.20	15.71
-10	-7.66	11.11	-0.77	10.73	-1.92	-3.07
-20	-15.33	24.90	-1.53	21.46	-3.83	-6.13
-30	-22.99	42.91	-2.68	32.18	-5.75	-9.58
-40	-30.65	66.67	-3.45		-7.66	-12.64
-50	-38.31	100	-4.21		-9.20	-15.71

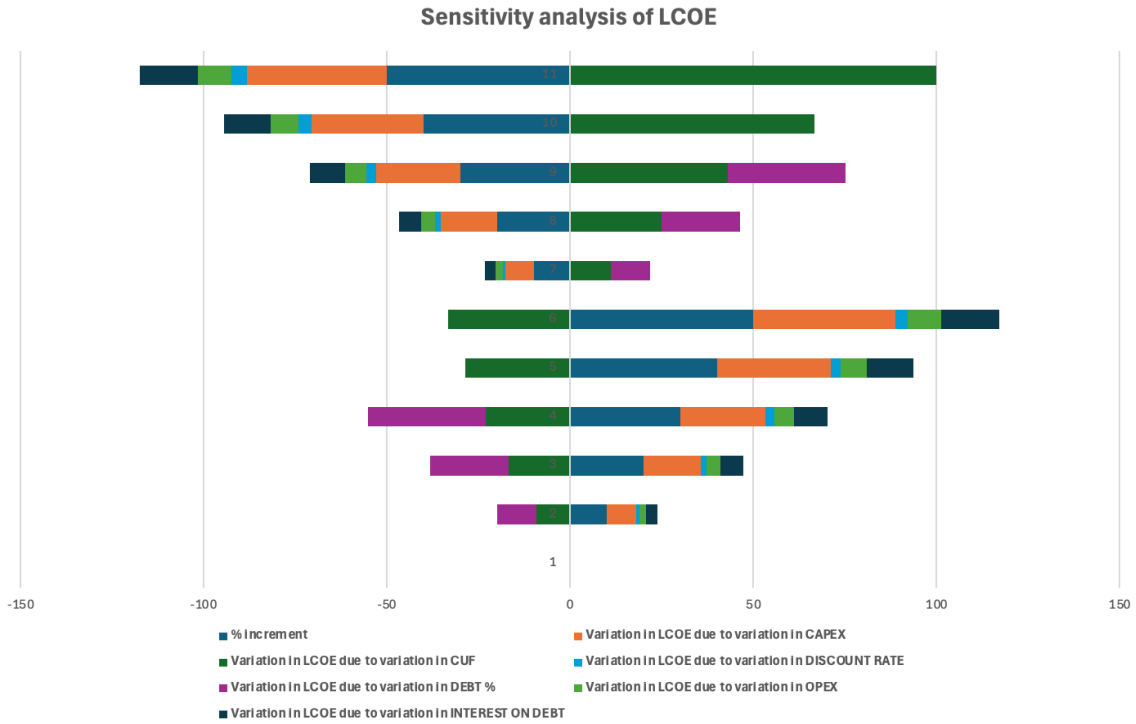

Figure. 6.4. Variation of LCOE with change in cost component of floating solar PV plant

The figure 6.4 showing the sensitivity analysis of LCOE with various cost components. The key insights derived from the sensitivity analysis of the Levelized Cost of Energy (LCOE):

Variation in LCOE due to CAPEX (Capital Expenditure)

A 10% increase in CAPEX results in an 8.05% increase in LCOE, while a 10% decrease leads to a 7.66% reduction.

LCOE is highly sensitive to CAPEX, with almost proportional changes across the range. Managing upfront capital costs is crucial to keeping LCOE competitive.

Variation in LCOE due to CUF (Capacity Utilization Factor)

- A 10% increase in CUF decreases LCOE by 9.20%, and a 10% decrease increases LCOE by 11.11%.
- This indicates that LCOE is highly sensitive to CUF changes, emphasizing the importance of optimizing system performance and efficiency to improve utilization.

Variation in LCOE due to Discount Rate

- A 10% increase in the discount rate raises LCOE by 0.77%, while a 10% decrease lowers LCOE by 0.77%.
- The impact of discount rate variation on LCOE is relatively minor compared to other factors, indicating lower sensitivity.

Variation in LCOE due to Debt Percentage

- A 10% increase in debt percentage reduces LCOE by 10.73%, while a 10% decrease raises LCOE by the same percentage.
- LCOE is highly sensitive to debt percentage. A higher proportion of debt financing can reduce LCOE but may increase financial risk.

Variation in LCOE due to OPEX (Operating Expenditure)

- A 10% increase in OPEX leads to a 1.92% increase in LCOE, while a 10% decrease reduces LCOE by 1.92%.
- OPEX has a moderate impact on LCOE. Keeping operational costs low is beneficial for long-term competitiveness.

Variation in LCOE due to Interest on Debt

- A 10% increase in the interest rate increases LCOE by 3.07%, while a 10% decrease reduces it by 3.07%.
- Interest rate variation has a moderate impact on LCOE, highlighting the need for favourable loan terms to manage costs effectively.

Overall Observations

- Most Sensitive Factors: CUF, CAPEX, and debt percentage have the highest impact on LCOE. Focus should be placed on optimizing performance, reducing capital expenditure, and evaluating financing options.
- Least Sensitive Factors: Discount rate and OPEX have relatively minor effects, though they should not be ignored in financial planning.
- Positive Trends: Improving CUF and reducing CAPEX or interest on debt significantly lowers LCOE, showcasing areas for cost-efficiency improvements.

6.3.4. FSPV- hydropower plant hybrid system

The combination of the floating solar PV (FSPV) system and the current hydroelectric facility at Rajghat Dam has the potential to significantly increase electricity output while also strengthening grid stability. This section evaluates the viability and advantages of integrating FSPV with the nearby hydroelectric facility, placing special emphasis on how hydropower-generating plants can be complemented by FSPV.

The 45 MW hydroelectric facility at Rajghat Dam now provides electricity to the 132 KV GSS. The plant produced about 87.6 million units (MU) of electricity in 2018. The hydropower plant runs at full capacity during the monsoon season when solar energy production is at its lowest. In contrast, the FSPV system shows peak generation during the

summer when Rajghat Dam's water availability declines. Because solar and hydropower generation are complementary, integrating the two is a practical strategy for ensuring a steady and well-balanced electricity supply all year long.

There are various benefits to integrating the FSPV system with the current hydropower plant. Firstly, it is possible to employ the extra solar energy produced throughout the summer months instead of letting it go unused. Pumped hydro storage systems, which entail pumping water to a raised reservoir during times of high solar generation and releasing it during times of high electricity demand, can store and use this surplus power. This integration enhances the overall effectiveness of the power generation system and allows for improved resource utilization.

The hydropower plant and FSPV together also improve grid stability and make it easier to satisfy the daily and seasonal variations in electricity demand. The hydropower plant can meet the increased electricity demand during the monsoon season when solar energy generation is lower. In contrast, during the summer when solar energy production is at its highest, the hydropower plant can run at a reduced capacity, saving water and providing a steady supply of electricity.

Additionally, there are financial and environmental advantages to integrating FSPV with the current hydroelectric facility. Surplus solar electricity can balance the requirement for additional conventional power production sources, lowering reliance on fossil fuels, as the cost of FSPV installations becomes more competitive. This integration helps to lower greenhouse gas emissions and is in line with India's ambitions for renewable energy.

In conclusion, there are substantial prospects for increasing power generation, enhancing grid stability, and maximizing the use of renewable energy resources with the combination of the FSPV system with the nearby hydropower plant at Rajghat Dam.

While minimizing environmental effects, the complementary nature of solar and hydropower generation and the possibilities for pumped hydro storage systems offer a steady and sustainable supply of electricity. This integration is an important tactic for developing a more reliable and effective power-producing system.

6.3.5. Findings and insights: Rajghat Dam Case Study

The findings from evaluating the potential installation capacity and advantages of floating solar PV (FSPV) on Rajghat Dam shown in Table 6.5, offer important new perspectives on the viability and benefits of putting this renewable energy solution into practice. In this section, we'll examine the results in more depth, evaluate them against the body of

knowledge and professional standards, and analyze how they relate to the application of FSPV to Rajghat Dam.

Rajghat Dam is located at 24.7625 N and 78.7500 E latitude and longitude, respectively. The dam gives a fantastic potential for the installation of FSPV due to its enormous open area, with a total submergence area at full reservoir level (FRL) of roughly 24,210 hectares.

The study took into account two suggested coverage zones, 10% and 25% of the entire submergence area, to evaluate the potential. This is equivalent to 2421 and 2603 ha, respectively.

The evaluation found that the proposed FSPV system had a large amount of potential for power generation. The specific yield was calculated to be 4,246,105 megawatt-hours (MWh) annually for the 25% coverage area, yielding an expected total power generation of 10,623,501 MWh. The power produced by the FSPV system for the 25% coverage area was calculated to be 6513.12 megawatts-peak (MWp), taking into account the fixed tilt arrangement. This indicates the significant energy contribution that FSPV may make to Rajghat Dam's overall capability for electricity generation.

In terms of economic evaluation, the cost per kilowatt-hour (kWh) of power produced by the FSPV system was determined using the levelized cost of electricity (LCOE). The proposed system at Rajghat Dam was expected to have an LCOE of Rs 2.61 per kWh, or roughly $0.036 per kWh. This suggests a cost that is competitive with other energy sources. Additionally, it was discovered that the project's internal rate of return (IRR) was 8.55%, proving the financial sustainability of the FSPV system.

The assessment's appraisal of the evaporation reduction achieved by the FSPV system was crucial. Water resources can be preserved by installing FSPV on water bodies to assist reduce evaporation losses.

According to the assessment, 0.9 litres of evaporation were reduced for every kWh of power produced. With this huge decrease in water loss, an estimated 9.084 million cubic metres of water will be saved overall. This illustrates the beneficial environmental impact of FSPV in terms of water saving and accounts for 0.47% of the total reservoir capacity.

The findings are consistent with the potential and advantages suggested by earlier studies when compared to the body of literature and industry standards. The planned FSPV system at Rajghat Dam has a power generation capacity of 6513.12 MWp and an annual energy generation of 10,623,501 MWh, which support the findings of similar studies carried out in various geographic areas. The system's financial viability is further supported by the LCOE

of Rs 2.61/kWh and IRR of 8.55%, which are within the range of economic statistics seen in other FSPV projects.

These results have important ramifications for Rajghat Dam's FSPV deployment. FSPV is a desirable renewable energy option for addressing the rising demand for electricity due to its significant power generation capacity and competitive cost. The FSPV system's success in reducing evaporation also aids in water resource management and conservation, tackling the urgent problem of water scarcity. These results demonstrate the importance of FSPV in attaining environmentally responsible energy production.

Policymakers, energy planners, and stakeholders involved in the decision-making process for renewable energy projects might benefit greatly from the findings of the study. The Rajghat Dam's FSPV supports its inclusion in the overall energy mix and water resource management policies due to its potential for power generation, cost effectiveness, and water conservation benefits. The research adds to the body of information about FSPV technology and the mounting evidence for its usefulness and benefits.

A positive outlook for the deployment of FSPV is revealed by the study of Rajghat Dam's PV installation capability and benefits. FSPV is a strong renewable energy option due to its significant power generating capacity, cost advantages, and water conservation advantages. The credibility of the findings is increased by the matching of the results with previous research and industry standards. The implications of these findings for the application of FSPV on Rajghat Dam highlight the significance of taking this technology into account as a sustainable energy and water resource management option. FSPV has the potential to be a crucial component of achieving a greener, more sustainable future by helping to meet our energy needs and tackle environmental issues.

Table 6.5. Summary of PV installation capacity and benefits at Rajghat dam.

Latitude	Longitude	Sub mergence area at FRL (ha)	10% Area proposed			25% area proposed			CUF	LCOE Rs / kWh	IRR %	Evaporation Reduction in liter/ kWh
			Area in ha	Power General for fixed tilt in MWp	Specific yield (MWh /Year	Area in ha	Power General for fixed tilt in MWp	Specific yield (MWh / Year				
24.7625 N	78.7500 E	24,210	2421	2603	4,246,105	6052.50	6513.12	10623501	18.62	2.61	8.55	0.9

6.3.6. Estimation of FSPV potential of major dams of the tropical region of Uttar Pradesh

The assessment of floating solar PV potential, initially conducted at Rajghat dam, has been extended to evaluate the potential installation capacity (MW) and electricity generation capacity (MWh) for all the reservoirs with a submergence area exceeding 500 hectares across Uttar Pradesh. Detailed findings regarding FPV potential and energy estimates for each reservoir are presented in Table 6.6. The energy generation potential for each reservoir is derived through the PVsyst energy simulation tool, as outlined in Table 6.6. Results indicate a substantial technical potential of 37,762 MWp for floating solar PV installation in major water reservoirs, surpassing the planned capacity for solar PV installation in Uttar Pradesh by 2022. The estimates project a potential energy generation of approximately 61,935,492 MWh, covering 25% of the surface area of reservoirs suitable for solar installation. Rihand water reservoir is identified with the largest capacity potential, estimated at 12,542 MWp. Notably, the study's estimates are conservative, based on covering only 25% of the reservoir surface area with FPV. The potential capacity and energy estimation could be doubled by increasing coverage to a maximum of 50 %. Additionally, an estimate of potential energy generation by covering 10% of the reservoir surface area is provided for reference. The location of each dam considered in this analysis is shown in Figure 6.5.

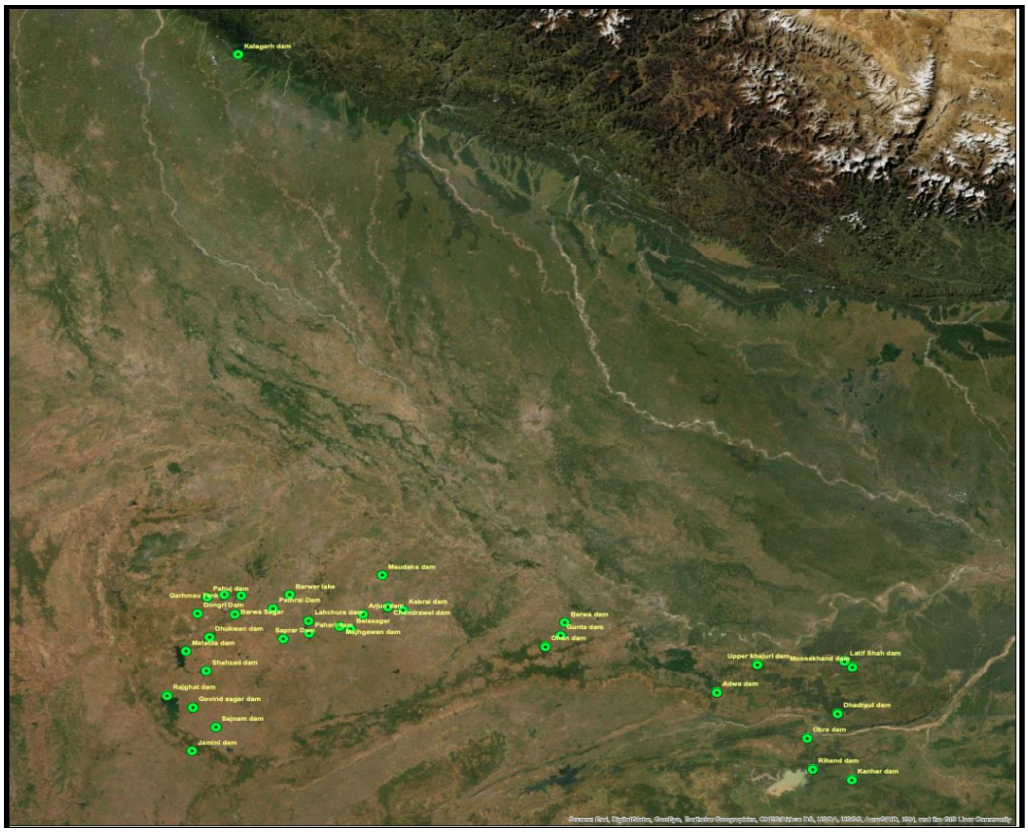

Figure 6.5. Map showing the location of all dams considered for analysis of FSPV assessment

Table 6.6. FSPV potential and energy generation of major dams of Uttar Pradesh

Name of Reservoir/Dams	Latitude	Longitude	Submergence area at Full Reservoir Level (ha)	10% Area proposed			25% area proposed			CUF
				Area in ha	Power Generation for fixed tilt in MWp	Specific yield (MWh/year)	Area in ha	Power Generation for fixed tilt in MWp	Specific yield (MWh/year)	
Saprar dam	25.2104 N	79.0831 E	2000.00	200.00	215	345718	500.00	538.05	864970	18.35
Barwa Sagar	25.3732 N	78.7220 E	520.00	52.00	56	88636	130.00	139.89	221761	18.10
Pathrai Dam	25.4148 N	78.9979 E	594.00	59.40	64	103800	148.50	159.80	259701	18.55
Dongri Dam	25.3844 N	78.4562 E	1920.00	192.00	206	335570	480.00	516.53	839576	18.55
Garhmau Tank	25.5238 N	78.6538 E	1467.00	146.70	158	255074	366.75	394.66	638180	18.46
Pahuj dam	25.5063 N	78.5260 E	543.00	54.30	58	94999	135.75	146.33	238084	18.57
Parichha dam	25.5171 N	78.7770 E	802.00	80.20	86	138658	200.50	215.76	346915	18.35
Dhukwan dam	25.1925 N	78.5347 E	1943.00	194.30	209	338880	485.75	522.72	847863	18.52
Barwar lake	25.5220 N	79.1307 E	1006.40	100.64	108	172357	251.60	270.75	431229	18.18
Matatila dam	25.0616 N	78.2506 E	12787	1278.7	1375	2242824	3196.75	3440.05	5611433	18.62
Sajnam dam	24.5253 N	78.5906 E	2375	237.5	255	413012	593.75	638.94	1033337	18.46
Govind sagar dam	24.6727 N	78.4266 E	2478.80	247.88	267	435196	619.70	666.86	1088840	18.64
Jamini dam	24.3403 N	78.4143 E	2472.65	247.265	266	433145	618.163	665.20	1083698	18.60
Shahzad dam	24.9502 N	78.5197 E	2993.00	299.30	322	527255	748.25	805.20	1319162	18.70
Arjun dam	25.3868 N	79.6763 E	1800.00	180.00	194	307709	450.00	484.25	769872	18.15
Belasagar	25.2642 N	79.5797 E	926.00	92.60	100	159324	231.50	249.12	398621	18.27
Pahari dam	25.2343 N	79.2836 E	803.00	80.30	86	138058	200.75	216.03	345414	18.25
Maudaha dam	25.5887 N	79.7048 E	5429.00	542.90	584	919728	1357.25	1460.54	2301109	17.99
Lahchura dam	25.3281 N	79.2796 E	897.27	89.727	96	154188	224.318	241.39	385773	18.24
Chandrawal dam	25.4308 N	79.8635 E	1192.00	119.20	128	203254	298.00	320.68	508533	18.10
Kabrai dam	25.4084 N	79.9769 E	505.30	50.53	54	86092	126.33	135.94	215404	18.09
Ohan dam	25.1319 N	81.0316 E	648.00	64.80	70	109158	162.00	174.33	273106	17.88
Barwa dam	25.3134 N	81.1737 E	648.00	64.80	70	109020	162.00	174.33	272761	17.86
Gunta dam	25.2173 N	81.1447 E	813.60	81.36	87	136263	203.40	218.88	340923	17.78
Majhgawan dam	25.2821 N	79.5099 E	830.00	83.00	89	141878	207.50	223.29	354969	18.15
Upper khajuri dam	24.9963 N	82.5960 E	1131.00	113.10	122	190458	282.75	304.27	476512	17.88
Moosakhand dam	24.9583 N	83.2917 E	1369.00	136.90	147	230639	342.25	368.30	577047	17.89
Latif Shah dam	25.025 N	83.2250 E	511.00	51.10	55	84171	127.75	137.47	210592	17.49
Dhadraul dam	24.6254 N	83.1695 E	3033.12	303.312	326	524471	758.28	815.99	1312202	18.36
Adwa dam	24.7861 N	82.3056 E	1667.00	166.70	179	284558	416.75	448.47	711950	18.12
Rihand dam	24.0236 N	82.7285 E	46620.00	4662.00	5013	8344114	11655.00	12542.04	20876572	19.00
Obra dam	24.4394N	82.9661 E	1800.00	180.00	194	317851	450.00	484.25	795248	18.75
Kanhar dam	24.1229 N	83.2946 E	3796.00	379.60	408	681008	949.00	1021.23	1703851	19.05
Kalagarh dam	29.5194 N	78.7586 E	7834.00	783.40	842	1461579	1958.50	2107.55	3656785	19.81
Total			**140365.14**	**14036.51**	**15093**	**24754751**	**35091.29**	**37762.21**	**61935492**	**18.72**

Note: Assumptions made- Albedo -0.10, Soiling -1%, Unavailability - 7.3 days/year, Meteorological data- Mateo norm, Module - Trina solar TSM-DE14H-(II)-350, Inverter- ABB-Core 500.0 TL, LID -2%, Fixed tilt 15 degree

6.4. Summary and Recommendations

The unique findings from the case study of Rajghat Dam, coupled with the extended assessment of the major dams in the tropical region of Uttar Pradesh, India, bring novel insights into the potential energy generation capabilities of Floating Solar Photovoltaic (FSPV) systems and their effectiveness in reducing evaporation rates.

The following is a summary of the key findings:

- According to the technical potential evaluation, Rajghat Dam can support a floating solar installation of 6513 MWp, which would produce an estimated 10,623,501 MWh of energy annually.
- The case study also evaluates the FSPV system's ability to reduce evaporation, estimating a reduction of 0.9 litres per kWh of power produced. This equals a cumulative water savings of about 9.08 million cubic metres.
- The levelized cost of energy (LCOE) for the FSPV system is determined by an economic analysis to be Rs 2.61 per kWh, or roughly $0.036/kWh. This illustrates how FSPV is more affordable than traditional energy sources. The project's 8.55% internal rate of return (IRR) further demonstrates its financial sustainability.
- Beyond Rajghat Dam, the consequences of the findings are broad. The study provides a basis for assessing the overall floating solar potential in Uttar Pradesh and maybe other locations. It also serves as a guide for planning FSPV installations on water bodies. FSPV is a potential option for the production of renewable energy and the management of water resources due to its economic allure and advantages for the environment.
- The extended study projects a potential energy generation of 37762.21 MWp and approximate specific yield of 61,935,492 MWh with capacity utilization factor (CUF) 18.72, by covering 25% of the reservoir surface area suitable for solar installations.
- Additionally, by adding electricity to the existing grid infrastructure, less new infrastructure construction is required, which benefits the local environment and lowers government costs.

In light of the findings of the current research, the following recommendations are offered:

- FSPV in Practise: Rajghat Dam's effective FSPV implementation serves as a model for comparable projects on other water bodies in Uttar Pradesh and throughout India. The government and pertinent parties should look for ways to replicate the FSPV model and take advantage of water bodies' untapped potential for producing renewable energy.
- Policy Support: It is essential to have favourable policies and laws in order to encourage the use of FSPV technology. The government ought to take into account reducing the approval procedure, expediting land and water leasing agreements, and offering incentives and subsidies for FSPV projects. Positive policy conditions will boost private investment and accelerate the expansion of FSPV installations.

Chapter 7

FSPV Installations at Varying Heights: Evaporation Reduction Estimation for Major Dams of Tropical Region of Uttar Pradesh, India

Abstract

The tropical region is well known for its high levels of sunshine and is suitable for PV installations with the associated disadvantage of high rates of evaporation. FSPV is an alternate approach for solar PV installations in such regions for harnessing maximum solar energy with and additional advantage of reducing evaporation from water bodies. The study on the estimation of the reduction in evaporation due to FSPV installations and associated panel height above the water surface is limited. This study aims to quantify the reduction in evaporation resulting from the deployment of floating solar photovoltaic (FSPV) systems above water surfaces. It also determines the panel height above water bodies to maximize evaporation reduction. These findings are then extended to evaluate the impact of FSPV installations on reducing evaporation over the major dams in the tropical region of Uttar Pradesh, India. The experimental results highlighted that the maximum evaporation reduction occurred from the water surface covered with a panel at a height of 300 mm above the water with an evaporation reduction of 23.44 %. The extrapolation of the study for 28 major dams of Uttar Pradesh, reveals an annual water saving of 92.56 million cubic meters (MCM) with FSPV coverage of 25%. Based on estimations, a 1 MWp FSPV installation considerable amount of water annually can fetch water for 67 individuals in a tropical region, assuming 100 lpcd. These research outcomes would provide valuable insights into FSPV technology and its potential to mitigate water evaporation, with implications for regional and national water and energy resource management policies.

7.1 Introduction

This chapter examines the possibility of floating solar photovoltaic (FSPV) installations in lowering evaporation in water bodies to address the concerns of water conservation and management. Floating solar PV plants present a promising alternative to conventional solar energy projects, which frequently compete for significant land allocations with agricultural or development needs. These installations could potentially reduce evaporation losses from the water bodies where they are installed in addition to reducing land use, addressing a frequently disregarded component of water conservation.

In addition to assisting in minimizing the growing demand for land, the novel concept of floating solar PV systems offers the advantage of increasing panel efficiency by lowering operating temperatures. A further advantage that highlights the need to conserve this priceless resource is the huge decrease in water evaporation losses. Any technique that reduces these losses might have a significant impact in tropical areas like Uttar Pradesh where water bodies utilized for agriculture experience significant water loss owing to evaporation. Although floating solar PV projects can solve this problem, limited research has examined how effective they are at lowering evaporation rates.

The present study addresses the need to investigate the reduction in evaporation resulting from the deployment of floating solar photovoltaic (FSPV) systems above water surfaces to fill existing gaps in knowledge. It aims to validate theoretical assertions regarding the benefits of such installations with empirical evidence. Furthermore, the study seeks to determine the panel height above water bodies to maximize evaporation reduction. These findings are then extended to evaluate the impact of FSPV installations on reducing evaporation over the major dams in Uttar Pradesh. These research outcomes would provide valuable insights into FSPV technology and its potential to mitigate water evaporation, with implications for regional and national water and energy resource management policies.

Water loss from reservoirs due to evaporation has become a challenge as water availability is becoming scarce due to climate change. An average water evaporation loss rate of 225 cm/year was estimated for major and medium dams of India as reported by the Central Water Commission, New Delhi (CWC,2006). Considering 225 cm as the annual evaporation loss rate, evaporation works out to be about 56,000 million cubic meter (MCM) every year. Hartzell (2016), estimated water evaporation losses to the tune of 4.4% per annum on dams & canals of the Central Arizona Project. Several techniques have been adopted and reported in the literature to mitigate evaporation losses. Cooley (1970) reviewed different evaporation reduction methods over the water surface and reported floating covers using foamed wax blocks, continuous wax and foamed rubber reduced evaporation losses between 36% and 84% for 8 years, and the estimate of the lowest cost for saving was USD 0.08-0.13 per kilo litre per year. Youssef & Khodzinskaya (2019), conducted a comprehensive review of evaporation reduction techniques and highlighted the significance of floating covers. Yao et al. (2010) studied suspended & floating covers for evaporation reduction, which estimated that if the Warenhoe dam was fully covered, the annual efficiency of evaporation reduction reached 76% for suspended covers and 68% for floating covers. The report also estimated the

cost per unit of water saved of the order of 1.14$ to 1.75$ per kilo litre. Such techniques are costly and not feasible for a country like India.

The dual advantage FSPV is a promising technology that generates power while reducing evaporation from water bodies. Melvin & Xiang (2015) studied the effect of solar panels on reducing water evaporation in Singapore reservoirs and reported a reduction effect of approximately 30% on evaporation rates. As per the experimental setup results, the average daily evaporation rate was about 7 mm/day which was reduced to about 5 mm/day by covering the water body surface using solar panels. Gaikwad & Deshpande (2017) studied the evaporation control using floating PV system and canal top system. However, the paper did not quantify the water evaporation loss factor. Farfan & Breyer (2018) also studied the impact of combining floating solar PV systems with hydropower systems and reported that 6.3% additional water is available through the prevention of water evaporation. Lopes et al. (2020) studied water evaporation reduction over Brazilian region reservoirs with FPVs coverage scenarios of 20%, 50%, and 70%, and reported 15.3%, 37%, and 55.2% reduction in evaporations respectively. FPV advantage in the context of evaporation reduction is reported up to 70% reduction of evaporation loss (Abdelal,2021; Bontempo Scavo et al.,2021; Redón Santafé et al.,2014; Santos et al.,2022). Ilgen et al. (2024) estimated evaporation reduction of 49.7% with FPV coverage of 90% over Aswan High Dam Reservoir and reported water savings of up to 5.9 billion cubic meters per year. The FSPV system not only reduces water evaporation but improves the water quality. Sahu et al. (2016) reported that the shading provided by the FPV can mitigate algal proliferation and improve the water quality. Cazzaniga et al. (2018) also recommended the use of FSPV over freshwater bodies since excessive algal growth significantly reduce water quality. Lower algal growth also reduces the likelihood of developing toxic species and the release of their toxins (Haas et. al.,2020). The area coverage for PV solar plant over water bodies remains debatable while Perez et al. (2018) proposed 24% of the total area and effective area for PV installations had been recommended at 20% but Acharya & Devraj (2019) has suggested 1 to 30% of the total surface area depending upon the type of water body.

Surface water evaporation is a complex phenomenon and various factors affects the water evaporation from open water surface, some of these factors include water surface area, temperature, vapour pressure difference, wind effect, atmospheric pressure and quality of water.

Various indirect estimating models for evaporation have been developed, such as the mass balance method and the Energy Budget method. The mass balance method calculates

evaporation as the disparity between inflow and outflow, as well as changes in stored water volume. However, its application is limited due to challenges in accurately measuring surface input, groundwater levels, and unknown seepage. On the other hand, the Energy Budget method, based on the conservation of energy principle, computes the available energy for evaporation once all other energy fluxes, including incoming and outgoing energy, and energy stored in the water body, have been determined. This method is considered highly accurate for estimating evaporation after direct measurement.

In this study, direct experimental observation using Pan Evaporimeters has been employed for measuring evaporation loss. Given their simplicity and widespread use for quantifying evaporation, Pan Evaporimeters serve as a reliable tool. Consequently, the Penman-Monteith equation has been chosen as the preferred method to estimate evaporation from 28 major dams in Uttar Pradesh. This decision is grounded in the belief that the Penman-Monteith equation provides the most accurate description of the evaporation process.

7.2 Methodology and Site Selection

The field study was carried out at BITS, Pilani Rajasthan India, which has a continental, semi-arid climate typical of Northwestern India. The region has hard summers and short monsoons, warm days and chilly nights in the winter, with a wide variety of environmental circumstances to consider in the study.

The field study is conducted in light of these climatic factors and the requirement to quantify the reduction in evaporation loss caused by the installation of floating solar PVs (FSPVs) over water bodies in any tropical region. The focus of the study is to determine the amount of evaporation loss reduction brought on by FSPV plants, determine the ideal height of panel installation above the water surface to maximize evaporation loss reduction and assess the viability of utilizing floating solar PV installation on a regional scale in Uttar Pradesh India.

7.3. Results and Discussions

7.3.1 Experimental Data and Analysis

The data collection commenced on April 1st, 2020, and continued until March 31st, 2023, for three annual cycles. It is crucial to note that some irregularities and omissions occurred because of the period's particular circumstances, particularly the global COVID-19 pandemic, which impacted the availability of data on particular days. Days with rainfall were also excluded because of the irregularity they contributed to the rainfall pattern over the evaporation pans, which also served as the covers for the solar panels. Maintenance intervals

for the evaporimeter and other crucial parts were also left out because they would have caused inconsistencies in the records.

7.3.1.1. Evaporation data

Based on the daily data, the resulting dataset was then utilized to calculate the evaporation rates for each month. The calculated daily average evaporation rates were then used to create a detailed picture of yearly evaporation trends. Table 7.1 provides a complete breakdown of this information for the years 2020 to 2023 and is also shown in Figure 7.1(a) to (c). In May and January, the highest and lowest rates of evaporation are observed, respectively. Low evaporation is observed during the winter period for water surfaces open to the sky.

Table 7.1. Average daily evaporation from water surface open to the sky and covered by solar panels vs panel height for the year 2020 to 2023

Month	Evaporation in mm/day											
	Solar panel 300 mm above water level			Solar panel 500 mm above water level			Solar panel 1000 mm above water level			Water Surface Open to sky		
	2020-21	2021-22	2022-23	2020-21	2021-22	2022-23	2020-21	2021-22	2022-23	2020-21	2021-22	2022-23
April	5.31	4.77	6.74	5.65	5.05	7.19	6.44	5.45	7.45	7.27	6.38	8.17
May	6.06	4.68	7.96	7.36	4.92	8.71	7.65	5.20	9.33	8.35	5.83	10.31
June	6.06	4.36	7.65	6.56	4.80	8.13	6.82	4.93	8.28	7.59	5.52	9.49
July	4.62	2.94	2.63	4.95	3.10	2.95	5.29	3.25	3.38	6.08	3.63	4.21
August	3.30	4.11	2.75	3.60	4.24	3.08	3.79	4.42	3.35	4.61	4.75	4.15
September	3.46	2.57	3.22	3.71	2.71	3.67	4.04	2.99	4.01	4.70	3.50	4.74
October	3.48	2.95	2.34	3.72	3.11	2.60	3.86	3.30	2.83	4.42	3.61	3.55
November	1.96	1.78	1.77	2.10	1.79	1.86	2.23	1.78	2.08	2.41	1.61	2.57
December	1.21	1.30	0.98	1.25	1.20	1.14	1.51	1.11	1.21	1.53	0.98	1.39
January	1.13	0.89	0.52	1.22	0.78	0.59	1.43	0.75	0.72	1.10	0.65	0.79
February	2.39	2.33	1.15	2.60	2.60	1.33	2.75	2.73	1.50	3.08	2.98	1.87
March	4.56	4.14	2.46	4.86	4.66	2.97	5.13	4.87	3.42	6.02	5.53	4.05

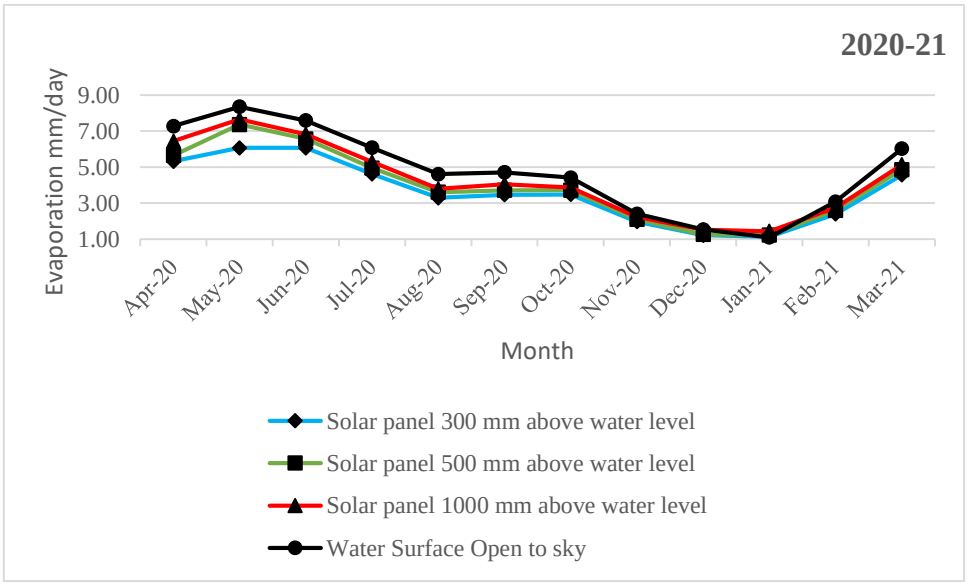

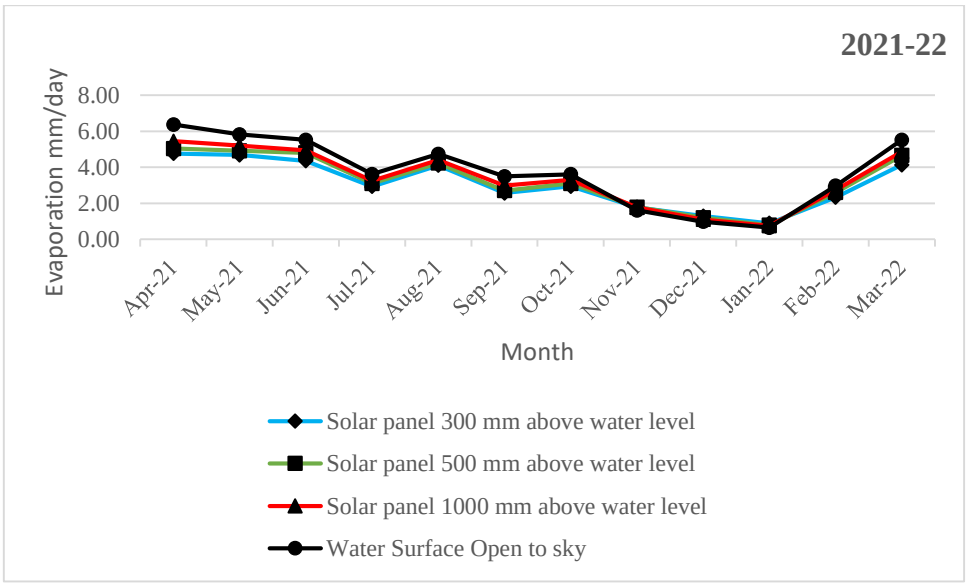

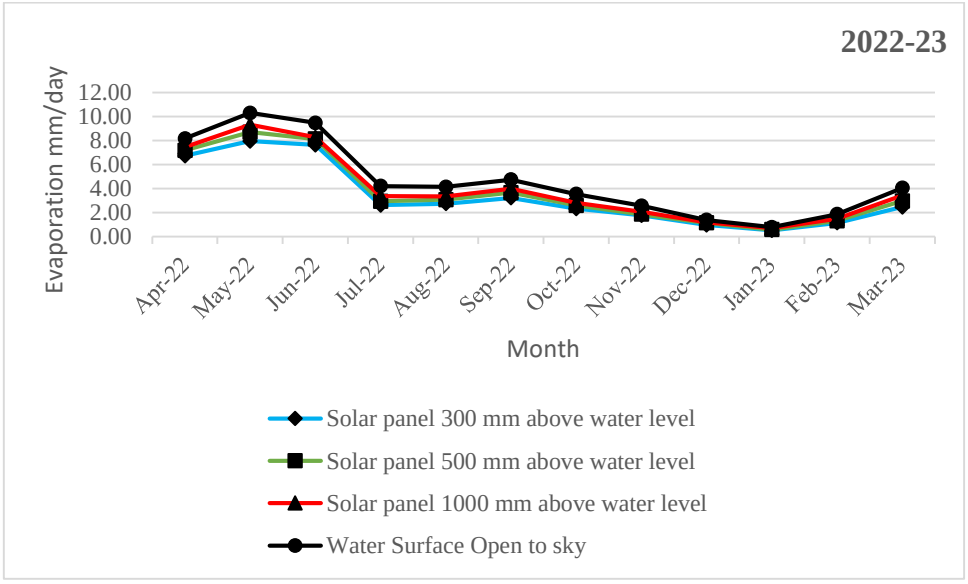

Figure. 7.1. Average daily rate of evaporation from water surface open to the sky and covered by solar panels of varying heights at Pilani, Rajasthan, India for (a) 2020-21, (b) 2021-22, (c) 2022-23.

Based on the findings illustrated in Figure 7.1, it is evident that the evaporation rate consistently remains at its lowest when the water surface is covered with a panel height of 300 mm. Therefore, a panel height of 300mm is deemed the most efficient in minimizing evaporation. To better understand the efficacy of this panel height, Figure 7.2 depicts the average daily evaporation rate from the water surface covered by the solar panel at 300 mm for the years 2020-23, contrasting it with the average daily evaporation rate from the water surface exposed to the sky.

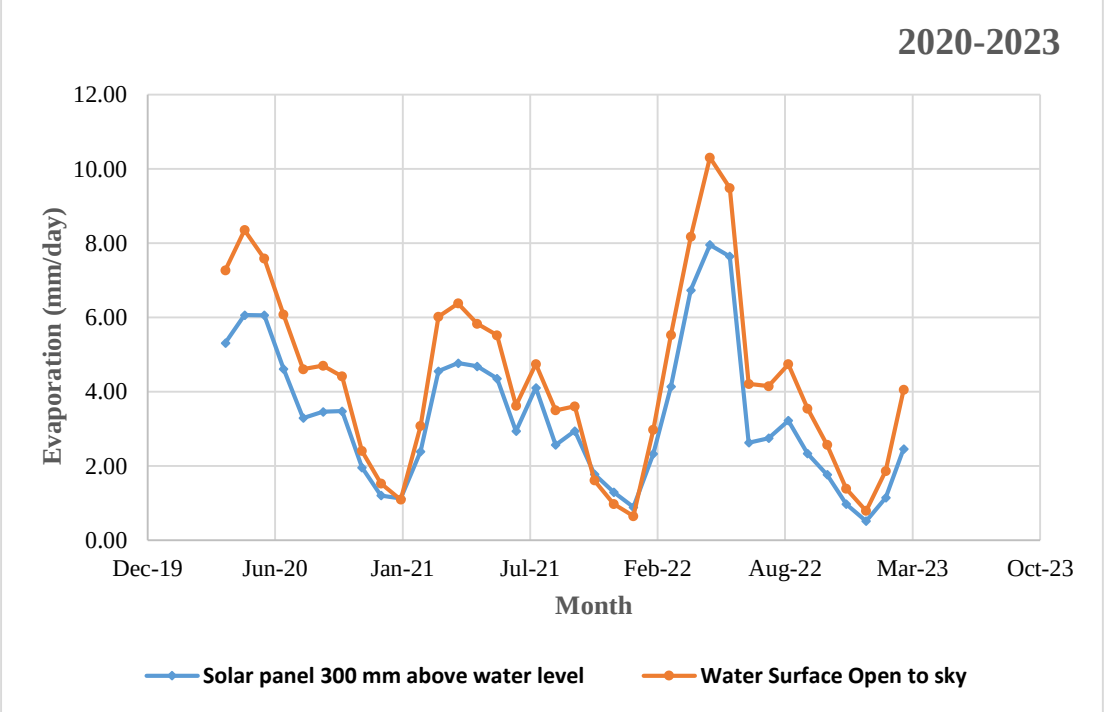

Figure. 7.2. Average daily rate of evaporation from water surface covered by solar panel at 300 mm at Pilani, Rajasthan, India for 2020-23.

7.3.1.2. Evaporation reduction analysis

The evaporation rates for each month were examined as given in Table 7.1, and an intriguing pattern emerged. The % evaporation reduction from water surface covered by panels at heights 300, 500 and 1000 mm was estimated for three consecutive years from 2020-2023 and the details are presented in Table 7.2. The study discovered an interesting correlation between the maximum evaporation reduction and the minimum panel height above the water (300 mm). This may be due to the panel's proximity to the water's surface, which may have an impact on microenvironmental aspects including heat transfer and humidity levels underneath the panel.

Table 7.2. Monthly average evaporation reduction (%) vs solar panel height for 2020-2023

Month	Evaporation reduction in %								
	When Solar panel 300 mm above water level			When Solar panel 500 mm above water level			When Solar panel 1000 mm above water level		
	2020-21	2021-22	2022-23	2020-21	2021-22	2022-23	2020-21	2021-22	2022-23
April	26.92	25.19	17.58	**22.30**	20.86	12.07	11.49	14.54	8.81
May	27.39	19.66	22.82	11.88	15.57	15.49	8.38	10.75	9.43
June	20.07	21.12	19.38	13.48	13.10	14.26	10.06	10.69	12.70
July	24.03	18.94	37.50	18.60	14.39	**29.88**	13.02	10.31	19.75
August	**28.51**	13.45	33.72	21.89	10.70	25.87	**17.76**	6.97	19.36
September	26.36	**26.57**	32.04	21.17	**22.57**	22.71	14.03	**14.57**	15.49
October	21.18	18.37	34.11	15.74	13.94	26.72	12.55	8.59	**20.31**
November	18.42	-10.33	31.12	12.74	-11.16	27.52	7.20	-10.12	19.16
December	21.09	-32.31	29.53	18.26	-22.79	17.67	1.30	-13.27	13.02
January	-2.83	-36.47	34.45	-11.48	-20.00	26.05	-30.66	-14.12	9.24
February	22.27	21.73	38.49	15.55	12.48	28.97	10.67	8.16	19.84
March	24.28	25.09	**39.25**	19.36	15.62	26.66	14.78	11.82	15.56
Average	**23.81**	**18.07**	**27.42**	**16.74**	**13.29**	**20.07**	**10.84**	**9.28**	**14.00**
Average (2020-23)	**23.44**			**16.93**			**11.51**		

Theoretically, the evaporation rate decreases because less solar radiation reaches the water surface due to the lower height, which increases the shade effect. Additionally, the panels might reduce the wind speed above the water's surface, which would help to decrease evaporation.

Notably, evaporation reduction rates in August were notably high despite a decline in the average daily evaporation rate. This unexpected tendency can be explained by August's increased relative humidity and water surface temperature, both of which have a significant impact on evaporation rates.

The average reduction in evaporation from the water surface covered with solar panels at a height of 300 mm was 23.44%. The reduction rates were 16.93% and 11.51% for the water surface covered with panel heights 500 mm and 1000 mm heights, respectively as shown in Table 7.2. The effect on evaporation reduction is substantial and inversely correlated with the height of the panels above the water as shown in Figure 7.3 (a) to (c).

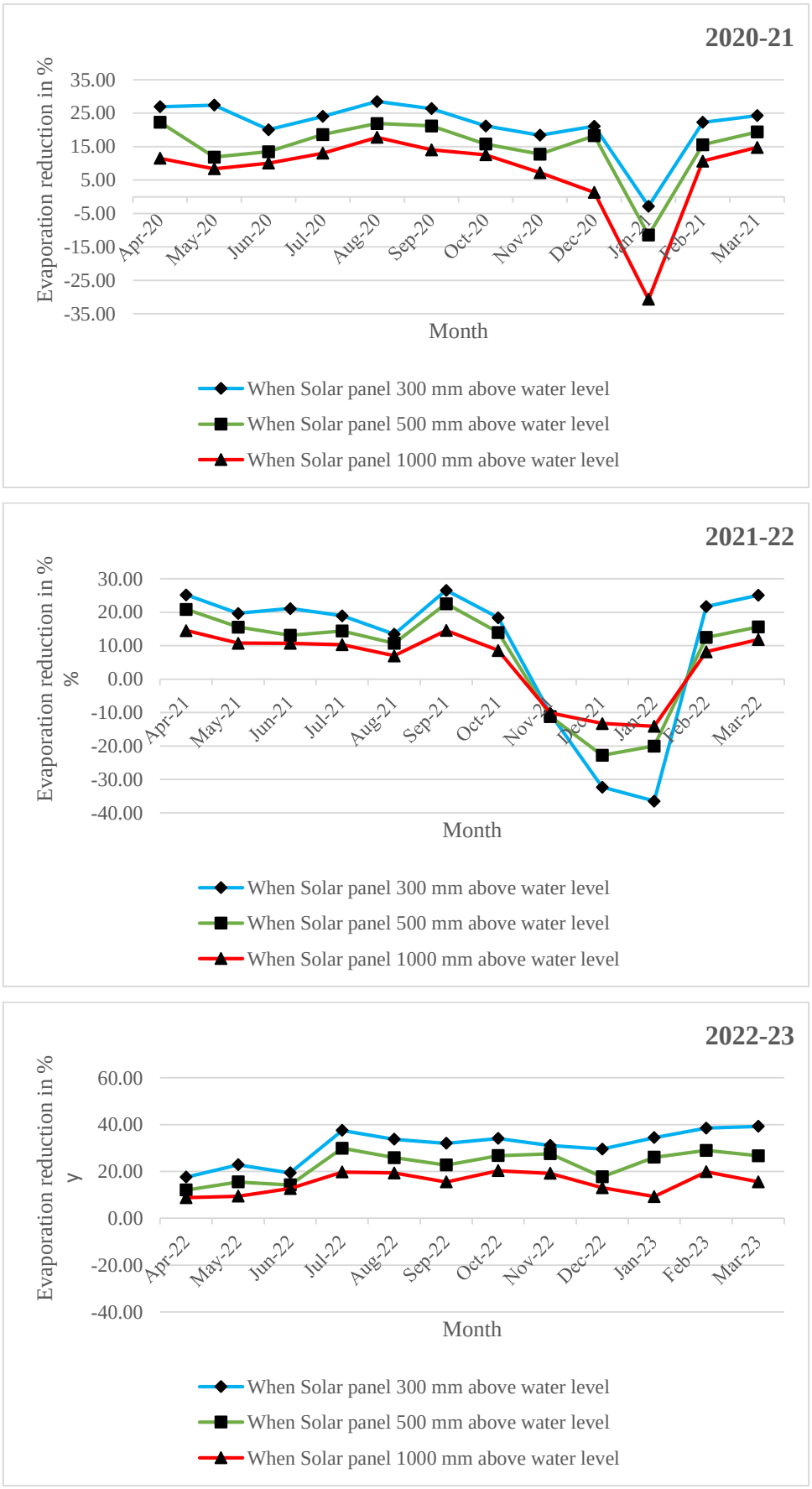

Figure 7.3. Percentage reduction in evaporation from water surface covered by solar panels with heights 300 mm,500 mm and 1000 mm above the water(a) for the year 2020-2021 (b) for the year 2021-2022 (c) for the year 2022-2023.

The estimations were carried out to find differences in water temperature between open water and water beneath solar panels. At each of the three tested heights, it is noted that the average temperature of the water exposed to the open sky was consistently greater than the water beneath the solar panels. For the solar panel placed 300 mm, 500 mm, and 1000 mm above the water surface, the average temperature of the water surface is cooler by 2.11°C, 1.86°C, and 0.66°C respectively than the water surface open to the sky. This information implies that the solar panels have a moderating effect by lowering the water's temperature, which therefore affects evaporation.

The investigation also includes ambient temperature as an influencing parameter. The ambient temperature over the water surface open to the sky is observed consistently higher compared to the ambient temperature over the water surface covered by solar panels. This temperature difference is developed as a result of the panels' shading effect, which decreased the amount of solar radiation impacting the water surface and air/ambient temperature above it.

It was discovered that the relative humidity was lower over the water surface open to the sky than it was over the water surface covered by panels. Lower relative humidity promotes evaporation, which accounts for the increased evaporation rates as observed in the water surface open sky. This result underlines the important advantage of solar panels in fostering a microenvironment that lowers water evaporation.

It is already observed that the amount of water evaporation is significantly decreased because of solar panels. It is also noticed that the panel heights above the water surface significantly impact the evaporation rate. Solar panels placed over the water surface control several variables, including the air/ambient temperature, water surface temperature, and relative humidity. This in turn influences this reduction in evaporation.

7.3.2. Evaporation reduction estimation due to FSPV installation over major dams of Uttar Pradesh

There are 132 reservoirs managed by the Uttar Pradesh Irrigation and Water Resources Department (UPIWRD) as per the database reported in the Public Data Portal. Database information such as the submergence area of the reservoir, depth of the dam, and water storage capacity were utilized for the estimation of evaporation for the major dams of Uttar Pradesh. Spatial data such as location and boundary information for each reservoir were obtained from Survey of India maps available in the public domain (https://soinakshe.uk.gov.in/). Out of these reservoirs, the reservoir with a submergence area

at full reservoir level (FRL) greater than 500 ha, has been considered suitable for floating PV installations. The rationale behind this is due to the minimum water depth requirement for the feasibility of FSPV installation. Based on this criterion, 28 dams/reservoirs are shortlisted for FSPV installation and water conservation estimation in this study. It can be observed that most of the reservoirs are concentrated in the Bundelkhand and Vindhyachal regions of Uttar Pradesh, India. These tropical regions with the highest sunlight turn these areas into the most susceptible to heat and therefore maximum rate of evaporation.

The evaporation rate data of selected 28 dams were not readily available. Hence, the above criteria and complete data requirements were assessed from meteorological data obtained from Meteonorm (Meteonorm 7.1 ,1991-2010). The monthly mean data of global horizontal irradiation, horizontal diffuse irradiation, wind velocity, temperature and relative humidity were taken from Meteonorm. The evaporation estimation was done by Penman-Monteith expression (Finch & Calver, 2008) as given by Equation 7.1 below.

$$E = (\Delta R'_n / (\Delta + \gamma)) + (\gamma f(u) (e_w - e_a) / (\Delta + \gamma)) \quad (7.1)$$

where, E is evaporation in mm/day

R'_n is the net radiation in units of equivalent depth of water mm/day

Δ is the slope of the saturated vapour pressure-temperature curve

γ is the psychometric constant

e_w is saturated vapour pressure of the air at the water surface temperature

e_a is the vapour pressure of the air

f(u) is a function of the wind speed

Evaporation estimation was done for 28 dams having a total surface area of 1,33,208 ha and a gross water storage capacity of 18,139.54 million cubic meters following the procedure described by (Zotarelli et. al, 2010). The evaporation estimated varied from 2246 mm at Kalagarh Dam to 2458 mm at Adwa Dam. The average annual evaporation from all the selected 28 dams is estimated to be 2374 mm and annual evaporation is 1577.47 million cubic meter, which is 8.7% of the gross storage capacity.

The insights from this study reveal that floating solar PV plants can be installed over these 28 major reservoirs of Uttar Pradesh which can reduce evaporation and save an accountable quantity of water. Building upon the findings of the evaporative water loss reduction observed at Rajghat dam as discussed in Chapter 6, the study extends its scope to assess the potential reduction in evaporation over major water bodies across Uttar Pradesh through the

installation of floating solar photovoltaic (FSPV) systems. By extrapolating the results from the Rajghat dam case study, estimates of evaporation and evaporation reduction are derived for various dams in the state.

The results, presented in Table 7.3, showcase the potential reduction in evaporation losses with FSPV coverage of both 25% and 10% of the reservoir surface area. Across a total of 28 dams, the analysis reveals an annual water saving of 92.56 million cubic meters (MCM) with FSPV coverage of 25%. Alternatively, with a 10% coverage of FSPV, an annual water saving of 37.02 MCM is estimated.

Table 7.3. Evaporation reduction due to FSPV installation on major dams of Uttar Pradesh

Name of Reservoir/Dams	Latitude	Longitude	Annual Evaporation in mm	Submergence area at Full Reservoir Level (ha)	Gross Water Storage capacity in MCM	Annual Evaporation loss from reservoirs (in MCM)		% evaporation(Annual evaporation) w.r.t.gross capacity	Reduction in evaporation if 25% is covered by solar panel @23.44% against annual evaporation	Reduction in evaporation if 10% is covered by solar panel @23.44% against annual evaporation
Saprar dam	25.2104 N	79.0831 E	2361.65	2000.00	76.20	23.62		30.99	1.38	0.55
Barwa Sagar	25.3732 N	78.7220 E	2350.00	520	10.2	6.11		59.90	0.36	0.14
Pahuj dam	25.5063 N	78.5260 E	2375.89	543	18.25	6.45		35.35	0.38	0.15
Parichha dam	25.5171 N	78.7770 E	2364.80	802	78.76	9.48		12.04	0.56	0.22
Dhukwan dam	25.1925 N	78.5347 E	2337.78	1943	57.8	22.71		39.29	1.33	0.53
Barwar lake	25.5220 N	79.1307 E	2368.55	1006.4	33.78	11.92		35.28	0.70	0.28
Matatila dam	25.0616 N	78.2506 E	2343.97	12787	1132.68	149.86		13.23	8.78	3.51
Sajnam dam	24.5253 N	78.5906 E	2336.42	2375	83.5	27.75		33.23	1.63	0.65
Govind sagar dam	24.6727 N	78.4266 E	2322.10	2478.8	96.8	28.78		29.73	1.69	0.67
Jamini dam	24.3403 N	78.4143 E	2346.75	2472.65	96.8	29.01		29.97	1.70	0.68
Shahzad dam	24.9502 N	78.5197 E	2310.01	2993	130	34.57		26.59	2.03	0.81
Arjun dam	25.3868 N	79.6763 E	2386.95	1800	68.35	21.48		31.43	1.26	0.50
Belasagar	25.2642 N	79.5797 E	2375.39	926	20.86	11.00		52.72	0.64	0.26
Pahari dam	25.2343 N	79.2836 E	2354.65	803	47.8	9.45		19.78	0.55	0.22
Maudaha dam	25.5887 N	79.7048 E	2408.19	5429	200	65.37		32.69	3.83	1.53
Lahchura dam	25.3281 N	79.2796 E	2371.99	897.27	15.29	10.64		69.60	0.62	0.25
Chandrawal dam	25.4308 N	79.8635 E	2425.00	1192	34.71	14.45		41.64	0.85	0.34
Kabrai dam	25.4084 N	79.9769 E	2418.16	505.3	13.22	6.11		46.21	0.36	0.14
Gunta dam	25.2173 N	81.1447 E	2451.30	813.6	28.8	9.97		34.62	0.58	0.23
Majhgawan dam	25.2821 N	79.5099 E	2355.09	830	26.8	9.77		36.46	0.57	0.23
Upper khajuri dam	24.9963 N	82.5960 E	2430.84	1131	44.74	13.75		30.73	0.81	0.32
Dhadraul dam	24.6254 N	83.1695 E	2364.44	3033.12	144.14	35.86		24.88	2.10	0.84
Adwa dam	24.7861 N	82.3056 E	2458.51	1667	57.7	20.49		35.51	1.20	0.48
Rihand dam	24.0236 N	82.7285 E	2395.02	46620	10600	558.28		5.27	32.72	13.09
Obra dam	24.4394N	82.9661 E	2441.03	1800	211	21.97		10.41	1.29	0.51
Kanhar dam	24.1229 N	83.2946 E	2415.41	3796	197.36	45.84		23.23	2.69	1.07
Kalagarh dam	29.5194 N	78.7586 E	2245.99	7834	2442	87.98		3.60	5.16	2.06
Rajghat dam	24.7625 N	78.7500 E	2352.67	24210	2172	284.79		13.11	16.69	6.68
			66468.56	**133208.1**	**18139.5**	**1577.47**		**8.70**	**92.56**	**37.02**
Average Evaporation				**2373.88**						

7.3.3. Major findings

The findings from the estimates of evaporation reduction due to FSPV installations on 28 selected dams of the Uttar Pradesh (UP) show that floating solar photovoltaic (FSPV) systems may generate sustainable electricity while also significantly reducing water evaporation.

These reservoirs were selected for their size as well as for their location in the tropical climate, which is distinguished by high sunlight exposure and consequently high evaporation rates. These reservoirs are predominantly found in the Bundelkhand and Vindhyachal regions of Uttar Pradesh.

The Penman-Monteith equation was used in the study to calculate the evaporation rates from these particular dams. Meteonorm provided information on global horizontal irradiation, horizontal diffuse irradiation, wind speed, temperature, and relative humidity. The overall surface area and gross water storage capacity of the dams are 133,208 hectares and 18,139.54 million cubic meter, respectively. The estimated evaporation ranged from 2246 mm at Kalagarh Dam to 2451 mm at Gunta Dam. According to estimates, the average annual evaporation is 2374 mm, which translates to an annual evaporation volume of 1577.47 million cubic meter, or 8.7% of the total storage capacity.

A potential approach to lower these excessive evaporation rates is to install FSPV systems on these reservoirs. The study estimates that annual water losses can be minimized up to 92.56 million cubic meters (MCM) with FSPV coverage of 25% of the surface area with FSPV plants. Even with a 10% area coverage, up to 37.02 million cubic metre (MCM) of water can be saved yearly. This assessment made using experimental data demonstrates a 23.44% decrease in evaporation from the water surface covered by FSPV systems with a panel height of 300 mm above the surface.

With this novel strategy, water security in the drought-prone Bundelkhand and Vindhyachal regions could be improved while also producing renewable energy.

The estimation of evaporation reduction from the dams of Uttar Pradesh emphasizes the dual advantages of floating solar PV arrays for both energy production and water conservation. These installations, especially in tropical areas with high evaporation rates, would mark a substantial advancement in sustainable water and energy management with careful planning and implementation.

7.4. Summary and Recommendations

The study of Floating Solar Photovoltaic (FSPV) installations in Uttar Pradesh (UP), India, has provided important insight into how this ground-breaking method might address the twin concerns of renewable energy generation and water conservation. In areas like the UP, which are renowned for their high levels of sunshine exposure and high rates of evaporation, FSPV presents a possible option for sustainable expansion by utilizing the capacity of already-existing water bodies, including dams and reservoirs.

- The study discovered an interesting correlation between evaporation reduction and panel heights. The experimental results highlighted that the maximum evaporation reduction occurred from the water surface covered with a panel at a height of 300 mm above the water.
- The evaporation reduction estimated was 23.44 % for a panel at a height of 300 mm above the water.
- The management and conservation of water resources are aided by the decrease in evaporation losses. The extension of the study for 28 major dams of Uttar Pradesh, reveals an annual water saving of 92.56 million cubic meters (MCM) with FSPV coverage of 25%.
- The benefits of FSPV extend to both environmental preservation and societal well-being. Beyond augmenting energy production, FSPV contributes to improving water quality by reducing algae proliferation. Moreover, its capacity to diminish evaporation losses presents a solution to water scarcity challenges. Based on estimations, a 1 MWp FSPV installation saves approximately 2451 cubic meters of water annually. Consequently, such an installation can provide water for 67 individuals annually in rural tropical areas, assuming a per capita daily requirement of 100 liters.

Based on the conclusions drawn from the study of FSPV installations at varying heights for evaporation reduction estimation for Major Dams of the tropical region of Uttar Pradesh, India, the following are recommended:

- The study recommends panel height of 300 mm above the water surface for installation of FSPV to maximize the evaporation reduction.
- The evaporation reduction with the recommended panel height above the water surface for installation of FSPV is 23.44% annually.

Chapter 8

Evaporation Dynamics: Analysis of experimental data and Model Development for open and PV covered water bodies.

Abstract

Addressing the pressing issue of water evaporation estimation and management within the context of India's water scarcity challenges, the significance of water as a vital resource for diverse sectors, encompassing agriculture, industry, and daily necessities, is underscored. Given the escalating water stress and climate uncertainties, effective water resource management, including the minimization of evaporation losses, has emerged as a critical priority. Surveying both traditional and innovative methods for estimating evaporation, it sheds light on the complexities inherent in diverse climatic conditions.

Focusing on the development of regression models for evaporation estimation under varied conditions, notably in Floating Solar Photovoltaic (FSPV) installations, it draws from experiments conducted in Pilani, India. The dynamics of evaporation and the validation of estimation models are highlighted. Furthermore, the influence of various meteorological parameters on evaporation rates is explored, providing insights into model selection based on data availability and precision.

The study extends its analysis to 28 dam sites, comparing evaporation rates under uncovered and FSPV-covered conditions. It underscores the efficacy of FSPV installations in reducing evaporation rates and provides recommendations for optimal coverage strategies. Decision-making charts are developed to aid practitioners and decision-makers in evaluating installation capacities, costs, evaporation reductions, and energy generation potential, facilitating informed decisions regarding FSPV installations. Finally, it offers a comprehensive exploration of water evaporation estimation and management, emphasizing the significance of precise modeling techniques and practical considerations for effective water resource conservation and energy generation strategies, particularly in the context of FSPV installations at dam sites.

8.1 Introduction

Water is an essential resource that sustains life on our planet. It is often referred to as the elixir of life. In India, water scarcity is a recurring challenge, and effective management of this finite and precious resource is crucial. One of the significant factors contributing to the loss of water resources is evaporation, especially in the drought affected regions, with high temperatures and prolonged dry spells. This chapter explores different methods used in India to estimate water evaporation and innovative approaches to manage this precious resource.

It is hard to overstate the importance of water as a resource for sustaining life, particularly in India where agriculture, a major factor in the economy, is heavily reliant on it. Water also plays a critical role in supporting ecosystems, meeting industrial demands, and fulfilling the daily needs of a growing population. As water stress and climate uncertainties continue to mount, effective water management has become more important than ever. One key strategy in this context is reducing water evaporation, which is a significant problem in arid and semi-arid regions like India. In this chapter, we'll explore various techniques used worldwide as well as in India to estimate water evaporation and innovative approaches to managing this precious resource.

In this study both conventional techniques like the pan evaporation method and other approaches are examined. The diversity of methodologies utilized across different regions is explored, and the strengths and limitations of each method are scrutinized. This sheds light on the complexities of estimating evaporation in India's heterogeneous climatic conditions.

In order to consider the impact of changing weather patterns and water scarcity, most appropriate methods of estimating water evaporation must be explored. This chapter delves into the development and application of new approaches, with a focus on how they can be adapted to meet India's specific needs. By incorporating advancements in meteorology, and data analytics, accuracy in evaporation estimation can be improved to better manage water resources.

It's important to have empirical evidence to guide the discussions on water evaporation estimation in India. This chapter presents the outcomes of an experimental study conducted in Pilani, a region known for its arid climate and persistent water scarcity issues. The study spanned three years and involved meticulous collection of pan evaporation data and atmospheric information. By comparing the recorded evaporation rates with estimates derived from established formulae, valuable insights into the accuracy and suitability of existing methods in a real-world is obtained on water-scarce scenario. It is crucial to

understand the role of water evaporation estimation in the broader context of water resource management and conservation. This chapter serves as a foundation for comprehending the challenges, opportunities, and innovations in the quest to conserve this precious resource. Ultimately, this knowledge contributes to a sustainable future for India's water landscape.

8.2 Model development and Methodology

There are various methods, which have been used to estimate evaporation from the water surface. The main methods are essentially based on the concepts of mass and energy transfer as discussed earlier. Evaporation values were estimated using these methods and were compared using field data mainly at American or European climatic conditions. However, these methods were rarely tested under Indian conditions. The emphasis of this research work was to develop a model which can be utilised to estimate the evaporation under Indian conditions. Hence data were collected and analysed for suitable action plans.

Each evaporation estimation methods have their own advantages and disadvantages. Choosing the most appropriate method for measuring evaporation rates can be challenging due to the wide range of equations available and the varying expertise required to use them correctly. Additionally, there are no objective criteria for selecting a model, and it is not always clear which method would be most suitable for a given study. To address these concerns, this study aims to analyse and develop a statistical model comparing with pan evaporation data collected and develop a form of generalized model. The ideal model should be analytical and simple, with easily measurable variables and the most important influencing factors. Other simple models should also be special cases of the generalized model, and the model parameters should be easily estimated with acceptable accuracy. Keeping in view of these facts, this Chapter aims to deal a simple and handy prediction model for evaporation. Thus, study is divided into five parts:

I. Evaporation Dynamics to understand key parameters

II. Existing Evaporation Estimation methods

III. Data collection

IV. Model development to estimate evaporation using regression analysis under two specific conditions: uncovered water surface area and provision of cover through FSPV panels.

V. Estimation of evaporation under above two site conditions at twenty-eight selected dam sites using a recommended model.

VI. Development of decision making charts, namely water surface area (ha) vs FSPV installation Capacity MWp (DC), FSPV cost of installation (Rs./Wp), evaporation reduction (TMC), and average annual energy generation (MWh).

The development of a model involves a number of important steps, starting from data collection, calibration, verification and its prediction. Therefore, it is important to analyse evaporation dynamics for a systematic model development, which are discussed in subsequent sections.

8.3 Evaporation Dynamics

A process by which liquid water is converted into vapour and transported away from the surface is known as evaporation. This phenomenon takes place from various surfaces such as river, lake, dam/reservoir etc. In this process water molecules obtains energy from solar radiation to convert into vapour and vapour deficit, difference between vapour pressure at evaporating surface and surrounding atmosphere, drives the vapours away from the water surface. The loss in water takes place only when these vapours are transported away from the surface and drier air is supplemented on the surface, where wind speed plays its role. So assessment of evaporation greatly depends on climatological factors Solar radiation, ambient temperature, humidity and wind speed. The evaporation rates are normally expressed in millimetres (mm) per unit time.

Radiation, ambient temperature, humidity and wind speed are principal weather components affects the evaporation, but the evaporation is also affected by site location, altitude above mean sea level, and latitude of the site.

The data required for the estimation of evaporation are

8.3.1 Temperature

The solar radiation absorbed by the air increases temperature of the air, which transfers the sensible heat to the water thereby controls the evaporation process. So, it is important to know the temperature of the air for estimation of evaporation. The temperature is measured from thermometer, thermistor or thermocouple kept inside shelters (Stevenson screens or ventilated radiation shields) placed in line with World Meteorological Organization (WMO) standards at 2 m above the ground. Daily maximum and minimum temperature and /or average daily temperature is required to estimate of vapour pressure. Due to non-linearity of humidity, the vapour pressure for a certain period is computed as the mean between the vapour pressure at the daily maximum and minimum air temperatures of that period. The slope of saturation vapour curve (Δ) is calculated by mean daily air Temperature (Tmean).

The mean daily air temperature is calculated by averaging maximum daily air temperature (Tmax) and minimum daily air temperature (Tmin) as given in equation (8.1).

$$Tmean = \frac{Tmax+Tmin}{2} \quad (8.1)$$

The temperature is measured in Celsius (°C) or Fahrenheit (°F) or in Kelvin(K) which can be obtained by adding 273.16 to the temperature recorded in degrees Celsius.

8.3.2 Humidity

While the solar radiations are driving force for evaporation while the vapour pressure deficit are the determining factor for vapour removal from the water surface. Humidity of air is the water content of the air, plays a crucial role in the process of evaporation, so it is important parameter required for estimation of evaporation. The actual vapour pressure if not readily available then it can be estimated by relative humidity utilising wet bulb and dry bulb temperature or wet bulb temperature.

8.3.3 Radiation

The solar radiation is the primary and largest source of energy reaching at evaporating surface, which converts water into vapours. The solar radiation reaching any place depends on the latitude, season and location of the place. The solar radiation reaching on earth also depends on turbidity in the atmosphere as well as clouds in the sky. The average daily net solar radiation is required for estimation of evaporation, which can be obtained either by pyranometer or from the (average) actual sunshine hour recorded at the site by Campbell-Stokes recorder.

8.3.4 Wind Speed

The process of removing water vapour depends heavily on wind and air turbulence, which transfer large quantities of air over the evaporating surface. If the air is not continuously replaced with drier air, the rate of evaporation decreases, which reduces the driving force for water vapor removal. For estimation of evaporation wind speed is an important parameter. The average daily wind speed is normally measured at 2 m height or 10 m above the height.

8.3.5 Atmospheric Parameters

There are several atmospheric parameters required for expressing principal weather parameters. Some of these parameters are

Atmospheric pressure

Atmospheric pressure (P) decreases with increase in altitude which in turn increases evaporation. As per gas law, at 20°C, standard atmospheric pressure is given by equation (8.2) (Burman et al.,1987).

$$P = 101.3\left(\frac{293-0.0065z}{293}\right)^{5.26} \quad (8.2)$$

where, P is atmospheric pressure (kPa),

z is elevation above sea level (m); for Pilani z = 299m has been utilised and atmospheric pressure at Pilani P = 97.82 kPa.

Latent Heat of vaporisation

The latent heat of vaporisation (λ) is the energy required to change unit mass of water from liquid state to vapour state at constant temperature and pressure. It is normally taken as 2.45 MJ/ kg^{-1} at 20°C. Harrison (1963) given an expression utilizing ambient temperature to estimate latent heat of vaporization.

Psychrometric constant

The psychrometric constant (γ) is given by equation (8.3) Brunt (1952):

$$\gamma = \frac{c_p\, P}{\varepsilon\, \lambda} = 0.665 \text{ x}10^{-3}\, P \quad (8.3)$$

where γ is a psychrometric constant [kPa $°C^{-1}$],

P is the atmospheric pressure [kPa],

λ is the latent heat of vaporization, 2.45 [MJ kg^{-1}],

c_p is the specific heat at constant pressure, 1.013X 10^{-3} [MJ kg^{-1} $°C^{-1}$], and

ε is the ratio molecular weight of water vapour/dry air = 0.622.

Vapour Pressure

The vapour pressure is the pressure exerted by the water vapour in the air, which is directly measure of the water content in the air. This pressure contributes to the total atmospheric pressure, measured in SI unit pascals (Pa). 1 Pa = $1N/m^2$.

Saturation Vapour Pressure

It is an equilibrium state of air, at a temperature, when water molecules in the air cannot be increased. This pressure of air is known as saturation vapour pressure ($e_0(T)$). As temperature

increases water holding capacity of air increases exponentially. So slope of saturation pressure curve (Δ)is very important in the process of evaporation (Tetens,1930;Murray,1967).

Actual Vapour Pressure

The actual vapour pressure (e_a) is the pressure due to vapour content at the given state of air, which is equal to or less than the saturation vapour pressure.

Relative Humidity

Relative humidity (Rh) is the ratio of actual vapour pressure(e_a) to the saturated vapour pressure ($e_0(T)$) is given in equation in (8.4).

$$\text{Rh} = \frac{e_a}{e_0(T)} \times 100 \quad (8.4)$$

The actual vapour pressure cannot be measured but estimated from relative humidity or dew point temperature. The dew point temperature is the temperature at which actual vapour becomes saturated vapour pressure.

Mean Saturation vapour pressure

The mean saturation vapour pressure (e_s) is estimated by air temperature is given in equation in (8.5) Tetens (1930)

$$e_0(T) = 0.6108 \exp\left(\frac{17.27\,T}{T + 237.3}\right) \quad (8.5)$$

where,

$e_0(T)$ is the saturation vapour pressure at the air temperature T [kPa],

T is the air temperature [°C],

exp[..] 2.7183 (base of natural logarithm) raised to the power [..].

The saturation vapour pressure for daily maximum e0 (Tmax) and daily minimum temperature (Tmin) are calculated from above expression and averaging the two values gives mean saturation vapour pressure is given in equation in (8.6)

$$e_s = \frac{e_0(Tmax) + e_0(Tmin)}{2} \quad (8.6)$$

Slope of saturation vapour pressure curve

The slope of saturation vapour pressure curve (Δ) at a given temperature is estimated by in equation in (8.7) (Tetens,1930; Murray,1967)

$$\Delta = \frac{4098\left(0.6108\ exp\left(\frac{17.27\,T}{T+237.3}\right)\right)}{(T+237.3)^2} \quad (8.7)$$

where,

Δ is the slope of saturation vapour pressure curve at air temperature T [kPa °C^{-1}],

T is the air temperature [°C],

exp[..] 2.7183 (base of natural logarithm) raised to the power [..].

The slope of saturation vapour pressure curve (Δ) has been estimated by using mean air temperature.

Actual vapour pressure

The actual vapour pressure (e_a) can be estimated by using dew point temperature in equation (8.5), though in the present case the actual vapour pressure is estimated using relative humidity data, using equation in (8.8).

$$e_a = \frac{e_0(Tmin)\frac{Rh_{max}}{100} + e_0(Tmax)\frac{Rh_{min}}{100}}{2} \quad (8.8)$$

where,

e_a is actual vapour pressure [kPa],

e_0 (Tmin) is the saturation vapour pressure at daily minimum temperature [kPa],

e_0 (Tmax) is the saturation vapour pressure at daily maximum temperature [kPa],

Rh_{max} is the maximum relative humidity [%],

Rh_{min} is the minimum relative humidity [%].

For periods of a month, Rh_{max} and Rh_{min} were obtained by dividing the sum of the daily values by number of days in that month.

Vapour Pressure Deficit

The difference between the saturation vapour pressure and actual vapour pressure is known as vapour deficit, which is given in Equation (8.9).

Vapour pressure deficit = e_s - e_a (8.9)

8.3.6 Solar Radiation

Extra-terrestrial Radiation

The solar radiation reaching on the top of earth's atmosphere is known as extra-terrestrial radiation (R_a). It's value on the perpendicular surface is 1367 W/m^2 or 0.082MJ/m^2 min, also called solar constant. The value changes as day proceeds as well as change in season due to change of sun's angle with the given location. R_a values for each day of the year have been derived for Pilani from the equation (8.10) given below (Allen,1996; Duffie & Beckman ,1991):

$$R_a = \frac{24(60)}{\pi} G_{sc}\, d_r\, [\omega_s\, sin(\varphi)\, sin(\delta) + \, cos(\varphi)\, cos(\delta)\, sin(\omega_s)] \quad (8.10)$$

where,

R_a is the extra-terrestrial radiation [MJ m^{-2} day^{-1}],

G_{sc} is the solar constant = 0.0820 [MJ m^{-2} min^{-1}],

d_r is the inverse relative distance Earth-Sun (Equation 8.12),

ω_s is the sunset hour angle [rad] (Equation 8.14),

ϕ is the latitude [rad] (Equation 8.11),

δ is the solar declination [rad] (Equation 8.13).

$$\text{Radian} = \frac{\pi}{180}(decimal\ degrees) \quad (8.11)$$

The inverse relative distance Earth-Sun, d_r and solar declination δ is given by Equation (8.12) and Equation (8.13) respectively.

$$d_r = \, 1 + \, 0.033\, cos\, \left(\frac{2\pi}{365}\, J\right) \quad (8.12)$$

$$\delta \, = \, 0.409\, sin\left(\frac{2\,\pi}{365}\, J - 1.39\right) \quad (8.13)$$

where,

J is the number of the day in the year between 1 (1 January) and 365 or 366 (31 December).

For Pilani latitude angle is 28.38 N.

The sunset hour angle, ω_s is given by Equation (8.14)

$$\omega_s = \, \, arccos\, [-tan(\varphi)\, tan(\delta)] \quad (8.14)$$

Daylight hours

The daylight hours are location dependent as well as season dependent. Its value changes as the sun's position changes every day, so daily daylight hours can be estimated by sunset hour angle ω_s in radian, using the Equation (8.15)

$$N = \frac{24}{\pi}\omega_s \tag{8.15}$$

Table 8.1 provides the estimated daylight hours and extra-terrestrial radiation for each month in Pilani. Meanwhile, Figure 8.1 and Figure 8.2 depict the plot of extra-terrestrial radiation and daylight hours, respectively.

Table 8.1. Monthly estimated daylight hours and extra-terrestrial radiation at Pilani

Month	**Daylight hours N(h)**	**R_a (MJ m^{-2} day^{-1})**
January	10.39	22.04
February	11.00	26.46
March	11.80	32.01
April	12.69	37.08
May	13.41	39.97
June	13.80	40.98
July	13.64	40.42
August	13.02	38.15
September	12.16	33.83
October	11.30	28.29
November	10.56	23.12
December	10.20	20.72

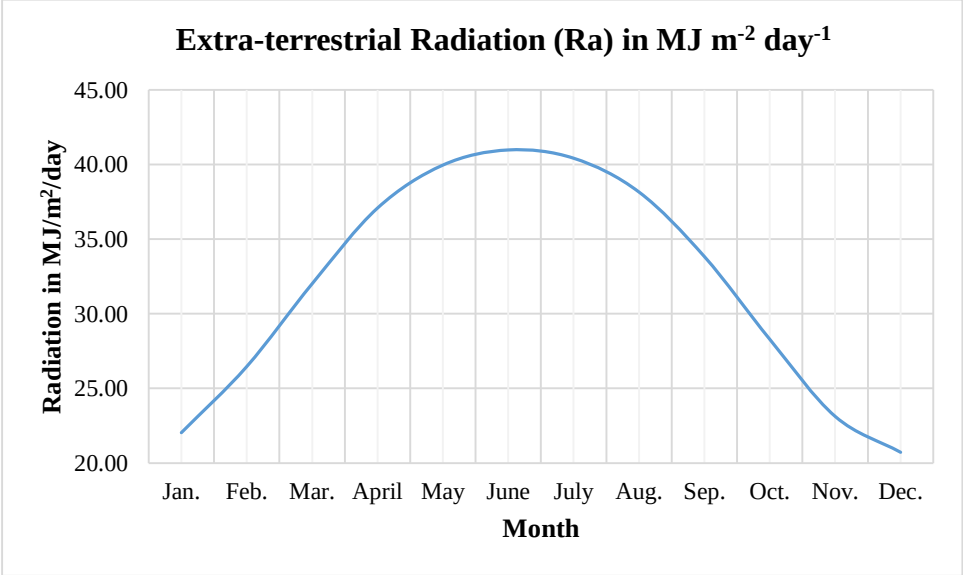

Figure 8.1. Average monthly Extra-terrestrial Radiation plot

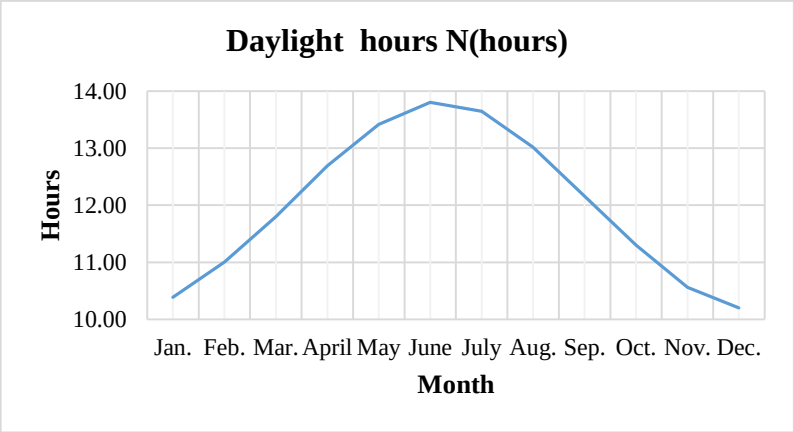

Figure 8.2. Average monthly daylight hours' plot

Solar or shortwave radiation

The Sun emits electromagnetic waves characterised by short wavelengths, so these radiations are known as shortwave radiations. The radiations emitted by sun while travelling through the atmosphere encounters with cloud, dust, gases etc. So, some part of these radiation scatters, reflected or absorbed by these atmospheric elements. The amount of energy/radiation reaches earth is known as solar or shortwave radiation (R_s). These radiations are measured by Pyranometer.

For recording these radiations Pyranometer was installed at Pilani campus. The pyranometer CMP11 was installed at an angle of 25 degree with the horizontal. These values recorded at an angle of 25 degree were converted to horizontal plane by cosine formula given in Equation (8.16)

$$I_2 = I_1 \, x \, \frac{cos\, \theta_1}{cos\, \theta_2} \tag{8.16}$$

where,

I_1 is Pyranometer recorded value at angle θ_1.

I_2 is Estimated pyranometer value at angle θ_2.

θ_1 is original angle of pyranometer.

θ_2 is Angle at which value is desired.

The readings from CMP11 were sometimes disrupted so records of pyranometer installed at Pilani solar power plant were utilised for unavailable period. However, this pyranometer is installed at 0.739 degree with the horizontal. So, values of this pyranometer were converted to horizontal plane by cosine formula given in Equation (8.16). Secondly, the readings of both pyranometer were observed for available period were observed to be having some differences, so a regression analysis was carried out and the following Equation (8.17) was obtained

$R_{s\,(CMP11)} = 1.91278 + 0.53476\ R_{s(pp)}$ (8.17)

where,

$R_{s(CMP11)}$ is Pyranometer reading of CMP11

$R_{s(pp)}$ is Pyranometer reading of Pilani Solar power plant

The values obtained are 99.99% significant and $R^2 = 0.7138$.

In the absence of pyranometer the solar or shortwave radiations are estimated by the Angstrom (1924) formula given in Equation (8.18)

$$R_s = \left(a_s + b_s \frac{n}{N}\right) R_a \quad (8.18)$$

where,

R_s is solar or shortwave radiation [MJ m^{-2} day^{-1}],

n is actual duration of sunshine [hour],

N is maximum possible duration of sunshine or daylight hours [hour],

n/N is relative sunshine duration [-],

R_a is extra-terrestrial radiation [MJ m^{-2} day^{-1}],

a_s is regression constant, expressing the fraction of extra-terrestrial radiation reaching the earth on overcast days (n = 0),

a_s+b_s is fraction of extra-terrestrial radiation reaching the earth on clear days (n = N) as are expressed in the above equation.

The Angstrom values a_s and b_s varies with atmospheric conditions and solar declination. In the absence of actual solar radiation, values for $a_s = 0.25$ and $b_s = 0.50$ were recommended by the Angstrom. However, to represent the field conditions correctly, regression constants (a_s = -0.1566 and $b_s = 0.95$) were derived from the solar data collected at Pilani. The data and code are provided in appendix (A-8.3.6).

Clear-sky Radiation R_{s0}

The amount of radiation that reaches earth's surface on cloudless day is known as clear sky radiation, which is approximately 75% of the extra-terrestrial radiation. This is the radiation received by earth surface when actual sunshine hour (n) is equal to daylight hours (N), estimated by Equation (8.19) given below (Allen et al.,1998):

$$R_{s0} = (a_s + b_s) R_a \quad (8.19)$$

Since the calibrated values of a_s and b_s were estimated, so above Equation (8.19) were used to estimate clear-sky radiation R_{s0}. Clear-sky radiation is utilised for estimation of longwave radiation.

Actual Sunshine hour

The actual sunshine hour (n) defined by World Meteorological Organisation (WMO, 2008; WMO,1983) as the duration in number of hours for which the direct solar irradiation is above 120 W/m^2 . In the absence of pyranometer, it can be measured with a Campbell Stokes sunshine recorder. A plot for actual sunshine hour and daylight hour for the month of April 2021 is plotted in Figure 8.3.

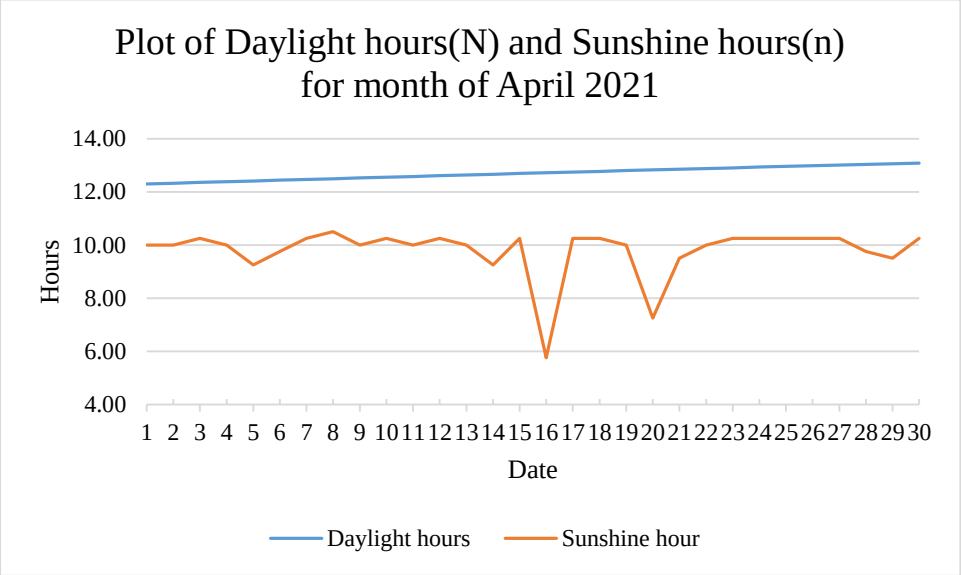

Figure 8.3. Plot of Daylight hour (N) and actual sunshine hour (n) for April 2021

Plot of a graph of Extra-terrestrial radiation Ra, Clear-sky radiation (R_{so}), and Shortwave radiation (R_s) is shown in Figure 8.4. It shows the relationship between these types of radiation and can provide useful information for studying radiation levels.

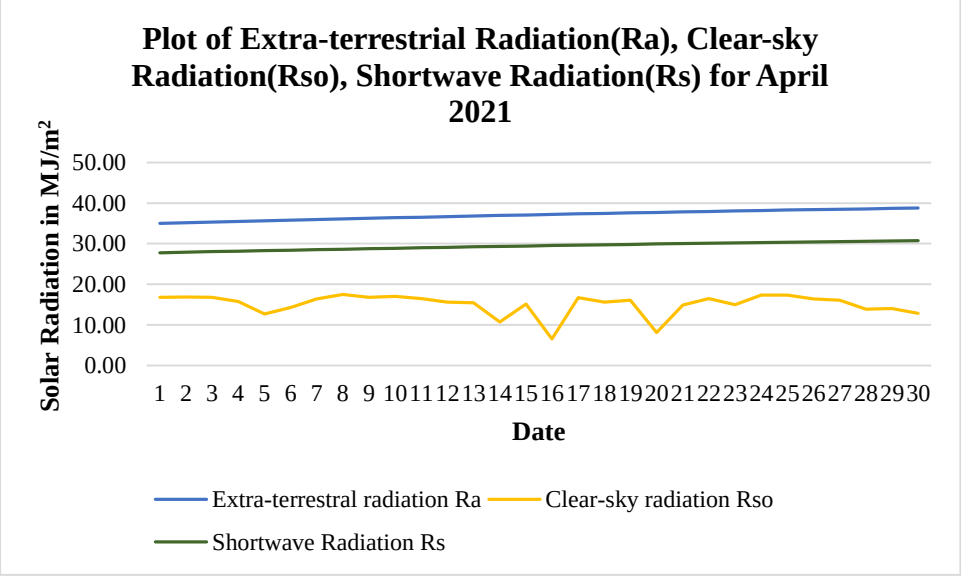

Figure 8.4. Plot of a graph of Extra-terrestrial radiation (R_a), Clear-sky radiation Rs_0, and Shortwave radiation (R_s)

Net longwave radiation

The earth receives heat energy from the sun through solar radiation. However, this energy is lost to the atmosphere through the emission of radiation from the surface of the earth. The radiation emitted by the earth has a longer wavelength than the radiation emitted by the sun, which is why it is called longwave radiation. As the radiation emitted by the earth (Rl,up) is absorbed by the atmosphere, it increases the temperature of the atmosphere, which in turn emits radiation (Rl,down). Part of this longwave radiation reaches the earth's surface, causing the earth to emit longwave radiation as well as receive it. The net longwave radiation (Rnl) is the difference between outgoing and incoming longwave adiation, with the sign convention for outgoing radiation being negative and for incoming radiation being positive. Generally, outgoing longwave radiation is higher than incoming longwave radiation.

Nowadays, the net longwave radiation can be recorded by the instruments but mostly these values are unavailable, so several formulations have been reported in the literature.

Downward Clear Sky Longwave radiation

Following Equations (8.20-8.28), have been used to simulate the downward longwave radiation ($R_{lo(down)}$) for clear sky:

$$R_{lo(down)} = \varepsilon_e(C_{cloud}, e_a, T_{aK})\, \sigma T_{aK}^4 \quad (8.20)$$

where,

C_{cloud} is cloud fraction

ε_e is effective emissivity of the atmosphere (under all sky conditions)

T_{aK} is air temperature in Kelvin

e_a is vapour pressure equation (8.8) [in hPa]

Crawford & Duchon (1999) , given equation (8.21) for estimation of cloud fraction

$$C_{cloud} = (1 - s) \quad (8.21)$$

where,

$$s = \frac{R_s}{R_{so}}$$

R_s is measured solar radiation [MJ m^{-2} day^{-1}],

R_{so} is calculated (Equation 8.19) clear-sky radiation [MJ m^{-2} day^{-1}].

Brunt (1932) did original work in Benson (UK) to develop a model and have given equation (8.22):

$$R_{lo(down)} = \left(a_1 + b_1 e_a^{1/2}\right)\sigma T_{aK}^4 \quad (8.22)$$

where,

a_1 is 0.55,

b_1 is 0.065 [$hPa^{-1/2}$]

These equations have empirical constants valid for original location, however values for empirical constants were derived for other places and the variation for a_1 varies up to 13% and b_1 varies up to 32%.

Swinbank (1963) developed equation (8.23) for Australia, Indian Ocean at low latitude, England and France, having annual average temperature ranging from 2-29 degree Celsius and utilised screen level temperature

$$R_{lo(down)} = (a_2 T_{aK}^2)\sigma T_{aK}^4 \quad (8.23)$$

where,

a_2 is 9.36 x10^{-6} [K^{-2}],

Idso & Jackson (1969), developed the equation (8.24) for Australia and Indian ocean with temperature range -29 to 37 degree Celsius.

$$R_{lo(down)} = (1 - a_3 exp\,[b_3(273 - T_{aK})^2]T_{aK}^2)\sigma T_{aK}^4 \quad (8.24)$$

where,

a_3 is 0.269,

b_3 is -7.77 x 10^{-4} [K^{-2}]

In equation (8.23) and (8.24) effective emissivity is function of air temperature.

Based on the research conducted by Brutsaert in 1975, equation (8.25) was developed using radiative transfer theory and data from various sources. This analytical equation considers screen level temperature and vapour pressure, providing a comprehensive understanding of the atmospheric conditions.

$$R_{lo(down)} = \left(a_4 \left[\frac{e_a}{T_{aK}}\right]^{b_4}\right)\sigma T_{aK}^4 \quad (8.25)$$

where,

a_4 is 1.24 [K/hPa] [b4],

b_4 is 1/7.

Idso (1981), developed equation (8.26) for Phoenix (Australia) for air temperature ranging -10 to 45 degree Celsius, utilising parameters air temperature in Kelvin and actual vapour pressure in hecto Pascal.

$$R_{lo(down)} = \left(a_5 + b_5\, e_a\, exp\left(\frac{1500}{T_{aK}}\right)\right)\sigma T_{aK}^4 \quad (8.26)$$

where,

a_5 is 0.7,

b_5 is 5.95 x 10^{-5} [hPa^{-1}]

Prata (1996) developed equation (8.27) based on Brutsaert(1975) equation and adjusted slab emissivity for temperature range -40 to 40 degree Celsius,

$$R_{lo(down)} = \left(1 - \left[(1+Y)exp\left(-(a_6 + b_6 Y)^{1/2}\right)\right]\right)\sigma T_{aK}^4 \quad (8.27)$$

where,

a_6 is 1.2,

b_6 is 3 [cm^2/g]

Y is 46.5 (e_a/T_{aK}) [g/cm^2].

According to Carmona et al. (2014), it is recommended to use the Swinbank (1963), Brutsaert (1975) and Idso (1981) models for estimating the downward clear sky longwave radiation. These models have been observed to result in an error within 10%. Dekok et al. (2019) though reported under estimation of clear sky downward longwave radiation estimate but suggested to use this equation as it incorporates vapour pressure in its equation. It was found that the Brutsaert (1975) equation considers both vapour pressure and air temperature produced the best results.

Brutsaert (1975) has given equation (8.25), which is expressed as equation (8.28):

$$R_{lo(down)} = \varepsilon_{clear}\, \sigma T_{aK}^4 \quad (8.28)$$

where,

$\varepsilon_{clear} = \left(a_4 \left[\frac{e_a}{T_{aK}}\right]^{b4}\right)$

Various researchers have recommended empirical values for a_4 and b_4 , these values are summarised below

Brutsaert (1975)	$a_4 = 1.24$	$b_4 = 1/7$
Sicart et al. (2010)	$a_4 = 1.15$	$b_4 = 1/7$
Konzelmann et al. (1994)	$a_4 = 0.443$	$b_4 = 1/$ value higher than7
Dekok et al. (2019)	$a_4 = 1.13$	$b_4 = 1/9.09$

So, Brutsaert (1975) equation with original empirical constant and value derived by Dekok et al. (2019) for Indian conditions have been utilised to estimate clear sky downward longwave radiation in this study.

Downward Cloudy Sky Longwave radiation

Based on these clear sky model, downward cloudy sky longwave radiation ($R_{l(down)}$) models were developed, resulting in the creation of Equations (8.29-8.34).

Maykut & Church (1973) model

$$R_{l(down)} = R_{lo(down)}\left(1 + 0.22C_{cloud}^{2.75}\right) \quad (8.29)$$

Jacobs (1978) model

$$R_{l(down)} = R_{lo(down)}(1 + 0.26\, C_{cloud}) \quad (8.30)$$

Sugnita & Brutsaert (1993) model

$$R_{l(down)} = R_{lo(down)}\left(1 + 0.0496C_{cloud}^{2.45}\right) \quad (8.31)$$

Konzelmann et al. (1994) model

$$R_{l(down)} = R_{lo(down)}(1 - C_{cloud}^4) + 0.952\, C^4 \sigma T_{aK}^4 \quad (8.32)$$

Crawford & Duchon (1999) model

$$R_{l(down)} = R_{lo(down)}(1 - C_{cloud}) + C_{cloud}\, \sigma T_{aK}^4 \quad (8.33)$$

Lhomme et al. (2007) model

$$R_{l(down)} = R_{lo(down)}(1.03 + 0.34\, C_{cloud}) \quad (8.34)$$

Durate et al. (2006) used the Equation (8.33) given by Crawford & Duchon (1999) for Brazil, Choil et al. (2008) also recommended Equation (8.33) after using it for Central Florida. Alados et al. (2011) used the Equation (8.33) at Taberna, Almeria, Spain and Palaiseau, France, where it performed well. Since Crawford & Duchon (1999) equation does not incorporate any coefficient in its expression, being able to ensure optimal results without previous calibrations under different climatic conditions.

So, (Crawford and Duchon ,1999) Equation (8.33) is being utilised for estimation of estimation of cloudy sky downward longwave estimation.

Longwave radiation Upward

The clear sky longwave radiation emitted by earth i.e. Longwave radiation Upward ($R_{lo(upward)}$) can be estimated by Penman (1948) Equation (8.35), which is based on Brunt (1939) equation:

$$R_{lo(upward)} = \sigma T_{aK}^4 \quad (8.35)$$

where,

σ is Stefan-Boltzmann constant [4.903 10-9 MJ K^{-4} m^{-2} day^{-1}],

T_{aK} is air temperature in Kelvin

This Equation (8.35) is based on two assumptions, the first one is that emissivity of earth surface is assumed to be unity and the other assumption is that temperature of earth is same as that of air. Hough (1997) and Allen et al. (1998) suggested Equation (8.36):

$$R_{lo(upward)} = \varepsilon_{land}\, \sigma T_{aK}^4 \quad (8.36)$$

where,

σ is Stefan-Boltzmann constant [4.903 10-9 MJ K^{-4} m^{-2} day^{-1}],

T_{aK} is air temperature in Kelvin.

ε_{land} is emissivity of land surface taken as 0.95.

Net Longwave radiation

Net longwave radiation (R_{nl}) is the difference between upward longwave radiation and downward longwave radiation.

Allen et al. (1999) reported a modified equation to estimate longwave energy emission follows Stefan-Boltzmann law, where energy emission is proportional to the fourth power of raised surface temperature. The modified equation also incorporates humidity and cloudiness

factors as they absorb and emits the longwave. The Equation (8.37) is proposed by them is given below:

$$R_{nl} = \sigma\left[\frac{T_{max,K}^4+T_{min,K}^4}{2}\right]\left(0.34 - 0.14\sqrt{e_a}\right)\left(1.35\frac{R_s}{R_{s0}} - 0.35\right) \quad (8.37)$$

where,

Rnl is net outgoing longwave radiation [MJ m^{-2} day^{-1}],

σ is Stefan-Boltzmann constant [4.903 10-9 MJ K^{-4} m^{-2} day^{-1}],

$T_{max,K}$ is maximum absolute temperature during the 24-hour period [K = °C +273.16],

$T_{min,K}$ is minimum absolute temperature during the 24-hour period [K = °C + 273.16],

e_a is actual vapour pressure [kPa],

R_s/R_{so} is relative shortwave radiation (limited to ≤ 1.0),

R_s is measured solar radiation [MJ m^{-2} day^{-1}],

R_{so} is calculated [Equation (8.19)] clear-sky radiation [MJ m^{-2} day^{-1}].

Rs/Rso term is limited to $Rs/R_{so} \leq 1.0$.

The other method given by Brutsaert (1975) , Equation (8.38) is utilised for estimation of longwave radiation

$$R_{nl} = \varepsilon_{land}\sigma[T_{aK}^4]\left(a_4\left[\frac{e_a}{T_{aK}}\right]^{b4} - 1\right)X\,[0.2 - 0.8\left(\frac{n}{N}\right)] \quad (8.38)$$

The equation for European condition reported by Finch & Hall (2001)

$$R_{nl} = \sigma[T_{aK}^4]\left(0.092\sqrt{e_a} - 0.56\right)X\left(1 - 0.09\left(\frac{n}{N}\right)\right) \quad (8.39)$$

All nomenclatures are described above. Equations (8.37-8.39) have been utilised for estimating longwave radiation. Original values of a_4 = 1.24 and b_4 = 1/7 in Equation (8.38) given by Brutsaert (1975) and a_4 = 1.12, b_4 = 1/7 for Indian conditions have also been utilised in our analysis.

The longwave estimates of different months from above mentioned methods are provided in the Table 8.2.

Table 8.2. Average Monthly net longwave radiation estimates from various methods at Pilani

Month	Net Longwave Radiation (MJ m^{-2} day^{-1}) By Allen et al. equation (8.37)	Net Longwave Radiation (MJ m^{-2} day^{-1}) clear sky radiation By Brutsaert equation (8.28) and cloudy sky radiation by Crawford and Duchon equation (8.33)	Net Longwave Radiation (MJ m^{-2} day^{-1}) By Brutsaert equation (8.38) with $a_4 = 1.12$, $b_4 = 1/7$	Net Longwave Radiation (MJ m^{-2} day^{-1}) By Finch and Hall equation (8.39)
Jan-21	2.28	0.30	3.64	-14.93
Feb-21	3.05	-1.00	4.71	-15.99
Mar-21	2.61	0.33	4.76	-17.12
Apr-21	3.02	3.09	5.38	-18.37
May-21	1.40	2.64	3.59	-18.14
Jun-21	1.08	1.86	3.29	-17.95
Jul-21	0.54	0.93	2.43	-17.13
Aug-21	1.00	0.90	2.90	-16.88
Sep-21	0.73	0.81	2.26	-16.37
Oct-21	2.56	0.97	3.34	-16.66
Nov-21	2.11	2.06	3.67	-16.19
Dec-21	2.09	2.08	2.89	-15.29
Jan-22	1.34	2.70	1.84	-14.92
Feb-22	3.10	1.55	3.56	-15.61
Mar-22	3.13	1.75	4.41	-17.33
Apr-22	3.07	3.48	5.44	-19.35
May-22	2.53	2.76	4.76	-19.37
Jun-22	3.41	0.91	4.38	-18.62
Jul-22	0.34	1.08	2.24	-16.72
Aug-22	0.52	1.10	2.51	-16.63
Sep-22	1.25	1.02	2.80	-17.07
Oct-22	2.08	1.64	2.80	-16.89
Nov-22	2.87	1.85	3.36	-16.40
Dec-22	3.20	1.48	3.83	-15.14
Jan-23	1.85	2.55	3.13	-14.81
Feb-23	3.97	0.80	4.26	-15.81
Mar-23	4.63	-0.08	4.19	-16.29

Plots of average monthly net Longwave estimates from January 21- March 23 at Pilani are shown in Figure 8.5.

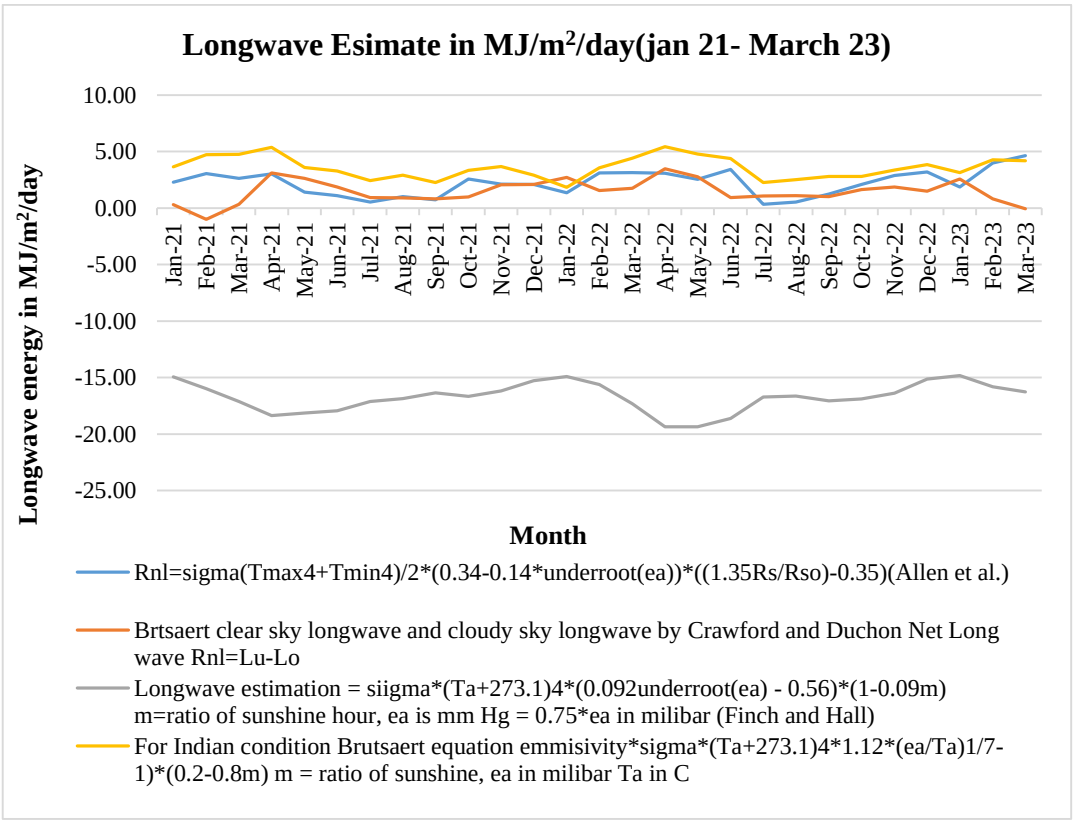

Figure 8.5. Plot of Longwave estimates from various methods at Pilani during January 2021 to March 2023

Based on the data, it seems that the Finch & Hall (2001),formula is not suitable for Indian conditions since the values obtained are quite low, ranging from -15 to -20 MJ m^{-2} day^{-1} and -6.12 to -8.16 mm/day in terms of water depth. On the other hand, the estimates from the other three methods fall within the 0 to 5 MJ m^{-2} day^{-1} range. It's worth noting that the Brutsaert (1975) equation, which includes an empirical constant for Indian conditions, yields slightly higher values compared to the Allen et al. (1998) and Brutsaert (1975), clear sky longwave radiation methods combined with Crawford & Duchon (1999), cloudy sky method. Based on the data presented, it appears that the estimated longwave radiation falls within the range of 0 to 2 mm/day in terms of water depth. Three methods were utilized to estimate the evaporation from a water body and compare it to the observed pan evaporation, using different methods of longwave estimation.

Albedo and net solar radiation

It is interesting to note that a significant portion of solar radiation that reaches the earth's surface is reflected. This reflection is known as the albedo and is denoted by the fraction α. The albedo varies significantly for different surfaces and for the angle of incidence or slope of the ground surface. For instance, the albedo can be as high as 0.95 for freshly fallen snow, while it can be as low as 0.05 for a wet bare soil. According to Cogley (1979), report, the

albedo of water surface varies for different altitudes. At 30-degree latitude, it ranges from 4.7% to 9.6% in different months. For our present work, we have adopted a value of 8% as the albedo of water. The net solar radiation, Rns, can be calculated using Equation (8.40):

$$Rns = (1-\alpha)\, Rs \tag{8.40}$$

where,

α represents the fraction of solar radiation that is reflected from the surface.

Soil heat flux

The soil heat flux, G, is something to consider when examining the energy used to heat the soil. It's important to note that G is positive when the soil is warming and negative when the soil is cooling. However, it's worth noting that the soil heat flux is typically small compared to Rn and may not always be a significant factor to consider. So, in present case it is ignored.

Net radiation

The net radiation, Rn, refers to the energy balance between incoming and outgoing radiation, both short and long wavelengths. It considers the energy absorbed, reflected, and emitted by the earth's surface. Essentially, it's the difference between the incoming net shortwave (Rns) and the net outgoing longwave (Rnl) radiation as given in Equation (8.41).

$$Rn = Rns - Rnl \tag{8.41}$$

8.3.7 Wind speed

When measuring wind, it is important to consider both its direction and velocity. Wind direction indicates the source from which the wind is coming, while wind speed is the variable that matters most when calculating evapotranspiration. However, since wind speed can fluctuate over time, it is necessary to determine an average over a specific period. Typically, wind speed is expressed in terms of metres per second or kilometres per day. Anemometers are used to measure wind speed.

Wind profile relationship

wind speeds can vary depending on the height above the soil surface. The surface friction slows down the wind that passes over it, causing the wind speed to be slowest at the surface and increase with height. To ensure accuracy in measurements, anemometers are placed at a chosen standard height. In meteorology, the standard height is 10 m, while in agrometeorology, it is typically 2 or 3 m.

To estimate wind speed data collected at different elevations, it's important to consider any potential discrepancies. One effective method is to apply a logarithmic wind speed profile. This technique can ensure that the wind speed data is accurate and reliable, even when collected at non-standard heights. Allen et al. (1998), Equation (8.42) is used to estimate wind speed at 2 m from varying height of measurement.

$$u_2 = u_z \frac{4.87}{ln(67.8z - 5.42)} \quad (8.42)$$

where,

u_2 is wind speed at 2 m above ground surface [m s^{-1}],

u_z is measured wind speed at z m above ground surface [m s^{-1}],

z is height of measurement above ground surface [m].

8.4 Existing Evaporation Methods

Evaporation is estimated/quantified by direct experimental observation, using Pan, also known as Evaporimeter. Pans containing water are exposed to atmosphere and water loss due to evaporation is measured at regular interval. Along with water loss meteorological data, parameters such as water temperature, ambient temperature, humidity, wind velocity, precipitation, sunshine hour are also measured. Pan estimation approach has been used worldwide due to their simplicity.

8.4.1 Pan Evaporation Method

Following types of Pans are commonly used for experimentally evaporation estimation:

A. **US Class A pan**- This is circular galvanized iron tank having diameter of 1.21m and 0.255m depth. It is mounted over wooden platform of height 15 cm above ground and water is kept 50mm below the rim. Water level is recorded every 24 hours along with water temperature and wind speed.

B. **USSR GGI-3000 Pan**-This is a cylindrical tank with a diameter of 0.618m, depth at walls 0.6m and at centre 0. 685m.The pan is sunk into the ground with rim 75mm above the ground.

C. **ISI Standard Pan**- This pan is commonly used in India, having almost same dimensions as US Class A pan, this pan diameter is1.22m and 0.255m depth. It is made up of copper sheet 0.9mm thick, mounted over wooden platform of height 10 cm above ground level. It is covered by hexagonal GI wire net to protect water from birds which also makes temperature of water more uniform during the day and night.

Pan evaporation estimates are corrected before it is applied to any water body, since heat transfer characteristics of pan material is different from that of reservoir. Pan coefficients and pan conversions are the factors which is multiplied to pan measurement to get lake evaporation. The coefficients are generally specific to pan type, its location, nature of water body and time.

8.4.2 Analytical Methods

There are several models to indirectly estimate evaporation. Most of the models are intended for use in climates similar to where they were developed and requires wide range of data. Some commonly used methods are briefly mentioned below:

8.4.2.1 Mass Balance

In this method evaporation is calculated as the change in the volume of water stored and the difference between inflow and outflow. General Equation (8.43) (Finch and Hall,2011), for mass balance is

$$E = R + \frac{(V_{is}+V_{ig})-(V_{os}+V_{og})-{}^{dQ}/_{dt}}{A_s} - ET \qquad (8.43)$$

where,

E is the evaporation rate from water body, R is the mean rate of precipitation, V_{is} is the surface inflow rate, V_{os} is surface outflow rate, V_{ig} is ground water and seepage inflow rate and V_{og} is ground water and seepage outflow rate, Q is water stored, ET is evapotranspiration and A_s is the surface area.

This method is suitable for large water bodies and large time scale. However, method is simple, but it is difficult to measure accurately surface inflow and volumes of ground water and seepage inflow and outflow are unknown. So this method is not generally used for evaporation estimation.

8.4.2.2 Energy Budget

This approach is based on law of conservation of energy, in which energy available for evaporation is estimated as the energy component required to close the energy budget when all the component of energy budget, incoming energy, outgoing energy and the energy stored in the water body over a known time interval are known. Two categories of energy are associated with evaporation are, first is the heat required to convert liquid water into water vapour, known as latent heat of vaporization and second is the energy carried by the water

vapour molecules through advection. After direct measurement of evaporation, the energy budget is considered as the most accurate method of estimating evaporation.

Energy budget of a water body is given by Equation (8.44) (Anderson,1954):

$$Q_n = R_s (1- \alpha_s)+R_{lo(down)} (1- \alpha_L) -R_{l(up)}- \lambda E-c_p (T_o-T_b) E-H+ F_{in} - F_{out}+ F_p – G_{sub}. \quad (8.44)$$

The net change in energy storage of water, denoted by Q_n is affected by various factors. These factors include the incident short and long wave radiation, represented by R_s and $R_{lo(down)}$ and the albedos of short and long wave, denoted by α_s and α_L, respectively. Additionally, the outgoing long wave, represented by $R_{l(\mathrm{up})}$ also influences Q_n. The latent heat flux, where λE is the product of the latent heat of vaporization (λ) and the evaporation in mass unit (E), also has an impact on Q_n. The specific heat of water, represented by cp, is another factor that contributes to Q_n. The temperature of evaporated water (T_o) and the base temperature of water (T_b) are also important components that affect Q_n. Furthermore, the sensible heat flux (H), which represents the energy used in warming the atmosphere in contact with the water and is convected upward, plays a role in Q_n. Heat flux from water inflow and outflow from the water body, represented by F_{in} and F_{out} respectively, as well as heat flux due to precipitation (F_p), also affect Q_n. Lastly, the heat conduction between water and its substrate, denoted by G_{sub}, is another factor that influences Q_n. All the aforementioned energy components are measured in units of energy per unit surface area of water.

Substituting, gives Equation (8.45)

$$R_n = R_s(1 - \alpha_s) + R_{lo(down)} (1 - \alpha_L) - R_{l(up)} \quad (8.45)$$

As per Equation (8.41)

$R_n = R_{ns} - R_{nl}$

in energy budget and rearranging gives Equation (8.46)

$$\lambda E + c_p (T_o - T_b) E = R_n + Q_n - H + F_{in} - F_{out} + F_p - Gsub \quad (8.46)$$

Bowen (1926) has given a ratio between sensible heat fluxes and latent heat, β can be expressed as Equation (8.47)

$$\beta = \frac{H}{\lambda E} = \frac{c_p P (T_s - T_a)}{\varepsilon \lambda (e_w - e_a)} \quad (8.47)$$

where c_p is specific of air at constant pressure, P atmospheric pressure while T_s and T_a are temperatures of water surface and air at reference height, ε is ratio of molecular weight of

water to that of dry air, e_w and e_a are saturated vapour pressure of air at water surface temperature and vapour pressure of the air at reference height. The ratio c_p P / ε λ = γ Equation (8.3), is known as psychometric constant. Substituting Bowen ratio, Energy budget equation can be expressed as Equation (8.48)

$$E = \frac{(R_n + Q_n - H + F_{in} - F_{out} + F_p - G_{sub})}{\lambda\,(1+\beta) + c_p(T_o - T_b)}. \quad (8.48)$$

Energy content of water is chiefly governed by the exchange of energy through the surface, so energy terms F_{in}, F_{out}, F_p and G_{sub} are neglected (Henderson-sellers,1986) and energy budget equation takes the form given in Equation (8.49), if we assume $T_o = T_b$,

$$E = \frac{(R_n + Q_n)}{\lambda\,(1+\beta)} \quad (8.49)$$

Also known as reduced energy budget equation. After direct measurement of evaporation, the energy budget is considered as the most accurate method of estimating evaporation.

8.4.2.3 Bulk or Mass Transfer

Bulk or mass transfer equation was given by Sene et al. (1991) which utilizes very few meteorological parameters such as wind speed, saturated vapor pressure, water surface temperature and vapor pressure to determine evaporation. However, empirical constant varies with site. Sene et al. (1991) gave simple derivation of bulk transfer equation as given in Equation (8.50):

$$E = C\,u\,(e_w - e_s) \quad (8.50)$$

Where C is mass transfer coefficient, u is wind speed, e_w and e_s are saturated vapour pressure of air at water surface temperature and vapour pressure of air at reference height. Mass transfer coefficient reflects the transfer characteristic of the particular water body which is determined by its geometry, plantation coverage, topography, land use and climate of surrounding land. So, a common value of C cannot be determined which can be applied to other water bodies. The mass transfer coefficient is determined empirically for a particular water body, so there are many formulations given by researchers for different water bodies. General form of mass transfer equation used is expressed as Equation (8.51):

$$E = f(u)\,(e_s - e_a) \quad (8.51)$$

where f(u) is wind speed function, f(u) = a + bu, a snd b are empirical constant allowing for free convection i.e. evaporation when there is no wind. (Sweers,1976) recommended wind function, derived by McMillan (1973), for temperate climate with adjustment for area of water body in relation to lake studied by McMillan (1973), given in Equation (8.52).

$$f(u) = (5 \times 10^6 / A_s)^{0.05} \times (3.6 + 2.5u_3) \quad (8.52)$$

Where u_3 is wind speed at 3 m above water surface. After establishing the value of C or f(u), the evaporation can be estimated by routine measurement of vapour pressure and wind speed at same height at which measurements used for determination of C. Singh & Xu (1997), evaluated free water evaporation using 13 mass transfer equations expressed in seven generalized equations. These seven equations compared with pan evaporation at four climatological stations in north-western Ontario, Canada, showed reasonable agreement with observed evaporation and effect of wind velocity was marginal for monthly evaporation assessment. However, equation with parameter obtained at one site utilized at other site showed disagreement with observed values. This shows that empirical constant C varies with site, so any one formulation cannot be generalized for estimating evaporation at other places.

8.4.2.4 Combined Equations

Various formulation has been established for estimation of evaporation, by combining mass transfer and energy budget equations. Most widely accepted formula for evaporation estimation based on combined equation was given by Penman. However, Penman Monteith equation is modified form of Penman equation does not contain empirical calibration factors inherent in the wind function of earlier equation. This method considered to represent the best description of the evaporation process and therefore preferred to other estimates.

Most widely accepted formula for evaporation estimation based on combined equation was given by Penman (Penman, H. L, 1948, 1956), the expression for evaporation in mm per day from open water is given in Equation (8.53):

$$E = \frac{\Delta R_n' + \gamma f(u)(e_w - e_s)}{\Delta + \gamma} \quad (8.53)$$

In this formula, R'_n represents net radiation in units of equivalent depth of water (mm / day), Δ represents the slope of the saturated vapour pressure-temperature curve, and γ represents the psychometric coefficient. By including the advected energy and subtracting the outflow energy, we can determine the available energy for the water body. However, it's important to note that this formula is only suitable for shallow water bodies as it does not consider heat storage.

According to Priestley & Taylor (1972), analysis of data collected over oceans and saturated land surfaces, when air flows over a body of water, it becomes saturated, causing the second term in Equation (8.12) to become zero. This means that the energy term dictates the

evaporation, which is the lower limit. They recommended an expression, given in Equation (8.54), for evaporation in millimetres per day.

$$E = \frac{\kappa(\Delta Q)}{\Delta+\gamma} \tag{8.54}$$

The equation that de Bruin (1978) came up with combination of the Penman and Priestly-Taylor equation, effectively eliminating the energy term and resolving the issue of adequately measuring Q_n, which represents the available energy stored in a water body. The parameter κ considers the evaporation caused by humidity deficit in addition to the equilibrium term.

The equation is

$$E = \left(\frac{\kappa}{\kappa-1}\right)\left(\frac{\gamma}{\Delta+\gamma}\right) f(u)(e_w - e_s) \tag{8.55}$$

This Equation (8.55) requires only measurements of wind speed at 2m height, air temperature and humidity deficit, to estimate the evaporation.

Penman Monteith equation is modified form of Penman equation (Penman, H. L, 1948, 1956) and Monteith (1965) equation, does not contain empirical calibration factors inherent in the wind function of earlier equation. Modified equation is (8.56):

$$E = \frac{1}{\lambda}\frac{\Delta R_n + \rho c_p f(u)\frac{(e_w - e_s)}{r_a}}{\Delta+\gamma} \tag{8.56}$$

When considering evaporation processes, it's important to account for aerodynamic resistance (r_a). This factor considers surface roughness, the size of the water body, and atmospheric stability. Essentially, it represents the resistance that water molecules face as they move from the water surface to a reference height in the atmosphere. It's worth noting that r_a is inversely proportional to wind speed, meaning that higher wind speeds will result in lower values of r_a. This method is widely considered to be the most accurate way of estimating evaporation and is preferred over other methods.

8.4.2.5 Comparison of different methods

Winter et al. (1995) estimated open water evaporation using 11 different equations for a small lake in the USA and compared the estimated monthly evaporation with that determined using the energy balance method. The equations included forms of the mass transfer and combination equation methods. Winter et al. (1995) found that the combination equations of Penman (1948), Priestley & Taylor (1972) and de Bruin & Keijman (1979) best described the evaporation in terms of close agreement with the energy budget values, small standard deviations from the energy budget values, lack of seasonal bias and similarity of results

whether using raft-based or land-based data. However, it's important to note that these equations used the available energy, which included a term for the change in heat storage of the water body based on repeated thermal surveys of the lake. Bozorgi et al. (2020), evaluated 12 alternative evaporation methods for evaluating evaporation from Karkheh reservoir with reference to the Bowen ratio energy budget (BREB) formula, the solar radiation-temperature based methods and the Blaney and Criddle method were best ranked based on their accuracy, sensitivity to input variables, and simplicity of application by means of the technique for order of preference by similarity to ideal solution (TOPSIS) multi-criteria decision analysis method. The evaporation estimates for deep water bodies have large uncertainty, like other methods. Sene et al. (1991), have suggested that heat storage in case of deep reservoirs can be neglected in tropical regions, due to constant water temperature of water throughout the year in tropical climates.

It's interesting to note that the use of pans of water for measuring evaporation dates to the 18th century. It makes sense that people were drawn to them since they provide a visible way to measure open water evaporation. However, despite the number of studies conducted, it's still difficult to use data from pans except in certain situations.

Measuring all the elements required for the mass balance is a difficult and expensive task, which is why it has only been applied in a few exceptional circumstances. Fortunately, developments in instrumentation have made the energy budget method a more practical option. However, both methods rely on calculating a balance, which can lead to errors in estimates of evaporation. Despite this, the energy balance method is considered the most accurate. It's important to note that estimates of evaporation are specific to the site where the measurements were taken and cannot be transferred to other water bodies. The bulk transfer method may appear attractive at first, as it uses easily measurable meteorological variables and the water body's surface temperature. However, the sensitivity to vapour pressure measurements combined with the difficulty of defining the wind function reduce the accuracy of this method. Combination equations are the most widely used method for estimating evaporation since they make use of readily available meteorological data. However, they don't take the heat storage of the water body into account if driven by net radiation data.

8.4.2.6 Methods proposed for analysis

The methods used to estimate evaporation rates can be challenging to apply accurately. Empirical methods that rely on regression analyses of pan evaporation, lake evaporation, or lysimeter measurements and meteorological factors can have a limited range of applicability

due to the difficulty of measuring certain variables and the fact that they are only accurate in a limited range. Additionally, comparing different empirical methods can be difficult due to method-specific model variables. Water budget methods are simple in theory but often produce unreliable results in practice due to the difficulty of measuring certain variables. Energy budget methods, such as the Penman combination method, are reliable in theory but require detailed meteorological data and are only suitable for research purposes in small areas. Despite efforts to simplify the Penman method, it still requires the evaluation of net radiation, which can be difficult to obtain for many practical applications.

Choosing the most appropriate method for measuring evaporation rates can be challenging due to the wide range of equations available and the varying expertise required to use them correctly. Additionally, there are no objective criteria for selecting a model, and it is not always clear which method would be most suitable for a given study. The ideal model should be analytical and simple, with easily measurable variables and the most important influencing factors. Other simple models should also be special cases of the generalized model, and the model parameters should be easily estimated with acceptable accuracy. Keeping in view of these facts all important data were collected and analysed as given in the subsequent sections.

8.5 Data Collection and Analysis

Though the significance of different parameters has been discussed in section 8.2.1 under evaporation dynamics, daily water evaporation was collected along with meteorological data including air temperature, water temperature, wet-bulb temperature, dry-bulb temperature, relative humidity, wind speed, wind direction, and solar insolation from 1st April 2020 to 31st March 2023. The monthly average evaporation rates and meteorological data were calculated accordingly, which is given in Table 8.3.

Table 8.3. Monthly Average evaporation rates and meteorological data from April 2021- March 2023

Month	Evaporation (mm/day)	Max Temperature (℃)	Min Temperature (℃)	Max Relatiive Humidity open air (Rhmax) in %	Min Relatiive Humidity open air (Rhmin) in %	Average Water Temperature open to sky (℃)	Day light Hours (N)	Ra MJ/m2/day	Sunshine hour in Hrs. (n)	Rs MJ/m2/day	Average Wind Velocity (m/s)	Average ambient temperature (℃)
Jan-21	1.10	20.59	6.20	77.34	51.03	12.58	10.39	22.04	7.33	8.92	0.15	13.40
Feb-21	3.08	28.80	10.36	64.46	32.00	17.66	11.03	26.65	8.94	12.08	0.13	19.58
Mar-21	6.02	34.16	16.15	51.24	25.50	22.79	11.80	32.01	9.34	13.18	0.48	25.16
Apr-21	6.63	37.98	18.54	34.56	14.74	25.44	12.69	37.08	9.79	15.05	0.43	28.26
May-21	5.83	38.80	22.99	47.70	27.16	27.96	13.41	39.97	8.90	12.84	0.53	30.89
Jun-21	5.52	39.73	26.20	55.19	33.16	30.29	13.80	40.98	9.28	12.77	0.51	32.97
Jul-21	3.63	37.39	27.02	70.90	52.32	30.91	13.64	40.42	8.32	10.79	0.43	32.20
Aug-21	4.89	36.14	25.84	71.80	51.16	30.53	13.02	38.15	8.86	12.42	0.42	30.99
Sep-21	3.50	33.30	24.55	82.55	62.78	28.47	12.16	33.83	7.45	10.26	0.38	28.93
Oct-21	3.61	33.39	18.03	67.07	40.74	23.01	11.30	28.29	7.76	12.56	0.25	25.71
Nov-21	1.61	29.28	9.64	60.90	31.14	15.45	10.56	23.12	7.23	8.73	0.12	19.46
Dec-21	0.98	22.66	6.50	71.92	44.45	10.90	10.20	20.72	6.26	7.95	0.18	14.58
Jan-22	0.65	18.10	7.08	83.03	62.51	11.30	10.39	22.04	5.14	7.28	0.32	12.59
Feb-22	2.98	25.53	8.92	71.83	38.67	15.34	11.03	26.65	7.61	12.41	0.38	16.84
Mar-22	5.53	35.45	16.37	54.78	25.29	22.81	11.80	32.01	8.86	14.56	0.44	25.91
Apr-22	8.17	41.78	21.76	27.89	10.44	27.24	12.69	37.08	9.49	14.76	0.47	31.77
May-22	10.31	42.60	26.56	35.75	16.30	30.55	13.41	39.97	9.85	14.13	0.64	34.58
Jun-22	9.78	40.59	26.95	45.60	27.02	31.06	13.80	40.98	17.67	19.14	0.63	33.77
Jul-22	4.21	35.30	26.32	78.32	57.33	31.29	13.64	40.42	8.24	10.14	0.58	32.09
Aug-22	4.15	34.60	25.58	77.90	56.05	30.15	13.02	38.15	8.33	10.40	0.53	30.09
Sep-22	4.74	36.14	24.52	73.78	47.68	28.87	12.16	33.83	7.99	11.87	0.50	30.33
Oct-22	3.55	33.16	17.55	69.58	37.52	22.34	11.30	28.29	6.72	10.82	0.28	25.35
Nov-22	2.57	29.65	11.49	61.66	31.16	16.84	10.56	23.12	6.84	8.93	0.22	20.57
Dec-22	1.39	23.58	5.81	75.57	42.99	11.36	10.20	20.72	7.47	7.22	0.19	14.70
Jan-23	0.80	19.82	4.39	80.90	51.96	10.48	10.39	22.04	6.77	6.25	0.29	12.41
Feb-23	1.15	29.55	11.08	70.79	30.79	17.85	11.03	26.65	8.53	9.50	0.36	18.99
Mar-23	4.05	31.15	15.53	66.27	33.93	20.63	11.80	32.01	9.13	12.23	0.45	22.45

8.5.1 Data presentation

These plots display the atmospheric data collected from January 2021 to March 2023, providing valuable insights into the climate at Pilani. The data is representative of the semi-arid climate of the tropical region. The atmospheric data is presented here in the form of plots for better understanding of variability of atmospheric parameters, ambient temperature, water temperature, humidity, wind velocity and solar radiation on every 15-minute basis for different seasons i.e. summer, winter and monsoon season.

8.5.1.1 Summer season

Data of May 15, 2021, is presented here to understand variability of parameters in summer season. Figure 8.6 (A) represents variation of ambient temperature with water temperature, Figure 8.6(B) represents plot of shortwaves recorded while Figure 8.6(C) is the plot of relative humidity and Figure 8.6(D) is the plot of wind speed recorded on a typical summer day 15th May 2021.

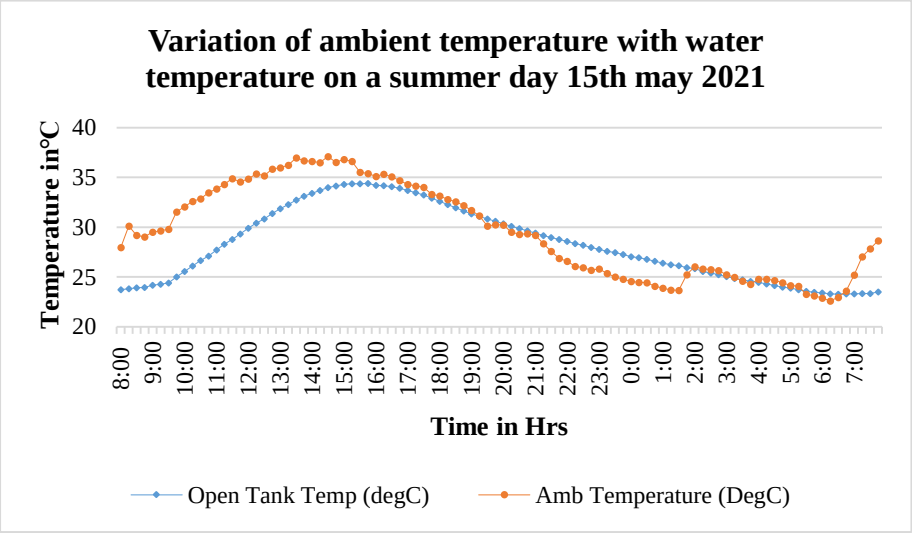

Figure 8.6(A). Variation of ambient temperature and water temperature on 15th May 2021

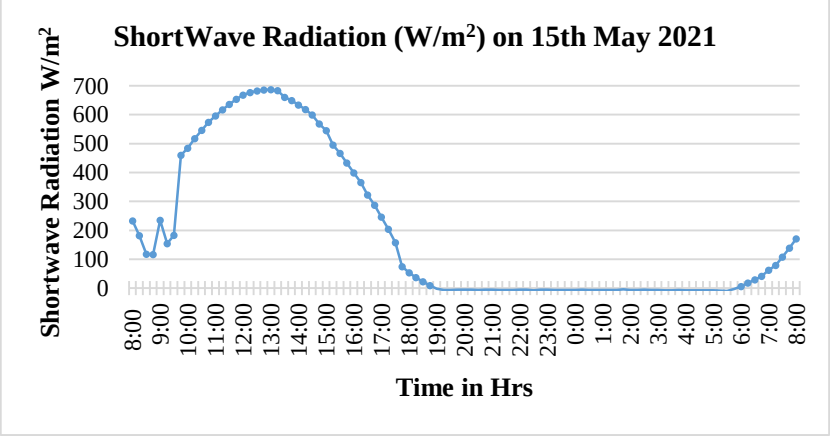

Figure 8.6(B). Variation of Shortwave radiation (Ra) in W/m2 on 15th May 2021

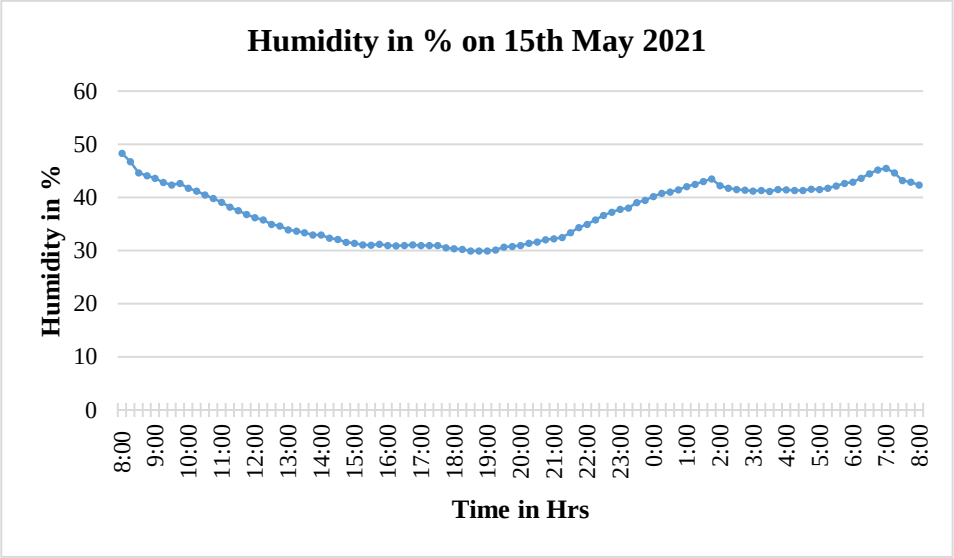

Figure 8.6(C). Variation of Humidity in % on 15th May 2021

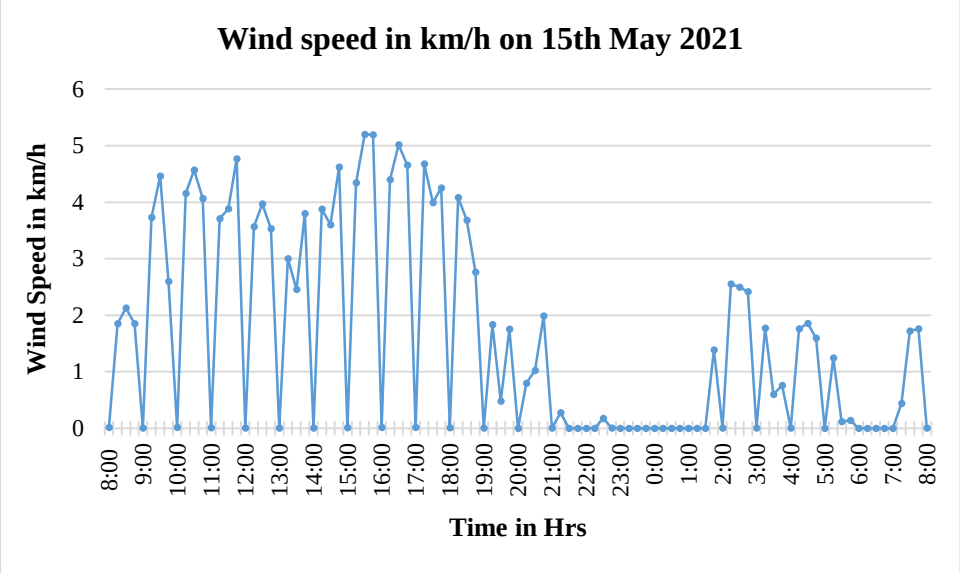

Figure 8.6(D). Variation of wind speed on 15th May 2021

Figure 8.6 Atmospheric parameters at Pilani on a summer day 15th May 2021

It appears that the highest ambient temperature was recorded at 36.7 degrees at 1345 hours, whereas the highest water temperature was recorded at 34.38 degrees at 1515 hours. This suggests that there is a time lag as well as a difference in the highest temperature between the two. The shortwave radiation was at its highest, measuring 686 W/m^2 at 1300 hours. It can be inferred that the increase in shortwave radiation led to an increase in ambient temperature, but with a time lag. As the sun sets, the ambient temperature decreases below the water temperature, while the temperature of water gradually reduces. The air temperature increases during the night owing to the warm wind blowing in the night. Wind speed is higher during the daytime due to an increase in ambient temperature making air light, with wind blowing during the daytime at a speed of 4-5 km/hr. It can be observed that the humidity decreases

during the daytime and due to the summer season, the humidity is maximum at 50% and low at 30%, clearly indicating dry summers.

8.5.1.2 Monsoon season

During a monsoon day of 26th July 2021, the atmospheric parameters behaviour can be seen in Figure 8.7.

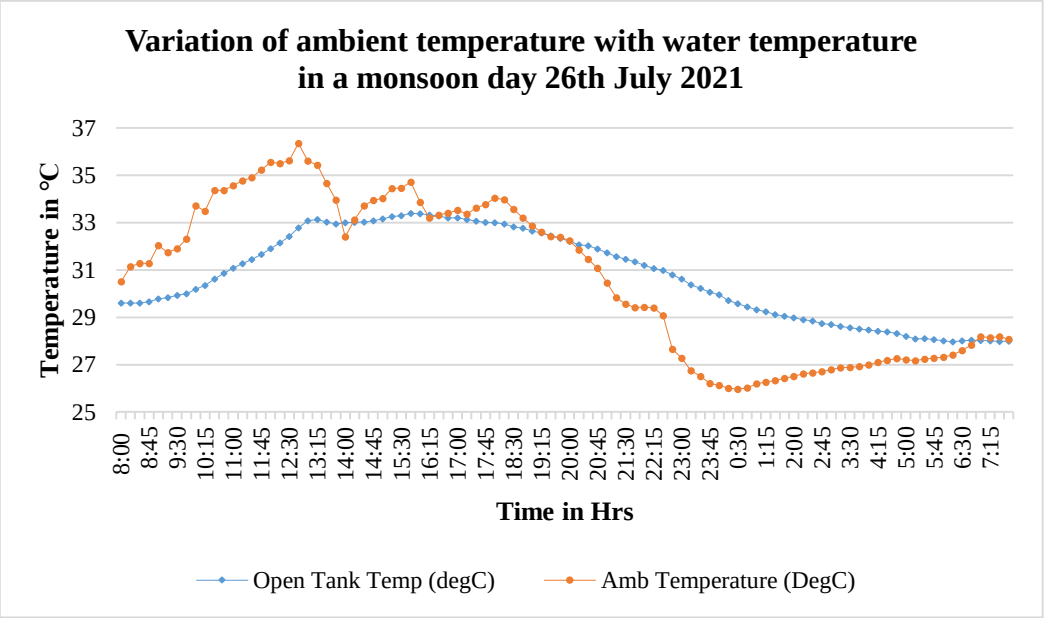

Figure 8.7(A) Variation of ambient temperature and water temperature on 26th July 2021

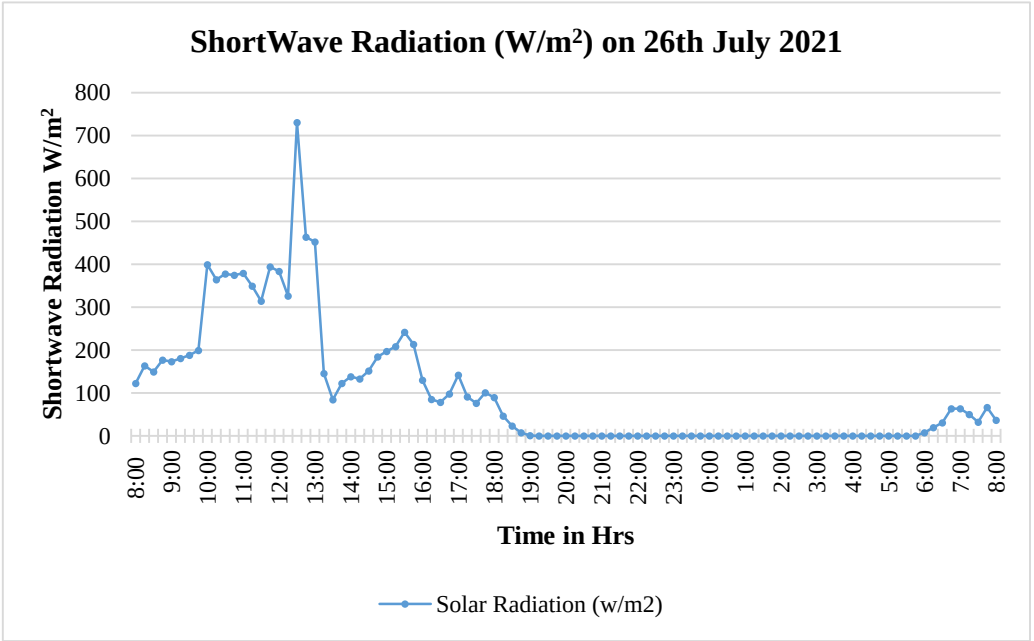

Figure 8.7(B) Variation of Shortwave radiation (Ra) in W/m^2 on 26th July 2021

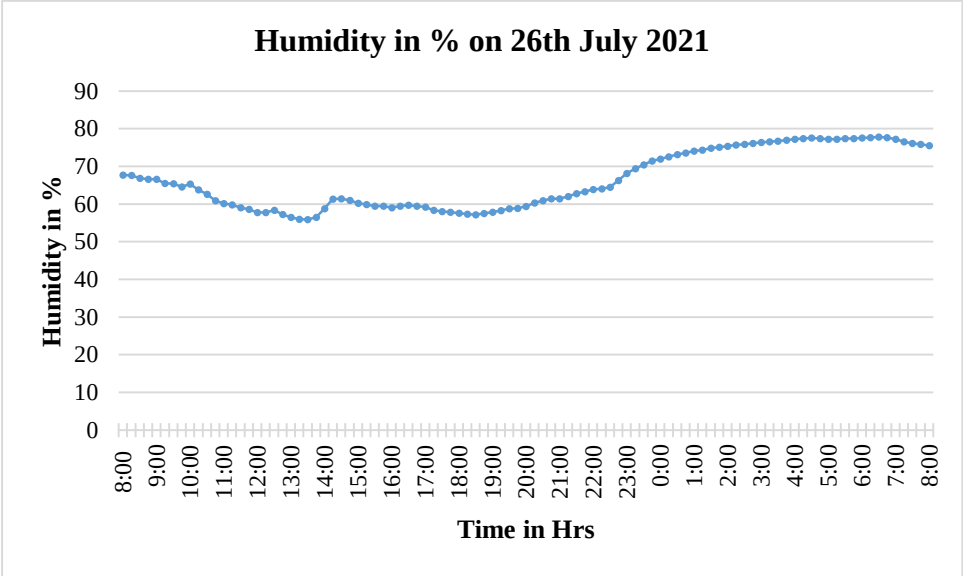

Figure 8.7(C) Variation of Humidity in % on 26th July 2021

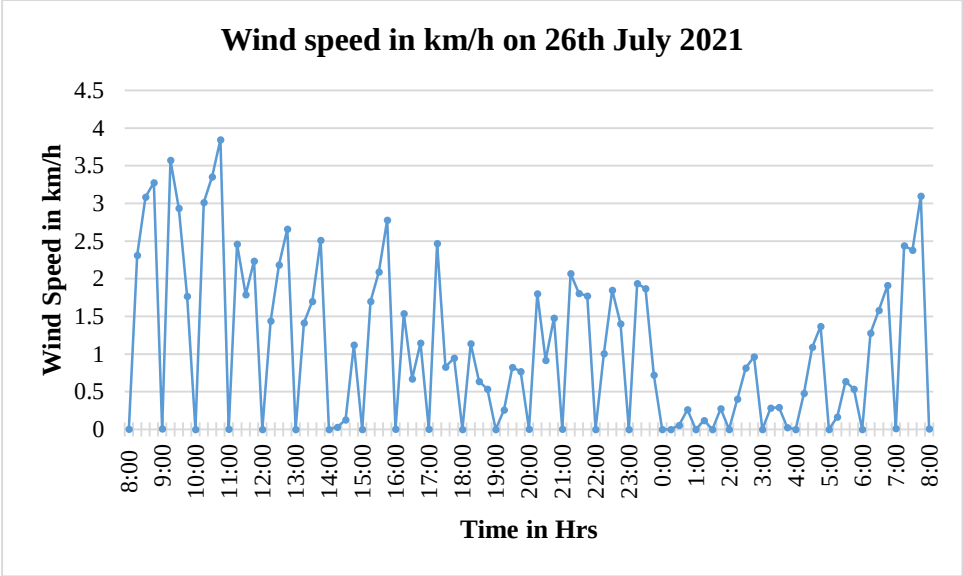

Figure 8.7(D). Variation of wind speed on 26th July 2021

Figure 8.7. Atmospheric parameters at Pilani during a monsoon day 26th July, 2021

During the monsoon season, it is common to observe high levels of humidity in the air, ranging from a high of 77% to a low of 55%. Despite the high solar insolation of 730 W/m^2, the ambient temperature can rise to a maximum of 35.6 degrees Celsius, while the maximum water temperature is around 33 degrees Celsius. At night, the wind may be blowing, but the air temperature tends to cool down due to the highly humid air. During monsoon season, the maximum wind speed is typically around 3.8 km/h.

8.5.1.3 Winter season

The atmospheric parameters on a typical winter day 3rd January 2021, at Pilani can be observed in following Figure 8.8.

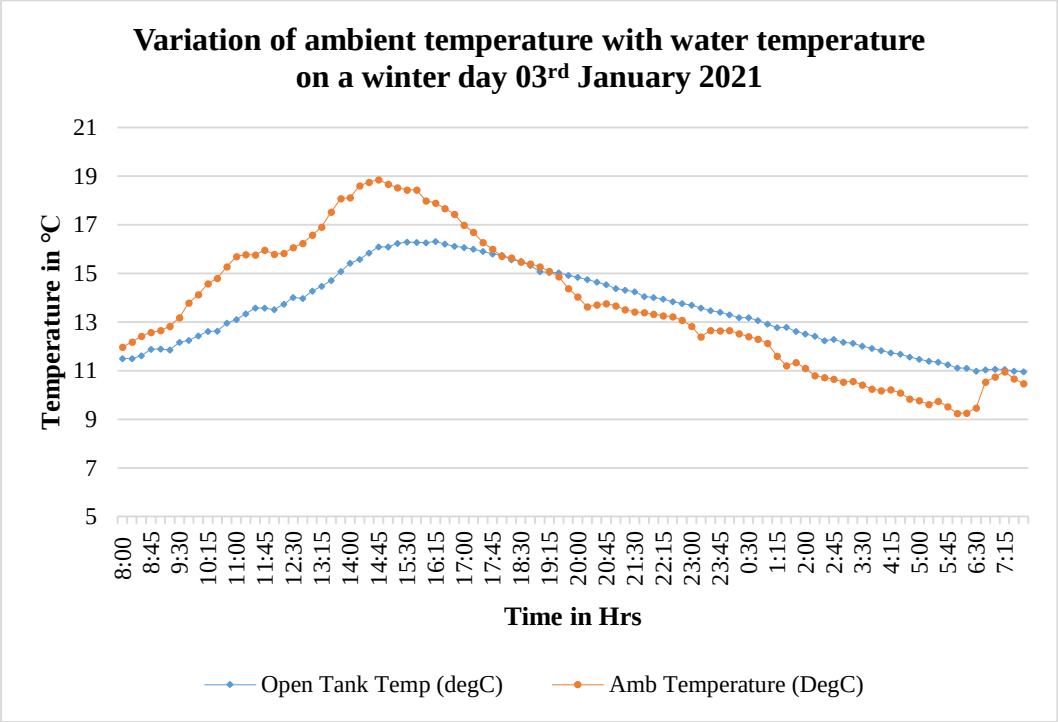

Figure 8.8(A). Variation of ambient temperature and water temperature on 03rd January 2021

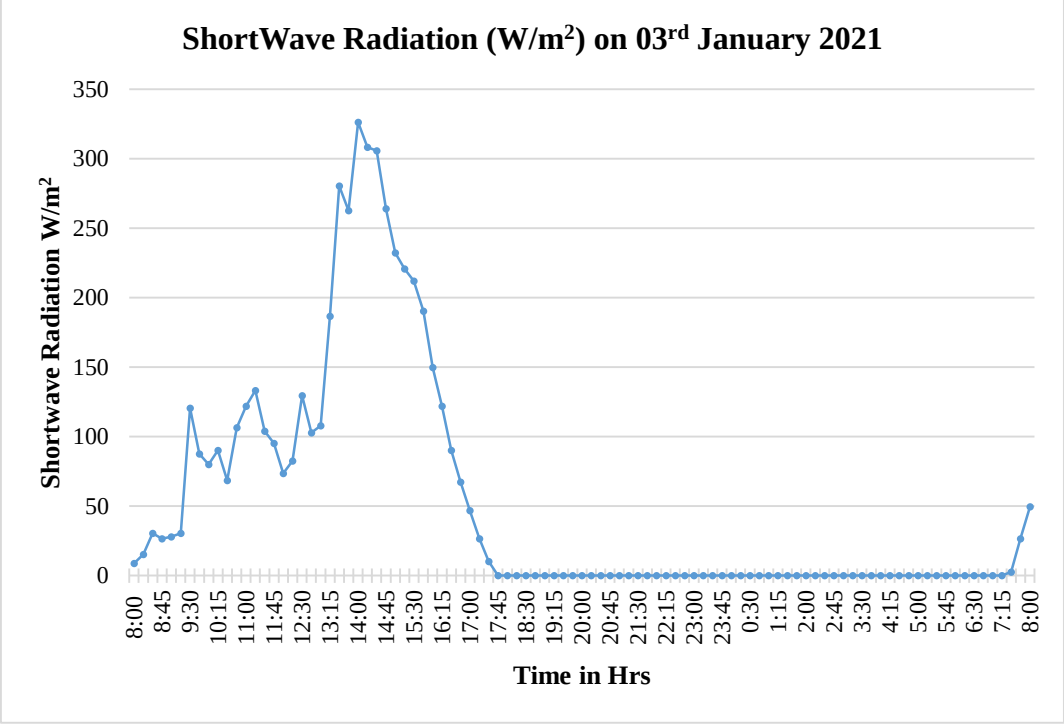

Figure 8.8(B). Variation of Shortwave or Solar Irradiation on 03rd January 2021

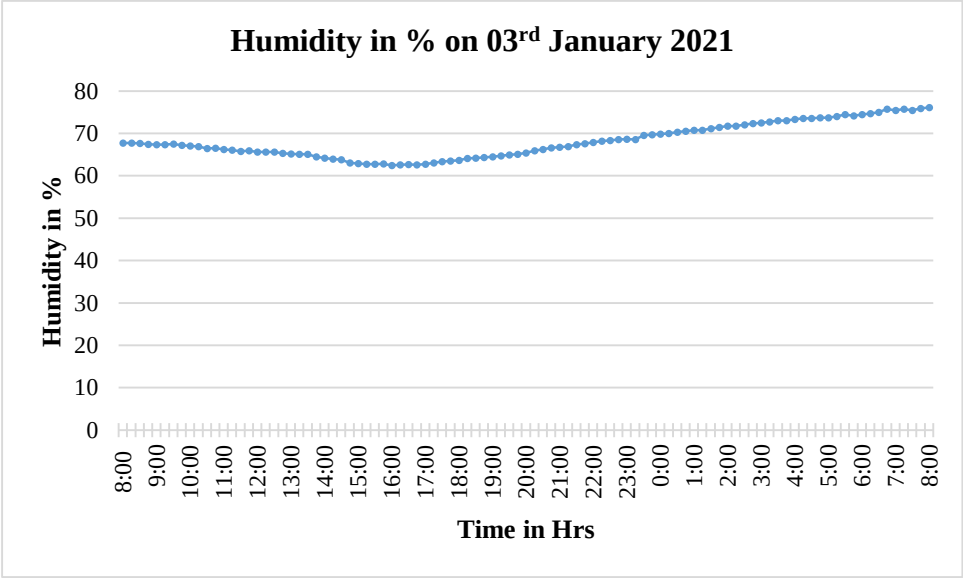

Figure 8.8(C). Variation of Humidity on 03rd January 2021

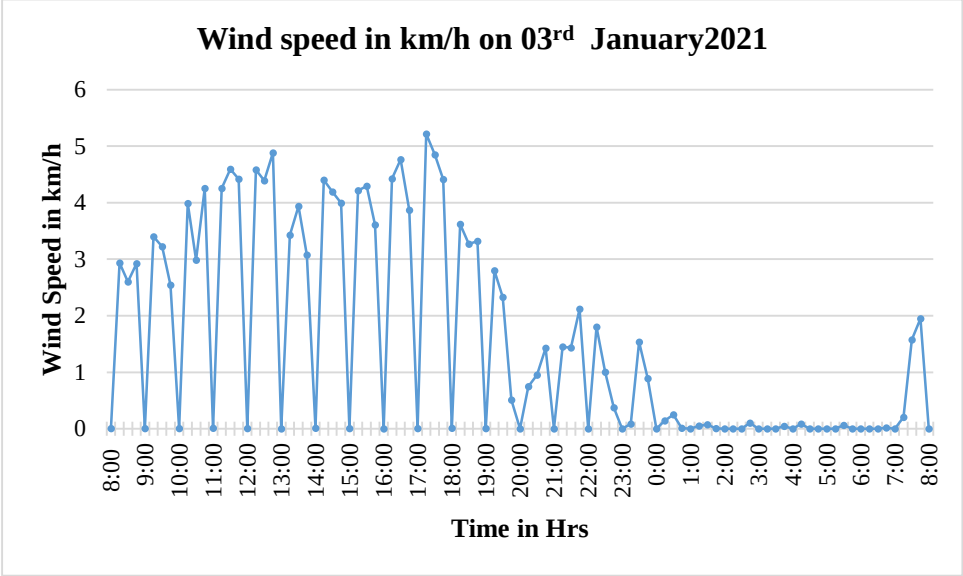

Figure 8.8(D). Variation of wind speed on 03rd January 2021

Figure 8.8. Atmospheric parameters at Pilani on a winter day 03rd January, 2021

During winter, the amount of solar radiation is at its lowest. On a typical day, the maximum solar radiation received is 326 W/m^2. This decrease in solar radiation has an impact on both the ambient temperature and water temperature. The highest ambient temperature during this time is 18.6 ℃, observed with a 1-hour lag after the maximum solar irradiation. The maximum water temperature is 16.29 ℃, observed at 1530 hrs with a 30-minute lag to the ambient temperature. It is worth noting that the time lag during winter is less than the time lag observed during summer. Wind speed during winter is similar to that during summer while humidity ranges between 62% and 76%.

8.5.2 Average Daily and Average Monthly data

It is evident that the atmospheric elements such as solar irradiation or shortwave radiation, wind velocity, humidity, ambient temperature, water temperature, and the combined effect of all the elements over evaporation are volatile in nature, even though the data is collected at every 1-minute interval and presented above at 15-minute intervals. Therefore, it is not possible to formulate any specific algorithm for such a dataset. However, calculating the daily average of all the elements can help in estimating the evaporation by utilizing the atmospheric parameters. The data presented below is for typical months of summer, winter, and monsoon, as well as monthly average data from Jan 2021 to March 2023.

8.5.2.1 Ambient temperature and Water temperature

As observed in Figures 8.6(A), 8.7(A), and 8.8(A), the difference in daily variation of water temperature and air temperature is evident. However, the hourly temperature variation displays a distinct difference. It can be noticed that the air temperature rises with an increase in sunlight and quickly reduces when clouds obscure the incoming sunlight. On the other hand, the temperature of water increases gradually, and the impact of shades or clouds is slow due to the inertia of water. The Figure 8.9(A) and 8.9(B), shows a marked difference between the daily average temperature of water and ambient temperature. However, based on the plot shown in Figure 8.10, the monthly average water temperature and air water temperature do not seem to be significantly different. Therefore, long period averaging of temperature forfeits the purpose of data collection and gives unreliable results.

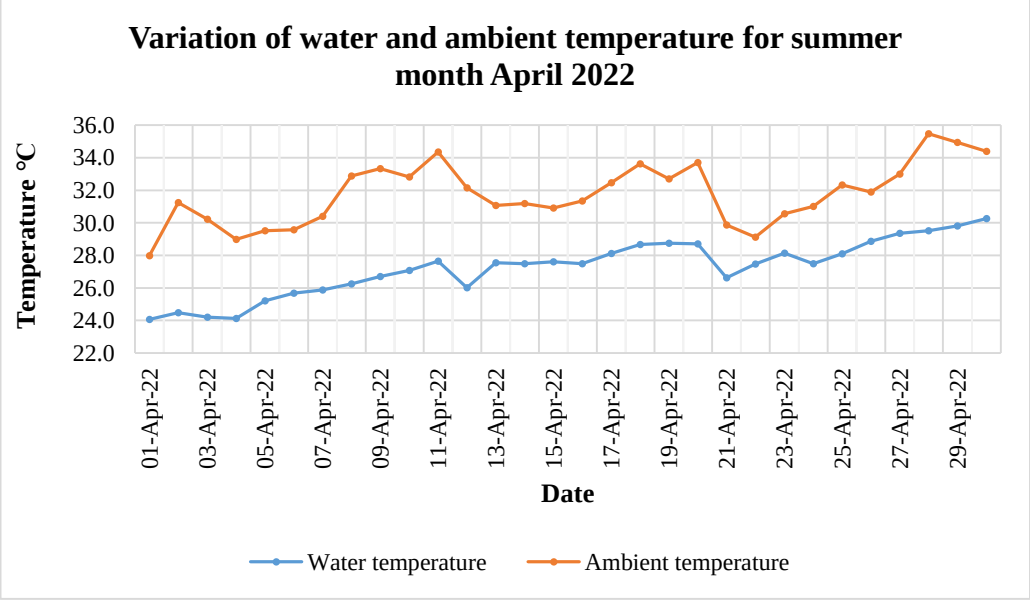

Figure 8.9(A). Average Daily water temperature and air temperature for summer month April 2022

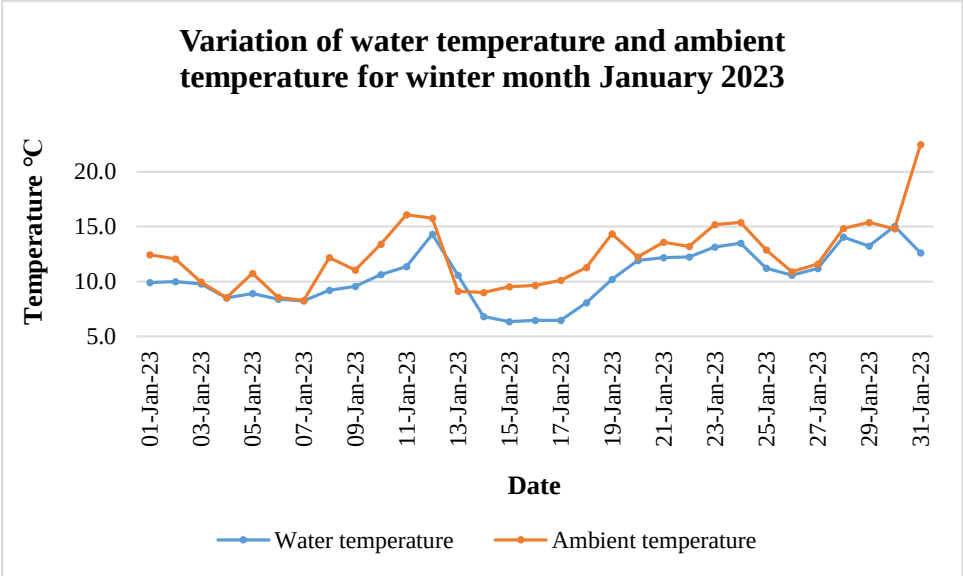

Figure 8.9(B). Average Daily water temperature and air temperature for winter month January 2023

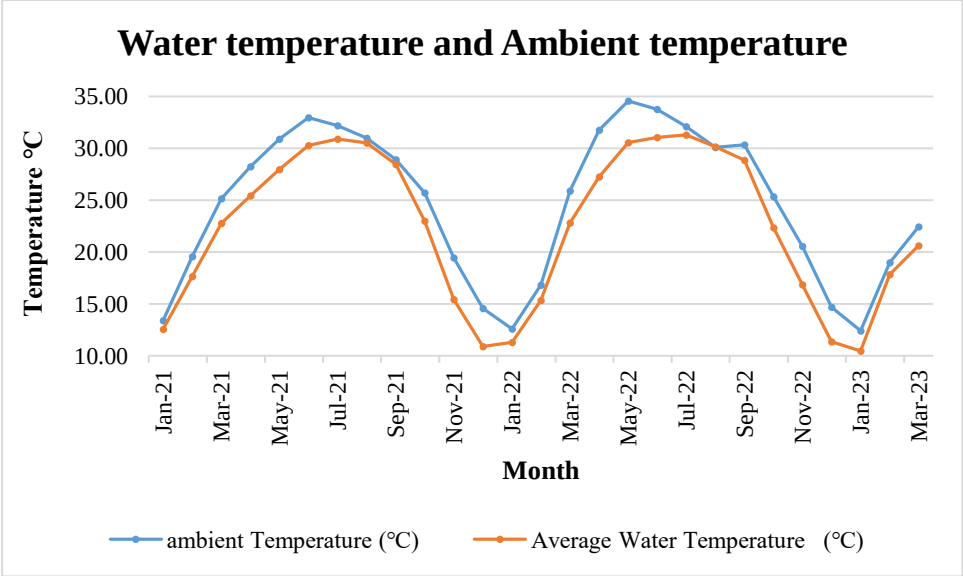

Figure 8.10 Monthly average water temperature and ambient temperature from January 2021-March 2023

8.5.2.2 Wind speed

According to the data presented in Figure 8.11, the average monthly wind speed fluctuates throughout the year. Notably, the month of May has the highest wind speed, while November and December, which are winter months, have the lowest. The annual wind speed ranges from 0.19 m/s to 0.64 m/s during the observation period. The prevailing wind direction is NE and NW, as observed throughout the year. Table 8.4 provides a breakdown of the frequency of wind direction during the observation period.

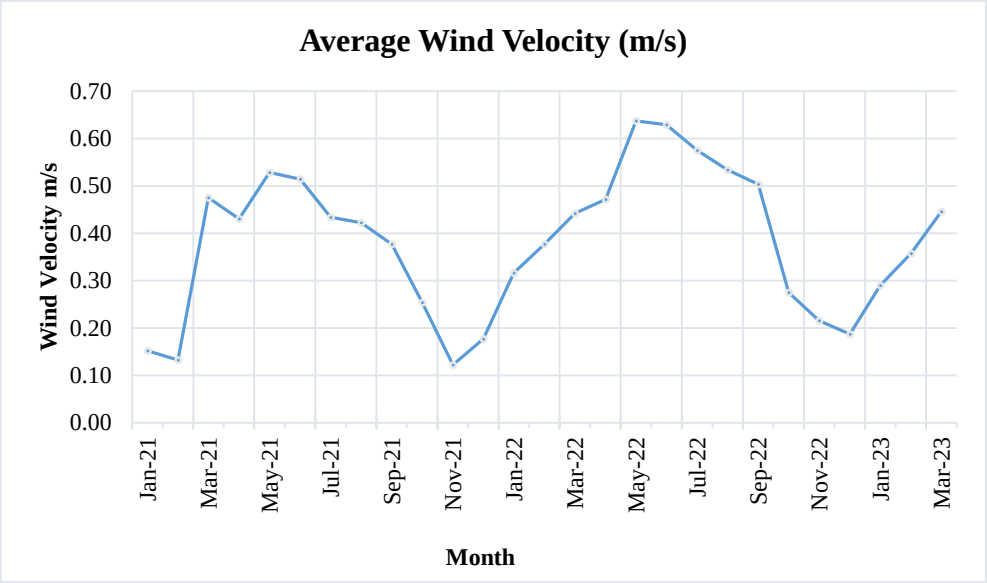

Figure 8.11. Monthly average wind velocity (m/s) from January 2021-March 2023

Table 8.4. Wind Direction Frequency Table - Frequencies for Wind Direction

Wind Direction	Frequency	Percent	Valid Percent	Cumulative Percent
E	57	1.656	1.681	1.681
EN	8	0.232	0.236	1.917
ES	3	0.087	0.088	2.005
EW	1	0.029	0.029	2.035
N	145	4.211	4.276	6.311
NE	1085	31.513	31.996	38.307
NW	1219	35.405	35.948	74.255
S	72	2.091	2.123	76.379
SE	315	9.149	9.289	85.668
SW	38	1.104	1.121	86.789
W	226	6.564	6.665	93.453
WE	3	0.087	0.088	93.542
WN	2	0.058	0.059	93.601
WS	214	6.216	6.311	99.912
se	1	0.029	0.029	99.941
w	1	0.029	0.029	99.971
ws	1	0.029	0.029	100.000
Missing	52	1.510		
Total	3443	100.000		

8.5.2.3 Humidity

Figure 8.12 displays the average monthly maximum and minimum humidity for the observation period. The highest humidity levels are observed in the winter months of January and the monsoon months of July, August, and September. On the other hand, the lowest humidity levels are observed in the summer month of April. After rains, the humidity levels reduce to a minimum during November, then gradually increase and reach their peak in January. They start declining again and reach the minimum in April.

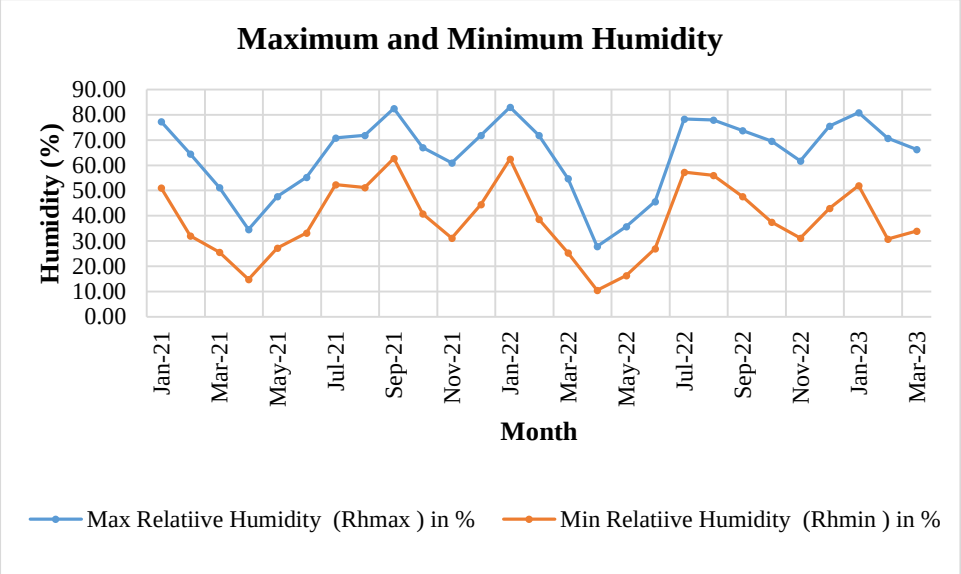

Figure 8.12. Monthly average maximum and minimum Humidity (%) from January 2021-March 2023

8.5.2.4 Daylight and Sunshine Hour

It is interesting to consider that every location has a theoretical maximum duration of daylight known as Daylight Hour. This refers to the total number of hours of illumination at a particular location. However, there is also a practical consideration of when the amount of daylight is sufficient to be considered a "sunshine hour". Furthermore, there are "bright" sunshine hours, which refer to the total number of hours when sunlight is stronger than a specified threshold of 120 W/m^2 (WMO,2008), as opposed to just "visible" hours. It is worth noting that "visible" sunshine occurs around sunrise and sunset but is not strong enough to activate the process of evaporation.

The day light hours and sunshine hour recorded for a period of January 2021 to March 2023 are plotted in the Figure 8.13.

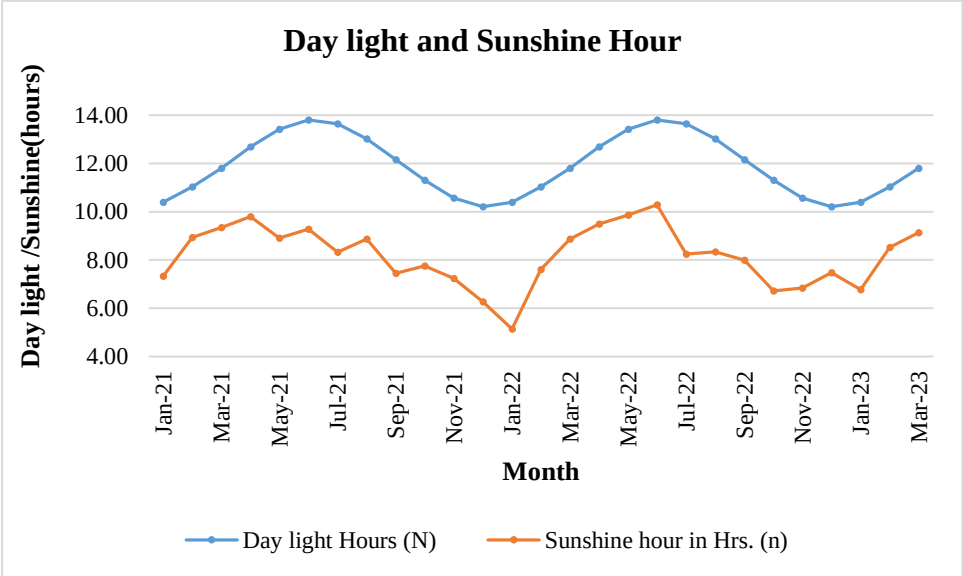

Figure 8.13. Monthly average Daylight hour and Sunshine hour (hour) from January 2021-March 2023

8.5.2.5 Extra-terrestrial Radiation and Short-Wave Radiation

The solar radiation that reaches a horizontal surface above the atmosphere of the earth is known as extra-terrestrial radiation. This radiation depends on the latitude, season, and time of day. The shortwave radiation that falls in the meteorologically significant spectral range of 300nm-3000nm is responsible for approximately 96% of the extra-terrestrial radiation. However, when this radiation reaches the earth, it is either reflected or absorbed by the clouds, dust, and gases present in the atmosphere. As a result, the energy that reaches the surface of the earth is less than the extra-terrestrial energy, as depicted in Figure 8.14.

The shortwave radiation recorded by pyranometer from January 2021 to March 2023 are plotted below in Figure 8.14.

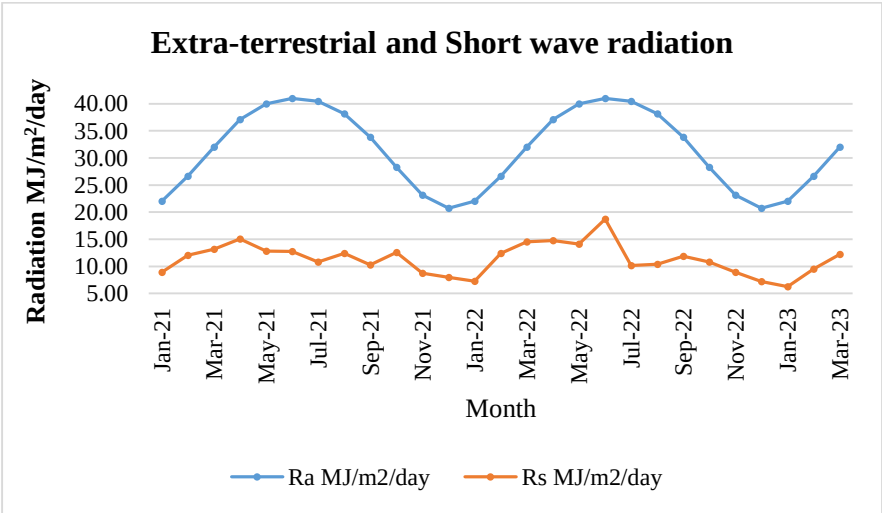

Figure 8.14. Monthly average Extra-terrestrial and Short wave Radiation (MJ/m^2/day) from January 2021-March 2023

8.5.2.6 Analysis of Evaporation data

The atmospheric parameters over water surface have a cumulative effect that results in evaporation. Figure 8.15 displays the monthly average evaporation from January 2021 to March 2023. It is evident from the plot that evaporation increases in summers and decreases in winters, following the trend of incoming solar radiation. While energy is the major cause of evaporation, other parameters such as humidity, ambient temperature, and wind speed also affect the process. To understand the impact of each parameter on evaporation, their variation is plotted below.

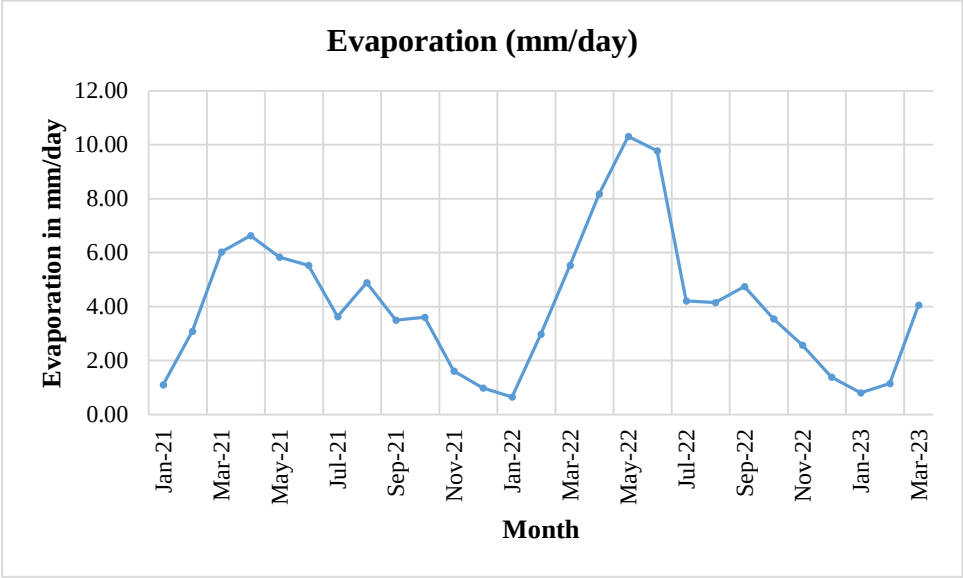

Figure 8.15. Monthly average evaporation From January 2021-March 2023

(i) Variation with ambient temperature

As ambient temperature increases, the evaporation increases. This can be seen in Figure 8.16.

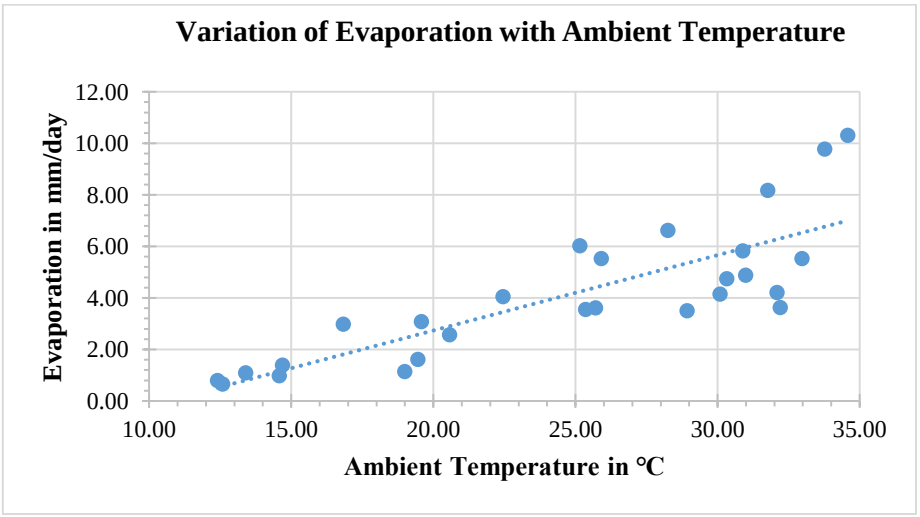

Figure 8.16. Variation of evaporation with average ambient temperature

(ii) Variation with water temperature

Figure 8.17 displays the relationship between water temperature and evaporation variability. As water temperature increases, evaporation also increases.

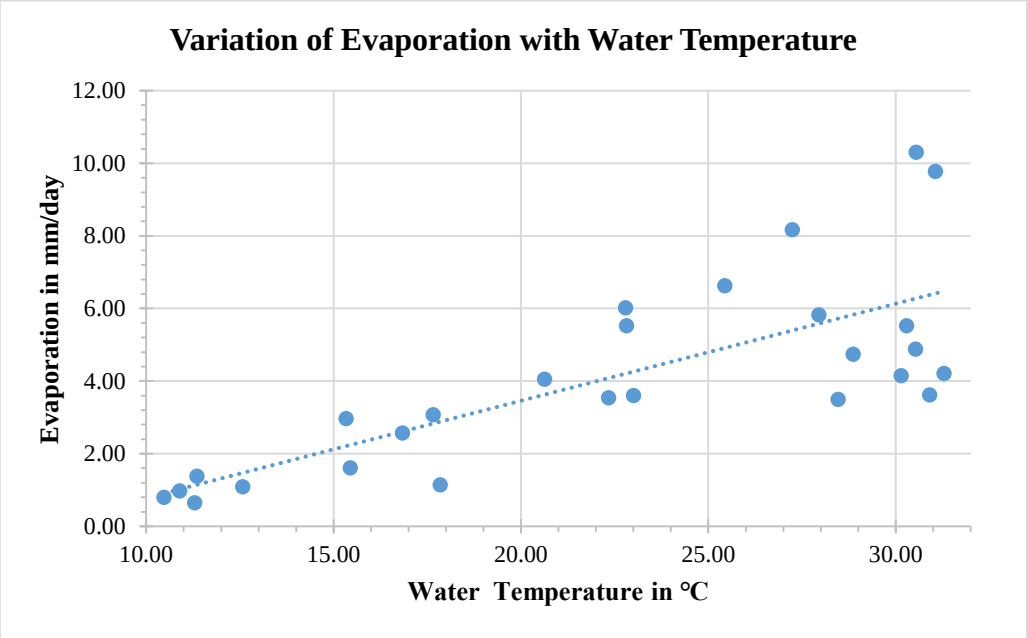

Figure 8.17. Variation of evaporation with average water temperature

(iii) Variation with wind velocity

Evaporation increases with increase in wind velocity, can be visualised in Figure 8.18.

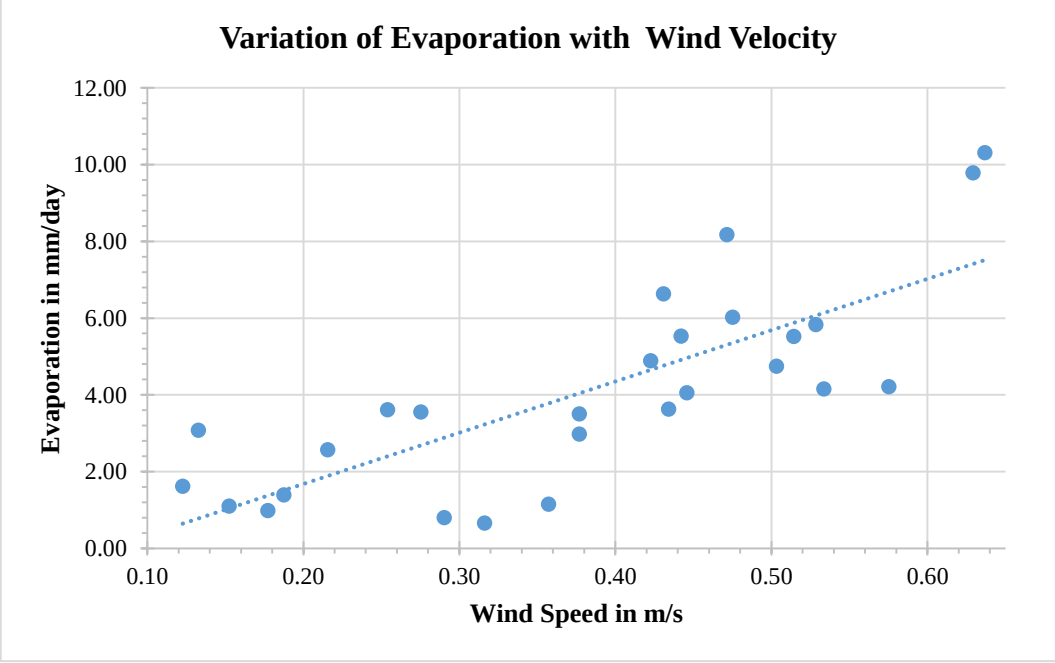

Figure 8.18. Variation of evaporation with wind velocity

(iv) Variation of evaporation with humidity

Figure 8.19 demonstrates the relationship between humidity and evaporation, indicating that as humidity increases, the rate of evaporation decreases. On the other hand, as the difference between maximum and minimum humidity decreases, the rate of evaporation increases, as shown in Figure 8.20**.**

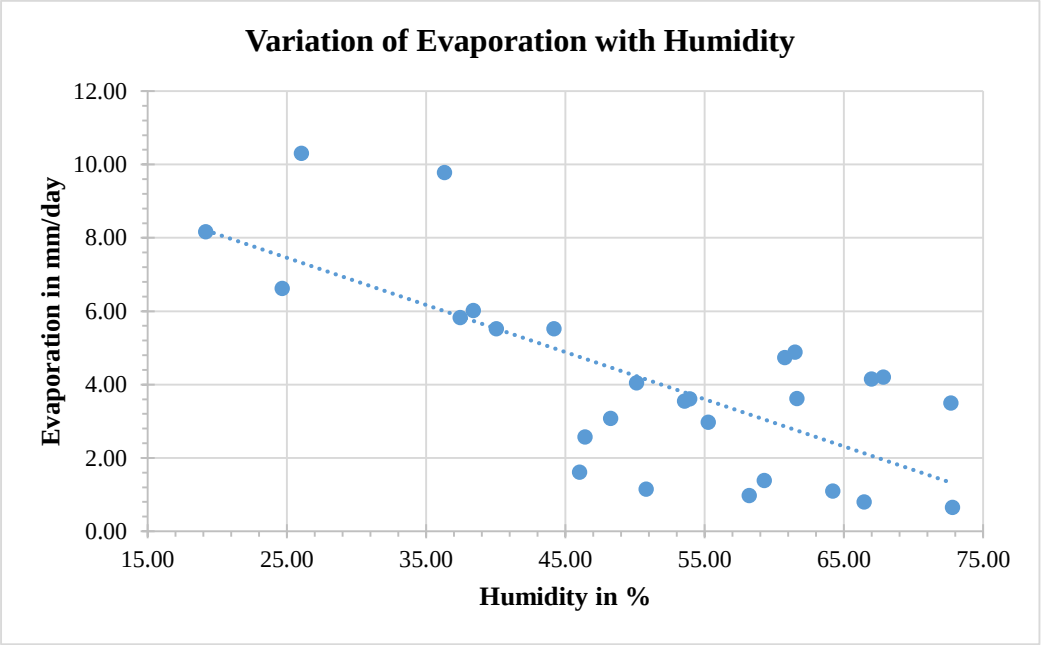

Figure 8.19. Variation of evaporation with average humidity

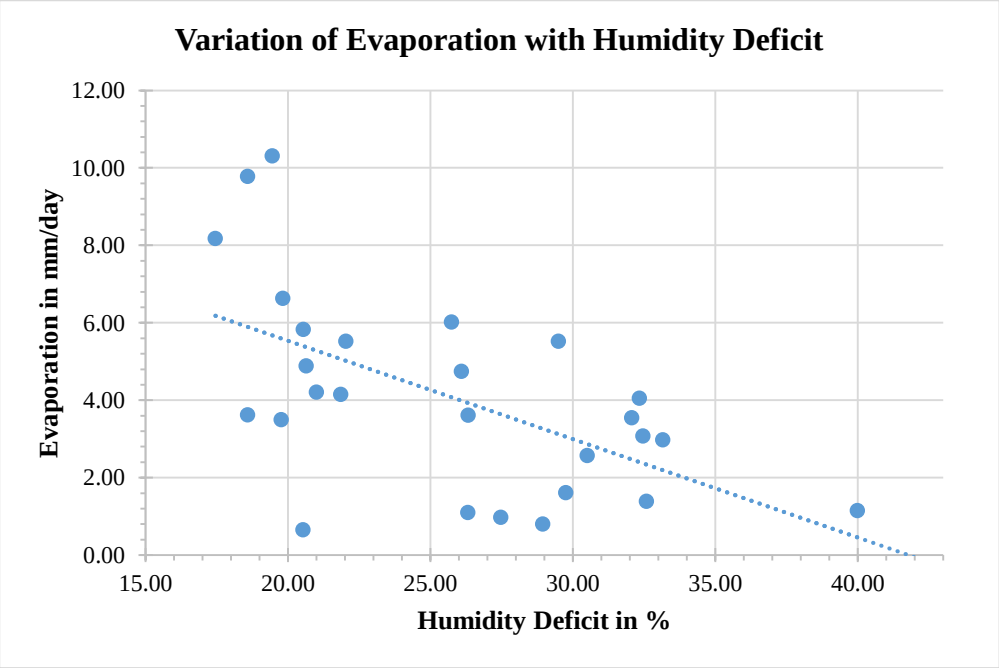

Figure 8.20. Variation of evaporation with difference between maximum and minimum humidity (humidity deficit) .

(v) Variation of Evaporation with Short-wave radiation

Figure 8.21 clearly demonstrates that there is a direct relationship between the increase in solar radiation and the increase in evaporation, which is not surprising given that solar radiation is the primary source of energy for evaporation.

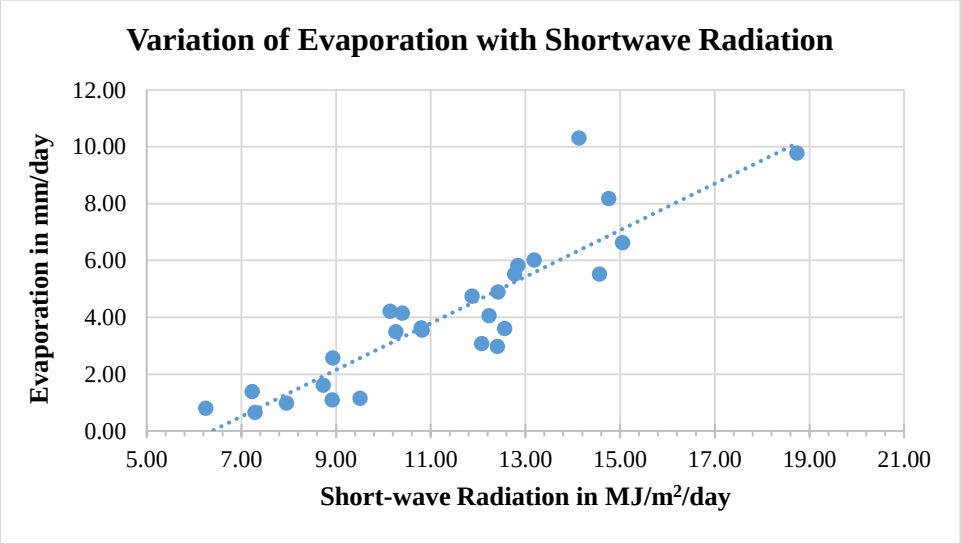

Figure 8.21. Variation of evaporation with shortwave radiation

8.6. Model development to estimate evaporation using regression analysis under two specific conditions: uncovered water surface area and provision of cover through FSPV panels

The evaporation from water bodies can be significantly reduced by covering the water surface. However, previous attempts to reduce evaporation have not been cost-effective. Given that water is a precious natural resource, conservation is crucial for the survival of living beings on Earth. That's why the installation of floating solar PV is an innovative way to harness energy while conserving water. The key objective is to quantify the reduction in evaporation resulting from the installation of solar PV and develop a formulation for estimating the evaporation of water bodies covered by floating solar PV.

Over the course of three years, starting from April 2020 and ending in March 2023, an experiment was conducted to observe the rate of evaporation from a standard class A pan that was open to the sky, as well as three pans covered with solar panels. The solar panels were placed at varying heights of 300 mm, 500 mm, and 1000 mm above the water surface, with the aim of determining the ideal panel height that would result in maximum evaporation reduction. The ideal panel height of 300mm above water surface has been determined in the chapter 7. The daily evaporation rates for a typical month of each season - summer, monsoon, and winter - were recorded and are presented below in Figure 8.22.

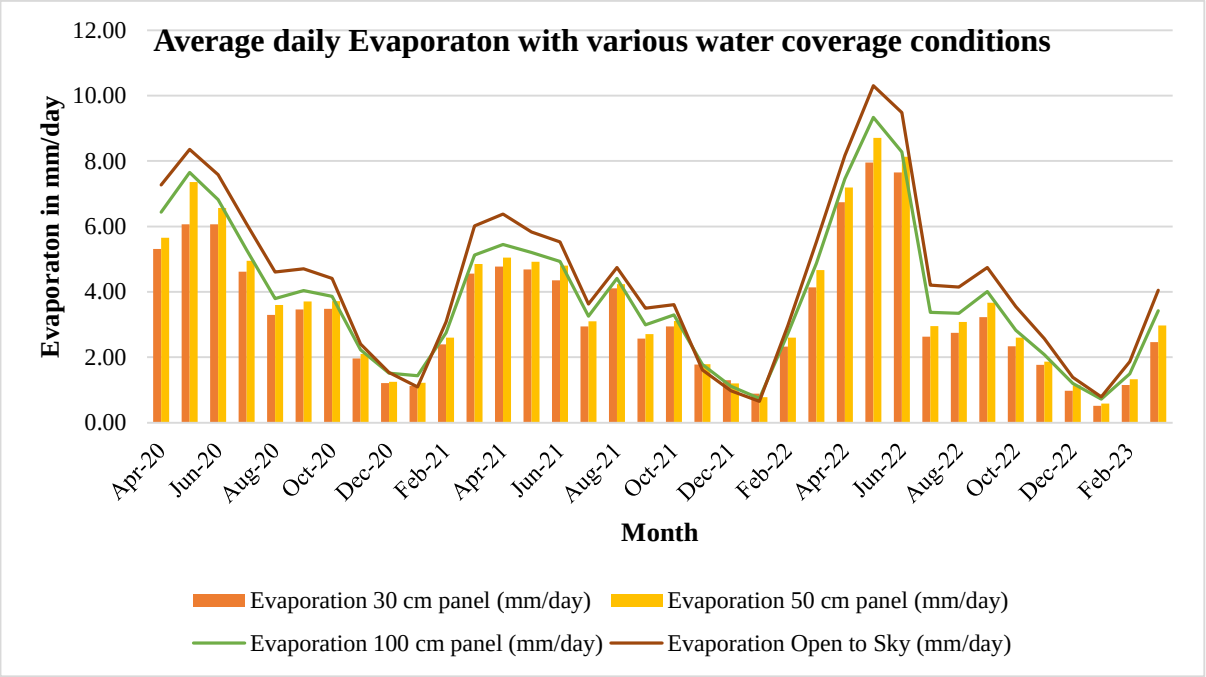

Figure 8.22. Average daily evaporation rates in monthly step April 2020 – March 2023

The data collected were analysed for recommendation of best formulation for Pilani and recommendation for Indian conditions. The formulations till now developed are for European or American conditions have not been modified or improved for Indian conditions. So present data collected at Pilani will provide an insight for best formulation that can be utilised for Pilani and further recommendation for Indian conditions.

8.6.1 Development of formulation for estimating evaporation from uncovered water body

The linear regression model has been developed for Pilani using several independent atmospheric parameters such as solar insolation (shortwave radiations), water temperature, ambient temperature, relative humidity, and wind speed. These parameters were utilised to develop model for estimating the dependent parameter evaporation. The Table 8.5(a) & (b) below provides details of the independent and dependent parameters along with the units of data collected.

Table 8.5(a). Independent variables

S. No.	Variable	Symbol	Unit
1	Solar Insolation	R_s	$MJ/m^2/day$
2	Ambient temperature	T_a	°C
3	Water temperature	T_w	°C
4	Humidity	Rh	%
5	Wind speed	V_w	m/s

Table 8.5(b). Dependent variable

S. No.	Variable	Symbol	Unit
1	Evaporation	E	mm/day

The regression model development experiment was carried out by considering six different designs-

1. The first model was developed by considering five parameters which include solar insolation, ambient temperature, water temperature, humidity, and wind speed.
2. The second model was developed by considering four parameters which include solar insolation, water temperature, humidity, and wind speed.
3. The third model was developed by considering four parameters which include solar insolation, ambient temperature, humidity, and wind speed.
4. The fourth model was developed by considering three parameters which includes solar insolation, humidity, and wind speed.
5. The fifth model was developed by considering three parameters which includes ambient temperature, humidity, and wind speed.
6. The sixth model was developed by considering three parameters which include water temperature, humidity, and wind speed.

8.6.1.1. Data summary for uncovered water body

The atmospheric data was collected at 15-minute intervals, including solar insolation, ambient temperature, humidity, wind velocity, and water temperature. However, pan evaporation was recorded on a daily basis. To use this data for analysis, the 15-minute interval data was averaged into daily time steps. The temperature data was recorded in degree Celsius, wind velocity in km/h, and humidity in percent. Solar insolation was measured in W/m^2 using a pyranometer. Any day that had missing data was excluded from analysis. The data used for analysis can be referred in the Appendix. A regression model was developed using the daily data collected from April 2021 to November 2022. The data from April 2021 to March 2022 was used for model development, while the data from April 2022 to November 2022 was used for testing. This time period was chosen as all the atmospheric parameter sensors were functioning properly during this period. The statistical summary of data is presented in Table 8.6 while correlation coefficient of all parameters with evaporation is given in Table 8.7.

Table 8.6. The statistical summary of modelling data

Statistical parameters	Evaporation (mm/day)	Water Temperature (°C)	Ambient Temperature (°C)	Wind Velocity (m/s)	Relative Humidity (%)	Solar Insolation (MJ/m2/day
Maximum	12.4	36.63	37.1	1.37	85.4%	17.5
Minimum	0.4	5.02	8.63	0.06	13.44%	1.5
Mean	4.00	22.75	25.08	0.3787	49.92%	12.276
Median	3.8	24.87	28.00	0.34	49.89%	12.9
Variance	5.6194	54.68	54.82	0.0416	276.20	10.41
Standard Deviation	2.37	7.39	7.40	0.2039	16.62	3.23

Table 8.7. Correlation coefficient of parameters with Evaporation

Parameters	Water Temperature	Ambient Temperature	Wind Velocity	Relative Humidity	Solar Insolation
Evaporation	0.6378	0.6961	0.4222	-0.7017	0.6184

It seems evident that most of the parameters show a strong correlation with evaporation, except for wind which has a weaker correlation. Additionally, relative humidity also exhibits a correlation with evaporation, but in a negative direction, unlike the other parameters.

8.6.1.2. Regression model development for uncovered water body

Following evaporation prediction regression models were developed

1. The model (E5) that employs five parameters, namely R_s, T_a, T_w, V_w, and R_h, was developed, and it resulted in obtaining Equation (8.57), which can be used for predicting evaporation.

$$E = 0.260961T_w + 0.016103R_s + 1.437038\ V_w - 0.136378T_a - 0.087122R_h + 5.097066. \quad (8.57)$$

The predicted evaporation values from the modelling and test data were also plotted against the actual values as shown in Figures A-8.6.1(1a) and A-8.6.1(1b), respectively. The adjusted R^2 value of the model is 0.7121.

2. The Equation (8.58) resulted after development of E4(T_w) model involves four parameters R_s, T_w, V_w, and R_h.

$$E = 0.133907T_w + 0.34992R_s + 1.368934\ V_w - 0.074295R_h + 3.719653. \quad (8.58)$$

The predicted evaporation values from the modelling and test data were also plotted against the actual values as shown in Figures A-8.6.1(2a) and A-8.6.1(2b), respectively. The adjusted R^2 value of the model is 0.7071.

3. Equation (8.59) was obtained by developing E4(T_a) model, which consist of four parameters R_s, T_a, V_w, and R_h.

$$E = 0.129173T_a + 0.067104R_s + 1.43272\ V_w - 0.061767R_h + 2.481629. \quad (8.59)$$

The predicted evaporation values from the modelling and test data were also plotted against the actual values as shown in Figures A-8.6.1(3a) and A-8.6.1(3b), respectively. The adjusted R^2 value of the model is 0.7121.

4 Equation (8.60) was obtained by developing E3(R_s) model, which consist of three parameters R_s, V_w, and R_h.

$$E = 0.175352R_s + 2.635177\ V_w - 0.070563R_h + 4.377117. \quad (8.60)$$

The predicted evaporation values from the modelling and test data were also plotted against the actual values as shown in Figures A-8.6.1(4a) and A-8.6.1(4b), respectively. The adjusted R^2 value of the model is 0.5862.

5 Equation (8.61) was obtained by developing E3(T_a) model, which consist of three parameters T_a, V_w, and R_h.

$$E = 0.137939T_a + 1.49557\ V_w - 0.068034R_h + 3.374499. \quad (8.61)$$

The predicted evaporation values from the modelling and test data were also plotted against the actual values as shown in Figures A-8.6.1(5a) and A-8.6.1(5b), respectively. The adjusted R^2 value of the model is 0.6857.

6 Equation (8.62) was obtained by developing E3(T_w) model, which consist of three parameters T_w, V_w, and R_h.

$$E = 0.138906T_w + 1.393587\ V_w - 0.077852R_h + 4.203714. \quad (8.62)$$

The predicted evaporation values from the modelling and test data were also plotted against the actual values as shown in Figures A-8.6.1(6a) and A-8.6.1(6b), respectively. The adjusted R^2 value of the model is 0.707.

8.6.2. Development of formulation for estimating evaporation from water body covered by the solar panel

The data collected were analysed for recommendation of best formulation for Pilani and recommendation for Indian conditions. The linear regression model has been developed for Pilani using several independent atmospheric parameters such as solar insolation (shortwave radiations), water temperature, ambient temperature, relative humidity, Panel temperature and wind speed. These parameters were utilised to develop model for estimating the dependent

parameter evaporation. Table 8.8(A) and 8.8(B) below provides details of the independent and dependent parameters along with the units of data collected.

Table 8.8(A). Independent variables

S. No.	Variable	Symbol	Unit
1	Solar Insolation	R_s	$MJ/m^2/day$
2	Ambient temperature	T_a	°C
3	Water temperature	T_w	°C
4	Humidity	Rh	%
5	Wind speed	V_w	m/s
6	Panel Temperature	T_p	°C
7	Humidity below panel	Rhp	%

Table 8.8(B). Dependent variable

S. No.	Variable	Symbol	Unit
1	Evaporation	Ep	mm/day

For the development of the regression model for a solar panel placed at 300 mm height, several experiments were designed. These parameters were the same as those collected for the open-air experiment and additional data of humidity under the panel and panel temperature were utilised for model development. The following experiments were conducted to develop different models:

1. A five parameter model was developed using solar insolation, ambient temperature, water temperature, humidity and wind speed. These parameters were collected in open-air.
2. Another five-parameter model was developed using solar insolation, ambient temperature, water temperature, humidity under panel and wind speed. In this model, humidity under the panel was considered to check the impact of humidity just above the water body.
3. A five-parameter model was developed by replacing solar insolation with panel temperature. As the pan was not directly receiving solar insolation, but rather receiving heat by radiating panel, the five parameters considered in this experiment were panel temperature, ambient temperature, water temperature, humidity and wind speed.
4. A four-parameter model was developed considering humidity under panel, solar insolation, ambient temperature, and wind speed.

5. Another four-parameter model was developed considering humidity under panel, solar insolation, water temperature, and wind speed.
6. A four-parameter model was developed considering humidity under panel, ambient temperature, water temperature, and wind speed.
7. A four-parameter model was developed by considering all four parameters recorded open to sky. These parameters were humidity, solar insolation, water temperature, and wind speed.
8. Another four-parameter model was developed considering humidity, solar insolation, ambient temperature, and wind speed. All data utilized for this model was recorded in open air.
9. A new model was developed by replacing solar insolation with four parameters: humidity, water temperature, ambient temperature, and wind speed, all of which were collected in open air.
10. Three parameter models were developed with humidity under panel and wind velocity as fixed parameters. Replacement variables such as solar insolation, water temperature, and ambient temperature were used. Three models were created, namely: a new model with three parameters solar insolation, wind velocity, and humidity under panel, a three parameter model utilizing ambient temperature, wind velocity, and humidity under panel, and a three parameter model with water temperature, wind velocity, and humidity.
11. Three parameter models were developed by fixing wind velocity and keeping humidity open to air. Replacement variables such as solar insolation, water temperature, and ambient temperature were used. The models developed were: a three parameter model with solar insolation, wind velocity, and humidity, a three parameter model with ambient temperature, wind velocity, and humidity, and a three parameter model with water temperature, wind velocity, and humidity.
12. When data is limited, it becomes difficult to estimate evaporation. To address this, models with two parameters were developed using available variables such as ambient temperature, humidity, wind velocity, and water temperature. Four models were created, namely: a two-parameter model with water temperature and humidity, a two-parameter model with water temperature and wind velocity, a two-parameter model with ambient temperature and humidity, and a two-parameter model with ambient temperature and wind velocity.

8.6.2.1. Data summary for water body covered by the solar panel

The atmospheric data was collected at 15-minute intervals, including solar insolation, ambient temperature, humidity, wind velocity, and water temperature. Solar panel temperature data were also recorded at 15-minute intervals using sensors. However, pan evaporation, which was covered with a solar panel fixed at a height of 30cm above the pan, was recorded once daily. Dry bulb and wet bulb temperature under the panel were recorded three times at 8:30am, 2:30 am, and 5:30 am. To use this data for analysis, the 15-minute interval data was averaged into daily time steps. The temperature data was recorded in degrees Celsius, wind velocity in km/h, and humidity in percent. Solar insolation was measured in W/m^2 using a pyranometer. Any day that had missing data was excluded from the analysis. The data used for analysis can be found in the appendix. A regression model was developed using the daily data collected from April 2021 to November 2022. The data from April 2021 to March 2022 was used for model development, while the data from April 2022 to November 2022 was used for testing. This period was chosen as all the atmospheric parameter sensors were functioning properly during this period.

Based on the collected data during the period, the statistical parameters have been estimated and are presented in the Table (8.9) below. As per the table, the highest rate of evaporation is 8.2 mm/day, whereas the lowest rate of evaporation is 0.5 mm/day. Moreover, the average maximum and minimum panel temperature is 6.75°C and 41.05°C, respectively. The maximum humidity beneath the panel has been recorded as 100%, while the maximum humidity in the open air is 85.40%. The high variance of humidity suggests the volatile nature of humidity. Also, there seems to be a high volatility in solar panel temperature.

Table 8.9. Statistical parameters of Meteorological data

Statistical Parameters	Evaporation (mm/day)	Water Temperature (°C)	Ambient Temperature (°C)	Solar insolation (MJ/m^2/day)	Panel Temperature (°C)	Wind Velocity (m/s)	Humidity (%)	Humidity (under panel)(%)
Min.	0.50	3.67	8.63	1.50	6.75	0.06	13.44	15.08
Max.	8.20	33.33	37.10	17.50	41.05	1.04	85.40	100.00
Range	7.70	29.66	28.47	16.00	34.30	0.98	71.96	84.92
Median	3.0	24.33	28.00	12.90	31.73	0.33	48.69	55.72
Mean	3.24	22.42	25.09	12.28	28.84	0.37	50.03	56.79
Variance	2.93	43.74	54.82	10.42	77.51	0.04	309.08	371.92
Standard Deviation	1.71	6.61	7.40	3.23	8.80	0.20	17.58	19.29

The correlation coefficients of all independent parameters were estimated with respect to dependent parameter Evaporation. Correlation coefficient is summarised in the Table (8.10) below.

Table 8.10. Correlation coefficient of parameters with Pan Evaporation covered with solar panel

Parameters	Water Temperature	Ambient Temperature	Wind Velocity	Relative Humidity	Solar Insolation	Panel temperature	Humidity (under Panel)
Evaporation	0.5928	0.6989	0.4463	-0.6926	0.5917	0.6912	-0.6713

Based on the correlation coefficient, it can be observed that ambient temperature, relative humidity, and panel temperature are showing a strong relationship with evaporation, while other parameters are having a moderate relationship with evaporation.

8.6.2.2. Regression model development for water body covered with solar panel

Following Regression model have been developed for evaporation estimation for water body covered with solar panel.

1. The model Ep5Rh(Rs) that employs five parameters, namely R_s, T_a, T_w, V_w, and R_h, was developed, and it resulted in obtaining Equation (8.63), which can be used for predicting evaporation. All data of open-air parameters were utilised for model development.

$$Ep = 0.136046T_w - 0.001573R_s + 1.412181V_w - 0.031922T_a - 0.6329R_h + 3.633706 \quad (8.63)$$

The predicted evaporation values from the modelling and test data were also plotted against the actual values as shown in Figures A-8.6.2(1a) and A-8.6.2(1b), respectively. The adjusted R^2 value of the model is 0.7227.

2. The model Ep5Rh(Tp) is being developed to estimate evaporation considering panel Temperature instead of solar radiation, so parameters considered in model development are T_p, T_a, T_w, V_w, and R_h. The Equation (8.64) has been developed, utilising all other parameters from open air.

$$Ep = 0.093722T_w + 0.081032T_p + 1.31707\,V_w - 0.08342228T_a - 0.059557R_h + 3.441718 \quad (8.64)$$

The predicted evaporation values from the modelling and test data were also plotted against the actual values as shown in Figures A-8.6.2(2a) and A-8.6.2(2b), respectively. The adjusted R^2 value of the model is 0.7088.

3. The model Ep5Rhp(Rs) is developed utilising parameter R_s, T_a, T_w, V_w recorded in open air and R_{hp} is the humidity recorded under the panel, just above the water surface. The Equation (8.65) is developed as follows

$$Ep = 0.021275T_w + 0.03202R_s + 1.29896\,V_w + 0.07908T_a - 0.037869R_{hp} + 2.043275 \quad (8.65)$$

The predicted evaporation values from the modelling and test data were also plotted against the actual values as shown in Figures A-8.6.2(3a) and A-8.6.2(3b), respectively. The adjusted R^2 value of the model is 0.6739.

4. The four parametric model is developed which took into account humidity under the panel, while all other parameter values were recorded in open air.

   (A) The Ep4Rhp(Tw) model resulted in Equation (8.66), which was developed using recorded values R_s, T_w, V_w in open air and R_{hp} under panel

   $$Ep = 0.097837T_w + 0.037859R_s + 1.45072\ V_w - 0.04329R_{hp} + 2.489682 \quad (8.66)$$

The predicted evaporation values from the modelling and test data were also plotted against the actual values as shown in Figures A-8.6.2(4a) and A-8.6.2(4b), respectively. The R^2 of the model is 0.6668.

(B) The Ep4Rhp(Ta) model resulted in Equation (8.67), which was developed using recorded values of Rs, Ta, and V_w in open air, with Rhp being recorded under panel. The R^2 value for this model is 0.6745. In Figure A-8.6.2(4c), the graph shows a comparison between the predicted evaporation values from the modelling data and the actual values. On the other hand, Figure A-8.6.2(4d) displays the predicted values from the testing data and the actual recorded values for comparison.

$$Ep = 0.032493R_s + 1.279266\ V_w + 0.098649T_a - 0.036484R_{hp} + 1.952207 \quad (8.67)$$

(C) The Ep4Rhp(TaTw) model resulted in Equation (8.68) was developed using parameters Ta, Tw, and V_w, which were recorded in open air, along with Rsp, which represents the humidity recorded just above the water surface. The R^2 value for this model is 0.6731, indicating a moderately strong correlation between the variables. In order to evaluate the accuracy of the modelling data, the predicted evaporation values were compared against the actual values and plotted in Figure A-8.6.2(4e). Similarly, the predicted values from the testing data were also compared against the actual recorded values and plotted in Figure A-8.6.2(4f). This analysis helps in assessing the performance of the model and its ability to make accurate predictions.

$$Ep = 0.022348T_w + 1.328705\ V_w + 0.082464T_a - 0.040453R_{hp} + 2.462838 \quad (8.68)$$

5. Based on the data recorded, a three parametric model was developed. The model includes one fixed parameter, which is humidity recorded under the panel. All other parameter values were recorded in open air. The model resulted in three different models, each with three parameters.

(A) The model Ep3Rhp(Tw) was developed using parameters Tw, V_w, and Rhp, and resulted in Equation (8.69) with an R^2 value of 0.6652. In Figure A-8.6.2(5a), the model's predicted evaporation values were compared to the actual values, using the modelling data. Similarly, Figure A-8.6.2(5b) shows the comparison between the predicted values from the testing data and the actual recorded values.

$$Ep = 0.103021T_w + 1.493906\ V_w - 0.046645R_{hp} + 3.012427 \quad (8.69)$$

(B) The Ep3Rhp(Ta) model has been developed and resulted in Equation (8.70) with parameters T_a, V_w, and R_{hp}. The R^2 value obtained for the model is 0.6736. In Figure A-8.6.2(5c), the predicted evaporation values from the model were compared to the actual values using the modelling data. Similarly, Figure A-8.6.2(5d) shows the comparison between the predicted values from the testing data and the actual recorded values.

$$Ep = 0.103089T_a + 1.308465\ V_w - 0.039037R_{hp} + 2.373624 \quad (8.70)$$

(C) The model Ep3Rhp(Rs) was developed with parameters R_s, V_w, and R_{hp}, resulting in Equation (8.71) and an R^2 value of 0.5587. Figure A-8.6.2(5e) displays the comparison between the model's predicted evaporation values and the actual values, using the modelling data. Similarly, Figure A-8.6.2(5f) shows the comparison between the predicted values obtained from the testing data and the actual recorded values.

$$Ep = 0.118474\ R_s + 2.201331\ V_w - 0.041461R_{hp} + 3.305054 \quad (8.71)$$

6. Based on the consideration of four parametric models, all parameters recorded in open air, following two models were developed with four parameters. These models are expected to be helpful in estimating evaporation losses, as the data is readily available with the meteorological department.

(A) The model Ep4Rh(Tw) was developed using parameters R_s, T_w, V_w and R_h, which were recorded in open air. This resulted in Equation (8.72) with an R^2 value of 0.7226, indicating a strong correlation between the variables (The details of plot between model's predicted evaporation values and the actual values are given in Appendix A-8). Figure A-8.6.2(6a) displays the comparison between the model's predicted evaporation values and the actual values, using the modelling data. Similarly, Figure A-8.6.2(6b) shows the comparison between the predicted values obtained from the testing data and the actual recorded values

$$Ep = 0.1046991T_w - 0.0004954R_s + 1.3587531\ V_w - 0.059813R_h + 3.368953 \quad (8.72)$$

(B) The model Ep4Rh(Ta) was developed using parameters R_s ,T_a, V_w and R_h, which were recorded in open air. Equation (8.73) was derived, which has an R^2 value of 0.7058, indicating a strong correlation between the variables. In Figure A-8.6.2(6c), the predicted evaporation values from the model were compared to the actual values using the modelling data. Similarly, Figure A-8.6.2(6d) shows the comparison between the predicted values from the testing data and the actual recorded values.

$$Ep = 0.094895T_a + 0.012928\ R_s + 1.289449\ V_w - 0.048998R_h + 2.656733 \quad (8.73)$$

7 Three parametric model were developed utilising data recorded in open air. Following are three models developed with three parameters.

A Model E3Rh(Rs) was developed using parameters R_s , V_w and R_h, which were recorded in open air. Equation (8.74) was obtained from this model, which has an R^2 value of 0.5992, indicating a moderate correlation between the variables. In Figure A-8.6.2(7a), the predicted evaporation values from the model were compared to the actual values using the modelling data. Similarly, Figure A-8.6.2(7b) shows the comparison between the predicted values from the testing data and the actual recorded values.

$$Ep = 0.092451\ R_s + 2.172817\ V_w - 0.055459R_h + 4.049228 \quad (8.74)$$

(B) The E3Rh(Tw) model was developed using parameters T_w , V_w and R_h recorded in open air. Equation (8.75) was obtained from this model and has an R^2 value of 0.7236, indicating a strong correlation between the variables. Figure A-8.6.2(7c) shows the comparison between the predicted evaporation values obtained from the model and the actual values, using the modelling data. Similarly, Figure A-8.6.2(7d) displays the comparison between the predicted values from the testing data and the actual recorded values.

$$Ep = 0.10463T_w + 1.35826\ V_w - 0.05976R_h + 3.36202 \quad (8.75)$$

(C) The Ep3Rh(Ta) model was developed using parameters T_a , V and R_h recorded in open air. Equation (8.76) was obtained from this model and has an R^2 value of 0.7065, indicating a strong correlation between the variables. In Figure A-8.6.2(7e), the predicted evaporation values from the model were compared to the actual values using the modelling data. Similarly, Figure A-8.6.2(7f) shows the comparison between the predicted values from the testing data and the actual recorded values.

$$Ep = 0.096584T_a + 1.301555\ V_w - 0.050205R_h + 2.828754 \quad (8.76)$$

8 Two variable models were developed, considering limited data availability in the field. Following are four models with two parameters

(A) The E2Rh(Tw) model was developed using parameters T_w , and R_h recorded in open air. Equation (8.77) was obtained from this model and has an R^2 value of 0.7021, indicating a strong correlation between the variables. In Figure A-8.6.2(8a), the predicted evaporation values from the model were compared to the actual values using the modelling data. Similarly, Figure A-8.6.2(8b) shows the comparison between the predicted values from the testing data and the actual recorded values.

$$Ep = 0.117294T_w - 0.062778R_h + 3.74309 \quad (8.77)$$

(B) The Ep2V(Tw) model was created by using the parameters T_w and V_w that were recorded in an open-air environment. The resulting Equation (8.78) has an R^2 value of 0.4141, which suggests a weak correlation between the variables. Due to this weak correlation, the model that uses these parameters may not be effective in establishing a relationship between the variables. As a result, comparative graphs of actual values against predicted values were not generated for this model.

$$Ep = 0.12885T_w + 2.30659\ V_w - 0.52315 \quad (8.78)$$

(C) The Ep2Rh(Ta) model was created by utilizing the parameters T_a and R_h that were observed in an open-air setting. The resulting Equation (8.79) has an R^2 value of 0.6874, which suggests a significant correlation between the variables. Figure A-8.6.2(8c) displays the comparison between the predicted evaporation values obtained from the model and the actual values, using the modelling data. Similarly, Figure A-8.6.2(8d) shows the comparison between the predicted values from the testing data and the actual recorded values.

$$Ep = 0.109689T_a - 0.05159R_h + 3.061951 \quad (8.79)$$

(D) Equation (8.80) was obtained from the model Ep2V(Ta), which utilizes the parameters T_a and V that were observed in an open-air setting. However, the resulting R^2 value for this model is 0.5172, which suggests a weak correlation between the variables. Hence, this model may not be effective in establishing a relationship between the variables. Consequently, no comparative graphs of actual values versus predicted values were created for this model.

$$Ep = 0.14317T_a + 1.64103\ V_w - 0.97471 \quad (8.80)$$

8.7. Results and discussion

8.7.1 Performance of Evaporation Models for Uncovered Water Bodies

The evaporation predictions for uncovered water body were made by all 6 models developed in section 8.6.1. To validate these values, they were compared with the recorded pan evaporation. To evaluate the accuracy of the models, root mean square error (RMSE), mean absolute error (MAE), mean square error (MSE), and mean biased error were estimated using both modelling and testing data. The Table 8.11 below presents the results of these evaluations.

Table 8.11. Model performance for predicted value and observed values using (model data and test data)

Model	**E5**	**E4(T_a)**	**E4(T_w)**	**E3(R_s)**	**E3(T_a)**	**E3(T_w)**
RMSE	0.119	0.076	0.074	0.088	0.077	0.074
MAE	1.087	1.026	0.978	1.190	1.040	0.984
MBE	-0.634	0.000	0.000	0.000	0.000	0.000
MSE	2.294	1.718	1.618	2.294	1.742	1.624
Test data						
Test	**E5**	**E4(T_a)**	**E4(T_w)**	**E3(R_s)**	**E3(T_a)**	**E3(T_w)**
RMSE	0.119	0.121	0.118	0.154	0.117	0.116
MAE	1.087	1.136	1.089	1.503	1.105	1.069
MBE	0.634	0.695	0.636	1.198	0.595	0.583
MSE	2.294	2.373	2.251	3.819	2.192	2.156

Based on the presented results, it is worth noting that the regression model that includes water temperature as a variable performs better than the other models that use solar insolation and ambient temperature as variables. Among all six models, the three-variable model E3(Tw) is the most accurate, with a mean absolute error of 1.07 mm/day. However, since water temperature data are not always available, it is challenging to estimate evaporation using this model. Therefore, a three-variable model was developed that includes air temperature or solar insolation, wind velocity, and humidity. From the RMSE and MAE results, it can be inferred that the model's estimation with ambient temperature can predict evaporation with equal accuracy. Models E4(Ta) and E3(Ta) are four and three-variable models with ambient temperature as one of the variables that have been developed. The R^2 value of E5 and E4(Ta) is 0.7121 and that of E3(Ta) is 0.6857. However, the three-variable model E3(Ta) performs better than the four and five-variable models E4(Ta) and E5, with an RMSE of 0.117 and MAE of 1.10 mm/day. The worst performing model is E3(Rs), with an R^2 value of 0.5862 and an RMSE and MAE of 0.154 and 1.503 mm/day, respectively.

Based on the analysis, two models for estimating evaporation are recommended. The first model, E3(Tw), which considers water temperature, wind velocity, and humidity, has an

RMSE of 0.116 and MAE of 1.07 mm/day. This model has an R^2 value of 0.707, making it a reliable choice for estimating evaporation.

In the absence of water temperature data, the second model, E3(Ta), is recommended which uses ambient temperature, wind velocity, and humidity to estimate evaporation. This model has an RMSE of 0.117 and MAE of 1.10 mm/day, with an R^2 value of 0.6857. This model can be a good alternative for estimating evaporation in situations where water temperature data is not available.

8.7.2 Performance of Evaporation Models for PV covered Water Bodies

A total of 18 different models were created, using all available parameters and their various combinations, to achieve the best possible results. However, out of these 18 models, only 16 were analysed, since the other two models showed very low correlation. Their R^2 values were less than 0.6, and therefore, they were excluded from the analysis. The 16 models that were analysed were rigorously tested with data, and the results were compared with actual values. A range of metrics, such as root mean square error (RMSE), mean absolute error (MAE), mean biased error (MBE), mean square error (MSE), and R^2, were used to evaluate the performance of each model. The accuracy of each model was showcased in a detailed Table 8.12, presenting the results of the analysis.

Table 8.12 Statistical Parameters obtained from Various Models.

Model	RMSE	MAE	MBE	MSE	R^2
Ep5Rh(Tp)	0.072	0.570	-0.416	0.482	0.709
Ep5Rhp(Rs)	0.133	1.259	0.204	2.850	0.674
Ep5Rh(Rs)	0.119	1.144	0.058	2.280	0.723
Ep4Rhp(Tw)	0.135	1.290	0.192	2.955	0.667
Ep4Rhp(Ta)	0.133	1.249	0.216	2.831	0.675
Ep4Rhp(TwTa)	0.133	1.270	0.157	2.829	0.673
Ep3Rhp(Rs)	0.145	1.312	0.610	3.370	0.559
Ep3Rhp(Tw)	0.135	1.306	0.137	2.940	0.665
Ep3Rhp(Ta)	0.132	1.259	0.170	2.807	0.674
Ep4Rh(Tw)	0.119	1.142	0.072	2.288	0.723
Ep4Rh(Ta)	0.121	1.134	0.162	2.358	0.706
Ep3Rh(Rs)	0.142	1.545	-0.862	3.227	0.599
Ep3Rh(Tw)	0.119	1.142	0.072	2.289	0.724
Ep3Rh(Ta)	0.121	1.135	0.143	2.342	0.707
Ep2Rh(Tw)	0.119	1.128	0.121	2.286	0.702
Ep2Rh(Ta)	0.121	1.130	0.189	2.358	0.687

The model Ep5Rh(Tp) utilises panel temperature instead of solar insolation and has the lowest RMSE value of 0.072 mm/day among all the models. Additionally, this model has a coefficient of determination R^2 of 0.7088, which is considered reasonable for the estimation of evaporation. The mean absolute error of this model is also lowest among all the models, with a value of 0.57 mm/day. Thus, this model performs the best among all the models. However, the availability of panel data required for estimation of evaporation is quite scarce. Hence, models utilising other parameters were developed.

The Ep5Rh(Rs) model with five variables, including solar insolation and other parameters recorded in open air, produced a slightly better coefficient of determination R^2 of 0.7227 than Ep5Rh(Tp). However, the RMSE and MAE values of this model were estimated to be 0.119 and 1.144, respectively. These values indicate that this model is not better than Ep5Rh(Tp). The hurdle in utilising this model is the unavailability of data for all the parameters.

To investigate the possibility of achieving better predictions with fewer parameters, a series of models were developed with four, three, and two parameters. The four-parameter model, Ep4Rh(Tw), outperformed the other four-parameter models, achieving a coefficient of determination (R^2) of 0.723, an RMSE of 0.119, and an MAE of 1.142. The three-parameter models outperformed the four-parameter models, with the Ep3Rh(Tw) model performing the best, achieving an R^2 of 0.7236, an RMSE of 0.119, and an MAE of 1.1421. Two-parameter models were also developed to account for situations where data availability is a constraint. These models performed equally well compared to higher-parameter models. Among the two-parameter models, the Ep2Rh(Tw) model performed the best, achieving an R^2 of 0.7021, an RMSE of 0.119, and an MAE of 1.128, which is better than the three- and four-parameter models. The best-performing models among all the variations have two common parameters: water temperature and relative humidity. Water temperature data is a rare resource from meteorological departments, which typically have ambient temperature data readily available. Therefore, models with ambient temperature were developed with varying numbers of parameters, and it was observed that the two-parameter model utilizing ambient temperature and humidity parameters performed equally well compared to the three- and four-parameter models. The model E2Rh(Ta) achieved an R^2 of 0.6874, an RMSE of 0.121, and an MAE of 1.130.

During the analysis, it was observed that using humidity measurements taken under the solar panel did not result in any significant improvement over the data recorded in open air. Additionally, models developed based on wind velocity instead of humidity did not yield promising results in terms of coefficient of determination and were hence disregarded for

analysis. Finally, solar insolation was found to be a poor parameter for model development as compared to ambient temperature and water temperature.

In order to estimate evaporation from water surfaces covered with solar panels, a total of 18 models were developed using linear regression analysis. These models were designed considering various parameters, including solar insolation, water temperature, ambient temperature, relative humidity recorded in open air, relative humidity recorded under the panel, wind velocity, and panel temperature. Among these parameters various combinations of parameters were considered and 18 models were developed. The models were analysed by utilising test data set and following are the recommendations

1. The Ep5Rh(Tp) model has proven to be the most precise and reliable among all other models. Its innovative approach utilizes panel temperature, as opposed to commonly used factor solar insolation, ambient temperature, water temperature, relative humidity, and wind velocity, to effectively estimate evaporation. With RMSE and MAE values of 0.072 mm/day and 0.57 mm/day, respectively, this model boasts the lowest error rates of all models. Additionally, its R^2 value of 0.7088 is considered quite reasonable for accurate evaporation estimation. The hurdle in utilising this model is the unavailability of panel temperature data.

2. When comparing the Ep5Rh(Rs) model to the Ep5Rh(Tp) model, it was found that the former produced a higher coefficient of determination R^2 of 0.7227. This model includes five variables, including solar insolation and other parameters recorded in open air. However, despite its higher R^2 value, the RMSE and MAE values of this model were estimated to be 0.119 and 1.144, respectively. It was concluded that the Ep5Rh(Rs) model is better than the Ep5Rh(Tp) model because atmospheric data has a better chance of availability. However, it should be noted that all five atmospheric parameters, including solar insolation, ambient temperature, water temperature, relative humidity, and wind velocity, are also rarely available.

3. The three-parameter Ep3Rh(Tw) model has outperformed all other models with an R^2 value of 0.7236. Additionally, it achieved an RMSE value of 0.119 and an MAE value of 1.142.

4. Two-parameter models were developed to account for situations where data availability is a constraint. Among the two-parameter models, the Ep2Rh(Tw) model was found to perform the best with an R^2 value of 0.7021. Additionally, it achieved an RMSE value of 0.119 and an MAE value of 1.127.

5. Due to the unavailability of water temperature data from meteorological departments, models with ambient temperature were developed. Among these models, the E3Rh(Ta) was found to perform well with an R^2 value of 0.7065. Additionally, it achieved an RMSE value of 0.120 and an MAE value of 1.134.

8.7.3 Estimation of evaporation under two water surface conditions at twenty-eight selected dam sites.

The model developed in section 8.6.1 for uncovered water surface area (open tank) evaporation using 4 parametric regression model (Equation 8.59) has been used to assess the evaporation at 28 different dam sites under uncovered water surface conditions. The geotagging of some specific location of these dams are shown in Table 8.13.

Table 8.13 Geolocations of Analysed dams for Uncovered and PV Covered Water Surfaces

Name of Reservoir/Dams	**Latitude**	**Longitude**
Saprar dam	25.2104 N	79.0831 E
Barwa Sagar	25.3732 N	78.7220 E
Pahuj dam	25.5063 N	78.5260 E
Parichha dam	25.5171 N	78.7770 E
Dhukwan dam	25.1925 N	78.5347 E
Barwar lake	25.5220 N	79.1307 E
Matatila dam	25.0616 N	78.2506 E
Sajnam dam	24.5253 N	78.5906 E
Govind sagar dam	24.6727 N	78.4266 E
Jamini dam	24.3403 N	78.4143 E
Shahzad dam	24.9502 N	78.5197 E
Arjun dam	25.3868 N	79.6763 E
Belasagar	25.2642 N	79.5797 E
Pahari dam	25.2343 N	79.2836 E
Maudaha dam	25.5887 N	79.7048 E
Lahchura dam	25.3281 N	79.2796 E
Chandrawal dam	25.4308 N	79.8635 E
Kabrai dam	25.4084 N	79.9769 E
Gunta dam	25.2173 N	81.1447 E
Majhgawan dam	25.2821 N	79.5099 E
Upper khajuri dam	24.9963 N	82.5960 E
Dhadraul dam	24.6254 N	83.1695 E
Adwa dam	24.7861 N	82.3056 E
Rihand dam	24.0236 N	82.7285 E
Obra dam	24.4394N	82.9661 E
Kanhar dam	24.1229 N	83.2946 E
Kalagarh dam	29.5194 N	78.7586 E
Rajghat dam	24.7625 N	78.7500 E

The predicted results of uncovered water surface area (open tank) evaporation are shown in Table A-8.7.1. Similarly, evaporation values have also been determined by taking into consideration of the covered areas with PV panels at these 28 dam sites using 4 parametric regression model (Equation 8.73). These values are also shown in Table A-8.7.2 (Appendix A-8).The highest evaporation rates for open sky and covered with PV panels were **2126.53 mm/year and 1567.63 mm/year** estimated for Ohan dam and lowest were **1783.29 mm/year and 1283.32 mm/year for Kalagarh dam.** The evaporation reduction due to coverage of dam surface area is estimated and presented in Table 8.14

Table 8.14 Evaporation Reduction due to total dam surface coverage by solar PV

Name of Reservoir/Dams	Latitude	Longitude	open surface water Evaporation estimation by 4 parametric Regression model by Equation 8.59 (in mm)	PV panel covered water surface Evaporation estimation by 4 parametric Regression model by Equation 8.73 (in mm)	% Reduction in evaporation by 4 parameter model
Saprar dam	25.2104 N	79.0831 E	1853.74	1300.52	29.84
Barwa Sagar	25.3732 N	78.7220 E	1834.51	1287.66	29.81
Pathrai Dam	25.4148 N	78.9979 E	1837.60	1291.58	29.71
Dongri Dam	25.3844 N	78.4562 E	1834.91	1286.79	29.87
Garhmau Tank	25.5238 N	78.6538 E	1840.95	1290.76	29.89
Pahuj dam	25.5063 N	78.5260 E	1844.74	1292.30	**29.95**
Parichha dam	25.5171 N	78.7770 E	1837.86	1289.10	29.86
Dhukwan dam	25.1925 N	78.5347 E	1848.81	1296.69	29.86
Barwar lake	25.5220 N	79.1307 E	1852.27	1304.30	29.58
Matatila dam	25.0616 N	78.2506 E	1882.36	1321.31	29.81
Sajnam dam	24.5253 N	78.5906 E	1945.43	1383.26	28.90
Govind Sagar dam	24.6727 N	78.4266 E	1906.55	1345.32	29.44
Jamini dam	24.3403 N	78.4143 E	2014.48	1448.90	28.08
Shahzad dam	24.9502 N	78.5197 E	1877.38	1322.45	29.56
Arjun dam	25.3868 N	79.6763 E	1933.11	1384.90	28.36
Belasagar	25.2642 N	79.5797 E	1912.29	1361.65	28.79
Pahari dam	25.2343 N	79.2836 E	1862.33	1313.23	29.48
Maudaha dam	25.5887 N	79.7048 E	1962.84	1411.82	28.07
Lahchura dam	25.3281 N	79.2796 E	1869.58	1319.73	29.41
Chandrawal dam	25.4308 N	79.8635 E	2008.42	1453.11	27.65
Kabrai dam	25.4084 N	79.9769 E	2022.24	1471.00	27.26
Ohan dam	25.1319 N	81.0316 E	**2126.53**	**1567.63**	**26.28**
Gunta dam	25.2173 N	81.1447 E	2117.15	1559.58	26.34
Majhgawan dam	25.2821 N	79.5099 E	1873.75	1321.17	29.49
Upper Khajuri dam	24.9963 N	82.5960 E	2094.16	1541.24	26.40
Moosakhand dam	24.9583 N	83.2917 E	2097.18	1536.62	26.73
Latif Shah dam	25.025 N	83.2250 E	2090.91	1532.84	26.69

Name of Reservoir/Dams	Latitude	Longitude	open surface water Evaporation estimation by 4 parametric Regression model by Equation 8.59 (in mm)	PV panel covered water surface Evaporation estimation by 4 parametric Regression model by Equation 8.73 (in mm)	% Reduction in evaporation by 4 parameter model
Dhadraul dam	24.6254 N	83.1695 E	1961.60	1429.85	27.11
Adwa dam	24.7861 N	82.3056 E	2100.24	1540.30	26.66
Rihand dam	24.0236 N	82.7285 E	1925.87	1382.44	28.22
Obra dam	24.4394N	82.9661 E	2044.25	1491.13	27.06
Kanhar dam	24.1229 N	83.2946 E	1971.73	1427.28	27.61
Kalagarh dam	29.5194 N	78.7586 E	**1783.29**	**1283.32**	28.04
Rajghat dam	24.7625 N	78.7500 E	1835.82	1289.60	29.75

As can be seen from Table 8.14, a significant reduction of evaporation has been observed when water surface at the dam sites is covered with PV panels. The reduction of evaporation varies from 26.28% to 29.95 at Ohan Dam and Pahuj dam, respectively. The results obtained from the model developed herein under two different conditions were compared with the some of the existing models.

As coverage of dam sites with PV panels not only dependent on variation of actual water surface area of the dam but also installation costs, therefore it has been decided to prescribe different percentages of coverage of water surface area with the PV panels under different scenarios.Table 8.15 represents the evaporation reduction for all selected dam sites with different percentage coverage of area with solar PV panels.

Table 8.15. Annual evaporation reduction due to various percentage coverage of water surface at selected dam sites

Name of Reservoir/Dams	Latitude	Longitude	Submergence Area of dam (ha)	Gross Water Storage capacity in MCM	Annual Evaporation loss from reservoirs (in MCM) (By Regression model Equation 8.59)	percent evaporation loss with respect to total storage	Reduction in evaporation (in MCM) against annual evaporation if 25% is covered by solar panel	Reduction in evaporation (in MCM) against annual evaporation if 20% is covered by solar panel	Reduction in evaporation (in MCM) against annual evaporation if 15% is covered by solar panel	Reduction in evaporation (in MCM) against annual evaporation if 10% is covered by solar panel
Saprar dam	25.2104 N	79.0831 E	2000.00	76.20	18.54	24.33	1.38	1.11	0.83	0.55
Barwa Sagar	25.3732 N	78.7220 E	520	10.2	4.77	46.76	0.36	0.28	0.21	0.14
Pahuj dam	25.5063 N	78.5260 E	543	18.25	5.01	27.44	0.37	0.30	0.22	0.15
Parichha dam	25.5171 N	78.7770 E	802	78.76	7.37	9.36	0.55	0.44	0.33	0.22
Dhukwan dam	25.1925 N	78.5347 E	1943	57.8	17.96	31.07	1.34	1.07	0.80	0.54
Barwar lake	25.5220 N	79.1307 E	1006.4	33.78	9.32	27.59	0.69	0.55	0.41	0.28
Matatila dam	25.0616 N	78.2506 E	12787	1132.68	120.35	10.63	8.97	7.17	5.38	3.59
Sajnam dam	24.5253 N	78.5906 E	2375	83.5	23.10	27.67	1.67	1.34	1.00	0.67
Govind sagar dam	24.6727 N	78.4266 E	2478.8	96.8	23.63	24.41	1.74	1.39	1.04	0.70
Jamini dam	24.3403 N	78.4143 E	2472.65	96.8	24.91	25.73	1.75	1.40	1.05	0.70
Shahzad dam	24.9502 N	78.5197 E	2993	130	28.09	21.61	2.08	1.66	1.25	0.83
Arjun dam	25.3868 N	79.6763 E	1800	68.35	17.40	25.45	1.23	0.99	0.74	0.49
Belasagar	25.2642 N	79.5797 E	926	20.86	8.85	42.44	0.64	0.51	0.38	0.25
Pahari dam	25.2343 N	79.2836 E	803	47.8	7.48	15.64	0.55	0.44	0.33	0.22
Maudaha dam	25.5887 N	79.7048 E	5429	200	53.28	26.64	3.74	2.99	2.24	1.50
Lahchura dam	25.3281 N	79.2796 E	897.27	15.29	8.39	54.86	0.62	0.49	0.37	0.25

Name of Reservoir/Dams	Latitude	Longitude	Submergence Area of dam (ha)	Gross Water Storage capacity in MCM	Annual Evaporation loss from reservoirs (in MCM) (By Regression model Equation 8.59)	percent evaporation loss with respect to total storage	Reduction in evaporation (in MCM) against annual evaporation if 25% is covered by solar panel	Reduction in evaporation (in MCM) against annual evaporation if 20% is covered by solar panel	Reduction in evaporation (in MCM) against annual evaporation if 15% is covered by solar panel	Reduction in evaporation (in MCM) against annual evaporation if 10% is covered by solar panel
Chandrawal dam	25.4308 N	79.8635 E	1192	34.71	11.97	34.49	0.83	0.66	0.50	0.33
Kabrai dam	25.4084 N	79.9769 E	505.3	13.22	5.11	38.65	0.35	0.28	0.21	0.14
Gunta dam	25.2173 N	81.1447 E	813.6	28.8	8.61	29.90	0.57	0.45	0.34	0.23
Majhgawan dam	25.2821 N	79.5099 E	830	26.8	7.78	29.02	0.57	0.46	0.34	0.23
Upper khajuri dam	24.9963 N	82.5960 E	1131	44.74	11.84	26.47	0.78	0.63	0.47	0.31
Dhadraul dam	24.6254 N	83.1695 E	3033.12	144.14	29.75	20.64	2.02	1.61	1.21	0.81
Adwa dam	24.7861 N	82.3056 E	1667	57.7	17.51	30.34	1.17	0.93	0.70	0.47
Rihand dam	24.0236 N	82.7285 E	46620	10600	448.92	4.24	31.67	25.33	19.00	12.67
Obra dam	24.4394N	82.9661 E	1800	211	18.40	8.72	1.24	1.00	0.75	0.50
Kanhar dam	24.1229 N	83.2946 E	3796	197.36	37.42	18.96	2.58	2.07	1.55	1.03
Kalagarh dam	29.5194 N	78.7586 E	7834	2442	69.85	2.86	4.90	3.92	2.94	1.96
Rajghat dam	24.7625 N	78.7500 E	24210	2172	222.23	10.23	16.53	13.22	9.92	6.61
		Total	**133208.14**	**18139.54**	1267.83	6.99	90.87	72.70	54.52	36.35
			100		0.95		0.0682	0.0546	0.0409	0.0273

Evaporation Reduction Scenarios for Different Coverage Areas

The generalization for evaporation reduction has been done based on estimates of evaporation reduction at twenty-eight dam sites. The evaporation reduction for various coverage scenario for 100 ha and variation of evaporation reduction with percent area coverage is shown in Figure 8.23

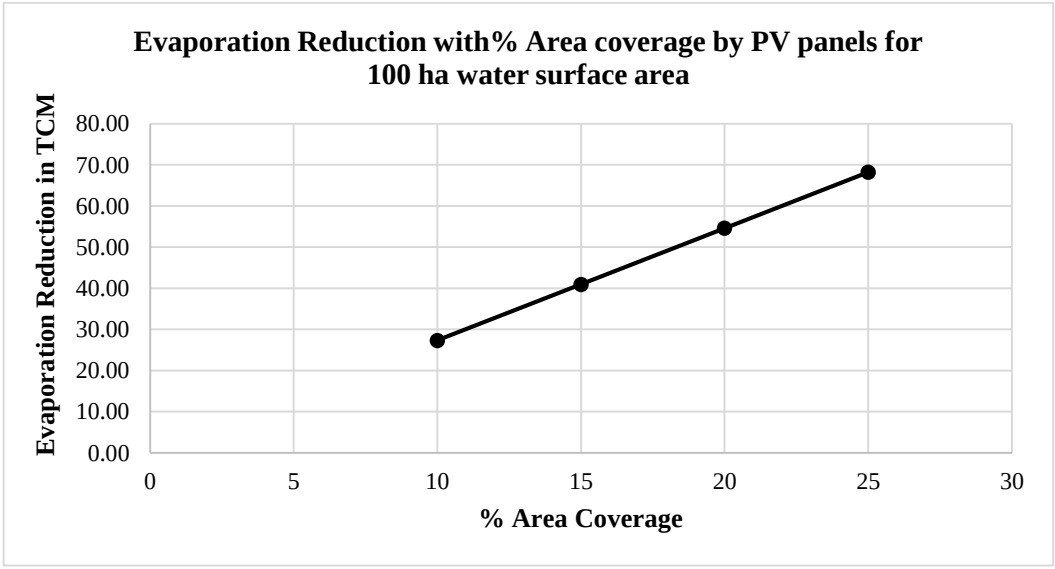

Figure 8.23 Plot of evaporation reduction vs Area coverage by FSPV panels

8.7.4 Development of decision-making charts

In response to the multifaceted considerations involved in floating solar photovoltaic (FSPV) installations, a comprehensive analysis has motivated to develop decision-making charts. These charts serve as indispensable aids for decision-makers, policymakers, and practitioners, offering important insights into critical parameters such as FSPV installation capacity (in

MWp) (DC), FSPV installation costs (Rs. /Wp), evaporation reduction (Thousand cubic meter TMC), and average annual energy generation (MWh) for a given water surface area (in hectares).

Water surface area (ha): The water bodies have open surface area varying size from few hectares to hundreds of kilo meters. These surface areas have potential to generate solar power by installation of floating solar PV over the unused surface. The potential estimation has been discussed in chapter 6. The water surface area available for installation have certain constraints. All the surface area available cannot be utilised for power generation as this area fluctuate month on month and least area is available during the summer season. So, an engineer should know the maximum area available in a dam for installation of solar PV over it. Engineers must determine the maximum usable area within a dam for FSPV installation, considering fluctuating seasonal dynamics.

FSPV installation Capacity MWp (DC): Depending upon the available area and knowing the weather parameters affecting the FSPV generation, maximum FSPV installation capacity in MWp can be estimated as discussed in chapter 6. The area required for MWp scale were estimated and a plot for area vs FSPV installation were prepared and shown in Figure 8.24

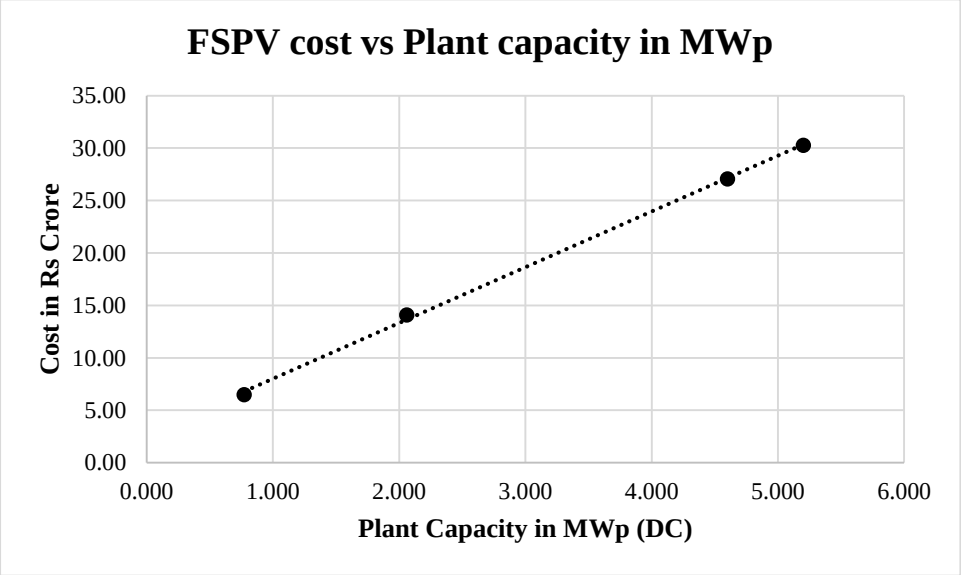

Figure 8.24. Plot showing total cost of FSPV plant for different installation capacity

FSPV cost of installation (Rs. / Wp): Project can only be viable when sufficient funds are available. So, success of project depends on funds availability. The cost of installation were obtained from vendors and estimation for various MWp capacity were carried out. Figure 8.25 shows the variation of cost in Rs/Wp with plant capacity and Figure 8.26 shows variation of cost in Rs/Wp with area of installation.

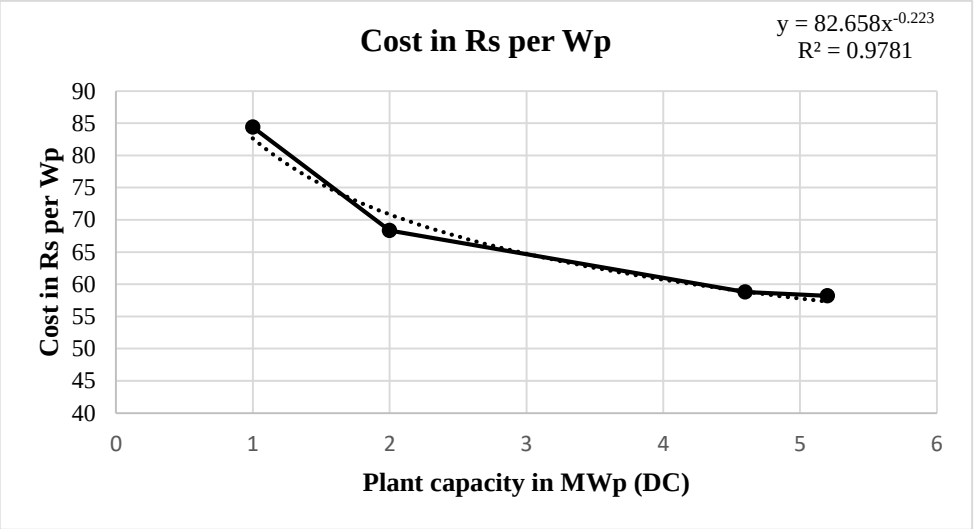

Figure 8.25. Variation of cost of FSPV in Rs/Wp with plant capacity in MW(DC)

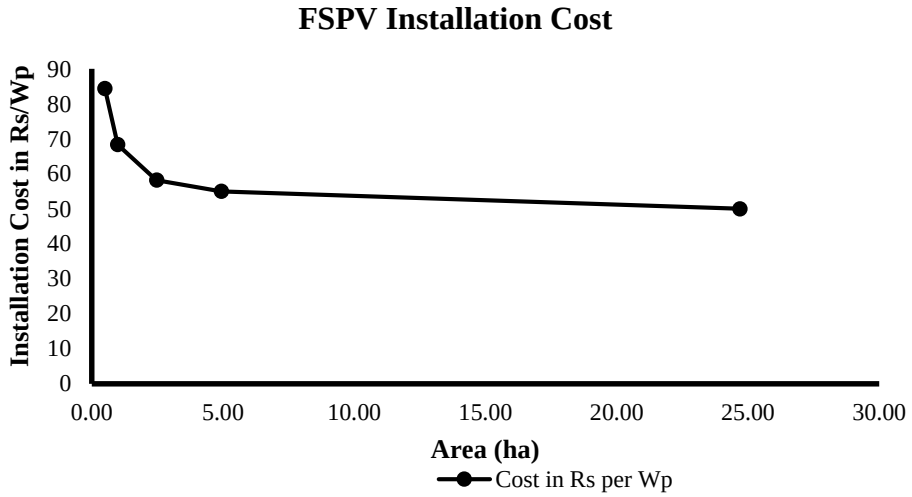

Figure 8.26. Variation of cost of FSPV in Rs/Wp with area of coverage in ha

Average annual energy generation (MWh): The power generation estimates for the given installation capacity can be estimated for FSPV plant as discussed in chapter 4. The annual power estimates have been prepared using temperature model developed in chapter 5. The estimates of average annual energy generation for different installation capacities have been derived, aiding in strategic decision-making. Estimates of annual power generation with area coverage were plotted in Figure 8.27.

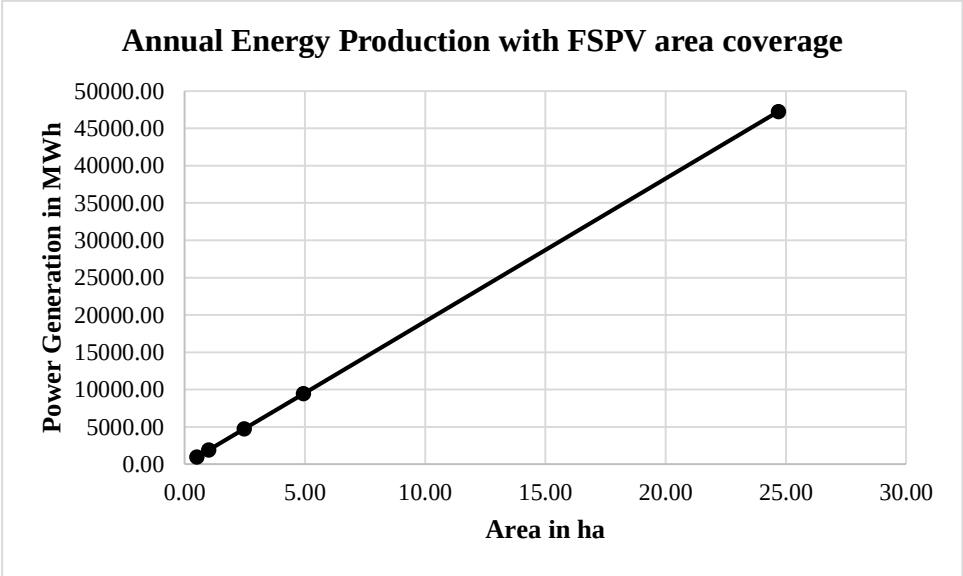

Figure 8.27. Power generation of FSPV in MWh with area coverage in ha

Evaporation Reduction due to FSPV installation: Since FSPV installation reduces evaporation as discussed in chapter 7, the water can be conserved. The model for evaporation estimation due to FSPV cover and without cover were developed in section 8.6.2 and 8.6.1 respectively. Recognizing the pivotal role of FSPV installations in reducing evaporation, models have been devised to estimate evaporation reduction corresponding to varying area coverage. These insights are encapsulated in charts delineating the relationship between area coverage and evaporation reduction. The evaporation estimates using these models were carried out and evaporation reduction due various area coverage and plotted in Figure 8.28.

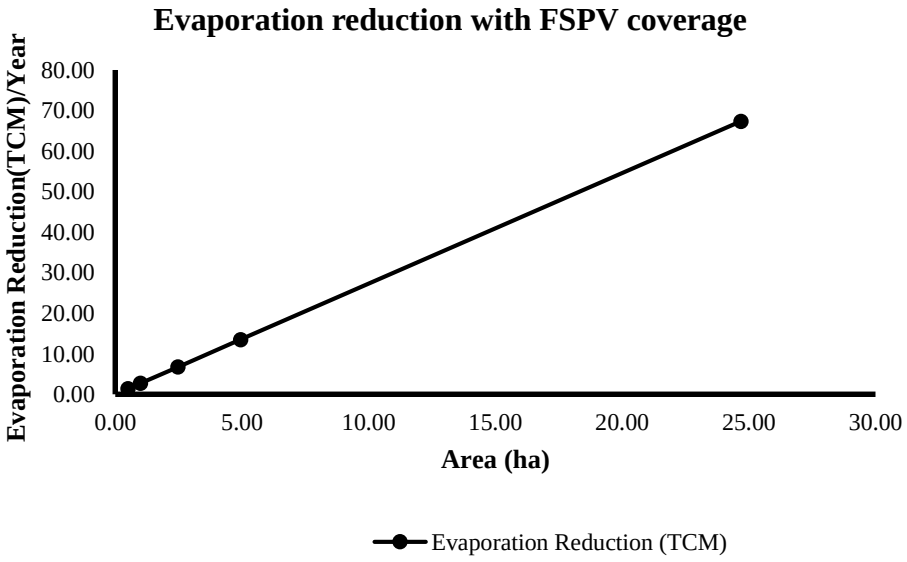

Figure 8.28. Evaporation reduction in TMC/year (Thousand cubic meter per year)with water surface area coverage

Keeping in view of above factors, individual plots with respect to area of coverage were prepared as shown in above Figures. Finally, a combined plot has been developed to take appropriate decision as given in Figure 8.29.

Table 8.16 showing variation of power generation, Evaporation reduction and cost variation with respect to area of coverage. While Table 8.17 gives variation of FSPV installation capacity, Evaporation reduction and cost variation with respect to area of coverage.

Table 8.16. Power Generation, Evaporation Reduction, and Cost Variation Relative to Coverage Area

Area (ha)	Annual Energy Production in MWh	Evaporation Reduction (TMC)	Cost in Rs per Wp
0.50	956.97	1.36	84.4
0.99	1890.15	2.69	68.35
2.47	4725.37	6.74	58.2
4.94	9450.74	13.47	55
24.69	47253.72	67.37	50

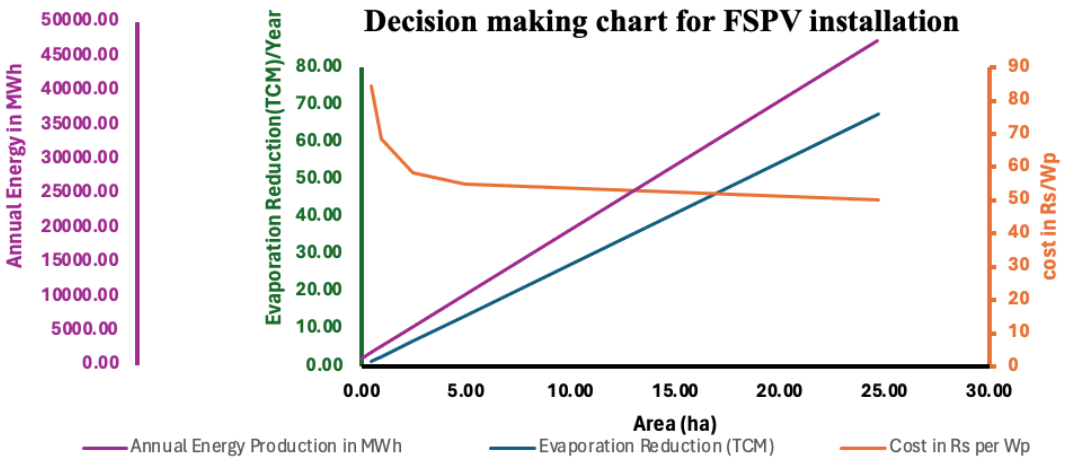

Figure 8.29. Integrated Evaluation of Power Generation, Evaporation Reduction, and Cost Variation Relative to Coverage Area

Table 8.17. FSPV Power Plant capacity, Evaporation Reduction, and Cost Variation Relative to Coverage Area

Area (ha)	Floating power capacity MWp	Evaporation Reduction (TCM)	Cost in Rs per Wp
0.50	1	1.36	84.4
0.99	2	2.69	68.35
2.47	5	6.74	58.2
4.94	10	13.47	55
24.69	50	67.37	50

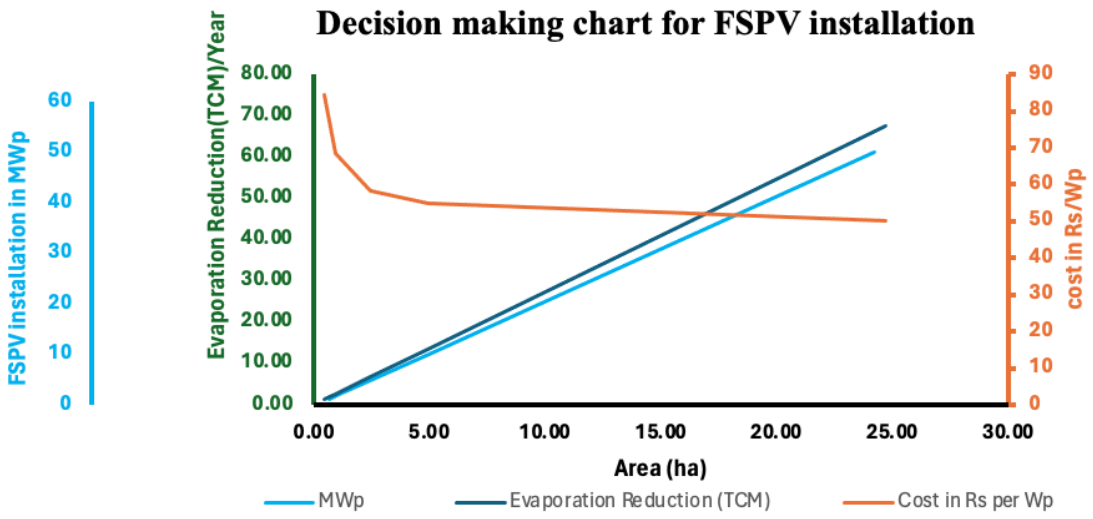

Figure 8.30. Integrated Evaluation of Power Plant Capacity, Evaporation Reduction, and Cost Variation Relative to Coverage Area

These plots are user-friendly decision-making tool for professionals working in this area. For example, if an irrigation officer wants to save water from reservoir to be utilised for industrial use or drinking water, which he/she would like to save through FSPV installation. So he wants to know how much water surface area coverage will serve the purpose, additionally he needs to know what should be the installation capacity, can easily be ascertained by this plot. For this purpose, he/she has to use the plot Figure 8.30 and select the corresponding line for required evaporation reduction desired and drop that line to area coverage required at area axis. Then knowing the area coverage, the desired installation capacity can be read by dropping the line from area coverage over the line of installation capacity for knowing the capacity. If it is required to estimate the cost, the drop from area coverage to cost line will directly provide the cost of installation instantly. If we want to know how energy will be generated, then it can be readily estimated from Figure 8.29. When we know the area coverage then directly dropping the line on energy generation line, the energy generation can be estimated. Another situation can be that capital cost for investment is known and want to estimate the capacity of plant that can be installed. The irrigation engineer can directly find the area that can be covered for the amount available, and subsequently the plant capacity. The engineer knowing the area required and area already been utilised can take a decision whether the permission can be granted or not. Knowing the proposed capacity, the decision can be taken with respect to availability of grid capacity. So these plots will be very handy tools for practitioners, professionals as well as government for taking decisions.

The creation of user-friendly decision-making charts marks a significant advancement in facilitating professionals within the field. If an irrigation officer seeking to conserve reservoir water for industrial or drinking purposes through FSPV installation. By utilizing these charts, they can determine the required water surface area coverage and corresponding installation capacity effortlessly. For instance, by referencing the appropriate chart and desired evaporation reduction, they can pinpoint the necessary area coverage and installation capacity. Similarly, these charts provide quick estimations of installation costs and energy generation potential. Such tools empower practitioners, professionals, and governmental bodies with streamlined decision-making capabilities, essential for navigating the complexities of FSPV deployment.

8.8. Summary and recommendations

In the absence of Pyranometer the shortwave radiation can be estimated by Angstorm equation, the fluctuation of Angstrom values (as and bs) in response to varying atmospheric conditions and solar declination highlights the critical need for precise representation of field conditions. Although there are general recommendations for situations lacking actual solar radiation data, calculating regression constants (as = -0.1566 and bs = 0.95) based on solar radiation data gathered at Pilani yields a more accurate depiction of the local environmental conditions.

Applying the (Swinbank ,1963; Brutsaert ,1975; Idso ,1981) models for estimating clear sky downward longwave radiation, as recommended by (Carmona et al. ,2013), resulted in less than 10% error, validating their accuracy for precise calculations. Although (Dekok et al. ,2019) pointed out the (Brutsaert,1975) model's tendency to underestimate, its inclusion of vapor pressure enhanced its precision. Tailoring this model with original empirical constants to Indian conditions further optimized its performance. (Crawford and Duchon's, 1999) equation (33) delivered consistent accuracy across varying climates, including Brazil, Central Florida, and Spain, proving its reliability for cloudy sky longwave radiation estimation without the need for preliminary calibration. Finch and Hall's approach, however, was found to be less effective under Indian conditions, producing consistently lower estimates than other methods. In contrast, methods adapted to Indian conditions, particularly the Brutsaert equation, provided estimates within an acceptable accuracy range. Comparative analysis of longwave radiation estimations, translating to 0 to 2 mm/day in water depth, revealed minimal differences among methods. This comparison with observed pan evaporation rates sheds light on the precision and dependability of each estimation technique.

Various models for estimating clear sky downward longwave radiation demonstrate promising accuracy, albeit with nuanced considerations for specific environmental contexts. Integrating water temperature into regression models emerges as a pivotal factor for enhancing evaporation rate prediction accuracy, offering valuable insights for model selection and application. Notably, the study's focus on crafting regression models for estimating evaporation rates from FSPV-covered water bodies underscores the importance of parameter selection and data availability. The resultant 4-parametric regression models, applied across 28 dam sites, reveal substantial reductions in evaporation rates under PV panel coverage, affirming the efficacy of such installations in water preservation efforts.

Selecting an appropriate method for estimating evaporation rates presents challenges due to the diverse range of equations available and the varying expertise required for their application. There is a lack of objective criteria for model selection, making it difficult to determine the most suitable method for a given study. As a result, adopting a regression model strategy has emerged as a viable alternative for deducing evaporation rates from meteorological observations. The conducted analysis leads to several insights regarding the creation and efficacy of linear regression models for estimating evaporation rates:

Integrating water temperature as a predictor in the regression model significantly enhances its accuracy over models that only consider solar radiation and air temperature. This indicates the critical role of water temperature in precise evaporation rate prediction. Out of the six models assessed, the model incorporating three variables, including water temperature (E3(Tw)), stands out for its precision, with a mean absolute error of 1.07 mm/day. Nonetheless, the sporadic availability of water temperature data might limit the practical use of this model. Given the challenges with water temperature data accessibility, an alternative three-variable model that includes either ambient temperature or solar radiation, along with wind speed and humidity, is recommended. This model shows a comparable level of accuracy for evaporation rate estimation and presents a feasible option.

The models E4(Ta) and E3(Ta), which include ambient temperature, show satisfactory performance, achieving R^2 values of 0.6857 and 0.7121, respectively. Remarkably, the model E3(Ta) surpasses the four and five-variable models in accuracy, evidenced by its lower root mean square error (RMSE) and mean absolute error (MAE). These models are therefore used for estimation of evaporation from uncovered water surface of twenty-eight dams of tropical region of Uttar Pradesh, India.

The model E3(Rs), which relies solely on solar radiation, ranks lowest in terms of performance among the models evaluated, indicated by its lower R^2 value and higher RMSE and MAE. This highlights the necessity of incorporating various atmospheric conditions to achieve precise estimates of evaporation. To conclude, the analysis underscores that adding water temperature to regression models significantly boosts their capability to accurately estimate evaporation rates. Nonetheless, when water temperature data is scarce, alternative models, E4(Ta) and E3(Ta), that use a combination of other atmospheric variables such as ambient temperature and/or solar radiation, wind speed, and humidity, can serve as effective tools for evaporation estimation.

This study focused on crafting models to estimate evaporation rates from water bodies equipped with Floating Solar Photovoltaic (FSPV) panels, successfully creating 16 viable models from an initial set of 18. The analysis identified the model Ep5Rh(Tp), which uses panel temperature, as the most accurate, recording the lowest RMSE of 0.072 mm/day and a solid R-square value of 0.7088. Although the model Ep5Rh(Rs) which replaces panel temperature by solar insolation in the Ep5Rh(Tp) model displayed a marginally higher R-square than Ep5Rh(Tp), its elevated RMSE and MAE indicate its lesser suitability for evaporation predictions.

Further exploration highlighted the efficiency of models with fewer variables, with Ep2Rh(Tw), which considers water temperature and relative humidity, standing out for its performance. Models that substituted ambient temperature for water temperature demonstrated similar effectiveness, pointing to the value of using easily accessible meteorological data. Parameters such as humidity under the solar panel and wind speed were deemed less impactful for model construction than ambient and water temperatures. Solar radiation was found to be a weaker predictor for these models compared to the more reliable ambient and water temperatures. In conclusion, this research highlights the critical role of selecting appropriate parameters and the availability of data in the development of precise evaporation estimation models for environments with FSPV-covered water surfaces.

The developed 4-parametric regression models were applied to assess evaporation rates at 28 different dam sites, both under uncovered and covered conditions with PV panels.

1. The highest evaporation rates were observed at Ohan dam, with 2126.53 mm/year for open sky and 1567.63 mm/year for covered with PV panels, while the lowest rates were at Kalagarh dam, with 1783.29 mm/year and 1283.32 mm/year, respectively.

2. A significant reduction in evaporation was noted when dam surfaces were covered with PV panels, ranging from 26.28% to 29.95% reduction at Ohan Dam and Pahuj dam, respectively.
3. Comparison with existing models revealed the efficacy of the developed models in accurately estimating evaporation rates under different conditions, highlighting the importance of considering PV panel coverage in such assessments.

Choosing to deploy Floating Solar Photovoltaic (FSPV) panels at dam locations requires more than just understanding changes in water surface area; it also involves evaluating installation expenses. Coverage recommendations for FSPV panels over water surfaces have been made by analysing evaporation reduction across twenty-eight dam sites, aiding in the decision-making process. Key factors such as the capacity of FSPV installations, cost implications, evaporation savings, and potential annual energy production have been thoroughly examined to support decision-makers and practitioners. To simplify the decision-making process, intuitive charts have been created that allow professionals to easily identify the best coverage strategy, installation capacity, associated costs, and estimated energy production tailored to their specific needs and limitations.

Beyond merely understanding water surface area changes, deploying FSPV panels at dam locations necessitates meticulous evaluation of installation expenses and associated benefits. Analysis of evaporation reduction across various dam sites informs decision-making processes, guiding recommendations for FSPV panel coverage. Factors such as installation capacity, cost implications, evaporation savings, and potential energy production are thoroughly examined to provide actionable insights for decision-makers. Through the creation of intuitive decision-making charts, tailored to specific needs and limitations, professionals are equipped with invaluable tools for making informed decisions regarding FSPV installations, serving both water preservation and energy generation goals effectively.

Chapter-9

Conclusions and Future Scope

9.1 Conclusions

Current research suggests predictive models for panel temperature and evaporation due to water surfaces covered with PV panels. It assesses PV panel performance, evaluates evaporation reduction attributed to FSPV installations, and extrapolates findings to major dams in tropical regions. The predictive models utilize data collected through experimentation for key parameters such as solar irradiance, wind speed, ambient temperature, module temperature, water temperature, dry and wet bulb temperature, evaporation loss, and relative humidity. Furthermore, it suggests the optimal height for PV panel installation over water bodies to maximize power output while minimizing evaporation loss attributed to FSPV installations.

Although photovoltaic modules are the most promising technology in renewable energy, their installation requires substantial land investment, which poses a significant loss from the perspective of agriculture and farming activities. Chapter one classifies and describes the floating photovoltaic system, its configuration, and working methodology, and compares the potential social, environmental, and economic benefits of installing Floating Solar PV (FSPV) systems with land-based PV installations. It also discusses the current status of floating solar systems in India and globally, highlighting the need for further research in this area. Additionally, the motivation for the present research, along with the objectives, scope, and organization of the proposed work, are established.

Floating solar PV systems are the appropriate environment-friendly alternatives to play their leading role in reducing greenhouse gas emissions in the power sector and water evaporation loss reduction in the water sector. Chapter two is organized to address the detailed review of the studies of floating solar systems in global scenarios, the recent advancements of floating solar systems in Indian scenarios, and the methodologies adopted to evaluate module temperature of the floating solar system, the methodologies adopted to evaluate evaporation loss reduction, the economics aspects of floating solar plants. Finally, the chapter presents the research gaps and scope of the current study.

The chapter three concludes by highlighting the approach taken in identifying critical parameters through an extensive review of existing literature and reports. This process was crucial in laying the groundwork for the successful design and execution of the experiment. By aligning the instruments, equipment, and data collection procedures with these identified

parameters, essential data on evaporation, panel performance, and meteorological conditions were systematically gathered over a period of three years. The collected data underwent thorough processing to meet the analytical requirements of the research, facilitating insightful analysis and meaningful conclusions regarding the performance and potential of floating solar photovoltaic systems in tropical regions.

This chapter provides a comprehensive overview of the key findings uncovered throughout this thesis, focusing primarily on the substantial potential of Floating Solar Photovoltaic (FSPV) installations. By synthesizing the results obtained from various analyses and experiments, this section highlights the significant benefits offered by FSPV installations, particularly in the realms of energy generation and water conservation. Through a systematic examination of the research outcomes, this chapter aims to elucidate the pivotal role of FSPV technology in addressing critical challenges related to sustainability and resource management. The key contributions from this thesis and consequent fulfilment of the identified research gaps (as stated in the literature review) are discussed as follows:

Comparative performance analysis of floating solar photovoltaic (FSPV) systems versus ground-mounted PV systems in tropical climates

A thorough analysis and comparison of the floating solar photovoltaic (FSPV) systems' performance in comparison to traditional ground-mounted PV systems in the climatic conditions of tropical regions like India were conducted in chapter four. The experimental study is focused on the characteristics of temperature and electricity generation from the FSPV modules mounted at various heights above the water surface. The modules are installed at varying heights of 300mm, 500mm, and 1000mm above water bodies to establish the best-performing height. The following are the principal findings:

Winter season observations

- Though there is a temperature difference between module temperatures of a ground-mounted solar panel and a floating or FSPV solar panel as high as about 4°C during peak sun time, an average temperature variation of 3.25°C was observed throughout the period.
- The average power output of FSPV solar panels is 1.73% higher compared to ground-mounted solar panels, highlighting that minor variations in the module operating temperature and lower operating temperature during winters do not significantly change the power output from solar panels.

Summer season observations

- The operating temperature of FSPV is about 10% lower compared to ground-mounted solar panels for panels at 500mm and about 6% for panels at other heights during peak solar hours.
- The average power output of FSPV is 2.5% higher compared to typical ground-mounted solar panels during summer, with the maximum power output 3.78% higher for the FSPV panel at 500mm above the water level.

Advantages and optimal installation height of FSPV

- Significant temperature variations were observed among the FSPV panels at varying heights with respect to water levels. The lowest module temperature observed was on the solar panel installed 500mm above the water body.
- Reducing the gap between the water body and the solar panel does not lead to further reduction of operating temperature due to reduced ventilation, resulting in higher operating temperatures, as observed in the panels operating 300mm above the water level.
- The panels should be installed 500mm above water bodies to maximize power output and minimize module operating temperature.
- The average operating temperature of modules mounted over the ground is six degrees higher than those mounted over water.
- The use of floating solar PV installation instead of ground-mounted PV installation can provide a higher power output of 2.5% annually.

Research Gap accomplished

1. Performance assessment of floating solar PV systems and comparative study with ground-mounted PV based on the recorded data for Uttar Pradesh, a tropical region has been achieved.
2. A comparative study of PV modules were addressed extensively based on experimental evidence for ground-mounted and floating PVs.
3. The optimal height for installation to achieve the best performance has been established.

Predictive model for FSPV panel temperature

The predictive models for panel temperature developed in Chapter Five utilized meteorological and PV panel performance data to analyse the significance of various meteorological parameters. A comparative study of PV panels over water bodies and ground-

mounted PV panels was conducted to quantify the benefits of Floating Solar Photovoltaic (FSPV) systems. Based on these findings, recommendations were made for the deployment of FSPV compared to ground-mounted PV in tropical climatic conditions.

Key findings from the study include:

Model Development and Validation

- Regression analysis was used to develop and validate models for predicting the operating temperature of floating solar PV modules. The models incorporated various meteorological parameters, including ambient temperature, solar insolation, wind velocity, water temperature, and humidity.
- The three-parametric models F3, which utilized ambient temperature, solar insolation, and wind velocity, predicted panel operating temperature the best, with a maximum root mean square error (RMSE) of 5.50°C.
- In contrast, the three-parametric models replacing ambient temperature with water temperature, F2 and F4, predicted panel operating temperature less accurately, with a maximum RMSE of 8.26°C and 9.43°C, respectively.
- The one-degree regression model with all five parameters did not significantly enhance the accuracy of the prediction model. However, the two-degree regression models were complex and had an RMSE of more than 20°C.The best-performing model was F3, which can be used to predict the operating temperature of the panel and power estimates, assessing the module's overall performance.

Research Gap accomplished

1. Predictive models for module temperature of FSPV panels were developed especially in the context of India and tropical region.
2. Most effective parameters for predicting module temperature of FSPV panels were established.

FSPV potential of tropical region of Uttar Pradesh (India)

The floating solar photovoltaic (FSPV) potential and water conservation were assessed in Chapter six, by conducting a similar case study in tropical regions, viz. a case study for Rajghat Dam and a Potential assessment for Uttar Pradesh, India. The unique findings from the case study of Rajghat Dam, coupled with the extended assessment of the major dams in the tropical region of Uttar Pradesh, India, bring novel insights into the potential energy

generation capabilities of Floating Solar Photovoltaic (FSPV) systems and their effectiveness in reducing evaporation rates. The following is a summary of the key findings:

- According to the technical potential evaluation, Rajghat Dam can support a floating solar installation of 6513 MWp, which would produce an estimated 10,623,501 MWh of energy annually.
- The case study also evaluates the FSPV system's ability to reduce evaporation, estimating a reduction of 0.9 litres per kWh of power produced. This equals a cumulative water savings of about 9.08 million cubic metres.
- The levelized cost of energy (LCOE) for the FSPV system is determined by an economic analysis to be Rs 2.61 per kWh, or roughly $0.036/kWh. This illustrates how FSPV is more affordable than traditional energy sources. The project's 8.55% internal rate of return (IRR) further demonstrates its financial sustainability.
- The extended study projects a potential energy generation of 37762.21 MWp and approximate specific yield of 61,935,492 MWh with capacity utilization factor (CUF) 18.72, by covering 25% of the reservoir surface area suitable for solar installations over major dams of Uttar Pradesh.
- Further, adding electricity to the existing grid infrastructure reduces the need for new infrastructure construction, benefiting the local environment and lowering government costs.

Research Gap accomplished

1. FSPV potential assessment is performed in the context of Uttar Pradesh.
2. Assessment of FSPV potential for major dams/reservoirs of Uttar Pradesh is conducted.

Evaporation reduction from FSPV installations and optimal panel height for minimizing evaporation

The study of Floating Solar Photovoltaic (FSPV) installations in Uttar Pradesh (UP), India, has provided important insight into how this ground-breaking method might address the twin concerns of renewable energy generation and water conservation. In areas like the UP, which are renowned for their high levels of sunshine exposure and high rates of evaporation, FSPV presents a possible option for sustainable expansion by utilizing the capacity of already-existing water bodies, including dams and reservoirs.

In chapter seven results of evaporation loss from uncovered water surface and solar PV covered water surface using an evaporimeter for the Indian atmospheric conditions were

analysed and evaporation reduction due to FSPV installations in some major dams located in the tropical region in Uttar Pradesh, India using experimental data were carried out. The results were analysed and the conclusion from this chapter is enumerated below

- The study discovered an interesting correlation between evaporation reduction and panel heights. The experimental results highlighted that the maximum evaporation reduction occurred from the water surface covered with a panel at a height of 300 mm above the water.
- The evaporation reduction estimated was 23.44 % for a panel at a height of 300 mm above the water.
- The management and conservation of water resources are aided by the decrease in evaporation losses. The extrapolation of the study for 28 major dams of Uttar Pradesh, reveals an annual water saving of 92.56 million cubic meters (MCM) with FSPV coverage of 25%.

The benefits of FSPV extend to both environmental preservation and societal well-being. Beyond augmenting energy production, FSPV contributes to improving water quality by reducing algae proliferation. Moreover, its capacity to diminish evaporation losses presents a solution to water scarcity challenges. Based on estimations, a 1 MWp FSPV installation saves approximately 2451 cubic meters of water annually. Consequently, such an installation can provide water for 67 individuals annually in rural tropical areas, assuming a per capita daily requirement of 100 litres.

Research Gap accomplished

1. The estimation of evaporation in tropical regions, especially semi-arid areas, with experimental evidence has been accomplished.
2. Evaporation reduction, including comparative studies between water surfaces covered by PV modules and water surfaces open to the sky with experimental data, has been established for tropical regions.
3. The optimal height above the water surface for FSPV installation to maximize evaporation reduction has been established.
4. The impact of seasonal and annual variations and the evaporation reduction assessment for major dams and reservoirs in Uttar Pradesh have been accomplished in this research.

Predictive evaporation models for open and PV-covered water bodies

Chapter eight deals with understanding of important insights about evaporation dynamics using experimental data in predictive evaporation models for open and PV-covered water bodies. The models were developed and validated in chapter eight for estimation of evaporation from PV covered and uncovered water surfaces utilising the meteorological data. These models were further extended to estimate evaporation reduction due to PV covers over major dams of Uttar Pradesh, the results were analysed, and decision-making tools were developed considering various coverage scenarios, cost, power generation and installation capacity. The conclusion from this chapter is summarised below

Shortwave radiation estimation

- In the absence of Pyranometer the shortwave radiation can be estimated by Angstorm equation, the fluctuation of Angstrom values (as and bs) in response to varying atmospheric conditions and solar declination highlights the critical need for precise representation of field conditions. Although there are general recommendations for situations lacking actual solar radiation data, calculating regression constants (as = -0.1566 and bs = 0.95) based on solar radiation data gathered at Pilani yields a more accurate depiction of the local environmental conditions.

Predictive evaporation models for uncovered water surface

- Integrating water temperature as a predictor in the regression model significantly enhances its accuracy over models that only consider solar radiation and air temperature. This indicates the critical role of water temperature in precise evaporation rate prediction. While the model which relies solely on solar radiation, ranks lowest in terms of performance among the models evaluated.
- Out of the six models assessed, the model incorporating three variables, including water temperature (E3(Tw)), stands out for its precision, with a mean absolute error of 1.07 mm/day. Nonetheless, the sporadic availability of water temperature data might limit the practical use of this model. The models E4(Ta) and E3(Ta), which include ambient temperature, show satisfactory performance, achieving R^2 values of 0.6857 and 0.7121, respectively.
- Remarkably, the model E3(Ta) which utilises parameters ambient temperature, wind speed, and humidity, surpasses the four and five-variable models in accuracy, evidenced by its lower root mean square error (RMSE) and mean absolute error (MAE). This

model is therefore used for estimation of evaporation from uncovered water surface of twenty-eight dams of tropical region of Uttar Pradesh, India.

Predictive evaporation models for PV covered water surface

- This study focused on crafting models to estimate evaporation rates from water bodies equipped with Floating Solar Photovoltaic (FSPV) panels, successfully creating 16 viable models from an initial set of 18.The analysis identified the model Ep5Rh(Tp), which uses panel temperature, as the most accurate, recording the lowest RMSE of 0.072 mm/day and a solid R^2 value of 0.7088. Although the model Ep5Rh(Rs) which replaces panel temperature by solar insolation in the Ep5Rh(Tp) model displayed a marginally higher R^2 than Ep5Rh(Tp), its elevated RMSE and MAE indicate its lesser suitability for evaporation predictions.
- Further exploration highlighted the efficiency of models with fewer variables, with Ep2Rh(Tw), which considers water temperature and relative humidity, standing out for its performance. Models that substituted ambient temperature for water temperature demonstrated similar effectiveness, pointing to the value of using easily accessible meteorological data. Parameters such as humidity under the solar panel and wind speed were deemed less impactful for model construction than ambient and water temperatures. Solar radiation was found to be a weaker predictor for these models compared to the more reliable ambient and water temperatures. In conclusion, this research highlights the critical role of selecting appropriate parameters and the availability of data in the development of precise evaporation estimation models for environments with FSPV-covered water surfaces.

Evaporation assessment by regression model for 28 dam sites in tropical region of Uttar Pradesh

- The highest evaporation rates were estimated at Ohan dam, with 2126.53 mm/day for open sky and 1567.63 mm/day for covered with PV panels, while the lowest rates were at Kalagarh dam, with 1783.29 mm/day and 1283.32 mm/day, respectively.
- A significant reduction in evaporation was noted when dam surfaces were covered with PV panels, ranging from 26.28% to 29.95% reduction at Ohan Dam and Pahuj dam, respectively.
- Comparison with existing models revealed the efficacy of the developed models in accurately estimating evaporation rates under different conditions, highlighting the importance of considering PV panel coverage in such assessments.

Decision-Making for FSPV Deployment

Choosing to deploy Floating Solar Photovoltaic (FSPV) panels at dam locations requires more than just understanding changes in water surface area; it also involves evaluating installation expenses. Coverage recommendations for FSPV panels over water surfaces have been made by analysing evaporation reduction across twenty-eight dam sites, aiding in the decision-making process. Key factors such as the capacity of FSPV installations, cost implications, evaporation savings, and potential annual energy production have been thoroughly examined to support decision-makers and practitioners. To simplify the decision-making process, intuitive charts have been created that allow professionals to easily identify the best coverage strategy, installation capacity, associated costs, and estimated energy production tailored to their specific needs and limitations.

Beyond merely understanding water surface area changes, deploying FSPV panels at dam locations necessitates meticulous evaluation of installation expenses and associated benefits. Analysis of evaporation reduction across various dam sites informs decision-making processes, guiding recommendations for FSPV panel coverage. Factors such as installation capacity, cost implications, evaporation savings, and potential energy production are thoroughly examined to provide actionable insights for decision-makers. Through the creation of intuitive decision-making charts, tailored to specific needs and limitations, professionals are equipped with invaluable tools for making informed decisions regarding FSPV installations, serving both water preservation and energy generation goals effectively.

Research Gap accomplished

1. Model development for the assessment of evaporation and evaporation reduction due to FSPV installations, along with comparative studies with open sky conditions, has been accomplished.
2. Evaporation with and without PV panel cover was assessed using a regression model for major dam sites in the tropical region of Uttar Pradesh, and the evaporation reduction due to FSPV installations was accomplished.
3. Decision-making strategies and tools to assess plant capacity, area coverage, installation cost, power generation, and evaporation reduction were developed.

9.2 Limitations and future work

Continued research and development in the field of FSPV are essential for advancing the technology and improving its efficiency and cost-effectiveness. Areas of focus should include the development of more efficient floating platforms, optimization of solar panel

configurations, and exploration of innovative storage solutions to enhance the reliability and dispatchability of FSPV systems.

As the study observed that climatic conditions significantly influence the performance evaluation of FSPV installation, hence, it is imperative to conduct more studies in different parts of the world for assessing the performance of floating solar PV systems in varied climatic conditions. These studies can aid in the generalization of the results on a global scale, which would enable to estimate the power output from floating solar PV plants more efficiently. Furthermore, conducting studies on panels made from various materials and comparing the results would be instrumental in recommending the maximum output.

Given that the models were created using data from a particular geographic area and under environmental conditions, their performance may differ in other places and circumstances. To improve their prediction capability and generalizability, future research might concentrate on evaluating and improving these models across multiple climatic and geographic contexts. Future studies could also investigate the inclusion of extra factors like ground albedo for ground-mounted systems or the speed and direction of water currents for floating PV installations. Predictive models based on artificial intelligence or more complicated machine learning may also be investigated to produce forecasts that are even more precise.

Based on the study of FSPV installations at varying heights for evaporation reduction estimation for Major Dams of the tropical region of Uttar Pradesh, India, the following limitations are identified:

- The current study was carried out with pans installed over land. The result may be more representative if floating pans are used over the water surface.
- The wind pressure guides the selection of minimum panel heights above the water surface; hence the minimum panel height selection is limited by this constraint.

It is crucial to carry out thorough environmental and social impact analyses as FSPV installations grow. These analyses should focus on the potential ecological consequences, particularly those affecting aquatic life and water quality, as well as the social repercussions for nearby communities and stakeholders. Optimizing FSPV design to minimize these impacts, along with implementing effective mitigation strategies, is necessary to reduce any negative effects. Additionally, assessing the socio-economic impacts, including local employment opportunities, energy access, and community well-being, will provide a comprehensive understanding of FSPV's role in sustainable development.

REFERENCES

[1] Abe, C.F., Dias, J.B., Notton, G., and Poggi, P. (2020), Computing solar irradiance and average temperature of photovoltaic modules from the maximum power point coordinates. IEEE Journal of Photovoltaics, 10(2), pp.655-663.

[2] Abe, C.F.; Dias, J.B.; Notton, G., and Faggianelli, G.A. (2020), Experimental Application of Methods to Compute Solar Irradiance and Cell Temperature of Photovoltaic Modules. Sensors, 20, 2490. https://doi.org/10.3390/s20092490.

[3] Abdelal, Q. (2021), Floating PV; an assessment of water quality and evaporation reduction in semi-arid regions. International Journal of Low-Carbon Technologies ctab001. https://doi.org/10.1093/ijlct/ctab001.

[4] Abeykoon, L. K., Aponsu, G. M. L. P., Gunathilaka, H. M. B. I., and Vimal Nadeera, H. A. (2018), Effect of temperature on the photovoltaic characteristics of polycrystalline silicon solar cells at Hambantota Solar Power Plant. proceedings of International Conference on Solar Energy Materials, Solar Cells & Solar Energy Applications Int. Conf., Institute of Fundamental Studies, Kandy Vol. 4 (pp. 270–275).

[5] Acharya, M. and Devraj, S. (2019), "Floating Solar Photovoltaic (FSPV): A Third Pillar to Solar PV Sector?", New Delhi, 2019. Accessed: Aug. 16, 2022. [Online]. Available: www.teriin.org.

[6] Adinoyi, M.J., and Said, S.A.M. (2013), Effect of dust accumulation on the power outputs of solar photovoltaic modules. Renew. Energy, 60, 633–636.

[7] Agrawal, K. K., Jha, S. K., Mittal, R. K., and Vashishtha, S. (2022), Assessment of Floating Solar PV (FSPV) Potential and Water Conservation: Case Study on Rajghat Dam in Uttar Pradesh, India. Energy for Sustainable Development, 66, 287–295, https://doi.org/10.1016/j.esd.2021.12.007

[8] Akhsassi, M., el Fathi, A., Erraissi, N., Aarich, N., Bennouna, A., Raoufi, M., and Outzourhit, A. (2018), Experimental investigation and modeling of the thermal behavior of a solar PV module. Solar Energy Materials and Solar Cells, 180, 271–279. https://doi.org/10.1016/j.solmat.2017.06.052.

[9] Akyuz, E., Coskun, C., Oktay, Z. and Dincer, I. (2012), A novel approach for estimation of photovoltaic energy efficiency. Energy, 44(1), pp.1059-1066.

[10] Alados, I., Foyo-Moreno, I., and Alados-Arboledas, L. (2011), Estimation of downwelling longwave irradiance under all-sky conditions. International Journal of Climatology 32, 781-793. https://doi.org/10.1002/joc.2307.

[11] Allen, R. G. (1996), Assessing integrity of weather data for use in reference evapotranspiration estimation. J. Irrig. and Drain. Engng. Div., ASCE 122 (2): 97-106.

[12] Allen, R. G., Pereira, L. S., Raes, D., and Smith, M. (1998), Crop Evapotranspiration-Guidelines for Computing Crop Water Requirements-FAO Irrigation and Drainage Paper 56, vol. 300 D05109 (Food and Agriculture Organization of the United Nations, Rome, 1998).

[13] Almaktar, M., Rahman, H.A., Hassan, M.Y., and Rahman, S. (2013), Climate-based empirical model for PV module temperature estimation in tropical environment. Applied Solar Energy, 49(4), pp.192-201.

[14] Anderson, E.R. (1954), Energy-Budget Studies. In: Water loss Investigations: Lake Hefner Studies, Technical Report, pp. 71-119.

[15] Ångström, A. (1918), A study of the radiation of the atmosphere. Smithso Inst Misc Collect 65:159–161.

[16] Angstrom, A. (1924), Solar and atmospheric radiation. Q. J. R. Meteorol. Soc. **50**, 121–126. https://doi.org/10.1002/qj.49705021008 .

[17] Anhui GCL (2023), "Anhui GCL, CHINA". *Ciel et Terre*. Retrieved 2023-02-16.

[18] Armstrong, A., Thackeray, S.J., Hernandez, R.R., Folkard, A.M., and Rocha S. M. (2024), Environmental impacts of floating solar panels on freshwater systems and their techno-ecological synergies. Environmental Research: Infrastructure and Sustainability. 4(4).

[19] Ayadi, F., Colak, I., Genc, N., and Bulbul, H.I. (2019), November. Impacts of wind speed and humidity on the performance of photovoltaic module. In 2019 8th International Conference on Renewable Energy Research and Applications (ICRERA) (pp. 229-233). IEEE.

[20] Baptista, J., and Vargas, P. (2020), Portuguese national potential for floating photovoltaic systems: a case study. In2020 IEEE International Conference on Environment and Electrical Engineering and 2020 IEEE Industrial and Commercial Power Systems Europe (EEEIC/I&CPS Europe) 2020 Jun 9 (pp. 1-5). IEEE.

[21] Barbuscia, M. (2018), Economic viability assessment of floating photovoltaic energy. Work Pap. 1(1):1-1.

[22] Barry, J., Böttcher, D., Pfeilsticker, K., Herman-Czezuch, A., Kimiaie, N., Meilinger, S., Schirrmeister, C., Deneke, H., Witthuhn, J., and Gödde, F. (2020), Dynamic model of photovoltaic module temperature as a function of atmospheric conditions. Advances in Science and Research, 17, pp.165-173.

[23] Bhattacharya, P., Dey, S., and Mustaphi, B. (2014), Some analytical studies on the performance of grid connected solar photovoltaic system with different parameters. Procedia materials science, 6, pp.1942-1950.

[24] Bhattacharya, T., Chakraborty, A.K., and Pal, K. (2014), Effects of ambient temperature and wind speed on performance of monocrystalline solar photovoltaic module in Tripura, India. Journal of Solar Energy, 2014.

[25] Bird, R.E., and Riordan, C. (1986), Simple solar spectral model for direct and diffuse irradiance on horizontal and tilted planes at the earth's surface for cloudless atmospheres. Journal of Applied Meteorology and Climatology, 25(1), pp.87-97.

[26] Blaney, H.F. and Criddle, W.D. (1962), Determining Consumptive Use and Irrigation Water Requirements. USDA Technical Bulletin 1275, US Department of Agriculture, Beltsville.

[27] Bloomberg (2023), "Floating Solar Panels Turn Old Industrial Sites Into Green Energy Goldmines". *Bloomberg.com*. 2023-08-03. Retrieved 2023-08-03.

[28] Bontempo Scavo, F., Tina, G.M., Gagliano, A., and Nižetić, S. (2021), An assessment study of evaporation rate models on a water basin with floating photovoltaic plants. International journal of energy research, 45(1), pp.167-188. https://doi.org/10.1002/ER.5170.

[29] Bowen, I.S. (1926), The ratio of heat losses by conduction and by evaporation from any water surface. Physical Review. **27** (6):779 787. Bibcode:1926PhRv...27..779B. doi:10.1103/PhysRev.27.779.

[30] Bozorgi, A., Bozorg-Haddad, O., Sima, S., and Loáiciga, H.A. (2020), Comparison of methods to calculate evaporation from reservoirs. International Journal of River Basin Management, 18(1), pp.1-12.

[31] Brunt D. (1932), Notes on radiation in the atmosphere. Quart J Roy Meteorol Soc 58:389–420.

[32] Brunt, D. (1939), Physical and dynamical meteorology, Univ. Press, Cambridge. 400 pp.

[33] Brunt, D. (1952), Physical and dynamical meteorology, 2nd ed., Univ. Press, Cambridge. 428 pp.

[34] Brutsaert W. (1975), On a derivable formula for long-wave radiation from clear skies. Water Resour Res 11:742–744.

[35] Brutsaert, W., and Stricker, H. (1979), An advection-aridity approach to estimate actual regional evapotranspiration. Water Resources. Res. 15, 443–450.

[36] Brutsaert W. (2013), Evaporation into the atmosphere: theory, history and applications. Springer Science & Business Media.

[37] Burgata (2022), "Profloating". www.profloating.nl. Retrieved 2023-08-22.

[38] Burman, R. D., Jensen, M. E., and Allen, R. G. (1987), Thermodynamic factors in evapotranspiration. In: James, L. G. and M. J. English (editors), Proc. Irrig. and Drain. Spec. Conf., ASCE, Portland, Ore., p. 28-30.

[39] Carmona, F., Rivas, R., and Caselles, V. (2014), Estimation of daytime downward longwave radiation under clear and cloudy skies conditions over a sub-humid region. Theoretical and applied climatology, 115, pp.281-295.

[40] Castillo, Carolina Perpiña, e Silva, Filipe Batista, and Lavalle, Carlo (2016), An assessment of the regional potential for solar power generation in EU-28. Energy Policy, 88, 86–99 ISSN 0301-4215https://doi.org/10.1016/j.enpol.2015.10.004.

[41] Castro-Santos, L., Martins, E., and Guedes Soares, C. (2016), Methodology to calculate the costs of a floating offshore renewable energy farm. Energies, 9(5), p.324.

[42] Cazzaniga, R., Cicu, M., Rosa-Clot, M., Rosa-Clot, P., Tina, G.M., and Ventura, C. (2018), Floating photovoltaic plants: Performance analysis and design solutions. Renewable and Sustainable Energy Reviews. 81:1730-41. https://doi.org/10.1016/j.rser.2017. 05.269.

[43] Chandra, S., Agrawal, S., and Chauhan, D.S. (2018), Effect of ambient temperature and wind speed on performance ratio of polycrystalline solar photovoltaic module: An experimental analysis. International Energy Journal, 18(2).

[44] Chandra, A., Shrikhande, V.J., and Kulshreshta, R. (1988), Relationship of pan evaporation with meteorological parameters. J. Indian Water Reso. Soc, 8(2), pp.41-44.

[45] Changbing (2023), "Changbing, TAIWAN". *Ciel et Terre*. Retrieved 2023-05-11."Hexa, Ciel & Terre complete Taiwan extension". 20 February 2024."Long popular in Asia, floating solar catches on in US". *AP NEWS*. 2023-05-10. Retrieved 2023-05-11.

[46] Charles Rajesh Kumar, J., and Majid, M. (2023), Floating solar photovoltaic plants in India – A rapid transition to a green energy market and sustainable future. Energy & Environment, 34(2), 304-358. https://doi.org/10.1177/0958305X211057185.

[47] Chenni, R., Makhlouf, M., Kerbache, T., and Bouzid, A., (2007), A detailed modelling method for photovoltaic cells. Energy, 32(9), pp.1724-1730.

[48] Chico Hermanu, B. A., Santoso, B., and Suyitno, W. (2019), Design of 1 MWp floating solar photovoltaic (FSPV) power plant in Indonesia. American Institute of Physics Conference Series vol. 2097. no. 1.

[49] Choi, M., Jacobs, J.M., and Kustas W.P. (2008), Assessment of clear and cloudy sky parameterizations for daily downwelling longwave radiation over different land surfaces in Florida. USA Geophys Res Lett 35: L20402. doi:10.1029/2008GL035731.

[50] Choi, Y.K. (2014), A study on power generation analysis of floating PV system considering environmental impact. International journal of software engineering and its applications, 8(1), pp.75-84.

[51] Cirata (2019), "Jokowi inaugurates Southeast Asia's largest floating solar farm". *The Jakarta Post*. Retrieved 2023-11-09.

[52] Cogley, J.G. (1979), The albedo of water as a function of latitude. Monthly Weather Review, 107(6), pp.775-781.

[53] Cooley, K. R. (1970), Energy Relationships in the Design of Floating Covers for Evaporation Reduction, Water Resource. *Res.*, 6(3), 717–727, doi:10.1029/WR006i003p00717.

[54] Cooley K.R. (1983) Evaporation reduction: summary of long-term tank studies. Journal of Irrigation and Drainage Engineering. 109(1):89-98.

[55] Coskun, C., Koçyiğit, N. and Oktay, Z. (2016), Estimation of PV module surface temperature using artificial neural networks. Mugla Journal of Science and Technology, 2(2), pp.15-18.

[56] Coskun, C., Toygar, U., Sarpdag, O. and Oktay, Z., 2017. Sensitivity analysis of implicit correlations for photovoltaic module temperature: A review. Journal of Cleaner Production, 164, pp.1474-1485.

[57] Crawford, T.M., and Duchon, C.E. (1999), An improved parameterization for estimating effective atmospheric emissivity for use in calculating daytime downwelling longwave radiation. Journal of Applied Meteorology and Climatology, 38(4), pp.474-480.

[58] CWC (2006), Evaporation control in reservoirs. Basin Planning and Management Organisation, Report. New Delhi: Central Water Commission, GoI. http://cwc.gov.in/ (Accessed November 2018).

[59] Da Mi Reservoir (2019), "Da Mi Floating Solar Power Plant successfully connected to grid". *en.evn.com.vn*. Retrieved 2023-06-07.

[60] Da Silva, Pimentel, Diogo, Gardenio, and Branco, David Alves Castelo (2018), Is floating photovoltaic better than conventional photovoltaic? Assessing environmental impacts. Impact Assessment and Project Appraisal, 36(5), 390–400.

[61] Darwish, Z.A., Kazem, H.A., Sopian, K., Alghoul, M.A., and Chaichan, M.T. (2013), Impact of some environmental variables with dust on solar photovoltaic (PV) performance: review and research status. International J of Energy and Environment, 7(4), pp.152-159.

[62] Dasgupta, Tina (2023). "EDF Group Unveils 1st Floating Solar Power Plant in Lazer, Hautes-Alpes". *SolarQuarter*. Retrieved 2023-07-07.

[63] Dash, P.K., and Gupta, N.C. (2015), Effect of Temperature on Power Output from Different Commercially Available Photovoltaic Modules. International Journal of Engineering Research and Applications, 5, 148–151.

[64] de Bruin, H. A. R. (1978), A Simple Model for Shallow Lake Evaporation. J. Appl. Meteor. Climatol., 17, 1132–1134, https://doi.org/10.1175/1520-0450(1978)017<1132:ASMFSL>2.0.CO;2.

[65] de Bruin, H.A.R., and Keijman, J. Q. (1979), The Priestley-Taylor evaporation model applied to a large, shallow lake in the Netherlands. Journal of Applied Meteorology. 18, 898-903. https://www.jstor.org/stable/26179219.

[66] de Kok, R.J., Steiner, J.F., Litt, M., Wagnon, P., Koch, I., Azam, M.F., and Immerzeel, W.W. (2020), Measurements, models and drivers of incoming longwave radiation in the Himalaya. International Journal of Climatology, 40(2), pp.942-956.

[67] Delacroix, Sylvain, Sylvain Bourdier, Thomas Soulard, Hashim Elzaabalawy, and Polina Vasilenko. 2023. "Experimental Modelling of a Floating Solar Power Plant Array under Wave Forcing" *Energies* 16, no. 13: 5198. https://doi.org/10.3390/en16135198.

[68] Deloitte, Lee, P., Loucks, J., Stewart, D., Jarvis, G., and Arkenberg C. (2019), Technology, Media, and Telecommunications Predictions, Deloitte, Insights, 2019.

[69] Dizier, A. (2018), Techno-economic analysis of floating PV solar power plants using active cooling technique: A case study for Taiwan [Internet]. [Dissertation]. (TRITA-ITM-EX). Available from: http://urn.kb.se/resolve?urn=urn:nbn:se:kth:diva-244320.

[70] DNV (2022), The future of floating solar, Drivers and barriers to growth Arnhem, The Netherlands.

[71] DNV (2023), The future of floating solar: Drivers and barriers to growth Arnhem, The Netherlands.

[72] Do T.N., Burke P.J., Nguyen H.N., Overland I., Suryadi B., Swandaru A., and Yurnaidi Z. (2021), Vietnam's solar and wind power success: Policy implications for the other ASEAN countries. Energy for Sustainable Development. 65:1-1.

[73] Dörenkämper M., Wahed A., Kumar A., de Jong M., Kroon J. and Reindl T. (2021), The Cooling Effect of Floating PV In Two Different Climate Zones: A Comparison of Field Test Data from The Netherlands and Singapore, Solar Energy, vol. 219, pp. 15-23.

[74] Du, Y., Fell, C.J., Duck, B., Chen, D., Liffman, K., Zhang, Y., Gu, M. and Zhu, Y. (2016), Evaluation of photovoltaic panel temperature in realistic scenarios. Energy Conversion and Management, 108, pp.60-67.

[75] Duarte, H.F., Dias, N.L., and Maggiotto, S.R. (2006), Assessing daytime downward long-wave radiation estimates for clear and cloudy skies in Southern Brazil. Agric For Meteorol 139:171–181.

[76] Duffie, J. A. and Beckman, W. A. (2020), *Solar engineering of thermal processes* 4th ed. Wiley: Madison, United States of America, 2020.

[77] Durković, Vladan, and Đurišić Željko (2017), Analysis of the Potential for Use of Floating PV Power Plant on the Skadar Lake for Electricity Supply of Aluminium Plant in Montenegro. *Energies* 10, no. 10: 1505. https://doi.org/10.3390/en10101505.

[78] Dzamesi, S.K.A., Ahiataku-Togobo, W., Yakubu, S., Acheampong, P., Kwarteng, M., Samikannu, R., and Azeave, E. (2024), Comparative performance evaluation of ground-mounted and floating solar PV systems. Energy for Sustainable Development, 80, p.101421.

[79] Eagleman, J. R. (1967), A New Approach for Calculating Evaporation Rates. Monthly Weather Review 95, no. 5: 335-340.

[80] El Hammoumi, A., Chalh, A., Allouhi, A., Motahhir, S., El Ghzizal, A., and Derouich, A. (2021), Design and construction of a test bench to investigate the potential of floating PV systems. Journal of Cleaner Production. 278:123917.

[81] Elminshawy, N.A., Osama, A., Saif, A.M. and Tina, G.M., 2022. Thermo-electrical performance assessment of a partially submerged floating photovoltaic system. Energy, 246, p.123444.

[82] Emery, K., Burdick, J., Caiyem, Y., Dunlavy, D., Field, H., Kroposki, B., Moriarty, T., Ottoson, L., Rummel, S., Strand, T., and Wanlass, M.W. (1996), Temperature dependence of photovoltaic cells, modules and systems. In Conference Record of the Twenty Fifth IEEE Photovoltaic Specialists Conference-1996 (pp. 1275-1278). IEEE.

[83] Essak, L., and Ghosh, A. (2022), Floating photovoltaics: A review. Clean Technologies, 4(3), pp.752-769. https://doi.org/10.3390/cleantechnol4030046

[84] Evans, D.L., and Florschuetz, L.W. (1978), Terrestrial concentrating photovoltaic power system studies. Solar Energy, 20(1), pp.37-43.

[85] Evans, D.L. (1981), Simplified method for predicting photovoltaic array output. Solar energy, 27(6), pp.555-560.

[86] Faiman, D. (2008), Assessing the outdoor operating temperature of photovoltaic modules. Progress in Photovoltaics: Research and Applications, 16(4), pp.307-315. https://doi.org/10.1002/PIP.813.

[87] Farrar, L.W., Bahaj, A.S., James, P., Anwar, A., and Amdar, N. (2022), Floating solar PV to reduce water evaporation in water stressed regions and powering water

pumping: Case study Jordan. Energy Conversion and Management, 260, p.115598.ISSN01968904,https://doi.org/10.1016/j.enconman.2022.115598.

[88] Farfan, J., and Breyer, C. (2018), Combining Floating Solar Photovoltaic Power Plants and Hydropower Reservoirs: Virtual Battery of Power Great Global Potential Combining Floating Solar Photovoltaic Plants and the 15th International Symposium on District Heatin. *Energy Procedia* 155, 403–411.

[89] Febrian H.G., Supriyanto A. and Purwanto H. (2023), Calculating the Energy Capacity and Capacity Factor of Floating Photovoltaic (FPV) Power Plant in The Cirata Reservoir Using Different Types of Solar Panels, *Journal of Physics*: *Conference Series*, vol. 2498, 012007.

[90] Ferrer-Gisbert C., Ferrán-Gozálvez, J.J., Redón-Santafé, M., Ferrer-Gisbert, P., Sánchez-Romero, F.J., and Torregrosa-Soler, J.B. (2013), A new photovoltaic floating cover system for water reservoirs. Renewable energy. 60:63-70.

[91] Finch, J. W., and Hall R. L. (2001), Estimation of open water evaporation, A Review of Methods. R&D Technical Report W6-043/TR, Environment Agency, Rio House, Waterside Drive, Aztec West, Almondsbury, Bristol, BS32 4UD.

[92] Finch J., and Calver A. (2008), Methods for the quantification of evaporation from lakes. World Meteorological Organization's Commission for Hydrology, https://nora.nerc.ac.uk/id/eprint/14359/1/wmoevap_271008.pdf.

[93] Florschuetz L.W. (1979), Extension of The Hottel-Whillier Model to The Analysis of Combined Photovoltaic/Thermal Flat Plate Collectors, *Solar energy*, vol. 22, pp. 361-66.

[94] Foster, R., Ghassemi, M., and Cota A. (2009), Solar Energy: Renewable Energy and the Environment. CRC Press, 2009. Accessed: Aug. 17, 2022. [Online]. Available: https://books.google.co.in/books?hl=en&lr=&id=DiNr-.

[95] Gaikwad, Omkar D., and Deshpande, U. L. (2017), Evaporation control using floating pv system and canal roof top solar system. International Research Journal of Engineering and Technology, 4(4).

[96] Garanovic, Amir (2021), "China connects 550MW combined floating solar and aquaculture project to power grid". *Offshore Energy*. Retrieved 2023-08-16.

[97] Garanovic, Amir (2023), "Multi-megawatt floating solar farm comes online in Thailand". *Offshore Energy*. Retrieved 2023-05-11.

[98] Garanovic, Amir (2023-02), "BayWa r.e. builds largest floating solar plant in Central Europe". *Offshore Energy*. Retrieved 2023-02-22.

[99] Ghosh, A. (2023), A comprehensive review of water-based PV: Flotavoltaics, under water, offshore & canal top. Ocean Engineering. 281:115044.

[100] Gorjian, S., Sharon, H., Ebadi, H., Kant, K., Scavo, F.B., and Tina, G.M. (2021), Recent technical advancements, economics and environmental impacts of floating photovoltaic solar energy conversion systems. Journal of Cleaner Production, 278, p.124285. ISSN 0959-6526, https://doi.org/10.1016/j.jclepro.2020.124285.

[101] Green, M., and Bremner, S. (2017), Energy conversion approaches and materials for high-efficiency photovoltaics. Nature Mater 16, 23–34. https://doi.org/10.1038/nmat4676.

[102] Gupta, Uma (2022). "NTPC's 92 MW Kayamkulam floating solar project now fully operational". *PV Magazine*. Retrieved 17 November 2023.

[103] Gurfude, S.S., and Kulkarni, P.S. (2019), Energy yield of tracking type floating solar PV plant. In 2019 National Power Electronics Conference (NPEC) (pp. 1-6). IEEE.

[104] Gwandu, B.A.L., and Creasey, D.J. (1995), Humidity: a factor in the appropriate positioning of a photovoltaic power station. Renewable Energy, 6(3), pp.313-316.

[105] Haas, J., Khalighi, J., De La Fuente, A., Gerbersdorf, S.U., Nowak, W., and Chen, P.J. (2020), Floating photovoltaic plants: Ecological impacts versus hydropower operation flexibility. Energy Conversion and Management. 206:112414.

[106] Hamon, W. R. (1960), Estimating potential evapotranspiration, (Doctoral dissertation). Retrieved from DSpace@MIT. (https://dspace.mit.edu/bitstream/handle/1721.1/79479/32827649-MIT.pdf?sequence=2). Cambridge, MA: Massachusetts Institute of Technology.

[107] Hapcheon dam (2021), "Giant Floating Solar Flowers Offer Hope for Coal-Addicted Korea". *Bloomberg.com*. 2022-02-28. Retrieved 2023-03-14.

[108] Harbeck, Jr. G.E., Kohler, M.A., and Koberg, G.E. (1958), Water-loss investigations; Lake Mead studies. U.S.G.S. Publications Warehouse Professional paper 298. https://doi.org/10.3133/pp298.

[109] Harrison, L. P. (1963), Fundamentals concepts and definitions relating to humidity. In Wexler, A (Editor) Humidity and moisture Vol 3, Reinhold Publishing Co., N.Y.

[110] Hartzell, Tynan Scott (2016), Evaluating potential for floating solar installations on Arizona water management infrastructure.

[111] Henderson-Sellers, B. (1986), Calculating the surface-energy balance for lake and reservoir modeling - a review. Reviews of Geophysics 24, 625-649.

[112] Hopson and Christopher (2020). "Floating solar going global with 10GW more by 2025: Fitch | Recharge". Recharge | Latest renewable energy news. Retrieved 2021-10-18.

[113] Hough, M.N., and Jones, R.J.A. (1997), The United Kingdom Meteorological Office rainfall and evaporation calculation system: MORECS version 2.0 - an overview. Hydrology and Earth System Science 1, 227-239.

[114] http://upneda.org.in/MediaGallery/Uttar_Pradesh_Solar_Energy_Policy-2017_English__0. pdf.

[115] https://www.ciel-et-terre.net/project/sugu-2-1133-kwp/ (Accessed September 2020).

[116] Huancheng Jining (2017), "Floating PV System - Commercial solar photovoltaic installers". *en.sungrowpower.com*. Retrieved 2023-03-14.

[117] Huang, G., Tang, Y., Chen, X., Chen, M., and Jiang, Y. A. (2023), Comprehensive Review of Floating Solar Plants and Potentials for Offshore Applications. J. Mar. Sci. Eng. 2023, 11, 2064. https://doi.org/10.3390/jmse11112064.

[118] Idso, S.B., and Jackson, R.D. (1969), Thermal radiation from the atmosphere. J Geophysical Res 74:5397–5403.

[119] Idso, S.B. (1981), A set of equations for full spectrum and 8 to 14 mm and 10.5 to 12.5 mm thermal radiation from cloudless skies. Water Resour Res 17:295–304.

[120] Ilgen K, Schindler D, Armbruster A, Ladwig R, Eppinger Ruiz de Zarate I, and Lange J. (2024), Evaporation reduction and energy generation potential using floating photovoltaic power plants on the Aswan High Dam Reservoir. Hydrological Sciences Journal. 2024 Mar 28(just-accepted).

[121] India RE-navigator (2018), https://india-re-navigator.com/utility/news/1581 (accessed 23 March 2023)

[122] Irodionov, A.E., Kurenkova, V.A., Potapov, V.N., and Strebkov, D.S. (1989), Choice of resistance for elements of photovoltaic system's external switching. Geliotechnika, 25, pp.18-21.

[123] IEA (2021), "India Energy Outlook 2021, IEA, Paris." https://www.iea.org/reports/india-energy-outlook-2021, License: CC BY 4.0 (accessed March 23, 2023).

[124] IEA-PVPS (2023), Trends in PV applications 2021. IEA-PVPS. https://iea-pvps.org/trends_reports/trends-in-pv-applications-2021/.

[125] "India Energy Information | Enerdata." https://www.enerdata.net/estore/energy-market/india/ (accessed Aug. 16, 2022).

[126] IPCC, I.P., on CC, 2018. Global warming of 1.5◦ C: an IPCC special report on the impacts of global warming of 1.5◦ C above pre-industrial levels and related global greenhouse gas emission pathways. The Context of Strengthening the Global Response to the Threat of Climate Change, Sustainable Development, and Efforts to Eradicate Poverty. Intergovernmental Panel on Climate Change.

[127] Irena (2021), Offshore renewables: An action agenda for deployment, International Renewable Energy Agency, Abu Dhabi, 2021.

[128] Jacobs, J.D. (1978), Radiation climate of Broughton Island. In: Barry RG, Jacobs JD (eds) Energy budget studies in relation to fast-ice breakup processes in Davis Strait. Inst. of Arctic and Alp. Res. Occas. Paper no. 26. University of Colorado, Boulder, pp 105–120.

[129] Jensen, M.E. and Haise, H.R. (1963), Estimating Evapotranspiration from Solar Radiation. Journal of the Irrigation and Drainage Division, 89, 15-41.

[130] Kala, Rishi Ranjan (2022), "India's annual power consumption to grow at 6.5% during 2022-24 - The Hindu BusinessLine.",18,January, 2022 https://www.thehindubusinessline.com/news/indias-annual-power-consumption-to-grow-at-65-during-2022-24/article64907816. ece (accessed Aug. 16, 2022).

[131] Kalogirou S.A. and Tripanagnostopoulos Y. (2006), Hybrid PV/T Solar Systems for Domestic Hot Water and Electricity Production, *Energy Conversion and Management,* vol. 47, pp. 3368-82.

[132] Kalogirou, S.A. (2013), Solar energy engineering: processes and systems. Academic press.

[133] Kamuyu, Charles Lawrence W., Lim J.R., Won, C.S., and Ahn, H.K. (2018), Prediction model of photovoltaic module temperature for power performance of floating PVs. Energies.11(2):447.

[134] Kaplani E. and Kaplanis S. (2014), Thermal modelling and experimental assessment of the dependence of PV module temperature on wind velocity and direction, module orientation and inclination. Solar Energy. 107:443-60.

[135] Kaplanis, S., and Kaplani, E. (2018), A new dynamic model to predict transient and steady state PV temperatures taking into account the environmental conditions. Energies. 12(1):2.

[136] Kaplani, E. and Kaplanis, S. (2020), PV module temperature prediction at any environmental conditions and mounting configurations. In Renewable Energy and Sustainable Buildings (pp. 921-933). Springer, Cham.

[137] Kapoor, M. and Garg, R.D. (2021a), Solar Potential Estimation and Management Using IoT, Big Data, and Remote Sensing in a Cloud Computing Environment. In *Artificial Intelligence* (pp. 117-125). Chapman and Hall/CRC.

[138] Kapoor, M. and Garg, R.D. (2021b), Evaluation of optimum PV tilt angle with generated and predicted solar electric data using geospatial open source software in cloud environment. *Sādhanā*, *46*(2), p.108.

[139] Kapoor, M. and Garg, R.D. (2021c), Solar potential assessment over canal-top using geospatial techniques. Arabian Journal of Geosciences, 14(4), p.254.

[140] Kapoor, M., Garg, R.D.(2018), Cloud computing for energy requirement and solar potential assessment. *Spat. Inf. Res.* **26**, 369–379 (2018). https://doi.org/10.1007/s41324-018-0181-3.

[141] Kassem Y., Camur H., Abdalla M. A. H. A. (2023), Assessment of Floating Photovoltaic (FPV) Systems as an Alternative Electricity Generation Source: A Case Study from Sudan, IOP Conf. Series: Earth and Environmental Science, vol. 1267, 012031.

[142] Kayamkulam (2022), "NTPC Kayamkulam, India". *Ciel et Terre*. Retrieved 2023-02-16.

[143] Kim, S.H., Yoon, S.J., Choi, W., and Choi, K.B. (2016), Application of floating photovoltaic energy generation systems in South Korea. Sustainability 8:1333. https://doi.org/ 10.3390/su8121333.

[144] Kim S.H., Baek S.C., and Choi K.B. (2020), Design and installation of 500- kW floating photovoltaic structures using high-durability steel. Energies, 13:4996.

[145] King, D.L., and Eckert, P.E. (1996), May. Characterizing (rating) the performance of large photovoltaic arrays for all operating conditions. In Conference Record of the Twenty Fifth IEEE Photovoltaic Specialists Conference-1996 (pp. 1385-1388). IEEE.

[146] King, D.L. (1997), February. Photovoltaic module and array performance characterization methods for all system operating conditions. In AIP conference proceedings (Vol. 394, No. 1, pp. 347-368). American Institute of Physics. https://doi.org/10.1063/1.52852.

[147] King D.L., Kratochvil J.A., and Boyson W.E. (1997), Temperature coefficients for PV modules and arrays: measurement methods, difficulties, and results. In Conference record of the twenty sixth IEEE Photovoltaic Specialists Conference-1997 29 (pp. 1183-1186). IEEE.

[148] King, D.L., Kratochvil, J.A., and Boyson, W.E. (2004), Photovoltaic array performance model. Sandia National Laboratories 2004. Report SAND2004-3535. Available from: http://prod.sandia.gov/techlib/access-control.cgi/2004/ 043535.pdf (accessed 30 July 2022).

[149] Kichou, S., Skandalos, N., and Wolf, P. (2022), Floating photovoltaics performance simulation approach. Heliyon, 8(12).

[150] Koehl, M., Heck, M., Wiesmeier, S. and Wirth, J. (2011), Modelling of the nominal operating cell temperature based on outdoor weathering. Solar Energy Materials and Solar Cells, 95(7), pp.1638-1646. https://doi.org/10.1016/j.solmat.2011.01.020.

[151] Konzelmann, T., van de Wal, R.S.W., Greuell, W., Bintanja, R., Henneken, E.A.C., and Abe-Ouchi, A. (1994), Parameterization of global and longwave

incoming radiation for the Greenland ice sheet. Global and Planetary Change, **9**(1–2), 143–164. https://doi.org/10.1016/0921-8181(94)90013-2.

[152] Kougias, I., Bódis, K., Jäger-Waldau, A., Moner-Girona, M., Monforti-Ferrario, F., Ossenbrink, H. and Szabó, S. (2016), The potential of water infrastructure to accommodate solar PV systems in Mediterranean islands. Solar Energy, 136, pp.174-182.

[153] Kumar, A., Purohit, I., and Kandpal T.C. (2021), Assessment of floating solar photovoltaic (FSPV) potential in India. In Proceedings of the 7th International Conference on Advances in Energy Research (pp. 973-982). Springer Singapore.

[154] Kumar M. and Kumar, A. (2019), Performance Assessment of Different Photovoltaic Technologies for Canal-Top and Reservoir Applications in Subtropical Humid Climate, in *IEEE Journal of Photovoltaics*, vol. 9, no. 3, pp. 722-732, May 2019, doi: 10.1109/JPHOTOV.2019.2892520.

[155] Kumar, N.M., Subramaniam, U., Mathew, M., Ajitha, A. and Almakhles, D.J., 2020. Exergy analysis of thin-film solar PV module in ground-mount, floating and submerged installation methods. Case Studies in Thermal Engineering, 21, p.100686.

[156] Kumar, M., Niyaz, H.M. and Gupta, R. (2021), Challenges and opportunities towards the development of floating photovoltaic systems. Solar Energy Materials and Solar Cells, 233, p.111408. ISSN 0927-0248, https://doi.org/10.1016/j.solmat.2021.111408.

[157] Kumar, S., Bhattacharyya B., and Gupta V. K. (2014), Present and Future Energy Scenario in India, Journal of The Institution of Engineers (India): Series B, vol. 95, no. 3, pp. 247–254, 2014, doi: 10.1007/s40031-014-0099-7.

[158] Kurtz, S., Whitfield, K., Miller, D., Joyce, J., Wohlgemuth, J., Kempe, M., Dhere, N., Bosco, N., and Zgonena, T. (2009), Evaluation of high-temperature exposure of rack-mounted photovoltaic modules. Conference Record of the IEEE Photovoltaic Specialists Conference, April 2016, 002399–002404. https://doi.org/10.1109/PVSC.2009.5411307.

[159] Lamaamar I., Tilioua A., Zaid Z.B., Babaoui A., Ettakni M., Alaoui M.A. (2021), Evaluation of different models for validating of photovoltaic cell temperature under semi-arid conditions. Heliyon. 7(12).

[160] Largue, Pamela (2023), "Israel's Teralight inaugurates 31MW floating solar project". *Power Engineering International*. Retrieved 2023-09-18.

[161] Lasnier, F., and Ang, T. G. (1990), Photovoltaic engineering handbook, 1st ed.; IOP Publishing LTD: Lasnier, France, 1990; pp. 258.

[162] Lee, Y.G., Joo, H.J., and Yoon, S.J. (2014), Design and installation of floating type photovoltaic energy generation system using FRP members. Solar Energy, 108, pp.13-27.

[163] Lee, Andrew (2022), "'Smooth operator': world's largest floating solar plant links with wind and storage". *Recharge | Latest renewable energy news*. Archived from the original on 11 March 2022."5 Largest Floating Solar Farms in the World in 2022". *YSG Solar*. 20 January 2022.

[164] Lhomme, J.P., Vacher, J.J., and Rocheteau, A. (2007), Estimating downward long-wave radiation on the Andean Altiplano. Agric For Meteorol 145:139–148.

[165] Liu, L., Wang, Q., Lin, H., Li, H., and Sun, Q. (2017), Power generation efficiency and prospects of floating photovoltaic systems. Energy Procedia. 105:1136-42.

[166] Liu, H., Krishna, V., Lun Leung, J., Reindl, T., and Zhao, L. (2018), Field experience and perfor- mance analysis of floating PV technologies in the tropics. Progress in Photovoltaics: Research and Applications, 26(12), 957–967.

[167] Liu, L., Sun, Q., Li, H., Yin, H., and Ren, X. (2019), Wennersten R. Evaluating the benefits of integrating floating photovoltaic and pumped storage power system. Energy Conversion and Management. 194:173-85.

[168] Llorens, D. (2017), Which direction should Solar Panel Face. 2017. Accessed: Aug. 17, 2022. [Online].

[169] Lopes, M.P.C., de Andrade Neto, S., Alves Castelo Branco, D., Vasconcelos de Freitas, M.A., and da Silva Fidelis, N. (2020), Water-energy nexus: floating photovoltaic systems promoting water security and energy generation in the semiarid region of Brazil. Journal of Clean Production. 273, 122010. https://doi.org/10.1016/j.jclepro.2020. 122010.

[170] Lopes, M.P., Nogueira, T., Santos, A.J., Branco, D.C., and Pouran, H. (2022), Technical potential of floating photovoltaic systems on artificial water bodies in Brazil. Renewable Energy. 181:1023-33.

[171] Magare, D., Sastry, O., Gupta, R., Bora, B., Singh, Y., and Mohammed, H. (2018), Wind effect modeling and analysis for estimation of photovoltaic module temperature. Journal of Solar Energy Engineering, 140(1), p.011008.

[172] Majid, Z.A.A., Ruslan, M.H., Sopian, K., Othman, M.Y., and Azmi, M.S.M. (2014), Study on performance of 80 watt floating photovoltaic panel. Journal of Mechanical Engineering and Sciences, 7, pp.1150-1156.

[173] Makhija, S.P., Shrivastava, P.K., Jena, P.K., Dubey, S.P. and Singh, P. (2024), Techno-Economic Comparative Analysis of On-Ground and Floating PV Systems: A Case Study at Gangrel Dam, India. *Photovoltaic Systems Technology*, pp.191-210.

[174] Makkink, G. F., and Heemst H.D.J. (1974), Resistance of leaves as a function of their water content and light. No. 774. Centre for Agricultural Publishing and Documentation Wageningen -1974.

[175] Mamatha, G., and Kulkarni, P.S. (2022), Assessment of floating solar photovoltaic potential in India's existing hydropower reservoirs, Energy for Sustainable Development, Volume 69,2022, Pages 64-76, ISSN 0973-0826, https://doi.org/10.1016/j.esd.2022.05.011.

[176] Markvart, Tomas, ed. Solar electricity. Vol. 6. John Wiley & Sons, 2000.

[177] Martín, José Rojo (2021), "5 Largest Floating Solar Farms in the World in 2022". *YSG Solar*. 20 January 2022. "Singaporean water utility in push for 50MW-plus floating PV". *PV Tech*. "Singapore launches large-scale floating solar farm in Tengeh Reservoir". *www.datacenterdynamics.com*. 27 July 2021. Archived from the original on 6 August 2021.

[178] Mattei, M., Notton, G., Cristofari, C., Muselli, M., and Poggi, P. (2006), Calculation of the polycrystalline PV module temperature using a simple method of energy balance. Renewable Energy 31: 553–567. DOI: 10.1016/j. renene.2005.03.010.

[179] Maykut, G.A., and Church, P.F. (1973), Radiation climate of Barrow, Alaska, 1962–66. J Appl Meteorol 12:620–628.

[180] McJannet, D.L., Cook, F.J., McGloin, R.P., McGowan, H.A., and Burn, S. (2011), Estimation of evaporation and sensible heat flux from open water using a large-aperture scintillometer. Water Resources Research, 47(5).

[181] McMillan, W. (1973), Cooling from open water surfaces. Final Report: Part 1; Lake Trawsfynydd cooling investigation. NW/SSD/RR/1204/73, pp.1-55.

[182] Mekhilef S., Saidur R. and Kamalisarvestani M. (2012), Effect of Dust, Humidity and Air Velocity on Efficiency of Photovoltaic Cells, *Renewable and sustainable energy reviews* vol. 16(5), pp. 2920-25.

[183] Melvin, Gair Kai, and Xiang. (2015), Experimental study of the effect of floating solar panels on reducing evaporation in Singapore reservoirs. *Trabalho de Conclusão de Curso (Engineering Department Of Civil & Environmental Engineering). Vol. 36*. University Of Singapore.

[184] Micheli, L. (2022), The temperature of floating photovoltaics: Case studies, models and recent findings. Solar Energy, 242, pp.234-245.

[185] Micheli, L., Talavera, D.L., Tina, G.M., Almonacid, F., and Fernández, E.F. (2022), Techno-economic potential and perspectives of floating photovoltaics in Europe. Solar Energy. 243:203-14.

[186] Ministry of New and Renewable Energy, “Cabinet approves Intra-State Transmission System – Green Energy Corridor Phase-II,” Jan. 2022. Accessed: Aug.16,2022. Available: https://pib.gov.in/PressReleaseIframePage.aspx?PRID=1788011.

[187] Ministry of Power, “Mission 500 GW by 2030: India takes one more step to reduce carbon emission and reduce the cost of power to consumers,” Nov. 2021. Accessed: Aug. 16, 2022. Available: https://pib.gov.in/PressReleaseIframePage.aspx? PRID=1772347.

[188] Mittal, D., Saxena, B.K. and Rao, K.V.S., 2017, April. Floating solar photovoltaic systems: An overview and their feasibility at Kota in Rajasthan. In 2017 international conference on circuit, power and computing technologies (ICCPCT) (pp. 1-7). IEEE.

[189] Mondol J.D., Yohanis Y.G., Smyth M., and Norton B. (2005), Long-term validated simulation of a building integrated photovoltaic system. Sol. Energy, 78 (2005), pp. 163-176.

[190] Mondol, J.D., Yohanis, Y.G., and Norton, B. (2007), Comparison of measured and predicted long term performance of grid a connected photovoltaic system. Energy conversion and management, 48(4), pp.1065-1080.

[191] Mongabay (2021), For net-zero by 2050, India needs 2.5 percent of its land for clean energy installation.” https://india.mongabay.com/2021/09/for-net-zero-by-2050-india-needs-2-5-percent-of-its-land-for-clean-energy-installation/ (accessed Aug. 16, 2022).

[192] Monteith, J.L. (1965), The state and movement of water in living organisms. In 19th Symposia of the Society for Experimental Biology. Cambridge University Press, London, 1965 (pp. 205-234).

[193] Mora Segado, P., Carretero, J., and Sidrach-de-Cardona, M. (2015), Models to predict the operating temperature of different photovoltaic modules in outdoor conditions. Progress in Photovoltaics: Research and Applications, 23(10), pp.1267-1282.

[194] Murray, F. W. (1967), On the computation of saturation vapor pressure. J. Appl. Meteor. 6: 203-204.

[195] Muzathik, A.M. (2014), Photovoltaic modules operating temperature estimation using a simple correlation. Int. J. Energy Eng., 4 (4) , pp. 151-158.

[196] Nagananthini, R., and Nagavinothini, R. (2021), Investigation on floating photovoltaic covering system in rural Indian reservoir to minimize evaporation loss. International Journal of Sustainable Energy, 40(8), pp.781-805.

[197] Nebey, A.H., Taye, B.Z., and Workineh, T.G. (2020), GIS-based irrigation dams potential assessment of floating solar PV system. Journal of Energy, 2020, pp.1-10.

[198] New Jersey (2022), "16,510 – Number of the Day". *NJ Spotlight News*. "Canoe Brook, USA". *Ciel et Terre*. Retrieved 2023-02-16.

[199] Niaki, A.H.M., and Davoodi, B. (2020), December. Proposing an Optimal Techno-Economic Scheme for a Hybrid Floating Photovoltaic-Hydro Power Plant. In 2020 10th Smart Grid Conference (SGC) (pp. 1-6). IEEE.

[200] Nisar, Hamza, Abdul, Kashif Janjua, Hamza, Hafeez, Sehar, Shakir, Nadia, Shahzad, and Adeel, Waqas (2022), Thermal and electrical performance of solar floating PV system compared to on-ground PV system-an experimental investigation, Solar Energy, Volume 241, Pages 231-247,ISSN 0038-092X, https://doi.org/10.1016/j.solener.2022.05.062.

[201] Nordmann, T., and Clavadetscher, L. (2003), Understanding temperature effects on PV system performance. In 3rd World Conference on Photovoltaic Energy Conversion, 2003. Proceedings of (Vol. 3, pp. 2243-2246). IEEE.

[202] Notton, G., Cristofari, C., Mattei, M., and Poggi, P. (2005), Modelling of a double-glass photovoltaic module using finite differences. Applied thermal engineering, 25(17-18), pp.2854-2877.

[203] Oliveira-Pinto, S., and Stokkermans, J. (2020), Assessment of the potential of different floating solar technologies–Overview and analysis of different case studies. Energy Conversion and Management, 211, p.112747.

[204] Omkareshwar (2023) "First block of 600MW floating solar plant phase-1 launched in Omkareshwar". The Times of India. 2023-08-21. ISSN 0971-8257. Retrieved 2023-11-17. N

[205] Omubo-Pepple, V.B., Israel-Cookey, C., and Alaminokuma, G.I. (2009), Effects of temperature, solar flux and relative humidity on the efficient conversion of solar energy to electricity. European Journal of Scientific Research, 35(2), pp.173-180.o.:SNS/N/13/32Student 1 SNS/N/13/320

[206] Osama, A., Elminshawy, N.A., and Saif, A.M. (2022), Design and construction of a test bench to investigate the potential of novel partially submerged PV system. Port-Said Engineering Research Journal, 26(1), pp.151-164.

[207] Owhaib W., Borett A., AlKhalidi A., Al-Kouz W. and Hader M. (2022), Design of a solar PV plant for Ma'an, Jordan, IOP Conf. Series: Earth and Environmental Science, vol. 1008, 012012.

[208] Pakyala, H.B.S. (2021), Floating solar potential assessment. In 2021 13th IEEE PES Asia Pacific Power & Energy Engineering Conference (APPEEC) (pp. 1-6). IEEE.

[209] Panjwani, M.K., and Narejo, G.B. (2014), Effect of humidity on the efficiency of solar cell (photovoltaic). International Journal of Engineering Research and General Science, 2(4), pp.499-503.

[210] Papadakis, J. (1965), Potential Evapotranspiration. Soil Science 100(1):p 76.

[211] Penman, H. L. (1947). Evaporation in nature. Reports on Progress in Physics, 11(1), 366. https://doi.org/10.1088/0034-4885/11/1/312.

[212] Penman, H.L. (1948), Natural evaporation from open water, bare soil and grass. Proceedings of the Royal Society of London. Series A. Mathematical and Physical Sciences, 193(1032), pp.120-145.

[213] Penman, H.L. (1956), Estimating evaporation, Eos Trans. AGU, 37(1), 43–50, doi:10.1029/TR037i001p00043.

[214] Perera, H.M.R., and Wen, H. (2020), September. Simulation Evaluation of Floating Photovoltaic Power System. In 2020 12th IEEE PES Asia-Pacific Power and Energy Engineering Conference (APPEEC) (pp. 1-6). IEEE.

[215] Perez, M., Perez, R., Ferguson, C. R., and Schlemmer, J. (2018), Deploying effectively dispatchable PV on reservoirs: Comparing floating PV to other renewable technologies. Solar Energy, 174, 837–847.

[216] "Power Sector at a Glance All India | Government of India | Ministry of Power." https://powermin.gov.in/en/content/power-sector-glance-all-india (Accessed 23March, 2023). Papadakis J. (1965), Potential evapotranspiration. Soil Science. 100(1):76.

[217] Prata, A.J. (1996), A new long-wave formula for estimating downward clear-sky radiation at the surface. Quart J. Royal Meteorological Soc. 122:1127–1151.

[218] Priestley C.H.B., and Taylor R.J. (1972), On the assessment of surface heat flux and evaporation using large-scale parameters. Monthly Weather Review 100(2):81–92. https://doi.org/10.1175/1520-0493(1972)1002.3.co;2

[219] PVsyst SA. (2021), PVsyst Contextual Help. Retrieved from https://www.pvsyst.com/help/index.html.

[220] Qintang (2019), "Floating PV System - Commercial solar photovoltaic installers". *en.sungrowpower.com*. Retrieved 2023-03-14.

[221] Rahaman, M.A., Chambers, T.L., Fekih, A., Wiecheteck, G., Carranza, G., and Possetti, G.R.C. (2023), Floating photovoltaic module temperature estimation: Modeling and comparison. Renewable Energy, 208, pp.162-180.

[222] Ramagundam (2022), "Power plant profile: NTPC Ramagundam Floating Solar PV Park, India". *Power Technology*. Retrieved 2023-11-19.*Correspondent, Special (2022-07-01).* "100 MW NTPC floating solar plant at Ramagundam fully operational". *The Hindu.* ISSN 0971-751X. Retrieved 2023-11-19.

[223] Rauschenbach, H.S. (1980), S*olar cell array design handbook*, 1st ed.; Van Nostrand Reinhold Company, New York, United States of America, 1980; pp: 390-391.

[224] REC Group (2022), Development of Canal-Top, Grid-Connected Solar Plants with Suspended Structure in Punjab, India.

[225] Richards, B.S. (2006), Enhancing the performance of silicon solar cells via the application of passive luminescence conversion layers. Solar energy materials and solar cells, 90(15), pp.2329-2337.

[226] Rim, C.S. (2017), Estimation of small pan evaporation using temperature data. Journal of Korea Water Resources Association. 50(1):37-53.

[227] Risser, V.V., and Fuentes, M. K. (1983), Linear regression analysis of flat-plate photovoltaic system performance data. Proceedings of the Fifth E.C. Photovoltaic Solar Energy Conference, Athens, Greece, October 17–21 (1983), pp. 623-627.

[228] Rizvi, T., Dubey, S.P., Tripathi, N. (2022), A Comparative Analysis of FSPV-Grid and Grid-Only Systems for an Industrial Subsection. In Proceedings of the IEEE Sponsored Second International Conference on Advances in Electrical, Computing, Communications and Sustainable Technologies (ICAECT 2022), Bhilai, India, 21–22 April 2022. [Google Scholar]

[229] Rizvi, T., Dubey, S.P., Tripathi, N., Srivastava, G., Makhija, S.P., and Mohiddin, M.K. (2023), "FSPV-Grid System for an Industrial Subsection with PV Price Sensitivity Analysis" *Sustainability* 15, no. 3: 2495. https://doi.org/10.3390/su15032495.

[230] Rizvi, T., Dubey, S.P., Tripathi, N., and Makhija, S.P. (2024), Assessment of FSPV-Grid System for Electrification of Industrial Sections with Shrinking Derating Factor. In: Dhote, N.K., Kolhe, M.L., Rehman, M. (eds) Recent Evolutions in Energy, Drives and e-Vehicles. REEDEV 2022. Lecture Notes in Electrical Engineering, vol 1162. Springer, Singapore. https://doi.org/10.1007/978-981-97-0763-8_22.

[231] Rodrigues, I.S., Ramalho G.L., and Medeiros P.H. (2020), Potential of floating photovoltaic plant in a tropical reservoir in Brazil. Journal of Environmental Planning and Management. 63(13):2334-56.

[232] Rosa-Clot, M., Tina, G.M., and Nizetic, S. (2017), Floating photovoltaic plants and wastewater basins: an Australian project. Energy Procedia, 134, pp.664-674.

[233] Rosa-Clot, M., and Tina, G.M. (2020), Current status of FPV and trends in Floating PV plants. (pp. 9-18). Academic Press.

[234] Rosenberry, D.O., Winter, T.C., Buso, D.C., and Likens, G.E. (2007), Comparison of 15 evaporation methods applied to a small mountain lake in the northeastern USA. Journal of hydrology, 340(3-4), pp.149-166.

[235] Ross, R.G. (1976), Interface design considerations for terrestrial solar cell modules. Proceedings of the 12th IEEE photo voltaic specialists conference, Baton Rouge, LA, November 15–18; 1976; 801–806.

[236] Ross, R.G., and Smokler, M. I. (1986), Flat-Plate solar array project final report, Volume VI: Engineering Sciences and Reliability, Report DOE/JPL-1012-125; JPL: California, United States of America, 1986.

[237] Ryan, P. J. and Harleman, D. R. F. (1973), An analytical and experimental study of transient cooling pond behavior. ralph M. Parsons laboratory for water resources and Hydrodynamics, Massachusetts Institute of Technology, Report no. 161. https://dspace.mit.edu/handle/1721.1/142973.

[238] Safarini, Al N., Akash, O., Mohsen, M., and Iqbal, Z. (2017), November. Performance evaluation of solar tracking systems for power generation based on simulation analysis: Solar Island concept. In 2017 International Conference on Electrical and Computing Technologies and Applications (ICECTA) (pp. 1-4). IEEE.

[239] Sahoo, B.C., Panda, S.N., and Panigrahi, B. (2009), January. Reduction of evaporation loss from the on-farm reservoir through biological shading. In Int. Conf. on "An International Perspective on Environmental and Water Resources" at AIT. EWRI and AIT.

[240] Sahu, A., Yadav, N., and Sudhakar, K. (2016), Floating photovoltaic power plant: A review. Renewable and sustainable energy reviews, 66, pp.815-824. https:// doi.org/10.1016/j.rser.2016.08.051.

[241] Sandnes, B., and Rekstad, J. (2002), A photovoltaic/thermal (PV/T) collector with a polymer absorber plate. Experimental study and analytical model. Solar Energy, 72(1), pp.63-73.

[242] Santafé -Redón, M., Ferrer-Gisbert, P.S., Sánchez-Romero, F.J., Torregrosa Soler, J.B., Ferrán Gozálvez, J.J., and Ferrer Gisbert, C.M. (2014), Implementation of a photovoltaic floating cover for irrigation reservoirs. Journal of cleaner production, 66, pp.568-570.

[243] Santafé, Redón M., Torregrosa Soler, J.B., Sánchez Romero, F.J., Ferrer Gisbert, P.S., Ferrán Gozálvez, J.J., and Ferrer Gisbert, C.M. (2014). Theoretical and experimental analysis of a floating photovoltaic cover for water irrigation reservoirs. Energy 67, 246–255. https://doi.org/10.1016/j.energy.2014.01.083.

[244] Santos, F.R. dos, Wiecheteck, G.K., Virgens Filho, J.S. das, Carranza, G.A., Chambers, T.L., and Fekih, A. (2022), Effects of a Floating Photovoltaic System on the Water Evaporation Rate in the Passaúna Reservoir, Brazil. Energies 15, 6274. https://doi.org/10.3390/en15176274.

[245] Sarver, T., Al-Qaraghuli, A., and Kazmerski L. L. (2013), A comprehensive review of the impact of dust on the use of solar energy: History, investigations, results, literature, and mitigation approaches, Renewable and Sustainable Energy Reviews, vol. 22, pp. 698–733, Jun. 2013, doi: 10.1016/J.RSER.2012.12.065.

[246] Schott, T. (1985), Operation temperatures of PV modules. Photovoltaic solar energy conference 1985, pp. 392-396.

[247] Schill, C., Brachmann, S., and Koehl, M. (2015), Impact of soiling on IV-curves and efficiency of PV-modules. Solar Energy, 112, 259–262. https://doi.org/10.1016/J.SOLENER.2014.12.003.

[248] Segado Mora P., Carretero J., and Sidrach-de-Cardona M. (2015), Models to predict the operating temperature of different photovoltaic modules in outdoor conditions. Progress in Photovoltaics: Research and Applications. 23(10):1267-82.

[249] Semeskandeh S., Hojjat M., Hosseini Abardeh M. (2022), Techno–economic–environmental comparison of floating photovoltaic plant with conventional solar photovoltaic plant in northern Iran. Clean Energy, 6(2):353-61.

[250] Sene, K.J., Gash, J.H.C. and McNeil, D.D. (1991). Evaporation from a tropical lake: comparison of theory with direct measurements. J. Hydrology. 127, 193-217.

[251] Servant, J.M. (1986), Calculation of the cell temperature for photovoltaic modules from climatic data, ISES 1986, pp. 1640-1643.

[252] Sharma, A. K., and Kothari, D. P. (2016), Uninterrupted green power using floating solar PV with pumped hydro energy storage & hydroelec- tric in India. *International Journal for Innovative Research in Science & Technology*, *3*(4), 2349–6010.

[253] Shirgure, P.S. (2012), Evaporation modeling with multiple linear regression techniques–a review. Scientific Journal of Review. 1(6):170-82.

[254] Shockley, William, and Queisser, Hans J. (1961), Detailed Balance Limit of Efficiency of *p-n* Junction Solar Cells. *J. Appl. Phys.* 1 March 1961; 32 (3): 510–519. https://doi.org/10.1063/1.1736034.

[255] Shrivastava, S. K., Singh, S. S., and Singh, R. (2001), Estimation of Evaporation Losses in India. Journal of the Indian Water Resources Society 21, no. 3: 11-16.

[256] Shyam, B., and Kanakasabapathy, P. (2022), Feasibility of floating solar PV integrated pumped storage system for a grid-connected microgrid under static time of day tariff environment: A case study from India,Renewable Energy,Volume 192,2022,Pages 200-215,ISSN 0960-1481, https://doi.org/10.1016/j.renene.2022.04.031.

[257] Sicart, J.E., Hock, R., Ribstein, P., and Chazarin, J.P. (2010), Sky longwave radiation on tropical Andean glaciers: parameterization and sensitivity to atmospheric variables. Journal of Glaciology, **56**(199), 854–860. https://doi.org/10.3189/002214310794457182.

[258] Singh, Raj, R.S., Bishnoi, O.P., and Ram Niwas, R.N. (1992), Relationship between evaporation from US class A open pan evaporimeter and meteorological parameters at Hisar.

[259] Singh, A.R., Kumar, R.S., Bajaj, M., Khadse, C.B., and Zaitsev, I. (2024), Machine learning-based energy management and power forecasting in grid-connected microgrids with multiple distributed energy sources. Scientific Reports. 14(1):19207.

[260] Singh, V. P., and Xu, C. Y. (1997), Evaluation and generalization of radiation-based methods for calculating evaporation. Hydrological Processes 11, no. 3: 339-349.

[261] Singh, V.P., and Xu, C. (1997), Evaluation and generalization of 13 mass-transfer equations for determining free water evaporation. J. Hydrology. Processes 11, 311-323.

[262] Singh, A.K., Boruah, D., Sehgal, L., and Ramaswamy, A.P. (2019), Feasibility study of a grid-tied 2MW floating solar PV power station and e-transportation facility using 'SketchUp Pro'for the proposed smart city of Pondicherry in India. Journal of Smart Cities, 2(2), pp.49-59.

[263] Sirindhorn dam (2021), "Thailand switches on 45MW floating solar plant, plans for 15 more". *RenewEconomy*. 11 November 2021."Thailand's massive floating solar farm lays the foundation for its emission-free future". *ZME Science*. 10 March 2022.

[264] Skoplaki, E., Boudouvis, A.G., and Palyvos, J.A. (2008), A simple correlation for the operating temperature of photovoltaic modules of arbitrary mounting. Solar Energy Materials and Solar Cells, volume 92, pp. 1393-1402.

[265] Skoplaski, E., and Palyvos, J.A. (2009), Operating temperature of photovoltaic modules: a survey of pertinent correlations. Renew. Energy, 34, pp. 23-29.

[266] Skoplaki, E., and Palyvos, J. A. (2009), On the temperature dependence of photovoltaic module electrical performance: A review of efficiency/power correlations. Solar Energy. https://doi.org/10.1016/j.solener.2008.10.008.

[267] Sohani, A., Sayyaadi, H., Cornaro, C., Shahverdian, M.H., Pierro, M., Moser, D., Karimi, N., Doranehgard, M.H., and Li, L.K. (2022), Using machine learning in photovoltaics to create smarter and cleaner energy generation systems: A comprehensive review. Journal of Cleaner Production, 364, p.132701.

[268] "Solar Target: India set to miss 2022 solar target by 27 per cent: Report - The Economic Times." https://economictimes.indiatimes.com/industry/renewables/india-set-to-miss-2022-solar-target-by-27-per-cent-report/articleshow/90790566.cms (accessed Aug. 16, 2022).

[269] Stephens, J.C., and Stewart, E.H. (1963), A comparison of procedures for computing evaporation and evapotranspiration. Publication 62, 123–133.

[270] Stultz, J. W. (1979), Thermal and other tests of photovoltaic modules performed in natural sunlight. Journal of Energy 3, no. 6: 363-372.

[271] Stultz, J.W., and Wen, L.C. (1977), Thermal Performance Testing and Analysis of Photovoltaic Modules in Natural Sunlight, LSA Task Report 5101-31, July 29, 1977.

[272] Sudhakar, K. (2019), SWOT analysis of floating solar plants. Sol. Photoenergy Syst. MOJ, 3–6.

[273] Sugita M., and Brutsaert W. (1993), Cloud effect in the estimation of instantaneous downward long-wave radiation. Water Resour Res 29:599–605.

[274] Sukarso, Adimas Pradityo, and Kyung, Nam Kim (2020), Cooling Effect on the Floating Solar PV: Performance and Economic Analysis on the Case of West Java Province in Indonesia. *Energies* 13, no. 9: 2126. https://doi.org/10.3390/en13092126

[275] Sulaeman, S., Brown, E., Quispe-Abad, R., and Müller, N. (2021), Floating PV system as an alternative pathway to the amazon dam underproduction. Renewable and Sustainable Energy Reviews, 135, p.110082.

[276] Sutanto B., Indartono Y.S., Wijayanta A.T. and Iacovides H. (2022), Enhancing the Performance of Floating Photovoltaic System by Using Thermosiphon Cooling Method: Numerical and Experimental Analyses, International Journal of Thermal Sciences, vol. 180, 107727.

[277] Swinbank, W.C. (1963), Long-wave radiation from clear skies. Quarterly Journal of the Royal Meteorological Society, 89(381), pp.339-348.

[278] Sweers, H.E. (1976), A nomogram to estimate the heat-exchange coefficient at the air-water interface as a function of wind speed and temperature, a critical survey of some literature. J. Hydrol. 30, 375-401.

[279] Tavakkoli, Mehdi, Adabi, Jafar, Zabihi, Sasan, Godina, Radu, and Pouresmaeil, Edris (2018), Reserve allocation of photovoltaic systems to improve frequency stability in hybrid power systems. Energies, 11(10), 2583.

[280] Tan C.S., Tan L.W. and Tan C.W. (2021), Floating Structure with Stabilised Buoyancy Control Device for Photovoltaic Application, IOP Conf. Series: Earth and Environmental Science, vol. 945, 012072.

[281] Tetens, O. (1930), Uber einige meteorologische Begriffe. Z. geophys, 6, pp.297-309.

[282] Three Gorges (2022), "5 Largest Floating Solar Farms in the World in 2022". *YSG Solar*. 20 January 2022. "Floating PV System - Commercial solar photovoltaic installers". *en.sungrowpower.com*. Retrieved 2023-03-14.

[283] Tina, G.M., Scavo, F.B., Merlo, L., and Bizzarri, F. (2021), Analysis of water environment on the performances of floating photovoltaic plants. Renewable Energy, 175, pp.281-295.

[284] Tina, G.M., Scavo, F.B., Micheli, L., and Rosa-Clot, M. (2023), Economic comparison of floating photovoltaic systems with tracking systems and active cooling in a Mediterranean water basin. Energy for Sustainable Development. 76:101283.

[285] Trapani, Kim, Redón Santafé, Miguel (2015), A review of floating photovoltaic installations: 2007-2013. Progress in Photovoltaics: Research and Applications.23 (4): 524-532. doi:10.1002/pip.2466. hdl:10251/80704. S2CID 98460653.

[286] Thornthwaite, C. W. (1948), An Approach toward a Rational Classification of Climate. Geographical Review, 38(1), 55. https://doi.org/10.2307/210739.

[287] Ubol Ratana dam (2024), "Hydro-floating Solar Hybrid at Ubol Ratana Dam starts commercial operation, driving Thailand toward Carbon Neutrality". *EGAT - Electricity Generating Authority of Thailand*. 2024-03-06. Archived from the original on 2024-03-23. Retrieved 2024-03-23.

[288] Uttar Pradesh Irrigation and Water Resources Department (UPIWRD) data, (http://idup.gov.in/pages/en/topmenu/existing-infrastructure/en-dams-and-reservoirs, accessed on 28.09.2020).

[289] Veldhuis, A.J., Nobre, A., Reindl, T., Rüther, R., and Reinders, A.H. (2013), June. The influence of wind on the temperature of PV modules in tropical environments, evaluated on an hourly basis. In 2013 IEEE 39th Photovoltaic Specialists Conference (PVSC) (pp. 0824-0829). IEEE.

[290] Wang, B., Wang, Z., Sun, Y., Wang, F., Zhen, Z., Zengqiang, M., and Ren, H. (2016), Research on influence between photovoltaic power and module temperature and ambient temperature. In 2016 IEEE International Conference on Power System Technology (POWERCON) (pp. 1-5). IEEE.

[291] Wasthage, Louise (2017), Optimization of floating PV systems : Case study for a shrimp farm in Thailand [Internet] [Dissertation]. Available from: https://urn.kb.se/resolve?urn=urn:nbn:se:mdh:diva-36015.

[292] Winter, T.C., and Rosenberry, D.O. (1995), Evaluation of 11 equations for determining evaporation for a small lake in the north central United States. Water Resour. Res. 31, 983- 993.

[293] WMO (1983), Guide to meteorological instruments and methods of observation, WMO-8, 5th edition, World Meteorological Organization, Geneva.

[294] WMO (2008), Guide to Meteorological Instruments and Methods of Observation.

[295] World Bank Group; ESMAP; SERIES (2019), Where Sun Meets Water (Vol. 2): Floating Solar Market Report (English). Washington, D.C.: World Bank Group. http://documents.worldbank.org/curated/en/670101560451219695/Floating-Solar-Market-Report.

[296] Worringham, Charles (2021), “IEEFA: Reducing land-use impacts of renewable generation could smooth the path for India’s energy transition | IEEFA.”, september2021. https://ieefa.org/articles/ieefa-reducing-land-use-impacts-renewable-generation-could-smooth-path-indias-energy (accessed Aug. 16, 2022).

[297] Xiong, L., Le, C., Zhang, P., Ding, H., and Li J. (2023), Harnessing the power of floating photovoltaic: A global review. Journal of Renewable and Sustainable Energy. Sep 1;15(5).

[298] Yadav, N., Gupta, M., and Sudhakar, K. (2016), December. Energy assessment of floating photovoltaic system. In 2016 International Conference on Electrical Power and Energy Systems (ICEPES) (pp. 264-269). IEEE.

[299] Yao, X., Zhang, H., Lemckert, C., Brook, A., and Schouten, P. (2010), Evaporation Reduction by Suspended and Floating Covers: Overview, Modelling and Efficiency. Urban Water Security Research Alliance Technical Report. http://hdl.handle.net/10072/37724http://www.urbanwateralliance.org.au/.

[300] Youssef, Y.W., and Khodzinskaya, A. (2019), A review of evaporation reduction methods from water surfaces. In E3S web of conferences (Vol. 97, p. 05044). EDP Sciences.

[301] Yuanziang yiyang (2019), "Floating PV System - Commercial solar photovoltaic installers". *en.sungrowpower.com*. Retrieved 2023-03-14.

[302] Zahedi, R., Ranjbaran, P., Gharehpetian, G.B., Mohammadi, F., and Ahmadiahangar, R. (2021), Cleaning of floating photovoltaic systems: a critical review on approaches from technical and economic perspectives. Energies, 14(7), p.2018.

[303] Zhao, J., Wang, A., Green, M.A., and Ferrazza, F. (1998), 19.8% efficient “honeycomb” textured multicrystalline and 24.4% monocrystalline silicon solar cells. Applied physics letters, 73(14), pp.1991-1993.https://doi.org/10.1063/1.122345.

[304] Zhao, Y., Zhang, R., Li, H., Shang, J., Hao, R., and Sun, X. (2024), Advancing floating photovoltaic systems: trends, challenges, and future directions in sustainable energy development. International Journal of Green Energy. 1-22.

[305] Zubair, M., Bilal Awan, A., Ghuffar, S., Butt, A.D., and Farhan, M. (2020), Analysis and selection criteria of lakes and dams of Pakistan for floating photovoltaic capabilities. Journal of Solar Energy Engineering, 142(3), p.031001.

[306] Zotarelli L., Dukes M.D., Romero C.C., Migliaccio K.W., and Morgan K.T. (2010), Step-by-step calculation of the Penman-Monteith Evapotranspiration (FAO-56 Method). Institute of Food and Agricultural Sciences. University of Florida. 8.

List of Publications

Publication in Journals

- Agrawal, K.K., Jha, S.K., Mittal, R.K., Singh, A.P., Vashishtha, S., (2022), Assessment of Floating Solar PV (FSPV) Potential and Water Conservation: Case Study on Rajghat Dam in Uttar Pradesh, India. **Energy for Sustainable Development,** 66, 287–295, (**Impact Factor: 4.4, Cite Score: 8.1, SNIP:1.244)**, https://doi.org/10.1016/j.esd.2021.12.007 https://www.sciencedirect.com/science/article/pii/S0973082621001514.
- Agrawal, K.K., Jha, S.K., Mittal, R.K., Singh, A.P., Vashishtha, S., Gupta, S., Soni, M.K.,(2024), Predictive Modeling of Solar PV Panel Operating Temperature over Water Bodies: Comparative Performance Analysis with Ground-Mounted Installations. **Energies** 2024, 17, 3489. https:// doi.org/10.3390/en17143489 **(Impact Factor: 3, Cite Score: 6.2, SNIP:0.947).**
- Agrawal, K.K., Mittal, R.K., Jha, S.K., Singh, A.P., Vashishtha, S., Soni, M.K.,(2024), Experimental Studies and Analysis for Performance Assessment of Floating Solar Photovoltaic Systems, **IOP Conference Series: Earth and Environmental Science**, 1375 (2024) 012023. doi:10.1088/1755-1315/1375/1/012023 **(SCOPUS, Cite Score: 1.0, SNIP:0.325).**

Conference Attended

- Agrawal, K.K., Mittal, R.K., Jha, S.K., Singh, A.P., Vashishtha, S., Soni, M.K. Experimental Studies and Analysis for Performance Assessment of Floating Solar Photovoltaic Systems. In Proceedings of the International Conference on Smart and Sustainable Energy Systems (Presented in ICSSES 2024), Vishnu Institute of Technology, Bhimavaram, Andhra Pradesh, India, 16–17 February 2024; Paper ID-47.
- Agrawal, K.K., Jha, S.K., Mittal, R.K., Singh, A.P., Vashishtha, S., (2024), Floating Solar Photovoltaic (FSPV) Installations at Varying Heights: Evaporation Reduction Estimation for Major Dams of Tropical Region of Uttar Pradesh, India. IoP Fourth International Conference on Sustainable Energy, Environment and Green Technologies, (ICSEEGT-2024). **(accepted and to be presented on 9th August 2024).**

Paper submitted for Journal Publication

- Agrawal, K.K., Jha, S.K., Mittal, R.K., Singh, A.P., Vashishtha, S., Joshi Hitesh (2024), Experimental Setup and Data Analysis for Assessing the Impact of Floating Solar PV (FSPV) on Water Temperature Reduction and Evaporation Loss Mitigation for Aquatic

Sustainability. Special issue on ‘Ecological, evolutionary and environmental implications of floating photovoltaics (floatovoltaics) on freshwater ecosystems’ Journal for Knowledge and Management of Aquatic Ecosystems **(Submitted, 2024)**.

- Agrawal, K.K., Singh, A.P., Mittal, R.K., Jha, S.K., Vashishtha, S., (2024), Evaporation Dynamics: Analysis of experimental data and Model Development for open and PV covered water bodies. Environmental Monitoring and Assessment **(Submitted, 2024)**.
- Agrawal, K.K., Singh, A.P., Mittal, R.K., Jha, S.K., Vashishtha, S., (2024), FSPV Installations and Decision making : A case study of major dams located in tropical region of Uttar Pradesh, India. Environment, Development and Sustainability **(Submitted, 2024)**.

Annexure A5

Plots of predicted panel temperature vs recorded panel temperature by best performing F3 model.

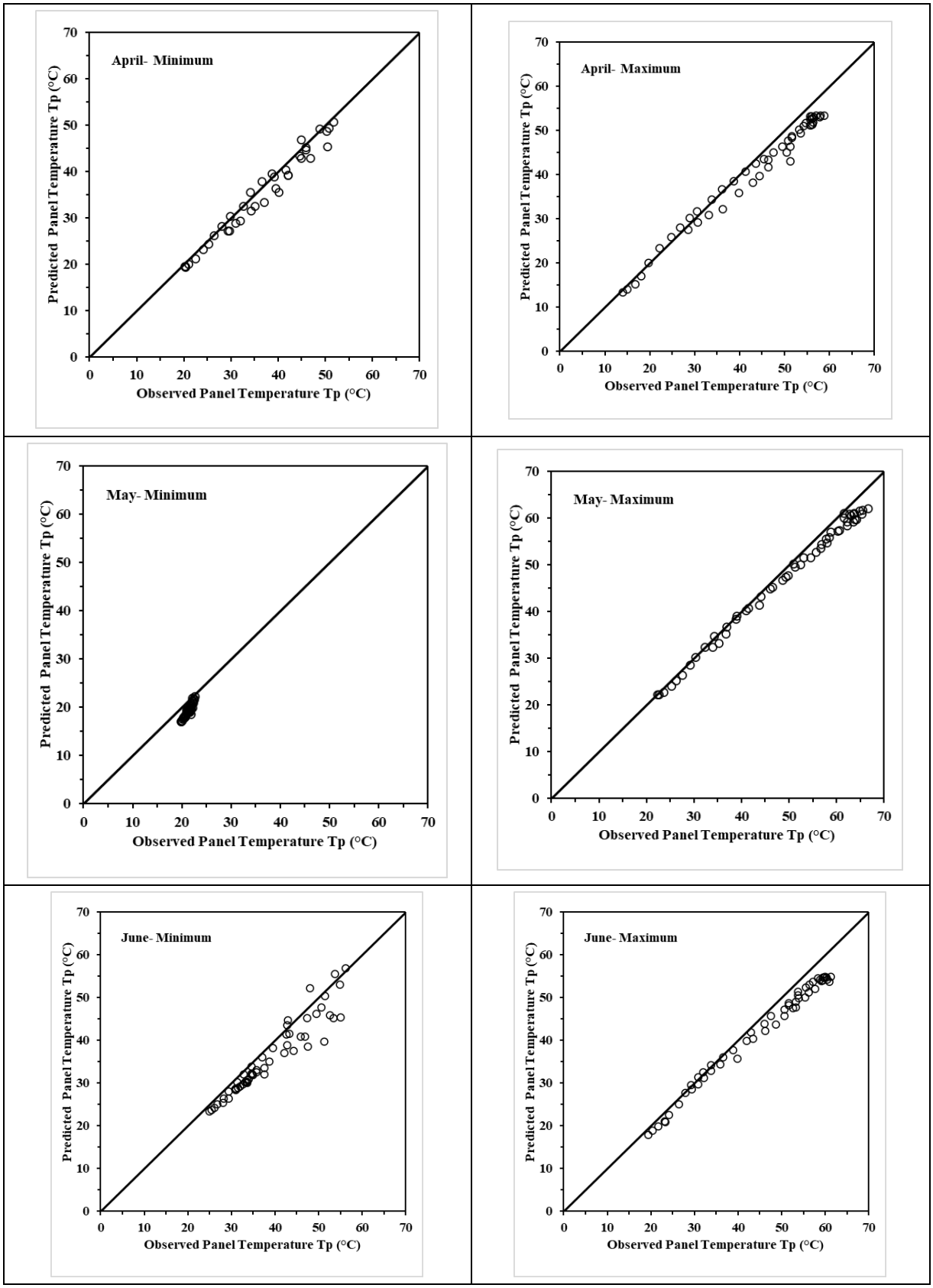

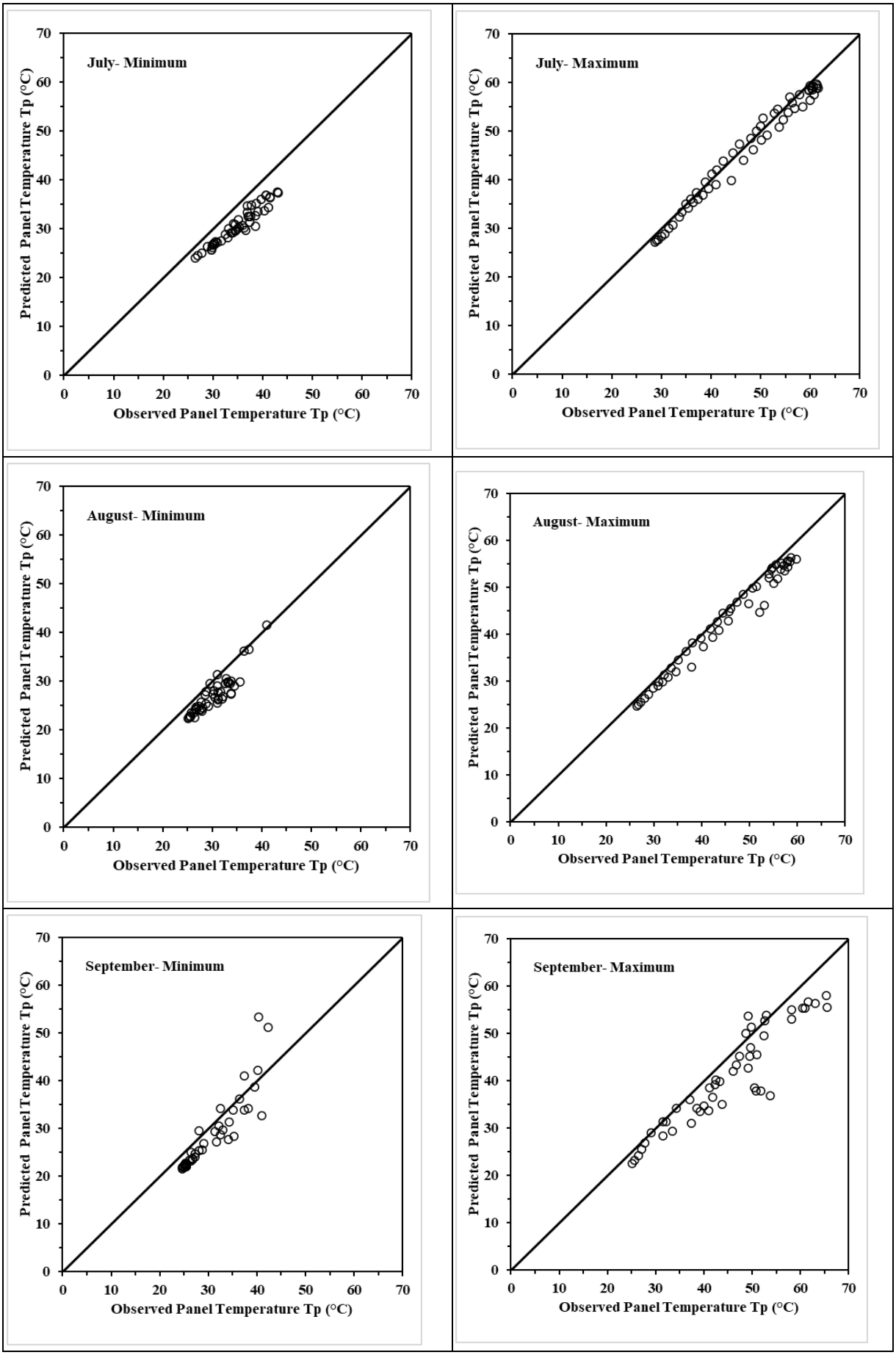
July- Minimum
Predicted Panel Temperature Tp (°C)
Observed Panel Temperature Tp (°C)
July- Maximum
Predicted Panel Temperature Tp (°C)
Observed Panel Temperature Tp (°C)
August- Minimum
Predicted Panel Temperature Tp (°C)
Observed Panel Temperature Tp (°C)
August- Maximum
Predicted Panel Temperature Tp (°C)
Observed Panel Temperature Tp (°C)
September- Minimum
Predicted Panel Temperature Tp (°C)
Observed Panel Temperature Tp (°C)
September- Maximum
Predicted Panel Temperature Tp (°C)
Observed Panel Temperature Tp (°C)

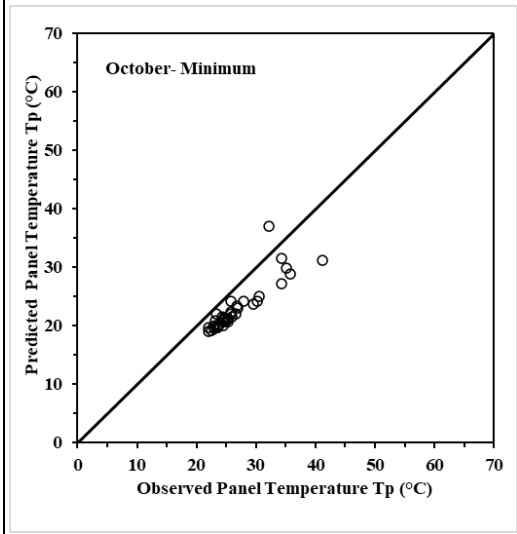
October- Minimum
Predicted Panel Temperature Tp (°C)
Observed Panel Temperature Tp (°C)
0
10
20
30
40
50
60
70

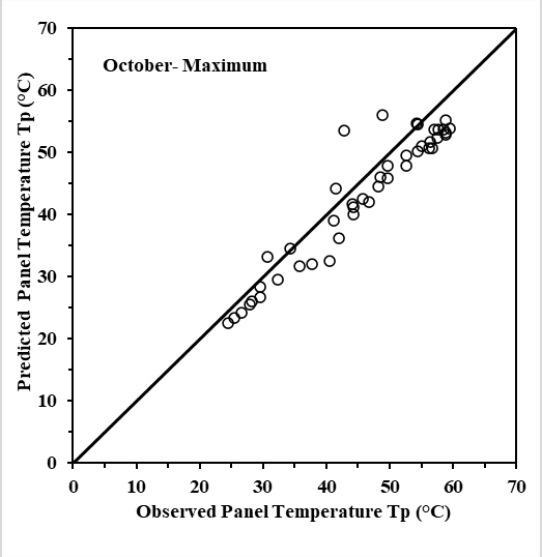
October- Maximum
Predicted Panel Temperature Tp (°C)
Observed Panel Temperature Tp (°C)
0
10
20
30
40
50
60
70

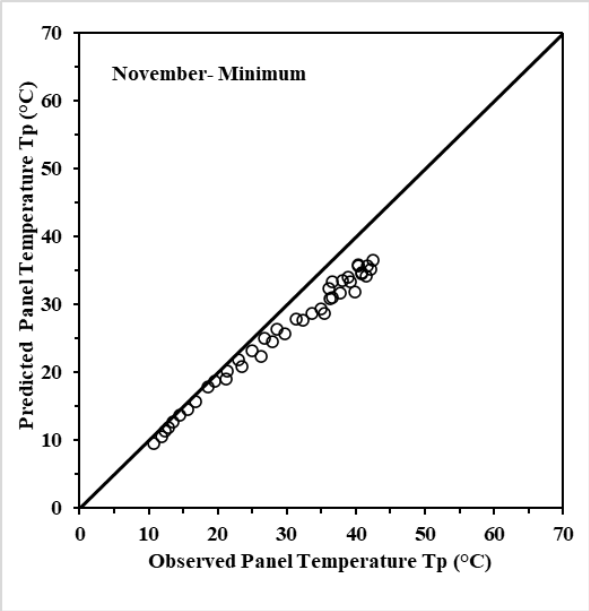
November- Minimum
Predicted Panel Temperature Tp (°C)
Observed Panel Temperature Tp (°C)
0
10
20
30
40
50
60
70

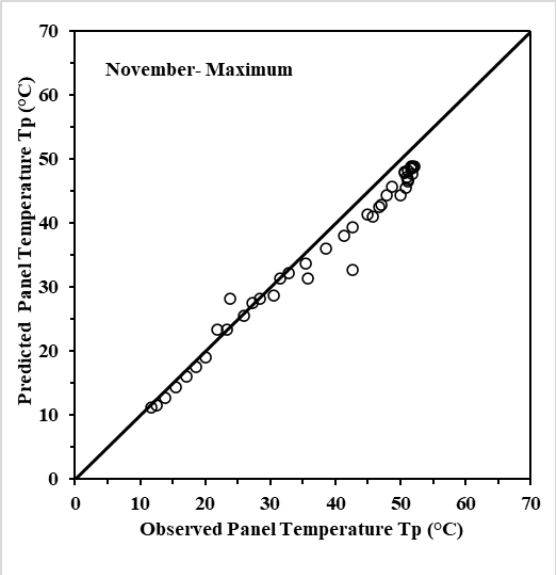
November- Maximum
Predicted Panel Temperature Tp (°C)
Observed Panel Temperature Tp (°C)
0
10
20
30
40
50
60
70

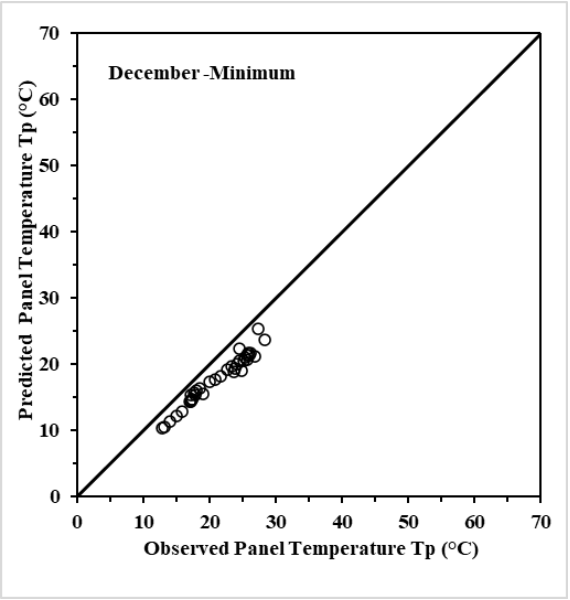
December -Minimum
Predicted Panel Temperature Tp (°C)
Observed Panel Temperature Tp (°C)
0
10
20
30
40
50
60
70

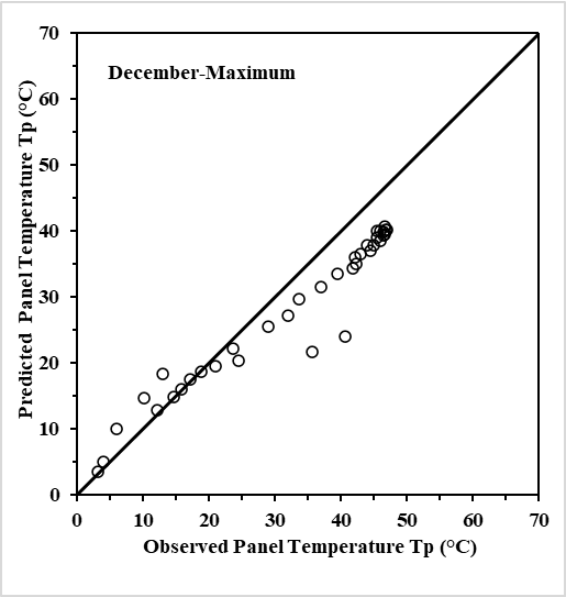
December-Maximum
Predicted Panel Temperature Tp (°C)
Observed Panel Temperature Tp (°C)
0
10
20
30
40
50
60
70

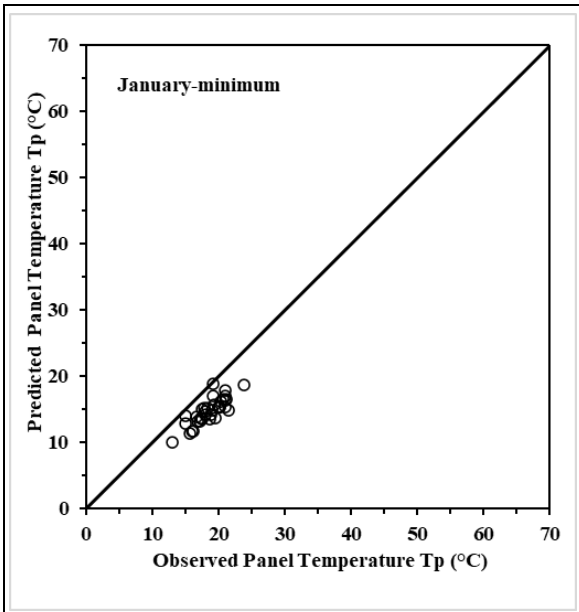
January-minimum
Predicted Panel Temperature Tp (°C)
Observed Panel Temperature Tp (°C)
0
10
20
30
40
50
60
70

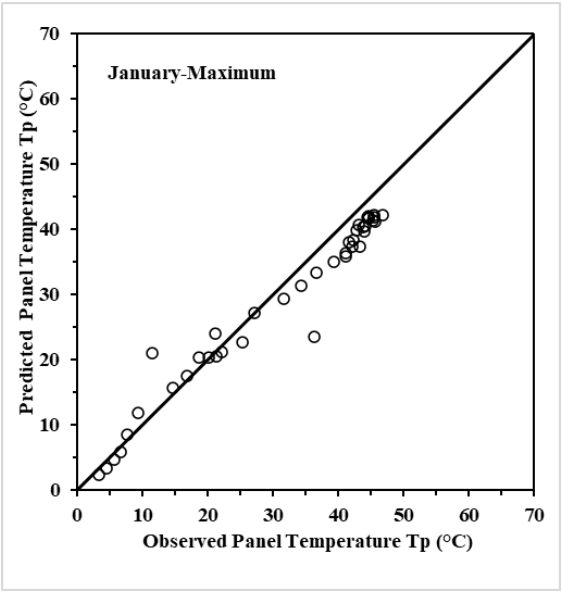
January-Maximum
Predicted Panel Temperature Tp (°C)
Observed Panel Temperature Tp (°C)
0
10
20
30
40
50
60
70

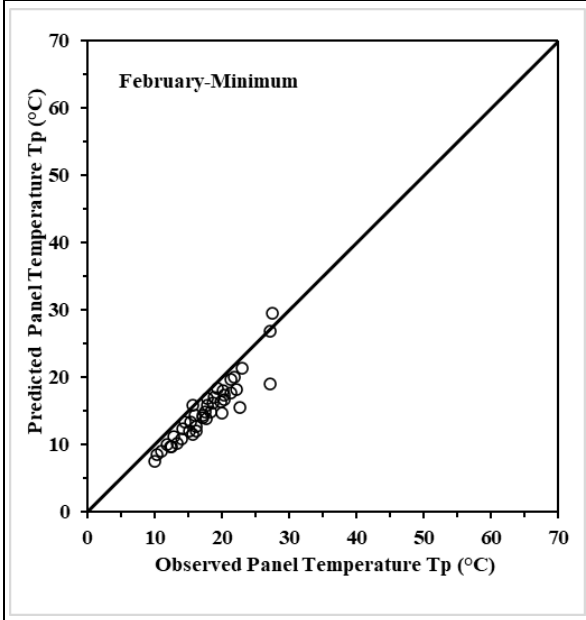
February-Minimum
Predicted Panel Temperature Tp (°C)
Observed Panel Temperature Tp (°C)
0
10
20
30
40
50
60
70

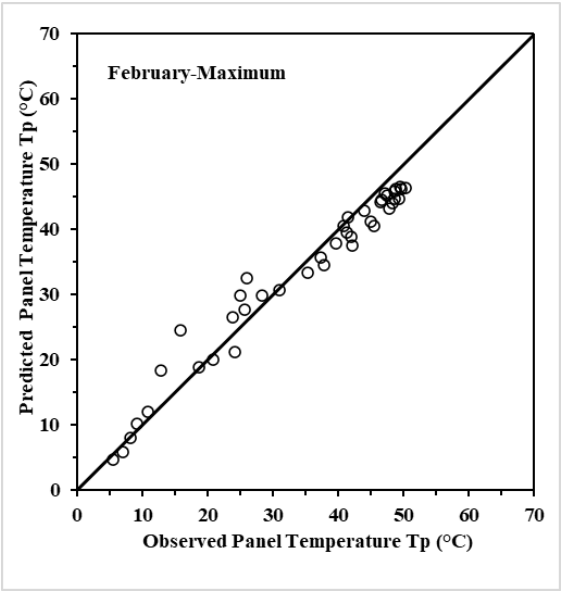
February-Maximum
Predicted Panel Temperature Tp (°C)
Observed Panel Temperature Tp (°C)
0
10
20
30
40
50
60
70

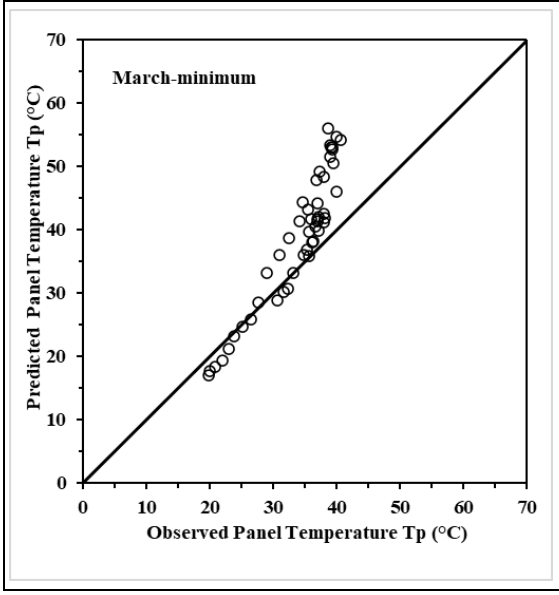
March-minimum
Predicted Panel Temperature Tp (°C)
Observed Panel Temperature Tp (°C)
0
10
20
30
40
50
60
70

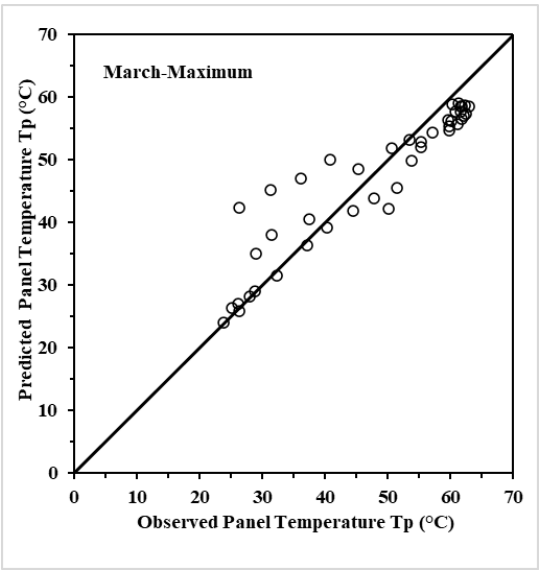
March-Maximum
Predicted Panel Temperature Tp (°C)
Observed Panel Temperature Tp (°C)
0
10
20
30
40
50
60
70

Appendix A8.3.6-A: Software Listing for Computation of Angstrom Constant

Source code for estimating values of a_s and b_s is

```
#!/usr/bin/env python
# coding: utf-8
# In[1]:
import pandas as pd
import glob
import os
from sklearn.metrics import r2_score
import math
from functools import partial
from sklearn.metrics import mean_absolute_error, mean_squared_error
import numpy as np
import scipy, scipy.optimize
# In[2]:
ls
# ## Read Data from CSV File and Analyzing it
# In[3]:
df_raw = pd.read_csv('Compiled Data_v1.csv', parse_dates=['Date'])
# In[4]:
df_raw.info()
# In[5]:
df_raw.head()
# In[6]:
df_raw.describe()
# In[7]:
df_raw.isna().sum()
# In[8]:
def global_formula(N, Ra, n, a= 0.25, b= 0.5):
 return Ra*(a + (b * (n/N)))
# ### Calculating the land solar temperature using global formula and global values of and b
# In[9]:
df_raw['Rs_Cal'] = df_raw.apply(lambda x: global_formula(x[3], x[4], x[5]), axis=1)
# In[10]:
```

```
df_raw.head()

# In[11]:

df_raw = df_raw[df_raw['Season']=='Monsoon']

# In[12]:

df_raw.head()

# In[13]:

print("R2 Score:", "%.3f" %r2_score(df_raw['Rs'], df_raw['Rs_Cal']))

print("Mean Squared Error:", "%.3f" %mean_squared_error(df_raw['Rs'], df_raw['Rs_Cal']))

print("Root Mean Squared Error:", "%.3f" %np.sqrt(mean_squared_error(df_raw['Rs'],
df_raw['Rs_Cal'])))

print("Mean Absolute Error:", "%.3f" %mean_absolute_error(df_raw['Rs'],
df_raw['Rs_Cal']))

# In[ ]:

# # Finding the value of a and b of global formula on our custom data

# In[14]:

def calculate_custom_a_b(X, a, b):

    N, Ra, n =  X[0], X[1], X[2]

    return Ra*(a + b * (n/N))

# In[15]:

x, y, z, p = df_raw['N'], df_raw['Ra'], df_raw['n'], df_raw['Rs']

# In[16]:

fittedParameters, pcov = scipy.optimize.curve_fit(calculate_custom_a_b, [x, y, z], p)

# In[17]:

fittedParameters

# In[18]:

df_raw['Rs_cal_fit'] = df_raw.apply(lambda x: global_formula(x[3], x[4], x[5],
a=fittedParameters[0], b=fittedParameters[1]), axis=1)

# In[19]:

print("R2 Score for custom a and b:", "%.3f" %r2_score(df_raw['Rs'], df_raw['Rs_cal_fit']))

print("Mean Squared Error for custom a and b:", "%.3f" %mean_squared_error(df_raw['Rs'],
df_raw['Rs_cal_fit']))

print("Root Mean Squared Error for custom a and b:", "%.3f"
%np.sqrt(mean_squared_error(df_raw['Rs'], df_raw['Rs_cal_fit'])))

print("Mean Absolute Error for custom a and b:", "%.3f"
%mean_absolute_error(df_raw['Rs'], df_raw['Rs_cal_fit']))

# In[ ]:

# In[ ]:

# In[ ]:
```

Appendix A8.3.6-B: Computational data for assessing Angstrom Constant

Date	Month	N	Ra	n	Rs
02/04/20	4.00	12.3	35.0	10.25	23.80
03/04/20	4.00	12.3	35.2	10.50	23.74
04/04/20	4.00	12.4	35.4	10.25	23.10
05/04/20	4.00	12.4	35.5	7.25	13.66
06/04/20	4.00	12.4	35.7	10.50	22.83
07/04/20	4.00	12.4	35.8	10.25	20.49
08/04/20	4.00	12.5	36.0	10.50	23.40
09/04/20	4.00	12.5	36.1	10.50	23.17
10/04/20	4.00	12.5	36.3	10.00	22.47
11/04/20	4.00	12.6	36.4	10.00	22.28
12/04/20	4.00	12.6	36.6	10.75	22.38
13/04/20	4.00	12.6	36.7	10.25	21.00
14/04/20	4.00	12.6	36.8	9.25	18.14
15/04/20	4.00	12.7	37.0	9.50	22.88
16/04/20	4.00	12.7	37.1	10.25	20.80
17/04/20	4.00	12.7	37.2	10.50	18.64
18/04/20	4.00	12.8	37.4	9.75	18.12
19/04/20	4.00	12.8	37.5	10.00	20.28
20/04/20	4.00	12.8	37.6	9.25	16.06
21/04/20	4.00	12.8	37.7	10.25	19.96
22/04/20	4.00	12.9	37.9	10.50	21.84
23/04/20	4.00	12.9	38.0	9.75	15.41
24/04/20	4.00	12.9	38.1	9.75	19.31
25/04/20	4.00	12.9	38.2	10.50	21.69
26/04/20	4.00	13.0	38.3	10.50	21.29
27/04/20	4.00	13.0	38.4	11.00	23.17
28/04/20	4.00	13.0	38.5	10.75	20.35
29/04/20	4.00	13.0	38.6	10.75	21.86
30/04/20	4.00	13.1	38.7	10.75	21.62
01/05/20	5.00	13.1	38.8	10.75	23.35
02/05/20	5.00	13.1	38.9	11.00	23.84
03/05/20	5.00	13.1	39.0	7.00	12.31
04/05/20	5.00	13.2	39.1	10.50	21.46
05/05/20	5.00	13.2	39.2	9.00	22.88
06/05/20	5.00	13.2	39.3	9.25	19.25
07/05/20	5.00	13.2	39.3	10.25	24.37
08/05/20	5.00	13.3	39.4	11.00	24.32
09/05/20	5.00	13.3	39.5	10.75	22.08
10/05/20	5.00	13.3	39.6	7.50	15.62
11/05/20	5.00	13.3	39.6	8.00	10.37
12/05/20	5.00	13.3	39.7	9.75	20.77
13/05/20	5.00	13.4	39.8	9.75	14.53
14/05/20	5.00	13.4	39.9	11.00	23.69
15/05/20	5.00	13.4	39.9	10.25	22.10
16/05/20	5.00	13.4	40.0	10.50	23.18
17/05/20	5.00	13.4	40.0	11.00	19.82
18/05/20	5.00	13.5	40.1	11.00	23.86

Date	Month	N	Ra	n	Rs
19/05/20	5.00	13.5	40.2	11.00	25.85
20/05/20	5.00	13.5	40.2	11.50	26.85
21/05/20	5.00	13.5	40.3	11.50	26.98
22/05/20	5.00	13.5	40.3	11.25	25.86
23/05/20	5.00	13.5	40.4	10.50	25.18
24/05/20	5.00	13.6	40.4	10.75	25.00
25/05/20	5.00	13.6	40.5	11.00	25.15
26/05/20	5.00	13.6	40.5	11.25	22.09
27/05/20	5.00	13.6	40.5	11.25	26.79
28/05/20	5.00	13.6	40.6	10.75	23.68
29/05/20	5.00	13.6	40.6	10.00	19.75
30/05/20	5.00	13.7	40.7	11.50	24.54
31/05/20	5.00	13.7	40.7	10.25	22.23
01/06/20	6.00	13.7	40.7	9.25	23.06
02/06/20	6.00	13.7	40.7	10.50	22.74
03/06/20	6.00	13.7	40.8	10.75	16.78
04/06/20	6.00	13.7	40.8	8.00	19.07
05/06/20	6.00	13.7	40.8	10.25	21.96
06/06/20	6.00	13.7	40.8	11.25	22.90
07/06/20	6.00	13.7	40.9	10.75	19.50
08/06/20	6.00	13.8	40.9	11.25	24.05
09/06/20	6.00	13.8	40.9	9.00	21.06
10/06/20	6.00	13.8	40.9	10.00	19.74
11/06/20	6.00	13.8	40.9	9.75	21.19
12/06/20	6.00	13.8	40.9	10.00	24.19
13/06/20	6.00	13.8	41.0	10.25	21.67
14/06/20	6.00	13.8	41.0	10.75	23.49
15/06/20	6.00	13.8	41.0	11.25	24.30
16/06/20	6.00	13.8	41.0	9.75	23.08
17/06/20	6.00	13.8	41.0	11.25	24.09
18/06/20	6.00	13.8	41.0	11.25	21.47
19/06/20	6.00	13.8	41.0	10.25	21.65
20/06/20	6.00	13.8	41.0	9.75	21.30
21/06/20	6.00	13.8	41.0	10.25	16.43
22/06/20	6.00	13.8	41.0	10.50	23.32
23/06/20	6.00	13.8	41.0	11.50	23.29
24/06/20	6.00	13.8	41.0	10.50	21.58
25/06/20	6.00	13.8	41.0	7.75	15.32
26/06/20	6.00	13.8	41.0	7.00	10.46
27/06/20	6.00	13.8	40.9	11.25	21.35
28/06/20	6.00	13.8	40.9	11.25	23.65
29/06/20	6.00	13.8	40.9	11.25	22.81
30/06/20	6.00	13.8	40.9	11.00	21.44
01/07/20	7.00	13.8	40.9	10.00	20.81
02/07/20	7.00	13.8	40.9	11.00	21.64
03/07/20	7.00	13.8	40.8	11.00	19.80
04/07/20	7.00	13.8	40.8	9.00	18.86
05/07/20	7.00	13.8	40.8	10.75	23.15

Date	Month	N	Ra	n	Rs
06/07/20	7.00	13.8	40.8	11.25	20.77
07/07/20	7.00	13.7	40.7	10.75	22.72
08/07/20	7.00	13.7	40.7	6.25	13.25
09/07/20	7.00	13.7	40.7	10.75	20.56
10/07/20	7.00	13.7	40.7	9.75	21.02
11/07/20	7.00	13.7	40.6	11.00	24.22
12/07/20	7.00	13.7	40.6	9.00	12.98
13/07/20	7.00	13.7	40.5	7.25	17.71
14/07/20	7.00	13.7	40.5	11.00	23.53
15/07/20	7.00	13.7	40.5	11.00	22.48
16/07/20	7.00	13.6	40.4	11.00	23.56
17/07/20	7.00	13.6	40.4	10.75	20.82
18/07/20	7.00	13.6	40.3	10.75	19.20
19/07/20	7.00	13.6	40.3	9.75	17.70
20/07/20	7.00	13.6	40.2	10.00	19.44
21/07/20	7.00	13.6	40.2	8.00	13.13
22/07/20	7.00	13.6	40.1	9.25	15.23
23/07/20	7.00	13.5	40.1	11.00	21.67
24/07/20	7.00	13.5	40.0	9.50	16.34
25/07/20	7.00	13.5	40.0	9.00	18.00
26/07/20	7.00	13.5	39.9	11.00	17.75
27/07/20	7.00	13.5	39.8	11.00	21.27
28/07/20	7.00	13.4	39.8	11.00	23.13
29/07/20	7.00	13.4	39.7	10.75	20.46
30/07/20	7.00	13.4	39.6	8.75	15.23
31/07/20	7.00	13.4	39.6	10.75	23.60
01/08/20	8.00	13.4	39.5	10.75	23.17
02/08/20	8.00	13.3	39.4	10.50	22.02
03/08/20	8.00	13.3	39.3	9.00	18.30
04/08/20	8.00	13.3	39.3	10.50	22.40
05/08/20	8.00	13.3	39.2	10.25	16.44
06/08/20	8.00	13.3	39.1	10.25	19.63
07/08/20	8.00	13.2	39.0	9.75	17.35
08/08/20	8.00	13.2	38.9	10.00	17.01
09/08/20	8.00	13.2	38.8	8.00	11.79
10/08/20	8.00	13.2	38.7	9.25	20.28
11/08/20	8.00	13.1	38.7	9.25	16.44
12/08/20	8.00	13.1	38.6	10.25	23.12
13/08/20	8.00	13.1	38.5	6.25	11.82
14/08/20	8.00	13.1	38.4	9.50	19.76
15/08/20	8.00	13.0	38.3	8.75	18.11
16/08/20	8.00	13.0	38.2	9.25	21.75
17/08/20	8.00	13.0	38.0	10.50	22.00
18/08/20	8.00	13.0	37.9	4.50	5.58
19/08/20	8.00	12.9	37.8	8.25	8.73
20/08/20	8.00	12.9	37.7	8.75	13.20
21/08/20	8.00	12.9	37.6	10.50	22.06
22/08/20	8.00	12.9	37.5	10.50	22.08

Date	Month	N	Ra	n	Rs
23/08/20	8.00	12.8	37.4	10.00	18.78
24/08/20	8.00	12.8	37.2	9.25	13.31
25/08/20	8.00	12.8	37.1	10.00	18.29
26/08/20	8.00	12.8	37.0	10.00	17.78
27/08/20	8.00	12.7	36.9	10.25	18.50
28/08/20	8.00	12.7	36.7	10.25	21.42
29/08/20	8.00	12.7	36.6	10.75	24.26
30/08/20	8.00	12.6	36.5	8.75	10.19
31/08/20	8.00	12.6	36.3	9.00	17.61
01/09/20	9.00	12.6	36.2	9.75	11.30
02/09/20	9.00	12.6	36.0	9.00	13.79
03/09/20	9.00	12.5	35.9	7.50	12.24
04/09/20	9.00	12.5	35.7	10.50	13.97
05/09/20	9.00	12.5	35.6	9.50	15.96
06/09/20	9.00	12.4	35.4	10.25	19.22
07/09/20	9.00	12.4	35.3	9.25	19.69
08/09/20	9.00	12.4	35.1	10.25	22.94
09/09/20	9.00	12.4	35.0	10.25	22.13
10/09/20	9.00	12.3	34.8	8.50	20.97
11/09/20	9.00	12.3	34.7	5.50	8.61
12/09/20	9.00	12.3	34.5	9.75	22.34
13/09/20	9.00	12.2	34.3	10.25	23.26
14/09/20	9.00	12.2	34.2	10.25	23.21
15/09/20	9.00	12.2	34.0	10.00	21.81
16/09/20	9.00	12.2	33.8	10.00	21.30
17/09/20	9.00	12.1	33.7	10.25	23.02
18/09/20	9.00	12.1	33.5	10.00	22.47
19/09/20	9.00	12.1	33.3	9.25	20.13
20/09/20	9.00	12.0	33.1	10.00	22.83
21/09/20	9.00	12.0	33.0	10.00	23.26
22/09/20	9.00	12.0	32.8	10.00	22.86
23/09/20	9.00	12.0	32.6	5.00	9.35
24/09/20	9.00	11.9	32.4	1.25	3.44
25/09/20	9.00	11.9	32.2	4.25	10.16
26/09/20	9.00	11.9	32.1	4.50	9.63
27/09/20	9.00	11.8	31.9	2.25	3.40
28/09/20	9.00	11.8	31.7	6.00	14.44
29/09/20	9.00	11.8	31.5	9.25	20.44
30/09/20	9.00	11.8	31.3	4.00	6.52
01/10/20	10.00	11.7	31.1	3.50	5.55
02/10/20	10.00	11.7	30.9	1.25	1.43
03/10/20	10.00	11.7	30.8	5.75	14.48
04/10/20	10.00	11.6	30.6	9.75	22.61
05/10/20	10.00	11.6	30.4	9.75	22.38
06/10/20	10.00	11.6	30.2	9.75	22.72
07/10/20	10.00	11.6	30.0	9.75	22.78
08/10/20	10.00	11.5	29.8	9.75	21.96
09/10/20	10.00	11.5	29.6	9.75	21.24

Date	Month	N	Ra	n	Rs
10/10/20	10.00	11.5	29.4	9.75	20.85
11/10/20	10.00	11.4	29.2	9.75	21.31
12/10/20	10.00	11.4	29.0	9.75	21.74
13/10/20	10.00	11.4	28.9	9.50	20.99
14/10/20	10.00	11.4	28.7	9.25	16.01
15/10/20	10.00	11.3	28.5	9.00	17.96
16/10/20	10.00	11.3	28.3	9.25	18.03
17/10/20	10.00	11.3	28.1	9.00	17.22
18/10/20	10.00	11.3	27.9	9.25	17.22
19/10/20	10.00	11.2	27.7	9.50	20.50
20/10/20	10.00	11.2	27.5	9.50	20.14
21/10/20	10.00	11.2	27.4	7.75	14.32
22/10/20	10.00	11.1	27.2	9.00	16.66
23/10/20	10.00	11.1	27.0	8.50	15.25
24/10/20	10.00	11.1	26.8	9.25	19.58
25/10/20	10.00	11.1	26.6	9.00	18.53
26/10/20	10.00	11.0	26.4	9.25	18.71
27/10/20	10.00	11.0	26.3	9.25	19.59
28/10/20	10.00	11.0	26.1	9.00	19.12
29/10/20	10.00	11.0	25.9	5.25	10.91
30/10/20	10.00	10.9	25.7	8.25	13.99
31/10/20	10.00	10.9	25.6	9.25	17.88
01/11/20	11.00	10.9	25.4	9.25	18.76
02/11/20	11.00	10.9	25.2	9.25	18.65
03/11/20	11.00	10.8	25.1	9.25	19.41
04/11/20	11.00	10.8	24.9	8.75	16.78
05/11/20	11.00	10.8	24.7	8.00	15.53
06/11/20	11.00	10.8	24.6	8.25	15.72
07/11/20	11.00	10.8	24.4	8.25	13.91
08/11/20	11.00	10.7	24.3	8.75	16.13
09/11/20	11.00	10.7	24.1	8.25	13.87
10/11/20	11.00	10.7	24.0	8.00	9.87
11/11/20	11.00	10.7	23.8	8.50	14.34
12/11/20	11.00	10.6	23.7	8.50	15.91
13/11/20	11.00	10.6	23.5	8.50	15.76
14/11/20	11.00	10.6	23.4	8.50	14.42
15/11/20	11.00	10.6	23.3	8.25	12.74
16/11/20	11.00	10.6	23.1	6.75	7.73
17/11/20	11.00	10.5	23.0	8.25	17.00
18/11/20	11.00	10.5	22.9	8.75	16.22
19/11/20	11.00	10.5	22.7	8.50	17.29
20/11/20	11.00	10.5	22.6	8.50	15.37
21/11/20	11.00	10.5	22.5	8.75	16.59
22/11/20	11.00	10.5	22.4	8.50	15.44
23/11/20	11.00	10.4	22.3	8.50	15.28
24/11/20	11.00	10.4	22.2	7.75	12.43
25/11/20	11.00	10.4	22.1	5.25	4.92
26/11/20	11.00	10.4	22.0	8.00	13.80

Date	Month	N	Ra	n	Rs
27/11/20	11.00	10.4	21.9	8.75	17.55
28/11/20	11.00	10.4	21.8	9.00	18.04
29/11/20	11.00	10.4	21.7	8.75	18.27
30/11/20	11.00	10.3	21.6	8.75	16.28
01/12/20	12.00	10.3	21.4	8.75	16.61
02/12/20	12.00	10.3	21.3	8.50	16.03
03/12/20	12.00	10.3	21.3	8.25	15.97
04/12/20	12.00	10.3	21.2	8.75	17.52
05/12/20	12.00	10.3	21.1	8.75	17.04
06/12/20	12.00	10.3	21.1	8.25	14.60
07/12/20	12.00	10.3	21.0	7.75	13.72
08/12/20	12.00	10.2	21.0	8.25	14.01
09/12/20	12.00	10.2	20.9	3.75	4.75
10/12/20	12.00	10.2	20.9	8.25	13.95
11/12/20	12.00	10.2	20.8	5.75	5.87
12/12/20	12.00	10.2	20.8	8.25	15.13
13/12/20	12.00	10.2	20.8	7.75	13.62
14/12/20	12.00	10.2	20.7	8.00	16.90
15/12/20	12.00	10.2	20.7	7.50	10.25
16/12/20	12.00	10.2	20.7	6.75	9.65
17/12/20	12.00	10.2	20.7	7.75	14.66
18/12/20	12.00	10.2	20.7	8.75	17.46
19/12/20	12.00	10.2	20.7	8.75	17.43
20/12/20	12.00	10.2	20.7	8.50	16.04
21/12/20	12.00	10.2	20.7	7.25	14.09
22/12/20	12.00	10.2	20.7	8.75	16.56
23/12/20	12.00	10.2	20.7	8.50	16.49
24/12/20	12.00	10.2	20.7	8.50	15.12
25/12/20	12.00	10.2	20.7	8.75	16.56
26/12/20	12.00	10.2	20.7	8.50	15.74
27/12/20	12.00	10.2	20.8	8.00	13.14
28/12/20	12.00	10.2	20.8	8.50	16.37
29/12/20	12.00	10.2	20.8	8.50	15.96
30/12/20	12.00	10.2	20.9	5.50	10.93
31/12/20	12.00	10.2	20.9	8.25	12.69
01/01/21	1.00	10.2	21.0	8.00	13.59
02/01/21	1.00	10.2	21.0	6.50	7.40
03/01/21	1.00	10.2	21.1	4.25	4.46
04/01/21	1.00	10.3	21.1	4.50	7.20
05/01/21	1.00	10.3	21.2	3.75	4.31
06/01/21	1.00	10.3	21.3	4.75	4.42
07/01/21	1.00	10.3	21.3	5.00	8.68
08/01/21	1.00	10.3	21.4	4.25	3.62
09/01/21	1.00	10.3	21.5	5.25	4.63
10/01/21	1.00	10.3	21.6	7.00	12.05
11/01/21	1.00	10.3	21.7	9.00	18.36
12/01/21	1.00	10.3	21.7	9.00	18.98
13/01/21	1.00	10.4	21.8	9.00	19.37

Date	Month	N	Ra	n	Rs
14/01/21	1.00	10.4	21.9	8.75	18.64
15/01/21	1.00	10.4	22.0	8.25	16.11
16/01/21	1.00	10.4	22.1	7.75	17.24
17/01/21	1.00	10.4	22.2	8.00	15.14
18/01/21	1.00	10.4	22.4	7.50	10.74
19/01/21	1.00	10.4	22.5	6.00	5.33
20/01/21	1.00	10.5	22.6	7.50	15.76
21/01/21	1.00	10.5	22.7	9.00	19.52
22/01/21	1.00	10.5	22.8	9.00	18.07
23/01/21	1.00	10.5	23.0	6.25	12.60
24/01/21	1.00	10.5	23.1	7.75	14.78
25/01/21	1.00	10.6	23.2	7.75	13.11
26/01/21	1.00	10.6	23.4	9.00	18.00
27/01/21	1.00	10.6	23.5	9.00	18.78
28/01/21	1.00	10.6	23.7	9.00	17.97
29/01/21	1.00	10.6	23.8	9.00	17.73
30/01/21	1.00	10.7	24.0	9.00	18.23
31/01/21	1.00	10.7	24.1	9.00	18.79
01/02/21	2.00	10.7	24.3	9.00	18.49
02/02/21	2.00	10.7	24.4	9.00	18.68
03/02/21	2.00	10.7	24.6	9.00	18.41
04/02/21	2.00	10.8	24.7	2.25	2.65
05/02/21	2.00	10.8	24.9	9.00	18.81
06/02/21	2.00	10.8	25.1	9.25	19.80
07/02/21	2.00	10.8	25.2	9.25	19.64
08/02/21	2.00	10.9	25.4	9.25	20.20
09/02/21	2.00	10.9	25.6	9.50	21.82
10/02/21	2.00	10.9	25.7	9.00	20.00
11/02/21	2.00	10.9	25.9	8.75	18.84
12/02/21	2.00	11.0	26.1	9.25	17.23
13/02/21	2.00	11.0	26.3	9.25	19.84
14/02/21	2.00	11.0	26.5	9.00	18.47
15/02/21	2.00	11.0	26.6	8.75	17.13
16/02/21	2.00	11.1	26.8	9.25	19.09
17/02/21	2.00	11.1	27.0	9.25	19.08
18/02/21	2.00	11.1	27.2	9.25	19.31
19/02/21	2.00	11.1	27.4	9.50	19.66
20/02/21	2.00	11.2	27.6	8.75	20.12
21/02/21	2.00	11.2	27.8	9.50	21.00
22/02/21	2.00	11.2	28.0	9.50	21.18
23/02/21	2.00	11.2	28.2	9.50	20.87
24/02/21	2.00	11.3	28.3	9.50	21.31
25/02/21	2.00	11.3	28.5	9.75	22.35
26/02/21	2.00	11.3	28.7	9.25	20.64
27/02/21	2.00	11.3	28.9	9.25	20.99
28/02/21	2.00	11.4	29.1	8.50	20.20
01/03/21	3.00	11.4	29.3	9.50	22.17
02/03/21	3.00	11.4	29.5	9.75	22.66

Date	Month	N	Ra	n	Rs
03/03/21	3.00	11.5	29.7	10.00	23.54
04/03/21	3.00	11.5	29.9	9.75	22.56
05/03/21	3.00	11.5	30.1	5.25	10.86
06/03/21	3.00	11.5	30.3	10.00	22.88
07/03/21	3.00	11.6	30.5	9.50	22.41
08/03/21	3.00	11.6	30.7	9.50	20.40
09/03/21	3.00	11.6	30.9	7.75	18.18
10/03/21	3.00	11.7	31.1	9.75	21.91
11/03/21	3.00	11.7	31.3	9.50	21.28
12/03/21	3.00	11.7	31.4	8.00	15.60
13/03/21	3.00	11.7	31.6	9.75	21.86
14/03/21	3.00	11.8	31.8	9.75	21.53
15/03/21	3.00	11.8	32.0	9.75	19.98
16/03/21	3.00	11.8	32.2	9.25	18.14
17/03/21	3.00	11.9	32.4	9.50	20.46
18/03/21	3.00	11.9	32.6	9.25	16.86
19/03/21	3.00	11.9	32.8	9.75	20.85
20/03/21	3.00	11.9	32.9	10.00	22.21
21/03/21	3.00	12.0	33.1	9.00	19.25
22/03/21	3.00	12.0	33.3	6.75	15.45
23/03/21	3.00	12.0	33.5	5.75	6.70
24/03/21	3.00	12.1	33.7	10.00	22.22
25/03/21	3.00	12.1	33.8	9.75	19.22
26/03/21	3.00	12.1	34.0	10.25	23.99
27/03/21	3.00	12.2	34.2	7.25	18.35
28/03/21	3.00	12.2	34.4	10.25	22.69
29/03/21	3.00	12.2	34.5	10.00	22.10
30/03/21	3.00	12.2	34.7	10.00	17.13
31/03/21	3.00	12.3	34.9	5.50	11.72

A8.6.1 Evaporation estimation models

Several models have been formulated to estimate evaporation from water surfaces exposed to the sky (uncovered) under diurnal conditions, utilizing data collected from field experiments. Preprocessing procedures were employed to remove any errors or ambiguities from the gathered data. This section includes both the data used for model development and the data themselves. Specifics regarding the different models developed can be found in Section A8.6.1.1, while modeling and testing data are presented in Section A8.6.1.2.

A.8.6.1.1. Evaporation estimation models for uncovered water surface

Following evaporation prediction regression models were developed for uncovered water surface.

1. The model (E5) that employs five parameters, namely R_s, T_a, T_w, V_w, and R_h, was developed, and it resulted in obtaining Equation (A8.1), which can be used for predicting evaporation.

$$E = 0.260961T_w + 0.016103R_s + 1.437038\ V_w - 0.136378T_a - 0.087122R_h + 5.097066. \quad (A8.1)$$

The predicted evaporation values from the modelling data were plotted against the actual values in Figure A8.6.1(1a), and the predicted values from the testing data were plotted against the actual recorded values in Figure A8.6.1(1b). The adjusted R^2 value of the model is 0.7121.

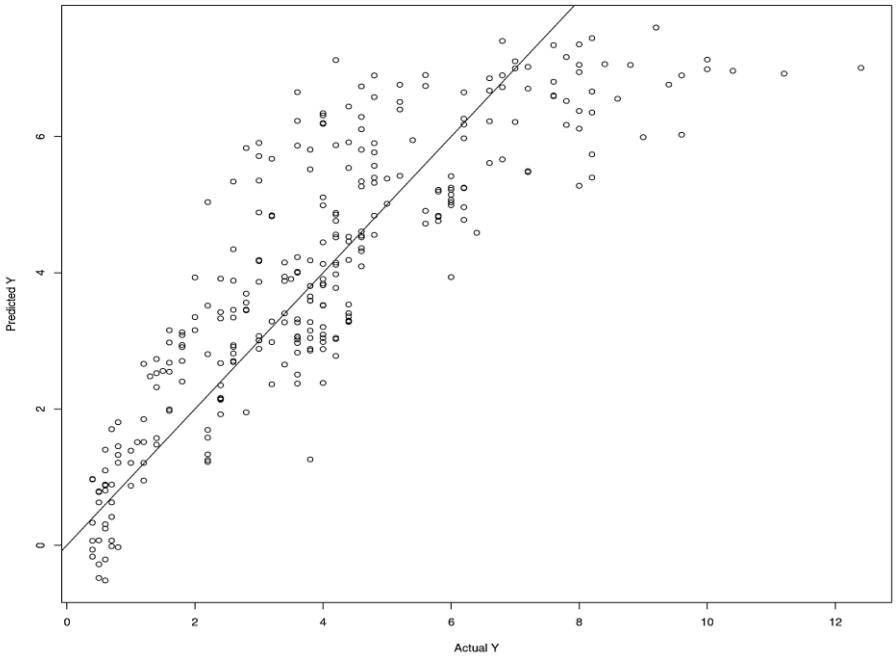

Figure A8.6.1. (1a) shows the predicted evaporation plotted against actual evaporation for Model E5, with the data used for modelling.

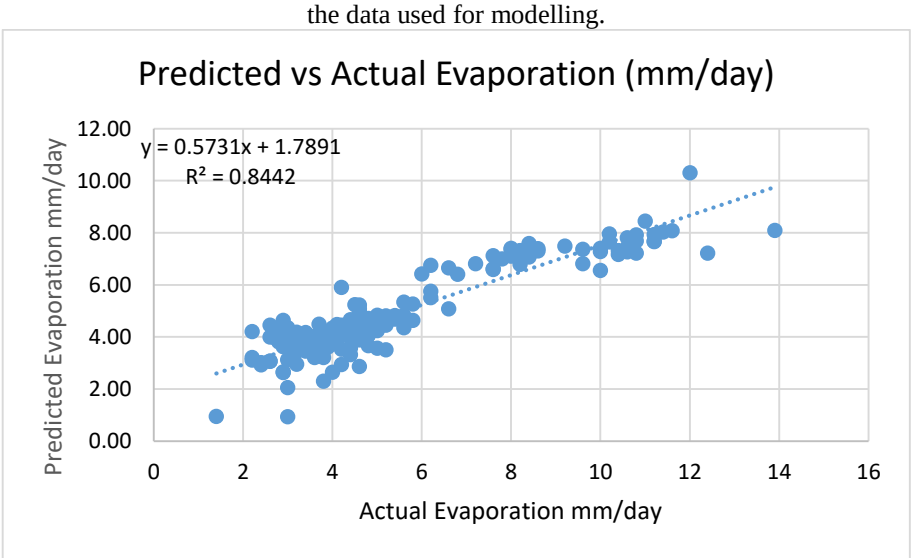

Figure A8.6.1. (1b) shows predicted evaporation plotted against actual evaporation for Model E5,with testing data (April22- Nov 22).

2. The Equation (A8.2) resulted after development of E4(T_w) model involves four parameters R_s, T_w, V_w, and R_h.

$$E = 0.133907T_w + 0.34992R_s + 1.368934\ V_w - 0.074295R_h + 3.719653. \quad \text{(A8.2)}$$

The predicted evaporation values from the modelling data were plotted against the actual values in Figure A8.6.1(2a), and the predicted values from the testing data were plotted against the actual recorded values in Figure A8.6.1(2b). The adjusted R^2 value of the model is 0.7071.

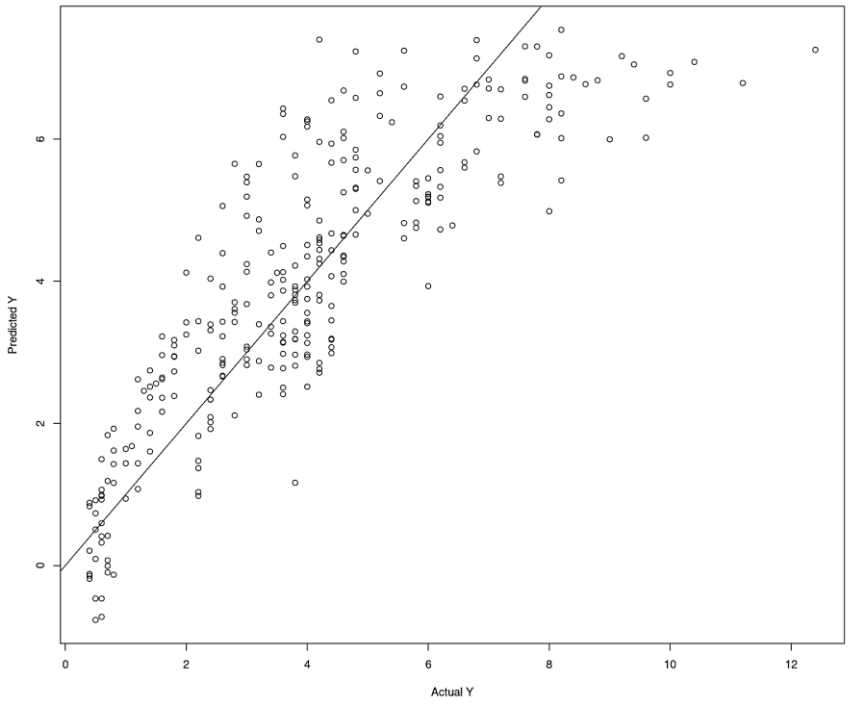

Figure A8.6.1(2a) shows the predicted evaporation plotted against actual evaporation for Model E4(T_w), with the data used for modelling

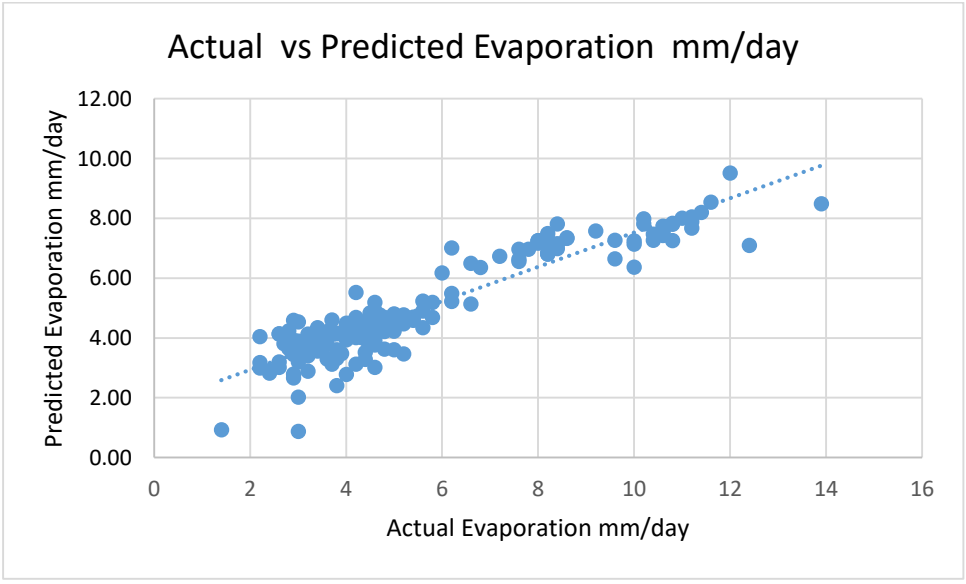

Figure A8.6.1(2b) shows predicted evaporation plotted against actual evaporation for Model E4(T_w),with testing data (April22- Nov 22).

3. Equation (A8.3) was obtained by developing E4(T_a) model, which consist of four parameters R_s, T_a, V_w, and R_h.

$$E = 0.129173T_a + 0.067104R_s + 1.43272\ V_w - 0.061767R_h + 2.481629. \quad \text{(A8.3)}$$

The predicted evaporation values from the modelling data were plotted against the actual values in Figure **A8.6.1(3a)**, and the predicted values from the testing data were plotted against the actual recorded values in Figure **A8.6.1(3b)**. The adjusted R^2 value of the model is 0.7121.

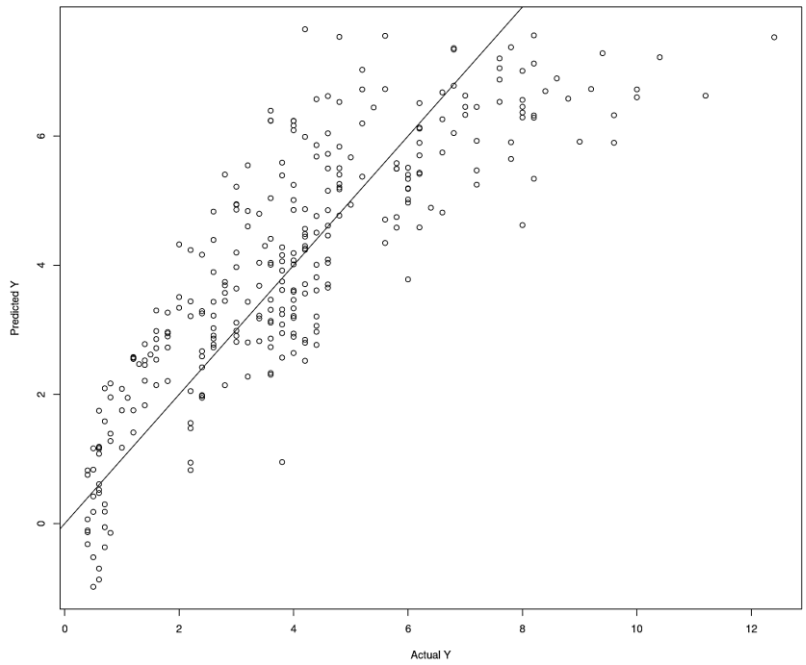

Figure A8.6.1(3a) shows the predicted evaporation plotted against actual evaporation for Model E4(T_a), with the data used for modelling

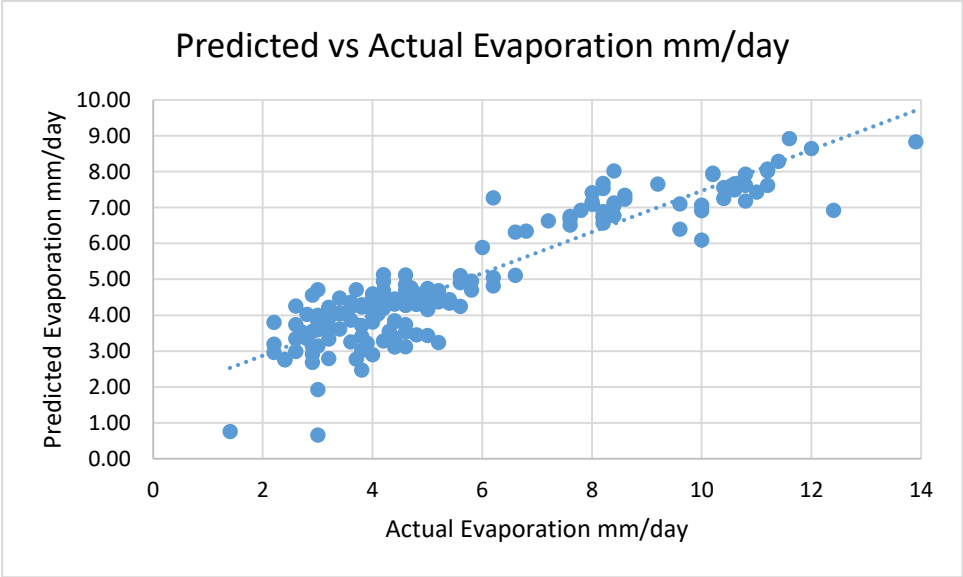

Figure A8.6.1(3b) shows predicted evaporation plotted against actual evaporation for Model E4(T_a),with testing data (April22- Nov 22).

4. Equation (A8.4) was obtained by developing E3(R_s) model, which consist of three parameters R_s, V_w, and R_h.

$$E = 0.175352R_s + 2.635177\ V_w - 0.070563R_h + 4.377117. \quad \text{(A8.4)}$$

The predicted evaporation values from the modelling data were plotted against the actual values in Figure **A8.6.1(4a)**, and the predicted values from the testing data were plotted against the actual recorded values in Figure **A8.6.1(4**b). The adjusted R^2 value of the model is 0.5862.

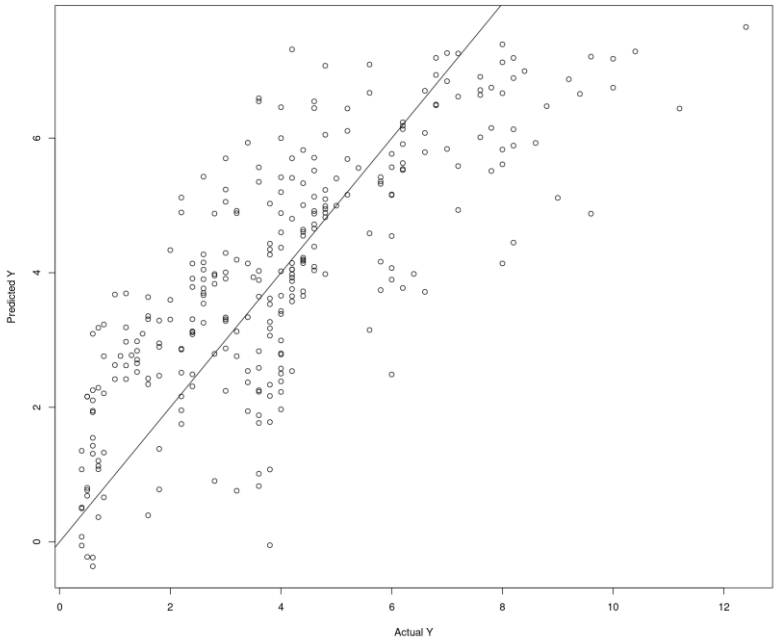

Figure A8.6.1(4a) shows the predicted evaporation plotted against actual evaporation for Model E3(R_s), with the data used for modelling

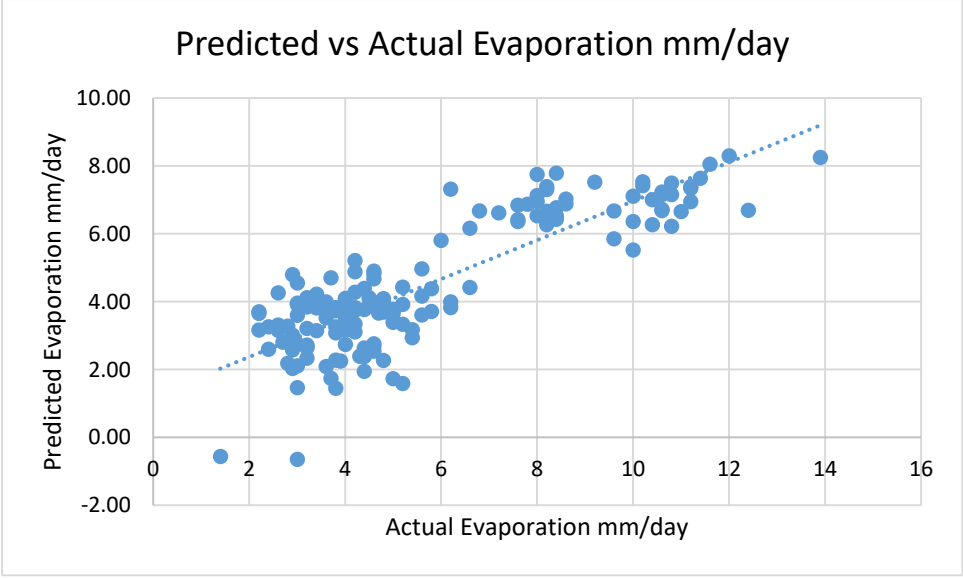

Figure A8.6.1(4b) shows predicted evaporation plotted against actual evaporation for Model E3(R_s),with testing data (April22- Nov 22).

5 Equation (A8.5) was obtained by developing E3(T_a) model, which consist of three parameters T_a, V_w, and R_h.

$$E = 0.137939T_a + 1.49557\ V_w - 0.068034R_h + 3.374499. \quad \text{(A8.5)}$$

The predicted evaporation values from the modelling data were plotted against the actual values in Figure **A8.6.1(5a)**, and the predicted values from the testing data were plotted against the actual recorded values in Figure **A8.6.1(5b)**. The adjusted R^2 value of the model is 0.6857.

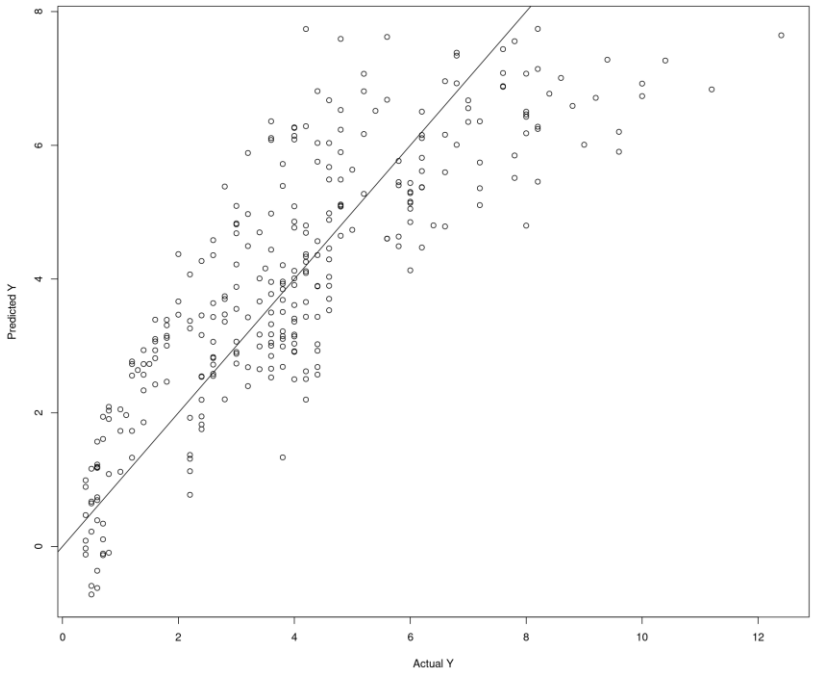

Figure A8.6.1(5a) shows the predicted evaporation plotted against actual evaporation for Model E3(T_a), with the data used for modelling

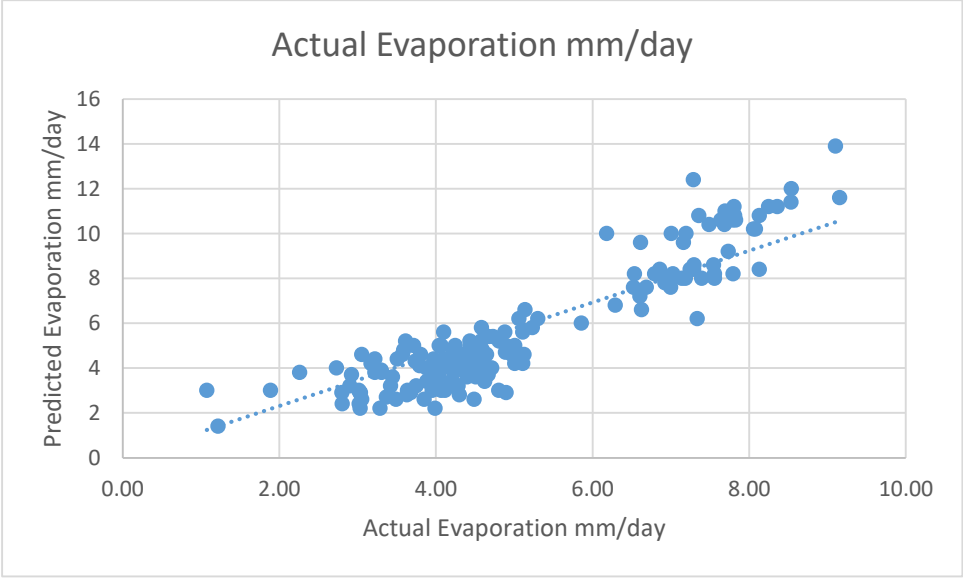

Figure A8.6.1(5b) shows predicted evaporation plotted against actual evaporation for Model E3(T_a),with testing data (April22- Nov 22).

6 Equation (A8.6) was obtained by developing E3(T_w) model, which consist of three parameters T_w, V_w, and R_h.

$$E = 0.138906T_w + 1.393587\ V_w - 0.077852R_h + 4.203714. \quad \text{(A8.6)}$$

The predicted evaporation values from the modelling data were plotted against the actual values in Figure **A8.6.1(6a)**, and the predicted values from the testing data were plotted against the actual recorded values in Figure **A8.6.1(6b)**. The adjusted R^2 value of the model is 0.707.

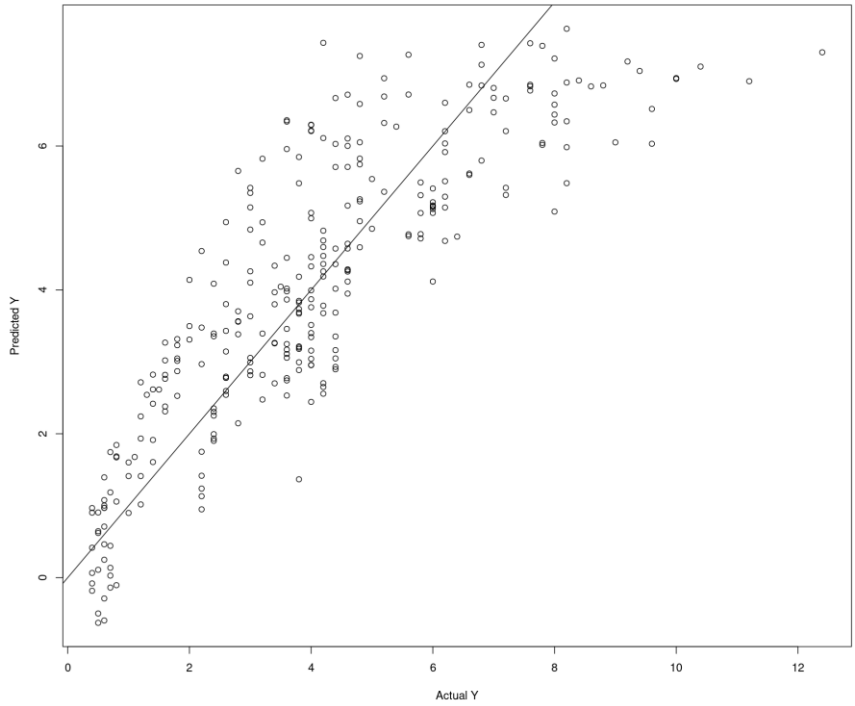

Figure A8.6.1(6a) shows the predicted evaporation plotted against actual evaporation for Model E3(T_w), with the data used for modelling

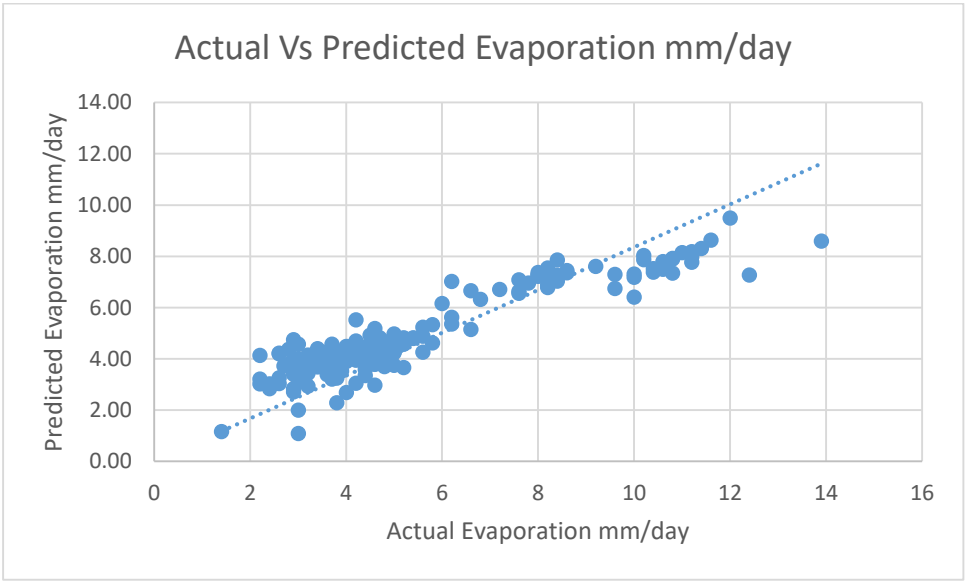

Figure A8.6.1(6b) shows predicted evaporation plotted against actual evaporation for Model E3 (T_w),with testing data (April22- Nov 22).

A8.6.1.2. Modelling and testing data for evaporation estimation models for uncovered water surface.

Date	Evaporation (mm)	Average Water Temperature (°C)	Rs at zero plane in $MJ/m^2/day$	Average Wind Velocity (m/s)	Average ambient temperature(°C)	Average humidity (%)
24/03/21	4.2	22.54	14.8	0.31	22.71	42.32
25/03/21	4.6	21.53	12.6	0.32	22.56	43.10
26/03/21	5	23.03	16.3	0.35	25.34	39.06
27/03/21	7.2	25.13	15.6	0.39	28.01	36.21
28/03/21	8.2	26.21	15.4	0.54	31.51	33.57
29/03/21	12.4	25.90	14.6	0.85	32.41	21.62
30/03/21	10	22.45	10.8	0.92	26.34	21.47
31/03/21	9.6	22.82	17.0	0.46	25.01	19.26
01/04/21	8	22.17	16.8	0.52	23.78	18.41
02/04/21	7.2	22.48	16.9	0.38	25.08	15.35
03/04/21	7	23.13	16.8	0.36	26.19	14.27
04/04/21	10.4	24.20	15.7	0.42	30.30	13.44
05/04/21	11.2	26.03	12.6	0.50	29.91	20.75
06/04/21	8.4	26.56	14.3	0.73	29.38	25.68
07/04/21	7.8	25.06	16.4	0.30	25.47	26.81
08/04/21	7.2	24.05	17.5	0.28	25.08	22.19
09/04/21	6.6	24.28	16.8	0.26	26.48	18.48
10/04/21	7	24.87	17.0	0.28	27.27	17.71
11/04/21	8	25.59	16.5	0.24	28.71	17.50
12/04/21	10	26.42	15.6	0.35	29.55	18.20
13/04/21	8.8	27.08	15.5	0.29	29.84	19.62
14/04/21	7.6	25.19	10.7	0.44	30.39	19.84
15/04/21	8	26.65	15.1	0.53	30.10	18.34
17/04/21	2.6	25.02	16.7	0.44	25.21	43.04
18/04/21	3	26.37	15.6	0.25	27.47	35.92
19/04/21	4	27.46	16.0	0.33	30.43	29.08
21/04/21	2.2	23.85	14.9	0.44	23.01	46.11
22/04/21	3.6	25.78	16.5	0.68	30.03	35.64
23/04/21	3	24.94	15.0	0.58	23.99	40.19
25/04/21	3.6	25.42	17.4	0.30	27.73	23.05
26/04/21	5.6	26.06	16.4	0.31	30.37	19.78
27/04/21	6.8	27.69	16.1	0.42	32.31	15.79
28/04/21	7.8	27.93	13.9	0.41	33.87	16.21
29/04/21	8.2	29.41	14.0	0.48	34.87	17.06
30/04/21	7.6	29.05	12.8	0.55	33.49	20.26

Date	Evaporation (mm)	Average Water Temperature (ºC)	Rs at zero plane in $MJ/m^2/day$	Average Wind Velocity (m/s)	Average ambient temperature(ºC)	Average humidity (%)
01/05/21	6.6	27.06	11.6	0.49	32.03	23.03
02/05/21	7	25.76	10.2	0.63	30.96	28.15
03/05/21	7.6	27.86	15.5	0.53	32.12	25.18
04/05/21	6.8	27.14	13.5	0.57	31.78	24.75
05/05/21	6.2	28.61	15.4	0.39	31.89	27.24
06/05/21	3.2	26.79	9.3	0.57	30.37	37.20
07/05/21	3.8	27.32	13.9	0.36	29.85	38.77
08/05/21	4	29.17	14.1	0.31	32.41	31.86
09/05/21	4.4	28.08	12.0	0.47	33.07	26.88
10/05/21	4.8	26.62	8.9	0.50	31.44	32.71
11/05/21	4.6	28.41	14.4	0.69	31.63	30.80
12/05/21	4.2	26.33	10.4	0.58	31.03	32.87
13/05/21	4	27.61	14.0	0.88	30.25	38.14
14/05/21	4.6	29.29	14.8	0.58	29.90	39.55
15/05/21	6.2	28.84	15.4	0.46	29.85	37.70
16/05/21	5.2	29.61	15.3	0.32	32.26	31.37
17/05/21	4.8	28.12	7.2	0.30	32.16	34.72
22/05/21	5.6	28.21	14.2	0.55	29.04	52.88
23/05/21	4.2	26.80	12.7	0.25	27.00	47.26
24/05/21	7.2	28.14	15.8	0.23	29.78	39.99
25/05/21	7.8	29.34	15.3	0.35	31.40	35.00
26/05/21	8.2	29.67	15.5	0.43	32.74	33.15
27/05/21	8	30.15	15.5	0.37	33.77	31.73
28/05/21	9.4	31.01	15.9	0.60	36.41	29.60
29/05/21	5.2	31.13	13.9	0.70	35.14	36.16
30/05/21	8	30.58	13.4	0.59	34.66	37.85
03/06/21	4	28.80	15.9	0.20	31.87	43.83
04/06/21	4.8	31.01	14.1	0.40	32.04	42.69
06/06/21	5	29.70	14.5	0.44	33.17	43.69
07/06/21	5.4	30.93	13.8	0.57	35.76	38.86
08/06/21	5.6	31.37	14.9	0.93	37.10	33.25
09/06/21	4.8	31.34	15.1	0.90	37.03	32.88
10/06/21	5.2	32.00	14.8	0.74	36.11	35.17
13/06/21	8	28.72	10.3	0.56	28.87	49.90
15/06/21	3.2	28.94	11.0	0.63	31.12	53.46
16/06/21	4.2	30.06	14.9	0.30	30.25	57.00
17/06/21	3	31.96	14.7	0.37	31.98	51.54

Date	Evaporation (mm)	Average Water Temperature (ºC)	Rs at zero plane in MJ/m^2/day	Average Wind Velocity (m/s)	Average ambient temperature(ºC)	Average humidity (%)
18/06/21	2.8	32.21	13.8	0.60	32.52	49.59
19/06/21	5.6	29.99	8.9	0.36	31.14	52.97
20/06/21	6	30.76	11.6	0.35	33.01	48.69
21/06/21	8.2	30.27	12.0	0.45	32.72	45.63
22/06/21	9	30.68	13.0	0.47	33.45	39.43
26/06/21	4.2	29.73	14.0	0.36	31.86	51.54
27/06/21	4.6	31.53	14.1	0.30	32.93	42.29
28/06/21	9.6	32.37	14.3	0.30	34.64	39.65
29/06/21	8.6	32.01	13.8	0.57	36.73	33.60
30/06/21	4.2	31.70	14.7	1.04	36.98	33.68
01/07/21	6.8	32.03	15.6	0.88	36.63	35.31
02/07/21	4.8	32.20	14.8	0.71	34.69	39.58
03/07/21	4.6	31.54	14.4	0.63	33.73	43.14
04/07/21	4.4	30.99	11.7	0.60	33.79	42.59
06/07/21	4.4	32.20	12.9	0.48	35.10	46.72
08/07/21	3.6	32.36	15.3	0.47	35.64	38.72
09/07/21	3.8	32.97	12.1	0.37	34.87	44.34
10/07/21	4	33.96	14.2	0.52	36.53	43.08
19/07/21	3.6	26.77	2.7	0.47	27.87	74.55
20/07/21	2.6	29.99	12.6	0.68	31.03	63.42
22/07/21	2.6	31.32	15.2	0.38	31.27	67.85
23/07/21	2.2	31.18	10.3	0.26	30.71	69.63
24/07/21	3	32.48	13.1	0.28	32.36	64.29
25/07/21	3	33.19	15.3	0.40	33.88	58.23
27/07/21	1.8	28.69	4.9	0.41	29.57	69.93
29/07/21	1.8	27.89	6.3	0.24	28.09	75.60
31/07/21	1.6	28.18	5.9	0.18	29.54	77.82
01/08/21	4	30.89	11.5	0.33	29.93	71.35
02/08/21	3.8	30.37	8.7	0.14	29.82	73.63
04/08/21	3.4	31.37	14.1	0.24	30.36	72.44
05/08/21	4.2	31.70	13.2	0.23	31.22	67.45
08/08/21	4	31.04	12.7	0.23	31.15	68.38
09/08/21	3	30.83	11.7	0.50	31.90	63.26
10/08/21	4	30.69	14.9	0.76	31.23	58.20
11/08/21	4.6	30.50	15.4	0.74	30.89	55.24
12/08/21	4.8	30.60	15.2	0.71	31.61	54.12
13/08/21	5.2	30.46	14.7	0.72	31.78	52.34

Date	Evaporation (mm)	Average Water Temperature (ºC)	Rs at zero plane in MJ/m^2/day	Average Wind Velocity (m/s)	Average ambient temperature(ºC)	Average humidity (%)
14/08/21	4.8	30.58	14.9	0.65	31.30	52.63
15/08/21	6	30.71	14.7	0.49	31.26	52.44
16/08/21	5.8	30.87	14.1	0.23	31.56	52.63
17/08/21	6.4	29.67	14.4	0.24	32.58	50.34
18/08/21	6.6	36.63	13.5	0.22	33.07	51.13
19/08/21	6	31.61	13.9	0.23	33.85	47.49
20/08/21	6	29.08	6.8	0.48	30.66	61.60
23/08/21	2.4	30.49	12.3	0.28	30.11	70.31
24/08/21	4.4	31.41	15.3	0.57	32.79	61.49
25/08/21	6.6	30.26	15.7	0.88	32.14	51.83
26/08/21	6	29.44	15.1	0.71	30.61	53.02
27/08/21	5.8	30.22	14.4	0.40	31.31	53.74
28/08/21	6.2	30.79	14.4	0.23	31.57	52.93
29/08/21	4.2	30.13	10.8	0.48	32.04	56.15
30/08/21	4	30.55	12.9	0.55	30.43	62.78
05/09/21	3.2	29.05	8.3	0.11	29.22	76.00
06/09/21	3.8	30.85	13.5	0.15	31.46	70.45
07/09/21	4	30.25	11.2	0.63	29.89	70.97
08/09/21	3.8	29.62	12.7	0.63	29.05	70.78
09/09/21	3.6	28.70	8.6	0.39	29.05	72.93
10/09/21	3.4	29.50	11.4	0.76	29.10	71.43
13/09/21	3.6	27.75	6.8	0.33	28.22	76.90
14/09/21	4	28.68	10.1	0.41	29.03	74.54
15/09/21	3.6	29.52	15.0	0.56	28.94	65.08
17/09/21	3.4	27.83	11.0	0.43	28.10	69.43
18/09/21	3.2	28.06	11.2	0.50	29.21	69.43
19/09/21	2.8	29.50	12.8	0.34	30.03	66.94
20/09/21	3.6	29.07	10.5	0.19	30.29	68.55
24/09/21	2.8	27.04	9.0	0.16	28.01	77.55
25/09/21	3.4	28.48	13.0	0.17	29.00	73.16
26/09/21	3	28.88	12.1	0.35	28.82	73.36
27/09/21	3.6	28.95	11.7	0.32	29.41	71.44
28/09/21	3.6	28.77	10.7	0.46	30.03	69.15
29/09/21	3.8	28.62	12.3	0.53	29.78	67.42
30/09/21	3.8	28.19	10.2	0.19	29.32	69.24
01/10/21	4	28.57	14.0	0.24	30.36	66.33
02/10/21	3.6	27.92	11.0	0.24	29.79	66.40

Date	Evaporation (mm)	Average Water Temperature (ºC)	Rs at zero plane in MJ/m^2/day	Average Wind Velocity (m/s)	Average ambient temperature(ºC)	Average humidity (%)
03/10/21	3.8	28.06	14.8	0.38	30.59	61.74
04/10/21	4	28.04	13.0	0.36	29.89	59.17
05/10/21	3.8	27.25	11.5	0.22	28.90	65.72
06/10/21	4	26.87	13.7	0.17	28.20	65.92
07/10/21	4	25.57	13.7	0.14	27.37	61.59
08/10/21	3.5	24.89	14.6	0.20	28.20	50.04
09/10/21	4.2	24.94	14.4	0.22	28.85	48.67
10/10/21	4	25.28	14.4	0.31	30.14	47.42
11/10/21	4.2	25.40	14.3	0.23	28.52	48.75
12/10/21	3.8	24.09	13.3	0.13	26.63	49.89
13/10/21	3.6	22.51	13.6	0.22	25.01	46.98
14/10/21	3.8	21.25	13.8	0.24	24.39	42.48
15/10/21	4	21.34	14.0	0.13	24.52	44.69
16/10/21	3.6	22.09	12.5	0.12	29.06	45.91
18/10/21	3.8	21.11	3.4	0.15	21.45	76.79
19/10/21	4	22.36	12.5	0.25	24.00	66.99
20/10/21	3.8	20.96	14.2	0.34	24.76	49.52
21/10/21	3.6	19.38	14.3	0.50	26.15	40.42
22/10/21	3.2	24.35	14.4	0.49	25.68	46.39
23/10/21	3.4	22.35	12.7	0.41	24.94	50.26
24/10/21	3.8	21.86	10.9	0.32	23.01	57.65
25/10/21	3.6	20.59	11.9	0.21	21.78	59.28
26/10/21	3.2	19.53	12.8	0.16	20.62	55.50
27/10/21	3	19.14	12.1	0.19	21.49	52.31
28/10/21	2.8	18.71	13.1	0.19	21.20	47.33
29/10/21	2.6	18.16	12.0	0.15	21.01	45.03
30/10/21	2.8	18.12	12.0	0.25	21.91	45.11
31/10/21	2.8	18.63	12.3	0.18	21.88	42.90
01/11/21	2	19.06	12.3	0.19	24.04	38.24
02/11/21	2.4	19.30	11.3	0.23	23.76	40.07
03/11/21	2.4	18.46	9.4	0.25	21.47	47.82
04/11/21	1.6	17.00	7.1	0.12	19.79	50.97
05/11/21	1.8	16.62	7.4	0.07	20.25	48.04
06/11/21	2	16.97	9.9	0.19	21.14	42.76
07/11/21	1.8	16.92	8.6	0.14	20.31	47.55
08/11/21	1.8	17.23	9.3	0.14	20.58	48.54
09/11/21	1.8	17.23	10.1	0.14	21.16	45.75

Date	Evaporation (mm)	Average Water Temperature (ºC)	Rs at zero plane in $MJ/m^2/day$	Average Wind Velocity (m/s)	Average ambient temperature(ºC)	Average humidity (%)
10/11/21	2	17.26	10.2	0.09	21.35	43.90
11/11/21	1.6	17.22	10.6	0.10	21.02	44.55
12/11/21	1.6	15.30	6.4	0.08	19.85	46.52
13/11/21	1.6	14.95	9.9	0.11	18.47	43.85
14/11/21	1.4	14.61	9.2	0.06	18.32	44.89
15/11/21	1.4	14.05	8.3	0.06	17.62	46.53
16/11/21	1.3	13.65	8.7	0.07	17.07	46.96
17/11/21	1.5	13.43	9.6	0.12	16.98	46.53
18/11/21	1.4	13.43	9.4	0.09	17.12	48.52
20/11/21	1.2	15.72	8.50	0.06	18.74	48.24
09/12/21	1.2	11.14	10.4	0.11	15.34	57.71
10/12/21	1.4	10.49	9.8	0.17	14.35	55.12
11/12/21	1	11.14	10.4	0.11	15.34	57.71
12/12/21	1.1	10.22	10.1	0.14	14.51	53.20
15/12/21	0.6	10.73	8.8	0.19	13.77	63.68
16/12/21	0.6	9.15	5.5	0.21	10.34	64.97
17/12/21	1	7.55	10.1	0.31	10.60	61.47
18/12/21	1.2	5.26	10.8	0.34	9.30	56.40
19/12/21	1	5.02	11.1	0.25	10.81	46.86
20/12/21	1.2	6.19	11.1	0.15	13.60	42.89
22/12/21	1.6	9.70	10.3	0.24	16.43	45.04
23/12/21	1.2	11.64	8.7	0.23	17.53	50.09
24/12/21	1.4	12.56	8.8	0.19	17.64	55.22
25/12/21	0.8	13.37	8.2	0.27	17.94	61.21
26/12/21	0.8	14.26	2.1	0.48	16.90	66.38
27/12/21	0.4	14.11	6.4	0.21	15.22	70.51
28/12/21	0.4	11.83	6.9	0.18	12.96	66.72
30/12/21	0.6	9.45	8.8	0.26	11.78	61.67
31/12/21	0.6	8.35	8.0	0.11	11.71	58.41
01-Jan-22	0.5	8.7	9.4	0.16	12.20	60.75
02-Jan-22	0.6	9.5	9.4	0.15	12.62	61.19
03-Jan-22	0.7	9.6	9.5	0.14	14.49	58.41
06-Jan-22	0.4	13.5	2.2	0.23	14.36	76.86
08-Jan-22	0.5	14.0	4.9	0.42	14.39	78.52
09-Jan-22	0.7	10.7	3.8	0.26	9.43	75.99
10-Jan-22	0.6	10.4	10.2	0.20	12.19	72.94
11-Jan-22	0.6	9.6	3.3	0.27	9.35	83.61

Date	Evaporation (mm)	Average Water Temperature (ºC)	Rs at zero plane in MJ/m^2/day	Average Wind Velocity (m/s)	Average ambient temperature(ºC)	Average humidity (%)
12-Jan-22	0.4	10.9	6.6	0.16	11.75	77.35
13-Jan-22	0.4	11.4	7.4	0.18	12.13	79.91
14-Jan-22	0.6	10.5	2.4	0.17	10.28	79.50
15-Jan-22	0.5	9.5	2.9	0.34	8.63	85.11
16-Jan-22	0.7	10.4	8.6	0.32	10.62	80.06
17-Jan-22	0.5	10.4	7.9	0.36	9.49	85.40
18-Jan-22	0.7	10.9	9.0	0.24	11.88	77.38
19-Jan-22	0.6	11.4	6.4	0.55	13.50	78.23
20-Jan-22	0.5	12.7	7.2	0.32	13.63	80.99
22-Jan-22	0.4	11.8	1.5	0.49	11.79	82.99
24-Jan-22	0.7	11.5	7.5	0.27	11.43	73.67
25-Jan-22	0.8	10.5	6.9	0.22	10.96	78.02
26-Jan-22	0.5	10.6	11.0	0.30	11.68	69.99
27-Jan-22	0.8	10.4	12.0	0.32	11.84	64.70
28-Jan-22	0.6	10.3	12.4	0.28	13.21	59.48
29-Jan-22	0.7	11.6	12.5	0.22	14.95	56.22
30-Jan-22	0.8	12.3	12.3	0.28	15.48	57.27
31-Jan-22	2.2	13.4	12.0	0.21	16.41	59.19
01-Feb-22	2.2	13.1	11.0	0.28	14.09	64.19
02-Feb-22	2.2	12.9	12.2	0.98	17.20	56.43
03-Feb-22	2.2	11.4	4.4	0.60	11.99	70.54
04-Feb-22	2.2	12.3	11.3	0.22	12.15	67.69
05-Feb-22	2.2	12.4	12.9	0.35	14.05	66.49
06-Feb-22	2.4	13.3	12.6	0.47	17.05	57.21
07-Feb-22	2.4	15.4	11.4	0.27	19.04	56.72
08-Feb-22	2.4	16.5	10.4	0.33	18.08	64.92
09-Feb-22	2.4	15.5	12.7	0.34	15.21	62.12
10-Feb-22	2.4	14.1	12.4	0.30	14.97	59.71
11-Feb-22	2.4	13.5	13.8	0.36	14.33	54.31
12-Feb-22	2.6	13.6	14.2	0.29	15.95	50.81
13-Feb-22	2.6	14.6	14.3	0.28	17.19	49.17
14-Feb-22	2.6	15.5	13.9	0.27	17.55	46.11
15-Feb-22	2.6	15.9	13.2	0.27	17.75	51.53
16-Feb-22	2.6	16.1	13.0	0.27	18.08	54.23
17-Feb-22	2.6	16.4	12.2	0.37	18.81	54.22
18-Feb-22	3	15.9	9.8	0.33	18.42	51.44
19-Feb-22	3	15.9	13.6	0.30	17.57	51.59

Date	Evaporation (mm)	Average Water Temperature (ºC)	Rs at zero plane in MJ/m^2/day	Average Wind Velocity (m/s)	Average ambient temperature(ºC)	Average humidity (%)
20-Feb-22	3	15.0	13.2	0.56	16.99	44.12
21-Feb-22	3.4	15.5	14.7	0.59	21.21	36.52
23-Feb-22	4.4	19.0	11.7	0.46	19.86	55.51
24-Feb-22	4	18.4	11.6	0.31	20.13	54.44
25-Feb-22	4.6	18.5	12.1	1.37	21.70	51.91
26-Feb-22	4.2	17.1	12.0	1.28	17.20	58.86
27-Feb-22	4.2	16.9	15.2	0.33	16.11	57.22
28-Feb-22	4.2	16.5	15.2	0.27	17.18	53.55
01-Mar-22	4.2	17.3	14.2	0.27	19.06	55.66
02-Mar-22	4.4	18.8	14.0	0.69	20.99	56.83
03-Mar-22	4.4	19.4	13.6	0.38	18.77	58.22
04-Mar-22	4.4	18.4	15.0	0.48	18.30	57.79
05-Mar-22	4.4	18.5	15.3	0.36	19.64	54.30
06-Mar-22	4.4	19.4	10.9	0.56	22.98	51.32
07-Mar-22	4.4	20.8	14.8	0.61	23.23	46.05
08-Mar-22	4.4	21.0	13.9	0.40	22.65	47.04
09-Mar-22	4.6	22.1	12.1	0.33	21.73	46.47
10-Mar-22	4.6	22.9	13.7	0.27	22.38	48.98
11-Mar-22	4.6	24.3	15.1	0.42	21.99	46.11
12-Mar-22	4.6	20.8	15.3	0.30	23.92	41.58
13-Mar-22	4.6	22.2	15.2	0.31	26.45	44.51
14-Mar-22	4.8	23.7	14.9	0.34	26.94	43.38
15-Mar-22	4.8	24.0	14.7	0.45	27.95	41.23
16-Mar-22	6	23.9	15.2	0.51	28.15	39.94
17-Mar-22	5.8	24.4	15.3	0.40	29.89	39.59
18-Mar-22	5.8	26.1	14.4	0.58	29.80	42.66
19-Mar-22	6.2	24.8	15.5	0.55	30.12	37.31
20-Mar-22	6.2	24.7	15.0	0.42	29.10	28.06
21-Mar-22	6	24.9	14.6	0.36	28.98	38.58
22-Mar-22	6.2	23.3	14.5	0.50	28.00	38.43
23-Mar-22	5.8	23.0	11.6	0.49	28.42	33.24
24-Mar-22	6	23.8	15.1	0.47	27.31	35.39
25-Mar-22	6.2	23.4	14.9	0.37	27.43	34.35
26-Mar-22	6.8	21.9	15.3	0.54	27.18	28.27
27-Mar-22	9.2	28.7	15.9	0.46	29.69	21.28
28-Mar-22	8.2	24.6	15.8	0.52	30.94	18.79
29-Mar-22	7.6	25.3	15.6	0.44	31.61	19.28

Date	Evaporation (mm)	Average Water Temperature (ºC)	Rs at zero plane in MJ/m^2/day	Average Wind Velocity (m/s)	Average ambient temperature(ºC)	Average humidity (%)
31-Mar-22	6.2	25.0	14.6	0.46	28.54	27.12
01-Apr-22	6.8	24.1	15.9	0.45	27.98	23.78
02-Apr-22	6.2	24.5	15.3	0.57	31.25	17.72
03-Apr-22	8	24.2	16.8	0.53	30.22	13.86
04-Apr-22	7.6	24.1	15.6	0.41	28.99	19.13
05-Apr-22	7.6	25.2	15.5	0.26	29.52	19.35
06-Apr-22	7.2	25.7	16.1	0.27	29.57	18.43
07-Apr-22	7.8	25.9	16.1	0.31	30.39	16.31
08-Apr-22	8.2	26.2	16.3	0.40	32.88	14.02
09-Apr-22	8.2	26.7	15.0	0.52	33.33	14.08
10-Apr-22	9.2	27.1	15.7	0.52	32.81	13.94
11-Apr-22	8.4	27.6	15.5	0.62	34.36	13.45
12-Apr-22	8	26.0	10.7	0.50	32.14	14.73
13-Apr-22	8	27.6	14.7	0.61	31.06	20.42
14-Apr-22	7.6	27.5	12.3	0.49	31.19	20.78
15-Apr-22	8.2	27.6	14.0	0.43	30.91	18.50
16-Apr-22	8	27.5	15.7	0.37	31.34	16.37
17-Apr-22	8.2	28.1	14.6	0.34	32.47	22.29
18-Apr-22	8.4	28.7	14.4	0.38	33.63	19.64
19-Apr-22	8.6	28.8	15.3	0.53	32.70	20.34
20-Apr-22	8.6	28.7	13.4	0.60	33.70	20.27
21-Apr-22	6.6	26.6	10.6	0.77	29.87	29.77
22-Apr-22	6	27.5	15.1	0.34	29.11	30.03
23-Apr-22	8.2	28.1	15.9	0.34	30.55	23.00
24-Apr-22	8.2	27.5	14.6	0.46	31.00	22.78
25-Apr-22	8.4	28.1	12.5	0.70	32.33	23.41
26-Apr-22	8.4	28.9	14.5	0.42	31.90	22.72
27-Apr-22	9.6	29.4	15.4	0.36	32.99	19.22
28-Apr-22	10.2	29.5	15.0	0.58	35.48	15.94
29-Apr-22	10.2	29.8	15.3	0.54	34.95	13.59
30-Apr-22	10.6	30.3	15.0	0.51	34.40	17.02
01-May-22	10.8	29.6	14.0	0.74	35.46	18.29
02-May-22	11.2	30.1	13.8	0.66	36.50	16.94
03-May-22	10.8	30.2	13.9	0.57	34.17	16.58
04-May-22	10	29.3	13.8	0.86	32.08	27.83
05-May-22	10	29.6	13.6	0.35	31.66	30.68
06-May-22	9.6	28.9	12.2	0.48	31.78	27.41

Date	Evaporation (mm)	Average Water Temperature (ºC)	Rs at zero plane in MJ/m^2/day	Average Wind Velocity (m/s)	Average ambient temperature(ºC)	Average humidity (%)
07-May-22	10	30.1	14.6	0.37	33.17	22.08
08-May-22	10.4	30.6	14.5	0.67	35.77	23.94
09-May-22	10.6	30.7	13.9	0.84	35.77	25.57
10-May-22	10.6	31.7	14.2	0.63	36.70	25.60
11-May-22	10.8	31.9	13.5	0.47	36.11	25.04
12-May-22	11.2	30.5	13.9	0.54	35.29	18.29
13-May-22	11.4	29.9	13.9	0.63	36.41	11.90
14-May-22	12	40.1	19.1	0.60	38.01	14.38
15-May-22	11.6	31.6	14.6	0.78	40.03	13.39
16-May-22	11.2	30.2	13.1	0.66	36.17	14.61
17-May-22	11	33.5	12.8	0.49	34.79	17.88
18-May-22	10.4	30.7	12.9	0.45	35.80	22.06
19-May-22	10.6	31.1	14.3	0.47	36.94	20.45
20-May-22	13.9	30.6	13.8	0.96	38.64	15.30
21-May-22	12.4	28.4	10.4	0.94	32.03	28.12
06-Jul-22	6.2	33.1	9.2	0.82	32.38	58.95
07-Jul-22	5.8	33.3	8.9	0.69	34.23	57.29
08-Jul-22	6.2	34.1	9.7	0.55	33.86	52.49
09-Jul-22	5.4	31.7	6.8	0.60	32.73	59.70
11-Jul-22	5	30.9	7.5	0.25	32.04	65.52
12-Jul-22	5.2	30.4	5.9	0.36	31.17	67.68
13-Jul-22	5.4	32.7	9.0	0.56	33.08	60.37
14-Jul-22	5	31.0	7.6	0.90	32.40	61.52
16-Jul-22	2.8	30.5	7.7	0.90	30.61	68.31
18-Jul-22	3.8	32.4	8.0	0.26	31.11	71.08
19-Jul-22	4.4	32.8	8.2	0.43	32.49	64.74
24-Jul-22	2.2	31.0	8.6	0.90	30.30	72.22
25-Jul-22	2.6	31.5	9.8	0.75	29.65	69.66
26-Jul-22	2.9	30.8	9.3	0.78	29.03	71.61
27-Jul-22	3.2	31.2	9.3	0.58	30.07	68.28
28-Jul-22	2.8	30.4	7.1	0.55	30.01	69.26
02-Aug-22	2.7	32.0	13.8	0.34	30.43	69.31
03-Aug-22	2.9	32.1	12.4	0.18	30.41	70.77
06-Aug-22	3	30.6	12.7	0.24	30.62	72.69
07-Aug-22	3.7	30.5	8.3	0.47	28.88	75.58
08-Aug-22	4.1	32.6	15.1	0.55	30.81	68.46
09-Aug-22	4.4	32.6	13.7	0.62	31.64	65.91

Date	Evaporation (mm)	Average Water Temperature (ºC)	Rs at zero plane in MJ/m^2/day	Average Wind Velocity (m/s)	Average ambient temperature(ºC)	Average humidity (%)
10-Aug-22	4.6	31.3	12.7	0.98	32.01	60.78
11-Aug-22	4.5	31.6	9.7	0.99	29.64	64.81
12-Aug-22	4.2	33.0	13.0	1.10	31.04	61.65
13-Aug-22	4	30.6	10.5	0.64	29.90	67.32
14-Aug-22	3.9	30.2	9.9	0.40	29.52	69.78
16-Aug-22	2.9	27.7	6.9	1.60	28.70	71.04
17-Aug-22	4.4	29.2	9.0	0.59	29.33	70.54
18-Aug-22	4.4	29.5	9.4	0.30	29.66	69.01
19-Aug-22	4.6	30.2	10.9	0.42	29.78	66.78
20-Aug-22	4.6	30.8	10.8	0.27	31.23	63.00
21-Aug-22	4.8	30.3	9.4	0.37	30.62	67.12
22-Aug-22	4.3	32.8	8.7	0.50	30.96	68.49
23-Aug-22	4.6	27.7	8.0	1.35	29.49	66.09
24-Aug-22	4.2	28.9	13.0	0.64	30.08	64.13
25-Aug-22	3.6	28.5	8.5	0.40	29.92	68.48
26-Aug-22	5	30.1	13.7	0.52	30.20	62.56
28-Aug-22	4.8	29.3	12.5	0.59	30.65	57.23
29-Aug-22	4.4	28.9	9.8	0.24	30.30	57.99
30-Aug-22	3.2	28.5	8.3	0.36	30.85	58.60
31-Aug-22	5.6	30.6	13.3	0.50	32.47	54.76
02-Sep-22	5.6	30.6	14.3	0.38	30.99	60.60
03-Sep-22	5.8	29.7	14.3	0.62	30.96	58.70
04-Sep-22	4.6	29.7	15.6	0.65	30.22	56.90
05-Sep-22	5	29.6	14.5	0.35	29.53	57.80
06-Sep-22	4.6	30.0	15.1	0.29	30.61	55.89
07-Sep-22	5	30.1	12.2	0.29	31.77	55.15
08-Sep-22	4.7	30.5	11.1	0.45	32.93	54.46
09-Sep-22	5	30.4	10.8	0.51	32.61	55.09
10-Sep-22	6.6	31.1	12.7	0.64	32.88	54.87
11-Sep-22	5.2	30.2	9.5	0.55	31.83	59.00
12-Sep-22	5.6	30.2	12.8	0.88	30.84	56.43
13-Sep-22	5.2	28.7	10.8	0.88	29.90	58.99
14-Sep-22	4.6	28.7	10.8	0.79	29.61	62.99
15-Sep-22	5	28.5	10.7	0.67	29.61	61.98
16-Sep-22	4.6	28.5	10.7	0.72	30.79	60.39
17-Sep-22	5.2	29.3	13.0	0.44	30.13	55.23
18-Sep-22	4.8	29.1	12.9	0.41	30.42	53.21

Date	Evaporation (mm)	Average Water Temperature (ºC)	Rs at zero plane in MJ/m^2/day	Average Wind Velocity (m/s)	Average ambient temperature(ºC)	Average humidity (%)
19-Sep-22	4.2	29.2	10.7	0.33	31.19	53.55
20-Sep-22	3.2	28.4	7.6	0.32	30.46	59.84
21-Sep-22	3	28.7	8.4	0.50	30.50	62.68
28-Sep-22	4.6	30.8	14.0	0.36	30.09	54.00
29-Sep-22	4.8	27.3	13.6	0.29	29.79	54.36
30-Sep-22	4	27.4	13.3	0.28	30.18	54.99
01-Oct-22	4.2	26.6	13.6	0.41	31.26	58.01
02-Oct-22	4	25.9	13.0	0.33	29.14	48.58
03-Oct-22	4.2	25.6	14.0	0.32	29.29	48.21
04-Oct-22	4	25.8	13.5	0.32	28.23	51.04
05-Oct-22	3.8	25.5	12.5	0.30	28.32	51.52
06-Oct-22	3.7	26.1	13.3	0.69	28.62	54.24
09-Oct-22	1.4	22.3	1.9	0.21	22.81	82.59
10-Oct-22	3	22.5	2.5	0.14	22.59	82.71
11-Oct-22	3	23.7	10.3	0.19	23.63	73.99
12-Oct-22	3.8	23.3	13.4	0.16	24.23	69.08
13-Oct-22	4	22.6	13.3	0.18	24.45	63.03
14-Oct-22	4.2	22.3	13.0	0.22	24.97	58.50
15-Oct-22	4.6	22.5	12.4	0.11	25.04	57.95
16-Oct-22	3.8	22.3	13.1	0.18	24.76	55.22
17-Oct-22	4	22.4	13.1	0.25	26.08	48.31
18-Oct-22	4.4	21.9	13.0	0.32	26.03	44.05
19-Oct-22	4.2	21.7	12.5	0.43	26.91	40.06
20-Oct-22	3	21.6	12.0	0.33	26.33	39.71
21-Oct-22	3.2	21.4	12.0	0.28	25.15	43.95
22-Oct-22	3.2	20.4	10.6	0.17	22.77	49.24
23-Oct-22	3	19.7	11.6	0.16	22.77	45.85
24-Oct-22	3	19.1	11.5	0.22	23.11	43.27
25-Oct-22	3	19.4	10.9	0.27	23.69	43.10
26-Oct-22	3.2	20.7	11.4	0.22	25.11	42.93
27-Oct-22	3.4	21.4	11.1	0.30	26.02	41.06
28-Oct-22	3.4	20.8	10.8	0.24	24.48	42.77
29-Oct-22	3.6	19.7	10.0	0.13	24.08	41.89
30-Oct-22	3.4	19.5	10.3	0.19	24.04	40.73
31-Oct-22	3.2	20.2	10.5	0.20	24.72	41.19
01-Nov-22	3.6	20.6	10.5	0.25	25.24	41.66
02-Nov-22	3.4	20.4	8.3	0.25	24.37	47.47

Date	Evaporation (mm)	Average Water Temperature (ºC)	Rs at zero plane in MJ/m^2/day	Average Wind Velocity (m/s)	Average ambient temperature(ºC)	Average humidity (%)
03-Nov-22	3.8	21.0	8.1	0.25	25.41	47.91
04-Nov-22	3.8	21.7	10.0	0.29	26.39	43.55
05-Nov-22	3.6	21.0	11.0	0.19	25.85	39.95
06-Nov-22	4	20.2	9.8	0.19	25.31	35.85
09-Nov-22	2.9	19.6	9.6	0.16	23.10	55.39
10-Nov-22	3.2	19.6	9.6	0.17	21.49	54.32
11-Nov-22	2.9	17.6	9.4	0.19	20.34	53.89
12-Nov-22	2.6	17.4	10.5	0.24	19.83	50.27
13-Nov-22	2.6	17.7	9.8	0.21	21.94	47.43
14-Nov-22	2.6	19.2	9.6	0.43	23.90	41.62
15-Nov-22	2.4	18.2	7.7	0.16	20.55	50.41
16-Nov-22	2.4	16.2	10.5	0.23	18.29	50.55
17-Nov-22	2.2	14.8	10.4	0.31	17.34	47.05
19-Nov-22	2.2	15.1	10.5	0.17	18.54	42.65

A8.6.2

Eighteen models were created to estimate evaporation from water surfaces covered with solar photovoltaic panels under diurnal conditions, utilizing data collected from field experiments. Prior to model development, the data underwent preprocessing to eliminate errors or ambiguities. The section includes both the data used for model development and testing, with details provided in Section A8.6.2.1 for the various models developed and in Section A8.6.2.2 for the modeling and testing data.

A.8.6.2.1. Evaporation estimation models for solar PV panel covered water surface

Following Regression model have been developed for evaporation estimation for water body covered with solar panel.

1.The model Ep5Rh(Rs), that employs five parameters, namely R_s, T_a, T_w, V_w, and R_h, was developed, and it resulted in obtaining Equation (A8.7), which can be used for predicting evaporation. All data of open air parameters were utilised for model development.

$$Ep = 0.136046T_w - 0.001573R_s + 1.412181\ V_w - 0.031922T_a - 0.6329R_h + 3.633706 \quad (A8.7)$$

The predicted evaporation values from the modelling data were plotted against the actual values in Figure A8.6.2(1a), and the predicted values from the testing data were plotted against the actual recorded values in Figure A8.6.2(1b). The adjusted R^2 value of the model is 0.7227.

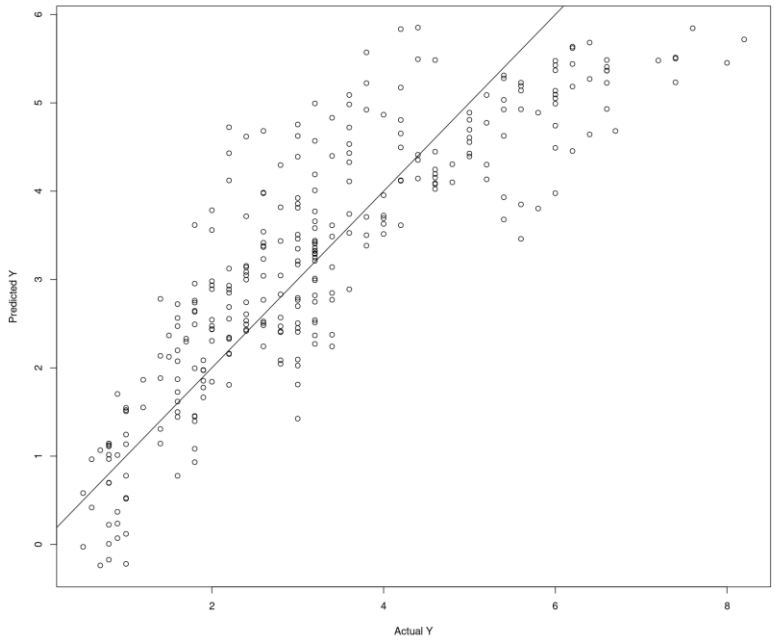

Figure A8.6.2(1a), plot of predicted evaporation values from equation (A8.7), against actual values from model data,

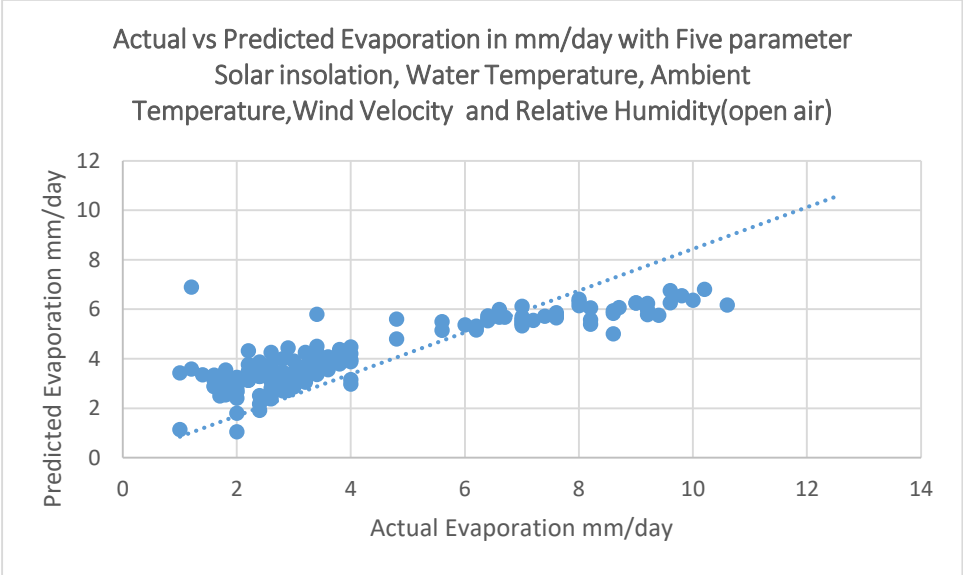

Figure A8.6.2(1b), plot of predicted evaporation values from equation (A8.7),against actual values from test data

2.The model Ep5Rh(Tp) is being developed to estimate evaporation considering panel Temperature instead of solar radiation , so parameters considered in model development are T_p, T_a, T_w, V_w, and R_h. The equation (A8.8) has been developed, utilising all other parameters from open air.

$$Ep = 0.093722T_w + 0.081032T_p + 1.31707\ V_w - 0.08342228T_a - 0.059557R_h + 3.441718 \quad (A8.8)$$

The predicted evaporation values from the modelling data were plotted against the actual values in Figure A8.6.2(2a),

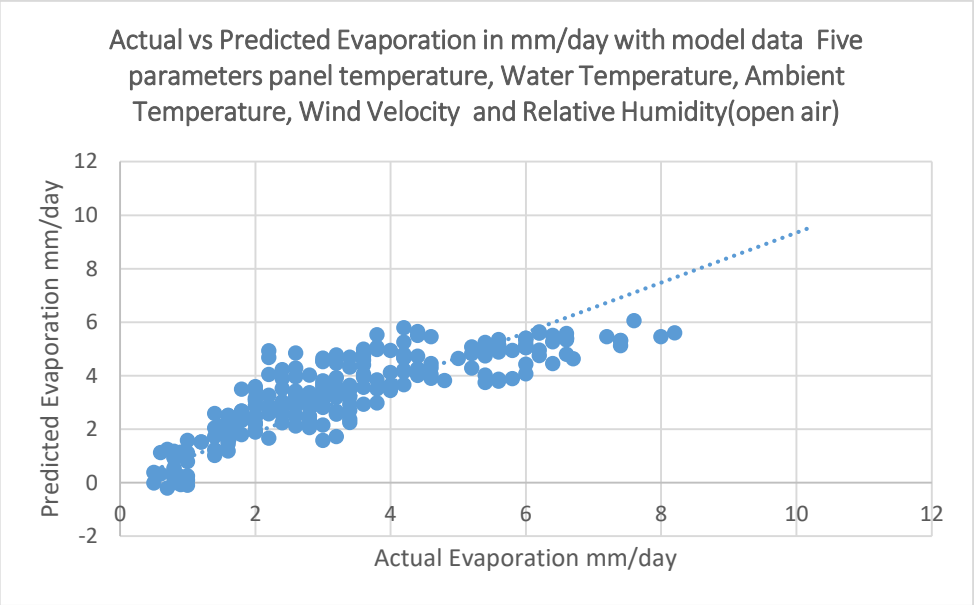

Figure A8.6.2(2a), plot of predicted evaporation values from equation (A8.8), against actual values from model data, and the predicted values from the testing data were plotted against the actual recorded values in Figure A-8.6.2(2b). The adjusted R2 value of the model is 0.7088.

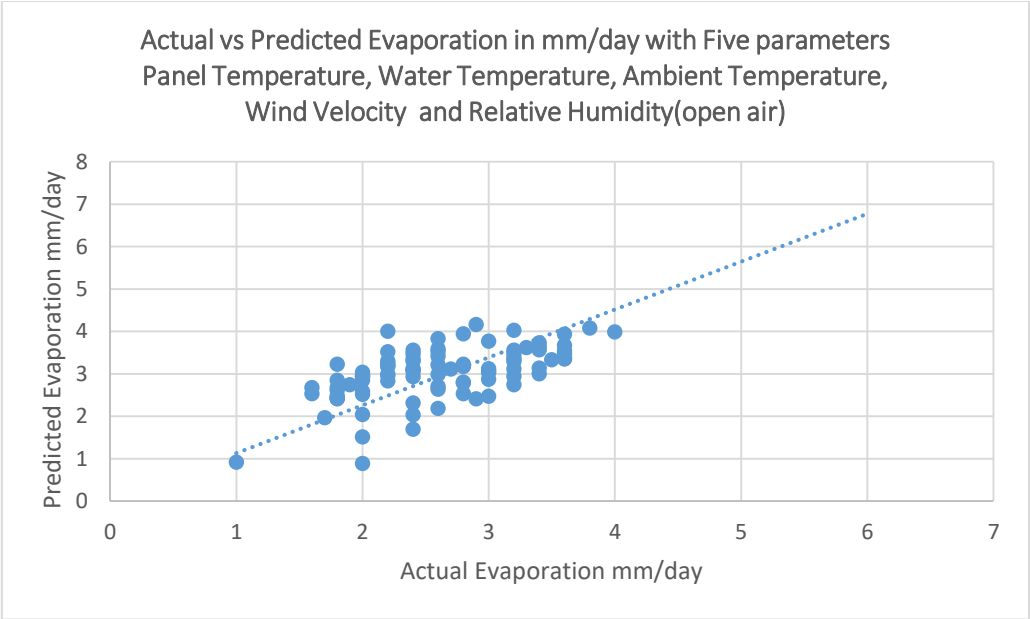

Figure A8.6.2(2b), plot of predicted evaporation values from equation (A8.8),against actual values from test data

3. The model Ep5Rhp(Rs) is developed utilising parameter R_s, T_a, T_w, V_w recorded in open air and R_{hp} is the humidity recorded under the panel, just above the water surface. The Equation (A8.9) is developed as follows

$$Ep = 0.021275T_w + 0.03202R_s + 1.29896\ V_w + 0.07908T_a - 0.037869R_{hp} + 2.043275 \quad \text{(A8.9)}$$

The predicted evaporation values from the modelling data were plotted against the actual values in Figure A8.6.2(3a),

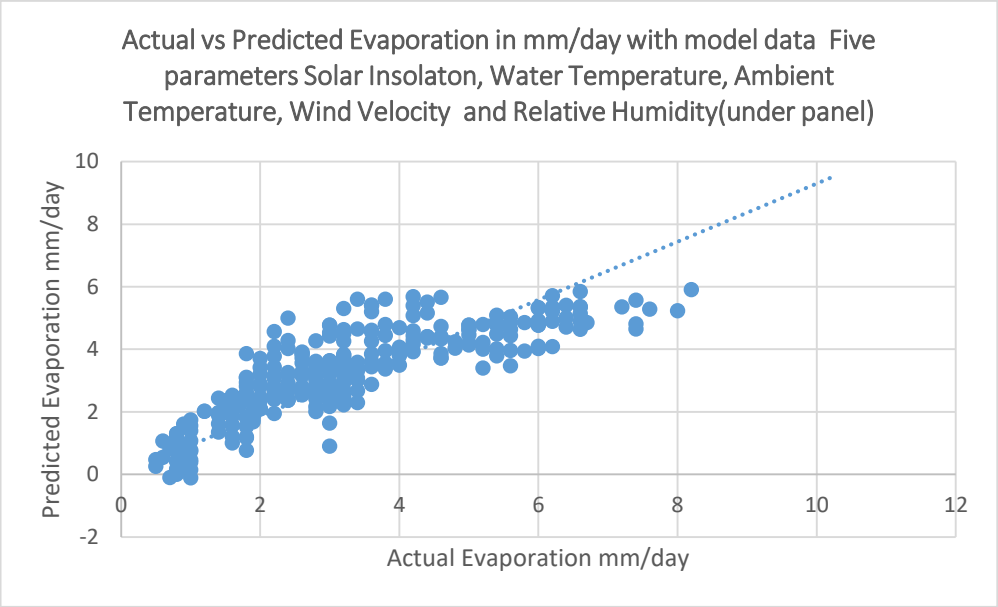

Figure A8.6.2(3a), plot of predicted evaporation values from equation (A8.9), against actual values from model data, and the predicted values from the testing data were plotted against the actual recorded values in Figure A8.6.2(3b). The adjusted R^2 value of the model is 0.6739.

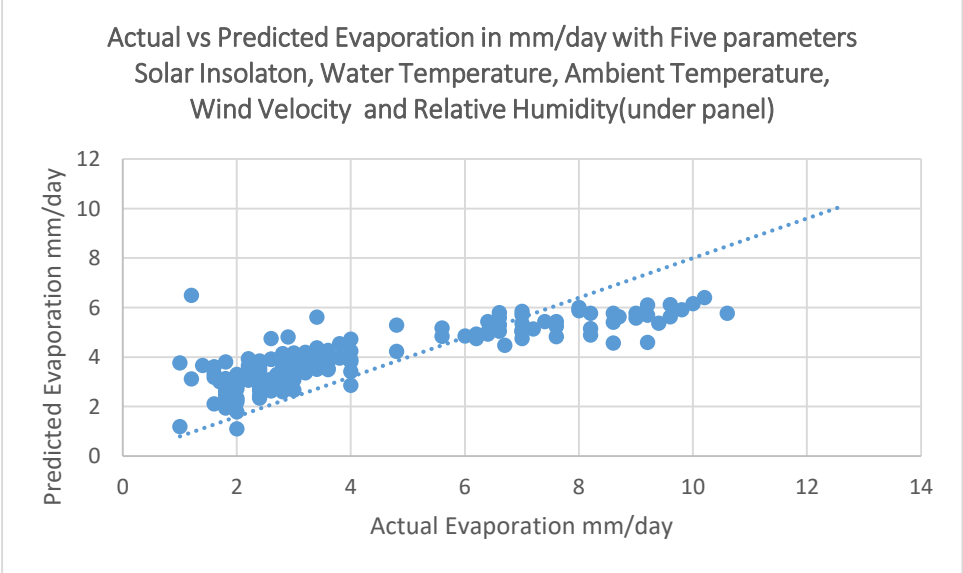

Figure A8.6.2(3b), plot of predicted evaporation values from equation (A8.9),against actual values from test data

4. The four parametric model is developed which took into account humidity under the panel, while all other parameter values were recorded in open air.

(D) The Ep4Rhp(Tw) model resulted in Equation (A8.10), which was developed using recorded values R_s, T_w, V_w in open air and R_{hp} under panel

$$Ep = 0.097837T_w + 0.037859R_s + 1.45072\ V_w - 0.04329R_{hp} + 2.489682 \qquad (A8.10)$$

The predicted evaporation values from the modelling data were plotted against the actual values in Figure A8.6.2(4a), and the predicted values from the testing data were plotted against the actual recorded values in Figure A8.6.2(4b) The R^2 of the model is 0.6668.

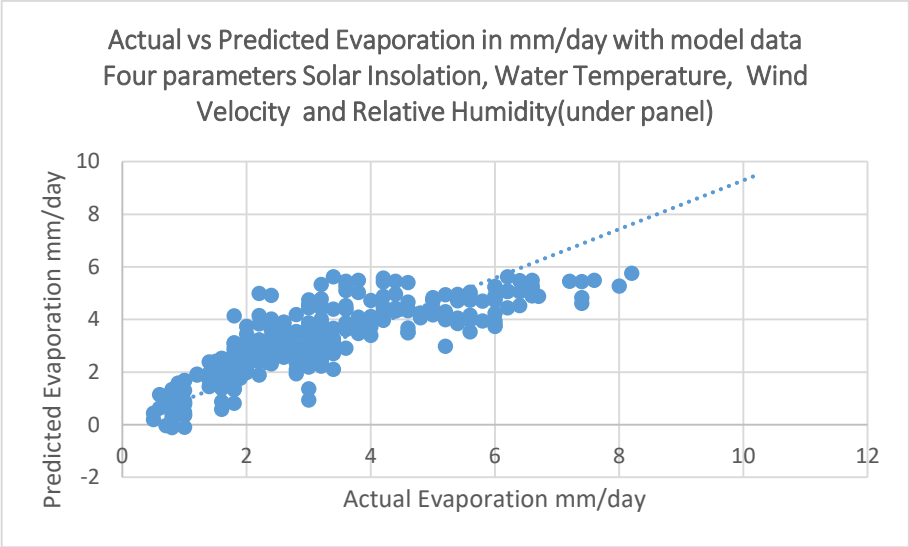

Figure A8.6.2(4a), plot of predicted evaporation values from equation (A8.10), against actual values from model data

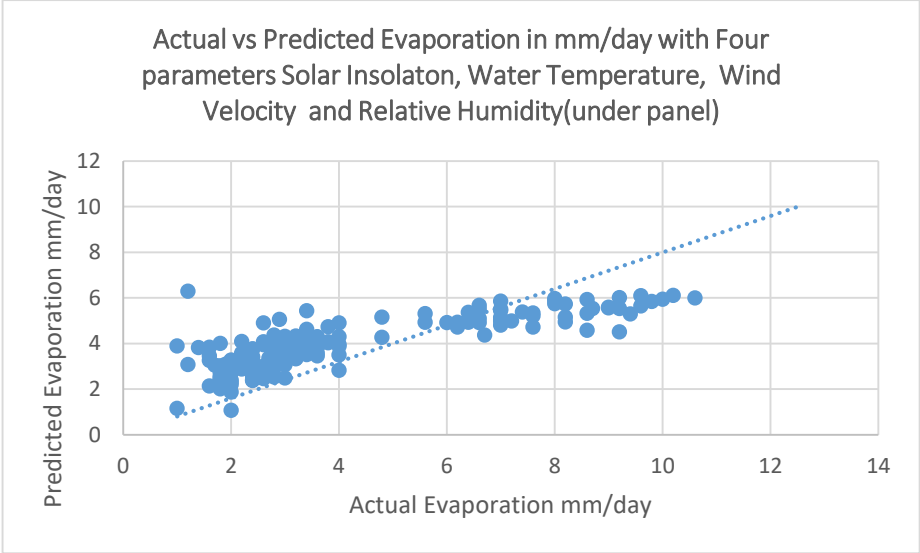

Figure A8.6.2(4b), plot of predicted evaporation values from equation (A8.10),against actual values from test data

(E) The Ep4Rhp(Ta) model resulted in Equation (A8.11), which was developed using recorded values of Rs, Ta, and V_w in open air, with Rhp being recorded under panel. The R2 value for this model is 0.6745. In Figure A8.6.2(4c), the graph shows a comparison between the predicted evaporation values from the modelling data and the actual values. On the other hand, Figure A8.6.2(4d) displays the predicted values from the testing data and the actual recorded values for comparison.

$$Ep = 0.032493R_s + 1.279266\ V_w + 0.098649T_a - 0.036484R_{hp} + 1.952207 \qquad (A8.11)$$

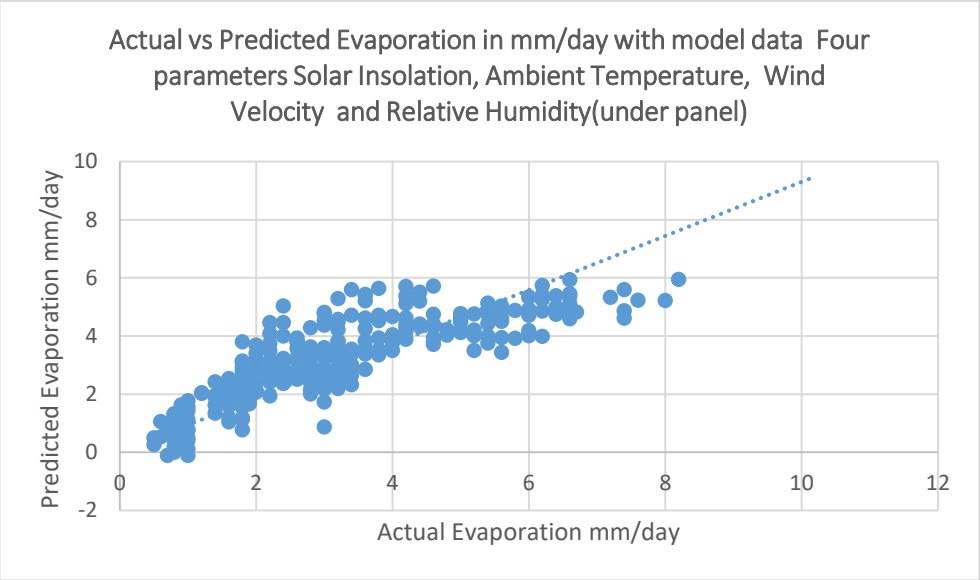

Figure A8.6.2(4c), plot of predicted evaporation values from equation (A8.11), against actual values from model data,

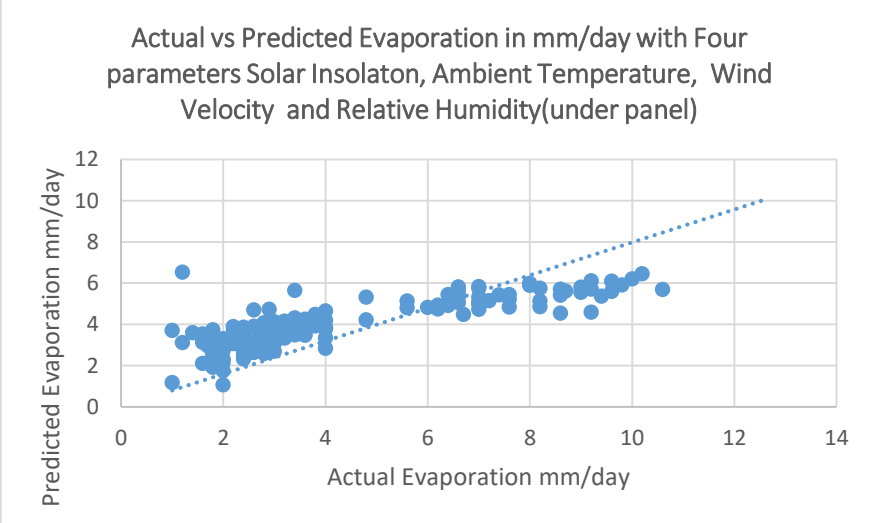

Figure A8.6.2(4d), plot of predicted evaporation values from equation (A8.11),against actual values from test data

(F) The Ep4Rhp(TaTw) model resulted in Equation (8.12) was developed using parameters Ta, Tw, and V_w, which were recorded in open air, along with Rsp, which represents the humidity recorded just above the water surface. The R^2 value for this model is 0.6731, indicating a moderately strong correlation between the variables. In order to evaluate the accuracy of the modelling data, the predicted evaporation values were compared against the actual values and plotted in Figure A8.6.2(4e). Similarly, the predicted values from the testing data were also compared against the actual recorded values and plotted in Figure A8.6.2(4f). This analysis helps in assessing the performance of the model and its ability to make accurate predictions.

$$Ep = 0.022348T_w + 1.328705\ V_w + 0.082464T_a - 0.040453R_{hp} + 2.462838 \quad \text{(A8.12)}$$

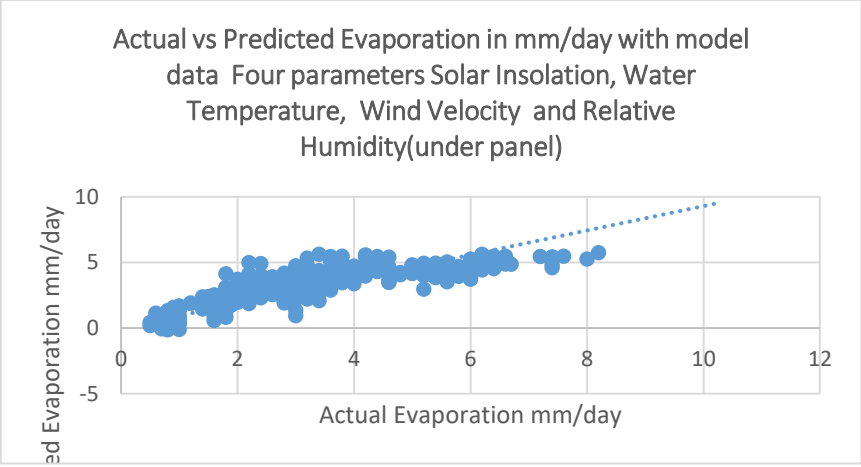

Figure A8.6.2(4e), plot of predicted evaporation values from equation (A8.12), against actual values from model data,

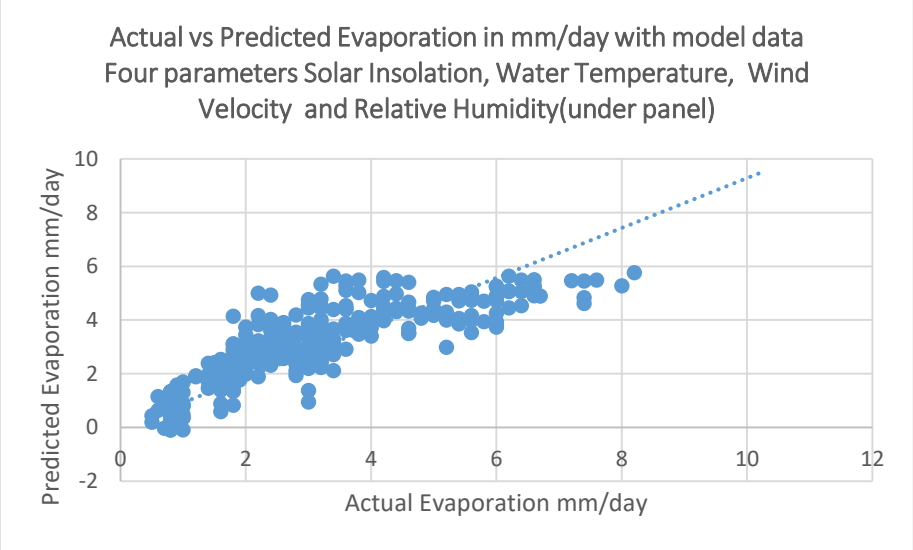

Figure A8.6.2(4f), plot of predicted evaporation values from equation (A8.12),against actual values from test data

5. Based on the data recorded, a three parametric model was developed. The model includes one fixed parameter, which is humidity recorded under the panel. All other parameter values were recorded in open air. The model resulted in three different models, each with three parameters.

(A) The model Ep3Rhp(Tw) was developed using parameters Tw, V_w, and Rhp, and resulted in Equation (A8.13) with an R^2 value of 0.6652. In Figure A8.6.2(5a), the model's predicted evaporation values were compared to the actual values, using the modelling data. Similarly, Figure A8.6.2(5b) shows the comparison between the predicted values from the testing data and the actual recorded values.

$$Ep = 0.103021T_w + 1.493906\ V_w - 0.046645R_{hp} + 3.012427 \quad \text{(A8.13)}$$

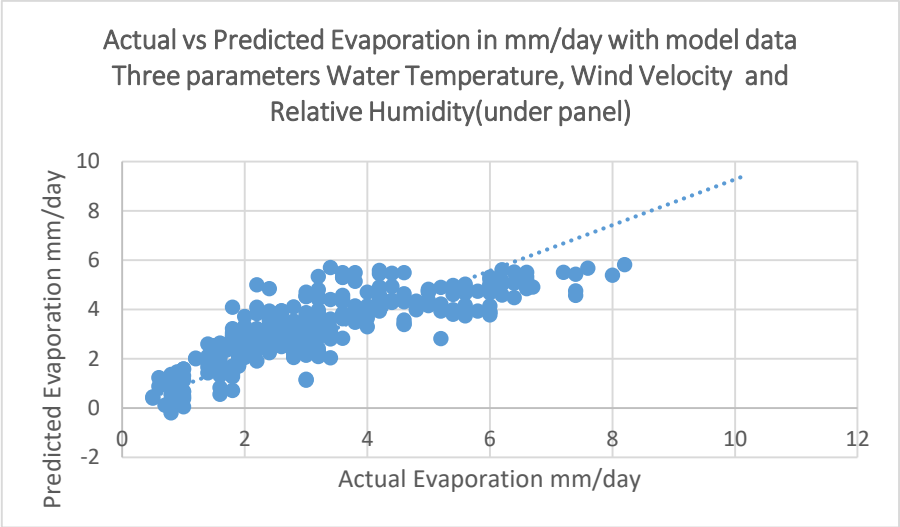

Figure A8.6.2(5a), plot of predicted evaporation values from equation (A8.13), against actual values from model data,

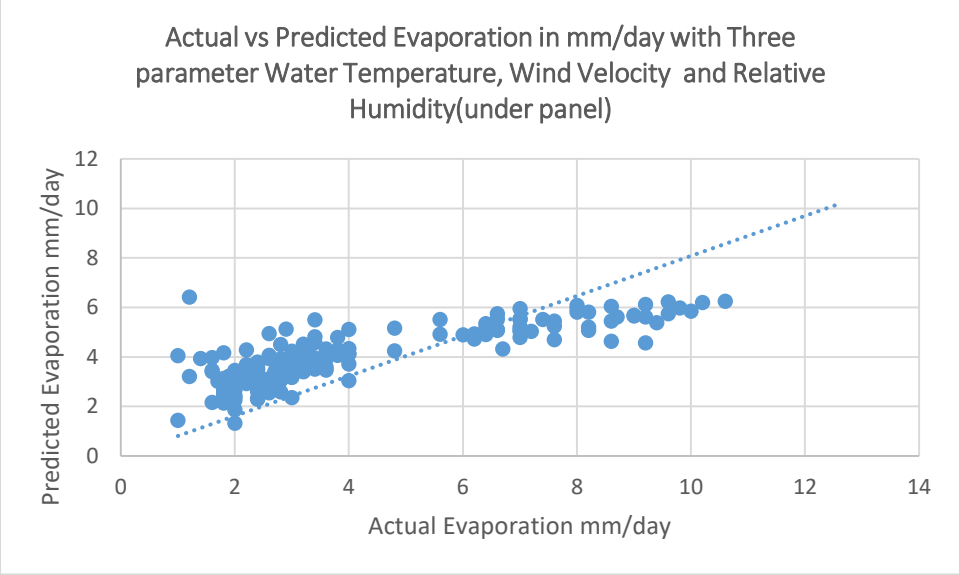

Figure A8.6.2(5b), plot of predicted evaporation values from equation (A8.13),against actual values from test data

(B) The Ep3Rhp(Ta) model has been developed and resulted in Equation (A8.14) with parameters T_a, V_w, and R_{hp}. The R^2 value obtained for the model is 0.6736. In Figure A8.6.2(5c), the predicted evaporation values from the model were compared to the actual values using the modelling data. Similarly, Figure A8.6.2(5d) shows the comparison between the predicted values from the testing data and the actual recorded values.

$$Ep = 0.103089T_a + 1.308465\ V_w - 0.039037R_{hp} + 2.373624 \qquad \text{(A8.14)}$$

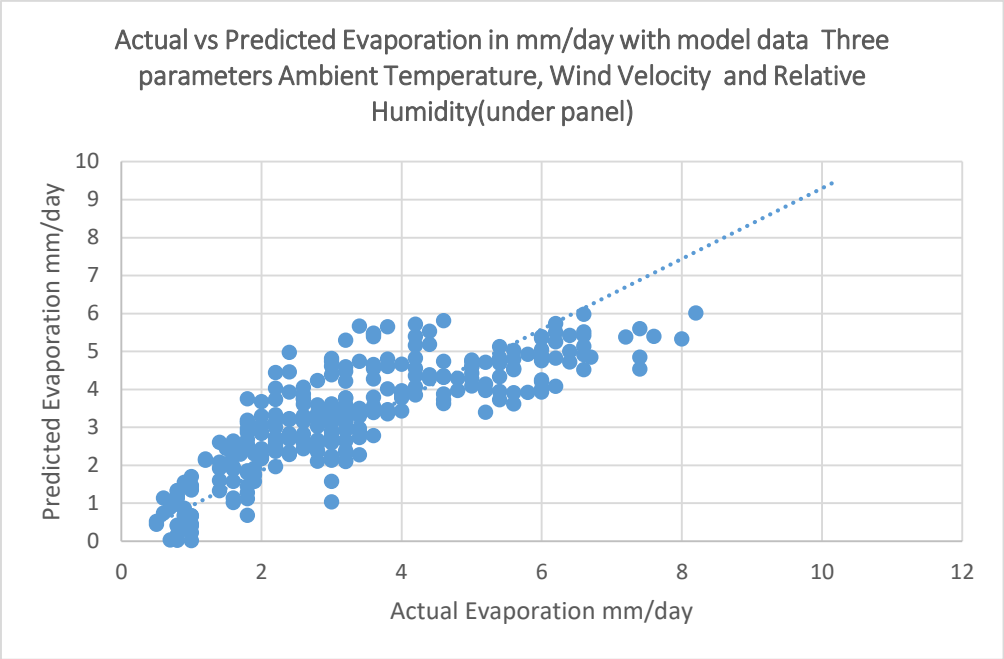

Figure A8.6.2(5c), plot of predicted evaporation values from equation (A8.14), against actual values from model data,

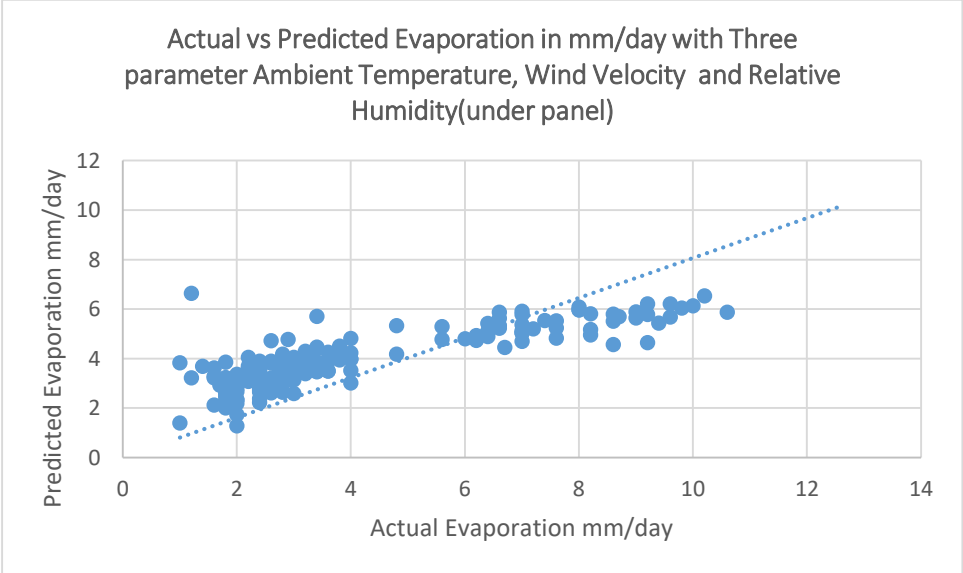

Figure A8.6.2(5d), plot of predicted evaporation values from equation (A8.14),against actual values from test data

(C) The model Ep3Rhp(Rs) was developed with parameters R_s, V_w, and R_{hp}, resulting in Equation (A8.15) and an R^2 value of 0.5587. Figure A8.6.2(5e) displays the comparison between the model's predicted evaporation values and the actual values, using the modelling data. Similarly, Figure A8.6.2(5f) shows the comparison between the predicted values obtained from the testing data and the actual recorded values.

$$Ep = 0.118474\ R_s + 2.201331\ V_w - 0.041461 R_{hp} + 3.305054 \qquad \text{(A8.15)}$$

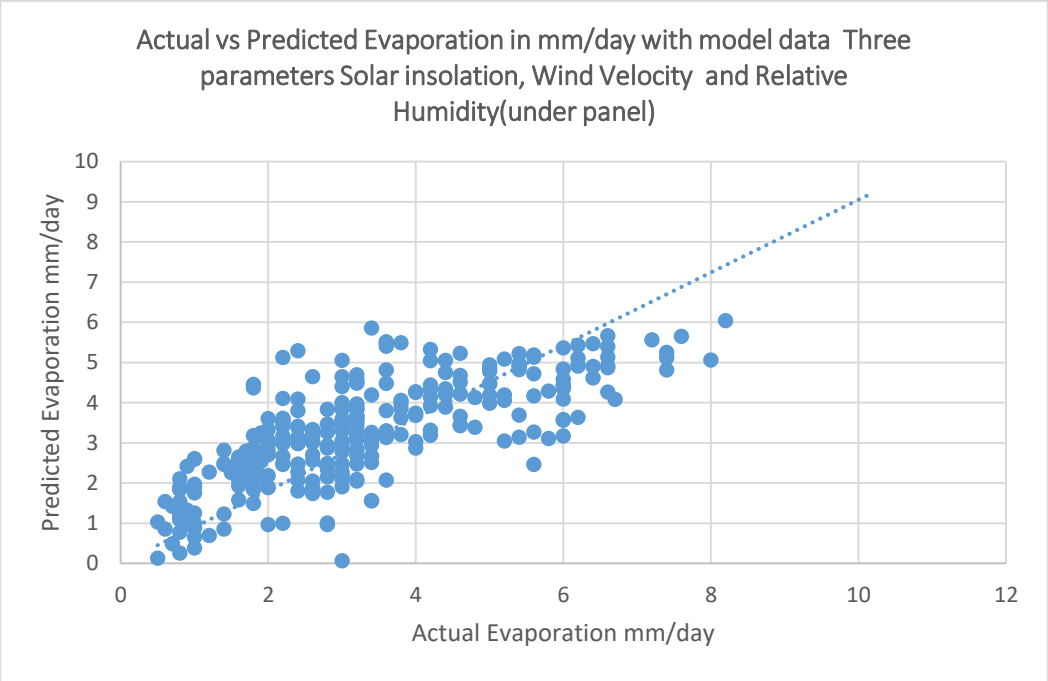

Figure A8.6.2(5e), plot of predicted evaporation values from equation (A8.15), against actual values from model data,

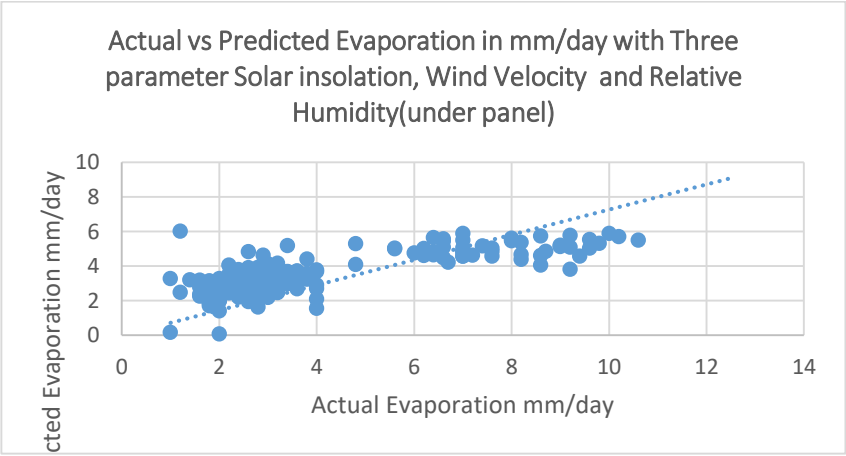

Figure A8.6.2(5f), plot of predicted evaporation values from equation (A8.15),against actual values from test data

6. Based on the consideration of four parametric models, all parameters recorded in open air, following two models were developed with four parameters. These models are expected to be helpful in estimating evaporation losses, as the data is readily available with the meteorological department.

(A) The model Ep4Rh(Tw) was developed using parameters R_s, T_w, V_w and R_h, which were recorded in open air. This resulted in Equation (A8.16) with an R^2 value of 0.7226, indicating a strong correlation between the variables (The details of plot between model's predicted evaporation values and the actual values are given in Appendix. Figure A8.6.2(6a) displays the comparison between the model's predicted evaporation

values and the actual values, using the modelling data. Similarly, Figure A8.6.2(6b) shows the comparison between the predicted values obtained from the testing data and the actual recorded values

$$Ep = 0.1046991T_w - 0.0004954R_s + 1.3587531\ V_w - 0.059813R_h + 3.368953 \quad \text{(A8.16)}$$

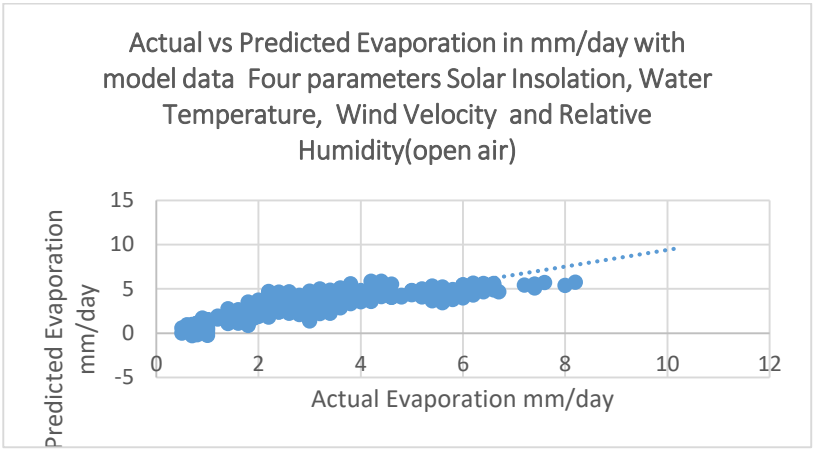

Figure A8.6.2(6a), plot of predicted evaporation values from equation (A8.16), against actual values from model data,

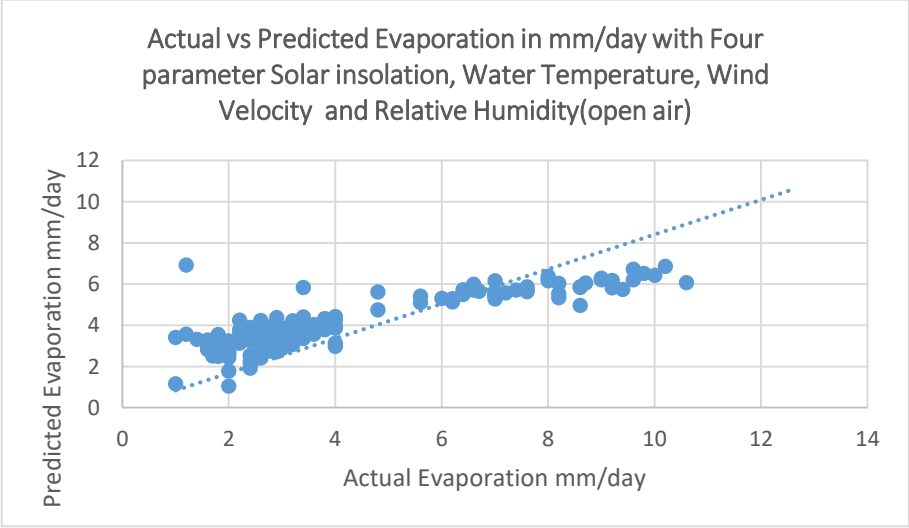

Figure A8.6.2(6b), plot of predicted evaporation values from equation (A8.16),against actual values from test data

B The model Ep4Rh(Ta) was developed using parameters R_s ,T_a, V_w and R_h, which were recorded in open air. Equation (A8.17) was derived, which has an R^2 value of 0.7058, indicating a strong correlation between the variables. In Figure A8.6.2(6c), the predicted evaporation values from the model were compared to the actual values using the modelling data. Similarly, Figure A8.6.2(6d) shows the comparison between the predicted values from the testing data and the actual recorded values.

$$Ep = 0.094895T_a + 0.012928\ R_s + 1.289449\ V_w - 0.048998R_h + 2.656733 \quad \text{(A8.17)}$$

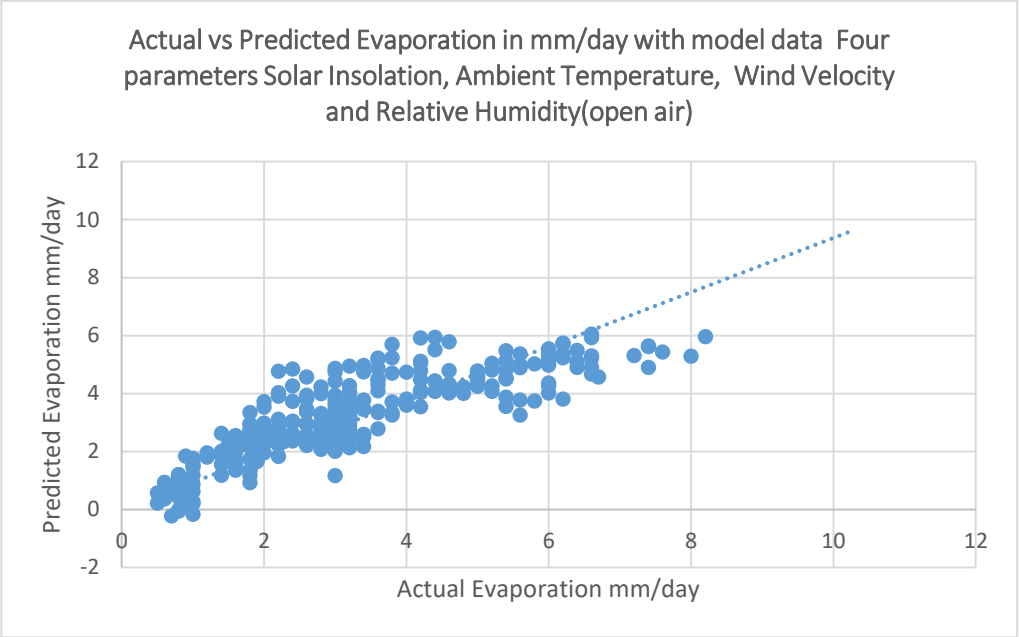

Figure A8.6.2(6c), plot of predicted evaporation values from equation (A8.17), against actual values from model data,

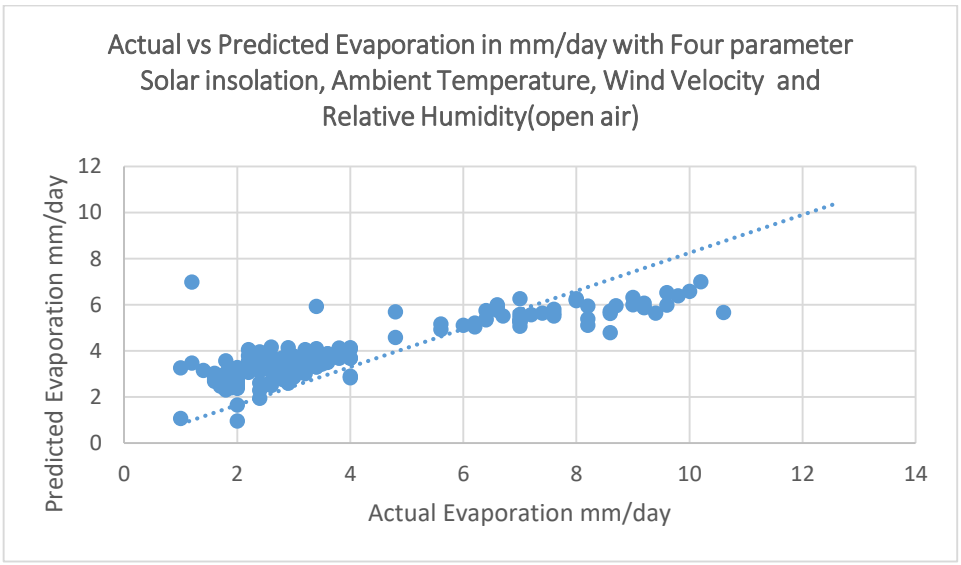

Figure A8.6.2(6d), plot of predicted evaporation values from equation (A8.17),against actual values from test data

7 Three parametric model were developed utilising data recorded in open air. Following are three models developed with three parameters.

A Model E3Rh(Rs) was developed using parameters R_s , V_w and R_h, which were recorded in open air. Equation (A8.18) was obtained from this model, which has an R^2 value of 0.5992, indicating a moderate correlation between the variables. In Figure A8.6.2(7a), the predicted evaporation values from the model were compared to the actual values using the modelling data. Similarly, Figure A8.6.2(7b) shows the comparison between the predicted values from the testing data and the actual recorded values.

$$Ep = 0.092451\ R_s + 2.172817\ V_w - 0.055459 R_h + 4.049228 \quad \text{(A8.18)}$$

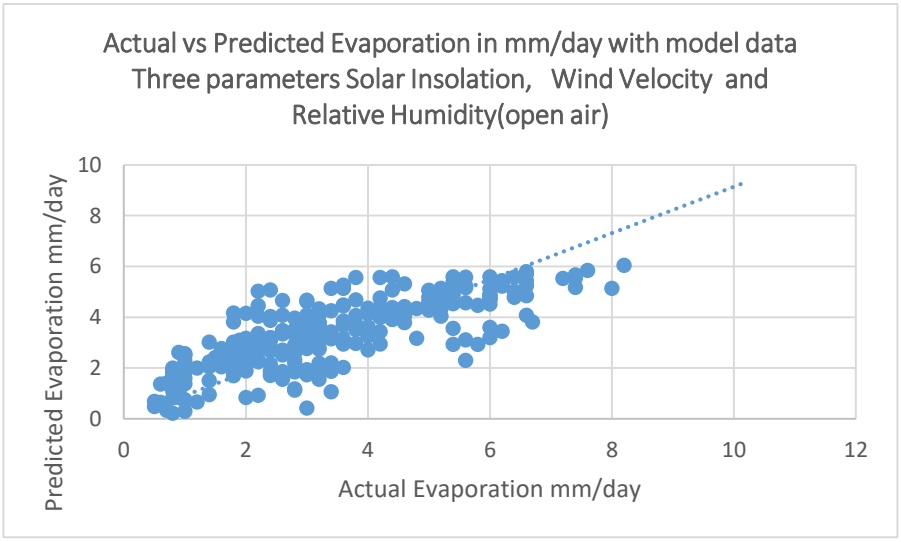

Figure A8.6.2(7a), plot of predicted evaporation values from equation (A8.18), against actual values from model data,

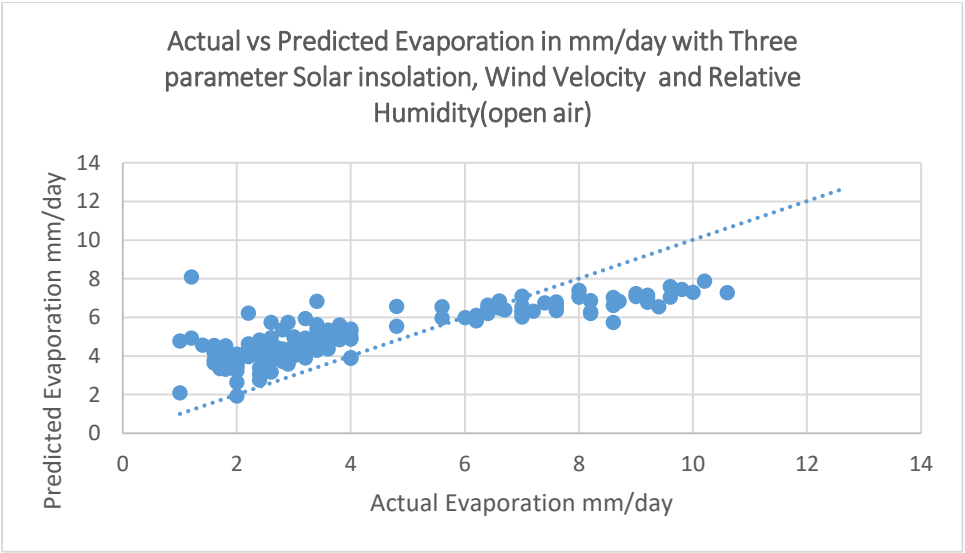

Figure A8.6.2(7b), plot of predicted evaporation values from equation (A8.18),against actual values from test data

B The E3Rh(Tw) model was developed using parameters T_w , V_w and R_h recorded in open air. Equation (A8.19) was obtained from this model and has an R2 value of 0.7236, indicating a strong correlation between the variables. Figure A8.6.2(7c) shows the comparison between the predicted evaporation values obtained from the model and the actual values, using the modelling data. Similarly, Figure A8.6.2(7d) displays the comparison between the predicted values from the testing data and the actual recorded values.

$$Ep = 0.10463 T_w + 1.35826\ V_w - 0.05976 R_h + 3.36202 \quad \text{(A8.19)}$$

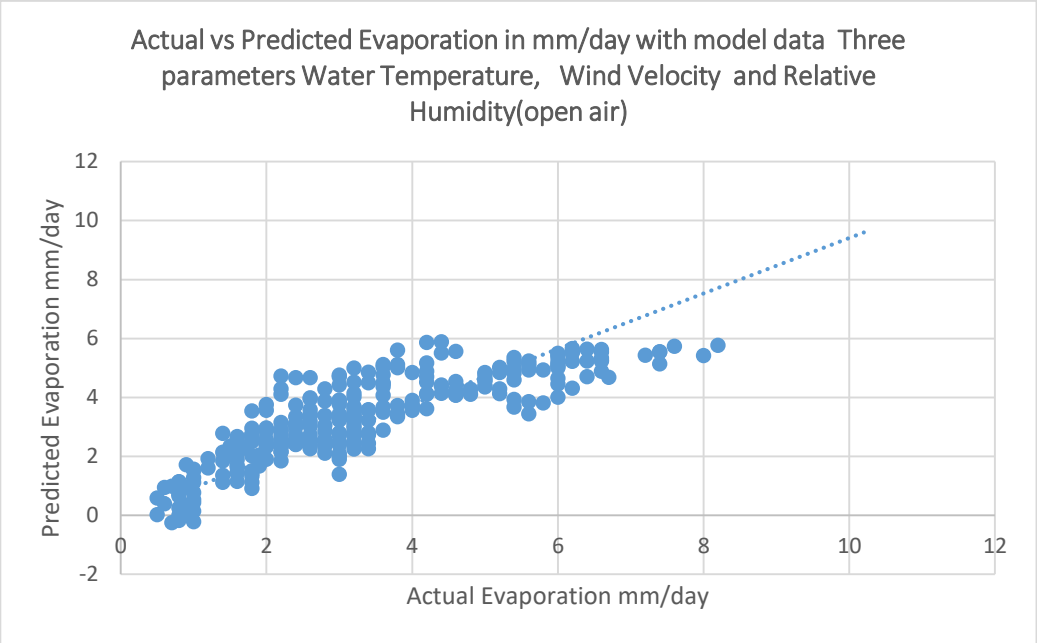

Figure A8.6.2(7c), plot of predicted evaporation values from equation (A8.19)), against actual values from model data,

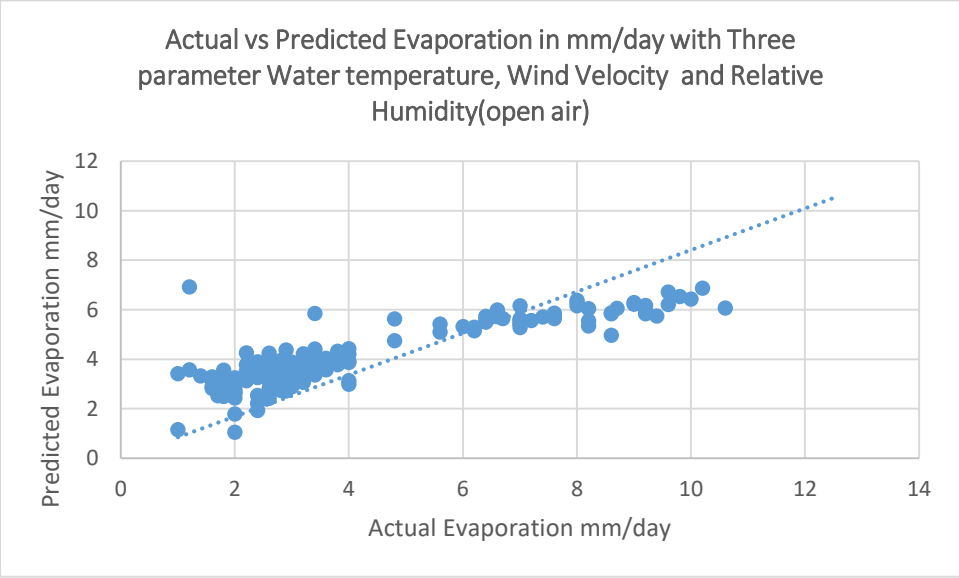

Figure A8.6.2(7d), plot of predicted evaporation values from equation (A8.19),against actual values from test data

C The Ep3Rh(Ta) model was developed using parameters T_a , V_w and R_h recorded in open air. Equation (A8.20) was obtained from this model and has an R^2 value of 0.7065, indicating a strong correlation between the variables. In Figure A8.6.2(7e), the predicted evaporation values from the model were compared to the actual values using the modelling data. Similarly, Figure A8.6.2(7f) shows the comparison between the predicted values from the testing data and the actual recorded values.

$$Ep = 0.096584T_a + 1.301555\ V_w - 0.050205R_h + 2.828754 \qquad (A8.20)$$

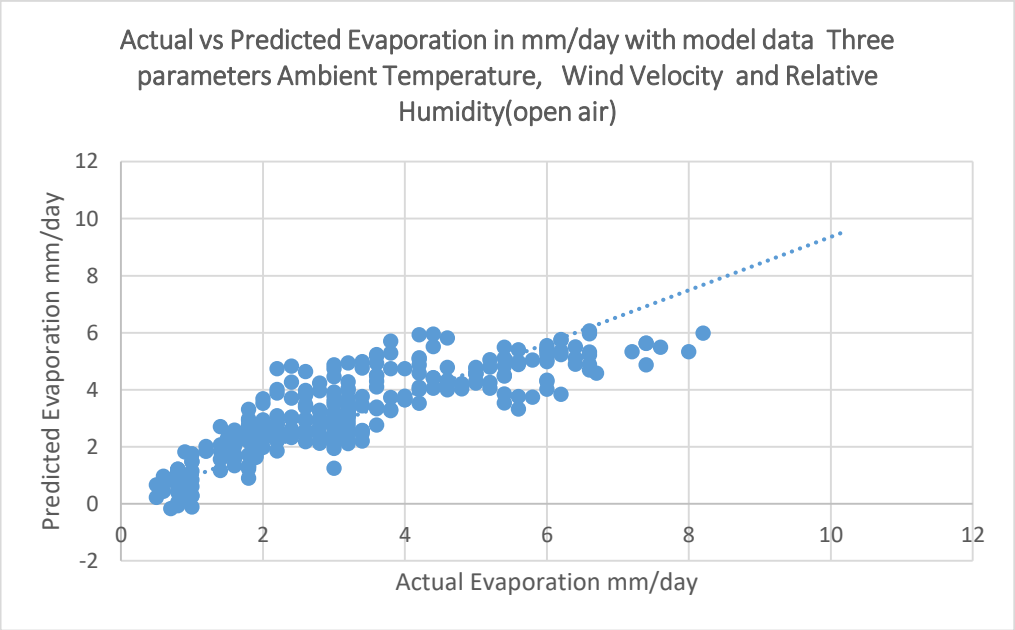

Figure A8.6.2(7e), plot of predicted evaporation values from equation (A8.20), against actual values from model data,

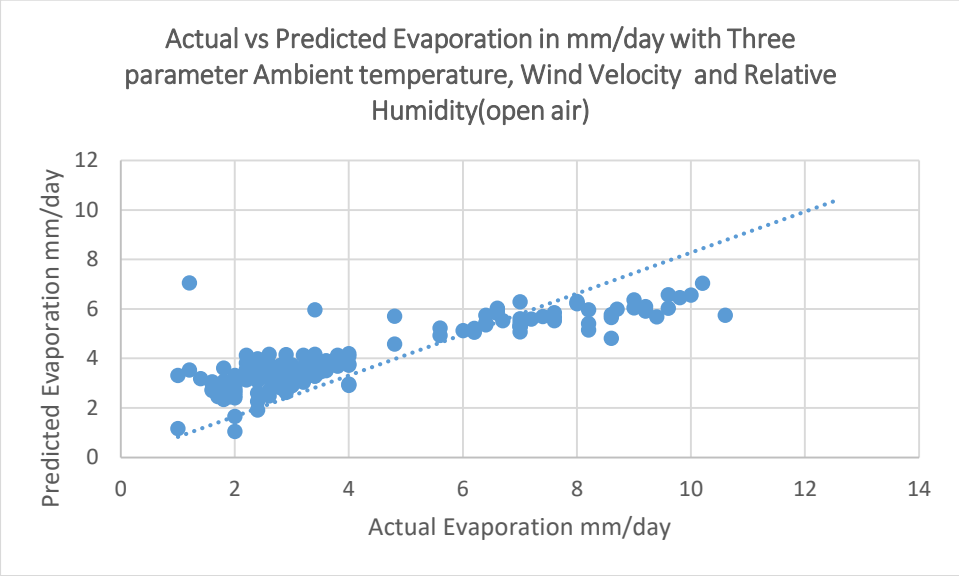

Figure A8.6.2(7f), plot of predicted evaporation values from equation (A8.20),against actual values from test data

8 Two variable models were developed, considering limited data availability in the field. Following are four models with two parameters

A The E2Rh(Tw) model was developed using parameters T_w , and R_h recorded in open air. Equation (A8.21) was obtained from this model and has an R^2 value of 0.7021, indicating a strong correlation between the variables. In Figure A8.6.2(8a), the predicted evaporation values from the model were compared to the actual values using the modelling data. Similarly, Figure A8.6.2(8b) shows the comparison between the predicted values from the testing data and the actual recorded values.

$$Ep = 0.117294T_w - 0.062778R_h + 3.74309 \quad \text{(A8.21)}$$

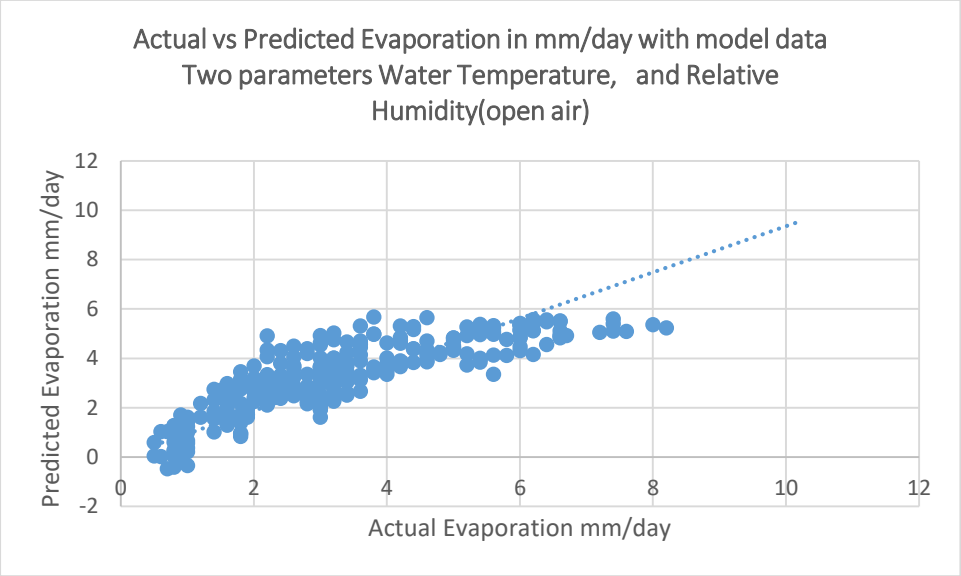

Figure A8.6.2(8a), plot of predicted evaporation values from equation (A8.21), against actual values from model data,

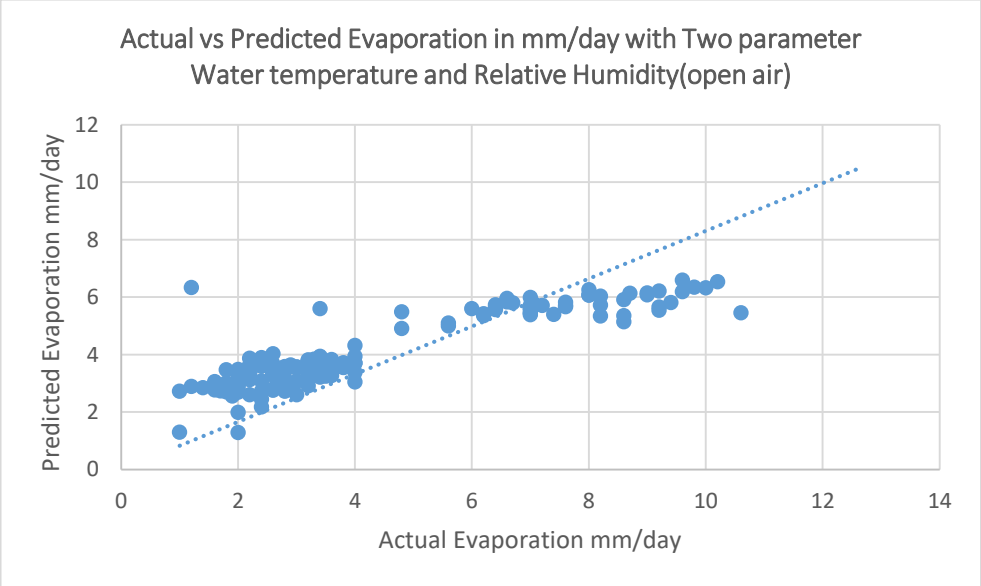

Figure A8.6.2(8b), plot of predicted evaporation values from equation (A8.21),against actual values from test data

B The Ep2V(Tw) model was created by using the parameters T_w and V_w that were recorded in an open-air environment. The resulting Equation (A8.22) has an R^2 value of 0.4141, which suggests a weak correlation between the variables. Due to this weak correlation, the model that uses these parameters may not be effective in establishing a relationship between the variables. As a result, comparative graphs of actual values against predicted values were not generated for this model.

$$Ep = 0.12885T_w + 2.30659\ V_w - 0.52315 \quad \text{(A8.22)}$$

C The Ep2Rh(Ta) model was created by utilizing the parameters T_a and R_h that were observed in an open-air setting. The resulting Equation (A8.23) has an R^2 value of

0.6874, which suggests a significant correlation between the variables. Figure A8.6.2(8c) displays the comparison between the predicted evaporation values obtained from the model and the actual values, using the modelling data. Similarly, Figure A8.6.2(8d) shows the comparison between the predicted values from the testing data and the actual recorded values.

$$Ep = 0.109689T_a - 0.05159R_h + 3.061951 \quad \text{(A8.23)}$$

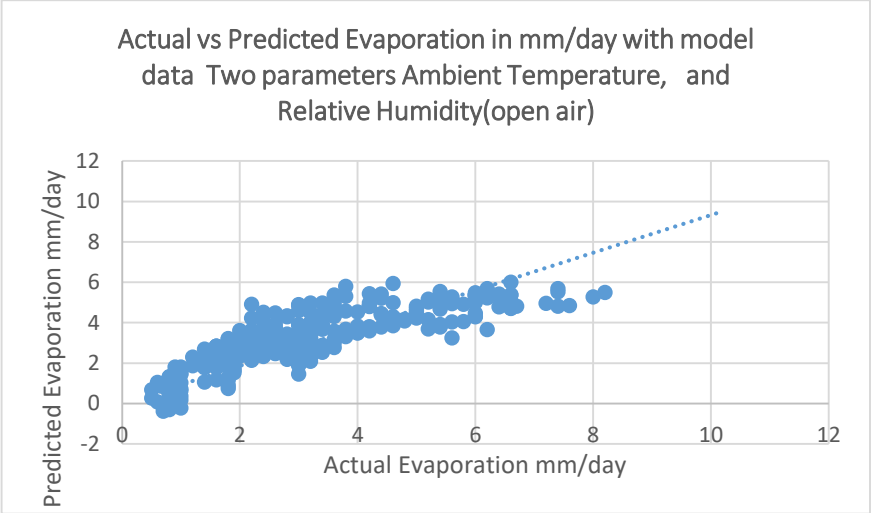

Figure A8.6.2(8c), plot of predicted evaporation values from equation (A8.23), against actual values from model data,

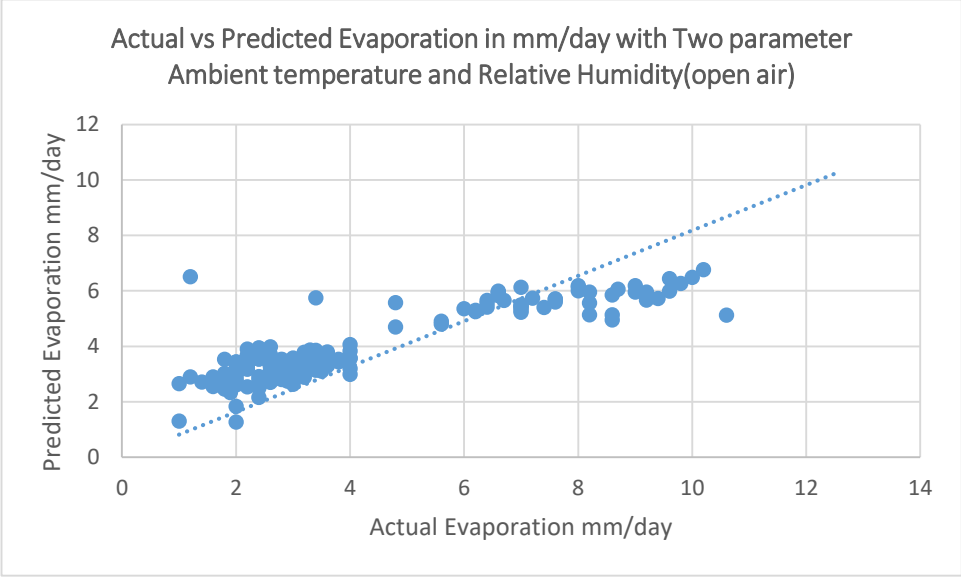

Figure A8.6.2(8d), plot of predicted evaporation values from equation (A8.23),against actual values from test data

D Equation (A8.24) was obtained from the model Ep2V(Ta), which utilizes the parameters T_a and V_w that were observed in an open-air setting. However, the resulting R^2 value for this model is 0.5172, which suggests a weak correlation between the variables. Hence,

this model may not be effective in establishing a relationship between the variables. Consequently, no comparative graphs of actual values versus predicted values were created for this model.

$$Ep = 0.14317T_a + 1.64103\ V_w - 0.97471 \quad \text{(A8.24)}$$

A8.6.2.2. Modelling and testing data for evaporation estimation models for solar PV panel covered water surface.

Date	evaporation (panel at height 300 mm) mm/day	Average Water Temp in °C	Rs in MJ/m^2/day	Average Wind speed (m/s)	Average daily ambient temp (°C)	Average daily humidity (%)	Average daily humidity under panel (%)	Panel temperature in °C
24.03.21	3.8	21.00	14.8	0.31	22.71	42.32	42.29	19.43
25.03.21	3.8	20.33	12.6	0.32	22.56	43.10	45.10	26.96
26.03.21	4	21.33	16.3	0.35	25.34	39.06	41.83	24.49
27.03.21	4.6	23.67	15.6	0.39	28.01	36.21	36.10	29.22
28.03.21	6.4	25.00	15.4	0.54	31.51	33.57	41.05	31.88
29.03.21	8.2	24.33	14.6	0.85	32.41	21.62	20.77	33.93
30.03.21	7.6	23.00	10.8	0.92	26.34	21.47	23.03	33.54
31.03.21	7.4	22.00	17.0	0.46	25.01	19.26	25.98	27.77
01.04.21	6.6	21.67	16.8	0.52	23.78	18.41	25.20	28.63
02.04.21	5.6	21.00	16.9	0.38	25.08	15.35	23.06	27.50
03.04.21	5.4	21.33	16.8	0.36	26.19	14.27	20.88	29.20
04.04.21	7.4	23.00	15.7	0.42	30.30	13.44	30.72	30.82
05.04.21	8	25.00	12.6	0.50	29.91	20.75	20.07	33.92
06.04.21	7.2	25.00	14.3	0.73	29.38	25.68	25.01	33.18
07.04.21	6	23.67	16.4	0.30	25.47	26.81	37.52	34.30
08.04.21	5.4	23.00	17.5	0.28	25.08	22.19	25.32	30.52
09.04.21	5.2	23.00	16.8	0.26	26.48	18.48	18.76	30.13
10.04.21	5.6	23.00	17.0	0.28	27.27	17.71	19.33	30.94
11.04.21	6	23.00	16.5	0.24	28.71	17.50	22.86	31.75
12.04.21	6.6	24.67	15.6	0.35	29.55	18.20	19.01	33.01
13.04.21	6.4	25.33	15.5	0.29	29.84	19.62	21.22	33.62
14.04.21	6	24.67	10.7	0.44	30.39	19.84	26.30	34.27
15.04.21	6.4	25.33	15.1	0.53	30.10	18.34	19.15	32.06
17.04.21	2	22.67	16.7	0.44	25.21	43.04	63.75	24.44
18.04.21	2.2	24.33	15.6	0.25	27.47	35.92	38.52	29.87
19.04.21	3	25.67	16.0	0.33	30.43	29.08	30.84	32.58
21.04.21	1.8	22.33	14.9	0.44	23.01	46.11	40.20	25.28
22.04.21	2.4	24.00	16.5	0.68	30.03	35.64	35.36	27.93
23.04.21	2.2	24.33	15.0	0.58	23.99	40.19	29.69	34.98
25.04.21	2.2	22.33	17.4	0.30	27.73	23.05	58.85	30.07
26.04.21	3.6	24.00	16.4	0.31	30.37	19.78	34.91	32.17

Date	evaporation (panel at height 300 mm) mm/day	Average Water Temp in °C	Rs in MJ/m^2/day	Average Wind speed (m/s)	Average daily ambient temp (°C)	Average daily humidity (%)	Average daily humidity under panel (%)	Panel temperature in °C
27.04.21	3.8	25.00	16.1	0.42	32.31	15.79	15.45	34.87
28.04.21	4.6	25.00	13.9	0.41	33.87	16.21	15.08	36.01
29.04.21	6.6	24.33	14.0	0.48	34.87	17.06	27.66	36.82
30.04.21	6.2	25.00	12.8	0.55	33.49	20.26	26.50	38.56
01.05.21	6	24.33	11.6	0.49	32.03	23.03	52.86	37.90
02.05.21	6	24.67	10.2	0.63	30.96	28.15	55.87	34.77
03.05.21	6.2	25.33	15.5	0.53	32.12	25.18	28.80	32.27
04.05.21	5.6	24.67	13.5	0.57	31.78	24.75	48.00	36.71
05.05.21	5.2	24.67	15.4	0.39	31.89	27.24	70.94	35.02
06.05.21	2.6	26.33	9.3	0.57	30.37	37.20	56.20	36.29
07.05.21	2.8	26.33	13.9	0.36	29.85	38.77	59.73	30.06
08.05.21	3.4	25.00	14.1	0.31	32.41	31.86	35.36	33.64
09.05.21	3.8	25.00	12.0	0.47	33.07	26.88	45.93	36.22
10.05.21	4.2	25.00	8.9	0.50	31.44	32.71	37.07	36.10
11.05.21	3.6	24.67	14.4	0.69	31.63	30.80	27.07	31.47
12.05.21	3.6	24.67	10.4	0.58	31.03	32.87	24.03	35.38
13.05.21	3.4	24.67	14.0	0.88	30.25	38.14	25.05	31.73
14.05.21	3.6	24.67	14.8	0.58	29.90	39.55	19.73	33.76
15.05.21	4.4	25.67	15.4	0.46	29.85	37.70	43.29	37.16
16.05.21	4.6	25.00	15.3	0.32	32.26	31.37	57.39	34.63
17.05.21	4.2	27.00	7.2	0.30	32.16	34.72	39.22	37.53
22.05.21	4	25.00	14.2	0.55	29.04	52.88	59.18	32.66
23.05.21	3.6	26.67	12.7	0.25	27.00	47.26	53.72	33.70
24.05.21	4.6	26.67	15.8	0.23	29.78	39.99	54.28	31.21
25.05.21	5	28.00	15.3	0.35	31.40	35.00	34.15	34.80
26.05.21	5.6	28.33	15.5	0.43	32.74	33.15	32.99	36.11
27.05.21	6	29.00	15.5	0.37	33.77	31.73	36.84	38.32
28.05.21	7.4	30.00	15.9	0.60	36.41	29.60	33.63	37.85
29.05.21	6.6	29.67	13.9	0.70	35.14	36.16	38.16	41.05
30.05.21	5.8	29.00	13.4	0.59	34.66	37.85	45.93	38.87
03.06.21	2.8	27.33	15.9	0.20	31.87	43.83	43.27	25.60
04.06.21	3.6	30.00	14.1	0.40	32.04	42.69	61.55	37.22
06.06.21	4.4	29.00	14.5	0.44	33.17	43.69	50.70	32.63
07.06.21	4.2	29.33	13.8	0.57	35.76	38.86	42.22	37.40
08.06.21	4.4	31.00	14.9	0.93	37.10	33.25	57.08	38.94
09.06.21	4.2	31.00	15.1	0.90	37.03	32.88	42.19	40.76
10.06.21	4.4	31.00	14.8	0.74	36.11	35.17	39.30	40.55
13.06.21	6.2	30.33	10.3	0.56	28.87	49.90	51.18	38.39
15.06.21	2.6	28.33	11.0	0.63	31.12	53.46	71.60	38.73

Date	evaporation (panel at height 300 mm) mm/day	Average Water Temp in °C	Rs in MJ/m^2/day	Average Wind speed (m/s)	Average daily ambient temp (°C)	Average daily humidity (%)	Average daily humidity under panel (%)	Panel temperature in °C
16.06.21	2.8	19.00	14.9	0.30	30.25	57.00	68.92	31.66
17.06.21	2.6	30.33	14.7	0.37	31.98	51.54	61.27	36.13
18.06.21	2.4	20.33	13.8	0.60	32.52	49.59	52.40	37.56
19.06.21	4	30.67	8.9	0.36	31.14	52.97	55.02	38.01
20.06.21	4.8	30.33	11.6	0.35	33.01	48.69	49.69	33.71
21.06.21	6	30.67	12.0	0.45	32.72	45.63	39.16	36.68
22.06.21	6.6	31.00	13.0	0.47	33.45	39.43	38.94	36.68
26.06.21	3	30.00	14.0	0.36	31.86	51.54	44.70	33.42
27.06.21	3.2	31.33	14.1	0.30	32.93	42.29	40.17	36.49
28.06.21	6.7	31.33	14.3	0.30	34.64	39.65	38.03	38.31
29.06.21	6	31.67	13.8	0.57	36.73	33.60	38.90	39.63
30.06.21	6.6	27.33	14.7	1.04	36.98	33.68	40.17	40.64
01.07.21	6.2	30.67	15.6	0.88	36.63	35.31	40.09	40.37
02.07.21	4.2	30.67	14.8	0.71	34.69	39.58	38.03	40.18
03.07.21	4	30.67	14.4	0.63	33.73	43.14	51.54	39.32
04.07.21	3.8	33.33	11.7	0.60	33.79	42.59	47.17	37.86
06.07.21	3.6	31.00	12.9	0.48	35.10	46.72	50.27	34.40
08.07.21	3.2	31.67	15.3	0.47	35.64	38.72	35.08	37.35
09.10.21	3	30.67	12.1	0.37	34.87	44.34	47.17	40.43
10.07.21	3	30.67	14.2	0.52	36.53	43.08	51.30	39.08
19.07.21	2.8	27.33	2.7	0.47	27.87	74.55	88.95	28.20
20.07.21	2	29.33	12.6	0.68	31.03	63.42	71.38	35.35
22.07.21	2	30.00	15.2	0.38	31.27	67.85	71.67	37.68
23.07.21	1.8	29.67	10.3	0.26	30.71	69.63	74.78	34.85
24.07.21	2.2	31.00	13.1	0.28	32.36	64.29	59.90	37.94
25.07.21	2.4	31.67	15.3	0.40	33.88	58.23	62.99	40.13
27.07.21	1.4	29.00	4.9	0.41	29.57	69.93	85.88	31.12
29.07.21	1.4	28.33	6.3	0.24	28.09	75.60	89.75	30.62
31.07.21	1.2	28.33	5.9	0.18	29.54	77.82	89.28	28.25
01.08.21	3.4	27.67	11.5	0.33	29.93	71.35	92.56	31.12
02.08.21	3.4	29.67	8.7	0.14	29.82	73.63	74.32	34.95
04.08.21	2.8	30.67	14.1	0.24	30.36	72.44	80.77	31.44
05.08.21	3.6	31.00	13.2	0.23	31.22	67.45	79.62	35.77
08.08.21	2.8	28.33	12.7	0.23	31.15	68.38	85.48	33.96
09.08.21	2.6	30.00	11.7	0.50	31.90	63.26	62.46	36.23
10.08.21	3	28.33	14.9	0.76	31.23	58.20	88.95	34.31
11.08.21	4.2	29.00	15.4	0.74	30.89	55.24	63.13	36.41
12.08.21	4.2	29.00	15.2	0.71	31.61	54.12	56.46	36.06
13.08.21	4.6	29.00	14.7	0.72	31.78	52.34	58.03	36.52

Date	evaporation (panel at height 300 mm) mm/day	Average Water Temp in °C	Rs in MJ/m^2/day	Average Wind speed (m/s)	Average daily ambient temp (°C)	Average daily humidity (%)	Average daily humidity under panel (%)	Panel temperature in °C
14.08.21	4.4	29.00	14.9	0.65	31.30	52.63	55.41	36.93
15.08.21	5.4	29.00	14.7	0.49	31.26	52.44	58.71	36.33
16.08.21	5.4	30.00	14.1	0.23	31.56	52.63	56.46	36.51
17.08.21	5.6	30.33	14.4	0.24	32.58	50.34	54.73	36.85
18.08.21	5.8	30.67	13.5	0.22	33.07	51.13	55.02	38.10
19.08.21	6	30.33	13.9	0.23	33.85	47.49	55.02	38.61
20.08.21	5.6	29.67	6.8	0.48	30.66	61.60	65.19	39.00
23.08.21	2	29.00	12.3	0.28	30.11	70.31	76.90	29.50
24.08.21	4	31.00	15.3	0.57	32.79	61.49	64.90	34.79
25.08.21	5.4	30.00	15.7	0.88	32.14	51.83	55.02	38.15
26.08.21	5.2	28.33	15.1	0.71	30.61	53.02	59.35	36.62
27.08.21	4	28.33	14.4	0.40	31.31	53.74	69.04	34.91
28.08.21	4.2	29.67	14.4	0.23	31.57	52.93	53.12	36.06
29.08.21	3.8	29.33	10.8	0.48	32.04	56.15	58.62	37.45
30.08.21	3.6	30.00	12.9	0.55	30.43	62.78	68.53	35.35
05.09.21	2	28.00	8.3	0.11	29.22	76.00	85.93	33.64
06.09.21	2.4	30.67	13.5	0.15	31.46	70.45	76.25	31.46
07.09.21	2.6	30.67	11.2	0.63	29.89	70.97	79.97	36.31
08.09.21	2.6	29.00	12.7	0.63	29.05	70.78	76.63	33.62
09.09.21	2.6	28.33	8.6	0.39	29.05	72.93	82.92	33.00
10.09.21	2.4	28.67	11.4	0.76	29.10	71.43	80.44	31.85
13.09.21	2.8	27.67	6.8	0.33	28.22	76.90	92.33	31.15
14.09.21	3	28.33	10.1	0.41	29.03	74.54	84.39	29.33
15.09.21	3	29.33	15.0	0.56	28.94	65.08	66.71	32.01
17.09.21	2.4	28.00	11.0	0.43	28.10	69.43	79.09	31.67
18.09.21	2.2	28.33	11.2	0.50	29.21	69.43	73.95	31.60
19.09.21	2.2	29.33	12.8	0.34	30.03	66.94	74.53	32.43
20.09.21	2.6	29.00	10.5	0.19	30.29	68.55	74.69	33.47
24.09.21	2.2	27.67	9.0	0.16	28.01	77.55	89.75	29.25
25.09.21	2.6	29.00	13.0	0.17	29.00	73.16	80.64	31.04
26.09.21	2.4	29.00	12.1	0.35	28.82	73.36	89.37	33.75
27.09.21	2.6	28.67	11.7	0.32	29.41	71.44	80.64	33.00
28.09.21	2.8	28.67	10.7	0.46	30.03	69.15	77.87	33.29
29.09.21	2.8	28.67	12.3	0.53	29.78	67.42	72.21	32.57
30.09.21	3.2	29.00	10.2	0.19	29.32	69.24	69.38	33.56
01.10.21	3.2	29.67	14.0	0.24	30.36	66.33	67.92	32.19
02.10.21	3	29.33	11.0	0.24	29.79	66.40	73.03	35.26
03.10.21	3	29.00	14.8	0.38	30.59	61.74	70.88	33.07
04.10.21	3.2	28.67	13.0	0.36	29.89	59.17	61.50	34.18

Date	evaporation (panel at height 300 mm) mm/day	Average Water Temp in °C	Rs in MJ/m^2/day	Average Wind speed (m/s)	Average daily ambient temp (°C)	Average daily humidity (%)	Average daily humidity under panel (%)	Panel temperature in °C
05.10.21	3	28.33	11.5	0.22	28.90	65.72	70.88	33.98
06.10.21	3.4	29.33	13.7	0.17	28.20	65.92	67.20	31.65
07.10.21	3.4	28.00	13.7	0.14	27.37	61.59	61.84	32.44
08.10.21	3.2	29.00	14.6	0.20	28.20	50.04	49.75	30.87
09.10.21	3.4	23.67	14.4	0.22	28.85	48.67	58.01	31.57
10.10.21	3.4	25.00	14.4	0.31	30.14	47.42	66.23	32.08
11.10.21	3.4	27.00	14.3	0.23	28.52	48.75	54.11	32.59
12.10.21	3.2	26.00	13.3	0.13	26.63	49.89	55.97	31.58
13.10.21	3	24.67	13.6	0.22	25.01	46.98	63.16	29.62
14.10.21	3.2	20.33	13.8	0.24	24.39	42.48	72.21	27.65
15.10.21	3.2	23.33	14.0	0.13	24.52	44.69	41.95	26.19
16.10.21	3	23.67	12.5	0.12	29.06	45.91	48.93	27.09
18.10.21	3	23.00	3.4	0.15	21.45	76.79	95.83	26.47
19.10.21	3.2	24.33	12.5	0.25	24.00	66.99	78.23	20.58
20.10.21	3.2	23.00	14.2	0.34	24.76	49.52	52.11	26.72
21.10.21	3.2	24.00	14.3	0.50	26.15	40.42	38.68	26.72
22.10.21	3	24.00	14.4	0.49	25.68	46.39	54.34	27.21
23.10.21	2.8	23.67	12.7	0.41	24.94	50.26	54.04	27.60
24.10.21	2.6	22.67	10.9	0.32	23.01	57.65	65.89	27.67
25.10.21	2.8	21.67	11.9	0.21	21.78	59.28	64.89	25.82
26.10.21	2	20.33	12.8	0.16	20.62	55.50	59.47	24.13
27.10.21	2.4	20.00	12.1	0.19	21.49	52.31	52.36	23.35
28.10.21	2.2	20.00	13.1	0.19	21.20	47.33	53.44	23.57
29.10.21	2	19.00	12.0	0.15	21.01	45.03	48.13	23.25
30.10.21	2.4	19.00	12.0	0.25	21.91	45.11	44.85	22.80
31.10.21	2.4	19.33	12.3	0.18	21.88	42.90	64.66	23.07
01.11.21	2.6	20.00	12.3	0.19	24.04	38.24	49.02	23.59
02.11.21	2.6	20.00	11.3	0.23	23.76	40.07	46.55	25.40
03.11.21	2	20.00	9.4	0.25	21.47	47.82	52.36	25.60
04.11.21	2	18.67	7.1	0.12	19.79	50.97	60.81	21.85
05.11.21	2	17.67	7.4	0.07	20.25	48.04	59.01	19.34
06.11.21	1.8	18.00	9.9	0.19	21.14	42.76	41.31	19.43
07.11.21	1.6	17.67	8.6	0.14	20.31	47.55	51.54	21.74
08.11.21	1.8	17.67	9.3	0.14	20.58	48.54	54.47	20.37
09.11.21	1.8	18.33	10.1	0.14	21.16	45.75	52.61	20.91
10.11.21	2.2	17.67	10.2	0.09	21.35	43.90	54.08	21.65
11.11.21	1.8	18.33	10.6	0.10	21.02	44.55	46.13	22.05
12.11.21	1.6	17.00	6.4	0.08	19.85	46.52	52.07	22.21
13.11.21	1.6	17.00	9.9	0.11	18.47	43.85	49.95	17.47

Date	evaporation (panel at height 300 mm) mm/day	Average Water Temp in °C	Rs in MJ/m^2/day	Average Wind speed (m/s)	Average daily ambient temp (°C)	Average daily humidity (%)	Average daily humidity under panel (%)	Panel temperature in °C
14.11.21	1.6	3.67	9.2	0.06	18.32	44.89	62.51	18.84
15.11.21	1.7	15.67	8.3	0.06	17.62	46.53	50.57	18.48
16.11.21	1.6	14.67	8.7	0.07	17.07	46.96	50.97	17.34
17.11.21	1.7	14.67	9.6	0.12	16.98	46.53	46.09	16.87
18.11.21	1.5	14.67	9.4	0.09	17.12	48.52	56.84	17.20
20.11.21	1.5	17.00	8.50	0.06	18.74	48.24	49.74	17.70
09.12.21	1.6	13.33	10.4	0.11	15.34	57.71	64.65	16.41
10.12.21	1.6	13.33	9.8	0.17	14.35	55.12	55.36	16.61
11.12.21	1.4	12.33	10.4	0.11	15.34	57.71	55.75	14.86
12.12.21	1.6	12.00	10.1	0.14	14.51	53.20	77.79	15.27
15.16.21	0.8	12.67	8.8	0.19	13.77	63.68	69.39	6.75
16.12.21	0.7	11.67	5.5	0.21	10.34	64.97	72.26	14.44
17.12.21	1.4	9.67	10.1	0.31	10.60	61.47	65.03	9.89
18.12.21	1.6	9.33	10.8	0.34	9.30	56.40	67.54	11.32
19.12.21	1.4	9.00	11.1	0.25	10.81	46.86	56.78	9.96
20.12.21	1.8	9.67	11.1	0.15	13.60	42.89	54.15	11.65
22.12.21	2	12.67	10.3	0.24	16.43	45.04	49.89	12.35
23.12.21	1.6	13.67	8.7	0.23	17.53	50.09	54.76	17.22
24.12.21	1.6	15.00	8.8	0.19	17.64	55.22	63.68	17.25
25.12.21	1.2	14.67	8.2	0.27	17.94	61.21	62.58	18.45
26.12.21	1	14.26	2.1	0.48	16.90	66.38	87.06	18.87
27.12.21	0.8	14.67	6.4	0.21	15.22	70.51	79.19	16.07
28.12.21	0.6	12.67	6.9	0.18	12.96	66.72	71.86	16.24
30.12.21	0.8	10.40	8.8	0.26	11.78	61.67	100.00	13.19
31.12.21	0.8	10.33	8.0	0.11	11.71	58.41	64.16	12.22
01-Jan-22	0.8	10.33	9.4	0.16	12.20	60.75	64.16	11.95
02-Jan-22	0.8	11.67	9.4	0.15	12.62	61.19	69.19	12.75
03-Jan-22	1	11.67	9.5	0.14	14.49	58.41	66.77	13.28
06-Jan-22	0.5	14.33	2.2	0.23	14.36	76.86	95.02	13.14
08-Jan-22	0.9	16.33	4.9	0.42	14.39	78.52	90.75	18.31
09-Jan-22	1	12.00	3.8	0.26	9.43	75.99	88.58	14.73
10-Jan-22	1	12.00	10.2	0.20	12.19	72.94	89.30	9.61
11-Jan-22	1	10.00	3.3	0.27	9.35	83.61	94.20	13.80
12-Jan-22	1	11.33	6.6	0.16	11.75	77.35	85.59	9.52
13-Jan-22	0.5	11.33	7.4	0.18	12.13	79.91	85.59	12.61
14-Jan-22	0.8	11.00	2.4	0.17	10.28	79.50	89.30	13.56
15-Jan-22	0.7	9.67	2.9	0.34	8.63	85.11	94.20	9.68
16-Jan-22	0.9	10.33	8.6	0.32	10.62	80.06	89.30	9.23
17-Jan-22	0.8	10.33	7.9	0.36	9.49	85.40	94.00	12.19

Date	evaporation (panel at height 300 mm) mm/day	Average Water Temp in °C	Rs in MJ/m^2/day	Average Wind speed (m/s)	Average daily ambient temp (°C)	Average daily humidity (%)	Average daily humidity under panel (%)	Panel temperature in °C
18-Jan-22	0.8	11.33	9.0	0.24	11.88	77.38	89.93	11.76
19-Jan-22	0.8	12.33	6.4	0.55	13.50	78.23	89.93	12.54
20-Jan-22	0.9	12.67	7.2	0.32	13.63	80.99	89.93	13.99
22-Jan-22	0.6	12.67	1.5	0.49	11.79	82.99	89.30	11.97
24-Jan-22	0.8	12.67	7.5	0.27	11.43	73.67	89.30	7.36
25-Jan-22	0.9	12.67	6.9	0.22	10.96	78.02	80.15	
26-Jan-22	1	11.33	11.0	0.30	11.68	69.99	84.70	
27-Jan-22	1	11.33	12.0	0.32	11.84	64.70	85.59	
28-Jan-22	1	12.67	12.4	0.28	13.21	59.48	67.56	
29-Jan-22	1	12.00	12.5	0.22	14.95	56.22	64.14	
30-Jan-22	0.9	13.33	12.3	0.28	15.48	57.27	71.33	
31-Jan-22	1.8	13.33	12.0	0.21	16.41	59.19	64.89	
01-Feb-22	1.8	14.33	11.0	0.28	14.09	64.19	89.93	
02-Feb-22	1.8	13.00	12.2	0.98	17.20	56.43	59.18	
03-Feb-22	1.8	13.00	4.4	0.60	11.99	70.54	79.78	
04-Feb-22	1.8	12.33	11.3	0.22	12.15	67.69	71.62	
05-Feb-22	1.8	12.00	12.9	0.35	14.05	66.49	72.57	
06-Feb-22	1.9	13.67	12.6	0.47	17.05	57.21	62.31	
07-Feb-22	1.9	16.00	11.4	0.27	19.04	56.72	61.10	
08-Feb-22	1.9	16.67	10.4	0.33	18.08	64.92	74.46	
09-Feb-22	1.9	16.00	12.7	0.34	15.21	62.12	67.80	
10-Feb-22	1.9	14.67	12.4	0.30	14.97	59.71	69.95	
11-Feb-22	1.9	13.67	13.8	0.36	14.33	54.31	61.56	
12-Feb-22	2.2	13.67	14.2	0.29	15.95	50.81	50.47	
13-Feb-22	2.2	14.67	14.3	0.28	17.19	49.17	51.04	
14-Feb-22	2.2	15.00	13.9	0.27	17.55	46.11	46.68	
15-Feb-22	2.2	16.00	13.2	0.27	17.75	51.53	49.20	
16-Feb-22	2.2	16.00	13.0	0.27	18.08	54.23	54.61	
17-Feb-22	2.2	16.33	12.2	0.37	18.81	54.22	62.16	
18-Feb-22	2.4	16.00	9.8	0.33	18.42	51.44	50.13	
19-Feb-22	2.4	16.33	13.6	0.30	17.57	51.59	58.79	
20-Feb-22	2.4	15.33	13.2	0.56	16.99	44.12	55.49	
21-Feb-22	2.6	15.33	14.7	0.59	21.21	36.52	40.94	
23-Feb-22	3.2	19.33	11.7	0.46	19.86	55.51	60.54	
24-Feb-22	3	18.67	11.6	0.31	20.13	54.44	69.69	
25-Feb-22	3.6	18.67	12.1	1.37	21.70	51.91	54.45	
26-Feb-22	3	17.00	12.0	1.28	17.20	58.86	60.05	
27-Feb-22	3	15.33	15.2	0.33	16.11	57.22	58.64	
28-Feb-22	3	15.00	15.2	0.27	17.18	53.55	57.81	

Date	evaporation (panel at height 300 mm) mm/day	Average Water Temp in °C	Rs in MJ/m^2/day	Average Wind speed (m/s)	Average daily ambient temp (°C)	Average daily humidity (%)	Average daily humidity under panel (%)	Panel temperature in °C
01-Mar-22	3	14.33	14.2	0.27	19.06	55.66	79.76	
02-Mar-22	3	18.00	14.0	0.69	20.99	56.83	50.24	
03-Mar-22	3	19.00	13.6	0.38	18.77	58.22	56.68	
04-Mar-22	3.2	18.33	15.0	0.48	18.30	57.79	71.33	
05-Mar-22	3.2	17.00	15.3	0.36	19.64	54.30	64.56	
06-Mar-22	3.2	19.00	10.9	0.56	22.98	51.32	72.57	
07-Mar-22	3.2	20.33	14.8	0.61	23.23	46.05	46.13	
08-Mar-22	3.2	20.67	13.9	0.40	22.65	47.04	53.00	
09-Mar-22	3.2	20.33	12.1	0.33	21.73	46.47	43.58	
10-Mar-22	3.2	20.67	13.7	0.27	22.38	48.98	53.74	
11-Mar-22	3.2	21.00	15.1	0.42	21.99	46.11	52.37	
12-Mar-22	3.2	20.33	15.3	0.30	23.92	41.58	46.80	
13-Mar-22	3.2	22.33	15.2	0.31	26.45	44.51	50.94	
14-Mar-22	3.2	23.33	14.9	0.34	26.94	43.38	46.65	
15-Mar-22	3.2	24.00	14.7	0.45	27.95	41.23	34.94	
16-Mar-22	4.8	25.00	15.2	0.51	28.15	39.94	50.53	
17-Mar-22	4.6	24.33	15.3	0.40	29.89	39.59	31.74	
18-Mar-22	4.6	24.33	14.4	0.58	29.80	42.66	63.41	
19-Mar-22	5	25.67	15.5	0.55	30.12	37.31	45.30	
20-Mar-22	5	24.33	15.0	0.42	29.10	28.06	29.44	
21-Mar-22	4.6	25.00	14.6	0.36	28.98	38.58	38.78	
22-Mar-22	5.2	24.33	14.5	0.50	28.00	38.43	49.79	
23-Mar-22	5	24.33	11.6	0.49	28.42	33.24	42.68	
24-Mar-22	5	24.00	15.1	0.47	27.31	35.39	30.91	
25-Mar-22	5	24.33	14.9	0.37	27.43	34.35	40.93	
26-Mar-22	5	23.33	15.3	0.54	27.18	28.27	32.94	
27-Mar-22	6.2	27.00	15.9	0.46	29.69	21.28	31.01	
28-Mar-22	6	24.33	15.8	0.52	30.94	18.79	23.00	
29-Mar-22	5.4	24.33	15.6	0.44	31.61	19.28	27.62	
31-Mar-22	5.4	25.00	14.6	0.46	28.54	27.12	27.84	
01-Apr-22	5.6	24.33	15.9	0.45	27.98	23.78	27.38	
02-Apr-22	4.8	24.33	15.3	0.57	31.25	17.72	25.86	
03-Apr-22	6.4	23.67	16.8	0.53	30.22	13.86	19.38	
04-Apr-22	6.2	24.00	15.6	0.41	28.99	19.13	25.01	
05-Apr-22	6.2	24.67	15.5	0.26	29.52	19.35	26.28	
06-Apr-22	6	25.67	16.1	0.27	29.57	18.43	25.04	
07-Apr-22	6.4	25.67	16.1	0.31	30.39	16.31	26.05	
08-Apr-22	6.6	25.33	16.3	0.40	32.88	14.02	24.64	
09-Apr-22	6.6	26.00	15.0	0.52	33.33	14.08	15.67	

Date	evaporation (panel at height 300 mm) mm/day	Average Water Temp in °C	Rs in MJ/m^2/day	Average Wind speed (m/s)	Average daily ambient temp (°C)	Average daily humidity (%)	Average daily humidity under panel (%)	Panel temperature in °C
10-Apr-22	6.6	26.33	15.7	0.52	32.81	13.94	20.83	
11-Apr-22	7	26.33	15.5	0.62	34.36	13.45	24.12	
12-Apr-22	6.6	26.00	10.7	0.50	32.14	14.73	28.68	
13-Apr-22	7	25.00	14.7	0.61	31.06	20.42	11.96	
14-Apr-22	6.4	26.67	12.3	0.49	31.19	20.78	28.77	
15-Apr-22	7	26.67	14.0	0.43	30.91	18.50	25.66	
16-Apr-22	6.7	26.33	15.7	0.37	31.34	16.37	42.15	
17-Apr-22	7	27.67	14.6	0.34	32.47	22.29	28.91	
18-Apr-22	7.2	27.33	14.4	0.38	33.63	19.64	29.20	
19-Apr-22	7.6	27.33	15.3	0.53	32.70	20.34	41.29	
20-Apr-22	7.6	27.67	13.4	0.60	33.70	20.27	28.31	
21-Apr-22	5.6	26.67	10.6	0.77	29.87	29.77	29.96	
22-Apr-22	4.8	26.00	15.1	0.34	29.11	30.03	41.96	
23-Apr-22	7	27.00	15.9	0.34	30.55	23.00	32.63	
24-Apr-22	7	26.67	14.6	0.46	31.00	22.78	28.99	
25-Apr-22	7.4	26.67	12.5	0.70	32.33	23.41	27.75	
26-Apr-22	7	28.00	14.5	0.42	31.90	22.72	21.46	
27-Apr-22	7.6	28.00	15.4	0.36	32.99	19.22	25.72	
28-Apr-22	8	28.33	15.0	0.58	35.48	15.94	21.32	
29-Apr-22	8	28.67	15.3	0.54	34.95	13.59	18.03	
30-Apr-22	8.2	28.67	15.0	0.51	34.40	17.02	19.91	
01-May-22	8	29.67	14.0	0.74	35.46	18.29	23.53	
02-May-22	9	29.00	13.8	0.66	36.50	16.94	28.57	
03-May-22	9	29.33	13.9	0.57	34.17	16.58	25.81	
04-May-22	8.6	28.67	13.8	0.86	32.08	27.83	26.04	
05-May-22	8.6	28.33	13.6	0.35	31.66	30.68	39.09	
06-May-22	8.2	28.33	12.2	0.48	31.78	27.41	33.84	
07-May-22	8.2	28.67	14.6	0.37	33.17	22.08	28.40	
08-May-22	3.4	28.67	14.5	0.67	35.77	23.94	31.63	
09-May-22	9.2	29.00	13.9	0.84	35.77	25.57	24.40	
10-May-22	9.2	30.00	14.2	0.63	36.70	25.60	30.86	
11-May-22	9.4	31.00	13.5	0.47	36.11	25.04	32.67	
12-May-22	9.6	30.67	13.9	0.54	35.29	18.29	26.61	
13-May-22	9.6	30.67	13.9	0.63	36.41	11.90	19.15	
14-May-22	10	29.67	19.1	0.60	38.01	14.38	24.09	
15-May-22	10.2	31.00	14.6	0.78	40.03	13.39	25.16	
16-May-22	9.8	30.00	13.1	0.66	36.17	14.61	23.86	
17-May-22	9.2	30.67	12.8	0.49	34.79	17.88	50.09	
18-May-22	8.6	30.33	12.9	0.45	35.80	22.06	29.28	

Date	evaporation (panel at height 300 mm) mm/day	Average Water Temp in °C	Rs in MJ/m^2/day	Average Wind speed (m/s)	Average daily ambient temp (°C)	Average daily humidity (%)	Average daily humidity under panel (%)	Panel temperature in °C
19-May-22	8.7	31.33	14.3	0.47	36.94	20.45	28.44	
20-May-22	1.2	30.33	13.8	0.96	38.64	15.30	24.91	
21-May-22	10.6	29.67	10.4	0.94	32.03	28.12	26.33	
06-Jul-22	3.4	33.00	9.2	0.82	32.38	58.95	60.74	
07-Jul-22	3.4	32.33	8.9	0.69	34.23	57.29	59.90	
08-Jul-22	4	33.00	9.7	0.55	33.86	52.49	45.54	
09-Jul-22	4	31.67	6.8	0.60	32.73	59.70	65.56	
11-Jul-22	4	32.00	7.5	0.25	32.04	65.52	63.69	
12-Jul-22	4	30.33	5.9	0.36	31.17	67.68	78.01	
13-Jul-22	4	32.00	9.0	0.56	33.08	60.37	64.90	
14-Jul-22	3.8	31.33	7.6	0.90	32.40	61.52	70.96	
16-Jul-22	1.2	29.33	7.7	0.90	30.61	68.31	89.37	
18-Jul-22	2	31.67	8.0	0.26	31.11	71.08	68.97	
19-Jul-22	2.8	32.00	8.2	0.43	32.49	64.74	68.97	
24-Jul-22	1	30.00	8.6	0.90	30.30	72.22	73.03	
25-Jul-22	1.4	29.67	9.8	0.75	29.65	69.66	69.92	
26-Jul-22	1.6	30.00	9.3	0.78	29.03	71.61	70.69	
27-Jul-22	1.8	30.33	9.3	0.58	30.07	68.28	61.00	
28-Jul-22	1.6	30.00	7.1	0.55	30.01	69.26	74.40	
02-Aug-22	1.6	30.67	13.8	0.34	30.43	69.31	70.21	29.99
03-Aug-22	1.8	30.33	12.4	0.18	30.41	70.77	80.48	32.57
06-Aug-22	1.7	30.33	12.7	0.24	30.62	72.69	74.69	27.71
07-Aug-22	1.9	30.33	8.3	0.47	28.88	75.58	77.55	33.89
08-Aug-22	2.4	31.00	15.1	0.55	30.81	68.46	72.21	30.90
09-Aug-22	2.6	31.67	13.7	0.62	31.64	65.91	67.42	33.91
10-Aug-22	2.9	31.67	12.7	0.98	32.01	60.78	56.07	33.91
11-Aug-22	2.8	29.67	9.7	0.99	29.64	64.81	65.31	33.89
12-Aug-22	2.6	29.33	13.0	1.10	31.04	61.65	58.62	30.21
13-Aug-22	2.7	29.33	10.5	0.64	29.90	67.32	76.76	31.83
14-Aug-22	2.6	29.33	9.9	0.40	29.52	69.78	79.51	31.32
16-Aug-22	2.2	28.33	6.9	1.60	28.70	71.04	86.60	29.84
17-Aug-22	3	28.00	9.0	0.59	29.33	70.54	77.40	28.05
18-Aug-22	2.9	29.33	9.4	0.30	29.66	69.01	68.67	29.71
19-Aug-22	3	30.00	10.9	0.42	29.78	66.78	61.36	31.13
20-Aug-22	3.2	29.67	10.8	0.27	31.23	63.00	65.53	31.09
21-Aug-22	2.8	29.67	9.4	0.37	30.62	67.12	86.60	32.41
22-Aug-22	2.8	30.67	8.7	0.50	30.96	68.49	82.39	30.67
23-Aug-22	3.2	28.33	8.0	1.35	29.49	66.09	73.76	31.38
24-Aug-22	3	28.67	13.0	0.64	30.08	64.13	68.89	29.45

Date	evaporation (panel at height 300 mm) mm/day	Average Water Temp in °C	Rs in MJ/m^2/day	Average Wind speed (m/s)	Average daily ambient temp (°C)	Average daily humidity (%)	Average daily humidity under panel (%)	Panel temperature in °C
25-Aug-22	2.8	28.00	8.5	0.40	29.92	68.48	73.80	30.95
26-Aug-22	3.4	29.00	13.7	0.52	30.20	62.56	66.15	29.60
28-Aug-22	3.8	29.00	12.5	0.59	30.65	57.23	60.46	
29-Aug-22	3.2	29.00	9.8	0.24	30.30	57.99	60.19	32.28
30-Aug-22	2.2	29.33	8.3	0.36	30.85	58.60	61.87	31.71
31-Aug-22	3.6	30.00	13.3	0.50	32.47	54.76	54.29	32.02
02-Sep-22	3.4	30.00	14.3	0.38	30.99	60.60	66.31	31.78
03-Sep-22	3.4	29.33	14.3	0.62	30.96	58.70	64.31	33.38
04-Sep-22	3	29.00	15.6	0.65	30.22	56.90	58.83	32.83
05-Sep-22	3.2	28.67	14.5	0.35	29.53	57.80	60.86	32.18
06-Sep-22	2.8	28.33	15.1	0.29	30.61	55.89	59.44	31.77
07-Sep-22	3.6	29.67	12.2	0.29	31.77	55.15	65.11	33.12
08-Sep-22	3.3	30.00	11.1	0.45	32.93	54.46	57.52	34.11
09-Sep-22	3.4	30.33	10.8	0.51	32.61	55.09	65.53	34.27
10-Sep-22	4	31.00	12.7	0.64	32.88	54.87	60.73	34.60
11-Sep-22	3.6	30.33	9.5	0.55	31.83	59.00	63.61	34.89
12-Sep-22	3.8	30.00	12.8	0.88	30.84	56.43	56.46	32.07
13-Sep-22	3.6	28.67	10.8	0.88	29.90	58.99	68.12	32.77
14-Sep-22	3.2	28.67	10.8	0.79	29.61	62.99	68.12	31.22
15-Sep-22	3.5	29.00	10.7	0.67	29.61	61.98	69.27	30.19
16-Sep-22	3.6	28.33	10.7	0.72	30.79	60.39	66.27	30.46
17-Sep-22	3.6	28.67	13.0	0.44	30.13	55.23	65.38	31.61
18-Sep-22	3.4	28.67	12.9	0.41	30.42	53.21	65.95	32.07
19-Sep-22	3.2	29.00	10.7	0.33	31.19	53.55	66.44	31.83
20-Sep-22	2.6	28.33	7.6	0.32	30.46	59.84	71.45	31.73
21-Sep-22	2.2	28.33	8.4	0.50	30.50	62.68	71.09	30.58
28-Sep-22	3	27.33	14.0	0.36	30.09	54.00	86.10	
29-Sep-22	3	27.33	13.6	0.29	29.79	54.36	58.27	30.28
30-Sep-22	3	27.67	13.3	0.28	30.18	54.99	56.63	30.28
01-Oct-22	3.2	26.67	13.6	0.41	31.26	58.01	51.56	31.09
02-Oct-22	3.2	26.67	13.0	0.33	29.14	48.58	51.56	30.87
03-Oct-22	3.2	26.00	14.0	0.32	29.29	48.21	48.01	29.06
04-Oct-22	2.8	26.00	13.5	0.32	28.23	51.04	48.38	28.63
05-Oct-22	2.8	26.00	12.5	0.30	28.32	51.52	56.12	28.87
06-Oct-22	2.6	26.00	13.3	0.69	28.62	54.24	59.81	29.10
09-Oct-22	1	23.33	1.9	0.21	22.81	82.59	92.17	22.56
10-Oct-22	2	23.33	2.5	0.14	22.59	82.71	92.33	23.20
11-Oct-22	2	24.67	10.3	0.19	23.63	73.99	85.24	23.22
12-Oct-22	2.4	23.67	13.4	0.16	24.23	69.08	73.03	24.15

Date	evaporation (panel at height 300 mm) mm/day	Average Water Temp in °C	Rs in $MJ/m^2/day$	Average Wind speed (m/s)	Average daily ambient temp (°C)	Average daily humidity (%)	Average daily humidity under panel (%)	Panel temperature in °C
13-Oct-22	2.4	22.67	13.3	0.18	24.45	63.03	70.58	24.96
14-Oct-22	2.4	22.67	13.0	0.22	24.97	58.50	66.10	24.95
15-Oct-22	2.6	22.67	12.4	0.11	25.04	57.95	63.74	24.78
16-Oct-22	2	22.67	13.1	0.18	24.76	55.22	63.85	25.51
17-Oct-22	2	22.33	13.1	0.25	26.08	48.31	61.82	25.10
18-Oct-22	2.2	22.33	13.0	0.32	26.03	44.05	51.69	25.67
19-Oct-22	2.4	22.33	12.5	0.43	26.91	40.06	46.49	25.77
20-Oct-22	2.2	22.33	12.0	0.33	26.33	39.71	46.49	26.06
21-Oct-22	2.2	22.33	12.0	0.28	25.15	43.95	57.90	26.08
22-Oct-22	2	22.33	10.6	0.17	22.77	49.24	67.15	24.91
23-Oct-22	2	22.33	11.6	0.16	22.77	45.85	55.01	23.65
24-Oct-22	2	20.00	11.5	0.22	23.11	43.27	50.69	22.58
25-Oct-22	2	20.00	10.9	0.27	23.69	43.10	46.13	22.48
26-Oct-22	2.2	20.00	11.4	0.22	25.11	42.93	53.26	23.14
27-Oct-22	2.4	21.67	11.1	0.30	26.02	41.06	48.04	25.86
28-Oct-22	2.4	21.67	10.8	0.24	24.48	42.77	44.70	25.89
29-Oct-22	2.4	21.33	10.0	0.13	24.08	41.89	58.91	24.53
30-Oct-22	2.4	21.00	10.3	0.19	24.04	40.73	49.74	23.31
31-Oct-22	2.4	21.00	10.5	0.20	24.72	41.19	58.91	23.48
01-Nov-22	2.2	21.33	10.5	0.25	25.24	41.66	44.70	24.77
02-Nov-22	2.2	21.67	8.3	0.25	24.37	47.47	51.11	25.29
03-Nov-22	2.6	21.67	8.1	0.25	25.41	47.91	64.86	23.16
04-Nov-22	2.6	22.67	10.0	0.29	26.39	43.55	67.10	25.33
05-Nov-22	2.4	22.67	11.0	0.19	25.85	39.95	55.98	26.99
06-Nov-22	2.6	21.67	9.8	0.19	25.31	35.85	51.71	26.05
09-Nov-22	2	20.67	9.6	0.16	23.10	55.39	67.19	20.67
10-Nov-22	2	21.67	9.6	0.17	21.49	54.32	67.32	23.60
11-Nov-22	1.8	20.00	9.4	0.19	20.34	53.89	68.02	21.87
12-Nov-22	1.8	18.67	10.5	0.24	19.83	50.27	58.19	19.99
13-Nov-22	1.8	18.67	9.8	0.21	21.94	47.43	57.13	19.76
14-Nov-22	1.8	20.00	9.6	0.43	23.90	41.62	55.47	22.35
15-Nov-22	1.8	20.33	7.7	0.16	20.55	50.41	68.97	24.77
16-Nov-22	1.8	18.67	10.5	0.23	18.29	50.55	61.47	21.17
17-Nov-22	1.8	16.67	10.4	0.31	17.34	47.05	59.18	17.92
19-Nov-22	1.6	17.00	10.5	0.17	18.54	42.65	61.29	18.53

A8.7(1)

The predicted results of uncovered water surface area (open tank) evaporation are shown in Table A8.7.1.

Table A8.7.1 Evaporation under uncovered water surface area (open tank) at 28 selected dam using Regression Equation (8.59)

Name of Reservoir/ Dams	Latitude	Longitude	Evaporation estimation under uncovered water surface using 4 parametric Regression model by Equation (8.59) (in mm)
Saprar dam	25.2104 N	79.0831 E	1853.74
Barwa Sagar	25.3732 N	78.7220 E	1834.51
Pathrai Dam	25.4148 N	78.9979 E	1837.60
Dongri Dam	25.3844 N	78.4562 E	1834.91
Garhmau Tank	25.5238 N	78.6538 E	1840.95
Pahuj dam	25.5063 N	78.5260 E	1844.74
Parichha dam	25.5171 N	78.7770 E	1837.86
Dhukwan dam	25.1925 N	78.5347 E	1848.81
Barwar lake	25.5220 N	79.1307 E	1852.27
Matatila dam	25.0616 N	78.2506 E	1882.36
Sajnam dam	24.5253 N	78.5906 E	1945.43
Govind sagar dam	24.6727 N	78.4266 E	1906.55
Jamini dam	24.3403 N	78.4143 E	2014.48
Shahzad dam	24.9502 N	78.5197 E	1877.38
Arjun dam	25.3868 N	79.6763 E	1933.11
Belasagar	25.2642 N	79.5797 E	1912.29
Pahari dam	25.2343 N	79.2836 E	1862.33
Maudaha dam	25.5887 N	79.7048 E	1962.84
Lahchura dam	25.3281 N	79.2796 E	1869.58
Chandrawal dam	25.4308 N	79.8635 E	2008.42
Kabrai dam	25.4084 N	79.9769 E	2022.24
Ohan dam	25.1319 N	81.0316 E	**2126.53**
Gunta dam	25.2173 N	81.1447 E	2117.15
Majhgawan dam	25.2821 N	79.5099 E	1873.75
Upper khajuri dam	24.9963 N	82.5960 E	2094.16
Moosakhand dam	24.9583 N	83.2917 E	2097.18
Latif Shah dam	25.025 N	83.2250 E	2090.91
Dhadraul dam	24.6254 N	83.1695 E	1961.60
Adwa dam	24.7861 N	82.3056 E	2100.24
Rihand dam	24.0236 N	82.7285 E	1925.87
Obra dam	24.4394N	82.9661 E	2044.25
Kanhar dam	24.1229 N	83.2946 E	1971.73
Kalagarh dam	29.5194 N	78.7586 E	**1783.29**
Rajghat dam	24.7625 N	78.7500 E	1835.82

Similarly, evaporation values have also been determined by taking into consideration of the covered areas with PV panels at these 28 dam sites using 4 parametric regression model (equation 8.73). These values are also shown in Table A8.7.2.

Table A-8.7.2. Evaporation estimation of selected 28 dams, by 4 parametric Regression model by Equation (8.73)

Name of Reservoir/Dams	Latitude	Longitude	PV panel covered tank Evaporation estimation by 4 parametric Regression model by equation (8.73) (in mm)
Saprar dam	25.2104 N	79.0831 E	1300.52
Barwa Sagar	25.3732 N	78.7220 E	1287.66
Pathrai Dam	25.4148 N	78.9979 E	1291.58
Dongri Dam	25.3844 N	78.4562 E	1286.79
Garhmau Tank	25.5238 N	78.6538 E	1290.76
Pahuj dam	25.5063 N	78.5260 E	1292.30
Parichha dam	25.5171 N	78.7770 E	1289.10
Dhukwan dam	25.1925 N	78.5347 E	1296.69
Barwar lake	25.5220 N	79.1307 E	1304.30
Matatila dam	25.0616 N	78.2506 E	1321.31
Sajnam dam	24.5253 N	78.5906 E	1383.26
Govind Sagar dam	24.6727 N	78.4266 E	1345.32
Jamini dam	24.3403 N	78.4143 E	1448.90
Shahzad dam	24.9502 N	78.5197 E	1322.45
Arjun dam	25.3868 N	79.6763 E	1384.90
Belasagar	25.2642 N	79.5797 E	1361.65
Pahari dam	25.2343 N	79.2836 E	1313.23
Maudaha dam	25.5887 N	79.7048 E	1411.82
Lahchura dam	25.3281 N	79.2796 E	1319.73
Chandrawal dam	25.4308 N	79.8635 E	1453.11
Kabrai dam	25.4084 N	79.9769 E	1471.00
Ohan dam	25.1319 N	81.0316 E	**1567.63**
Gunta dam	25.2173 N	81.1447 E	1559.58
Majhgawan dam	25.2821 N	79.5099 E	1321.17
Upper khajuri dam	24.9963 N	82.5960 E	1541.24
Moosakhand dam	24.9583 N	83.2917 E	1536.62
Latif Shah dam	25.025 N	83.2250 E	1532.84
Dhadraul dam	24.6254 N	83.1695 E	1429.85
Adwa dam	24.7861 N	82.3056 E	1540.30
Rihand dam	24.0236 N	82.7285 E	1382.44
Obra dam	24.4394N	82.9661 E	1491.13
Kanhar dam	24.1229 N	83.2946 E	1427.28
Kalagarh dam	29.5194 N	78.7586 E	**1283.32**
Rajghat dam	24.7625 N	78.7500 E	1289.60

The highest evaporation rates for open sky and covered with PV panels were **2126.53 mm/day and 1567.63 mm/day** estimated for Ohan dam and lowest were **1783.29 mm/day and 1283.32 mm/day for Kalagarh dam.**

PROFILE OF CANDIDATE

KARMENDRA KUMAR AGRAWAL

Superintending Engineer
UP Irrigation and Water Resources Department, Lucknow (UP)-226001, India
+91-9005747472 (Mobile)
Email: p20170105@pilani.bits-pilani.ac.in
karmendra.agrawal@gmail.com

Karmendra Kumar Agrawal, presently, functioning as a Superintending Engineer in UP Irrigation and Water Resources Department, Lucknow (UP) and posted as General Manager at Zone-6, UP Projects Corporation Limited, Noida (UP).

He has carved a niche for himself in the irrigation department while he worked in various capacities and has immensely contributed towards planning, execution, and monitoring of an assortment of irrigation projects. He has been associated with excellence, commitment, time-bound accomplishment of seemingly impossible projects. His remarkable feat in construction of complexed Lahchura dam is like a folklore to upcoming budding aspiring engineers. He also has documented the humongous task of entire paradigm and modus operandi of construction of Lahchura Dam which has become a revered epic book and précis for future references. His other significant commendable works have been towards planning and execution of Arjun Sahayak Irrigation Project, Augasi Irrigation Pump house, Bhaurat dam and Madhya Ganga Canal Project phase-II. He has also contributed towards construction of 5.92 MWp canal top solar power plant, which was unprecedented in Uttar Pradesh.

He holds a very vast experience in conceptualizing, planning, monitoring, and executing various administrative works and has won accolades in almost every project he has ever taken on for accomplishment.

BRIEF PROFILE OF SUPERVISOR

Dr. Ravi Kant Mittal

Professor,
Department of Civil Engineering,
Birla Institute of Technology & Science, Pilani-Rajasthan-333031, India
Tel. No.: +91-9887692025 (Mobile)
Email: ravimittal@pilani.bits-pilani.ac.in
Website: https://www.bits-pilani.ac.in/pilani/ravi-kant-mittal/
,

Dr. Ravi Kant Mittal is currently Professor, Department of Civil Engineering, Birla Institute of Technology & Science, Pilani. Dr. Mittal obtained B.E., M.E. and Ph.D. in Civil Engineering from I.I.T., Roorkee. He has more than 30 years of teaching and research experience. His research interests include sustainable development, cleaner energy, utilization of waste material, environmental geotechnics, optimization and economical design. He has authored more than 80 research publications of national and international repute. Prof Mittal has guided 3 doctoral Thesis and over 35 PG and UG Dissertations/Thesis and currently guiding 4 Ph.D. scholars in research areas of real-life importance. He has completed 2 sponsored projects in the field of Civil Engineering such as Design and development of fixed and floating solar PV installation for water management infrastructures and working on one ongoing project in the area of waste utilization using MICP technique. Prof. Mittal has taught more than 30 different courses of Civil Engineering.

He has served as head of the Civil Engineering department of the institute from 2016-2018. As HoD he Co-ordinated, NAAC team visit in 2016 and team visit in 2017. As HoD, he contributed to the development of curriculum, new course, labs, experiments, content, etc. He played key role in developing M.Tech. (Transportation) and M.Tech. (Structures) for WILP for PWD Goa. He was member of task force for curriculum development for UG and PG programmes of Civil Engineering. He is Life member Indian Society of Earthquake Technology and Indian Geotechnical Society, India.

BRIEF PROFILE OF CO-SUPERVISOR

Prof. Shibani Khanra Jha
Associate Professor, Department of Civil Engineering
Faculty In-Charge, Teaching Learning Centre, BITS Pilani, Pilani Campus

Professor Shibani Khanra Jha currently work as a faculty member in the Department of Civil Engineering at BITS Pilani. Additionally, she leads the Teaching Learning Centre (TLC) at the Pilani Campus as the Faculty-In-Charge. She earned her Doctoral and Master's degrees from IISc, Bangalore, and a B.E. (Hons) in Civil Engineering from Jadavpur University, Kolkata.

With over 15 years of experience in teaching, research, and administrative roles, her expertise lies in water resources, environmental engineering, renewable/geothermal energy etc. Her notable publications can be found in respected journals such as the International Journal of Geomechanics, Water Science and Technology, Geothermics, Geothermal Energy, Energy, Renewable Energy, Energies, Energy for Sustainable Development, and more. Her research on geothermal energies has garnered attention from publications like India Science Wire, TECH EXPLORIST, and Geothermal Resources Council News.

In addition to supervising PhD, postgraduate, and undergraduate theses, she actively contributes as a technical reviewer for various reputed journals like Sadhna by Springer, Journal of Earth System Sciences by Springer, Current Sciences by Indian Academy of Sciences, Environmental Earth Sciences by Springer, Geothermal Energy: Science, Society, and Technology by Springer, International Journal of Green Energy by Taylor and Francis, Energy, Sustainability and Society by Springer Nature, Geothermics and others. She also serves as a technical advisor for international conferences. She holds memberships in esteemed organizations like the Institute of Engineers India (IEI), International Association for Water, Environment, Energy, and Society (IAWEES), Women in Geothermal (WING) by Geothermal Resource Council, and The International Society for Porous Media (InterPore). She contributes as a Member of the Programme Advisory Group (PAG) Committee of DST sponsored Technology Enabling Centre (TEC) at Pandit Deendayal Energy University (PDEU), an External Expert Member of the Doctoral Committee (DC), Pandit Deendayal Energy University. She contributes as an expert resource person in the FDP on "Synergizing Academic Success: A Comprehensive Skill Development Program for Faculty" by Institute of Pharmacy, Nirma University under the Auspices of IQAC.

Furthermore, she has organized the International Conference on Best Innovative Teaching Strategies (ICON BITS 2023), conducted several workshops, Faculty Development Programs (FDPs), and mentorship programs for faculty and research students, conducted Leadership exposure program for CBSE Principals. As the Institute-Wide Coordinator of SWAYAM courses at BITS Pilani, she plays a key role in advancing education and learning strategies for 21st century education. She is also credited as the potential editor of the book "Perspective and Strategies on Newage Education and Creative Learning, Springer 2024" as an outcome of the ICON BITS 2023 conference.

BRIEF PROFILE OF CO-SUPERVISOR

Dr. AJIT PRATAP SINGH
Senior Professor, Civil Engineering Department,
Dean, Academic-Undergraduate Studies
Birla Institute of Technology and Science(BITS)-Pilani,
Vidya Vihar Campus, Pilani-Rajasthan-333031, India
Tel. No.: +91-1596-515235 (Office)
+91-9664031566 (Mobile)
Email: aps@pilani.bits-pilani.ac.in, apsbits@gmail.com
Website: https://www.bits-pilani.ac.in/pilani/aps/profile

Ajit Pratap Singh presently working as a **Senior Professor** of the Civil Engineering Department and **Dean, Academic-Undergraduate Studies** (Institute-wide for Pilani, Goa, Hyderabad, and Dubai Campuses) at Birla Institute of Technology and Science, Pilani (BITS Pilani)-Pilani Campus, Rajasthan.

He has published over **130** research papers and reports. He has also served as the Professor and Head of Department, Civil Engineering, BITS Pilani-Dubai Campus, UAE for 2 years from September 2015 to August 2017. He has more than **28 years** of teaching and research experience in the area of sustainable water resources management, hydraulics, and water resources engineering with a special focus on surface water-quality modeling and advanced computer applications: water quality and quantity assessment, water pollution analysis, solid waste management, prediction and management of surface waters, and groundwater contaminant transport modeling, climate change, pavement management systems, soft computing techniques, fuzzy-based decision making, and simulation and modeling.

Prof. Singh has taught as many as **25** different courses of Civil Engineering such as Hydrology & Water Resources Engineering, Environmental Engineering, Hydraulics, and Fluid Mechanics, Water and Wastewater Treatment, Waste Management Systems, Environmental Pollution Control, Transportation Engineering, Transport Phenomena I, Pavement Analysis and Design, Pavement Material Characterization, Engineering Optimization, Geographical Information Systems and so on. From time to time Dr. Ajit has also delivered invited talks for various training programs and workshops. Prof Singh has guided **10** doctoral Thesis and over **50** Master's Dissertations/Thesis and currently guiding **4** Ph.D. scholars in research areas of real-life importance. Prof Singh has also evaluated **20** Ph.D. Thesis. He has completed **5** sponsored project in different field of Civil Engineering and working on one ongoing projects in the area of water resources engineering and societal development. He has also been actively involved in various consultancy projects related to water quality assessment, water pollution analysis, prediction and management of surface waters, groundwater contaminant transport modeling, traffic safety of National highways, district

environmental management plans, etc. He is a fellow of the Institution of Engineers (India), Fellow of Indian Association of Hydrologists (FIAH), Member of the International Water Association, the Indian Society of Hydraulics, the Indian Water Works Association (IWWA), and the Institution of Public Health Engineers, India, and a Member of Eastern Asia Society for Transportation Studies (EASTS), Japan, etc. He has been actively involved in reviewing various research papers submitted in his field to more than 35 Journals of International and National repute. He has also worked as the commissioner/member of high powered committee/monitoring committee appointed by the Hon'ble National Green Tribunal, New Delhi for assessing the status of environmental quality in different rivers and industrial clusters. He is an expert member of the State Level Environment Appraisal Committee (SEAC) in Rajasthan to examine environmental issues before clearing developmental projects proposed in the state of Rajasthan.

Prof. Singh applies engineering concepts with a sound mathematical foundation to maintain a high-quality environment in a sustainable and cost-efficient manner and used to share knowledge through his teaching, training programs, workshops, and quality publications.